Sulfur copolymers for coatings, composites, and mining applications

by

Maximilian Mann

Thesis

Submitted to Flinders University

for the degree of

Doctor of Philosophy

College of Science and Engineering

22 April 2022

Contents

Summary

The discovery of inverse vulcanisation has renewed the interest in sulfur polymers. Since sulfur is produced in vast quantities by the oil and gas industry as a co-product of petroleum refining, inverse vulcanisation also opened new ways to take advantages of this low-cost feedstock.

With a focus of using renewable, abundant, or low-cost materials, the process chemistry of upscaling the synthesis of a poly(S-*r*-canola) polymer from a laboratory scale to an industrial scale was explored.

To utilise another low-cost feed stock from the petroleum industry, the protocol for synthesising polymer made from sulfur and dicyclopentadiene (DCPD) was revisited to establish a robust method that was safer than methods previously reported. This method produced a solvent processable pre-polymer that could be rendered insoluble by thermal curing. Further, the material was coated onto silica gel and metal and displayed excellent solvent and acid resistance along with mercury sorption properties.

Since the construction industry is one of the biggest consumers of resources globally this sector would benefit greatly from the use of renewable or abundant building materials. A polymer made from sulfur, DCPD and canola oil was investigated as a bulk structural material. The ability of this material to be bonded together through amine-catalysed S-S metathesis makes it a unique candidate for construction as it can be the mortar and bulk structural material simultaneously. The strength of this adhesion was evaluated as well as ways to improve the mechanical properties though the addition of various carbon materials.

Since an ever-increasing amount of plastic waste is produced, end of life solutions for plastics have become increasingly important. With this in mind, a simple carbonisation method for the poly(S-*r*-canola) polymer was developed. The resulting carbon showed a high sulfur content resulting in efficient mercury removal from aqueous solutions. Additionally, carbonising the polymer after it has been used to remove oil from water, its mercury sorption ability actually improved. After mercury uptake, the material could be regenerated and used again to remove mercury. Importantly, prolonged exposure to acidic solution resulted in minimal mercury leaching from the carbon.

The use of mercury in artisanal and small-scale gold mining (ASGM) is damaging to environment and detrimental to the health of the miners and their communities. Therefore, alternatives to mercury are urgently needed. In preliminary experiments a poly(S-*r*-canola) polymer displayed gold sorption capabilities. Consequently, a more thorough investigation into this interesting aspect of the polymer was undertaken. Firstly,

a new gold oxidation method using cost effective and relatively benign chemicals was developed to leach solid gold into aqueous solution. This method was then used to extract gold from a range of different ores and ore concentrates. This method was also applied to remove gold from e-waste. The poly(S-*r*-canola) polymer was able to recover the leached gold to a high degree of purity from the ore and e-waste samples. Hence, it can be said that a mercury free gold extraction method has been developed using a new gold oxidation method in conjunction with a polymer sorbent to recover the gold which has applications in ASGM and e-waste processing.

Declaration

I certify that this thesis does not incorporate without acknowledgment any material previously submitted for a degree or diploma in any university; and the research within will not be submitted for any other future degree or diploma without the permission of Flinders University; and that to the best of my knowledge and belief it does not contain any material previously published or written by another person except where due reference is made in the text.

Signed:…Maximilian Mann

Date: 22 April 2022

Acknowledgements

I want to thank my supervisor Justin Chalker for allowing to undertake my PhD in his laboratory and under his supervision. Comparing myself to when I began my research made me realise how much I have grown as a scientist. For most of this I must thank my supervisor, for his attention to detail (to which I hope someday I come close) and for helping me to see the positive in seemingly negative results. I learned so much from him and will be forever grateful.

A thank you to all the members of the Chalker group, past and present for all the chats, help and support.

Without the support of my wife, I would have never been able to do my PhD (or undergraduate degree) but her unwavering support and faith in me made all the difference.

I also like to thank my parents for supporting me in every decision I made in many ways.

Lastly, I'd like to thank all the people at Flinders and Liverpool universities that helped me during my research with their expertise and knowledge of instruments, methods, analysis and much more.

My candidature was supported by a Research Training Program scholarship.

Publications and patents

Publications 1-4 are directly related to the research contained in this thesis.

Publications 5-6 are co-authored publications to which I contributed to but are not directly related to this thesis.

1. **Mann, M.**; Luo, X.; Tikoalu, A. D.; Gibson, C. T.; Yin, Y.; Al-Attabi, R.; Andersson, G. G.; Raston, C. L.; Henderson, L. C.; Pring, A.; Hasell, T.; Chalker, J. M., Carbonisation of a polymer made from sulfur and canola oil. *Chem Commun* **2021,** *57* (51), 6296-6299.

2. **Mann, M.**; Zhang, B.; Tonkin, S.; Gibson, C.; Jia, Z.; Hasell, T.; Chalker, J. Process for coating surfaces with a copolymer made from sulfur and dicyclopentadiene. *Polym. Chem.* **2022**

3. **Mann, M.**; Pauling, P. J.; Tonkin, S. J.; Campbell, J. A.; Chalker, J. M., Chemically Activated S-S Metathesis for Adhesive-Free Bonding of Polysulfide Surfaces. *Macromol. Chem. Phys.* **2021**, 2100333

4. Materials and process for recovering precious metals. **Mann, M**.; Chalker, J.M. Patent No. WO 2020/198778 A1, March 31, 2020

5. Chalker, J. M.; **Mann, M.**; Worthington, M. J. H.; Esdaile, L. J., Polymers Made by Inverse Vulcanization for Use as Mercury Sorbents. *Organic Materials* **2021,** *03* (02), 362-373.

6. Lundquist, N. A.; Tikoalu, A. D.; Worthington, M. J. H.; Shapter, R.; Tonkin, S. J.; Stojcevski, F.; **Mann, M.**; Gibson, C. T.; Gascooke, J. R.; Karton, A.; Henderson, L. C.; Esdaile, L. J.; Chalker, J. M., Reactive Compression Molding Post-Inverse Vulcanization: A Method to Assemble, Recycle, and Repurpose Sulfur Polymers and Composites. Chem. Eur. J. 2020, 26 (44), 10035-10044.

Chapter 1

Synthesis and applications of materials made by inverse vulcanisation

The element sulfur and its abundance

Sulfur is the 16th most abundant element on our planet and makes up around 0.1% of our earth's crust in weight and has been mined for thousands of years for multiple uses.[1, 2] Coincidentally, sulfur is also the 16th element in the periodic table. Sulfur has an atomic weight of 32.066 g mol^{-1} and exists in four stable isotopes, ^{32}S (95%), ^{33}S (0.76%), ^{34}S (4.22%) and ^{36}S (0.014%).[3] The molecular structure of elemental sulfur is that of an eight-membered ring and melts at around 119 °C.[3, 4] Sulfur is also an important element for living organisms.[5] In its native form, sulfur is a relatively nontoxic, odourless, and brittle solid of pale yellow color.[3, 4] Sulfur can be found it its native form around hot springs and volcanoes, or more commonly in metal sulfide ores in the form of minerals like sulfates (SO_4^{2-}) or sulfides (S^{2-}).[3, 6] However the most important geological source of sulfur are the sulfides, of which the pyrites are prominent.[6] These minerals have been a major industrial source of sulfur for the production of sulfuric acid beside elemental sulfur.[6]

Today, sulfur is mainly a co-product from sour gas and crude oil processing, smelting of nonferrous metal ores and other industrial processes.[7, 8] While the composition of oil is dominated by hydrocarbons, metals, oxygen, and nitrogen, sulfur containing species are also present in various amounts.[9] Sulfur content of oil has an impact on its value and presents an obstacle during the refining process.[9] Sulfur in fuels such as kerosene, diesel and gasoline presents itself in the form of sulfides, disulfides and thiophenes.[10] The need to remove these compounds from fossil fuels arises from the SO_x formation during their combustion.[10] These sulfur oxides can cause environmental pollution, acid rain, smog, and contribute to global warming when released into the atmosphere.[11, 12] Further, SO_2 is also linked to human health problems. [13] Therefore, strict regulations regarding the sulfur release of fuels have been enforced by governments round the world.[10] According to the British geological survey of 2014-2018, over 70 million metric tonnes of sulfur have been recovered in 2018 alone, mainly from petroleum and gas refining.[14] The enormous production of sulfur lead to massive stockpiles around the world (Figure 1.1).[15]

Figure 1.1: Sulfur piles from oil refining. Image credit: Ed Uthman, this image was reproduced under a Creative Commons Licence: CC BY 2.0

Much of the recovered sulfur is used in the production of sulfuric acid while smaller amounts are used in the synthesis of pharmaceutical, industrial and agricultural chemicals or other applications in chemical synthesis.[7] Nevertheless, the supply of sulfur still outweighs the demand and sulfur is stored in large quantities (Figure 1.1).[7] This excess sulfur can be stored in block form for a long time but environmental concerns like groundwater contamination with sulfuric acid (through the oxidation of sulfur) can arise if storage is not carried out with suitable precautions.[16, 17] Considering this challenge with surplus sulfur, it becomes apparent that alternative uses of this element need to be investigated.

Polymers made by inverse vulcanisation

The rubber industry has a long history of sulfur use. Using the vulcanisation process, rubber resins are chemically crosslinked to yield elastic rubbers.[18] Rubber products made using vulcanisation include tires for cars and planes.[19] Rubbers are polymeric materials that return to their original shape after a mechanical external force has been applied.[18, 20] These characteristics are attained by a process called vulcanisation. During this process the elasticity of a material is enhanced while the degree of plasticity is reduced.[20] This is usually achieved by crosslinking polymer chains. (Figure 1.2).[20] The crosslink can be in the form of a single sulfur atoms or a short chain of sulfur atoms.[20] The most common vulcanisation method is sulfur vulcanisation.[18]
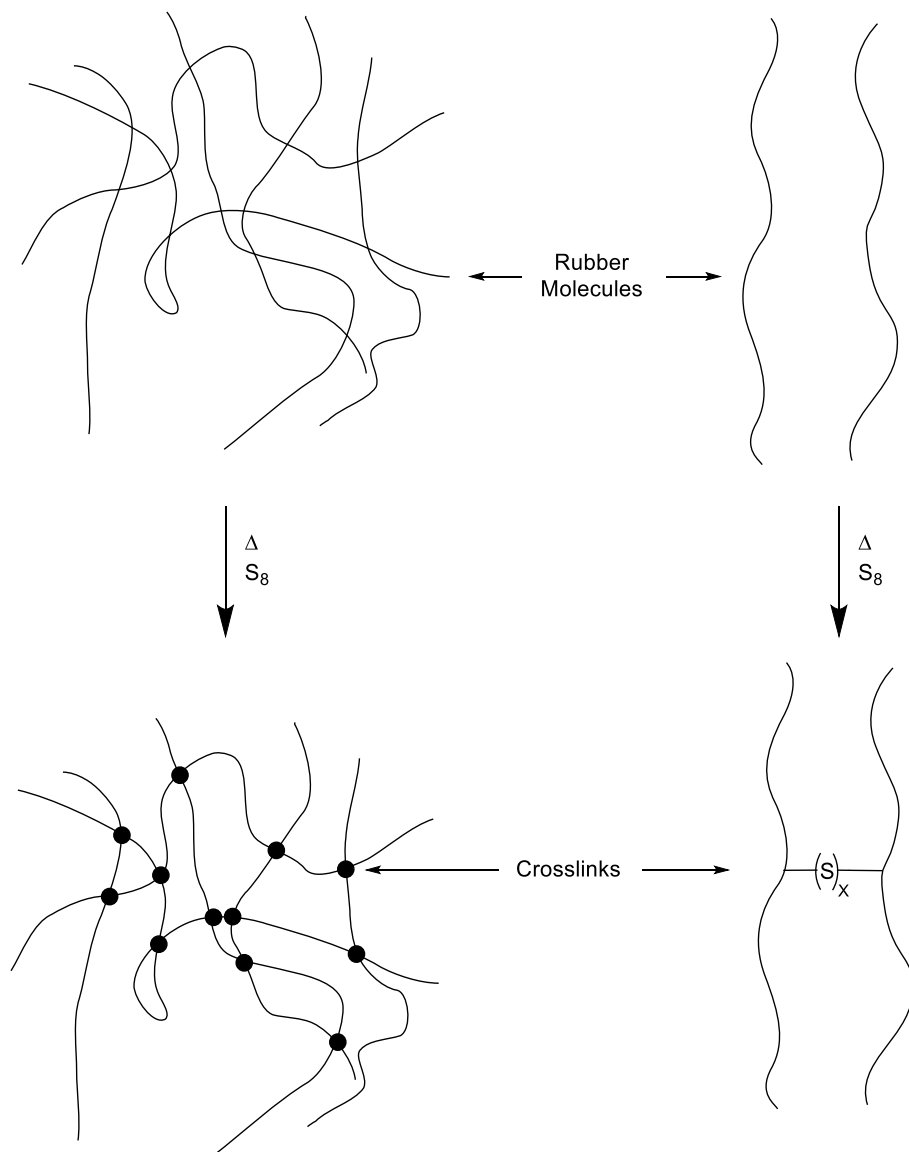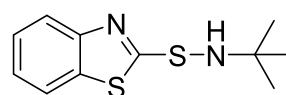

Figure 1.2: During conventional vulcanisation rubber molecules are crosslinked using small amounts of sulfur to form synthetic rubber.[20]

To facilitate a fast and effective formation of crosslinked material, accelerators and activators are commonly used.[21, 22] Not only does the addition of accelerators increase the speed of the reaction but the number of crosslinks and their density is also improved.[18] Commonly used accelerators are dithiocarbamates, quinones, thiurames, amines, sulfenamides and benzothiazoles (Figure 1.3).[23] Most accelerators contain one or two sulfur atoms between organic end groups and have a N=C-S group.[24]
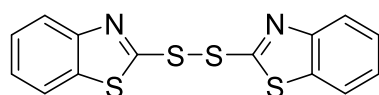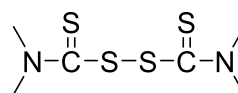

2,2'-Dithiobenzothiazole   N-tert-butylbenzothiazole-2-sulfenamide

Zinc dimethyldithiocarbamate   Tetramethylthiuram disulfide

Figure 1.3: Examples of a benzothiazole, sulfenamide, dithiocarbamate and thiuram commonly used as accelerators.[24]

Activators used today are metal oxides or hydroxides in conjunction with co-activators which are usually fatty acids.[23] The most commonly used activator is zinc oxide combined with a fatty acid such as stearic or lauric acid.[18] Although the vulcanisation process has been used for over 150 years, the mechanism of the accelerated vulcanisation process is not yet fully understood.[18] It is thought that increasing the amount of accelerators reduces modifications in the main chain which decreases the formation of cyclic structures as well as the sulfur rank between crosslinks, leading to a more efficient vulcanisaton.[22] Further, it is believed that the activators (such as zinc oxide) together with the fatty acid, form salts. This salt combined with the accelerators used, results in intermediate complexes, which aid the activation of the sulfur present, hence increasing the reaction rate.[18]

The vulcanisation process results in changes in the molecular structure of previously unvulcanised rubber molecules. Typically, unvulcanised rubber molecules have a molecular weight of between 100,000 and 500,000 daltons.[20] After the vulcanisation process is complete, cross links have been introduced with an average molecular weight between these junctures of 4000 to 10.000 daltons.[20] This results in

practically insoluble rubbers whose shape cannot be permanently altered after they have been made.[20] Early vulcanisations used 8 parts of sulfur per 100 parts of rubber (phr) and took 5 hours at 140 °C to complete.[20] However, the use of accelerators and activators decreased the reaction time to under 3 minutes while only requiring 0.4-3.5 phr of sulfur depending on the type of rubber made.[18]

Lately, new applications for sulfur in the synthesis of polymers have emerged, specifically the synthesis of polymers by inverse vulcanisation. The term 'inverse vulcanisation was first coined by Pyun and colleagues in 2013.[15] In this process, copolymers are synthesised by a direct polymerisation with sulfur and an unsaturated organic compound.[15] In traditional vulcanisation only small amounts of sulfur (0.4-3.5 phr)[18] are used to crosslink polydienes.[15] This is in stark contrast to inverse vulcanisation where larger quantities of sulfur (50-90 wt%) are polymerised by ring-opening polymerisation followed by reaction of the radical end groups with the organic crosslinker (Figure 1.4).[25, 26] Termination, for instance by radical recombination, provides isolable polymers with polysulfide backbones.[26, 27] This mechanism was postulated by Pyun et al[15] and will be discussed in more detail below. However, other mechanisms can also be operative like in the case of sulfur and dicyclopentadiene polymerisation which are discussed in Chapter 4 of this thesis.
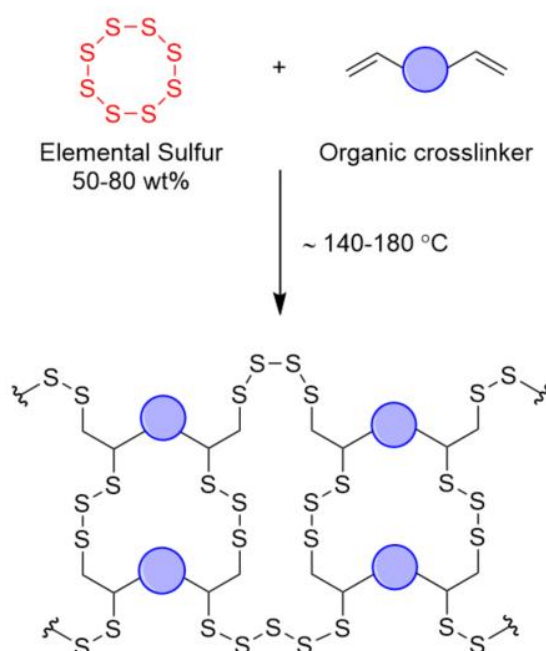
Figure 1.4: Copolymerisation of elemental sulfur and an organic crosslinker (for example a polyene).

Recently, many different unsaturated crosslinkers have been investigated regarding their utilisation in inverse vulcanisation. Many of these crosslinkers have been chosen because they are natural abundant products like canola oil[28] or they are low-cost products like dicyclopentadiene which is produced during the steam cracking process in ethylene plants.[29] Further, the investigated crosslinkers have unsaturated sites which react with the thiyl radicals formed in inverse vulcanisation. These crosslinkers range from natural products like plant oils to petroleum derived alkenes.[26, 28] Natural crosslinkers include triglycerides like canola[28, 30-33], castor[30], linseed[34], soybean[35] and other[30, 34, 36-39] oils. Also used are other natural unsaturated fatty acids [40] sourced from plant and animals like farnesene and farnesol[41] or rubber seed oil[42, 43] as well as natural polymers such as lignin[44] and natural small molecules found in garlic[45] and onion[46], thyme[45], orange peel[47], algae[48] and cloves.[49] Further, efforts have been made to modify natural molecules to make them available for use in polysulfide synthesis.[50, 51] Other monomers used include 1,3-diisopropenylbenzene (DIB)[15, 52-58], divinylbenzene[54, 55, 57, 59-62] benzoxazines and poly benzoxazines[51, 63-66], styrene and styrene derivatives[67-69] and dicyclopentadiene (DCPD).[41, 70, 71] Figure 1.5 below shows additional crosslinkers that have been recently used in polysulfide synthesis.
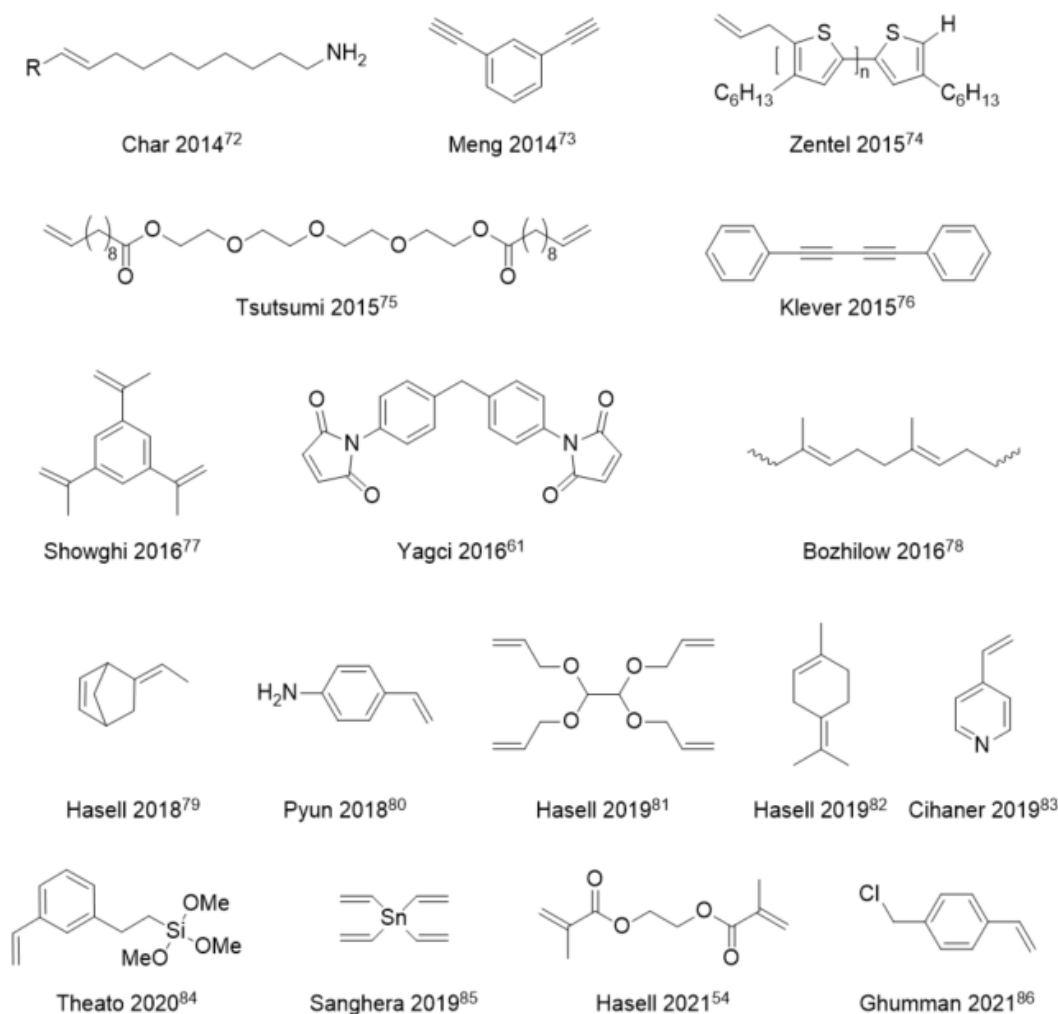
Figure 1.5: A selection of crosslinkers used in inverse vulcanisation to produce polysulfide polymers. The corresponding authors and the relevant citations are included for reference.

Clearly, a substantial amount of research has been made to explore a wide range of crosslinkers that can be utilised in inverse vulcanisation and the crosslinker library is still growing.

Inverse vulcanisation mechanism

The mechanism by which inverse vulcanisation occurs is not yet fully understood and can potentially be different depending on the conditions of the reaction, the choice of crosslinker or the use of a catalyst.[27] Nonetheless, one possible mechanism by which the inverse polymerisation may proceed is as follows (Figure1.6): As elemental sulfur is heated to over 159 °C, homolytic ring opening of the S_8 sulfur rings occurs, leading to a

polymerisation reaction between sulfur molecules.[87] Then, the thiyl radical end groups on the polymerised sulfur can react with a pi bond of an alkene or alkyne used as crosslinker during the propagation sequence.[25] Finally, the radical polymerisation could be terminated through radical recombination, as was proposed by Pyun et al.[15]
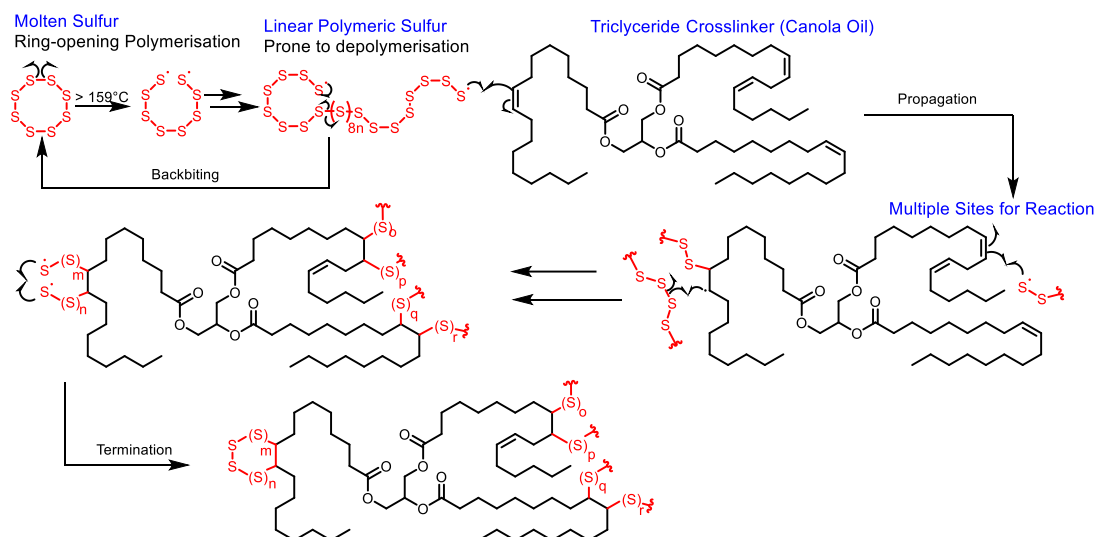

Figure 1.6: Possible mechanism of inverse vulcanisation of sulfur and canola oil (canola oil was chosen as representative crosslinker since this polymer was extensively used by the author). Homolytic ring opening of the S_8 sulfur rings is induced as elemental sulfur is heated above 159 °C. At this point the just generated thiyl radicals can react with another S_8 ring or react with an alkene or alkyne (in this case canola oil). However, the thiyl radical can also depolymerise through backbiting and revert back to the more thermodynamically stable S_8.[26] Termination is thought to proceed though radical recombination.[15]

Evidence that inverse vulcanisation proceeds via a radical mechanism includes electron paramagnetic resonance detection of radicals in liquid sulfur,[87] and in the polymer before termination.[25] NMR studies conducted by Pyun and Chalker confirmed that the sulfur radicals indeed react with pi bonds in the crosslinker by monitoring the alkene consumption during the polymerisation.[15, 47] Additionally, Raman spectroscopy, mass spectrometry, and degradation studies with reducing agents have been used to show the presence of S-S bonds, which is consistent with the proposed mechanism.[27] However, several studies indicate that the mechanism can vary.[27, 62] For instance this can happen when the crosslinker homopolymerises with itself, when branching occurs due to C-H abstraction, substitution with sulfur[62] or when nucleophilic additives are added to activate sulfur.[27]

Although investigating different crosslinkers is an important step toward expanding our knowledge of these new materials, finding potential application for these materials is equally as important. Consequently, a flurry of research has been conducted in recent years to identify potential applications of inverse vulcanised polysulfides. The following summary is designed to give the reader an overview of some of these applications:

Precursor for carbonised materials

Hasell and colleagues carbonised polysulfides and investigated possible applications for these carbonaceous materials.[88, 89] In one of their studies, they focused on S-DIB and S-Limonene polysulfides which was carbonised after synthesis via inverse vulcanisation (Figure 1.7).
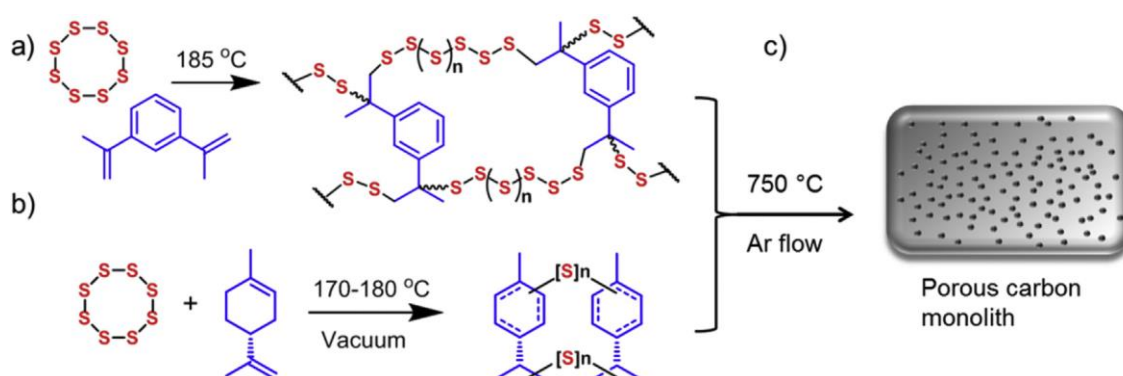

Figure 1.7: **a)** DIB or **b)** limonene were inverse vulcanised with sulfur and carbonised under Ar atmosphere to yield porous carbon. ©2016 Elsevier Inc. Images were reproduced under an RightsLink license.[88]

The same group also used a polymer made form sulfur and DCPD.[89] Their carbonisation method involves heating the polymer to temperatures of 750 °C to 850 °C under nitrogen flow. Additionally, some of the materials were activated using KOH.[89] More recently, Chalker and co-workers used carbonisation as an end of life use for a sulfur polymer already used to remove oil from water.[33] However, during the carbonisation at 600 °C no inert atmosphere was used and the materials were not chemically activated. Chapter 3 of this thesis details this research on sulfur polymers as a precursor to functional carbon materials. The materials made by the Hasell and Chalker groups exhibited surface areas ranging from 111 m^2 g^{-1} [88] to over 2200 m^2 g^{-1} [89]

and excellent gold[89] and mercury[33, 89] uptake. Further, the carbonaceous materials showed micro-porosity and displayed gas selectivity.[88, 89]

Adhesives

Regarding the use of inversed vulcanised polymers in adhesion applications, two different strategies have been employed. Jenkins et al set out and combined elemental sulfur with garlic essential oil and other sulfides to make a novel glue (Figure 1.8).[90]
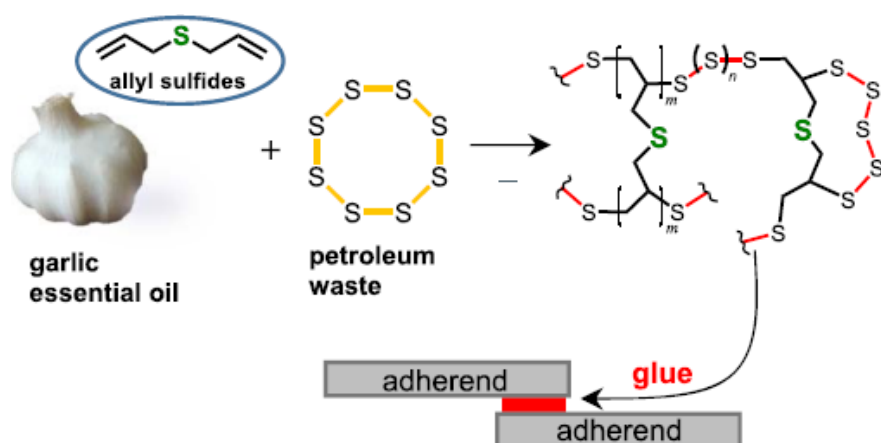
Figure 1.8: Garlic derived allyl sulfides and sulfur were inversely vulcanised. This reaction resulted in adhesive polymers. ©2019 American Chemical Society Image reproduced under a RightsLink licence.[90]

The results show that polysulfides based on garlic can indeed act as an adhesive. The adhesive was deposited onto aluminium sheets and hardened upon curing, achieving adhesive strength higher than that of hide glue.[90] Chalker and collaborators used a different strategy to utilise sulfur polymers as adhesive.[70, 91] In their work, a terpolymer synthesised by the direct reaction of DCPD, canola oil and sulfur, was used as a building block as well as a glue. This was accomplished by inducing a S-S bond metathesis between two polymer pieces using a catalyst containing an amine or phosphine. By adding the nucleophile to the surface, this metathesis is stimulated, resulting in an adhesion between the polymer pieces.[70, 91] This work is the focus of Chapter 5 of this thesis.

Antimicrobial / antibacterial materials

Polymers made via the inverse vulcanisation of DIB and elemental sulfur were spin coated onto silicon wafers resulting in thin films by Lienkamp and co-workers.[92] The materials were then assessed regarding their antimicrobial activity and found to be moderately active against *Escherichia coli*.[92] A more comprehensive study was conducted by Hasell et al by probing onto the antibacterial properties of inverse vulcanised polymers made from sulfur and DIB or DCPD.[93] For their work, interactions of their polysulfides with a Gram-negative and Gram-positive bacterium, namely *Escherichia Coli* and *Staphylococcus aureus* were investigated. The results show a higher antibacterial activity of the DIB containing polymer which the authors attribute to a higher sulfur rank of the material.[93] The same group also investigated the antibacterial properties of polysulfide polymers using DIB, perillyl alcohol DCPD, divinyl benzene (DVB) and triglycerides from rapeseed and linseed oil as crosslinkers on *Staphylococcus aureus* and *Pseudomonas aeruginosa*.[94] The polymers showed an inhibitory effect on the bacteria which was dependent on the crosslinker used. Hasell et al also postulate a correlation of the antimicrobial activity and the glass transition temperature of the polymers.[94]

Coating applications

Several reports explore the use of inverse vulcanised polymers as a coating. In an earlier work by Pyun et al, a sulfur DIB copolymer was used to produce thin films via spin coating.[95] Since then different coating techniques like spray coating, [83] dip coating, and solution casting[84] have been deployed to coat substrates with inverse vulcanised polymers. At times a curing process is needed after the coating process to stabilise the polymeric material. This can be done by thermal curing,[95] or by provoking a polycondensation post coating under mild conditions as has been recently reported by Theato and collaborators (Figure 1.9).[84] Notably, advantage has been taken of the solubility of sulfur-limonene[81] and *net*-poly(S_n-*r*-StyTMS)[84] systems to coat silica gel. The resultant coated silica gels proved excellent in removing mercury from aqueous solution.[81, 84] In chapter 4 of this thesis, a copolymer made from sulfur and dicyclopentadiene is described, along with its application as functional, protective and repairable coating.[96]
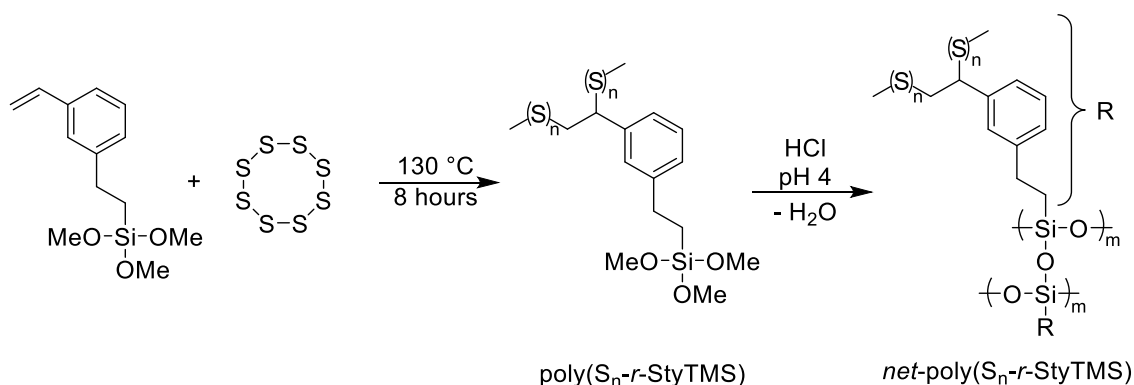
Figure 1.9: Synthesis scheme by Theato et al of the inverse vulcanisation of sulfur and styrylethyltrimethoxysilane (StyTMS) followed by hydrolysis and polycondensation to give *net*-poly(S_n-*r*-StyTMS).[84]

Composites

Polysulfides have also been made into composites. In a report by Zhang and associates, cottonseed oil and sulfur were inversely vulcanised, with the addition of fillers like active carbon, active clay, elm, cattail and carboxymethyl cellulose during the reaction.[36] Although the thermal properties did not change significantly between the different fillers, the morphology was greatly affected. This allowed tuneable densities for the composites.[36] A report by the Chalker group described a new way of making polysulfide composites.[31] In their work the authors co-polymerise canola oil and sulfur via inverse vulcanisation and use the pre-synthesised ground up polymer to form composites (Figure 1.10). To do that, filler materials are mixed with ground polymer and hot-pressed (100 °C, 40 MPa).
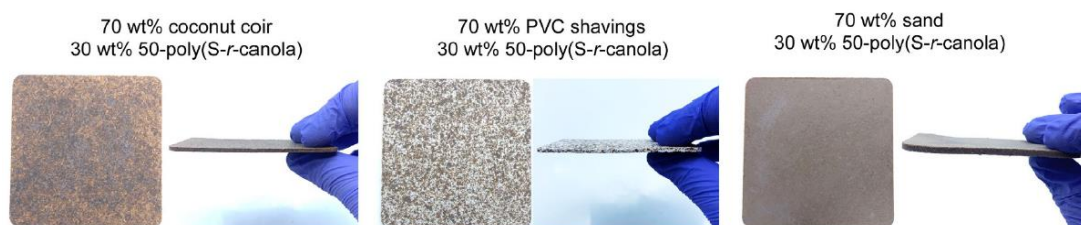

Figure 1.10: Composites made by Chalker et al using a polymer made by hot-pressing a polymer made from sulfur and canola oil (50-poly(S-*r*-canola)) and filler material like coconut coir, PVC shavings or sand. ©2020 Whiley-VCH Verlag GmbH&Co. KGaA, Weinheim. This image was reproduced under a RightsLink license.[31]

However, instead of a melting process, the authors propose a thermally induced homolytic cleavage of S-S bonds to induce S-S bond rearrangements. The advantage of the process is the comparatively low temperatures of ≈100 °C needed to form the composites. As fillers, coconut coir, PVC, sand, and powdered carbon fibre were used resulting in materials with varying moduli of elasticity, therefore presenting the opportunity for tuneable properties.[31] Similarly, Chalker et al demonstrated that wool can be used as a filler.[97] To ground up canola oil and sulfur polymer, wool fibres were added to produce composites using a hot press. Interestingly, the wool increased the insulating properties, tensile strength and reduced the flammability of the composite.[97]

Energy storage

Lithium-sulfur (Li-S) batteries are on the forefront of new energy storage technologies.[69]. Although Li-S batteries offer many advantages such as high capacities, low cost, and higher energy density,[98] there are some substantial drawbacks to that technology. These drawbacks include the poor electrical conductivity of elemental sulfur, the volume expansion during cycling and the dissolving of sulfur and polysulfide intermediates into the electrolyte.[99] Immobilisation of sulfur is thought to overcome this diffusion of sulfur species with in the battery[100]. With this in mind, polysulfides for energy storage and energy harvesting applications have been actively researched. A wide range of crosslinkers and synthesis pathways are used in the polysulfide synthesis to be used as cathode material in Li-S batteries.[15, 49, 69, 98-114] For example Pyun et al used a simple inverse vulcanisation of elemental sulfur and DIB to synthesise a polysulfide,[15] whereas Demir-Cakan and co-workers first synthesise their monomer (hexakis(styreneoxy) cyclotriphosphazene) by reacting hexachlorocyclotriphosphazene (HCCP) with p-hydroxystyrene which is then inverse vulcanised with elemental sulfur (Figure 1.11).[69] Both of these materials were evaluated as Li-S battery cathode.
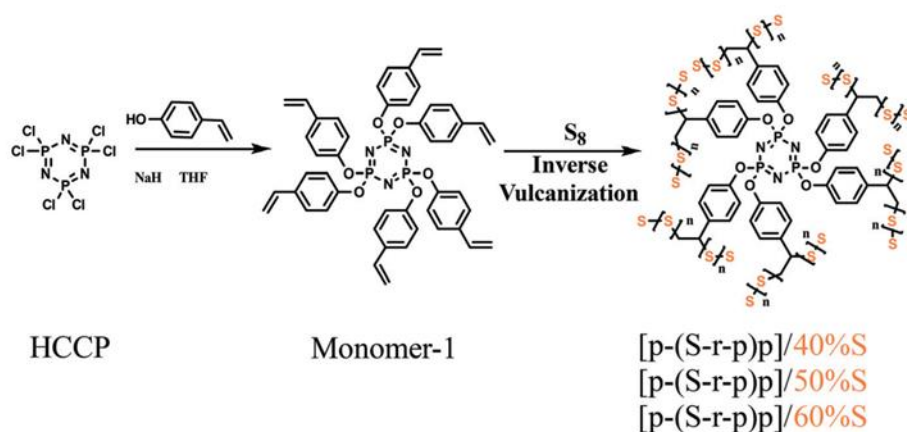
Figure 1.11: Synthesis pathway of poly(S-random-phenoxy)cyclotriphosphazene as described by Demir-Cakan. © 2020 The Royal Society of Chemistry. This image was reproduced under a Marketplace™ licence.[69]

Compared to the material made by Demir-Cakan, elemental sulfur showed a capacity fade up to the 60th cycle whereas the polysulfide showed a stable performance for over 100 cycles.[69] There are also various ways by which the polymers are used as cathode materials. For instance, just to mention two approaches, Zhang et al integrated the polysulfide into the cathode by mixing the polymer with carbon material and binders to form a cathode,[114] or as Chen and colleagues have shown, the polymer can be directly used as cathode.[107] In addition to energy storage applications, Wie et al have shown that polysulfides could also serve as new generation of triboelectric materials to generate energy.[115] Thus, polysulfides my play an integral part in future generations of Li-S batteries or energy harvesting applications.

Fertiliser

Inverse vulcanised polymers have also been utilised in the use of fertilisers. Chalker et al reported a sulfur polymer composite as controlled release fertiliser. A NPK fertiliser ((NH_4)$_2$$SO_2$, $CaHPO_4$, KCl) was directly added during the synthesis of a canola oil-sulfur polymer (Figure 1.12).[116] This allowed for the NPK nutrients to be encapsulated and released at a slow rate, proving advantageous to plant growth compared to free fertiliser.[116]
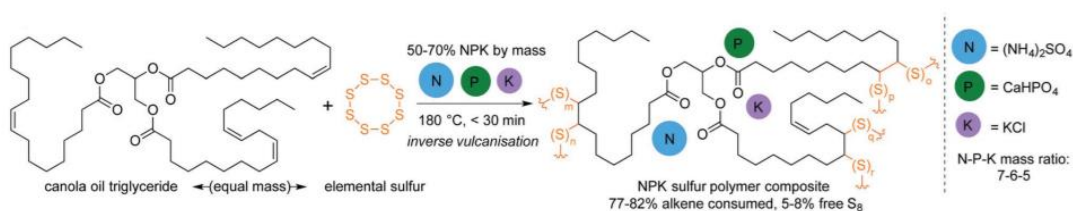
Figure 1.12: Chalker et al added nutrients directly during the synthesis of their canola oil-sulfur polymer which resulted in the nutrients being encapsulated within the polymer and release at a slow rate as shown by plant growth studies. © 2018 The Royal Society of Chemistry. This image was reproduced under a Marketplace™ licence.[116]

Ribeiro et al followed a similar concept to make fertiliser composites.[117] In their study they integrated ground Bayóvar rock (phosphate rock) or struvite ($MgNH_4PO_4 \cdot 6H_2O$) into the polymer matrix directly during the polysulfide synthesis. The resulting fertiliser composite was used in a growth study and found to release sulfur and phosphate. Since sulfur is a plant nutrient itself, the same group investigated if a sulfur and soybean polymer could increase sulfate release, compared to elemental sulfur. The results show that the copolymers were over 50% better compared to sulfur alone. [35]

Infrared optics and sensors

Another important use of polysulfides is in optical applications. While inverse vulcanised polymers have been used in polarisers,[118] the majority of optical applications lie in infrared lenses.[85, 95, 119-125] Many current lenses are made from material such as germanium or zinc-selenium which are expensive, toxic and fragile.[119, 124, 125] Further, plastics like polycarbonate or poly(methyl methacrylate) do not transmit infrared light in the 1-5 µm range due to strong C-H, O-H and N-H bond vibrations.[124] However, due to the high sulfur content polysulfide polymers are highly transmissive in the mid-wavelength range (3-5 µm)[125] as well as in the long range (7-14 µm)[122] which are ranges used for thermal imaging (Figure 1.13).[122, 125] In many cases DIB is the preferred choice of crosslinker,[95, 118-121] sometimes in conjunction with selenium[119-121] or ZnS nanoparticles (to improve thermal stability)[124].
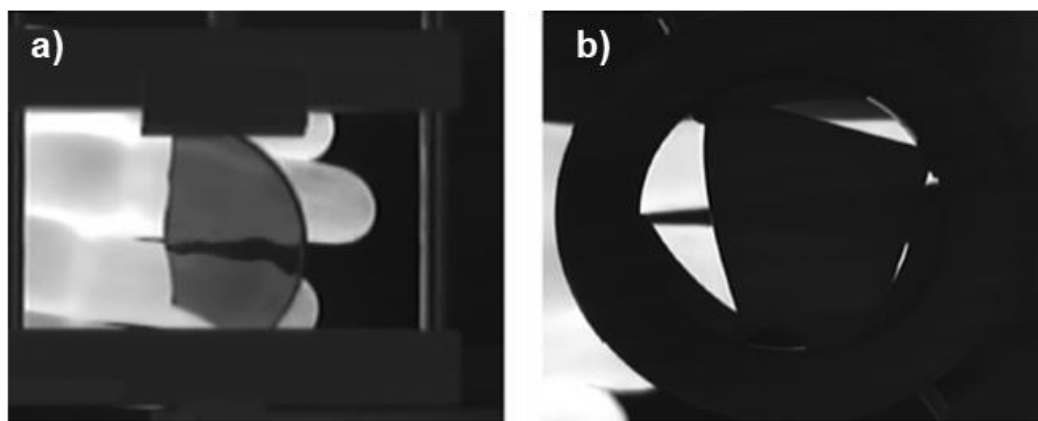
Figure 1.13: a) Sanghera and colleagues have shown that a polymer made from sulfur and DIB (30 wt%) is transmissive in the long wave infrared region (7-14 µm) whereas **b)** a polymethyl methacrylate polymer is not transmissive at that wavelength. © 2019 American Chemical Society. This image was reproduced under a RightsLink licence.[85]

Other crosslinkers include tetravinyltin,[85] a norbornadiene dimer derivative,[122] DVB[123] or a combination of algal oils and natural, plant based monoterpene compounds like limonene or myrcene[125]. These materials can have high refractive indices in the order of 1.9 in the case of a material made by Sanghera et al, which is excellent considering that polymers with a refractive index of over 1.5 in the visible region are considered high refractive index polymers.[85] And yet many inverse vulcanised polymers exceed a refractive index of 1.8.[85, 119, 123] There is a need for low cost thermal imaging lenses for defence, medical diagnosis, agriculture and autonomous vehicles.[126] Ideally, the new materials are plastic-type materials that can be made easily without the need of high-cost processing. Sulfur polymers are good candidates for these purposes and can have an exciting future in infrared optics and sensors.

Metal binding

Extensive research has also been conducted in the use of inverse vulcanised polysulfides in metal binding applications. The binding of many metals (in the form of metal salts) like Pd, Cd, Co, Cu, Pb, Zn, Fe, Cr, Mn, Ni, Ga, Ag, In, Ba, Ti, Bi and Au have been investigated.[47, 127, 128] However, of greatest interest in this regard, has been the binding of mercury.[28, 41, 47, 81, 129-137] In early efforts to capture Hg^{2+}, Chalker et al used a sulfur-limonene polymer.[47] In this study a plate of polymer was exposed to a mercury solution (10 mM of $HgCl_2$) which has shown to reduce the Hg concentration by 55%.[47] To increase surface area, Hassell and associates, coated silica gel with a sulfur-

limonene polymer, which resulted in a capacity of 716 mg of mercury per gram of polymer.[81] Different pathways have been devised to increase mercury uptake of inversed vulcanised polymers. Most of these pathways aim to increase the surface area of the polysulfide. Theato and colleagues, used electrospinning with a mixed polymer solution of S-DIB and polymethyl methacrylate (PMMA) to produce polymer fibres.[130] These fibres showed an excellent mercury (Hg^{2+}) uptake of 440 mg per g of fibres. Supercritical CO_2 has been used by the Hasell group to increase the surface area of polysulfide polymers.[41, 129] This strategy has been shown to greatly increase the uptake of Hg^{2+} from aqueous solution. Liu and co-workers took advantage of CO_2 evolved within their polysulfide to foam the material and thus increase its surface area.[134] Other strategies involve the use of salt ($NaCl_2$) which is added during the polymer synthesis as a porogen, to be removed after synthesis to leave a highly porous material.[128, 137, 138] Most work has been done with aqueous Hg^{2+}. However, the uptake of mercury vapour has also been investigated, for example by the Alhassan and Chalker groups.[28, 132] Additionally, the Chalker group has also used elemental mercury (Figure 1.14), inorganic mercury bound to organic materials as well as alkylmercury found in a organomercury fungicide.[28]
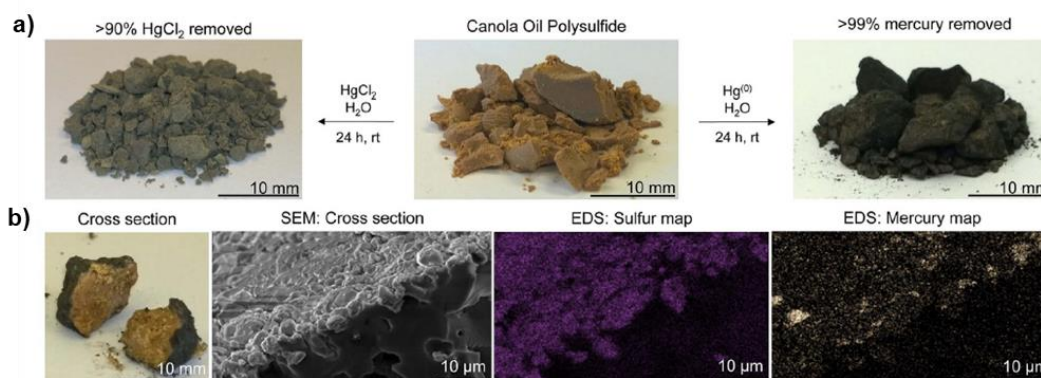

Figure 1.14: a) Chalker et al have shown that a canola oil polysulfide can remove over 99% of Hg^{2+} or Hg^0 from an aqueous solution. b) The removed mercury was bound to the surface of the polymer as was confirmed using energy dispersive X-ray analysis. © 2017 Wiley-VCH Verlag GmbH & Co. KGaA, Weinheim. This image was reproduced under a Creative Commons CC BY licence.[28]

Oil spill clean-up

The Chalker group has also pioneered the use of polysulfide in oil spill applications.[139] The hydrophobicity of a polymer made from sulfur and canola oil has been exploited to remove oil from seawater. Interestingly, the polymer forms an aggregate with the oil which facilitates easy separation from water using a net (Figure

1.15). After the oil – polymer aggregate has been removed, the oil could be recovered by simple mechanical compression. The polysulfide has also proved useful as a filter media in a continuous separation process of oil from water.[139] In Chapter 3 of this thesis, carbonisation of the polymer after use in oil spill remediation was investigated as a route to extend the lifetime of the material and repurpose it for new applications.
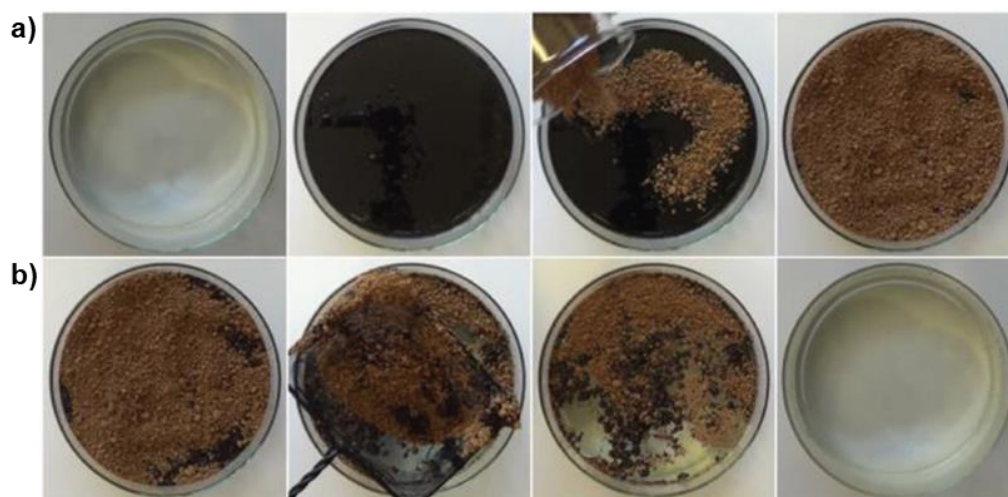
Figure 1.15: a) 100 mL of cure oil is added to 1.5 L of seawater before 100 g of a polymer made from sulfur and canola oil is added. **b)** In under one minute the polymer and oil formed an aggregate with was removed using a net. © 2017 Wiley-VCH Verlag GmbH & Co. KGaA, Weinheim. This image was reproduced under a Creative Commons CC BY licence.[139]

Repairable and healable materials

Studies have also been undertaken to investigate if inverse vulcanised polymers can be healed or repaired after they have been damaged. Various crosslinkers have been used in the synthesis of these polymers, such as DIB[140, 141], polybenzoxazines,[64] oleic acid[142] or canola oil and DCPD.[70] In many cases the healing of the material occurs due to S-S bond formation, while the material is heated (Figure 1.16).[64, 140, 142, 143]
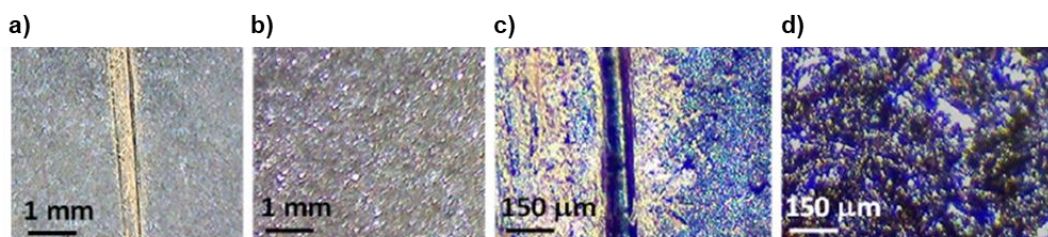
Figure 1.16: Tennyson et al used a polysulfide containing sulfur oleic acid and zinc oxide to show thermal annealing. **a)** and **c)** show scratches on the material. **b)** and **d)** show the area of the scratch after thermal annealing at 100 °C for 5 minutes. © 2019 Whiley Periodicals, Inc. This image was reproduced under a RightsLink licence.[142]

Interestingly, a report by Zhang et al describes a self-healing process at ambient conditions for a composite that contains a liquid metal embedded on the sulfur polymer.[141] Zhang and co-workers attribute the repair to chain entanglement as well as to the dynamic nature of the bonds between the ligands of the polysulfide and the liquid metal.[141] Another strategy was followed by Chalker and co-workers.[70] In their work, repair of a polymer made by inverse vulcanisation of DCDP, canola oil and sulfur was chemically induced. A phosphene or amine catalyst was used to provoke S-S bond metathesis within the polymer to join two polymer surfaces. Additional concepts in polymer repair are investigated in this thesis in Chapters 4 and 5.

Thermal insulation

A recent application for inverse vulcanised polymers is that of thermal insulation. Alhassan et al tested the thermal conductivity of a porous polymer made of sulfur and DVB and showed that the thermal conductivity was lower than that of pristine sulfur while having a stable thermal conductivity up to 100 °C.[132] The same group also showed that polymers made with a range of cyclic crosslinkers (such as cycloheptane or cyclodecene) exhibit a lower thermal conductivity at 10-50 °C compared to pristine sulfur.[144] Chalker et al used a different approach to thermal insulation.[97] A polymer made of canola oil and elemental sulfur was ground up, blended with raw wool and hot-pressed into a composite (Figure 1.17). Not only did this composite show a lower thermal conductivity than sulfur, but additionally the composite demonstrated excellent flame resistance compared to the polymer alone.
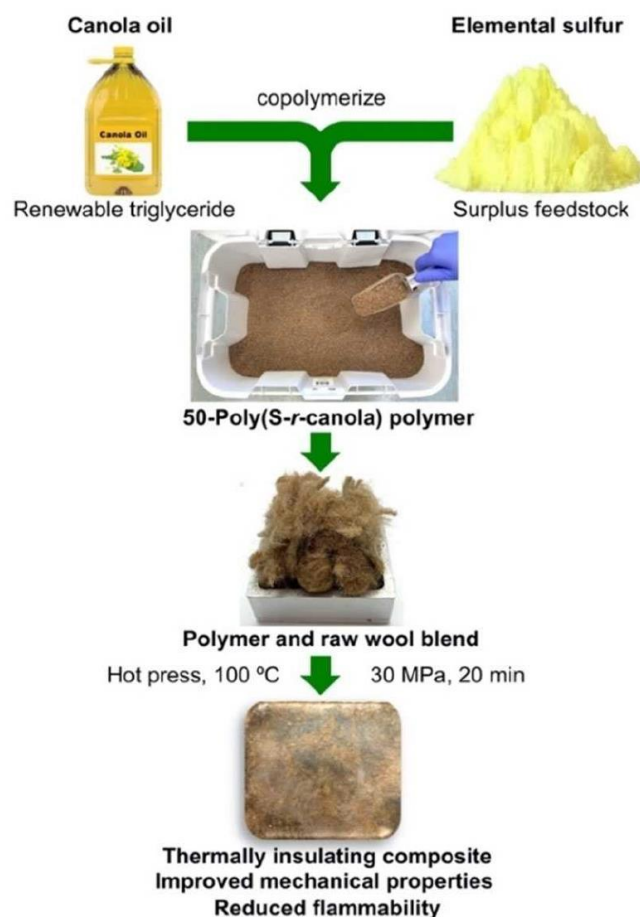
Figure 1.17: Chalker et al combined wool to a sulfur and canola oil polymer to make a thermally insulating composite. © 2021 Whiley-VCH GmbH. This image was reproduced under a RightsLink licence.[97]

Research aims and summary of research in thesis

Extensive research has been conducted in recent years in the field of inverse vulcanisation. The focus of the Chalker lab has been the use of inexpensive and/or renewable or even waste materials to make useful polysulfides, which has informed the research described in this thesis. During my Honours year I worked extensively with a sulfur polymer made of canola oil and sulfur, for use as a vehicle for slow-release fertilisers.[116] For my PhD I explored more applications of sulfur polymers and learned more about the mechanistic aspects of inverse vulcanisation.

It has been previously shown that polysulfide polymers are capable of removing metals, including gold from an aqueous solution.[89, 145] Since mercury is often used to remove gold from gold tailings in the small scale and artisanal gold mining sector, the polymer was seen as a potential alternative to gold recovery by mercury

amalgamation.[146] Our aim also extended to the development of a novel gold leaching technique tailored for the small scale and artisanal gold mining and electronic waste sector that can be used in conjunction with gold uptake using the polysulfide to encourage mercury free small scale and artisanal gold mining. The focus of Chapter 2 therefore was to develop a safe, cheap, and reliable gold extraction method without the use of mercury or cyanide that can be implemented into the artisanal and small-scale gold mining and informal electronic waste recycling sector. The result of this research was a patented novel gold oxidation method that has proven successful in extracting gold from gold ore tailings, gold ore and electronic waste. A polysulfide made from sulfur and canola oil was used to successfully remove the gold from the leach solutions. Lastly, the gold was recovered in high yields and quality by incinerating the polysulfide.

Already, efforts have been made to use polysulfides as precursors for carbonised materials.[88, 89] However, some of these materials underwent activation using KOH therefore adding complexity to the carbonisation process. Additionally, only two polysulfide systems (S-DCPD[89] and S-DIB[88]) have been used in these studies. Since a polymer made form sulfur and canola oil has been extensively researched in the Chalker lab, we posed the question if carbonisation of this polymer can present and end of life application for that material though an easy and simple carbonisation pathway. We also wanted to explore potential mercury removal applications using the newly carbonised material. Therefore, in Chapter 3, end of life uses for the sulfur and canola oil polysulfide were explored. To do that, the polymer was firstly used to remove oil from water, a useful application of this polymer that had been previously explored by the Chalker lab,[139] before the polymer was carbonised. The carbonised polymer showed a high sulfur content and was successfully used as sorbent to remove aqueous mercury from solution. Further it has been shown that only minimal mercury leached off the carbonised polymer when exposed to acidic water as compared to commercially available carbon materials.

Some inverse vulcanisation polymerisations are prone to runaway reactions.[81] One such reaction is that of sulfur and DCPD which was observed first hand by the author. While efforts have been made to limit the risk of runaway reactions through the use of catalysts, the catalyst (1 wt%) remains in the material after the synthesis.[81] This gave rise to the question if this particular reaction can be optimised and performed without the use of catalysts in a safe and reliable way to produce a processable material. With this in mind, Chapter 4 discusses the successfully optimised reaction between sulfur and dicyclopentadiene to yield a shelf stable and soluble oligomer. After thermally curing this material at 140 °C, it was rendered resistant to acid and solvents. Advantage was taken of the solubility of the oligomer and silica gel was coated with the oligomer

and the coated silica gel has displayed excellent mercury removal properties. The oligomer was also used to coat metal, concrete, and polyvinyl chloride to further illustrate protection from acids and solvents. Finally, it was shown that the coating was repairable as surface scratches were removed by applying heat.

Recently, the Chalker lab developed a novel catalytic adhesion method to bond polysulfides together.[70] Since the previous study was undertaken on small polymer blocks, we wanted to explore this adhesion on larger polymer blocks by upscaling the reaction and by quantifying the bond strength. Moreover, the question if the polymer can be reinforced in order to improve its structural strength was posed. To answer these questions, a polysulfide terpolymer made from sulfur, canola oil and dicyclopentadiene was evaluated as bulk structural material in Chapter 5. The structure of this material allowed bonding of two polymer blocks by the application of an amine-based catalyst without the use of an exogenous adhesive. The strength of this bond was evaluated and shown to be stronger than that of commercially available super glue. In order to increase the mechanical properties of the terpolymer, carbon fibres and carbon nanorods were used. Adding carbon fibres to the polymer resulted in a nearly 16-fold increase in flexural strength.

References:

1.   Hocking, M. B., 9 - Sulfur and Sulfuric Acid. In *Handbook of Chemical Technology and Pollution Control (Third Edition)*, Hocking, M. B., Ed. Academic Press: San Diego, 2005; pp 253-287.

2.   Boyd, D. A., Sulfur and Its Role In Modern Materials Science. *Angew. Chem. Int. Ed.* **2016,** *55*, 15486-15502.

3.   Räisänen, J., SULFUR. In *Encyclopedia of Analytical Science (Second Edition)*, Worsfold, P.; Townshend, A.; Poole, C., Eds. Elsevier: Oxford, 2005; pp 415-423.

4.   Mokhatab, S.; Poe, W. A.; Mak, J. Y., Chapter 8 - Sulfur Recovery and Handling. In *Handbook of Natural Gas Transmission and Processing (Fourth Edition)*, Mokhatab, S.; Poe, W. A.; Mak, J. Y., Eds. Gulf Professional Publishing: 2019; pp 271-305.

5.   Mackenzie, F. T., Volume Editor's Introduction. In *Treatise on Geochemistry (Second Edition)*, Holland, H. D.; Turekian, K. K., Eds. Elsevier: Oxford, 2014; pp xxiii-xxxii.

6.   Kutney, G., *Sulfur: History, Technology, Applications & Industry*. 2nd ed.; ChemTec Publishing: Toronto, 2013.

7.   Wagenfeld, J.-G.; Al-Ali, K.; Almheiri, S.; Slavens, A. F.; Calvet, N., Sustainable applications utilizing sulfur, a by-product from oil and gas industry: A state-of-the-art review. *Waste Manage.* **2019,** *95*, 78-89.

8.   Ober, J. A. *Materials flow of sulfur*; 2331-1258; 2002.

9.   Clayton, C., PETROLEUM GEOLOGY | Chemical and Physical Properties. In *Encyclopedia of Geology*, Selley, R. C.; Cocks, L. R. M.; Plimer, I. R., Eds. Elsevier: Oxford, 2005; pp 248-260.

10.   Ibrahim, M. H.; Hayyan, M.; Hashim, M. A.; Hayyan, A., The role of ionic liquids in desulfurization of fuels: A review. *Renew. Sust. Energ. Rev.* **2017,** *76*, 1534-1549.

11.   Hayyan, M.; Ibrahim, M. H.; Hayyan, A.; Alnashef, I. M.; Alakrach, A. M.; Hashim, M. A., Facile Route for Fuel Desulfurization Using Generated Superoxide Ion in Ionic Liquids. *Ind. Eng. Chem. Res.* **2015,** *54* (49), 12263-12269.

12.   Saikia, B. K.; Khound, K.; Baruah, B. P., Extractive de-sulfurization and de-ashing of high sulfur coals by oxidation with ionic liquids. *Energy Convers. Manage.* **2014,** *81*, 298-305.

13. Boniek, D.; Figueiredo, D.; Dos Santos, A. F. B.; De Resende Stoianoff, M. A., Biodesulfurization: a mini review about the immediate search for the future technology. *Clean Techn. Environ. Policy* **2015,** *17* (1), 29-37.

14. Brown, T.; Idoine, N.; Raycraft, E.; Shaw, R.; Hobbs, S.; Everett, P.; Deady, E.; Bide, T. *World Mineral Production 2014-20118*; British Geological Survey: Nottingham, **2020**.

15. Chung, W. J.; Griebel, J. J.; Kim, E. T.; Yoon, H.; Simmonds, A. G.; Ji, H. J.; Dirlam, P. T.; Glass, R. S.; Wie, J. J.; Nguyen, N. A.; Guralnick, B. W.; Park, J.; Somogyi, Á.; Theato, P.; Mackay, M. E.; Sung, Y.-E.; Char, K.; Pyun, J., The use of elemental sulfur as an alternative feedstock for polymeric materials. *Nat. Chem.* **2013,** *5*, 518-524.

16. Birkham, T. K.; Hendry, M. J.; Barbour, S. L., Advective and Diffusive Gas Transport through Fractured Sulfur Blocks. *Vadose Zone J.* **2010,** *9* (2), 451-461.

17. Gosselin, P.; Hrudey, S. E.; Naeth, M. A.; Plourde, A.; Therrien, R.; Van Der Kraak, G.; Xu, Z., Environmental and health impacts of Canada's oil sands industry. *Royal Society of Canada, Ottawa, ON* **2010,** *10.*

18. Kruželák, J.; Sýkora, R.; Hudec, I., Sulphur and peroxide vulcanisation of rubber compounds – overview. *Chem. Pap.* **2016,** *70* (12).

19. Ikeda, Y.; Higashitani, N.; Hijikata, K.; Kokubo, Y.; Morita, Y.; Shibayama, M.; Osaka, N.; Suzuki, T.; Endo, H.; Kohjiya, S., Vulcanization: New Focus on a Traditional Technology by Small-Angle Neutron Scattering. *Macromolecules* **2009,** *42* (7), 2741-2748.

20. Coran, A. Y., Chapter 7 - Vulcanization. In *The Science and Technology of Rubber (Fourth Edition)*, Mark, J. E.; Erman, B.; Roland, C. M., Eds. Academic Press: Boston, 2013; pp 337-381.

21. Heideman, G.; Noordermeer, J. W. M.; Datta, R. N.; Ben van, B., Effect of Zinc Complexes as Activator for Sulfur Vulcanisation in Various Rubbers. *Rubber Chem. Technol.* **2005,** *78* (2), 245-257.

22. Aprem, A. S.; Joseph, K.; Mathew, T.; Altstaedt, V.; Thomas, S., Studies on accelerated sulphur vulcanization of natural rubber using 1-phenyl-2, 4-dithiobiuret/tertiary butyl benzothiazole sulphenamide. *Eur. Polym. J.* **2003,** *39* (7), 1451-1460.

23. Mostoni, S.; Milana, P.; Barbara Di, C.; Massimiliano, D. A., Zinc-Based Curing Activators: New Trends for Reducing Zinc Content in Rubber Vulcanization Process. *Catalysts* **2019,** *9* (8), 664.

24. Heideman, G.; Datta, R. N.; Noordermeer, J. W. M.; Ben van, B., Activators in Accelerated Sulfur Vulcanisation. *Rubber Chem. Technol.* **2004,** *77* (3), 512-541.

25. Shankarayya Wadi, V. K.; Jena, K. K.; Khawaja, S. Z.; Yannakopoulou, K.; Fardis, M.; Mitrikas, G.; Karagianni, M.; Papavassiliou, G.; Alhassan, S. M., NMR and EPR Structural Analysis and Stability Study of Inverse Vulcanized Sulfur Copolymers. *ACS Omega* **2018,** *3* (3), 3330-3339.

26. Worthington, M. J. H.; Kucera, R. L.; Chalker, J. M., Green chemistry and polymers made from sulfur. *Green Chem.* **2017,** *19*, 2748-2761.

27. Chalker, J. M.; Mann, M.; Worthington, M. J. H.; Esdaile, L. J., Polymers Made by Inverse Vulcanization for Use as Mercury Sorbents. *Organic Materials* **2021,** *03* (02), 362-373.

28. Worthington, M. J. H.; Kucera, R. L.; Abuquerque, I. S.; Gibson, C. T.; Sibley, A.; Slattery, A. D.; Campbell, J. A.; Alboaiji, S. F. K.; Muller, K. A.; Young, J.; Adamson, N.; Gascooke, J. R.; Jampaiah, D.; Sabri, Y. M.; Bhargava, S. K.; Ippolito, S. J.; Lewis, D. A.; Quinton, J. S.; Ellis, A. V.; Johs, A.; Bernardes, G. J. L.; Chalker, J. M., Laying Waste to Mercury: Inexpensive Sorbents Made from Sulfur and Recycled Cooking Oils. *Chem. Eur. J.* **2017,** *23*, 16219-16230.

29. Cheung, T. T. P., Cyclopentadiene and Dicyclopentadiene. In *Kirk-Othmer Encyclopedia of Chemical Technology*.

30. Tikoalu, A. D.; Lundquist, N. A.; Chalker, J. M., Mercury Sorbents Made By Inverse Vulcanization of Sustainable Triglycerides: The Plant Oil Structure Influences the Rate of Mercury Removal from Water. *Adv. Sustain. Syst.* **2020,** *4* (3), 1900111.

31. Lundquist, N. A.; Tikoalu, A. D.; Worthington, M. J. H.; Shapter, R.; Tonkin, S. J.; Stojcevski, F.; Mann, M.; Gibson, C. T.; Gascooke, J. R.; Karton, A.; Henderson, L. C.; Esdaile, L. J.; Chalker, J. M., Reactive Compression Molding Post-Inverse Vulcanization: A Method to Assemble, Recycle, and Repurpose Sulfur Polymers and Composites. *Chem. Eur. J.* **2020,** *26* (44), 10035-10044.

32. Lundquist, N. A.; Chalker, J. M., Confining a spent lead sorbent in a polymer made by inverse vulcanization prevents leaching. *SM&T* **2020,** *26*, e00222.

33. Mann, M.; Luo, X.; Tikoalu, A. D.; Gibson, C. T.; Yin, Y.; Al-Attabi, R.; Andersson, G. G.; Raston, C. L.; Henderson, L. C.; Pring, A.; Hasell, T.; Chalker, J. M., Carbonisation of a polymer made from sulfur and canola oil. *ChemComm* **2021,** *57* (51), 6296-6299.

34. Hoefling, A.; Lee, Y. J.; Theato, P., Sulfur-Based Polymer Composites from Vegetable Oils and Elemental Sulfur: A Sustainable Active Material for Li–S Batteries. *Macromol. Chem. Phys.* **2017,** *218*, 1600303.

35. Valle, S. F.; Giroto, A. S.; Klaic, R.; Guimarães, G. G. F.; Ribeiro, C., Sulfur fertilizer based on inverse vulcanization process with soybean oil. *Polym. Degrad. Stab.* **2019,** *162*, 102-105.

36. Liu, Y.; Chen, Y.; Zhang, Y.; Chen, Y.; Wang, L.; Zan, X.; Zhang, L., Density-Adjustable Bio-Based Polysulfide Composite Prepared by Inverse Vulcanization and Bio-Based Fillers. *Polymers* **2020,** *12* (9), 2127.

37. Lauer, M. K.; Karunarathna, M. S.; Tennyson, A. G.; Smith, R. C., Robust, remeltable and remarkably simple to prepare biomass–sulfur composites. *Mater. Adv.* **2020,** *1* (7), 2271-2278.

38. Lyu, Y.; Hu, Q.; Chen, L.; Luo, T.; Liu, J.; Yin, X., Using conjugated system from natural sources for the synthesis of sulfur copolymers by bi-function catalysts at mild temperatures. *J. Appl. Polym. Sci.* **2021,** *138* (36), 50925.

39. Abbasi, A.; Nasef, M. M.; Yahya, W. Z. N.; Moniruzzaman, M.; Ghumman, A. S., Preparation and characterization of green polymer by copolymerization of corn oil and sulphur at molten state. *Polym. Polym. Compos.* **2020**, 096739112095953.

40. Smith, A. D.; McMillen, C. D.; Smith, R. C.; Tennyson, A. G., Copolymers by Inverse Vulcanization of Sulfur with Pure or Technical-Grade Unsaturated Fatty Acids. *J. Polym. Sci.* **2020,** *58* (3), 438-445.

41. Parker, D. J.; Jones, H. A.; Petcher, S.; Cervini, L.; Griffin, J. M.; Akhtar, R.; Hasell, T., Low cost and renewable sulfur-polymers by inverse vulcanisation, and their potential for mercury capture. *J. Mater. Chem. A* **2017,** *5* (23), 11682-11692.

42. Ghumman, A. S. M.; Shamsuddin, M. R.; Nasef, M. M.; Yahya, W. Z. N.; Ayoub, M.; Cheah, B.; Abbasi, A., Synthesis and Characterization of Sustainable Inverse Vulcanized Copolymers from Non-Edible Oil. *ChemistrySelect* **2021,** *6* (6), 1180-1190.

43. Ghumman, A. S. M.; Shamsuddin, R.; Nasef, M. M.; Nisa Yahya, W. Z.; Abbasi, A., Optimization of synthesis of inverse vulcanized copolymers from rubber seed oil using response surface methodology. *Polymer* **2021,** *219*, 123553.

44. Karunarathna, M. S.; Tennyson, A. G.; Smith, R. C., Facile new approach to high sulfur-content materials and preparation of sulfur–lignin copolymers. *J. Mater. Chem. A* **2020,** *8* (2), 548-553.

45. Gomez, I.; Leonet, O.; Blazquez, J. A.; Mecerreyes, D., Inverse Vulcanization of Sulfur using Natural Dienes as Sustainable Materials for Lithium–Sulfur Batteries. *ChemSusChem* **2016,** *9* (24), 3419-3425.

46. Khawaja, S. Z.; Vijay Kumar, S.; Jena, K. K.; Alhassan, S. M., Flexible sulfur film from inverse vulcanization technique. *Mater. Lett.* **2017,** *203*, 58-61.

47.   Crockett, M. P.; Evans, A. M.; Worthington, M. J. H.; Albuquerque, I. S.; Slattery, A. D.; Gibson, C. T.; Campbell, J. A.; Lewis, D. A.; Bernardes, G. J. L.; Chalker, J. M., Sulfur-Limonene Polysulfide: A Material Synthesized Entirely from Industrial By-Products and Its Use in Removing Toxic Metals from Water and Soil. *Angew. Chem. Int. Ed.* **2016,** *55*, 1714-1718.

48.   Oishi, S.; Oi, K.; Kuwabara, J.; Omoda, R.; Aihara, Y.; Fukuda, T.; Takahashi, T.; Choi, J.-C.; Watanabe, M.; Kanbara, T., Synthesis and Characterization of Sulfur-Based Polymers from Elemental Sulfur and Algae Oil. *ACS Appl. Poly, Mater.* **2019,** *1* (5), 1195-1202.

49.   Hoefling, A.; Nguyen, D. T.; Lee, Y. J.; Song, S.-W.; Theato, P., A sulfur–eugenol allyl ether copolymer: a material synthesized via inverse vulcanization from renewable resources and its application in Li–S batteries. *Mater. Chem. Front.* **2017,** *1* (9), 1818-1822.

50.   Lauer, M. K.; Tennyson, A. G.; Smith, R. C., Inverse vulcanization of octenyl succinate-modified corn starch as a route to biopolymer–sulfur composites. *Mater. Adv.* **2021,** *2* (7), 2391-2397.

51.   Shukla, S.; Ghosh, A.; Roy, P. K.; Mitra, S.; Lochab, B., Cardanol benzoxazines – A sustainable linker for elemental sulphur based copolymers via inverse vulcanisation. *Polymer* **2016,** *99*, 349-357.

52.   Zhang, Y.; Konopka, K. M.; Glass, R. S.; Char, K.; Pyun, J., Chalcogenide hybrid inorganic/organic polymers (CHIPs) via inverse vulcanization and dynamic covalent polymerizations. *Polym. Chem.* **2017,** *8* (34), 5167-5173.

53.   Choudhury, S.; Srimuk, P.; Raju, K.; Tolosa, A.; Fleischmann, S.; Zeiger, M.; Ozoemena, K. I.; Borchardt, L.; Presser, V., Carbon onion/sulfur hybrid cathodes via inverse vulcanization for lithium–sulfur batteries. *Sustain. Energy Fuels* **2018,** *2* (1), 133-146.

54.   Dodd, L. J.; Omar, Ö.; Wu, X.; Hasell, T., Investigating the Role and Scope of Catalysts in Inverse Vulcanization. *ACS Catalysis* **2021,** *11* (8), 4441-4455.

55.   Diez, S.; Hoefling, A.; Theato, P.; Pauer, W., Mechanical and Electrical Properties of Sulfur-Containing Polymeric Materials Prepared via Inverse Vulcanization. *Polymers* **2017,** *9* (12), 59.

56.   Wadi, V. S.; Jena, K. K.; Halique, K.; Rožič, B.; Cmok, L.; Tzitzios, V.; Alhassan, S. M., Scalable High Refractive Index polystyrene-sulfur nanocomposites via in situ inverse vulcanization. *Sci. Rep.* **2020,** *10* (1).

57.   Gomez, I.; Mecerreyes, D.; Blazquez, J. A.; Leonet, O.; Ben Youcef, H.; Li, C.; Gómez-Cámer, J. L.; Bondarchuk, O.; Rodriguez-Martinez, L., Inverse vulcanization of sulfur with divinylbenzene: Stable and easy processable cathode material for lithium-sulfur batteries. *J. Power Sources* **2016,** *329*, 72-78.

58. Parreño, R. P.; Liu, Y.-L.; Beltran, A. B., A Sulfur Copolymers (SDIB)/Polybenzoxazines (PBz) Polymer Blend for Electrospinning of Nanofibers. *Nanomaterials* **2019,** *9* (11), 1526.

59. Chung, W. J.; Simmonds, A. G.; Griebel, J. J.; Kim, E. T.; Suh, H. S.; Shim, I.-B.; Glass, R. S.; Loy, D. A.; Theato, P.; Sung, Y.-E.; Char, K.; Pyun, J., Elemental Sulfur as a Reactive Medium for Gold Nanoparticles and Nanocomposite Materials. *Angew. Chem. Int. Ed.* **2011,** *50* (48), 11409-11412.

60. Salman, M. K.; Karabay, B.; Karabay, L. C.; Cihaner, A., Elemental sulfur-based polymeric materials: Synthesis and characterization. *J. Appl. Polym. Sci.* **2016,** *133* (28).

61. Arslan, M.; Kiskan, B.; Cengiz, E. C.; Demir-Cakan, R.; Yagci, Y., Inverse vulcanization of bismaleimide and divinylbenzene by elemental sulfur for lithium sulfur batteries. *Eur. Polym. J.* **2016,** *80*, 70-77.

62. Orme, K.; Fistrovich, A. H.; Jenkins, C. L., Tailoring Polysulfide Properties through Variations of Inverse Vulcanization. *Macromolecules* **2020,** *53* (21), 9353-9361.

63. Arslan, M.; Kiskan, B.; Yagci, Y., Combining Elemental Sulfur with Polybenzoxazines via Inverse Vulcanization. *Macromolecules* **2016,** *49* (3), 767-773.

64. Arslan, M.; Kiskan, B.; Yagci, Y., Recycling and Self-Healing of Polybenzoxazines with Dynamic Sulfide Linkages. *Sci. Rep.* **2017,** *7* (1).

65. Akkus, B.; Kiskan, B.; Yagci, Y., Combining polybenzoxazines and polybutadienes via simultaneous inverse and direct vulcanization for flexible and recyclable thermosets by polysulfide dynamic bonding. *Polym. Chem.* **2019,** *10* (42), 5743-5750.

66. Bayram, O.; Kiskan, B.; Demir, E.; Demir-Cakan, R.; Yagci, Y., Advanced Thermosets from Sulfur and Renewable Benzoxazine and Ionones via Inverse Vulcanization. *ACS Sustain. Chem. Eng.* **2020,** *8* (24), 9145-9155.

67. Martin, T. R.; Mazzio, K. A.; Hillhouse, H. W.; Luscombe, C. K., Sulfur copolymer for the direct synthesis of ligand-free CdS nanoparticles. *ChemComm* **2015,** *51* (56), 11244-11247.

68. Zhang, Y.; Griebel, J. J.; Dirlam, P. T.; Nguyen, N. A.; Glass, R. S.; Mackay, M. E.; Char, K.; Pyun, J., Inverse vulcanization of elemental sulfur and styrene for polymeric cathodes in Li-S batteries. *J. Polym. Sci., Part A: Polym. Chem.* **2017,** *55* (1), 107-116.

69. Yeşilot, S.; Küçükköylü, S.; Demir, E.; Demir-Cakan, R., Phosphazene based star-branched polymeric cathode materials via inverse vulcanization of sulfur for lithium–sulfur batteries. *Polym. Chem.* **2020,** *11* (25), 4124-4132.

70.   Tonkin, S. J.; Gibson, C. T.; Campbell, J. A.; Lewis, D. A.; Karton, A.; Hasell, T.; Chalker, J. M., Chemically induced repair, adhesion, and recycling of polymers made by inverse vulcanization. *Chem Sci* **2020,** *11* (21), 5537-5546.

71.   Zhang, B.; Petcher, S.; Hasell, T., A ternary system for delayed curing inverse vulcanisation. *ChemComm* **2019,** *55* (72), 10681-10684.

72.   Kim, E. T.; Chung, W. J.; Lim, J.; Johe, P.; Glass, R. S.; Pyun, J.; Char, K., One-pot synthesis of PbS NP/sulfur-oleylamine copolymer nanocomposites via the copolymerization of elemental sulfur with oleylamine. *Polym. Chem.* **2014,** *5* (11), 3617.

73.   Sun, Z.; Xiao, M.; Wang, S.; Han, D.; Song, S.; Chen, G.; Meng, Y., Sulfur-rich polymeric materials with semi-interpenetrating network structure as a novel lithium–sulfur cathode. *J. Mater. Chem. A* **2014,** *2* (24), 9280.

74.   Oschmann, B.; Park, J.; Kim, C.; Char, K.; Sung, Y.-E.; Zentel, R., Copolymerization of Polythiophene and Sulfur To Improve the Electrochemical Performance in Lithium–Sulfur Batteries. *Chem. Mater.* **2015,** *27* (20), 7011-7017.

75.   Itaoka, K.; Kim, I.-T.; Yamabuki, K.; Yoshimoto, N.; Tsutsumi, H., Room temperature rechargeable magnesium batteries with sulfur-containing composite cathodes prepared from elemental sulfur and bis(alkenyl) compound having a cyclic or linear ether unit. *J. Power Sources* **2015,** *297*, 323-328.

76.   Dirlam, P. T.; Simmonds, A. G.; Kleine, T. S.; Nguyen, N. A.; Anderson, L. E.; Klever, A. O.; Florian, A.; Costanzo, P. J.; Theato, P.; Mackay, M. E.; Glass, R. S.; Char, K.; Pyun, J., Inverse vulcanization of elemental sulfur with 1,4-diphenylbutadiyne for cathode materials in Li–S batteries. *RSC Adv.* **2015,** *5* (31), 24718-24722.

77.   Kleine, T. S.; Nguyen, N. A.; Anderson, L. E.; Namnabat, S.; Lavilla, E. A.; Showghi, S. A.; Dirlam, P. T.; Arrington, C. B.; Manchester, M. S.; Schwiegerling, J.; Glass, R. S.; Char, K.; Norwood, R. A.; Mackay, M. E.; Pyun, J., High Refractive Index Copolymers with Improved Thermomechanical Properties via the Inverse Vulcanization of Sulfur and 1,3,5-Triisopropenylbenzene. *ACS Macro Lett.* **2016,** *5* (10), 1152-1156.

78.   Fu, C.; Li, G.; Zhang, J.; Cornejo, B.; Piao, S. S.; Bozhilov, K. N.; Haddon, R. C.; Guo, J., Electrochemical Lithiation of Covalently Bonded Sulfur in Vulcanized Polyisoprene. *ACS Energy Lett.* **2016,** *1* (1), 115-120.

79.   Smith, J. A.; Wu, X.; Berry, N. G.; Hasell, T., High sulfur content polymers: The effect of crosslinker structure on inverse vulcanization. *J. Polym. Sci., Part A: Polym. Chem.* **2018,** *56* (16), 1777-1781.

80.   Zhang, Y.; Kleine, T. S.; Carothers, K. J.; Phan, D. D.; Glass, R. S.; Mackay, M. E.; Char, K.; Pyun, J., Functionalized chalcogenide hybrid inorganic/organic polymers (CHIPs) via inverse vulcanization of elemental sulfur and vinylanilines. *Polym. Chem.* **2018,** *9* (17), 2290-2294.

81.   Wu, X.; Smith, J. A.; Petcher, S.; Zhang, B.; Parker, D. J.; Griffin, J. M.; Hasell, T., Catalytic inverse vulcanization. *Nat. Commun.* **2019,** *10* (1), 647.

82.   Smith, J. A.; Green, S. J.; Petcher, S.; Parker, D. J.; Zhang, B.; Worthington, M. J. H.; Wu, X.; Kelly, C. A.; Baker, T.; Gibson, C. T.; Campbell, J. A.; Lewis, D. A.; Jenkins, M. J.; Willcock, H.; Chalker, J. M.; Hasell, T., Crosslinker Copolymerization for Property Control in Inverse Vulcanization. *Chem. Eur. J.* **2019,** *25* (44), 10433-10440.

83.   Berk, H.; Balci, B.; Ertan, S.; Kaya, M.; Cihaner, A., Functionalized polysulfide copolymers with 4-vinylpyridine via inverse vulcanization. *Mater. Today Commun.* **2019,** *19*, 336-341.

84.   Scheiger, J. M.; Direksilp, C.; Falkenstein, P.; Welle, A.; Koenig, M.; Heissler, S.; Matysik, J.; Levkin, P. A.; Theato, P., Inverse Vulcanization of Styrylethyltrimethoxysilane–Coated Surfaces, Particles, and Crosslinked Materials. *Angew. Chem. Int. Ed.* **2020,** *59* (42), 18639-18645.

85.   Boyd, D. A.; Nguyen, V. Q.; McClain, C. C.; Kung, F. H.; Baker, C. C.; Myers, J. D.; Hunt, M. P.; Kim, W.; Sanghera, J. S., Optical Properties of a Sulfur-Rich Organically Modified Chalcogenide Polymer Synthesized via Inverse Vulcanization and Containing an Organometallic Comonomer. *ACS Macro Lett.* **2019,** *8* (2), 113-116.

86.   Abbasi, A.; Nasef, M. M.; Yahya, W. Z. N.; Moniruzzaman, M.; Ghumman, A. S. M., Preparation and characterization of sulfur-vinylbenzyl chloride polymer under optimized reaction conditions using inverse vulcanization. *Eur. Polym. J.* **2021,** *143*, 110202.

87.   Meyer, B., Elemental sulfur. *Chem. Rev.* **1976,** *76* (3), 367-388.

88.   Bear, J. C.; McGettrick, J. D.; Parkin, I. P.; Dunnill, C. W.; Hasell, T., Porous carbons from inverse vulcanised polymers. *Microporous Mesoporous Mater.* **2016,** *232*, 189-195.

89.   Lee, J.-Sing M.; Parker, D. J.; Cooper, A. I.; Hasell, T., High surface area sulfur-doped microporous carbons from inverse vulcanised polymers. *J. Mater. Chem. A* **2017,** *5* (35), 18603-18609.

90.   Herrera, C.; Ysinga, K. J.; Jenkins, C. L., Polysulfides Synthesized from Renewable Garlic Components and Repurposed Sulfur Form Environmentally Friendly Adhesives. *ACS Appl. Mater. Interfaces* **2019,** *11* (38), 35312-35318.

91.   Mann, M.; Pauling, P. J.; Tonkin, S. J.; Campbell, J. A.; Chalker, J. M., Chemically Activated S-S Metathesis for Adhesive-Free Bonding of Polysulfide Surfaces. *Macromol. Chem. Phys.* **2021**, 2100333.

92.   Deng, Z.; Hoefling, A.; Théato, P.; Lienkamp, K., Surface Properties and Antimicrobial Activity of Poly(sulfur-co -1,3-diisopropenylbenzene) Copolymers. *Macromol. Chem. Phys.* **2018,** *219* (5), 1700497.

93.   Smith, J. A.; Mulhall, R.; Goodman, S.; Fleming, G.; Allison, H.; Raval, R.; Hasell, T., Investigating the Antibacterial Properties of Inverse Vulcanized Sulfur Polymers. *ACS Omega* **2020,** *5* (10), 5229-5234.

94.   Dop, R. A.; Neill, D. R.; Hasell, T., Antibacterial Activity of Inverse Vulcanized Polymers. *Biomacromolecules* **2021**.

95.   Griebel, J. J.; Namnabat, S.; Kim, E. T.; Himmelhuber, R.; Moronta, D. H.; Chung, W. J.; Simmonds, A. G.; Kim, K.-J.; van der Laan, J.; Nguyen, N. A.; Dereniak, E. L.; Mackay, M. E.; Char, K.; Glass, R. S.; Norwood, R. A.; Pyun, J., New Infrared Transmitting Material via Inverse Vulcanization of Elemental Sulfur to Prepare High Refractive Index Polymers. *Adv. Mater.* **2014,** *26* (19), 3014-3018.

96.   Mann, M.; Zhang, B.; Tonkin, S. J.; Gibson, C. T.; Jia, Z.; Hasell, T.; Chalker, J. M., Processes for coating surfaces with a copolymer made from sulfur and dicyclopentadiene. *Polym. Chem.* **2022**.

97.   Bu Najmah, I.; Lundquist, N. A.; Stanfield, M. K.; Stojcevski, F.; Campbell, J. A.; Esdaile, L. J.; Gibson, C. T.; Lewis, D. A.; Henderson, L. C.; Hasell, T.; Chalker, J. M., Insulating Composites Made from Sulfur, Canola Oil, and Wool. *ChemSusChem* **2021,** *14* (11), 2352-2359.

98.   Wang, J.; Zhang, S., A Novel Sulfur-Based Terpolymer Cathode Material for Lithium–Sulfur Battery. *Energy Technol.* **2020,** *8* (5), 2000057.

99.   Sahu, T. S.; Choi, S.; Jaumaux, P.; Zhang, J.; Wang, C.; Zhou, D.; Wang, G., Squalene-derived sulfur-rich copolymer@ 3D graphene-carbon nanotube network cathode for high-performance lithium-sulfur batteries. *Polyhedron* **2019,** *162*, 147-154.

100.   Royuela, S.; Almarza, J.; Mancheño, M. J.; Pérez-Flores, J. C.; Michel, E. G.; Ramos, M. M.; Zamora, F.; Ocón, P.; Segura, J. L., Synergistic Effect of Covalent Bonding and Physical Encapsulation of Sulfur in the Pores of a Microporous COF to Improve Cycling Performance in Li-S Batteries. *Chem. Eur. J.* **2019,** *25* (53), 12394-12404.

101.   Bhargav, A.; Bell, M. E.; Cui, Y.; Fu, Y., Polyphenylene Tetrasulfide as an Inherently Flexible Cathode Material for Rechargeable Lithium Batteries. *ACS Appl. Energy Mater.* **2018,** *1* (11), 5859-5864.

102. Chang, C.-H.; Manthiram, A., Covalently Grafted Polysulfur–Graphene Nanocomposites for Ultrahigh Sulfur-Loading Lithium–Polysulfur Batteries. *ACS Energy Lett.* **2018,** *3* (1), 72-77.

103. Dong, P.; Han, K. S.; Lee, J.-I.; Zhang, X.; Cha, Y.; Song, M.-K., Controlled Synthesis of Sulfur-Rich Polymeric Selenium Sulfides as Promising Electrode Materials for Long-Life, High-Rate Lithium Metal Batteries. *ACS Appl. Mater. Interfaces* **2018,** *10* (35), 29565-29573.

104. Gomez, I.; Mantione, D.; Leonet, O.; Blazquez, J. A.; Mecerreyes, D., Hybrid Sulfur−Selenium Co-polymers as Cathodic Materials for Lithium Batteries. *ChemElectroChem* **2018,** *5* (2), 260-265.

105. Gracia, I.; Ben Youcef, H.; Judez, X.; Oteo, U.; Zhang, H.; Li, C.; Rodriguez-Martinez, L. M.; Armand, M., S-containing copolymer as cathode material in poly(ethylene oxide)-based all-solid-state Li-S batteries. *J. Power Sources* **2018,** *390*, 148-152.

106. Hoefling, A.; Nguyen, D. T.; Partovi-Azar, P.; Sebastiani, D.; Theato, P.; Song, S.-W.; Lee, Y. J., Mechanism for the Stable Performance of Sulfur-Copolymer Cathode in Lithium–Sulfur Battery Studied by Solid-State NMR Spectroscopy. *Chem. Mater.* **2018,** *30* (9), 2915-2923.

107. Jiang, Q.; Li, Y.; Zhao, X.; Xiong, P.; Yu, X.; Xu, Y.; Chen, L., Inverse-vulcanization of vinyl functionalized covalent organic frameworks as efficient cathode materials for Li–S batteries. *J. Mater. Chem. A* **2018,** *6* (37), 17977-17981.

108. Shen, K.; Mei, H.; Li, B.; Ding, J.; Yang, S., 3D Printing Sulfur Copolymer-Graphene Architectures for Li-S Batteries. *Adv. Energy Mater.* **2018,** *8* (4), 1701527.

109. Wu, F.; Chen, S.; Srot, V.; Huang, Y.; Sinha, S. K.; Aken, P. A.; Maier, J.; Yu, Y., A Sulfur–Limonene-Based Electrode for Lithium–Sulfur Batteries: High-Performance by Self-Protection. *Adv. Mater.* **2018,** *30* (13), 1706643.

110. Zeng, S.; Li, L.; Yu, J.; Wang, N.; Chen, S., Highly crosslinked organosulfur copolymer nanosheets with abundant mesopores as cathode materials for efficient lithium-sulfur batteries. *Electrochim. Acta* **2018,** *263*, 53-59.

111. Zhao, F.; Li, Y.; Feng, W., Recent Advances in Applying Vulcanization/Inverse Vulcanization Methods to Achieve High-Performance Sulfur-Containing Polymer Cathode Materials for Li–S Batteries. *Small Methods* **2018,** *2* (11), 1800156.

112. Chen, Z.; Droste, J.; Zhai, G.; Zhu, J.; Yang, J.; Hansen, M. R.; Zhuang, X., Sulfur-anchored azulene as a cathode material for Li–S batteries. *ChemComm* **2019,** *55* (61), 9047-9050.

113. Li, Z.; Fang, C.; Qian, C.; Zhou, S.; Song, X.; Ling, M.; Liang, C.; Liu, G., Polyisoprene Captured Sulfur Nanocomposite Materials for High-Areal-Capacity Lithium Sulfur Battery. *ACS Appl. Poly, Mater.* **2019,** *1* (8), 1965-1970.

114. Liu, X.; Lu, Y.; Zeng, Q.; Chen, P.; Li, Z.; Wen, X.; Wen, W.; Li, Z.; Zhang, L., Trapping of Polysulfides with Sulfur-Rich Poly Ionic Liquid Cathode Materials for Ultralong-Life Lithium–Sulfur Batteries. *ChemSusChem* **2020,** *13* (4), 715-723.

115. Lee, J. H.; Kim, K. H.; Choi, M.; Jeon, J.; Yoon, H. J.; Choi, J.; Lee, Y.-S.; Lee, M.; Wie, J. J., Rational molecular design of polymeric materials toward efficient triboelectric energy harvesting. *Nano Energy* **2019,** *66*, 104158.

116. Mann, M.; Kruger, J. E.; Andari, F.; McErlean, J.; Gascooke, J. R.; Smith, J. A.; Worthington, M. J. H.; McKinley, C. C. C.; Campbell, J. A.; Lewis, D. A.; Hasell, T.; Perkins, M. V.; Chalker, J. M., Sulfur polymer composites as controlled-release fertilisers. *Org. Biomol. Chem* **2018**.

117. Do Valle, S. F.; Giroto, A. S.; Reis, H. P. G.; Guimarães, G. G. F.; Ribeiro, C., Synergy of Phosphate-Controlled Release and Sulfur Oxidation in Novel Polysulfide Composites for Sustainable Fertilization. *J. Agric. Food Chem.* **2021,** *69* (8), 2392-2402.

118. Berndt, A. J.; Hwang, J.; Islam, M. D.; Sihn, A.; Urbas, A. M.; Ku, Z.; Lee, S. J.; Czaplewski, D. A.; Dong, M.; Shao, Q.; Wu, S.; Guo, Z.; Ryu, J. E., Poly(sulfur-random-(1,3-diisopropenylbenzene)) based mid-wavelength infrared polarizer: Optical property experimental and theoretical analysis. *Polymer* **2019,** *176*, 118-126.

119. Anderson, L. E.; Kleine, T. S.; Zhang, Y.; Phan, D. D.; Namnabat, S.; Lavilla, E. A.; Konopka, K. M.; Ruiz Diaz, L.; Manchester, M. S.; Schwiegerling, J.; Glass, R. S.; Mackay, M. E.; Char, K.; Norwood, R. A.; Pyun, J., Chalcogenide Hybrid Inorganic/Organic Polymers: Ultrahigh Refractive Index Polymers for Infrared Imaging. *ACS Macro Lett.* **2017,** *6* (5), 500-504.

120. Boyd, D. A.; Baker, C. C.; Myers, J. D.; Nguyen, V. Q.; Drake, G. A.; McClain, C. C.; Kung, F. H.; Bowman, S. R.; Kim, W.; Sanghera, J. S., ORMOCHALCs: organically modified chalcogenide polymers for infrared optics. *ChemComm* **2017,** *53* (1), 259-262.

121. Kleine, T. S.; Diaz, L. R.; Konopka, K. M.; Anderson, L. E.; Pavlopolous, N. G.; Lyons, N. P.; Kim, E. T.; Kim, Y.; Glass, R. S.; Char, K.; Norwood, R. A.; Pyun, J., One Dimensional Photonic Crystals Using Ultrahigh Refractive Index Chalcogenide Hybrid Inorganic/Organic Polymers. *ACS Macro Lett.* **2018,** *7* (7), 875-880.

122. Kleine, T. S.; Lee, T.; Carothers, K. J.; Hamilton, M. O.; Anderson, L. E.; Ruiz Diaz, L.; Lyons, N. P.; Coasey, K. R.; Parker, W. O.; Borghi, L.; Mackay, M. E.; Char, K.; Glass, R. S.; Lichtenberger, D. L.; Norwood, R. A.; Pyun, J., Infrared Fingerprint Engineering: A Molecular-Design Approach to Long-Wave Infrared Transparency with Polymeric Materials. *Angew. Chem. Int. Ed.* **2019,** *58* (49), 17656-17660.

123. Park, S.; Lee, D.; Cho, H.; Lim, J.; Char, K., Inverse Vulcanization Polymers with Enhanced Thermal Properties via Divinylbenzene Homopolymerization-Assisted Cross-Linking. *ACS Macro Lett.* **2019,** *8* (12), 1670-1675.

124. Islam, M. D.; Liu, S.; Boyd, D. A.; Zhong, Y.; Nahid, M. M.; Henry, R.; Taussig, L.; Ko, Y.; Nguyen, V. Q.; Myers, J. D.; Baker, C. C.; Kim, W.; Sanghera, J. S.; Smith, E. M.; Derov, J. S.; Ye, X.; Amassian, A.; Ade, H.; Genzer, J.; Ryu, J. E., Enhanced mid-wavelength infrared refractive index of organically modified chalcogenide (ORMOCHALC) polymer nanocomposites with thermomechanical stability. *Opt. Mater.* **2020,** *108*, 110197.

125. Kuwabara, J.; Oi, K.; Watanabe, M. M.; Fukuda, T.; Kanbara, T., Algae-Inspired, Sulfur-Based Polymer with Infrared Transmission and Elastic Function. *ACS Appl. Poly, Mater.* **2020,** *2* (11), 5173-5178.

126. Meem, M.; Banerji, S.; Majumder, A.; Vasquez, F. G.; Sensale-Rodriguez, B.; Menon, R., Broadband lightweight flat lenses for long-wave infrared imaging. *Proc. Natl. Acad. Sci. USA* **2019,** *116* (43), 21375-21378.

127. Lundquist, N. A.; Worthington, M. J. H.; Adamson, N.; Gibson, C. T.; Johnston, M. R.; Ellis, A. V.; Chalker, J. M., Polysulfides made from re-purposed waste are sustainable materials for removing iron from water. *RSC Adv.* **2018,** *8*, 1232-1236.

128. Ren, Z.; Jiang, X.; Liu, L.; Yin, C.; Wang, S.; Yang, X., Modification of high-sulfur polymer using a mixture porogen and its application as advanced adsorbents for Au(III) from wastewater. *J. Mol. Liq.* **2021,** *328*, 115437.

129. Hasell, T.; Parker, D. J.; Jones, H. A.; McAllister, T.; Howdle, S. M., Porous inverse vulcanised polymers for mercury capture. *ChemComm* **2016,** *52*, 5383-5386.

130. Thielke, M. W.; Bultema, L. A.; Brauer, D. D.; Richter, B.; Fischer, M.; Theato, P., Rapid Mercury(II) Removal by Electrospun Sulfur Copolymers. *Polymers* **2016,** *8*, 266.

131. Akay, S.; Kayan, B.; Kalderis, D.; Arslan, M.; Yagci, Y.; Kiskan, B., Poly(benzoxazine-co-sulfur): An efficient sorbent for mercury removal from aqueous solution. *J. Appl. Polym. Sci.* **2017,** *134* (38), 45306.

132. Abraham, A. M.; Kumar, S. V.; Alhassan, S. M., Porous sulphur copolymer for gas-phase mercury removal and thermal insulation. *Chem. Eng. J.* **2018,** *332*, 1-7.

133. Lee, J.; Lee, S.; Kim, J.; Hanif, Z.; Han, S.; Hong, S.; Yoon, M.-H., Solution-based Sulfur-Polymer Coating on Nanofibrillar Films for Immobilization of Aqueous Mercury Ions. *Bull. Korean Chem. Soc.* **2018,** *39* (1), 84-89.

134. Lin, H.-K.; Lai, Y.-S.; Liu, Y.-L., Cross-Linkable and Self-Foaming Polysulfide Materials for Repairable and Mercury Capture Applications. *ACS Sustain. Chem. Eng.* **2019,** *7* (4), 4515-4522.

135. Petcher, S.; Parker, D. J.; Hasell, T., Macroporous sulfur polymers from a sodium chloride porogen—a low cost, versatile remediation material. *Environ. Sci.: Water Res. Technol.* **2019,** *5* (12), 2142-2149.

136. Chen, Y.; Yasin, A.; Zhang, Y.; Zan, X.; Liu, Y.; Zhang, L., Preparation and Modification of Biomass-Based Functional Rubbers for Removing Mercury(II) from Aqueous Solution. *Materials* **2020,** *13* (3), 632.

137. Wadi, V. S.; Mittal, H.; Fosso-Kankeu, E.; Jena, K. K.; Alhassan, S. M., Mercury removal by porous sulfur copolymers: Adsorption isotherm and kinetics studies. *Colloids Surf. Physicochem. Eng. Aspects* **2020,** *606*, 125333.

138. Ko, L.-A.; Huang, Y.-S.; Lin, Y. A., Bipyridine-Containing Polysulfide Materials for Broad-Spectrum Removal of Heavy Metals from Water. *ACS Appl. Poly, Mater.* **2021,** *3* (7), 3363-3372.

139. Worthington, M. J. H.; Shearer, C. J.; Esdaile, L. J.; Campbell, J. A.; Gibson, C. T.; Legg, S. K.; Yin, Y.; Lundquist, N. A.; Gascooke, J. R.; Albuquerque, I. S.; Shapter, J. G.; Andersson, G. G.; Lewis, D. A.; Bernardes, G. J. L.; Chalker, J. M., Sustainable Polysulfides for Oil Spill Remediation: Repurposing Industrial Waste for Environmental Benefit. *Adv. Sustain. Syst.* **2018,** *2* (6), 1800024.

140. Griebel, J. J.; Nguyen, N. A.; Namnabat, S.; Anderson, L. E.; Glass, R. S.; Norwood, R. A.; Mackay, M. E.; Char, K.; Pyun, J., Dynamic Covalent Polymers via Inverse Vulcanization of Elemental Sulfur for Healable Infrared Optical Materials. *ACS Macro Lett.* **2015,** *4* (9), 862-866.

141. Xin, Y.; Peng, H.; Xu, J.; Zhang, J., Ultrauniform Embedded Liquid Metal in Sulfur Polymers for Recyclable, Conductive, and Self-Healable Materials. *Adv. Funct. Mater.* **2019,** *29* (17), 1808989.

142. Smith, A. D.; Thiounn, T.; Lyles, E. W.; Kibler, E. K.; Smith, R. C.; Tennyson, A. G., Combining agriculture and energy industry waste products to yield recyclable, thermally healable copolymers of elemental sulfur and oleic acid. *J. Polym. Sci., Part A: Polym. Chem.* **2019,** *57* (15), 1704-1710.

143. Thiounn, T.; Lauer, M. K.; Bedford, M. S.; Smith, R. C.; Tennyson, A. G., Thermally-healable network solids of sulfur-crosslinked poly(4-allyloxystyrene). *RSC Adv.* **2018,** *8* (68), 39074-39082.

144.   Omeir, M. Y.;   Wadi, V. S.; Alhassan, S. M., Inverse vulcanized sulfur–cycloalkene copolymers: Effect of ring size and unsaturation on thermal properties. *Mater. Lett.* **2020,** *259*, 126887.

145.   Alboaiji, S. Porous Polysulfide Polymer in Removing Perfluorooctanoic acid from Water and Extracting Gold. Flinders University, **2017**.

146.   Esdaile, L. J.; Chalker, J. M., The Mercury Problem in Artisanal and Small-Scale Gold Mining. *Chem. Eur. J.* **2018,** *24*, 6905-6916.

Chapter 2

Polysulfides and their application in mercury free artisanal gold mining and e-waste recycling

Introduction

A total of 187,000 tons of gold have been mined in history.[1] For the last 10 years the global gold production has increased consecutively. In 2019 the gold production hit a new record high of 3107 tones.[2] While formal gold mining is regulated to a degree and is responsible for the majority of the global gold production, the artisanal and small scale gold mining (ASGM) sector is largely unregulated and contributes up to 25% to the global gold production.[3] Unfortunately, many of these small scale mining operations use mercury[4-6] or in the case of larger operations, cyanide.[7-9] This chapter aims to give an overview of the work undertaken to develop a mercury- and cyanide-free gold extraction and recovery process that can be implemented by the ASGM sector as well in e-waste applications.

AGSM and Mercury

A small vessel full of metallic mercury was found in a grave in Egypt dating back to 1600 to 1700 years B. C., indicating that mercury has been known to man for thousands of years.[5] The use of mercury in precious metal mining started around 750 B. C. when the Phoenicians and Carthaginians used mercury from Spain to amalgamate and concentrate precious metals, but it was not before 50 B. C. that mercury was used widely by the Romans. Mercury amalgamation remained one of the most used techniques to mine for precious metals up to the 16th century.[5] Nevertheless, in colonial America over 70% of Mexican silver in 1870 was mined using mercury. In the years between 1700 and 1820 over 100,000 tons of mercury were used in mining operations in the Americas.[5] Even between 1850 and 1900, 70,000 tons of mercury were used for gold mining in the USA. The development of cyanidation in the 1880's and abundant alluvial gold sources in the USA rendered the use of mercury amalgamation mostly

redundant.[5] However, a resurgence of the use of mercury occurred in the 1970's when it found renewed use in the tropics.[5]

Worldwide, in over 70 countries around 10-19 million miners are involved in AGSM mining along with 80-100 million people who are economically dependent on this mining activity.[10] Mining operations can be conducted on a small, medium or large scale by only a handful of individuals. Larger operations involve thousands of men, women and children. Along with organised legal operations, illegal, informal mining often occurs due to the fact that many operations are poverty driven.[10] While AGSM is responsible up to 25% of the world's gold production many of these operations are taking place in low income nations using only rudimentary techniques.[11] Many of these rudimentary techniques involve the use of elemental mercury. It is estimated that the mercury emission from AGSM amounts to >30% of the total mercury released worldwide translating to up to 1400 tons of mercury (Figure 2.1). Many of these operations take place in developing nations in Asia, Africa or South America as can be seen in Figure 2.1 below.[3]
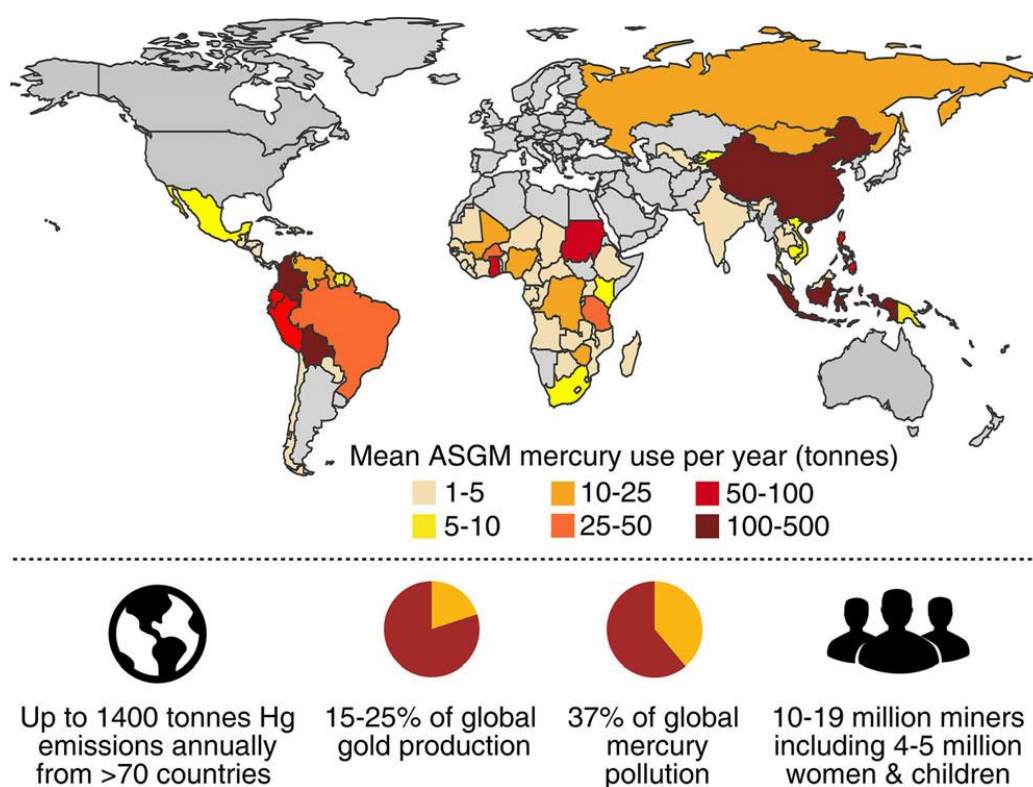
Figure 2.1: Annual mercury use in ASGM. Image reproduced under a Creative Commons CC-BY-NC license.[3]

Mercury has the ability to from a dense amalgam with gold hence rendering it very useful for the AGSM sector. Moreover, mercury is freely available from geological

sources like cinnabar, and it can be acquired relatively cheaply through industrial processes or the black market.[3, 12] Esdaile and Chalker described one particularly harmful way in which gold is mined using mercury (Figure 2.2).[3] The first step involves crushing the gold bearing ore or sediment into fine particles. This is commonly done by adding the ore into motor or hand-powered mills filled with water and steel balls functioning in a similar way as ball mills. The mills are operated until the ore is crushed to a fine powder. Following that, between 0.3 to 1.0 kg of elemental mercury is added to 20 kg of ore inside the mills, with milling continuing for another couple of hours after which the mercury and the gold have formed an amalgam,[3] which is an alloy of mercury and gold.[13] The dense amalgam is then removed from the mills, and excess mercury is recovered by hand. The isolated gold-mercury amalgam material contains up to 80% mercury. Next, the gold is recovered by heating the amalgam over a stove or using a handheld torch. During this process the amalgam breaks down to gold and mercury metal, with mercury boiled off leaving only the gold behind.[3] During this process the mercury vapors are often inhaled by the unprotected miners.[14] Virtually no safety equipment is used in this process.

Figure 2.2: Gold recovery process in ASGM. **a)** Gold bearing material is crushed and mixed with water in mills. **b)** Mercury is added to the crushed material (up to 1 kg per 20 g of ore). **c)** After the amalgamation process the remaining mercury is recovered. **d)** Gold-mercury amalgam is recovered. **e)** The mercury in the amalgam is removed by a blow torch. **f)** Isolated gold from an artisanal mine. Image reproduced under a Creative Commons CC-BY-NC license.[3]

Mercury is one of the most toxic elements[15] and exists in several forms: elemental or metallic mercury (Hg^0), organic mercury and inorganic mercury. At room temperature Hg presents as a liquid metal with a low vapor pressure which makes it easily released into the environment and atmosphere.[16] Organic mercury is often found as methyl- or ethylmercury in the environment after microbial metabolism. Inorganic mercury can form solid state compounds with oxygen, sulfur, or chlorine. In these compounds the inorganic mercury exists in mercurous (Hg^+) or mercuric (Hg^{2+}) oxidation states.[16] Human exposure to mercury most commonly occurs though inorganic mercury from food, methylmercury from seafood or mercury vapor exposure from dental amalgam restorations or other direct uses of mercury metal.[16] While elemental mercury is not readily absorbed into the body, inhalation of mercury vapor poses a significant health risk. Upon inhalation into the lungs the toxic metal is swiftly taken up by the blood and is dispersed to all the other organs. Although metal mercury is readily oxidised into Hg^{2+} in the red blood cells within several minutes rendering it unable to cross the blood-brain barriers, vaporised mercury will stay as a vapor in the blood long enough that a significant amount can cross the blood-brain barrier before it is oxidised. Once the barrier is crossed, the mercury is oxidised and accumulates in the brain.[16] The half-life of inorganic mercury in the brain is estimated to be years or decades long.[17] The other primary organ for mercury accumulation is the kidney, where the greatest amount can be found after exposure.[16] The health effects of acute mercury exposure can be as severe as lung damage and death due to hypoxia. In the case of chronic mercury vapor exposure, the target organs are the central nervous system and the kidneys. Chronic exposure can lead to gingivitis, erethism, tremors, psychological disturbances and memory and other adverse health effects.[16]

Adverse health effects due to mercury exposure in the AGSM have been well documented. Bose-O'Reilly and colleagues examined 200 children between 9 and 17 years of age shedding light on the health hazard for children in gold mining areas.[18] The findings show excessive salivation, metallic taste in the mouth, ataxia, abnormal reflexes, dysdiadochokinesia and other symptoms.[18] Laboratory test showed elevated mercury levels in urine (6.49 µg/L) and blood (5.25 µg/L) of children just living in the mining areas compared to the control group (0.4 µg/L in urine and 3.47 µg/L in blood). Children working with mercury had peak concentration of 941 µg/L in urine and 101 µg/L in blood.[18] The fact that children who are just living in the vicinity in which mercury is used have elevated mercury levels highlights the problem of mercury being spread through communities near ASGM activity. Cordy et al. investigated and mapped the mercury vapor emissions in four mines located in Chile, Peru, Ecuador, Suriname and Colombia.[19] Results show that mercury fumes persist for around 15 minutes, the same

time it usually takes to burn the amalgam. Measurements around the processing centers revealed that some areas had a mercury concentration that exceeded the maximum detection limit (> 999 µg m^{-3}) of the instrumentation. Although further studies are needed to confirm this, measurements showed that the mercury is dispersed to elevations that could make it possible to transport the mercury to other areas.[19] Studies conducted on soil at artisanal mining sites in China showed heavy metal pollution.[20] Besides mercury, high levels of cadmium in the soil as well as elevated levels of mercury and lead were found in grains and vegetables. The authors of that study recommend urgent soil remediation together with the removal of tailings from farmland. For this reason, farmers should not grow crops near the contaminated areas and locals should avoid eating local agricultural products due to contamination caused by nearby mining.[20] Taking all of this into account it becomes evident that a change in practices surrounding AGSM are urgently needed.

On the 10th of October 2013, the Minamata Convention on Mercury was signed by 128 countries,[21] and entered onto force on the 16th of August 2017.[22] The aim of the convention is to reduce anthropogenic Hg emission and make the public more aware of mercury exposure and its impacts. Further, signatory countries are required to improve Hg monitoring in the environment thereby reducing human exposure.[23] As such, the convention provides provisions to reduce Hg sources. Besides other strategies, it seeks to do that by reducing or eliminating the supply and trade of mercury, its use in AGSM, and by appropriately dealing with contaminated sites.[21] The convention also specifically addresses the use of Hg in AGSM. Under the convention, the parties agreed to reduce and where possible eliminate the use, release, and emissions of mercury. Parties to the convention must also develop and implement an action plan to address mercury related problems. The problem is further exaggerated since AGSM takes predominately place in developing counties and as such are mostly informal, unregulated operations.[22]

Such implementations have proven difficult. A study by Spiegel et al. found that an increase of mercury prices was the expected result of restrictions in the mercury trade.[24] However, the example in Indonesia shows that that is not the case. There, new cinnabar mining operations not only make mercury more accessible but also cheaper.[24] In light of all this it seems imperative that alternative, mercury free, AGSM methods are developed, investigated and implemented. While mercury free methods are already available, most of them are difficult to implement into the ASGM sector.

Mercury free gold mining methods for ASGM

The first stage if these methods usually involves concentration to gold into a ore concentrate by gravity separation like shaker tables or sluices before the gold is extracted and recovered by one of the following methods.[25]

Cyanide

While the first cyanide based leaching processes were introduced in New Zealand over 100 years ago, it was not before the 1970's that major operations in the U.S. began to use cyanide.[26] Before cyanide processes were introduced to mining, only lode, high yield placer deposits or vein gold could be profitably mined. With the introduction of cyanide low grade ore deposits could now be also exploited.[26]

The most common form of cyanide used in mining is sodium cyanide (NaCN).[26] Because it contains a single negatively charged cyanide ion (NC$^-$) and a single positively charged sodium ion (Na$^+$), sodium cyanide is colloquially referred to as simply "cyanide" in the mining sector. Cyanide can easily convert into hydrogen cyanide (HCN) and a free cyanide ion (CN$^-$), when in water.[26] The toxicity of cyanide is correlated to the amount of free cyanide present (in contrast to cyanide complexed to other metals).[26] Simple cyanides like sodium cyanide are preferred in leaching solutions since they have the ability to dissolve metals and form complex cyanides. Generally, complex cyanides are less toxic and more stable than simple cyanides.[26] During the leaching process the toxicity of the solution heavily depends on the pH since it is related to the amount of toxic free cyanide. Free, toxic cyanide exists at a neutral pH of 7, and more HCN is formed at lower pH values. However, the most efficient gold leaching with cyanide takes place at a basic pH. Also, the most toxic form of cyanide, HCN is predominately seen at a pH at or under 9.36. Therefore, the ideal pH for mining falls between 9.5 and 11 with 10.5 being optimal.[26] That mining operations ensure to maintain the correct pH of the leach solution is paramount considering that HCN is gaseous and therefore highly toxic for the workers while no longer available for the leaching process.[26]

For ores of lower gold grade or when the gold is scattered in a large amount of rock, heap leaching is a commonly used extraction method. Around 13-20 % of the cyanide used in gold mining in used in heap leaching[27] For this method, the crushed ore is placed in an especially engineered pad and irrigated with a 0.01% to 0.05% NaCN solution which is kept at a pH between 9.5 and 11.[26] This cyanide solution trickles though the ore and leaches the gold before it is collected at the bottom of the ore heap.[27] The resulting gold bearing solution is termed "pregnant".[26] After collection the gold is recovered by zinc cementation or carbon adsorption whereas the latter is the preferred method (these methods of gold recovery after cyanidation are briefly discussed below).[28]

A major drawback of this technique is that the process can take from several weeks to months. The mechanism of cyanidation involves several reactions at the solid liquid interface. The process begins with the uptake of oxygen by the solution, followed by the transportation of the oxygen and dissolved cyanide to the liquid-solid interface. It is at that interface where the CN^- and O_2 are adsorbed to the surface and the redox reactions take place. Gold is oxidised to Au^+ and forms a $Au(CN)_2^-$ complex while oxygen and water are reduced to H_2O_2 and OH^-. Next, the gold-cyanide complex is desorbed from the surface and released into the liquid phase.[28] The mechanism proceeds as seen below in Figure 2.3.
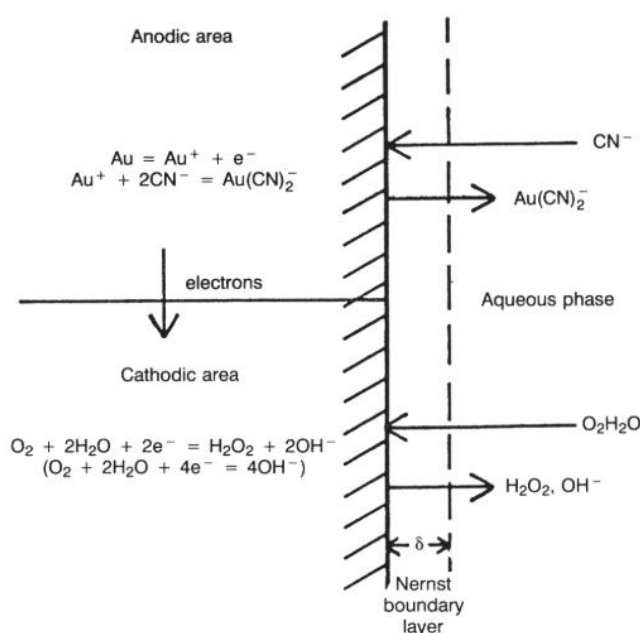
Figure 2.3: Cyanidation process of gold dissolution at the solid-liquid interface. © 1991 Van Nostrand Reinhold. Image reproduced under a RightsLink license. [28]

Gold recovery from the leach solutions can take place using a variety of methods, however only three will be discussed briefly here.

Zinc cementation is a reductive precipitation process during which the gold is reduced on the surface of zinc metal which is lower in the galvanic series than gold.[27] Since hydrogen gas is evolved during the process, which can aid gold precipitation, the chemical reaction can be summarised as follows:[27]

$$Au(CN)_2^- + Zn^0 + H_2O + 2CN^- = Au^0 + Zn(CN)_4^{2-} + OH^- + \frac{1}{2}H_2$$
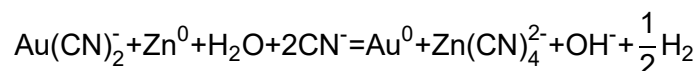
The precipitates from this reaction are then collected and smelted and refined.[27]

Another way to recover gold from cyanidation is by carbon absorption.[27] During this process, the gold-cyanide solution is passed through agitation tanks to enrich the

carbon with gold.[27] The adsorption mechanism of gold from the cyanide solution is not yet fully understood.[28] However, some theories involve a gold adsorption mechanism that proceeds by the adsorption of the gold-cyanide complex through van der Waals or electrostatic forces.[27, 28] Nevertheless very little is known about the of gold absorption onto carbon and much controversy still exits around the absorption mechanism.[28, 29]

These days the majority of the worlds gold is recovered with the use of cyanide.[30] The byproduct of this type of gold extraction have been billions of tons of cyanide tailings so far. These tailings contain toxic cyanides and are mainly stored in tailing dams since detoxification is often not economically viable.[30] Storing enormous amounts of toxic tailings in dams can lead to devastating disasters as was the case in the Baia Mare, Romania, cyanide spill in 2000.[31] High levels of rain caused a holding pond to beak, releasing 10000 cubic meters of cyanide and heavy metal containing tailings. These tailings found their way into river ways in Romania, Hungary, Yugoslavia and Bulgaria before ending up in the black sea causing the death of fish and other wildlife in its wake. Additionally, the drinking water of an estimated 2.5 million people in Hungary alone was poisoned.[31] Even seemingly intact tailing dams can pose a risk to human health in the environment as the example of the mining community in Kenyasi, Ghana, shows. Opoku et al found that water, cassava and fish samples near dams had heighted levels of cyanide and were not fit for consumption.[32]

As has been previously discussed in this chapter, mercury has a detrimental effect on ASGM communities. Hence it does not come as a surprise that alternative methods are being explored, including the use of cyanide.[33] Therefore cyanide has found its way from large scale gold mining operations into the ASGM sector.[34] This however comes with considerable risks. In some cases, tailings that have been already treated with mercury are reprocessed with cyanide.[35] This practice leads to the formation of anionic mercury cyanide complexed which, at a certain pH values, become bioavailable and easily methylated. In turn, this can result in bioaccumulation of mercury potentially harming the environment as well as human health.[34] Another factor adding to the risk of using cyanide in ASGM is its lack the lack of treatment or control of cyanide. For instance, Yacouba and colleagues have reported illegal use of cyanide at a rate of 20 kg per week in an ASGM catchment in Burkina Faso, resulting in the direct release of cyanide containing tailings into the environment.[35]

Additional mercury free methods

Other mercury- and cyanide-free methods for gold extractions are being developed. Many use alternative leach solutions. One such approach is that of using

sulfur containing lixiviants such as thiosulfate.[36] Another is that of using chlorine to process ores. In this process hydrochloric acid and bleach are used to leach to gold from the ore.[37] However, the handling of strong acid and the chlorine gas formation during the leaching process pose a potential risk. Unfortunately, many mercury- and cyanide-free methods are limited by higher costs and complicated processes. Further, many of these methods require trained personnel which decreases their chances of uptake by ASGM miners.[38] A review by Meech confirms that the most used treatments for gold concentrates are cyanide, lixiviants like thiourea, chlorine including electro-chlorination.[25]

<u>Electronic waste (e-waste)</u>

Another area that would greatly benefit from non-toxic gold extraction methods is that of informal e-waste recycling. Included in e-waste are electronical and electrical scraps like computers, scientific equipment, X-ray machines, cell phones, scanners, printers, tablets and more.[39] The amount of electronic waste produced globally is rising rapidly, with 50 million tons produced in 2018 alone.[40] Developed countries are responsible for the majority of that waste with countries in Europe, USA, Canada and Australia generating 20-28 kg of e-waste per capita per year. (Figure 2.4).[41] Conversely, low income countries in Africa or Asia only produce 0.1-1 kg per capita per year (Figure 2.4) Further, electronic waste is poised to grow by around 5 % annually making it the fastest growing waste stream globally.[42, 43]
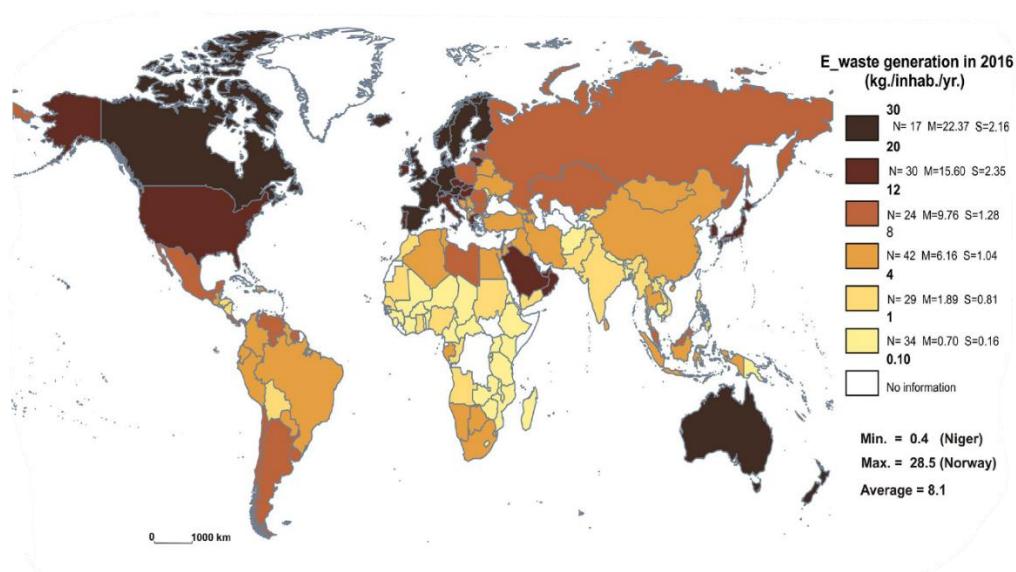
Figure 2.4: Global e-waste generation rate per capita per year in 2016. © 2019 Elsevier Inc. Image reproduced under a RightsLink license.[41]

Printed circuit boards contain a multitude of elements with gold being one of them.[40] Recent surveys suggest that around 340g of gold can be recovered from 1 ton of mobile phones.[40] This translates to a gold concentration of between 10 and 1600 ppm of gold in electronic waste which greatly surpasses the concentration of mined gold ores with an average of 18 ppm.[40] The electronics industry used 245 tons of gold, over 40 tons of palladium and nearly 13,000 tons of silver in 2015 alone.[44] Estimations by the National Institute for Materials Science found that 60,000 tons of silver and 6,800 tons of gold, which equates to 16 % and 22 % of the worlds reserves respectively can be found in urban mines (e-waste).[44] Hence there is enormous potential for precious metal recovery from e-waste. Due to the hazards associated with precious metal recovery from e-waste, and the many instances in which this is done in an unregulated informal economy leads to many parallels with ASGM. In some cases, e-waste recycling has been referred to as "urban mining."

Only 20% of e-waste generated around the world is collected and processed via an official system.[45] And as of 2016, policies to manage electronic waste were not established in 113 countries.[45-47] Hence, the remaining vast amounts are part of an informal or illegal sector of e-waste processing.[45] In this way, there are many challenges similar to those faced in ASGM, as mentioned above. A report by Ratti et al tracked e-waste from the United States to different ports in Asia, with a high likelihood of not being recorded in official trade data.[48] Since most developing countries have strict environmental legislation and higher cost of labor, e-waste is often shipped to developing countries.[49] The reuse of used electronics is stated as the reason for developed countries to send e-waste to developing countries. However, this is not always the case as an example from Nigeria shows. Of the 100,000 tons of electronic products received, 30% were not re-usable and were essentially waste.[45]

Although some countries like China and India have banned the import of e-waste, illegal import and smuggling still continues, leading to increasing informal e-waste processing activities.[48] For example 95% of e-waste generated in India is processed by informal operations.[50] It is estimated that 80% of the global e-waste is recycled in informal sectors in countries such as Vietnam, China, Nigeria, Brazil, Mexico, Ghana, India or the Philippines (Figure 2.5).[51] The illegal nature of e-waste smuggling makes it very hard to quantify the extent of this activity however it is known that China and West Africa receive large amounts of electronic waste.[47]

Figure 2.5: Major informal e-waste recycling sites around the world. © 2019 Elsevier Inc. Image reproduced under a RightsLink license.[52]

While informal e-waste processing provides income and employment,[53] concerns arise over the dangerous methods employed to recycle e-waste.[51] Often, undocumented e-waste is manually dismantled and processed.[51] Many of the current e-waste processing methods in developing countries have an detrimental impact on the environment and human health.[49] Incineration of e-waste is frequently used to remove combustible components, leading to the release of various phthalic acids (PAEs).[50] Incomplete combustion can also lead to the buildup of carcinogenic organic compounds like polycyclic hydrocarbons.[50] Peijnenburg et al show that informal e-waste recycling sites in Nigeria are contaminated with polybrominated diphenyl esters which can have a negative effect on thyroid function as well as reproductive system and can lead to endocrine disruption.[51]

Heavy metals in e-waste are also a concern, since metals such as lead, cadmium and chromium are frequently found in electronic waste.[43] A study by Chen and co-workers, investigated links between birth outcomes and metal exposure at an e-waste recycling site in Guiyu, China.[43] The study found that mothers had higher concentrations of cadmium, lead and chromium than those from a control site.[43] Studies of an informal e-waste processing site in Ghana show a high levels of copper, zinc and lead contamination in the working areas where the dismantling and burning of e-waste takes place.[54] Similar trends have been observed in three other sites in Nigeria, where metal concentrations where up to 1000 times higher as at control sites.[53] These informal e-waste recycling activities not only affect human health but also lead to contamination of the environment. Air tested close to e-waste processing sites in China proved to be contaminated with chlorinated and brominated compounds and a range of heave metals

was found in the air around processing centres in India.[49] Another method by which the informal e-waste recycling community processed e-waste is by acid leaching.[55, 56] After using incineration to burn off as much flammable material from the e-waste as possible, acid leaching is used to recover precious metals such as gold, silver, platinum and palladium.[57] Using these processes, harmful acids such as nitric acid as well as cyanide are used leading to large amounts of contaminated waste water which is often released into adjacent rivers.[55, 57] A sample of acid waste collected from a leaching site in India showed high levels of nickel, tin, lead, copper, antimony and zinc as well as organic pollutants (phthalate esters, chlorophenols).[56]

<u>Current e-waste recycling strategies</u>

There are some parallels between formal and informal e-waste recycling. In both sectors pyrometallurgical and hydrometallurgical recovery methods[55] are used while biometallurgical methods are mostly used in the formal sector.[58]

Pyrometallurgy is used to extract metals using elevated temperatures which includes the preparation, smelting and refining of e-waste.[59, 60] During this process most organic components are volatilised leaving glass fibres and metal oxides behind which need to be further processed and refinded.[61] While pyrometallurgical methods to recover precious metals from e-waste are simple and effective,[61] it also released toxic gases, dust and smoke.[59] Another disadvantage is the relatively heigh energy consumption.[62]

Although hydrometallurgy has been predominantly used to extract metals from ore, it is also used in e-waste processing.[58] These processes include chemical leaching and bioleaching.[62] Usually, the process starts with pre-treatment of the e-waste such as shredding, sorting and the separation of magnetic components (Figure 2.6).[63] This is followed by the leaching step and the final metal recovery (Figure 2.6).[62] Chemical leaching can be done using a variety of lixiviant systems. One of them is cyanide leaching which was already discussed above. Others include leaching using halides, thiourea, thiosulfate and acid leaching.[62]
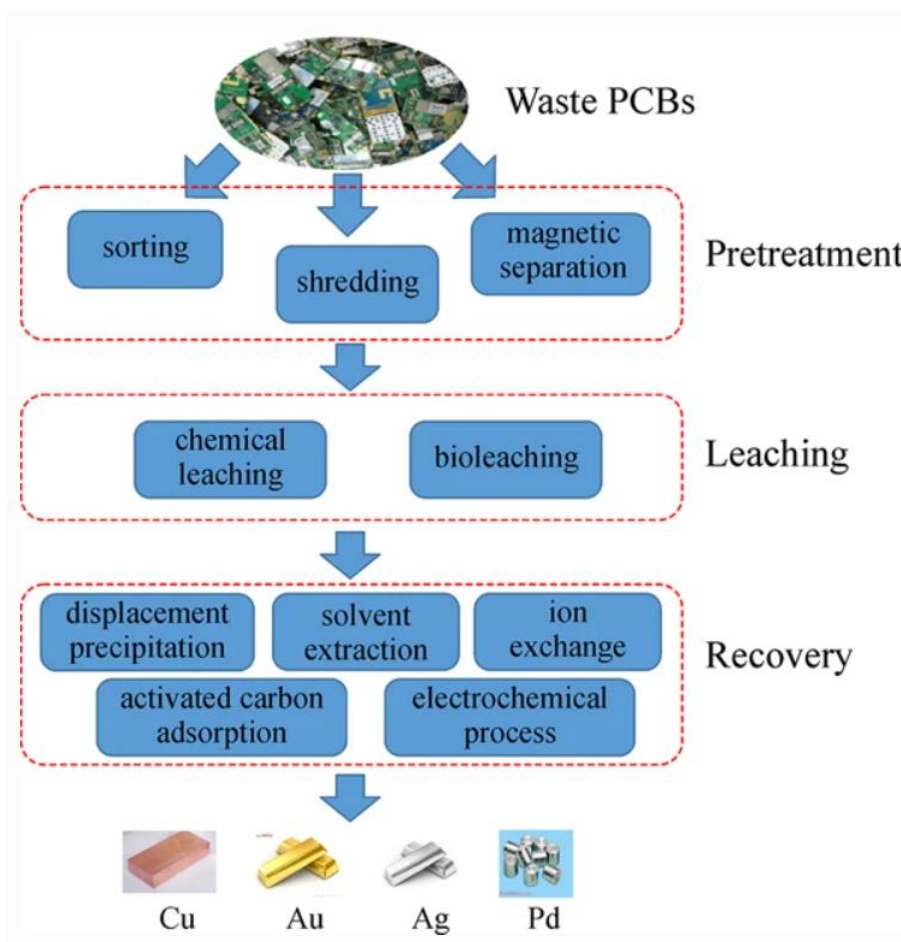
Figure 2.6: Process flow of hydrometallurgical precious metal recovery from electronic waste as proposed by Wang et al. © 2017 Higher Education Press and Springer-Verlag GmbH Germany. Image reproduced under a RightsLink license.[62]

A more recent pathway of precious metal recovery form e-waste is that of biometallurgy, which utilises various acidophilic bacteria capable of sulfur- and iron oxidation.[64] Using this method high leaching rates for copper, zinc, nickel and lead and moderate leaching rates for silver and gold were achieved. [64]

As has been briefly discussed, the main strategies used in precious metal recovery from electronic waste are pyrometallurgy, hydrometallurgy and biometallurgy. However, each of these methods had advantages and disadvantages. While pyrometallurgical methods can be applied to any type of e-waste and do not require pretreatment, plastic cannot be recovered and the combustion of electronic waste leads to the formation of toxic fumes detrimental to human health and the environment (Figure 2.7).[39]

Figure 2.7: Burning of e-waste to recovery copper is producing toxic fumes. © 2020 Informa UK Limited. Image reproduced under a RightsLink license.[65]

Hydrometallurgical leaching methods reduce the risk of air pollution but rely on large amounts of liquids which contain hazardous chemicals like cyanide and acids which can contaminate bodies of water.[39] Whereas biometallurgy is cheap and environmentally friendly, the leaching process is lengthy and leads to the production of harmful chemicals like sulfuric acid which can pollute the environment.[39] While these methods are viable options offering a high recovery rate and low initial investment,[63] they are technically challenging, hard to perform for untrained personnel and often involve strong acids.[62]

In summary it can be said that there are parallels between ASGM and informal e-waste recycling. Most of the activities take place in developing or low-income countries. While mercury use is a problem in ASGM, the informal e-waste methods also include harmful chemicals such as acids. Further, incineration of e-waste releases toxic fumes which are harmful to human health. Both ASGM and informal e-waste recycling result in environmental pollution. Although safter methods to extract gold exist for both areas, many are not practical for informal settings and require training or specialised personnel.

The goal for this chapter is twofold. A polymer made from sulfur and canola oil (50-poly(S-*r*-canola)) has been shown to remove oxidised gold from aqueous solutions in precious experiments in the Chalker research group. Keeping this in mind, the first aim is to develop a novel gold oxidation technique specifically tailored to be used in the small scale and artisanal gold mining and informal e-waste recycling sectors. Such a technique must be non-toxic, easy to perform and robust to be able to be applied to

various ore types as well as in order to be used by the informal mining community. The second goal is to validate the 50-poly(S-*r*-canola) polymer as a material to successfully remove and recover gold in high yields from the leach solutions.

Therefore, this chapter will discuss a novel, patented gold oxidation method that can be used in ASGM as well as informal e-waste scenarios which does not involve the use of mercury, cyanide or harsh acids. Further it will be shown that the leached gold can be recovered using a 50-poly(S-*r*-canola) polymer made from highly abundant or renewable resources: sulfur and canola oil.

Gold oxidation

The first step was to develop a method to oxidise gold and leach it into aqueous solution. For our goals in sustainability and effort to support the ASGM and informal e-waste recycling sector, the gold oxidation method had to be simple, low-cost, robust, rapid, and use chemicals that are relatively safe. Accordingly, the first oxidant to be tested was household bleach. Although similar procedures had been reported,[37] it was an important first step to trial this to get an indication of rate of gold oxidation and difficulty of this process. Bleach was chosen since it is a readily available household product and contains hypochlorite (ClO^-), an oxidant that can be used to oxidise gold metal.

For the first experiment 1 mg of gold wire (99.9% purity, 0.1 mm diameter) was added to solutions containing pure bleach (pH 13) but no reaction was observed after several hours. This result was not surprising since the hypochlorite ion alone is not reactive enough to oxidise gold at a useful rate. In order to speed up the reaction, the pH had to be lowered so that hypochlorous acid (HOCl) can form. HOCl is a stronger oxidising agent than ClO^-, able to oxidise gold.[66] The acid will protonate the ^-OCl ion to give hypochlorous acid (HOCl), as seen in Scheme 2.1.
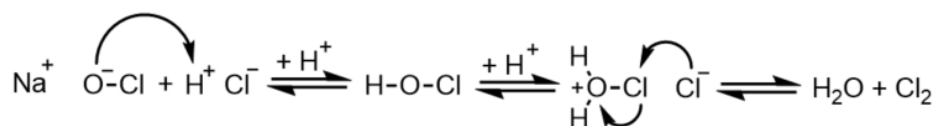
Scheme 2.1: Reaction mechanism for the reaction of sodium hypochlorite (NaOCl) and hydrochloric acid HCl to yield hypochlorous acid (HOCl), water and chlorine gas (Cl_2) after a second protonation.

However, a second protonation can take place to form Cl_2 gas, also a strong oxidant, able to oxidise gold (Scheme 2.1). The product of the oxidation is tetrachloroauric acid as seen in Scheme 2.2.[66, 67]

$$2Au + 3Cl_2 + 2HCl \longrightarrow 2HAuCl_4$$

Scheme 2.2: Reaction scheme of the oxidation of gold to tetrachlorauric acid ($HAuCl_4$) using chlorine gas (Cl_2) and hydrochloric acid (HCl).

To test the oxidation of bleach combined with HCl, 1 mg of gold wire was added to a solution of NaOCl and HCl with a pH of 1.5. Immediately, formation of bubbles could be seen, and the gold wire was oxidized and completely dissolved after 1 hour. Conversely, the gold wire in a pH 6 solution took overnight to oxidise and dissolve under otherwise identical conditions. Next, the effect pH had on the rate of gold dissolution was investigated more thoroughly. To do this, 5 solutions with a pH of 2, 4, 6, 8 and 10 were prepared using HCl (aq. 37 %). An equal mass of gold wire was placed in the solutions. After the first wire dissolved (1 hour 7 minutes, pH 2) the remaining gold wires were removed, dried, and weighed. The results showed a relationship between the weight loss of the gold wire by gold oxidation and pH (Figure 2.8). This result agrees with the literature in that gold oxidation using bleach is highly pH dependent.[66, 68]
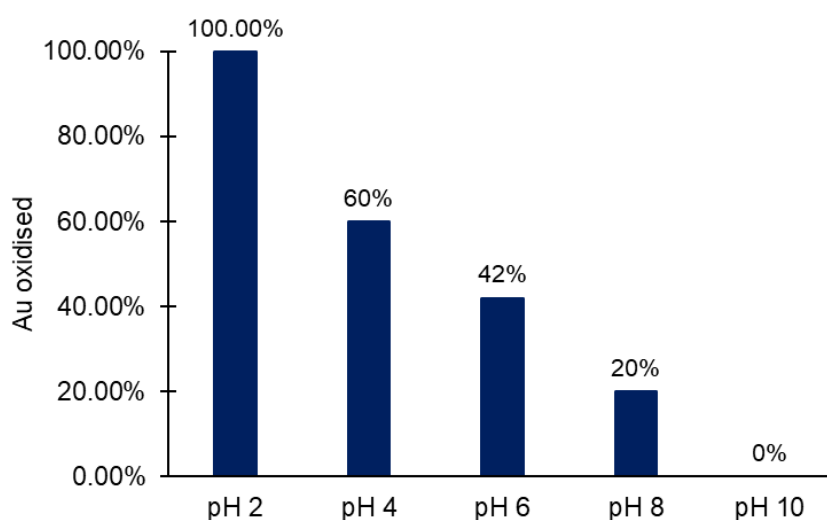
Figure 2.8: Percentage of gold oxidised and dissolved in solutions containing bleach and HCl of various pH value after the first gold wire had completely dissolved (1 hour and 7 minutes).

Although this process works well, it has limitations which include the formation of hazardous Cl_2 gas as seen below in Scheme 2.3. Further, the reaction is very pH

sensitive which requires the handling of acids and corrosive conditions. All these factors make it unlikely that this process will be taken up by the subsistence gold mining community. Hence, easier to handle, less toxic and more robust oxidants were sought out in this project.[69]

$$NaOCl + 2HCl \longrightarrow Cl_2 + NaCl + H_2O$$

Scheme 2.3: Reaction scheme of chlorine gas formation from NaOCl and HCl.

The goal was to find oxidants that are low-cost, relatively safe, and fast. Many pool sanitation chemicals contain halides (Cl, Br) and oxidants that are cheap, widely available, and relatively safe. Therefore, four pool chemicals were purchased as potential bleach surrogates to test their ability to oxidise gold. Their active constituents can be seen in Figure 2.9: bromochloromethylhydantoin (BCDHM), trichloroisocyanuric acid (TCCA), calcium hypochlorite ($Ca(OCl)_2$) and sodium dichloroisocyanurate plus sodium bromide (SDIC+NaBr). To investigate the effect of these chemicals on gold, individual solutions (15 mL) with a concentration of 6.66 mg/mL of each pool chemical were prepared and 1 mg of gold wire was added. After 43 hours all the gold had dissolved except in BCDMH solution. Since the gold oxidation using BCDMH took the longest it was excluded as a potential gold oxidant in subsequent experiments. While the initial results seemed promising, the gold oxidation was very slow. To explore if an increased concentration of halides would speed up the reaction, the effect of adding NaCl, NaBr or HCl as an additional halide source was investigated. The hypothesis was that the halide could react with the pool chemical and generate a more reactive oxidant such as BrCl, Br_2, or HOBr.
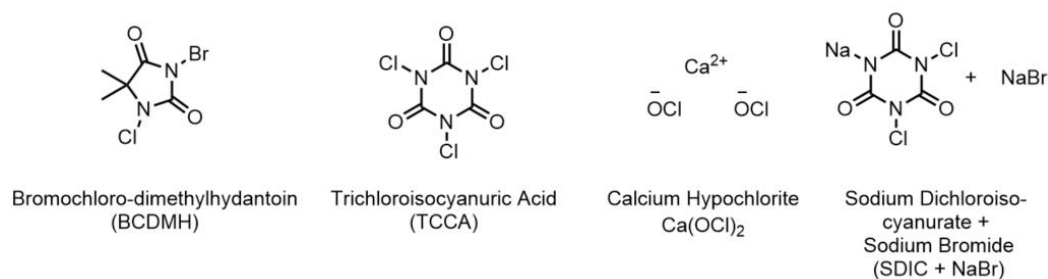
Figure 2.9: Name and structure of active constituent of commercial pool chemicals.

To test this hypothesis, different solutions containing one pool chemical, and one or two additional halide sources like HCl, NaBr or NaCl were prepared (Figure 2.10 and Figure 2.57). To each chemical that already had a hypochlorite group, HCl (since it has been previously established that the hypochlorite alone is not strong enough of oxidise gold) and an additional halide source like NaBr or NaCl was added. To chemicals without a hypochlorite group, NaBr or NaCl were added individually without the addition of HCl. The concentration of individual chemicals was chosen so that 50% of halide came from the pool chemical and 50% of the halide from an additional source. The concentration of total halides was 186 mM (93 mM of halide from the pool chemical and 93 mM of the halide from and additional halide source. If the solution contained more than one additional halide source, their concentrations were 46.6 mM each to make up 93 mM) and the volume of the solutions was 15 mL. To each solution 1 mg of gold wire was added. The pH of the solution was not controlled in order to determine which combination was the easiest to use without the need of any further adjustments. After the gold wires had been in the solution for 8 hours, the weight loss of the wires was calculated. Also, the pH of these solutions was monitored over the experiment time of 8 hours and the pH of the solution at the beginning of the experiment and at the end is recorded in Figure 2.10. However, it was decided to use only two solutions going forward. These solutions were $Ca(OCl)_2$ plus HCl and TCCA plus NaBr. The rationale for this was that the $Ca(OCl)_2$ plus HCl solution showed the fastest gold oxidation and could be used as a benchmark reaction. Although the TCCA plus NaBr solution did not show the fastest oxidation, this combination contained a source of bromide rather than chloride, lowering the risk of chlorine gas evolution. Additionally, the pH of a TCCA and NaBr solution is approximately 6.5 which also contributes to safety considerations. Calcium hypochlorite is very similar to bleach and the dissolving of gold using bleach has been the subject of previous studies.[66, 68] However, adding HCl to a $Ca(OCl)_2$ solution will evolve toxic Cl_2 gas as previously discussed.[70] Further, the reaction involved the handling of HCl, which can be dangerous. Furthermore, the reaction is quite pH sensitive.[66, 68] These factors render the use of calcium hypochlorite in conjunction with hydrochloric acid in a ASGM setting unlikely.
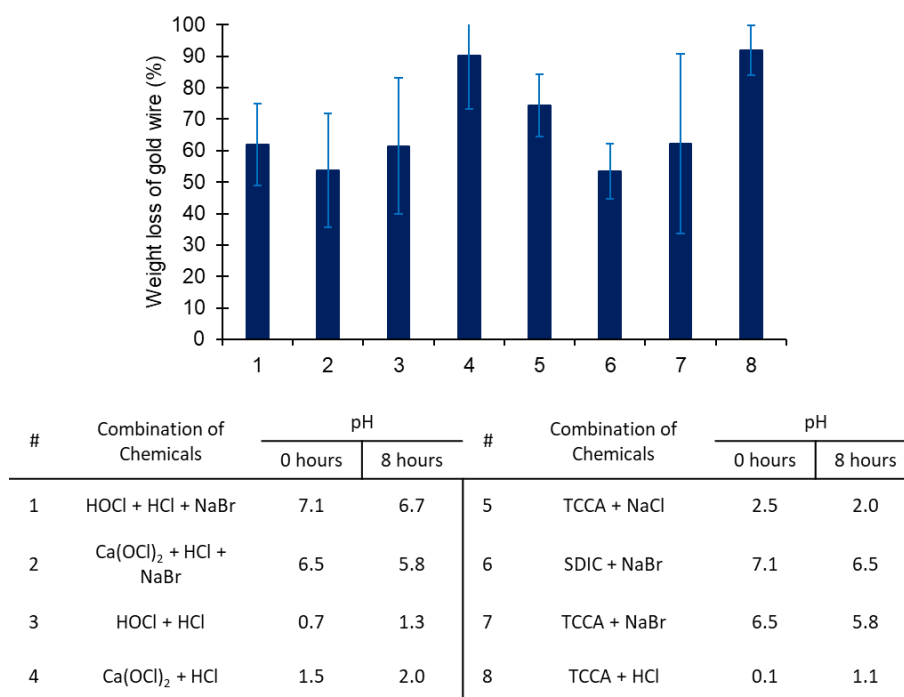
Figure 2.10: Gold oxidation (measured by the weight loss of gold wire) of a 1 mg gold wire in various combination of pool chemicals and additional halide sources.

#	Combination of Chemicals	pH		#	Combination of Chemicals	pH	
		0 hours	8 hours			0 hours	8 hours
1	HOCl + HCl + NaBr	7.1	6.7	5	TCCA + NaCl	2.5	2.0
2	Ca(OCl)$_2$ + HCl + NaBr	6.5	5.8	6	SDIC + NaBr	7.1	6.5
3	HOCl + HCl	0.7	1.3	7	TCCA + NaBr	6.5	5.8
4	Ca(OCl)$_2$ + HCl	1.5	2.0	8	TCCA + HCl	0.1	1.1

The use of TCCA and NaBr involves no acid handing but only two solids, which could be a benefit for storage and transport in a mining context. TCCA is a slow dissolving *N*-chlorinated isocyanurate used as a swimming pool sanitiser,[71] and has a low solubility of 12 g/L at 20 °C.[72] The basic structure is that of a s-triazine.[73] In an aqueous solution, TCCA forms cyanuric acid and hypochlorous acid (Scheme 2.4).[74] Interestingly, previous studies have shown that cyanuric acid is biodegradable, breaking down into CO_2 and NH_3.[75] In that context, a spent leaching solution containing cyanuric acid might be used to fertilize plants. A study by Ensminger et al investigated the use of cyanuric acid as fertiliser and showed promising results.[76] Therefore, more research needs to be undertaken to fully understand the benefits of using cyanuric acid as fertilizer, but the prospect of using spent leach reagent as a fertiliser is intriguing as it could potentially facilitate land rehabilitation after mining.
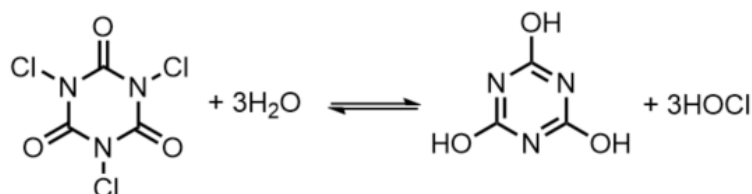
Scheme 2.4: Reaction mechanism of TCCA in water, forming cyanuric acid and hypochlorous acid.

However, it was anticipated that the addition of NaBr can result in different reactions. A proposed mechanism in an aqueous solution is shown in Scheme 2.5 below.

1)

2)
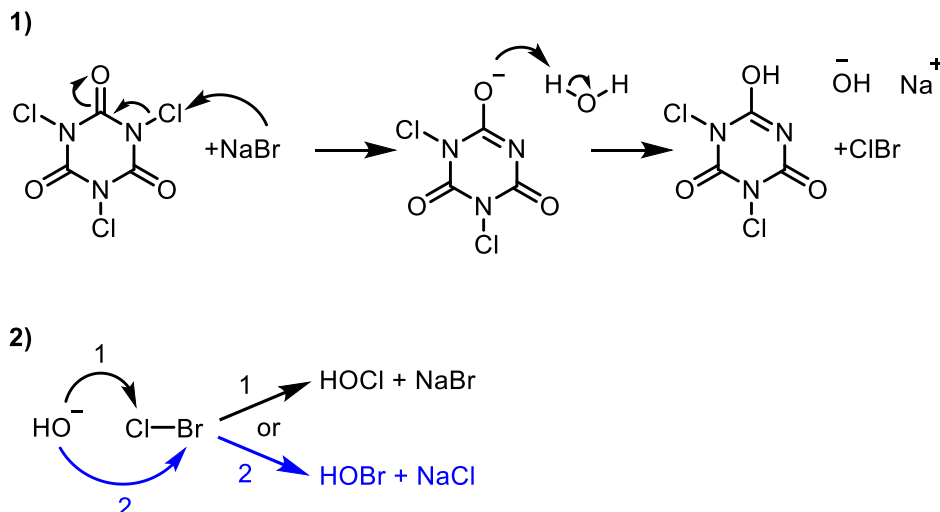
Scheme 2.5: Proposed reaction mechanism of the reaction of TCCA and NaBr in an aqueous solution. First, reaction of TCCA with NaBr to from ClBr, followed by the formation of hypobromous or hypochlorous acid and NaBr or NaCl.

It is proposed that ClBr is formed first but is only short-lived. ClBr can then react in two ways to form either HOCl and NaBr or HOBr and NaCl. A reaction scheme by which HOBr can dissolve gold to form the gold complex has been described by Dinis, et al (Scheme 2.6).[77] Therefore, the TCCA and NaBr reaction is a potentially useful method for the *in situ* generation of hypobromous acid, which is known to oxidise gold.

$$HOBr + H^+ + Br^- \rightleftharpoons Br_2 + H_2O$$

$$2Au + 3HOBr + 5Br^- + 3H^+ \longrightarrow 2AuBr^-_4 + 3H_2O$$
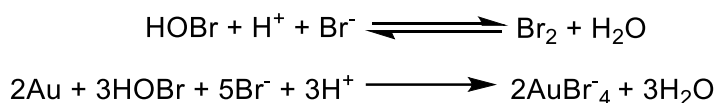
Scheme 2.6: Reaction scheme of the reaction of hypobromous acid to form water and bromine followed by the reaction of hypobromous acid, bromine and gold to form gold (III) bromide.[77]

To see if there is any evidence for HOBr formation, TCCA (108 mg, 0.03M) and NaBr (144 mg 0.09 M) were dissolved in water (15 mL), and a UV-Vis spectrum was taken. Control spectra of only NaBr (144 mg 0.09 M) or only TCCA (108 mg, 0.03M) dissolved in 15 mL of water were also taken (Figure 2.11). The spectrum of the TCCA and NaBr solution is consistent with the spectrum of HOBr seen in a study by Orlando,

et. al.[78] This suggests the presence of HOBr and it is consistent with the proposed mechanism. Although the presence of Br_2 could not be confirmed spectroscopically, a small amount of Br_2 might still form, as it is expected to be in equilibrium with HOBr in aqueous solution. The composition of this equilibrium would also be influenced by the pH of the solution.
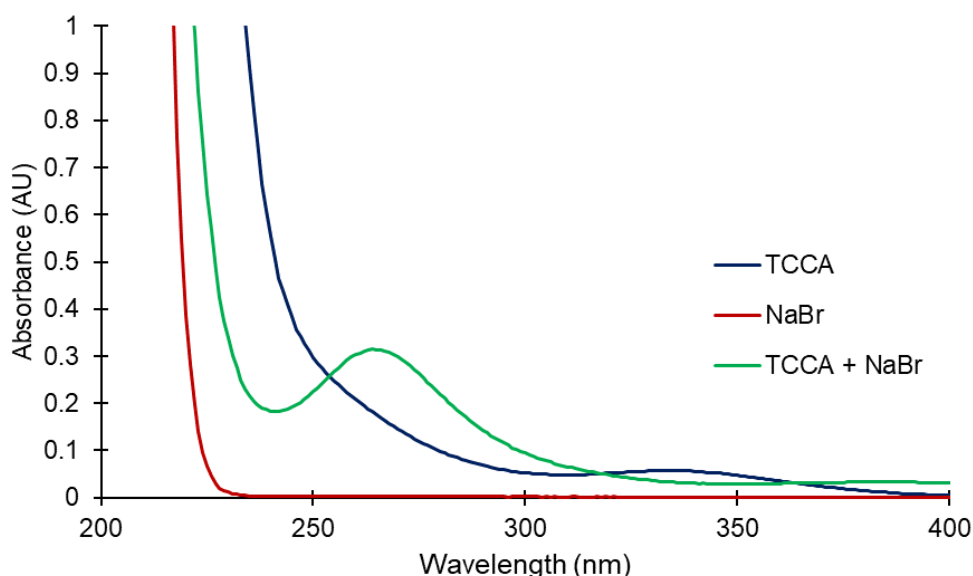
Figure 2.11: UV-vis spectra of aqueous TCCA, NaBr and TCCA plus NaBr.

The TTCA plus NaBr solution had a characteristic orange color whereas the $Ca(OCl)_2$ solution was slightly yellow (Figure 2.12). However, as previously stated a $Ca(OCl)_2$ plus HCl oxidation would not be useful in a ASGM setting due to the handling of strong acids and potential Cl_2 production.

Further, TCCA can be acquired on a commodity scale for as little as 1 USD per kilogram and NaBr for as little as 2 USD per kilogram. The low cost of TCCA is due to its widespread use in water sanitation.
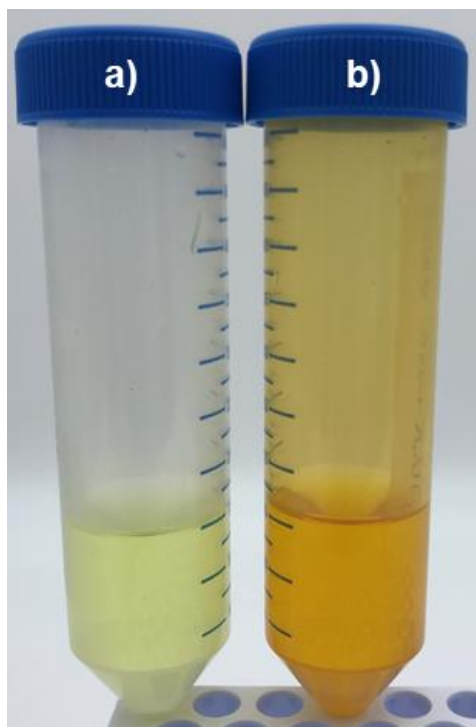
Figure 2.12: a) Ca(OCl)$_2$ plus HCl solution **b)** TCCA plus NaBr solution.

So far it has been shown that a solution of TCCA (0.03M, 15mL) and NaBr (0.09M, 15 mL) is able to oxidise gold wire at an average rate of 0.125 mg/hour. At this concentration, the concentration of halides is 186 mM, 93 mM bromide from NaBr and 93 mM chloride from TCCA. Is it hypothesised that TCCA and NaBr form hypobromous and hypochlorous acid *in situ*. It is thought to be the hypobromous acid which is then oxidising the gold to form gold(III) bromide. This was a promising result since both reagents, TCCA and NaBr are relatively benign and available in large quantities on the commodities market at low costs. Further, this method is acid free and only involves the handling of two solid reagents. Additionally, steps were taken to optimise the conditions of this gold oxidation method which will be discussed later in this chapter. Next, ways of gold recovery from a TCCA plus NaBr solution will be explored.

Gold and metal uptake by 50-poly(S-*r*-canola) polymer using aqueous gold and metal salts as model systems

To remove and recover the gold from the leach solution a polysulfide polymer made from sulfur and canola oil was used (Figure 2.13). This polymer (made from equal masses of sulfur and canola oil) has been thoroughly characterised by the Chalker group for other application in environmental remediation.[79] It is referred to as 50-poly(S-*r*-canola) in this thesis.
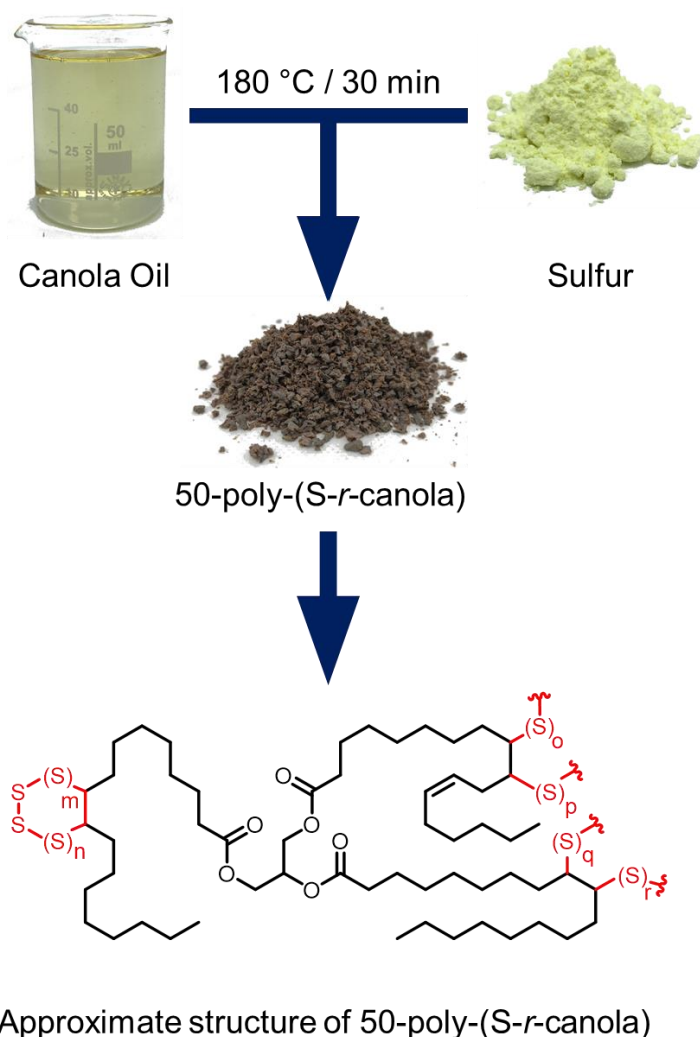
Figure 2.13: Reaction scheme and approximate structure of 50-poly(S-*r*-canola). Equal masses of canola oil and elemental sulfur were directly reacted at 180 °C together for 30 minutes. After the gel point of the reaction was reached the polymer was isolated as friable rubber. Reproduced with permission from the Royal Society of Chemistry.[80]

For preliminary experiments samples of the polymer were obtained from multi-kg synthesis prepared by a collaborative team in the Chalker lab (see later in this chapter for more details for this large-scale synthesis which was performed by the author). This polymer was made by directly reacting equal masses of canola oil and elemental sulfur at 180 °C for 30 minutes. During this reaction, NaCl was added as a porogen. After the reaction, the polymer was ground using a meat grinder, and the NaCl was removed by repeated rinsing with water. The final product was a porous friable rubber. The polymer that was synthesised in a multi-kg scale was characterised using ^{1}H NMR, IR, Simultaneous Thermal Analysis (STA) which included thermogravimetric analysis (TGA) and differential scanning calorimetry (DSC), powder X-ray diffraction (XRD), scanning

electron microscopy (SEM) and energy dispersive X-ray analysis (EDX) as can be seen in Figure 2.58 to Figure 2.62 in the experimental section.

All these analyses were consistent with what has been previously published.[81] Further, elemental analysis for carbon, hydrogen, nitrogen and sulfur (CHNS analysis) has been performed (Figure 2.63 in experimental section).

Additionally, preliminary results in a Masters project in the Chalker lab had shown that the 50-poly(S-r-canola) polymer is capable of removing aqueous gold (Au^{3+}) from solution followed by gold recovery through incineration,[82] however this was only done with pure AuCl$_3$. Therefore, it was necessary to determine if this polymer could capture gold from the TCCA-based leach solution. Additional, information on the rate and mechanism of gold uptake were unknown at the outset of this project.

Firstly, gold uptake studies using 50-poly(S-r-canola) were performed. To do this a 5 ppm solution of Au^{3+} from HAuCl$_4 \cdot$ H$_2$O was made. A cotton bag containing 1 g of polysulfide was added to 50 mL of gold solution in a plastic tube and rotated end over end at 25 RPM for 10 hours (Figure 2.14).

1 cm

Figure 2.14: 1 g of 50-poly(S-r-canola) polymer sewn into a cotton bag with the dimensions of 9 cm × 2 cm.

Every 2 hours a 1.9 mL sample was taken using a micropipette and stabilised in 5% HCl before the samples were analysed using ICP-MS. After the 10 hours 99.8% of gold had been removed as can be seen Figure 2.15. This was an encouraging result and was in line with the preliminary experiments performed in the Chalker laboratory.[82] However, it was also important to compare the gold uptake of the 50-poly(S-r-canola) polymer to the gold uptake of elemental sulfur to validate the polymer as a superior gold sorbent. Thus, the same experiment was performed with elemental sulfur as sorbent. Only 0.5 g of sulfur was used which is the same amount of sulfur in 1 g of poly(S-r-canola). The results showed that only 10% of gold was removed using elemental sulfur as sorbent compared to 99.8% using the polysulfide (Figure 2.15). This highlighted that sulfur alone is not efficient in removing gold but that the polysulfide chains on the 50-poly(S-r-canola) polymer significantly enhance gold uptake.
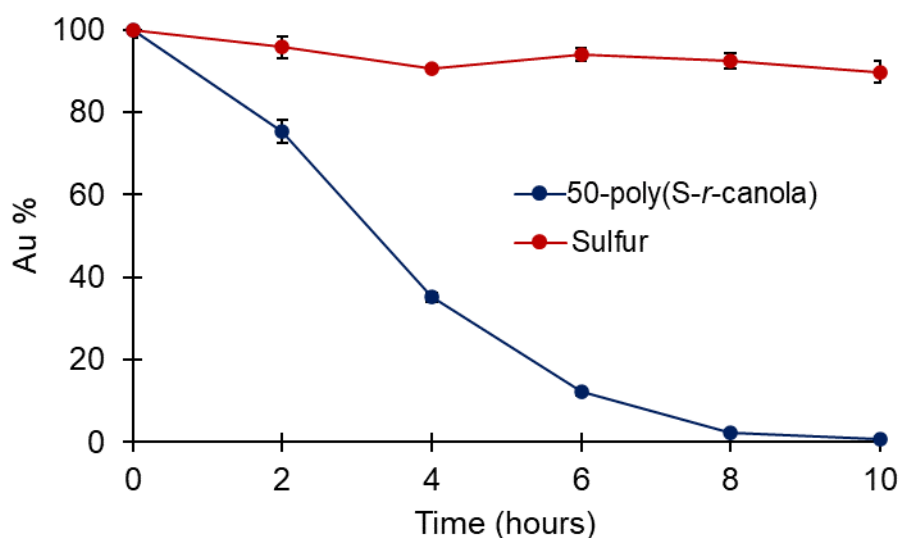
Figure 2.15: Uptake of Au³⁺ from aqueous solution by 1 g of 50-poly(S-*r*-canola) polymer and 0.5 g of sulfur over 10 hours.

To learn more about the form of gold on the 50-poly(S-*r*-canola) polymer, 1g of polymer was exposed to a 500 ppm gold solution (40 mL, made from AuCl₃) and analysed using SEM and EDX (Figure 2.16). Surprisingly, clusters of gold could be seen on the surface of the polymer (Figure 2.16).
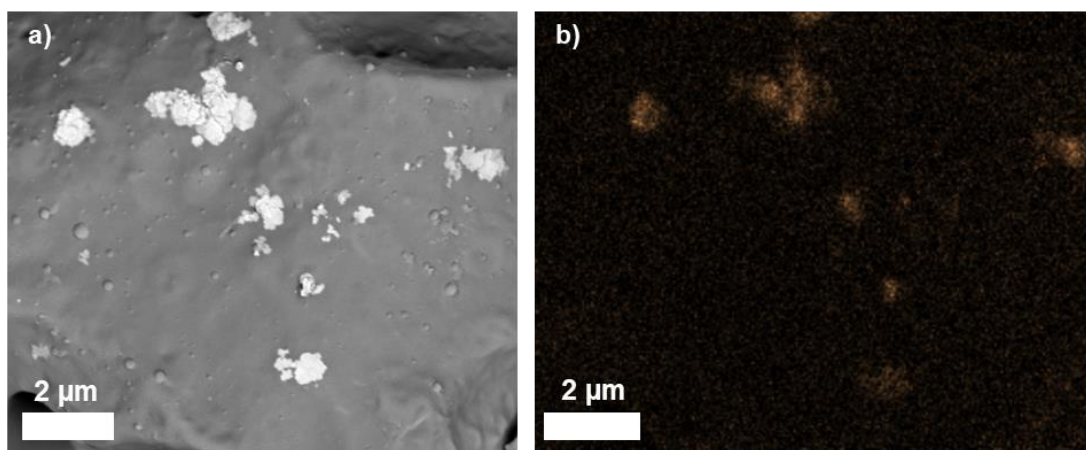
Figure 2.16: a) SEM micrograph using a backscattered electron detector and **b)** EDX gold map of polymer exposed to a 500 ppm gold solution.

Intrigued by this result, more work was done to determine the nature of gold on the 50-poly(S-*r*-canola) polymer as well as the gold-polymer interactions. To do this angle resolved X-ray photoelectron spectroscopy (ARXPS) analysis was performed (analysis performed by Yanting Yin). The 50-poly(S-*r*-canola) Polymer (1g) that had been exposed to 1, 5, 25, 250 and 500 ppm gold solutions (40 mL, made from AuCl₃)

was used for this experiment. The high-resolution scans of carbon, oxygen, sulfur, and gold of the samples were recorded. In Figure 2.17, the fittings of Au and S via a range of insertion angles are shown.
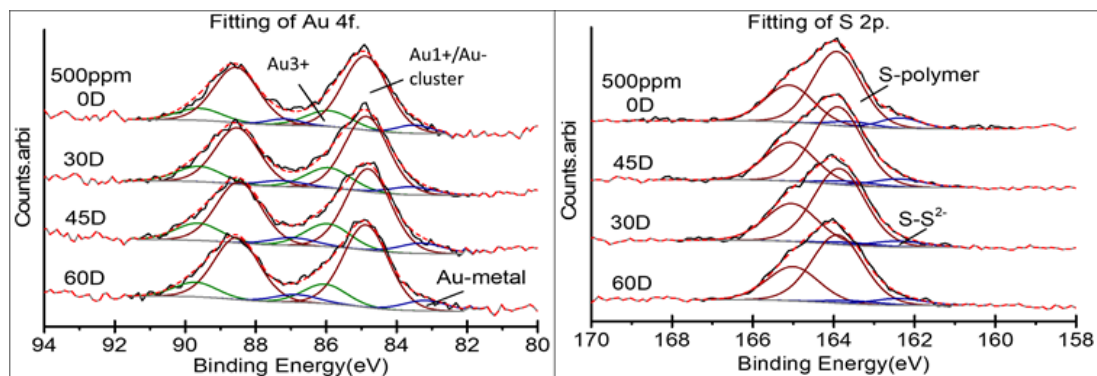
Figure 2.17: Fitting of Au and S high resolution scans as a function of different angles.

The fitting of Au 4f7/2 resulted in three individual peaks. The peak of an Au-metal/cluster was found at 83.6eV while the Au^{1+}/Au cluster was fitted at 84.8eV. The peak occurring at 86.1eV thus represented the high oxidation form of Au^{3+}, which is likely to be an Au-S bond. The fitting of S2p3/2 results in two distinguishable components. The one fitted at 164.0eV is from the polysulfide, while the other one fitted at 162.6eV represents the binding form of Au-S (S^{2-}).

The plots of relative concentration and fraction of different Au/S components can be seen in Figure 2.18 below. The increase of the concentration of Au on the 50-poly(S-*r*-canola) polymer correlates with the increase of concentration of gold in the solution to which the polymer was exposed to. A solution with a higher gold concentration resulted in a higher adsorption rate of gold onto the polymer. It is important to note, that if the polymer is exposed to a gold solution with a gold concentration of over 250 ppm S^{2-} can be observed. The S^{2-} is likely to be in a binding form with Au. The fraction can be increased to 11% when the polymer is exposed to a 500 ppm gold solution.
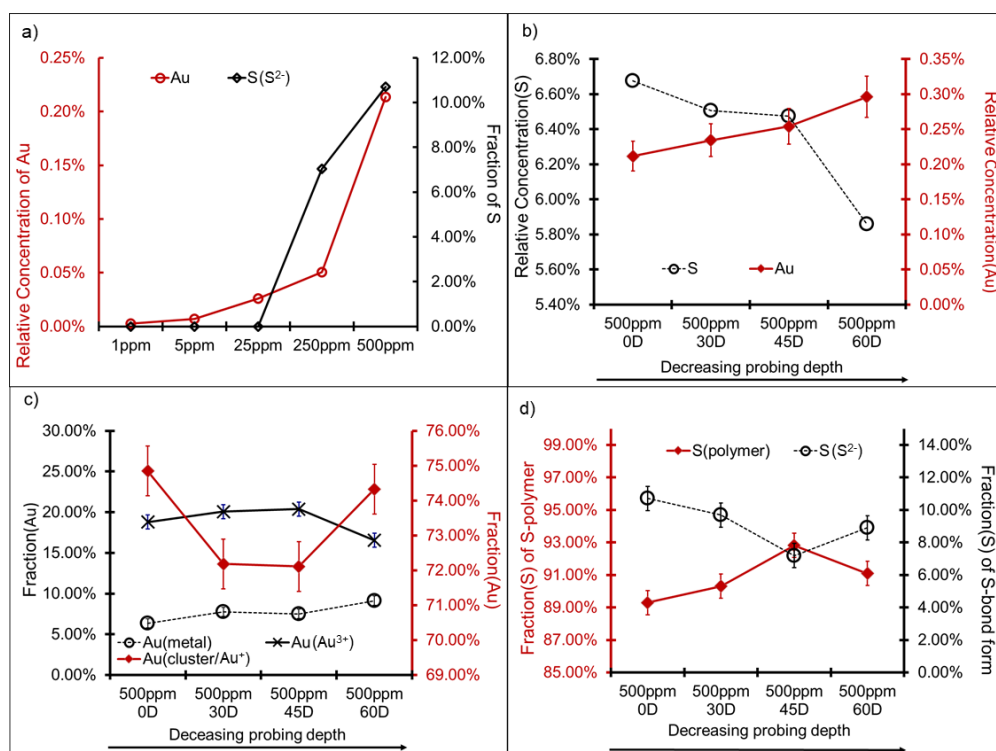
Figure 2.18: a) Relative concentration of Au and fraction of S^{2-} as a function of gold concentration. **b)** Relative concentration of Au and S via a range of depth. **c)** Fraction of Au(metal/cluster/Au^{1+}/Au^{3+}) as a function of different angles. **d)** Fraction of S(polymer/S^{2-}) as a function of different angles.

Angle resolved XPS was employed on the 500 ppm sample, the scans were conducted at 0º (deepest), 30 º, 45 º and 60 º(outmost), indicating the insertion angle. The results show an increase in the relative concentration of Au with the decrease of probing depth and that the concentration of S was decreased correspondently (Figure 2.18). Notably, the gold bound onto the polymer does not follow the change in gold concentration, which implies that the gold sorption process if more efficient at higher gold concentrations. It is obvious that the Au tends to aggregate on the outmost layer while the majority of S was from the polysulfide. Further, the fraction assigned to Au-metal increases with the decrease of probing depth, while the fraction of Au^{3+} (Au-S) shows a slight decrease. On the other hand, the fraction of S^{2-} shows a downwards trend, which is in agreement with the change of Au^{3+}. Following ARXPS analysis the following can be concluded: i) exposure of the polymer to a solution with a higher gold concentration resulted in higher amount of gold on the polymer, ii) both physical and chemical gold adsorption of gold to the polymer was observed resulting an Au^{3+}, Au^{1+}/cluster and Au metal on the polymer. An important implication of these findings is that the 50-poly(S-*r*-canola) is a *reactive* sorbent, which can bind to ionic gold, and reduce it to gold metal. This was also supported by the presence of S^{-2} which suggests a chemical bond of sulfur

63

to gold, and iii) gold in the form of clusters aggregates in the outmost surface of the polymer while gold in the form of Au-S (chemically bound) appears deeper within the polymer.

Previously, the 50-poly(S-*r*-canola) polymer has been extensively used in the uptake of mercury,[79] therefore it was important to compare the uptake of mercury to that of gold. To do this 1 g polymer bags were added to 40 mL solutions containing both, 5 ppm of gold (from $HAuCl_4$) and mercury (from $HgCl_2$) for 10 hours while being rotated. As can be seen in Figure 2.19 both mercury and gold are taken up by the polymer. After 2 hours the gold concentration was reduced by 99.7% whereas the mercury concentration was only reduced by 73.5%. Interestingly the gold was removed faster during this experiment than in the experiment comparing the polymer to elemental sulfur which is likely due to the variable polymer particle size or the mercury could bind to the gold as it is taken from solution having a synergistic effect (Figure 2.15).
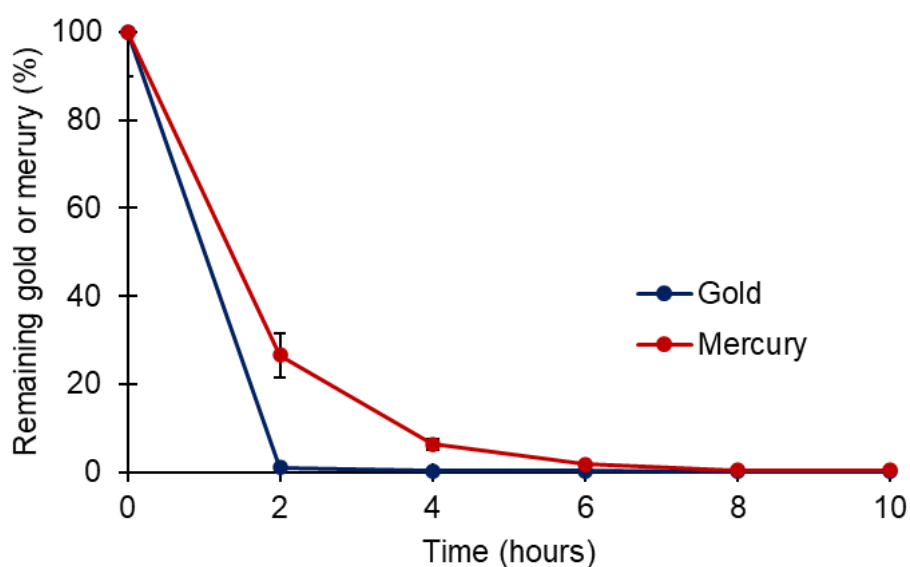
Figure 2.19: Uptake of Au^{3+} and Hg^{2+} from aqueous solution by 1 g of 50-poly(S-*r*-canola) polymer in a cotton bag.

If the 50-poly(S-*r*-canola) polymer is to be used in real world mining scenarios, the gold will be in the presence of many other elements in a leach solution. Therefore, the next step was to assess if the polymer is selective for gold in the presence of other common metals. This was important to explore since the polymer has already shown to bind to mercury and iron, though binding to iron was not very efficient.[79, 83] Sorption selectivity for elements abundant in the earth's crust like copper, iron, aluminium, and zinc were evaluated in a competition experiment with gold. Accordingly, a 5 ppm solution (50 mL) of Au^{3+} ($AuCl_3$), Al^{3+} ($AlCl_3$), Cu^{2+} ($CuBr_2$), Fe^{3+} ($FeCl_3$), and Zn^{2+} ($ZnSO_4$) was

prepared. To that solution, a cotton tea bag containing 1 g 50-poly(S-*r*-canola) was added, and the solution was agitated end over end for 72 hours at 25 RPM. After 72 hours samples were taken and analysed using ICP-MS. As can be seen in Figure 2.20, over 99% of the gold has been removed whereas the polymer did only take up negligible amounts of Al, Cu, Fe and Zn. This is an important finding since these elements can be found in gold ore deposits[84-86] and it is preferable that the 50-poly(S-*r*-canola) polymer has a high selectivity for gold.
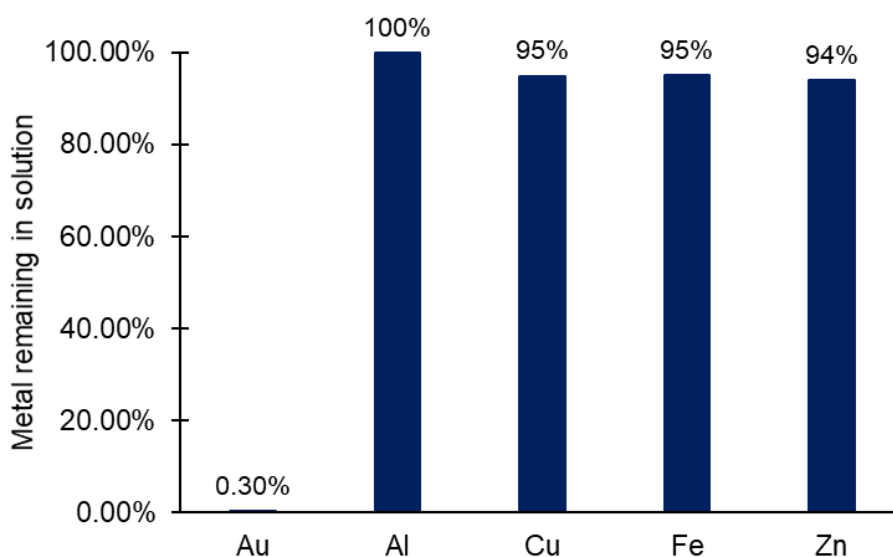
Figure 2.20: Au^{3+}, Al^{3+}, Cu^{2+}, Fe^{3+}, and Zn^{2+} remaining on solution after adding 1g of 50-poly(S-*r*-canola) polymer for 72 hours.

It was next investigated if metals closer to the electronic configuration of gold would influence the gold uptake of the 50-poly(S-*r*-canola) polymer. Arsenic, lead, and cadmium were chosen in this experiment. Firstly, a solution containing 5 ppm of Au^{3+} ($AuCl_3$), As^{5+} (As_2O_5), Pb^{2+} ($Pb(NO_3)_2$) and Cd^{2+} ($Cd(NO_3)_2$) was made. To this solution (50 mL) a 1 g 50-poly(S-*r*-canola) polymer bag was added and rotated end over end for 42 hours. After that time the samples were analysed using ICP-MS. The majority of the gold had been removed (96%) whereas the arsenic concentration remained the same, the lead concentration only dropped by 6% and the cadmium concentration only by 1% (Figure 2.21).
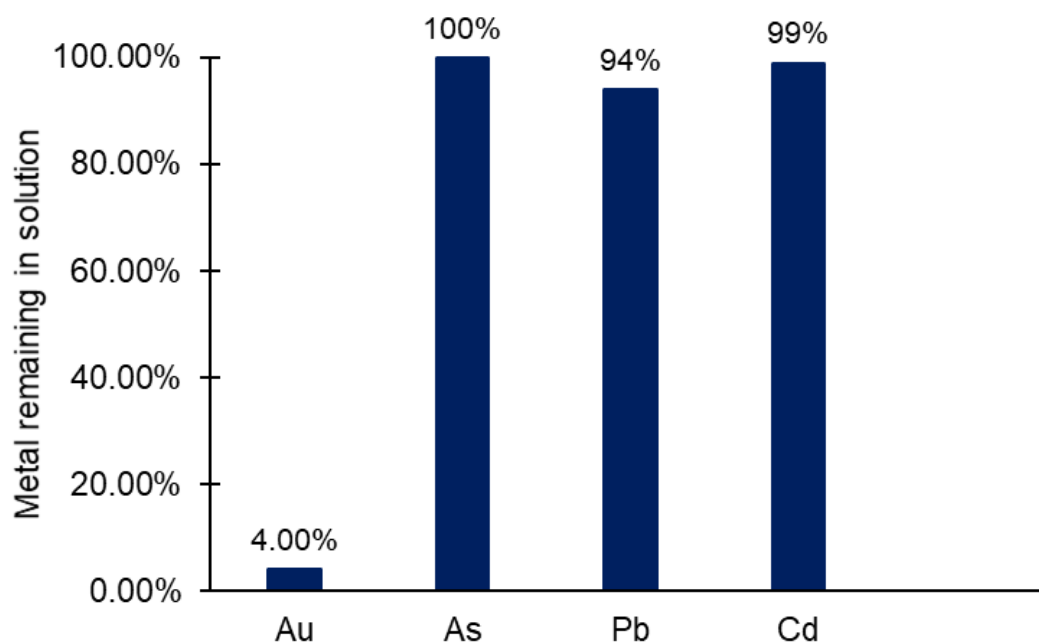
Figure 2.21: Au^{3+}, As^{5+}, Pb^{2+} and Cd^{2+} remaining on solution after adding 1g of 50-poly(S-*r*-canola) polymer for 42 hours.

These results were very encouraging and showed that if elements other than mercury are present in the ore or e-waste leachate, then selective gold uptake may be possible. Since it had been established that the polymer is highly effective in removing gold from a AuCl$_3$ solution, gold uptake from a TCCA-derived leach solution as well as additional aspects of the full process were investigated in more detail, as described in the following sections.

Gold recovery

It has been previously shown that $AuCl_3$ bound to the 50-poly(S-*r*-canola) polymer can be recovered by incinerating the polymer.[82] Nevertheless, it is not known if the oxidants would have any effect on the polymer during this final gold recovery step. For comparative reasons $Ca(OCl)_2$ plus HCl solutions and TCCA plus NaBr will be tested throughout this section. To determine if the oxidant solutions have an effect on the polymer, a 15 mL $Ca(OCl)_2$ plus HCl and a 15 mL TCCA plus NaBr solution was made each with a total halide concentration of 186 mM (93 mM form each chemical in solution). To these solutions 150 mg of polysulfide was added. After the solutions were left undisturbed for 24 hours a white layer had formed on the surface of the polymer, likely from a slight oxidation of the polymer. However, this layer was confined to the surface of the polymer and as the polymer was broken up it could be seen that the inside of the polymer was still dark brown without any discoloration. This qualitative evaluation suggested that the polymer can react partially with the leach solution. This could potentially be an advantage in that the polymer also serves as a quenching reagent. This also means that the amount of polymer required to recover gold may depend on the concentration of the leach reagents.

Model gold recovery experiments

To assess gold recovery, two 15 mL oxidising solutions were prepared, and 50 mg of gold metal was added. One solution contained $Ca(OCl)_2$ (100 mg) plus HCl (0.138 mL) and the other NaBr (144 mg) plus TCCA (108 mg) resulting in a total halide concentration of 186 mM (93 mM from each chemical). All samples were prepared in triplicate. After 6 days no gold in the TCCA and NaBr was visible indicating that the Au^0 had been oxidised to Au^+ or Au^{3+}, both soluble in aqueous solution. The gold in the $Ca(OCl)_2$ and HCl solution was oxidised after an additional 5 days indicating that the TCCA plus NaBr oxidation was faster. All the solutions had an average gold concentration of 2855 ppm (as determined by ICP-MS). One gram of 50-poly(S-*r*-canola) polymer was then added to the solutions and rotated (20 RPM) for 96 hours. To determine how much gold was removed from the solution, samples for ICP-MS analysis were taken at 25 and 96 hours. After 25 hours 83 % of the gold had been removed from the TCCA and NaBr solutions and 78% from The $Ca(OCl)_2$ and HCl solutions. After 96 hours 93.3 % of gold was removed from the TCCA and NaBr solutions and 99 % from the $Ca(OCl)_2$ and HCl solutions. Interestingly, the polymer was not able to remove 100 % of the gold. A possible explanation for this is that the polymer may be approaching

saturation or that the some of the surface of the polymer was oxidised, therefore rendering some of it unable to remove gold.

The method of gold recovery using incineration of the 50-poly(S-*r*-canola) polymer had to be rudimental to make uptake by ASGM miners feasible. Consequently, the polymer was placed in a ceramic crucible and incinerated by heating up the crucible with a Bunsen burner (Figure 2.22). As the polymer started to burn a lid was placed on the crucible to extinguish the flames to ensure a more controlled burn of the polymer.

Figure 2.22: Gold bearing 50-poly(S-*r*-canola) polymer incineration set-up. The wet or dry polymer was placed into the crucible and a Bunsen burner was used to heat the crucible until the polymer was incinerated.

Incineration of the 50-poly(S-*r*-canola) polymer resulted in recovery of 94 – 95 % of the gold oxidised with TCCA and NaBr and 99% of the gold oxidised with $Ca(OCl)_2$. The samples were analysed using SEM/EDX and the results showed residual sodium, bromide, and calcium. These residues are likely from the use of NaBr and $Ca(OCl)_2$ during the oxidation and the NaCl used as porogen during the polysulfide synthesis. In order remove the residues, the samples were purified by washing in deionised water. As can be seen in Figure 2.23, the purification process was successful and no elements

other than oxygen and gold were seen. Under an optical microscope, the recovered material had the visual appearance of gold (Figure 2.23).
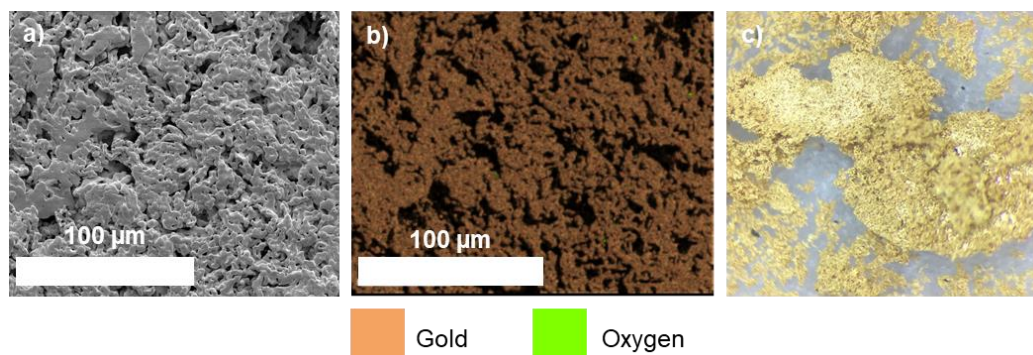
Figure 2.23: a) SEM micrograph of recovered and purified gold. b) EDX elemental map of the purified gold showing only gold and oxygen. c) Recovered and purified gold under an optical microscope.

Since it has been established that the 50-poly(S-*r*-canola) polymer is able to remove gold that had been oxidised using TCCA plus NaBr, it was investigated if the form of gold on the polymer was different when compared to a gold uptake from a $AuCl_3$ solution. Therefore, ARXPS analysis was performed on a polymer sample that has been used to remove gold from a TCCA plus NaBr oxidant solution. Besides gold, this analysis also revealed bromine on the polymer which is not surprising since bromine is part of the oxidant solution (Figure 2.24).
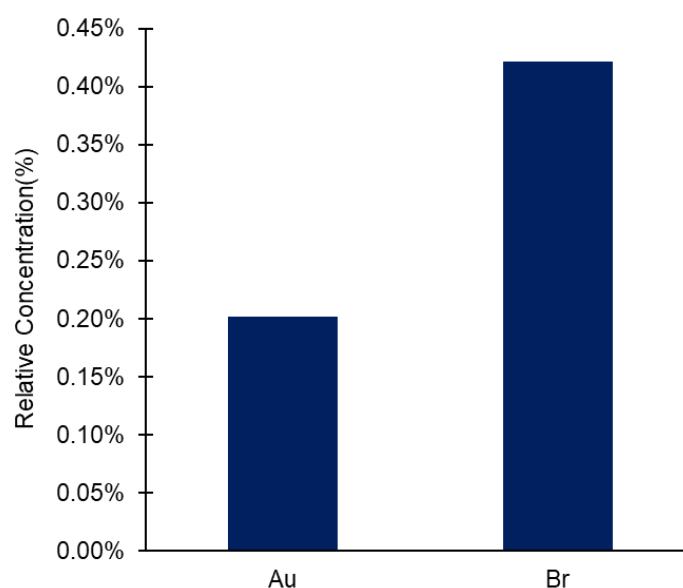
Figure 2.24: Relative concentration of Au and Br on the 50-poly(S-*r*-canola) polymer determined by ARXPS.

The form of gold found on the 50-poly(S-*r*-canola) polymer is very similar the that found on the polymer that had been exposed to a $AuCl_3$ solution. An increase of the fraction of Au-metal can be seen with the decreasing probing depth. It is also obvious that the Au tends to aggregate on the outmost layer (Figure 2.25).
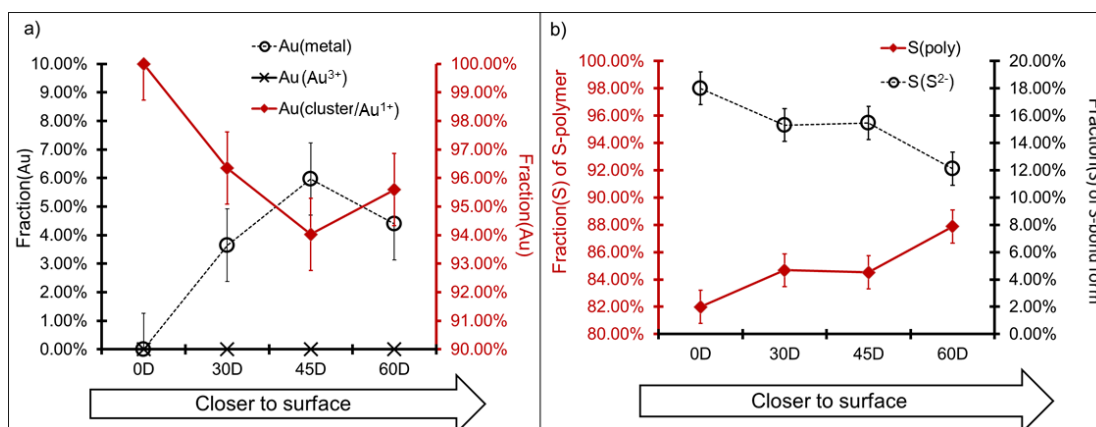
Figure 2.25: a) The fraction of Au in the sample and **b)** the fraction of S in the sample.

Therefore, the conclusions that can be drawn are that both a physical and chemical adsorption of gold to the polymer was observed resulting in gold metal, Au^{3+} and gold cluster/Au^{1+} forms. Further, gold in a cluster or metal form tends to aggregate on the outmost surface while gold bonded to sulfur appears further within the polymer.

Gold ore simulation

Given the success for oxidants TCCA plus NaBr as well as $Ca(OCl)_2$ plus HCl, the next step was to simulate a more realistic mining scenario. Shale rock collected from the university grounds was crushed using mortar and pestle, a similar procedure to that used to crush ore in ASGM. Crushed rock particles with sizes between 20-38 µm were isolated using a series of sieves to reflect a particle size commonly used in AGSM. The 50-poly(S-*r*-canola) polymer's ability to recover the gold in the presence of the shale rock was then tested. To do that samples of crushed shale, gold sheets (20 mg) and the oxidants were prepared for both the TCCA (108 mg) plus NaBr (144 mg) and $Ca(OCl)_2$ (100 mg) plus HCl (0.138 mL) oxidants, each repeated in triplicate (15 mL volume). After 6 days the gold in the TCCA plus NaBr solutions had completely dissolved. However, the gold in the $Ca(OCl)_2$ and solutions had not dissolved. A possible reason for that could be that carbonates are present in the shale rock since they are commonly found in sedimentary rock such as shale.[87] Upon analysing the shale using X-ray powder diffraction it was confirmed that magnesium calcium carbonate was in the shale rock. When carbonates come into contact with acids, they neutralise the acid and form soluble

salts and CO_2. If the acid in the $Ca(OCl)_2$ and HCl oxidising solution is neutralised, then the solution will not be acidic enough to produce the HOCl and Cl_2 needed to oxidise the gold. Therefore, the pH of the $Ca(OCl)_2$ plus HCl solutions was tested and found to be at a pH of 5.25 which is much higher than in the oxidant solution without the rock which had a pH of 2.0 after gold oxidation (Figure 2.10). In order to decease the pH, 0.138 mL of HCl and an additional 100 mg of $Ca(OCl)_2$ were added. After that, the gold in these solutions was oxidised after 6 days. This highlights a problem with using acids. Acids will react with carbonates essentially quenching the reaction. However, this is not an issue then using the TCCA plus NaBr oxidation method.

Meanwhile, 1 g of 50-poly(S-*r*-canola) polymer was added to the TCCA plus NaBr solutions and rotated for 6 days. The gold concentration (determined by ICP-MS) before the polymer addition was 1444 ± 25 ppm, 734 ± 10 ppm after 24 hours and 260 ± 12 ppm after 6 days indicating that 82% of gold had been removed. The polymer from the TCCA plus NaBr solutions was then removed from solution by filtration and incinerated. It was found that the average yield for all the experiments was above 350% which meant that something other than gold was recovered during the incineration, likely crushed shale that was not removed during the filtration. This was also visible by looking at the product of incineration which was a red solid. SEM/EDX analysis confirmed that O, Fe, Na, Mg, Al, Si, S, and Ca were in the incineration product besides Au and Ag (coating) (Figure 2.26)
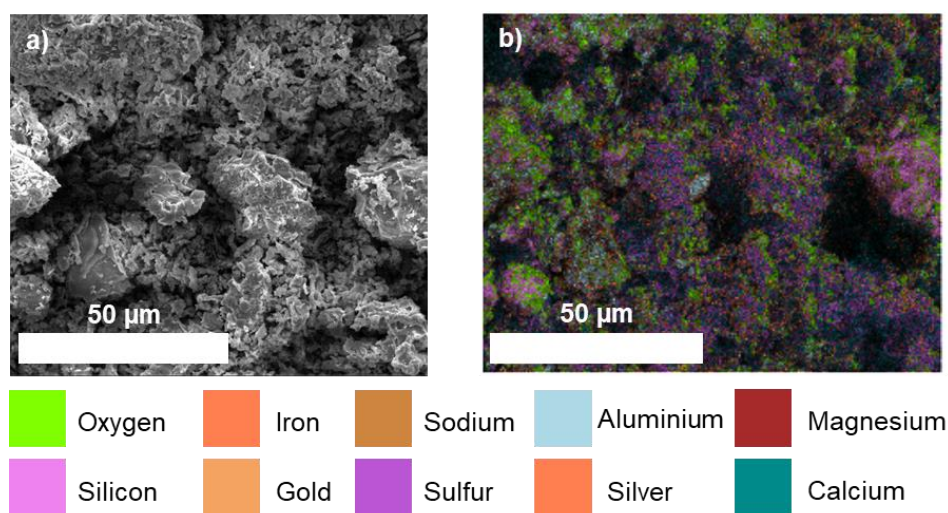
Figure 2.26: a) SEM micrograph and **b)** elemental map of representative incineration product of simulated ore oxidised with TACCA plus NaBr.

The presence of Ca and Mg was not unusual since XRD analysis confirmed that calcium magnesium carbonate is present in the crushed shale. The contaminations can be contributed to mixing the 50-poly(S-*r*-canola) polymer freely in the solutions. The EDX map showed that Al is in the sample, however, further investigation revealed that it was Br, as the accelerating voltage of the SEM was increased more Br lines could be seen. This experiment showed that it is difficult to remove all the impurities if the polymer was added directly to the solution containing the oxidant and crushed shale. Therefore a different strategy was be used to recover the gold from the simulated ore experiment with $Ca(OCl)_2$ plus HCl as oxidant.

After the gold had dissolved in the remaining $Ca(OCl)_2$ and HCl solutions, one sample was filtered and adjusted to a volume of 50 mL prior to adding 1 g of 50-poly(S-*r*-canola) polymer sewn into a bag and rotated for 6 days. After 24 hours the gold concentration was reduced from 298 ppm to under the detection limit of 2 ppm, a decrease of over 99%. SEM/EDX analysis of that sample showed primarily gold after incineration and only small amounts of Na. However, since the filtration of such finely ground rock is quite challenging, the other two samples oxidised with $Ca(OCl)_2$ and HCl were not filtered but adjusted to a volume of 50 mL and a 1 g 50-poly(S-*r*-canola) polymer bag was added and left sitting on top of the settled crushed shale. After 24 hours, one sample showed reduction of gold concentration from 301 ppm to 107 ppm (65% reduction) whereas the other sample only showed a reduction from 320 ppm to 265 ppm (13% reduction). To remove more gold from the solutions, the samples were left for an additional 5 days. After that the gold concentration had been reduced to 4 ppm in one solution, a reduction of 99%. However, the last solution still had a gold concentration of 100 ppm, having only removed 62% of gold. Following that the polymers were incinerated, and the product analysed using SEM and EDX. Although the samples were cleaner than the ones with the polymer was added loosely, without being in a cotton bag, some contamination from sulfur and calcium were still present.

Overall, regarding the simulated ore experiments the following conclusions could be drawn. While both oxidation pathways using TCCA plus NaBr or $Ca(OCl)_2$ plus HCl oxidise gold, the TCCA plus NaBr method is easier to perform. This is because the carbonates in the rock reacted with the hydrochloric acid and neutralised it, reducing the oxidation strength. Further, the percentage of gold removed from the solutions had wide variations. The reason for these variations could be that the 50-poly(S-*r*-canola) polymer is not a homogeneous product. As the polymer is ground up, washed and dried, the particles have different sizes hence the polymer used in one solution will have more or less particles than in another solution, resulting in different surface areas of polymer in different solutions. Additionally, it became clear that the polymer is able to remove gold

the fastest in a filtered solution and under rotation. Filtering the solutions before adding the polymer also greatly increased to purity of the recovered gold.

Small scale gold ore oxidation

The leaching methods were also tested on a gold ore sample form the Aurora Australis mine in Kalgoorlie WA. The crushed ore (750 mg at 20-38 µm) was added to 15 mL TCCA (108 mg) plus NaBr (144 mg) solutions and three $Ca(OCl)_2$ (100 mg) plus HCl (0.183 mL) solutions. After 8 days, the volume was adjusted to 50 mL and the gold concentration was determined to be 35.6 ± 0.7 ppm. After that, 1 g of 50-poly(S-r-canola) polymer sewn into cotton bags were added to each sample. The samples were left undisturbed on the bench for 13 days. Samples for ICP-MS were taken after 0, 1, 7 and 13 days and analysed for old concentration. The gold uptake was initially faster in the $Ca(OCl)_2$ plus HCl solutions, however after 13 days the gold uptake was similar with 98.6% removed in the TCCA plus NaBr solutions and 99.9% of gold removed in the $Ca(OCl)_2$ plus HCl solutions (Figure 2.27).
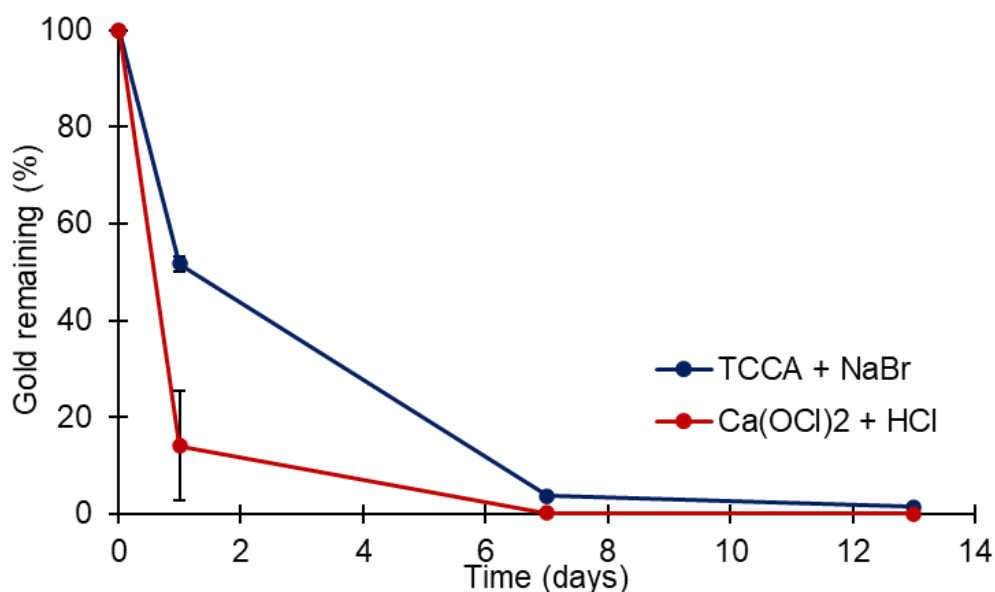
Figure 2.27: Gold removed using the 50-poly(S-r-canola) polymer from TCCA plus NaBr solutions and $Ca(OCl)_2$ plus HCl solutions over a time of 13 days from oxidised gold ore.

Since the total gold on the 50-poly(S-r-canola) polymer would only be around 2 mg, the polymer was not incinerated since such a small mass of gold would be very difficult to recover. However, so far it has been shown that by using TCCA plus NaBr in an oxidising solution, gold can be successfully oxidised from gold ore and that over 98%

of gold can be recovered using the polysulfide as sorbent. Next, steps were taken to optimise the oxidation conditions.

Oxidation optimisation

Oxidant concentration

The first variable to be optimised was the oxidant concentration. This was done in order to assess whether the rate of gold oxidation is dependent on the oxidant concentration. The hypothesis was that a higher oxidant concentration would result in faster gold oxidation. At the same time, the goal was to minimize the cost of reagents, so understanding the effect of oxidant concentration was important.

Accordingly, 40 mL solutions with different oxidant (TCCA) concentrations were made. To each oxidant concentration a molar equivalent of NaBr according to the chloride concentration was added. To perform these experiments oxidant (TCCA) concentrations of 16.6 mM, 83.5 mM and 166.7 mM were chosen (Table 2.1).

Table 2.1: Concentrations of oxidant (TCCA) and concentration of chloride and added bromide (from NaBr) as well as their molar mount used to determine the effect of the oxidant concentration on the gold oxidation rate in a solution with the volume of 40 mL.

TCCA conc.	16.6 mM	83.5 mM	166 mM
TCCA mass	0.155 g	0.775 g	1.55 g
Chloride conc.	0.05 mM	0.25 mM	0.5 mM
Chloride amount	2.00×10^{-3} moles	10.0×10^{-3} moles	20.0×10^{-3} moles
NaBr mass	0.206 g	1.02 g	2.06 g
Bromide conc.	0.05 mM	0.25 mM	0.5 mM
Bromide amount	2.00×10^{-3} moles	9.91×10^{-3} moles	20.0×10^{-3} moles
Gold Mass	5 mg	5 mg	5 mg
Gold amount	2.53×10^{-5} moles	2.53×10^{-5} moles	2.53×10^{-5} moles

All solutions were prepared in deionised water and in triplicate to a volume of 40 mL. To each solution, 5 mg of gold sheet was added, and the solutions were left unagitated until the gold had dissolved. That mass of gold resulted in a calculated gold

74

concentration of 0.65 mM. As the NaBr was added it could be observed that a higher oxidant concentration resulted in a more orange colored solution. After an average of 24 hours all the gold had been oxidised in the 166 mM TCCA solutions, however some TCCA was still not dissolved. The gold in two of the 83.5 mM TCCA concentration solutions had dissolved at a similar time as the 166 mM concentrations. However, the gold in one of the 83.5 mM TCCA concentrations took another 23 hours to dissolve. By far the slowest gold oxidation was observed in the 16.6 mM TCCA solution. Figure 2.28 shows this data displayed in the average mg of gold oxidised per hour (calculated by using the time it took to oxidise the gold and the mass of gold used). It can be clearly seen that the fastest oxidation was observed in the 166 mM TCCA concentration with around 0.2 mg of gold oxidised per hour which is twice as fast as in the 16.6 mM TCCA concentration solutions. However, two of the gold samples in the 83.5 mM solutions were oxidised as similar rates than those in the 166 mM solution. The molar amounts of available chloride for each concentration were calculated and found to be 2 mmol in the 16.6 mM TCCA solution, 10 mmol in the 83.5 mM TCCA solution and 20 mmol in the 166 mM TCCA solutions. Comparing that to the molar amount of gold in solution (0.63 mM), it can be said that the oxidation is most effective when at least 16 molar equivalents of oxidant are used.
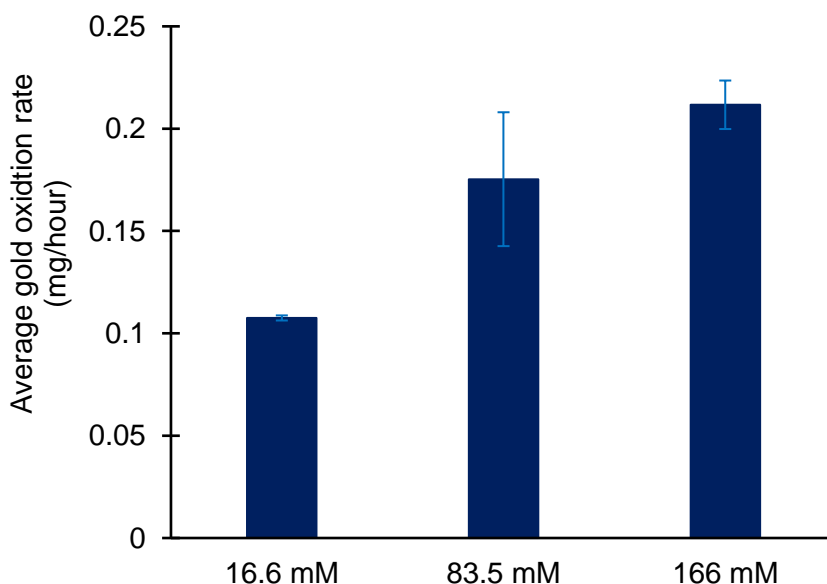
Figure 2.28: Average gold oxidation rate in mg/hour in solutions with different TCCA concentrations. Complete contents of solutions can be seen in Table 2.1.

Only one gold sample in the 83.5 mM TCCA solutions took longer which is reflected in the large error of the 83.5 mM TCCA sample. Further, there seems to be no significant difference between the 83.5 mM and 166 mM TCCA solution to warrant

doubling the oxidant concentration since that would also double to cost of oxidant. However, the rate of gold oxidation can also be influenced by the composition of the ore or e-waste from which the gold is to be extracted. Therefore, this experiment established that an increased oxidant concentration would increase the rate of gold oxidation, but the concentration of oxidant used must be determined at a case-to-case level by taking the nature of the ore or e-waste into consideration. Further, this experiment showed that there was no significant difference in gold oxidation between the 83.5 mM and 166 mM TCCA concentrations, indication that after a certain oxidant concentration is reached, adding more oxidant will not speed of the gold oxidation. The reason for that is that at a 83.5 mM TCCA solutions contains 19.4 g of TCCA per liter which means that the solution is saturated with TCCA (solubility of TCCA at 20 °C is 12 g/L[72]). Running the oxidation in a saturated solution can be of advantage in a ASGM or informal e-waste recycling scenarios since it would be easy to tell when the solution is ready to be used based on visibly undissolved TCCA. This could simplify measuring operations for this leaching method, as it simply can be run with TCCA at saturation.

Oxidation temperature

The next variable to be optimised was the temperature of the reaction. For these experiments various reaction temperatures and oxidant concentrations were used. As such, temperatures 45 °C and 80 °C were chosen. No temperatures over that were tested since heating the samples further would need more energy and therefore increase the cost of the oxidation step. Also, many ASGM miners might not have access to electricity. Further, 45 °C were chosen since many ASGM activities take place in hot climates. Therefore, 45 °C would not be unreasonable if the gold oxidation would take place in a dark container in the sun, which could significantly heat the solution. The TCCA and NaBr concentrations were the same as mentioned in Table 2.1. For each temperature, the experiment was performed in triplicates for each oxidant concentration and 5.0 mg of gold sheet was used for each sample. For this experiment the tubes were closed to see if any pressure build up would occur. After 20 minutes reaction time the solutions kept at 80 °C had a more vibrant orange color than the solutions at 45 °C. To determine if any gas had built up, the lids of the tubes were carefully loosened after 30 minutes reaction time. All the solutions at 80 °C build up a considerable amount of pressure and a dark orange gas (likely bromine gas) was observed exiting the reaction tube upon opening the lid (at no time did the pressure appear high enough to burst the tube). In contrast, hardly any pressure build up was observed in the solutions kept at 45 °C and only a small amount of gas was observed. In terms of oxidation rate of the added

gold, it was observed that higher temperatures resulted in faster gold oxidation (Figure 2.29). The average rate of gold oxidation was calculated from the time taken to dissolve the 5 mg of gold in each solution. Heating the samples to 45 °C resulted in a gold oxidation of around 1 mg per hour. At 80 °C substantially more gold is oxidised per hour. While not much variation of oxidation rate was observed between the different oxidant concentrations at 45 °C, the results at 80 °C show large variations, likely because oxidant is lost through volatilisation in the low oxidant concentration sample (16.6 mM).
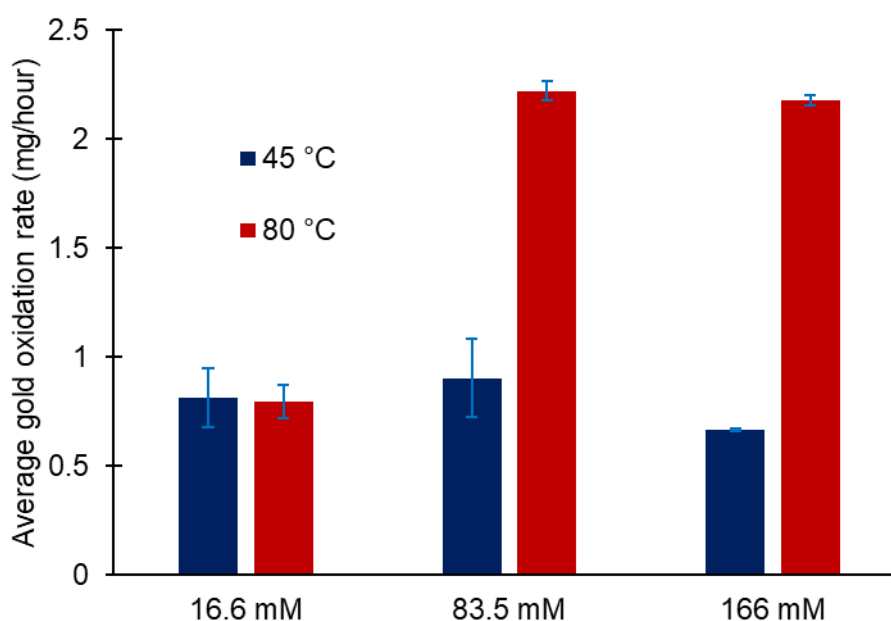
Figure 2.29: Average gold oxidation rate in mg/hour in solutions with different TCCA concentrations and temperatures. Complete contents of solutions can be seen in Table 2.1.

The gold in the 40 mL, 16.6 mM TCCA concentration sample at 80 °C was oxidised at a rate of 0.8 mg/hour, very similar to that rate at 45 °C. However, at both higher TCCA concentrations of 83.5 mM and 166 mM (both 40 mL) the rate of gold oxidation is 2.2 mg/hour. This result showed that the reaction temperature has an impact on the gold oxidation rate and that there is no noticeable difference in the oxidation rate at the 83.5 mM and 166 mM TCCA concentrations. Interestingly, this was also observed previously, in the oxidation concentration optimisation section. Further, increasing the temperature also increased the solubility of TCCA since less undissolved TCCA was seen in the reactions run at higher temperature as those run at room temperatures. This means that at higher temperatures more active chloride is available. However, oxidation at 80 °C was concerning since pressure build up and gas release was observed with can

prove dangerous for AGSM miners inexperienced with this method. Further, heating to higher temperatures would also increase costs. However, since the goal was to also implement this method for gold recovery from e-waste at a commercial scale, heating could and should be considered in such cases.

Next, the effect sonication has on the rate of gold oxidation was examined. This was done since sonication in a commercial setting is viable and can potentially speed up the gold oxidation process. This was considered of relevance to the processing of ore concentrates or e-waste in a formal, regulated setting.

Effect of sonication on oxidation rate

Three identical 45 mL oxidant solutions (0.05 M TCCA and 0.15 M NaBr) were prepared in plastic tubes into which 10 mg of gold were added each. These concentrations were chosen according to some more optimisation done under a Honours project at the Chalker laboratory.[88] The samples were then heated to 50 °C and sonicated using a VWR USC500TH sonicator (45 kHz, 100W) until the gold was oxidised. After 8 hours all the gold had been oxidised. During the oxidation samples for ICP-MS analysis were collected. As can be seen in Figure 2.30, after 4 hours most of the gold has been oxidised at an average rate of 2.3 mg/hour (The calculation was based on the time it took for the gold to be fully oxidised and the mass of gold used). As can be seen a sharp increase in gold concentration occurred between 2 and 4 hours which indicated that the gold oxidation rate was not constant, rendering a more detailed kinetic analysis difficult. A reason for that could be that the surface area of the gold increases as the gold is oxidised, this would result in a faster rate of gold oxidation. This rate matched the rate of gold oxidation when unagitated at 80 °C. This was an excellent result that showed that sonication at lower temperatures can increase to gold oxidation to levels previously only seen when the oxidation was heated to 80 °C.
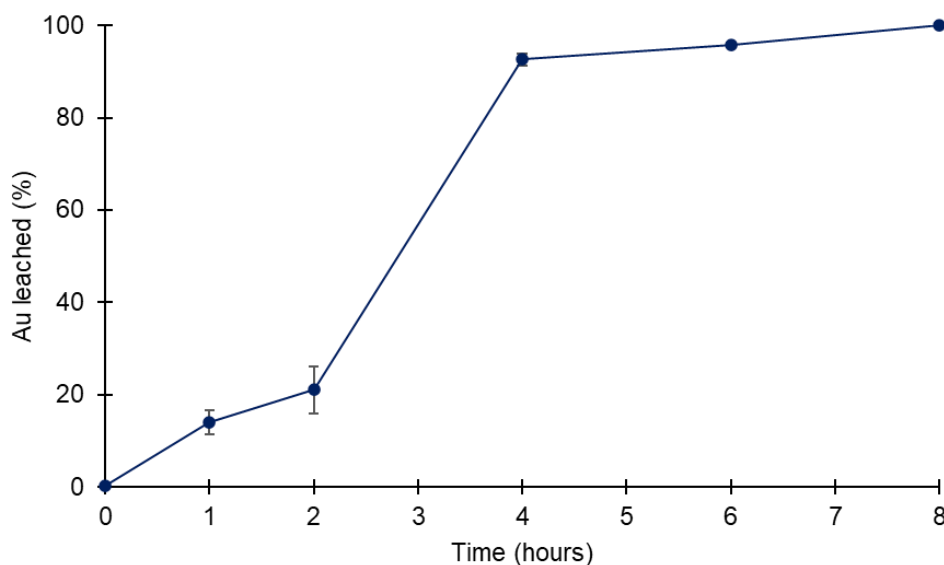
Figure 2.30: Percentage of gold (10 mg) leached while sample was heated to 50 °C and sonicated.

Scrubbing off gases generated during polysulfide incineration

Since the primary recovery method of the gold from the 50-poly(S-*r*-canola) polymer was the incineration of the polymer, noxious gases like SO_2 are released. In an industrial setting, scrubbing techniques are available to mitigate this risk. For instance flu gases can be converted to sulfate,[89, 90] sulfuric acid[91] or sulfur.[92] However, in ASGM settings it is likely that this technology is not available. Hence, it was important to investigate possible ways to convert the off gases to something less harmful albeit being simple enough to be implemented in an ASGM setting. Since TCCA is an oxidising agent, it was reasoned that TCCA might be able to convert SO_2 to sulfates. To test this, a retort was built through which the gases from burning the polymer can be bubbled into a solution of water and TCCA. This would allow for TCCA to have a dual purpose: part of the gold leaching solutions as well as part of a simple wet scrubber during the gold recovery by polymer incineration. Metal pipes were used to construct this retort. As can be seen in Figure 2.31, the compartment holding polymer was placed above a Bunsen burner. The end of the pipe was completely submerged in the TCCA and water mixture. As the Bunsen burner heated up the polymer compartment, yellow off gases came out of the submerged end of the pipe and bubbled through the solution. The mass of polymer and TCCA was chosen so that the molar ratio of TCCA to sulfur was 5:1 to allow for an excess of oxidant. After no more bubbles were observed the polymer compartment was opened and showed small amounts of carbonised material left over.
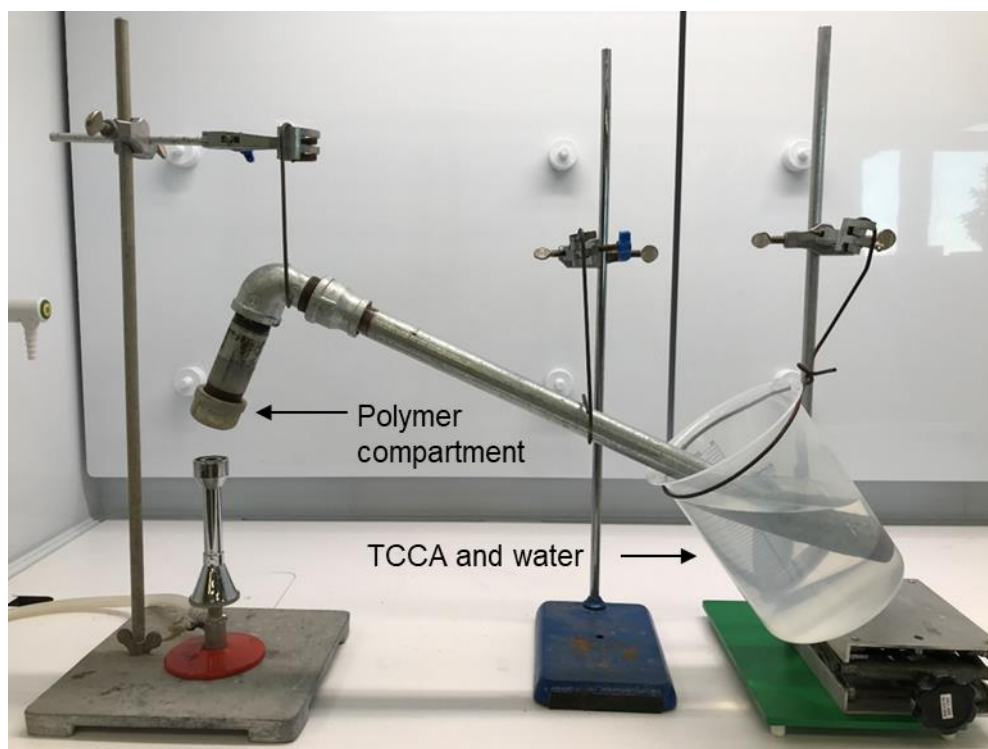
Figure 2.31: Set up to test gas conversion by water and TCCA mixture. 50-poly(S-*r*-canola) polymer was incinerated by heating the polymer compartment with a Bunsen burner and the off gasses were passed through the solution.

The hypothesis was that some of the off gases are converted to sulfates by the TCCA and water mixture. To test this the solution was analysed using ion chromatography (IC) after the incineration. Analysis of the solution showed chloride (from TCCA) and sulfate which supported the hypothesis that conversion of off gases to sulfate is possible (Figure 2.32).
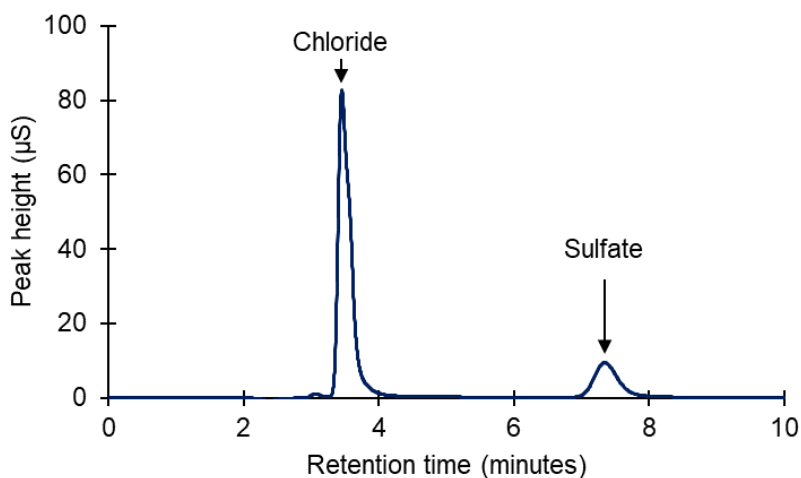
Figure 2.32: Ion chromatogram of the TCCA and water solution after the 50-poly(S-*r*-canola) polymer incineration gas was passed through.

A fresh TCCA and water solution was prepared for this experiment. However, to reduce the TCCA usage, the possibility of using old, gold deficient leach solution can also be considered. This way the same solution can be used in two stages, in the oxidation stage after that the convert off gases from the polymer incineration. Further, the results were only examined qualitatively as a proof of concept. Nevertheless, future work should include quantitative analysis to determine how much of the off gases are converted to sulfates.

Battery sand oxidation and recovery

For this experiment tailings were acquired from Menzies (Western Australia) at a decommissioned stamp mill. Those tailings had been previously processed and were called battery sand. Part of that processing included running the crushed ore over a sluice containing mercury. Therefore, the tailings were expected to contain mercury. The aim was to test the leaching method as a remediation process to leach gold but also to leach and recover mercury in the future. The ore was processed and analysed by a commercial metallurgy laboratory. Firstly, the commercial service pulverized the sample using a ring mill so that 85 % of the sample particles are below 75 µm (P85 < 75µm). To determine the gold concentration fire assay was used. This was done by firstly adding a flux (sodium carbonate, borax, silica, lead oxide and carbon) to the sample. Next, the flux and sample mix were melted and the lead and the precious metals are collected in the slag in the form of a lead button. A furnace is than used to remove the lead to produce a metal prill. Using nitric acid, the silver is then removed from the prill leaving behind gold and platinum group metals. Following that, aqua regia is used to dissolve the remaining precious metals. Lastly, the dissolved metal solution is analysed using ICP-OES. For elements besides gold or platinum group metals a four-acid digest (hydrochloric acid, nitric acid, perchloric acid and hydrofluoric acid) or sodium peroxide fusion was used followed by ICP-OES analysis of the solution. The measurement errors of the commercial service are 5% or lower. Table 2.2 below shows the result of the assay. Since previous experiments have shown that the filtration of finely crushed ore on a laboratory scale is very challenging, the ore for this experiment was not crushed but used as received without further milling.

Table 2.2: Assay (performed by commercial service) of battery sands showing the concentration of various elements found in the sand.

Ag (ppm)	Al (ppm)	Au (ppm)	Ba (%)	Be (ppm)	Bi (ppm)
<2	6	1.72	0.05	<5	<10
Cr (ppm)	Cu (ppm)	Fe (%)	Hg (ppm)	K (%)	Li (ppm)
160	220	9.22	8.6	1.03	45
Pb (ppm)	S (%)	Si (%)	Sr (ppm)	Ti (%)	V (ppm)
180	1.44	26.8	108	0.69	232
Mg (%)	Mn (%)	C org (%)	Ca (%)	Cd (ppm)	Co (ppm)
2.07	0.12	0.09	2.89	5	50
Y (ppm)	Zn (ppm)	Mo (ppm)	Na (%)	Ni (ppm)	P (ppm)
15	404	<5	1.52	60	700

As can be seen (Table 2.2), the gold concentration in the battery sands is 1.72 ppm. Further, the mercury concentration is 8.9 ppm. Also, other elements that can potentially be oxidised during the oxidation process such as iron and copper are also present in high concentrations. Through a series of experiments in collaboration with an industry partner some test reactions were run facilitated by the industry partner and a collaborator based in the work presented in this thesis. This work showed that higher oxidant concentrations (0.25 M TCCA, 0.45 M NaBr) were needed in order to oxidise all the gold from these tailings since high concentrations of other metals were also present. While that concentration was a lot higher than previously used, this concentration was maintained in an effort to leach out as much as possible with the plan to optimise the conditions for these tailings at a later stage. Also, since TCCA was at saturation, the excess TCCA served as a reservoir in case all the dissolved TCCA was consumed. At this stage the goal was to leach as much as possible form the tailings by using a concentrated leach solution. For this reaction 200 g of ore and 2L of water was used.

For all these lab scale experiments the following set up was used (Figure 2.33). An overhead stirrer was place above a bucket. The size of the bucked varied between 5 and 20 L. To stir the solution a stainless-steel impeller was attached to the stirring unit (Figure 2.33).

Figure 2.33: General set up for ore oxidation experiment and gold recovery experiment using the polysulfide. (20 L bucket is shown here but 5 L buckets were also used).

Magnetic material can be found in gold ores. While pure gold and many gold alloys are not of magnetic nature, gold alloys with cobalt, nickel and iron are ferromagnetic.[28] Additionally, gold is often found in iron oxide copper gold (IOCG) deposits which can contain magnetite.[93] Since magnetic material present it ore would be oxidised along with the gold, unnecessarily consuming oxidant, the magnetic material was removed first using magnets. This was done by attaching magnets to the impeller and stirring the mixture at 100 RPM for 5 minutes. After that, the magnets were removed, water (2 L) and oxidants (TCCA: 120 g, 0.25 M; NaBr: 93 g, 0.45 M) were added. Following that, the solution was stirred at 250 RPM. Using the gold concentration from the tailings assay and the volume of solution the estimated total gold concentration is 0.172 ppm. After 24 hours the gold concentration had increased to 0.2 ppm which was higher than expected. However, of the over 20 kg of tailings that were received only 200 g were sent to be tested for gold and other mineral content (performed by commercial service as has been previously described). Therefore, the tailings might not be homogenous, and the gold concentration can vary. As the stirring was discontinued and

the tailings had settled, a layer of fine white material was on top of the ore, likely unreacted TCCA or cyanuric acid (a byproduct of the reaction as seen in Scheme 2.4). Next, the sample had to be filtered. This was done by vacuum filtration. This step proved to be very challenging since the TCCA and cyanuric acid layer had the consistency of a very fine powder. Nevertheless, the sample was filtered and washed with deionised water to wash off as much gold as possible. After the filtration only 65% (0.13 ppm) of the expected gold was seen (as determined by ICP-OES). A possible reason was that the gold was lost during the filtration process since it was very slow and it is possible that not enough water was used to wash the tailings, hence some gold was still left on the discarded ore. The next step was the use the polysulfide to remove the gold from the solution which had a volume of 3.35 L after filtering and washing the tailings. Since the solution contained only 0.2 mg of gold and excess of 50-poly(S-*r*-canola) polymer (2 g) was used. After 24 hours no reduction in the gold concentration was observed. The aim was to remove the gold within 1-2 days however this was not the case. Therefore, this experiment was stopped and was revisited after 15 days. Out of interest, the solution was then again tested for gold, and it was seen that the gold concentration had been reduced by only 40%. It is possible that not enough polymer (2 g) was used taking into account the volume of the solution (3.25 L) and the possible high concentration of other elements. Further, the concentration of gold might have been too low for the polymer to remove the gold efficiently.

However, this experiment has shown that the oxidation method is able to leach gold from these tailings. Additionally, this experiment has shown that filtration of the leach solution is difficult and requires further research into engineering solutions if this method is used at a larger scale. Also, the mass of polymer used needs be adjusted to an amount capable to capture sufficient gold from a tailings leach solution. Further research must be conducted to investigate if the same leach solution could be used multiple times to build up the gold concentration to a level from which the polymer is able to remove the gold.

Gold removal from 5 ppm gold solution in oxidant matrix

During the previous section, the 50-poly(S-*r*-canola) polymer was added to a tailings leach solution with a gold concentration of 0.13 ppm and only removed 40 % after 15 days. Experiments during the oxidation development have shown the polymer to remove 93.3 % of gold from a TCCA solution. However, only 10 mg of gold were in that solution. Therefore, the next step was to assess if the polymer is able to remove gold from solutions with such small concentrations of gold.

This was done by oxidising 50 mg of pure gold using TCCA and NaBr and diluting that solution to a gold concentration of 5 ppm. This concentration was relevant to formal mining scenarios since cyanide leach solutions can have gold concentrations between 2-15 ppm.[28] Since 30 mL of 5 ppm gold solution was used, the mass of gold in the solution was 0.15 mg which was less than the 0.2 mg of gold in the battery sand leach. To that solution (30 mL), TCCA (0.582 g, 0.25 M) and NaBr (1.390 mg, 0.45 M) were added to increase their concentrations to what was used on the battery sand leach to see if the 50-poly(S-*r*-canola) polymer can remove gold from a high oxidant solution. After that, 1 g of polymer was added and rotated using and end over end mixer for 6 days. ICP-OES analysis showed gold removal of 99.9%. This was an encouraging result that showed that the polymer is able to remove a very small amount of gold from solution in the presence of high concentrations of oxidant.

It is possible that the problem with the battery sand leach was the liquid to polymer ratio. In the case of the battery sand leach 2 g of polymer have been used for 3.25 L of liquid which is 1.625 L of liquid per gram of polymer. In this experiment however 1 g of polymer was used for 30 mL of liquid which is 0.03 L per gram of polymer. Also, other elements were present in the leach solution that can potentially interfere with the polymer. These issues could be overcome by concentrating the gold concentration in solution, for example by using the same solution to oxidise multiple batches of tailings. Further, a higher liquid to polymer ratio might result in better uptake, or the solution can be circulated through a polymer filter. Additionally, the solution could be pre-treated in order the remove some of the interfering elements. This could be done by chemical precipitation or electrochemically. These issues are all relevant areas of study in future work.

Alternative gold recovery pathways

Given that the 50-poly(S-*r*-canola) polymer is most effective at higher gold concentrations, it was desirable to explore other potential methods of gold recovery from the TCCA/NaBr leach solution. This was investigated by the use of reducing agents. As possible candidates, ascorbic acid (Vitamin C), oxalic acid, sodium bisulfite, sodium metabisulfite and hydrogen gas were considered (Figure 2.34).
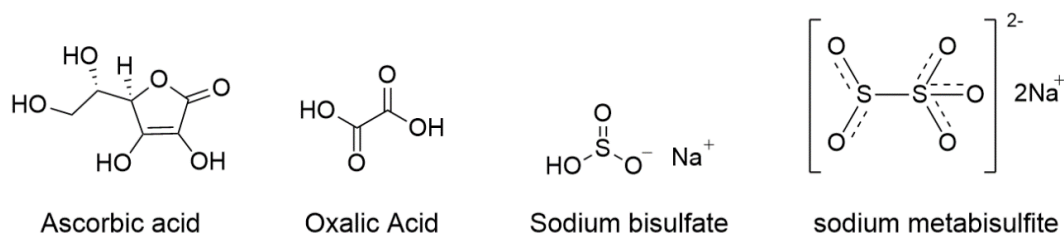
Figure 2.34: Chemical structures of ascorbic acid, oxalic acid, sodium bisulfate and sodium metabisulfite.

A 1 M or saturated solution was prepared from each reducing agent to ensure an excess of reducing agent compared to the gold concentration (solutions of ascorbic acid, sodium bisulfate and sodium metabisulfite had a concentration of 1 M whereas the oxalic acid solution reached saturation at a concentration of 0.7 M). After that, 50 mL from each solution was added to individual 50 mL aliquots of a 1770 ppm gold solution (gold oxidised with TCCA plus NaBr). The mass of gold in the gold solution was 88.5 mg so that if gold was reduced and was to precipitate out of solution it could be clearly seen and isolated by filtration. As the ascorbic acid solution was added to the gold solution, the color of the solution turned from a darker orange to gray. After a couple of minutes, a black precipitate formed (Figure 2.35). No change was observed as the oxalic acid solution was added to the gold solution (Figure 2.35). As the sodium bisulfite solution was added to the gold solution the solution turned from orange into a cloudy white color, but no dark precipitation was observed (Figure 2.35). The addition of sodium metabisulfite resulted in the same reaction as was observed with sodium bisulfate (Figure 2.35).
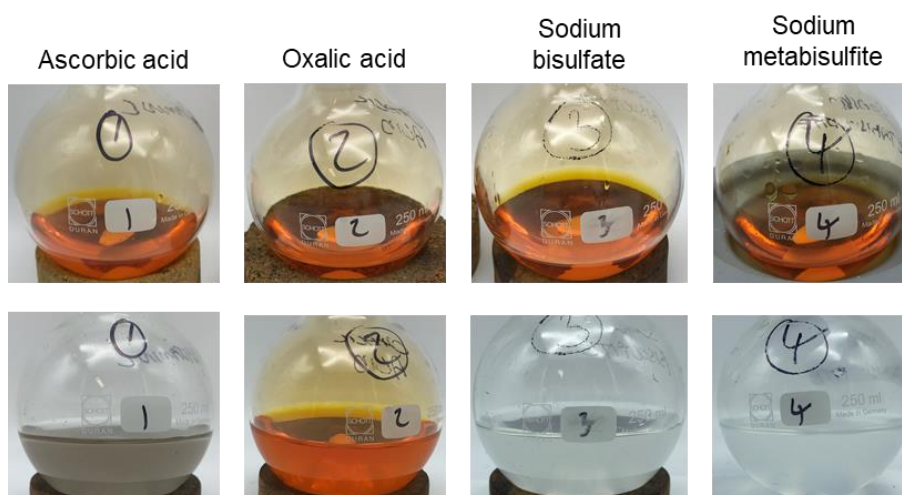
Figure 2.35: Top: 1770 ppm gold solution before reducing solution was added. Bottom: Gold solution 1 hour after solution containing reducing agent was added.

Lastly, hydrogen gas was directly bubbled through 50 mL of gold solution. After 2 hours the solution was noticeably darker, and a black precipitate formed. The most promising leads were ascorbic acid and hydrogen since a dark material precipitated from both solutions. Therefore, the precipitate of both solutions was recovered and analysed using SEM and EDX. This analysis confirmed that the dark precipitate was indeed gold (Figure 2.36). Interestingly, when the gold solution was treated with ascorbic acid the precipitated gold metal presented itself in small spheres approximately 2.5 µm in diameter (Figure 2.36). Hydrogen gas treatment of the gold solution resulted in a differently shaped material (Figure 2.36).
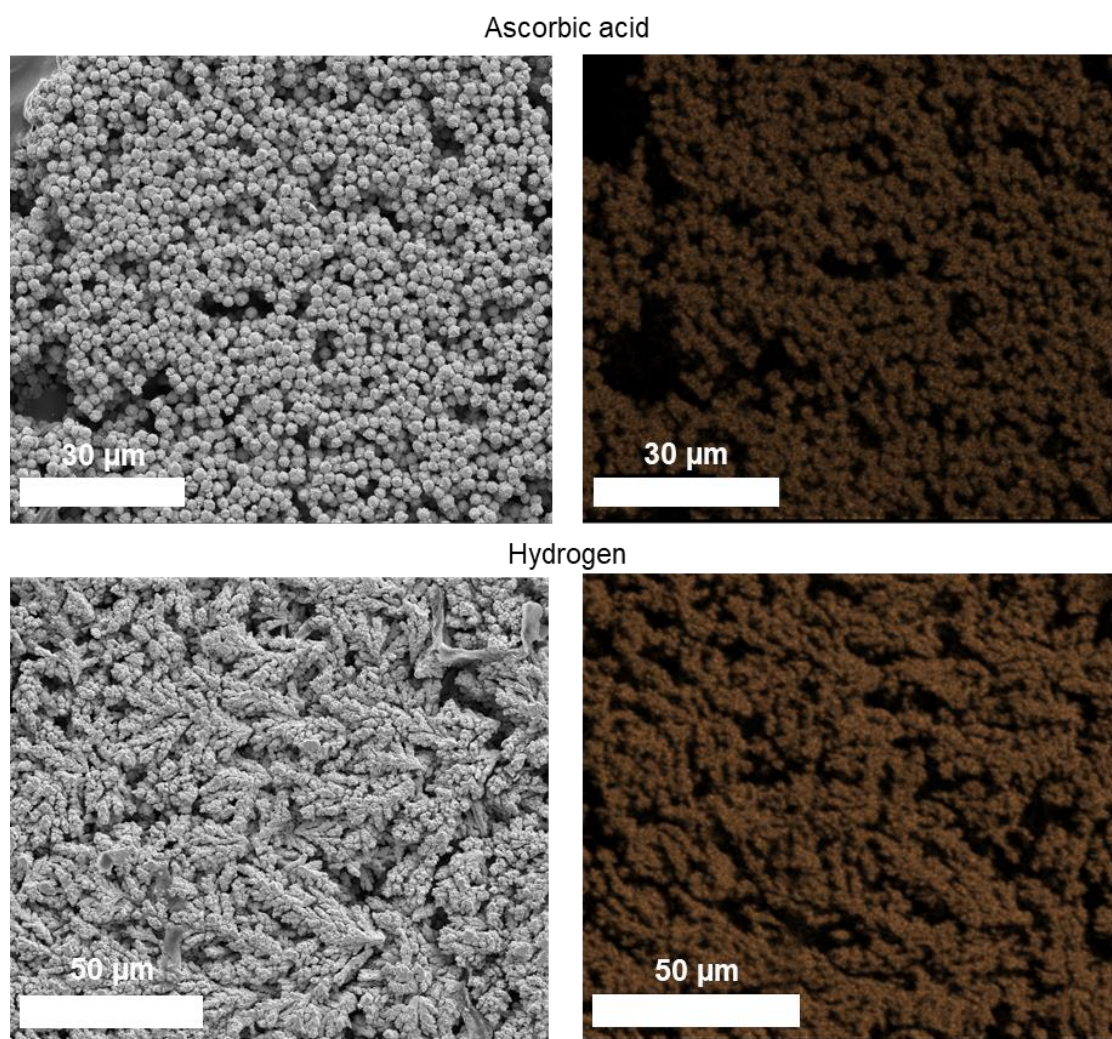
Figure 2.36: SEM micrographs (left) and gold elemental map (right) of the precipitates of ascorbic acid or hydrogen treatment of concentrated gold solutions.

This experiment showed that ascorbic acid as well as hydrogen gas can be used to reduce and precipitate gold from a TCCA plus NaBr leach solution. On the other hand, oxalic acid, sodium bisulfate or sodium metabisulfite were not able to reduce the gold in solution. Recovery of gold from the leach solutions using hydrogen gas or ascorbic acid

might be a complimentary final step to the recovery using the 50-poly(S-*r*-canola) polymer. Using hydrogen gas as reducing agent took longer than ascorbic acid but does not involve the handling of another solid reagent. Further, if too much ascorbic acid were used, the reducing agent could lead to a solid material co-isolated with the gold. No such issue was observed with hydrogen gas as the reducing agent. However, safety concerns have to be raised regarding the use of hydrogen given that hydrogen gas is highly flammable. Gold reduction using ascorbic acid was faster than using hydrogen gas and is less hazardous. As can be seen in Figure 2.36, reduction of gold with hydrogen gas results in a different gold morphology as reduction with ascorbic acid. Nevertheless, in both cases the reduced gold could be easily isolated using simple vacuum filtration. That renders reduction with ascorbic acid or hydrogen gas into an easy pathway to reduce and recover gold from solution. However, in this experiment the gold solution was obtained from pure gold without any other metals dissolved in it. Therefore, further studies have to be conducted to determine of ascorbic acid or hydrogen gas will reduce other metals present and a leach solution from mining tailings or gold ore.

Low grade ore concentrate oxidation and gold recovery

For this experiment gold ore concentrates were acquired from the Linger and Die gold mine in the Mertondale Goldfields in Western Australia. Firstly, the ore was analysed by fire assay and acid digestion (performed by commercial service as previously described) to determine an approximate elemental composition. This was used as a benchmark to anticipate which elements could potentially leach out upon reaction with the TCCA plus NaBr oxidant system (Table 2.3).

Table 2.3: Assay (fire assay for gold content and acid digestion followed by ICP-OES for non-platinum group element content) of low-grade ore concentrate showing the concentration of various elements found in the ore.

Ag (ppm)	Al (%)	Au (ppm)	Ba (%)	Be (ppm)	Bi (ppm)
6	3.86	75.3	0.27	<5	<10
Cr (%)	Cu (ppm)	Fe (%)	Hg (ppm)	K (%)	Li (ppm)
0.11	156	19.3	3.1	0.9	15
Pb (ppm)	S (%)	Si (%)	Sr (ppm)	Ti (%)	V (ppm)
295	0.08	25.5	50	0.93	158
Mg (%)	Mn (%)	C org (%)	Ca (%)	Cd (ppm)	Co (ppm)
0.23	0.62	0.11	0.16	<5	85
Y (ppm)	Zn (ppm)	Mo (ppm)	Na (%)	Ni (ppm)	P (ppm)
155	224	10	2940	60	1200

As can be seen in Table 2.3 the gold concentration is considerable higher (75.3 ppm) then in the previous ore sample (1.72 ppm, Table 2.2).

An honours project focusing on leaching gold from e-waste had discovered that NaBr can be used in much lower concentrations in the TCCA and NaBr leaching method.[88] Therefore, less NaBr was used for this experiment. Also, KBr was tested as a bromide source. The reason for that was that the spent leachate was investigated as fertiliser due to its cyanuric acid content, as discussed previously. Since sodium can be harmful to plants but potassium can be beneficial, KBr was used. Thus, cyanuric acid can serve as a nitrogen source whereas KBr acts as the potassium source. Further, sodium thiosulfate could be used to quench any free chlorine or bromine remaining in solution in order to make to solution more suitable as fertiliser.[94] Additionally, since sulfur itself is a secondary plant nutrient, the quenching with thiosulfate adds sulfur to the prospective fertiliser solution.

The adjusted concentrations were 0.05 M TCCA and 0.015 M NaBr or KBr. A total of 4 kg of ore was added to 2 L of deionised water in a plastic bucket. To conserve oxidant, as much magnetic material as possible was removed. This was done as described previously by placing magnets in plastic bags and tying them to the stirrer bar (Figure 2.37).

Figure 2.37: Magnetic material was removed before oxidants were added.

After removing magnetic material, TCCA (23.2 g, 0.05 M) and NaBr (3.8 g, 0.015M) were added to the solution and the solution was stirred at 200 RPM. This time a lid was placed on the bucket with a hole for the stirrer bar. This was done for two reasons. Firstly, it would contain any leaching solution that may splash during agitation and secondly, it would reduce the amount of evaporation. The estimated gold concentration based on the mass of ore and volume of water used was 151 ppm. After 4 days of oxidation the concentration was 67 ppm. Since KBr was catalytic more TCCA (23.2 g) was added to leach the remaining gold. After another 3 days (total of 7 days) the gold concentration had increased to 157 ppm which was near to the expected value. This discrepancy is likely due to the error of the ICP-OES measurement (error associated with the instrument in typically less than 5%). It was therefore concluded that the majority of gold had been leached. In an effort to conserve water, as little water as possible was used resulting in an ore to water ratio of 2 to 1. This resulted in a thick mud like consistency of the leach solution. Even after letting the solution settle for 5 hours the solution was still a thick mud, and no separation of the ore and water could be seen. Next, the leachate was vacuum filtered using laboratory filter paper. This was a long and tedious process since the remaining TCCA and cyanuric acid had a powder like consistency. Further the ore was rinsed with an additional 1.5 L of deionised water to remove as much gold as possible. After the filtration process the estimated gold concentration was adjusted, taking into account the dilution through the rinse water. The calculated concentration was 86 ppm, and the actual concentration was 80 ppm (as

measured by AAS). This suggest that about 7% of gold were lost during the filtration process. Rinsing the ore with more water might result in less gold lost.

Next, 50-poly(S-*r*-canola) polymer was added to remove the gold. Initially 10 g of polymer was added, and the solution was stirred at 200 RPM. However, after 24 hours only 2.4% of gold has been removed. Consequently, more polymer was added. In total 40 g of polymer was added over 6 days. At that stage 93% of gold was removed as has been determined by ICP-OES analysis. Next, the polymer was recovered by vacuum filtration and incinerated. This resulted in 384 mg of brown powder. However, the expected mass of gold was only 280 mg. To analyse the sample SEM and EDX analysis was performed. This analysis showed gold to be the main element of the incineration product (Figure 2.38).
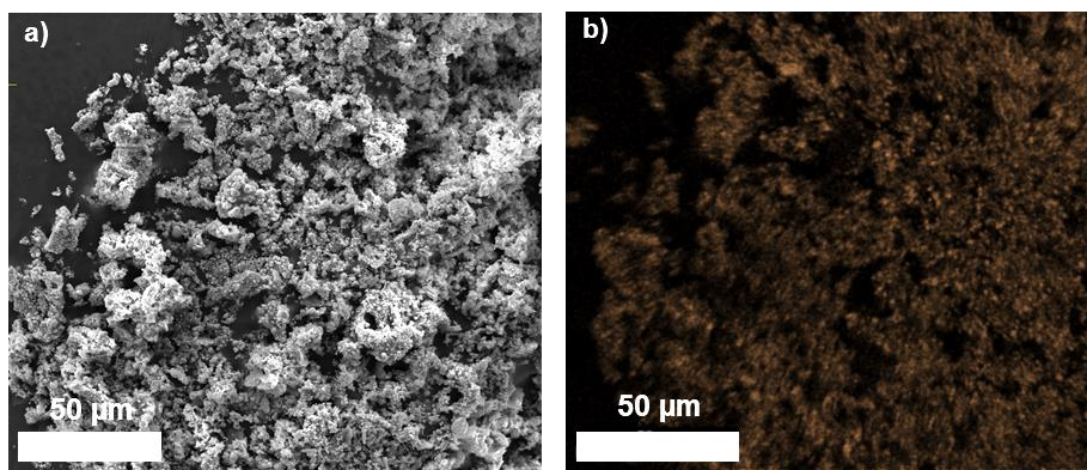
Figure 2.38: a) SEM micrograph of incineration product and **b)** EDX elemental gold map.

However, other elements such as iron, magnesium and silicon could also be observed, confirming that the sample was contaminated. However, these contaminants are commonly removed in standard smelting operations, so the gold recovery method from ore concentrations was a promising result.

This experiment has shown a complete gold recovery process from gold ore concentrate using the TCCA plus KBr leach. The process is very simple (no pH adjustment or any other adjustments needed to be made), a high gold yield was achieved during the leaching step (expected: 151 ppm, actual: 157 ppm) and good gold recovery was observed after the full process (93%). The purity of the recovered gold was relatively high and suitable for refining by smelting. Performing a successful complete gold recovery from gold ore concentrate was a highly promising achievement and provided motivation to further optimise and test this new process. In particular, the separation of solids from the liquid leach solution was very slow. Therefore, future

research will need to focus on suitable filtration technology (such as a belt filter) that is able to filter the leach solution from the tailings on a useful scale and timeframe.

Comparison of ore panning and ore oxidation

The gold oxidation and recovery method presented here will only be viable in ASGM if it is better or comparable to already used methods in the ASGM sector. For this reason, a comparison to traditional gold panning was made, as this method is commonly used in ASGM.[95] Hence an effort was made to compare the TCCA and NaBr mediated gold oxidation and 50-poly(S-*r*-canola) polymer recovery of the gold to gold panning. Firstly, 300 g of gold ore with a gold concentration of 1.72 ppm was spiked with 22.4 mg of finely cut up gold sheets. Then, panning was used to recover the gold. After developing a good panning routine, up 92% of gold was recovered. This positive control with added pure gold was done to ensure the panning technique was satisfactory. Next panning was tried on 300 g gold ore containing 75.3 ppm gold metal (without any added gold). Of the 22.6 mg estimated gold in that ore only 0.5 mg or 2% could be recovered by panning (Figure 2.39). This led to the conclusion that the vast majority of gold would be lost if panning was used as gold recovery method. The reason for this loss is typically due to gold particles that are very fine and not as easy to separate as larger particles.
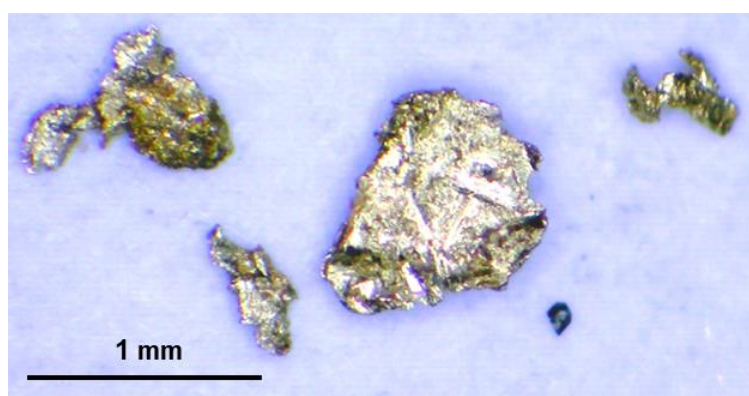
Figure 2.39: Optical microscope image of recovered gold using panning.

Further, the analysis with and optical microscope, SEM and EDX analysis was also performed on the panned gold and confirmed the panned material is indeed gold. No other elements besides gold and silver (the coating material) were detected (Figure 2.40).
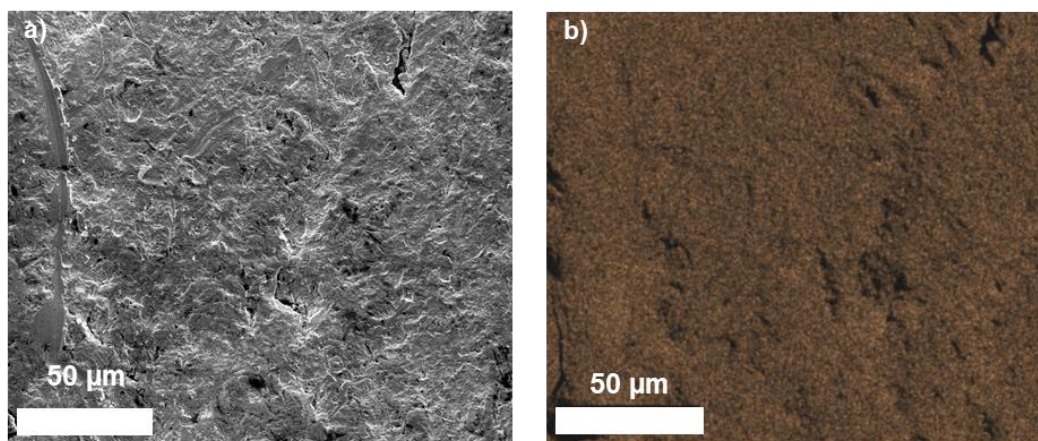
Figure 2.40: a) SEM micrograph and **b)** elemental gold EDX map of panned gold.

The remaining ore (246 g) was then oxidised using TCCA (5.25 g, 0.15M) plus KBr (285 mg, 0.015 M). A higher concentration of TCCA was chosen since more TCCA was needed to oxidise all the gold in the previous low grade ore concentrate oxidation experiment. After the magnetic material was removed the ore was mixed with 150 mL of deionised water, TCCA and KBr in a 5 L bucket. After the solution had been stirred for 24 hours the gold concentration was 113.5 ppm and the expected concentration was 123 ppm. Therefore, more TCCA (1.76 g) was added to increase the concentration by 0.05 M. Following an additional 24 hours of stirring the gold concentration had increased to 174 ppm which was higher than expected but as already discussed this could be due to inhomogeneous gold distribution in the ore. Next, the sample was filtered, and 2.5 g of 50-poly(S-*r*-canola) polymer was added to recover the gold. However, after 24 hours the gold concentration had only decreased by 18 % hence more polymer was added every 24 hours until the gold recovery was satisfactory. After a total of 9.5 g of polymer had been added over 8 days, 97% of gold had been removed. Incineration of the polymer confirmed the gold recovery by SEM and EDX analysis (Figure 2.41). However, some impurities like calcium, magnesium or silica were also observed indicating additional smelting would be required, which is common in both ASGM and formal mining. This experiment clearly showed that the use of the TCCA plus KBr oxidant in conjunction with the polymer as gold sorbent is able to leach and recovery over 97% of the gold, which was more efficient then panning for gold.
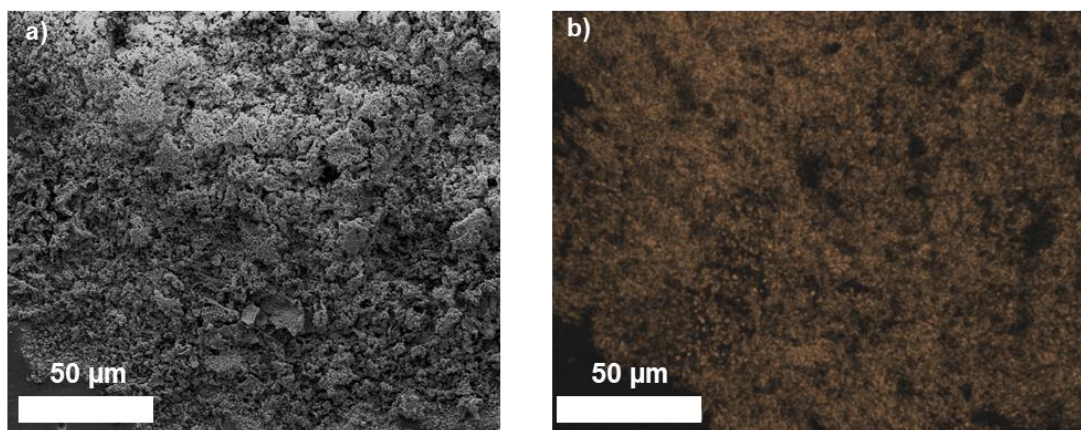
Figure 2.41: a) SEM micrograph and **b)** elemental gold EDX map of incineration product.

Determination of other leachable elements

Another important step in the validation of the TCCA plus NaBr oxidations method was the determination of other leachable elements. This would give an insight of what can be oxidised and how leach solutions should be treated after they have been depleted of gold. To do that, ore from a 100 kg ore sample from Linger and Die was used (this ore will be called 100 kg ore for this section). Before any experiments were conducted the ore was assayed using fire assay for gold content and acid digest followed by ICP-OES for the other elements (performed by commercial service as previously described). Table 2.4 shows the composition of the ore.

Table 2.4: Assay of 100 kg ore showing the concentration of various elements found in the ore.

Ag (ppm)	Al (%)	Au (ppm)	Ba (%)	Be (ppm)	Bi (ppm)
<2	5.87	40	425	<5	<10
Cr (ppm)	Cu (ppm)	Fe (%)	Hg (ppm)	K (%)	Li (ppm)
180	44	3.07	0.6	1.76	25
Pb (ppm)	S (%)	Si (%)	Sr (ppm)	Ti (%)	V (ppm)
70	N/A	34.5	34	0.21	76
Mg (%)	Mn (ppm)	C org (%)	Ca (%)	Cd (ppm)	Co (ppm)
0.61	460	0.28	0.28	<5	15
Y (ppm)	Zn (ppm)	Mo (ppm)	Na (ppm)	Ni (ppm)	P (ppm)
45	126	<5	5860	30	200

The aim of this experiment was to leach as much as possible from the ore, gold as well as all other elements. A total of 400 g or ore and 800 mL of water was used. The

TCCA concentration was 0.25 M (46.4 g) and the KBr concentration was 0.04 M (3.8 g). This increased concentration of TCCA and KBr was used to leach out as much as possible from the ore. After 2 days of oxidation the same amount of TCCA (46.6 g) and KBr (3.8 g) was added again to ensure complete oxidation of the ore. Following an additional 6 days of reaction time the sample was filtered and the filtrate volume was adjusted to the original reaction volume of 800 mL. Next, the sample was analysed using inductively coupled plasma atomic emission spectroscopy (ICP-AES), ICP-MS and cold vapor atomic absorption spectroscopy (performed by a commercial service). Based on the ore assay (Table 2.4), the mass of ore used, and the volume of the solution, the maximum concentrations of elements in the sample were calculated based on a complete leach of all elements present (Table 2.5). These concentrations were then compared to the concentration of elements present after the TCCA plus KBr leach (Table 2.5)

Table 2.5: Maximum and measured concentration of total ore oxidation.

Maximum concentration (if fully leached)		Measured concentration (after TCCA plus KBr leach)	
Element	ppm	Element	ppm
Ag	1	Ag	0.046
Al	29350	Al	8
As	148	As	0.004
Au	20	Au	6.2
Ba	212.5	Ba	9.8
Be	2.5	Be	0.035
Bi	5	Bi	<0.001
Ca	1400	Ca	810
Cd	2.5	Cd	0.034
Cr	90	Cr	<0.001
Co	7.5	Co	0.039
Cu	22	Cu	0.12
Fe	15350	Fe	0.39
Hg	0.3	Hg	0.17
K	8800	K	130
Li	12.5	Li	0.034
Mg	3050	Mg	340
Mn	230	Mn	0.008
Mo	2.5	Mo	<0.001
Na	2930	Na	200
Ni	15	Ni	0.75
P	100	P	<0.05
Pb	35	Pb	0.002
Sr	17	Sr	4.8
Ti	1050	Ti	<0.001
V	38	V	<0.001
Y	22.5	Y	0.12
Zn	63	Zn	0.62

In Table 2.5, elements of concern are highlighted in red whereas gold as the target element is highlighted in green. Only 31% of the expected gold concentration had been leached. This could be due to the gold being locked in the ore's larger particles. This might be characteristic of this type of ore, since higher percentages of gold have been leached from other ore batches as described in this chapter. However, what this experiment also showed was that the concentration of toxic elements like arsenic, cadmium, chromium, mercury, and lead were leached at levels far below the amount contained in the ore. This could indicate that they are also locked in larger ore particles or that these elements are already in a higher oxidation state and cannot be oxidised further using TCCA plus KBr. As was mentioned, a reason for the low gold leaching could be the large particle size of the ore. Therefore, SEM was used to determine the average particle size (Figure 2.42). This analysis showed very large variations of particle size within that ore sample. The largest measures particle had a length of 1444 µm and the smallest a length of 2.5 µm.
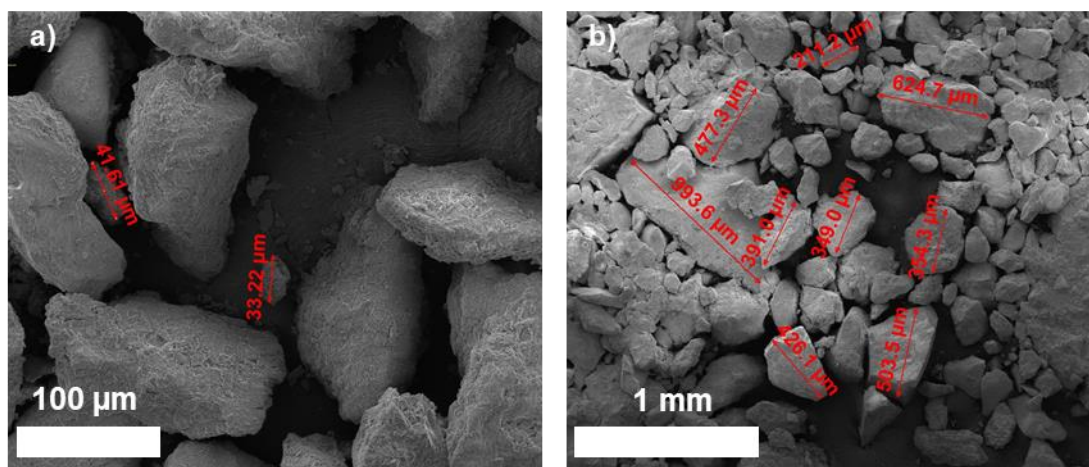
Figure 2.42: Representative SEM micrographs of the ore at a) 800 × magnification and b) 100 × magnification.

Therefore, it is plausible that the large particle size and distribution might be responsible for the low gold leaching result. Another reason could have been uneven distribution of the gold within the sample since the ore had arrived in five 20 L buckets from our industry partner. Next, the ore was homogenised by adding a layer of each bucket in a 100 L drum while each layer was mixed with the one below. After that the ore was split up into four 20 L buckets. Small samples from each bucket were combined and sent for gold analysis. The results showed 26 ppm of gold, less than the original analysis result of 40 ppm. If a gold concentration of 26 ppm is estimated the expected concentration in the leach solution would have been 13 ppm. If that were the case 47%

of gold would have been leached. An improvement of 16%. In an effort to attain more accurate results the ore was then classified to a particle size of ≤ 90 μm (Figure 2.43). Of the 100 kg of ore received only 4.1 kg had a particle size of ≤ 90 μm. The finer ore was also analysed for gold (fire assay) and other elements (acid digest followed by ICP-OES, both analysis were performed by a commercial service) and returned a gold concentration of 190 ppm, a stark increase of the unclassified 100 kg bulk ore (40 ppm) analysed preciously or the homogenised 100 kg bulk ore (26 ppm). A reason for this discrepancy could be that the gold is found in the fine particles which were isolated from the bulk ore.
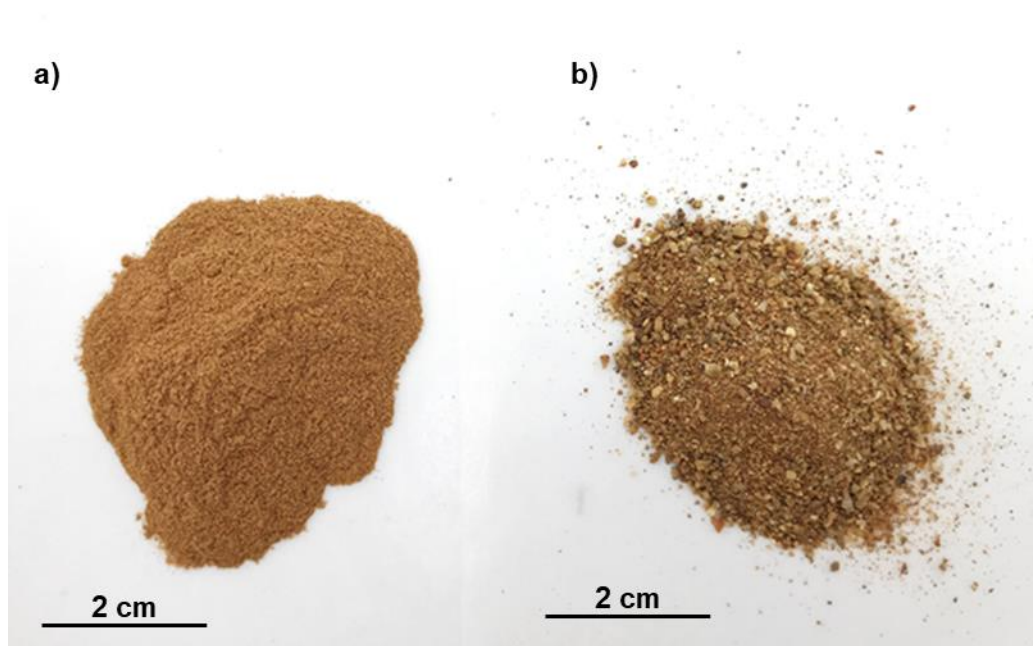
Figure 2.43: a) ore after being sieved to a size of ≤ 90 μm and **b)** remaining ore after particles with the size of 90 μm or under have been removed.

Small scale gold recovery from ore with a particles size of ≤ 90 μm

The ore with particle sizes of ≤ 90 μm had a high gold concentration and was used for gold recovery experiments. For possible uptake of this technique in the ASGM sector, it had to be reliable and fast. The goal of the next experiments was to determine after how much oxidation time the peak gold concentration was reached. For this leach a leach solution with the oxidant concentrations of 0.4 M TCCA and 0.02 M KBr was made. These concentrations were used to ensure fast oxidation of the ore. To 20 mL of this solution 25 g of ore was added. Since it has been previously shown that increased temperatures can speed of the leaching process, the deionised water that had been used was at a temperature of 60 °C. The gold concentration was measured using

ICP-OES and peaked at 2 hours with 40 ppm and slightly decreased thereafter to 36 ppm and remained constant (Figure 2.44).
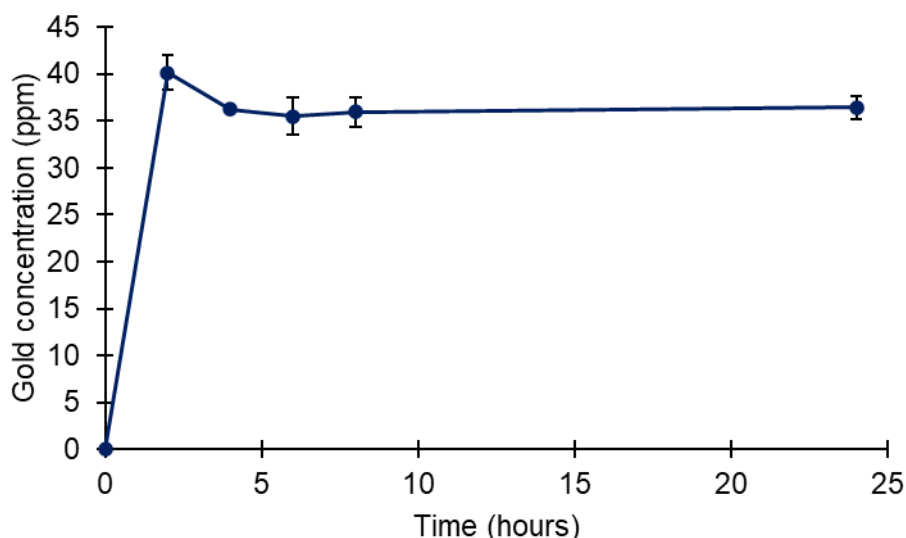
Figure 2.44: Gold concentration of oxidised ore over 24 hours.

This was an encouraging result, showing that the gold is leached very rapidly. The estimated gold concentration was 237 ppm, however only 36.5 ppm were leached. This again could be due to the gold being locked into the ore and occluded from the leach solution. If this were the case, crushing the ore into finer particles would liberate more gold and increase the yield. Further, the gold might have been inaccessible for the leach solution or due to the concentrations of the oxidants in the leach solution being too low. Another possibility was that the magnetic material in the ore consumed the oxidant before more of the gold could be leached. This hypothesis was tested by leaching ore samples in parallel that had magnetic material removed or that still contained magnetic material. The same mass of ore and volume of water (at 60 °C) was used as in the previous experiment. This time however, the magnetic material was removed from one set of samples pre oxidation and double the mass of oxidant was added to the other sample set. This was done for two reasons. Firstly, to find out if removing the magnetic materials increased the gold leached and secondly to determine if an increase of oxidant leached more gold from this batch of ore. As with the previous experiment the gold concentration was monitored using ICP-OES and peaked after only 2 hours. The gold concentrations in the samples which had their magnetic material removed was higher (46 ppm) then in the sample with double the mass of oxidant (34 ppm, Figure 2.45). This experiment showed that removing magnetic material before leaching the sample has a

higher impact on the mass of gold leached as when the oxidant concentration in increased.
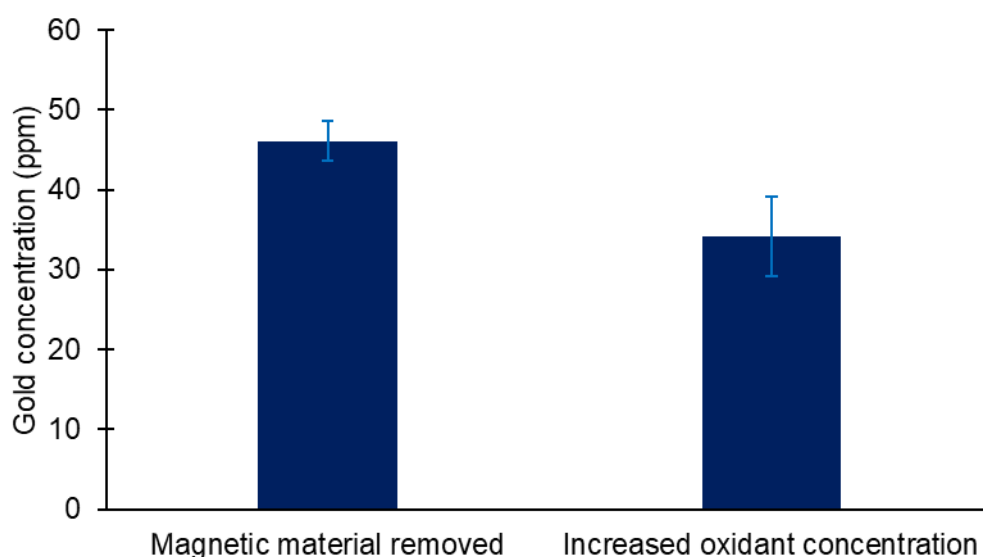
Figure 2.45: Gold concentration of samples from which the magnetic material was removed and form samples which had an increased oxidant concentration.

However, the gold concentration was still a lot lower than the expected 237 ppm predicted from the commercial fire assay. The reason for that could be that the gold was in a form which cannot be oxidised using TCCA and KBr . Nevertheless, these results proved useful in establishing that the amount of gold leached can be increased when magnetic material is removed from the ore before the oxidation step.

Large scale gold oxidation and recovery (5 kg ore)

A gold leach and recovery experiment using approximately 5 kg of ore was conducted next. The equipment to conduct this experiment was supplied by Adelaide Control Engineering. This experiment served as a proof of concept to aid the development of a compartmentalised ASGM kit that is in development since the gold concentration of the ore was not accurately known. For this experiment the oxidants were pre-dissolved by sonication and heating. To do that, two 800 mL solutions were prepared beforehand, each containing 180 g of TCCA and 7 g of KBr. A total of 1.6 L of leach solution with a TCCA concentration of 0.97 M and a KBr concentration of 0.07 M was prepared beforehand. This was done in order to save time for a full operation from start to final gold recovery. Also, the higher concentration of TCCA was chosen to compensate for the large amount elements that could be leached form 5 kg or ore. Prior to starting the reaction, the oxidant solutions were pre-heated to 50 °C while an

additional 2 L of deionised water were pre heated to 70 °C. The ore used had particle sizes of up to 104 µm and a total mass of 4759.4 g. Before the ore was oxidised, it was passed over a strong magnet to remove as much magnetic material (such as nickel-, iron- and cobalt-gold alloys and magnetite) as possible (Figure 2.46).

Figure 2.46: Magnetic material was removed by pouring the ore over a strong tubular magnet.

During this process 5.4 g of magnetic material was removed, leaving 4755 g of ore to be oxidised. After the ore, water and oxidant solution were added to a 20 L drum Resulting in a TCCA concentration of 0.43 M and a KBr concentration of 0.03 M. A PVC block was added to aid in agitation of the leach mixture (it essentially served as a baffle). The drum was then placed on a roller and rotated at 4.5 RPM (Figure 2.47). This equipment was designed by Adelaide Control Engineering and was part of upscaling the gold extraction method using TCCA plus NaBr or KBr. The drum was on a variable speed roller to that the rotation speed could be adjusted. Further the assembly was on plastic bunding to catch the leach contents if a spill was to occur. The temperature of the mixture at the beginning of the process was 40 °C and the temperature was monitored during the oxidation process. The reaction was continuously heated via a small fan heater. This was done to increase the rate of the reaction. Since it had been previously shown that the peak gold concentration was reached after 2 hours, this reaction was also stopped after 2 hours. At this stage the temperature of the reaction was still 36 °C. At that time a strong chlorine odour was detected, so this operation had to be performed in an area with adequate ventilation. The generation of chlorine was expected with the elevated temperature and in-situ formation of hypochlorous acid in addition to hypobromous acid.
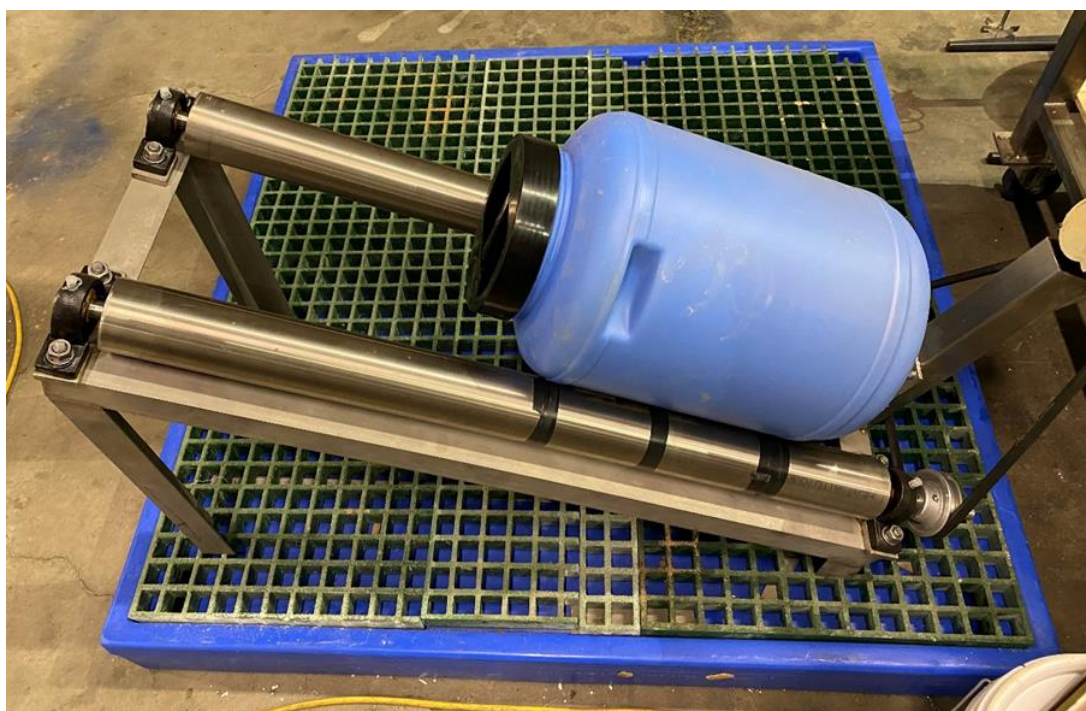
Figure 2.47: Set up of roller with 20 L drum containing leach reagents and ore.

Since the filtration of the sample had been the main challenge of the project, a different approach was used. This time the ore was filtered in two steps. The first step involved gravity filtration of the ore using a 50 µm nylon filter bag. Since the filtrate was still cloudy it was filtered again using vacuum filtration. Doing this, 2697.7 mL were recovered. The ore was then washed with deionised water to wash as much solubilised gold of the ore as possible. The total recovered liquid had a volume of 4066.9 mL. Next, 150 g of 50-poly(S-*r*-canola) polymer was added to the solution and stirred for 30 minutes after which an additional 150 g of polymer was added and stirred for 4 hours. This was done because it was thought that the leach solution is quenched by the first polymer addition. After a total of 4.5 hours of stirring, the polymer was removed by filtration through a cotton cloth on a sieve. Next the polymer was incinerated using a muffle furnace which was more controlled than a crucible and Bunsen burner. Incineration of 300 g of polymer resulted in 374 mg of remaining material. SEM and EDX analysis of this material showed gold together with other elements such as sulfur, calcium or magnesium—consistent with other lab-scale leaching trials. The ore used for this experiment was the same as previously used. The gold concentration of that homogenised ore was 28 ppm as estimated by fire assay. However, after that analysis the ore was sieved and particles with a size of ≤ 90 µm collected. The gold concentration in that ore was a lot higher than in the 100 kg bulk are with 190 ppm. Since no further

gold analysis was conducted on the bulk ore (which has been used for this experiment) after removing the particles with a size of ≤ 90 µm no accurate comment can be given on the gold content. Therefore, it is important to note that this experiment was performed as a proof as concept to assess if the TCCA plus KBr can be performed at a larger scale within a day, and also to test the equipment designed for an artisanal operation. Nevertheless, the gold concentration during the experiment was measured using ICP-OES. The concentration after the leach process was found to be 8 ppm. After the filtration process and taking the dilution factor into account the gold concentration had dropped by 18% indicating that this gold had been lost during the filtration process. The solution to which the polymer was added had a gold concentration of 5.8 ppm which was reduced to 4.5 ppm, 4.5 hours after the polymer was added. This equates to a gold reduction of 29%. This low percentage of gold removal could be due to several factors. This was the first reaction at this scale and was performed in one day only. From the addition of the oxidant to the ore to the end of the gold removal by the polymer only 10 hours had passed. A longer oxidation and gold removal time might have resulted in higher gold yields. However, this experiment was an important step toward upscaling of this reaction and understanding its time requirements. Currently, the engineering company is working on a small pilot plant that addresses the filtration problems and aims to have modular and containerised plant design suitable for use in ASGM, as well as small and medium formal mines.

This experiment has shown a complete gold leach and gold recovery using TCCA plus KBr can be performed within one day. Additionally, this experiment served to evaluate newly developed equipment (by Adelaide Control Engineering) for applications in ASGM operation. Further this was the largest scale experiment to date in an effort to continuously scale up gold oxidation from gold ore using TCCA plus KBr together with gold recovery using the 50-poly(S-*r*-canola) polymer. Additional testing is required to quantify the yield of the gold recovery using these techniques. Due to the chlorine odour, any larger scale operations need to be performed in a well-ventilated area. Further, continuous monitoring of the gold concentration is paramount of maximum efficiency of the process, which could be a bottleneck for artisanal operations that do not have access to spectroscopic techniques such as AAS. This experiment also highlighted the ongoing difficulty of filtering the leachate after the oxidation. Further research needs to be undertaken to understand and improve to uptake of gold from the solution using the 50-poly(S-*r*-canola) polymer. A solution could be to use more polymer or to further enrich the gold concentration by using the same liquid to oxidise more than one batch of ore.

The next steps of this project will involve the setup of real time gold concentration monitoring at the location of the large-scale experiments. Further, any newly developed strategies to filter the leachate need to be validated and tested.

Electronic waste applications

As has been discussed in the introduction of this chapter, e-waste presents a problem around the world. Nevertheless, e-waste contains precious metals like gold and silver. Since the TCCA plus NaBr gold leach method was discovered with the ASGM sector in mind, it could also be implemented into the informal (or even formal) e-waste recycling sector. Therefore, the use of the TCCA and NaBr gold leach and gold recovery using the 50-poly(S-*r*-canola) polymer in the context of e-waste was investigated.

Decommissioned computers were acquired and taken apart to determine what parts to use for initial experiments. The parts that were best suited for that were the random-access memory (RAM) pins since they were small in size and contained gold that was clearly visible (Figure 2.48). The goal of these experiments was to learn how much gold was contained in the RAM pins, what other elements would be released by leaching with TCCA plus NaBr, and if the leached gold could be successfully recovered. Several factors distinguished the ore experiments from the e-waste experiments. The RAM pins used were not a homogenous material and were not crushed in order to keep the procedure as simple as possible. Further, as has been discussed in the introduction, electronic waste contains many other metals besides gold. Additionally, e-waste contains plastic, which was not the case in gold ore experiments.

It had been previously shown in an Honours project[88] that the copper in the leach solution can interfere with the gold uptake by the polymer and the literature has shown that substantial amounts of copper can be found in e-waste.[40] As has been shown earlier in this chapter, gold is selectively bound to the polymer in the presence of copper (Figure 2.20). However, for these experiments the copper concentration was only 5 ppm. E-waste may have orders or magnitude more copper than gold. Therefore, ways to limit the interference of copper were investigated. An Honours[88] project found that complexing the copper with ethylenediaminetetraacetic acid (EDTA) can lessen the effect of copper on the gold removal. Building on this knowledge this section of the thesis will examine what elements are commonly encountered in electronic waste and will focus on a complete process to recover gold from electronic waste. For these studies random-access memory (RAM) modules were used since the gold was clearly visible (Figure 2.48).

Gold rich area

Figure 2.48: RAM module with gold rich area highlighted in box.

A total of 10 RAM modules were placed into 500 mL oxidant solution (TCCA: 11.6 g, 0.1 M; KBr: 892 mg, 0.015 M) and heated to 50 °C while sonicating. Sonication was used here since previous experiments in this thesis have shown that sonication speeds up the gold oxidation. After 6 hours the visible gold had been oxidised (Figure 2.49). The gold concentration in the leachate was at 139 ppm which equates to 69.5 mg of gold in the solution (Figure 2.50). However, a drop in gold concentration was observed after two hours. A reason for that could be that the copper of the RAM pin that is situated under the gold begins to be oxidised into Cu1+ which may reduce and precipitate gold. However, as the oxidation continues the gold is oxidised again resulting in a subsequent rise on gold concentration.

Figure 2.49: Representative RAM module **a)** before and **b)** after oxidation.

Following the oxidation, EDTA was added until the solution was saturated (EDTA was added until no more dissolved). This was done since it is known that EDTA binds to cupric ions.[96] Since the amount of copper in the solution was unknown, the solution was saturated with EDTA (50 g) in order to ensure all the copper in the solution was bound

104

to EDTA and to simplify the procedure. Next, the solution was gravity filtered to remove any undissolved EDTA and debris. The gold concentration was determined before and after the filtration using ICP-OES analysis. As can be seen in Figure 2.50, small amount (5%) of gold has been lost during the filtration process. This could be due to insufficient rinsing of the debris and undissolved EDTA or to gold adhering to the glassware. Further, instrumental inaccuracies can also lead to the different gold concentration after the filtration as before. Next, 12 g of 50-poly(S-r-canola) polymer was added to remove the gold from solution. After only 3 hours the gold concentration had been reduced by 99% (Figure 2.50).
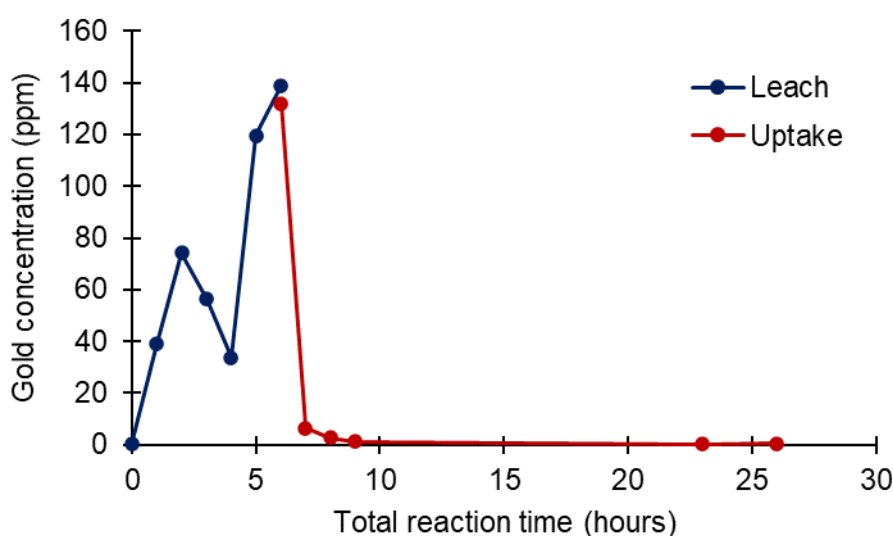
Figure 2.50: Gold concentration over the entirety of RAM module gold recovery, beginning from the leaching and continuing throughout the gold uptake stage as measured by ICP-OES.

After the 50-poly(S-r-canola) polymer was recovered via filtration, it was incinerated in a muffle furnace. The incineration product had a mass of 97 mg which was more than the expected mass of recovered gold with 65 mg. This is likely due to contamination and was investigated using SEM and EDX. Besides gold this analysis only showed copper, aluminium, and tin. To determine how much of the mass of the material was gold, the sample was microwave digested using aqua regia. This digestion showed 42 mg of gold in the incineration product which equates to 64 wt% of the incineration product. This is lower than expected since some difficulties were encountered during the digestion process. Some of the incineration product was very difficult to remove and some was still stuck to the crucible. Further, the final product was susceptible to static charge which complicated transfer to the digestion tubes and lead

to loss of material. Nevertheless, it has been shown that over 99% of leachable gold has been recovered by using the polymer as a sorbent.

During the aqua regia digestion not all of the material had been dissolved, so the remaining material was recovered and analysed using XRD. This analysis showed the presence of tin oxide which was not surprising since SEM and EDX analysis of the incineration product also showed tin. In future studies, it may be possible to remove tin first, as it can be removed at relatively low temperatures when it is used in soldering. This could be done, for instance, before the leaching process. Alternatively, tin oxide has a much higher melting point than gold, so smelting is a realistic alternative for the final gold purification.

In conclusion, a method of gold oxidation and recovery developed in this thesis can be successfully used to recover gold from electronic waste. Using a leach solution of TCCA and NaBr while sonicating the surface gold was removed from the RAM pins within 5 hours. EDTA was used to form a complex with copper in solution so that the 50-poly(S-*r*-canola) polymer could remove the solubilised gold more efficiently from the leach solution. Further, it has been shown that sonication was effective in this oxidation. Following the oxidation, the gold was recovered using the 50-poly(S-*r*-canola) polymer within 3 hours. Isolation of the recovered gold through incineration of the polymer showed contamination (mainly in the form of tin oxide). In order to further optimise and refine the process, research has to be undertaken to determine additional ways by which copper can be removed from the solution before the polymer is added. This could be done by first electroplating the copper out of solution. Further investigation has to be done into the contents of the leach solution (what metals are present in the solution) and what to do with the leach solution after the gold has been removed. One solution could be to use the solution again for additional oxidation cycles, or the solution can be filtered (though a carbon filter) to remove other metals before the solution is being used again. Currently efforts are under way to construct a pilot plant to process electronic waste using TCCA and NBr as oxidant and 50-poly(S-*r*-canola) as gold sorbent.

Large scale 50-poly(S-*r*-canola) polymer synthesis

The reagents needed (TCCA, NaBr, KBr) for the gold oxidation developed in this thesis can be ordered at a large scale. However, that was not the case with the 50-poly(S-*r*-canola) polymer. Since the 50-poly(S-*r*-canola) polymer has many applications, interest was expressed from commercial enterprises. However, to fill the need for larger quantities of this material, upscaling of the reaction was important. Dr Louise Esdaile has done extensive work on developing an upscaled synthesis to a reaction yielding kilogram scales, and research in this thesis contributed in part to these advances.[81]

For instance, working with Dr Esdaile, we developed the first kilogram-scale reactions for the production of 50-poly(S-*r*-canola). The reaction was performed in a 4L stainless steel cooking pot fitted with an overhead stirrer bar on a hotplate. A funnel placed on the side of the pot was used to add the sulfur and sodium chloride, the porogen (Figure 2.51). First, 375 g of canoa oil was added to the pot and heated to 170 °C. Next 375 g of elemental sulfur was added. During the sulfur addition care was taken not to let the temperature drop to under 160 °C in order to ensure sulfur-ring opening. As the sulfur was added two phases were initially observed. However, upon longer reaction time and vigorous stirring, the reaction became one phase.

Figure 2.51: a) Set-up of 700 g poly(S-*r*-canola) synthesis. **b)** Reaction after some sulfur was added, two phases can be seen with molten sulfur at the bottom and canola oil at the top.

Next, the reaction temperature was increased to 180 °C and 1.75 kg of salt was added. The salt was added as a porogen to increase the surface area of the final polymer. Prior to the salt addition a blender was used to blend the salt to ensure no clumps were present. As the salt was added, special care was taken to keep the temperature at or above 160 °C. This process took usually around 20 minutes. After that the reaction continued to be heated to around 180 °C. The completion of the reaction was assessed based on the torque reading of the overhead stirrer. At a measured torque

of 40 N•cm or more, the reaction was a viscous brown liquid. At this point the reaction had to be removed quickly from the heat source since heating it any longer could result a continued exothermic reaction and thermal decomposition of the product. While the product was still hot, a large spatula was used to break the polymer up before it was ground to a particle size of 0.4–4.0 mm using a meat grinder. Lastly, the polymer was added to 19 L of deionised water and stirred in order the remove the salt. After the polymer was air dried, it was ready for use. (Figure 2.52). Characterisation can be seen in the experimental details (Figure 2.58 to Figure 2.63).
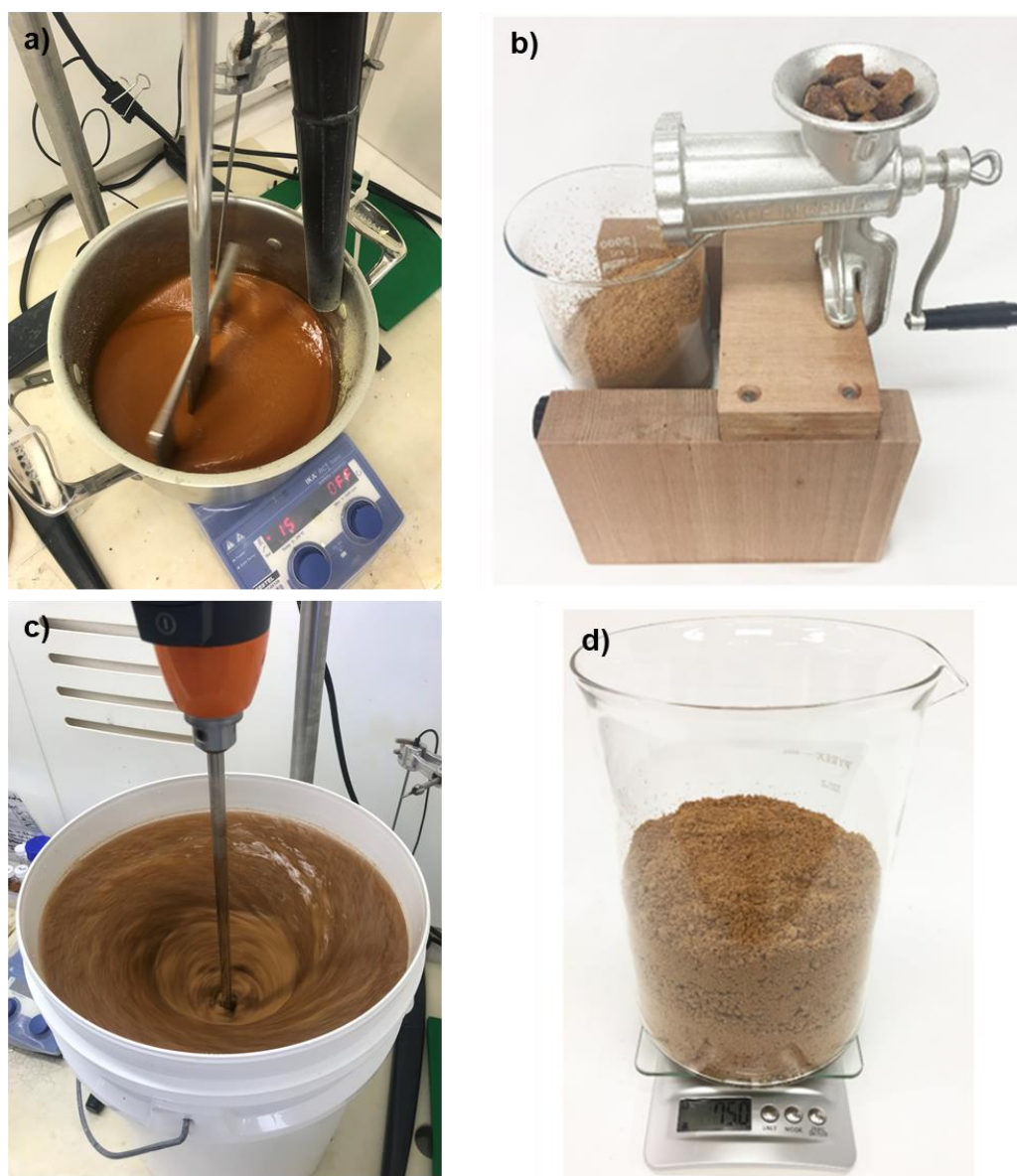
Figure 2.52: a) Reaction mixture after salt was added. **b)** Polymer is being ground using meat grinder. **c)** Salt is removed by washing the polymer in deionised water. **d)** Final dried product.

Using this process, more than 20 kg of polymer were made. However, as more commercial interest was registered, larger quantities of polymer were required for which a 750 g reaction was not a viable option. These experiments were crucial in the upscaling of the 50-poly(S-*r*-canola) polymer. The experiments described above were therefore critical in the first commercial production methods of this polymer. Since then, a proprietary plant used these results to produce the polymer at a 500 kg scale as can be seen in Figure 2.53. The results in this thesis were used in consultation with the company to develop this reactor and manufacturing process.

Figure 2.53: 500 kg of 50-poly(S-*r*-canola).

The determine of the large-scale polymer was the same as the laboratory scale polymer TGA analysis was performed which corresponded to that of the laboratory scale polymer which has been previously published (Figure 2.54).[81]
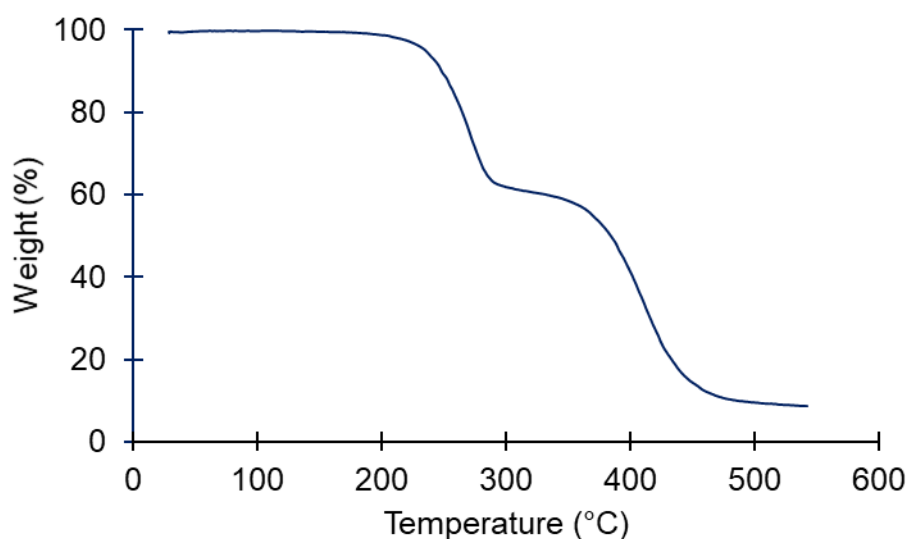
Figure 2.54: TGA analysis of large scale polymer

As has been described in this chapter the 50-poly(S-*r*-canola) polymer is able to remove gold from aqueous solution. Hence, the large-scale polymers gold capture capabilities were benchmarked against that of the laboratory scale polymer. Briefly, to do that, 1 g of polymer was sown into a 2 cm × 9cm cotton bag, added to 50 mL of a 5 ppm Au^{3+} and rotated end over end at 25 RPM for 28 hours with samples taken in between. Gold uptake was initially faster for the large-scale polymer. However, after 10 hours, the gold uptake of both polymers was very similar with 98.3% gold removal for the large-scale polymer and 99.5 % for the laboratory polymer (Figure 2.55). This result indicated that the large-scale polymer performed very similar to the laboratory scale polymer, which was an important step toward further upscaling of the polymer synthesis.
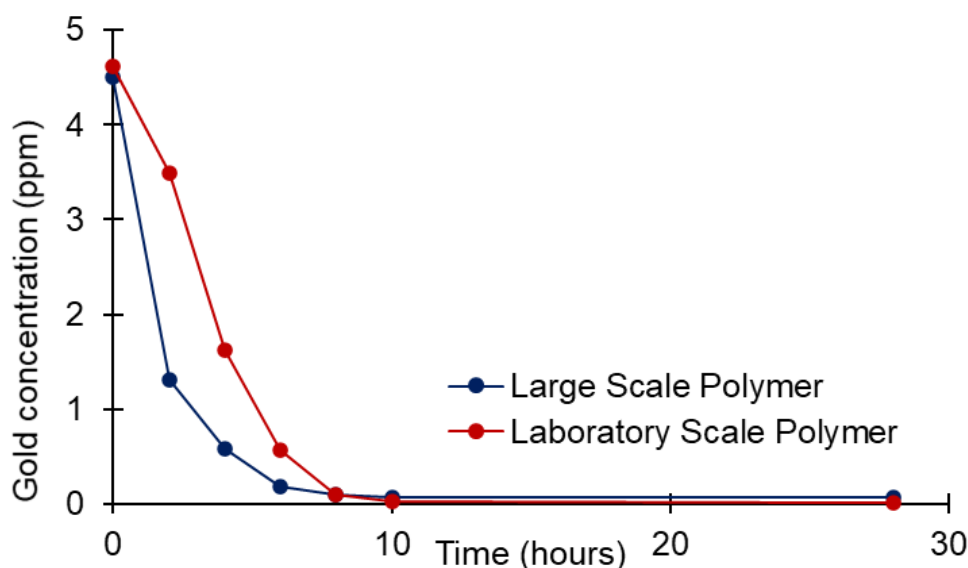
Figure 2.55: Gold (Au^{3+}) uptake of large scale and laboratory scale polymer.

Hence it has been shown that the 50-poly(S-*r*-canola) polymer can be made on a large scale using a proprietary continuous process. This was an important step to implement the TCCA plus NaBr gold leach and the gold recovery using the 50-poly(S-*r*-canola) polymer in ASGM and informal e-waste recycling. This is just one use for polysulfides polymers. The following chapters of this thesis will explore the applications of there polysulfide polymer systems.

Patent that resulted from the research in this paper:

Materials and process for recovering precious metals. **Mann, M**.; Chalker, J.M. Patent No. WO 2020/198778 A1, March 31, 2020

Experimental details

Materials: TCCA was purchased from Sigma Aldrich at a small scale (250 g) and from ACE Chemical Company at a large scale (20 kg). NaBr was purchased from ACE chemicals and KBr, EDTA, Gold(III) chloride, NaBr ascorbic acid, oxalic acid, sodium bisulfite and sodium metabisulfite was purchased from ChemSupply. Gold wire (0.1 mm diameter), 1000 ppm gold standard was purchased from Sigma-Aldrich. Canola oil was purchased from Just Fry Oil Australia.

ARXPS (Angle-resolved X-ray photoelectron spectroscopy) was applied for determining the chemical and valence states of a sample across a variation of depth. The apparatus was built by SPECS, which was operated in an ultra-high vacuum (UHV) condition at a base pressure of low 10-10 mbar. A no-monochromatic X-ray source (12kV-200W) with Mg anode was used for the measurements and survey and high-resolution scans were operated at a pass energy of 40eV and 10eV respectively and recorded. The X-ray is generated by a Tungsten filament. The emission of a core electron from the sample surface is caused by the X-ray photon absorption. The electron is then detected, and the variation of kinetic energy is correspondent to the elemental characterization. The XPS can be operated at a range of different intersection angle. In this work, the intersection angle between the surface normal and the electron path was 0º while the measuring depth was maximized. With the increase of intersection angle, the electrons were not capable of reaching the sample surface due to the limits of the electron mean free path. Consequently, the measuring depth was diminished.

Inductively coupled plasma mass spectrometry (**ICP-MS)** was performed using a Perkin Elmer NexION 350D spectrometer. The instrument had a quartz cyclonic temperature controlled (2 °C) spray chamber and a glass concentric nebuliser (300 µL/minute). The radio frequency power was set to 1600 W with the plasma flow being 16 L/minute, the auxiliary flow 1.2 L/minute, the nebuliser flow 0.9 L/minute. The dwell time was 100 ms with 3 replicates. The KED mode had a helium flow of 4.7 L/minute. Before use the instrument was tuned to standard mode using 1 ppb tuning solution to within Perkin Elmer specifications. The KED mode was tuned with KED Mode solution to within Perkin Elmer specifications. The analysis was performed in KED (Kinetic Energy Discrimination) mode with Internal Standard correction using Indium. The internal standard was added externally through a T-junction for standard and samples. The flow rate of the sample was set to 0.25 mL/minute and the flow rate of the internal standard to 0.02 mL/minute. The error is the instrument is typically 5% or lower.

Scanning electron microscopy (SEM) and energy dispersive X-ray spectroscopy (EDX) were performed using a FEI Inspect F50 SEM fitted with a EDAX energy dispersive X-Ray detector. Samples were sputter coated with silver metal (20 nm thickness) before analysis.

Powder X-ray diffraction (XRD) patterns were recorded on a Bruker D8 Advance Eco diffractometer (Bragg-Brentano geometry) using Co-Kα radiation (λ = 1.78897 Å). The Bragg angle (2θ) was varied from 10° to 90° with a step size of 0.019°, measurement time of 0.6 s per step and sample rotation at 10 rpm. The samples were deposited onto a sample holder well before analysis.

Ion Chromatography (IC) was conducted using a Dionex ICS-1500 ion chromatograph fitted with a Dionex AS 40 automated sampler. The column used was a Dionex Ion Pac™ AS14A, RFIC™, 4 × 250 mm. The eluent was 0.8 mM sodium carbonate / 1.0 mM sodium bicarbonate.

pH was measured using a Sper Scientific Benchtop Water Quality Meter. The meter was calibrated with pH 4, 7 and 10 buffer solutions.

Atomic absorption spectroscopy (AAS) was performed using a GBC Savant AA flame atomic absorption spectrometer fitted with a Photron hollow cathode lamp (Au). As fuel and air and acetylene mixture was used with an air flow rate of 10.0 L/minute and an acetylene flow rate of 1.0 L/minute. The lamp current was set to 40. mA and the wavelength chosen for gold analysis was 267.6 nm. The slid with was set to 0.5 nm and the sample read time was set to 5s. As measuring mode integration was used.

Incineration of 50-poly(S-*r*-canola) was performed in a ceramic crucible by heating it up with a Bunsen burner, or in a Carbolite Gero CWF 1200 furnace. The protocol for incineration in the furnace was as follows except otherwise stated. The 50-poly-(S-r-canola) sample was heated to 1100 °C using a 5 °C / minute heating rate. After the target temperature was reached the temperature was held for 30 minutes. Next, the oven was left to cool down naturally. The crucibles used in the furnace were made from Al_2O_3.

Inductively coupled plasma – optical emission spectroscopy (ICP-OES) was conducted using a Perkin Elmer Optima 8000 ICP-OES fitted with a Perkin Elmer S10 autosampler. For the analysis an external standard of all the target elements was used. After the calibration solutions were prepared, the samples were diluted within the calibration range (sample concentration was estimated if not know). As quality control measured spikes and additional known concentrations were run. Further, an internal

standard using an element not likely to be in the sample or to interfere was continually run to assess performance of the instrument.

Simultaneous thermal analysis (STA) which included TGA and DSC analysis was performed using a Perkin Elmer STA 8000. Between 5-10 mg of sample were held at 40 °C for 4 minutes before the temperature was increased by 10 °C/minute to 800 °C. This was done under a 20 mL/min nitrogen flow.

^{1}H NMR spectra were recorded on a 600 MHz Bruker spectrometer with $CDCl_3$ as solvent. Spectra were referenced to residual solvent peaks (δ_H = 7.19, 7.44 and 8.71 for pyridine-d5).

Infrared (IR) spectra were recorded using a FTIR Perkin Elmer Frontier spectrometer between 4000 and 500 cm^{-1}.

CHNS elemental analysis was performed by The Campbell Microanalytical Laboratory at the University of Otago in New Zealand.

Gold oxidation

Gold wire (99.9 %, 0.1 mm ø, 0.5 cm) was placed in 15 mL of pure bleach (pH 13). Two fresh 15 mL batches of bleach were acidified to pH 1.5 and 5.96 using concentrated aqueous hydrochloric acid (37 %) and 5 mm of gold wire was added to each solution. Five solutions with a pH of 2.04, 3.96, 6.08, 8 and 9.93 were prepared and gold wires with the weight of 0.9, 0.81, 1.02, 1.05 and 0.89 mg were added respectively. After the gold wire in one solution had been fully oxidised (1 hr. 7 min) the wires in the remaining solutions were removed, rinsed with deionised water, dried under vacuum, and weighed.

For the next step, the oxidation of gold using pool chemicals, the following chemicals were purchased from a hardware store:

1) Hy-Clor Spa Sanitiser Tablets (Active constituent: 650 g/kg available bromide and 280 g/kg available chlorine present as bromochlorodimethylhydantoin **(BCDHM)**).

2) Hy-Clor Long Lasting Swimming Pool Tablets (Active constituent: 850 g/kg available chlorine present as trichloroisocyanuric acid **(TCCA)**).

3) Hy-Clor Super-Shock Granular Pool Chlorine (Active constituent: 700 g/kg chlorine present as calcium hypochlorite **(Ca(Ocl)$_2$)**).

4) Hy-Clor Spa Granular Bromine (Active constituent: 510 g/kg chlorine present as sodium dichloroisocyanurate and 150 g/kg sodium bromide **(SDIC + NaBr)**).

To assess if the pool chemicals could oxidise gold, the following solutions of each chemical were made and gold wire was added to each solution, the solutions were then left undisturbed for 43 hours. At that time the gold had dissolved in all solutions but in the BCDMH solution. Therefore, the experiment was stopped and BCDHM was discarded as useful oxidant.
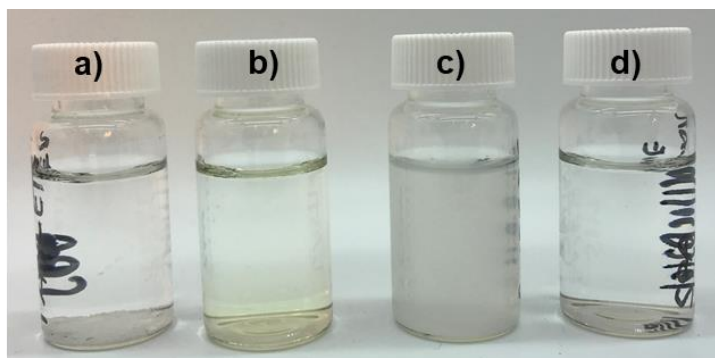
Solution	Active Constituent	Mass (mg)	Deionised Water (mL)	Gold Wire (mg)	pH
a)	BCDMH	100	15	1.125	6.6
b)	TCCA	100	15	1.144	3.6
c)	Ca(OCl)$_2$	100	15	1.308	11.5
d)	SDIC+ NaBr	100	15	0.9	6.6

Figure 2.56: Solutions made of each pool chemical, the amounts of chemical, water and gold wire added as well as the pH of the solutions.

After 43 hours the BCDMH still had some undissolved solid at the bottom of the vial, also the Ca(Ocl)$_2$ solution had a cloudy white color. The chemicals in the other two solutions were completely dissolved. In order to speed up the gold oxidation halides in the form of HCl, NaBr and NaCl were added. A total of 8 solutions with various combinations of pool chemical and halides were made. The concentration of total halides was 186 mM (93 mM of halide from the pool chemical and 93 mM of the halide from and additional halide source. If the solution contained more than one additional halide source, their concentrations were 46.6 mM each to make up 93 mM and the volume of the solutions was 15 mL.
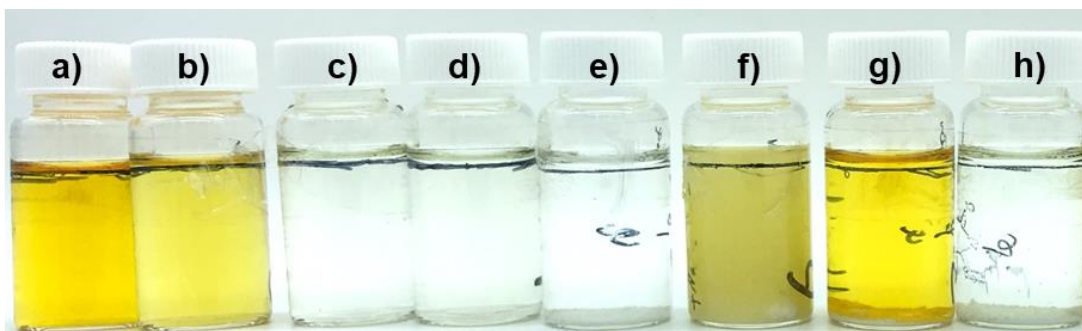
Solution	Oxidant	Halide source	pH		Repetition 1 Gold loss (%)	Repetition 2 Gold loss (%)
			0 hours	8 hours		
a)	Bleach	HCl / NaBr	7.1	6.7	58.8	50.7
b)	Ca(OCl)$_2$	HCl / NaBr	6.5	5.8	44.3	42.4
c)	Bleach	HCl	0.7	1.3	74.4	36.6
d)	Ca(OCl)$_2$	HCl	1.5	2.0	70.7	100.0
e)	TCCA	NaCl	2.5	2.0	75.0	84
f)	SDIC + NaBr	NaBr	7.1	6.5	47.7	49.3
g)	TCCA	NaBr	6.5	5.8	30.8	69.3
h)	TCCA	HCl	0.6	1.1	100.0	91.3

Figure 2.57: Solutions (15 mL) made from pool chemicals with added halide sources, their pH values before and after the gold had been oxidised as well as their respective gold loss.

These solutions were made so that the additionally added halide had the same concentration as the halide from the pool chemical. For example, if 0.2 moles of TCCA was used (TCCA contains 3 Cl species) then 0.6 moles of NaBr would be used in order to add the same amount of bromide to chloride ions. This was done for all solutions.

After the gold wire had been completely oxidised in either of the solutions, the reaction was stopped by removing and rinsing the gold wire with deionised water. After that the wire was dried under vacuum and weight. The weight before and after the oxidation as used to determine the weight loss percentage.

Gold recovery by 50-poly(S-*r*-canola) polymer

The polymer made in the laboratory at a multi-kg scale was characterised using ^{1}H NMR, IR, Simultaneous Thermal Analysis (STA) which included thermogravimetric analysis (TGA) and differential scanning calorimetry (DSC), powder X-ray diffraction (XRD), scanning electron microscopy (SEM) and energy dispersive X-ray analysis (EDX).
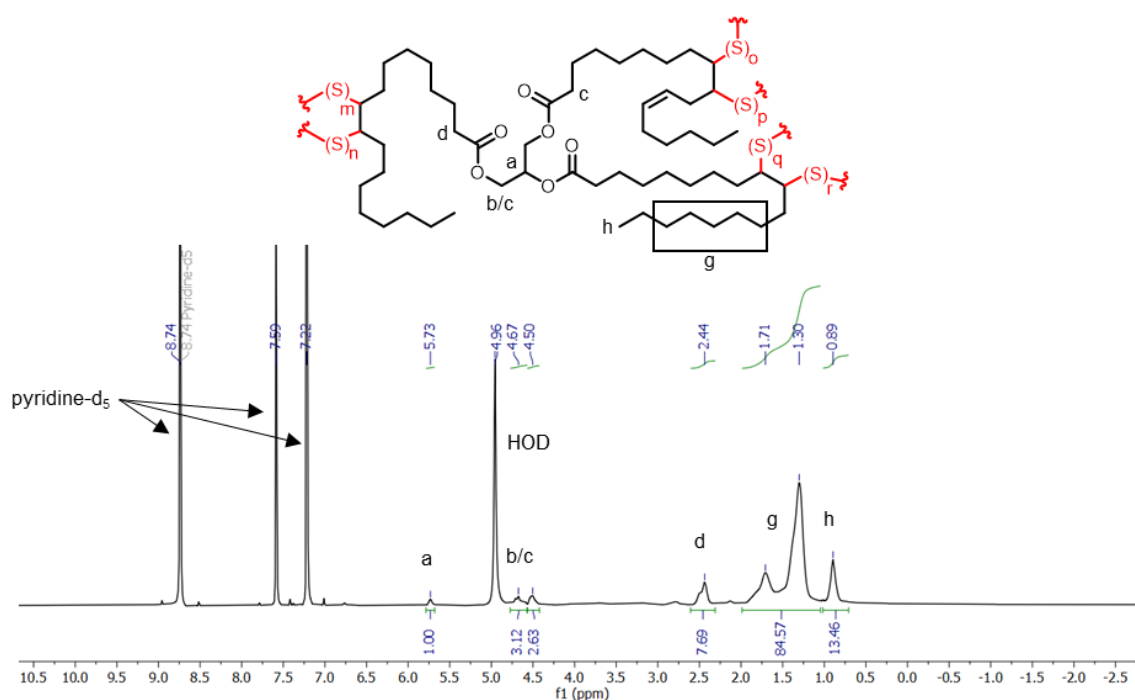
Figure 2.58: ^{1}H NMR of 50-poly-(S-*r*-canola) in pyridine-d5 was consistent with that previously reported.[81]
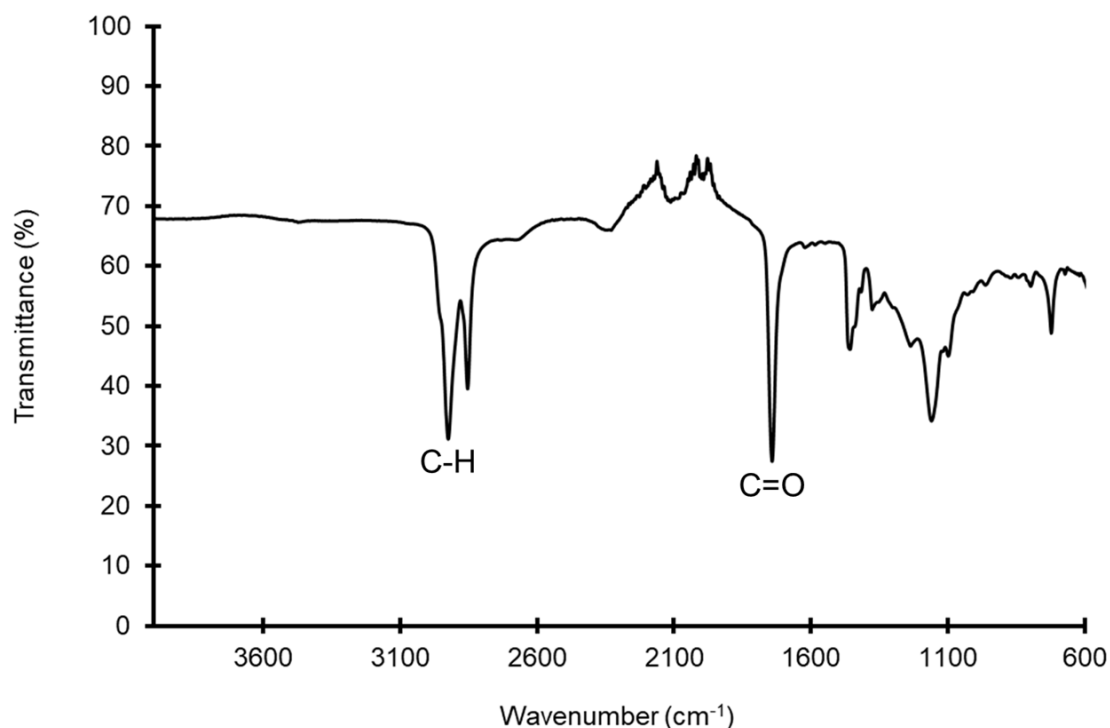
Figure 2.59: IR spectra of 50-poly-(S-*r*-canola). IR analysis of 50-poly-(S-*r*-canola) showed C=O stretching at 1742 cm^{-1} which corresponds to the triglyceride structure of the canola oil and was consistent with that previously reported.[81]

The STA analysis shows that the degradation of 50-poly-(S-r-canola) occurs over 2 steps. The first mass loss event has an onset temperature of 180 °C and continues to around 315 °C. This is followed by a second mass loss starting at 315 °C. Most of the second mass loss is over at around 500 °C. At this stage a total mass loss of 88 % has occurred. For the remainder of the DSC protocol (500 °C – 800 °C) an additional mass loss of only 4 % was observed.
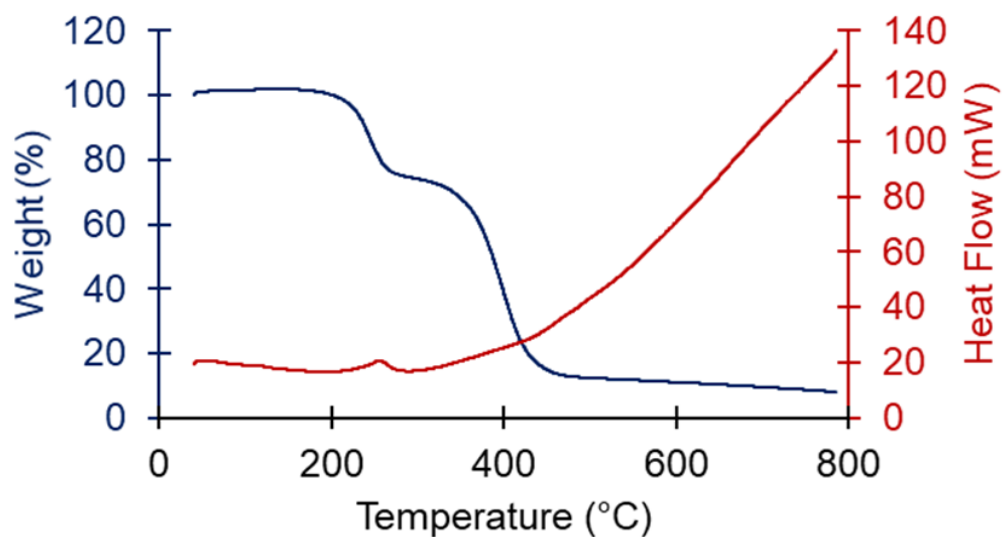
Figure 2.60: STA (DSC and TGA) of 50-poly-(S-r-canola) was consistent with that previously reported.[81]
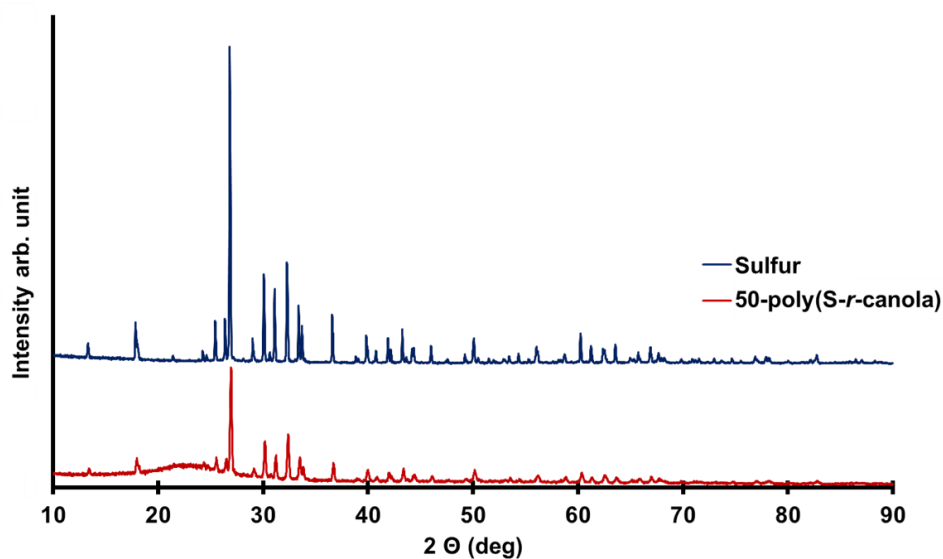
Figure 2.61: XRD analysis of 50-poly(S-*r*-canola) compared to sulfur showed similar peaks indicating that some free sulfur is embedded in the polymer.

Sulfur   Carbon   Oxygen
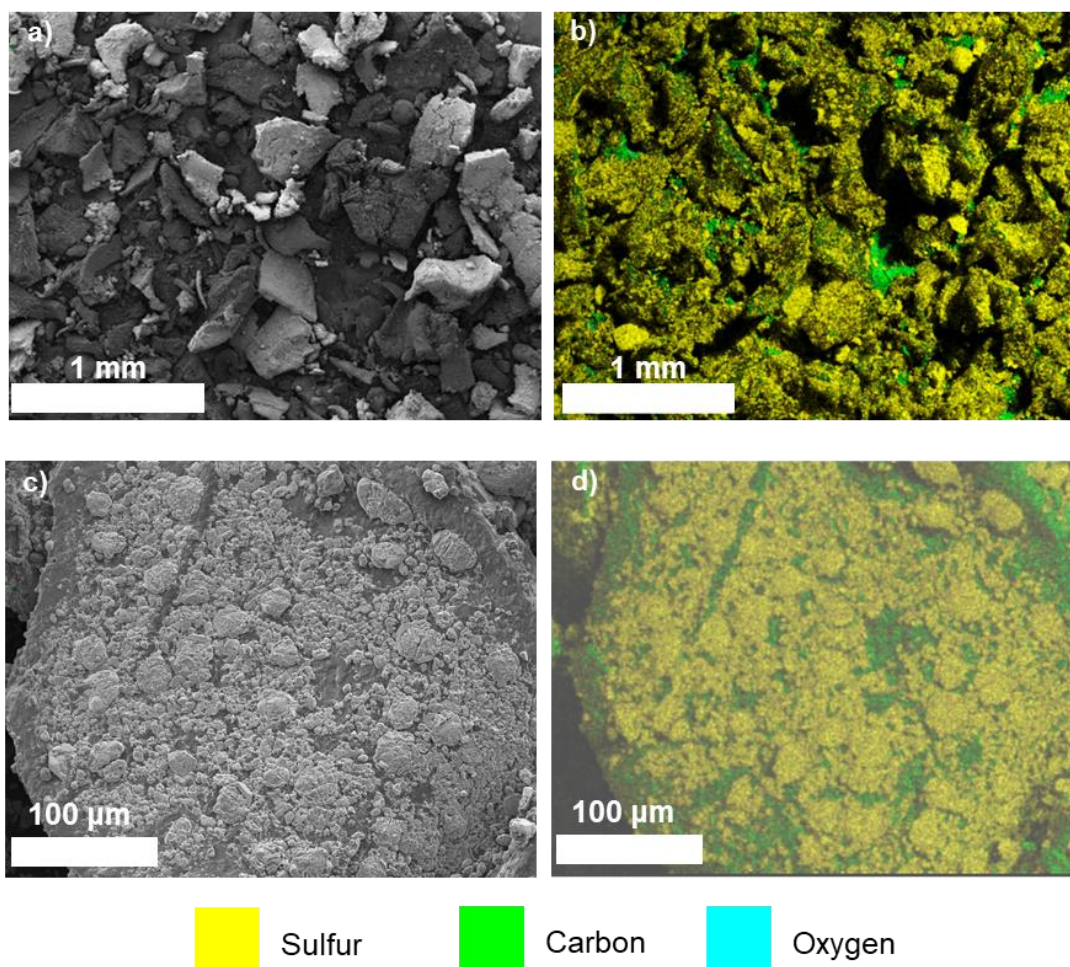
Figure 2.62: a) SEM micrograph of 50-poly(S-*r*-canola) at 100 × magnification. **B)** EXD elemental map of 50-poly(S-*r*-canola) at 100 × magnification. **C)** SEM micrograph of 50-poly(S-*r*-canola) at 800 × magnification. **D)** EXD elemental map of 50-poly(S-*r*-canola) at 800 × magnification.
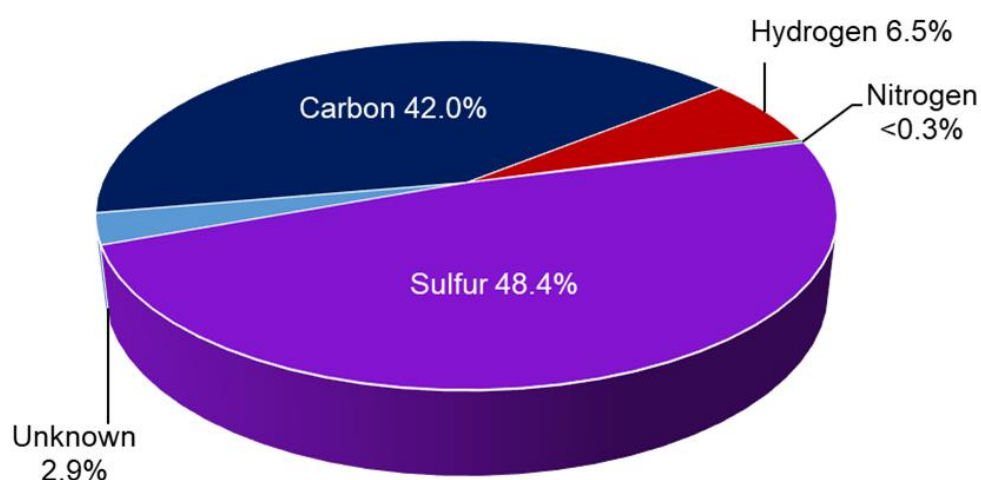
Figure 2.63: CHNS elemental analysis of 50-poly(S-*r*-canola).

Unless otherwise stated, the 50-poly(S-*r*-canola) polymer used for these experiments was sown into cotton teabags in 1 g portions. The same was done for 0.5 g of sulfur. This was done for easy collection of the polymer

For the kinetic uptake 1.9 mg of $HauCl_4 \cdot H_2O$ was dissolved in 200 mL of deionised water in order to give a 5 ppm Au^{3+} solution. The experiment was performed in triplicate and the samples were rotated end over end at 25 RPM. After the cotton bags containing 50-poly(S-*r*-canola) polymer or sulfur were added to the gold solutions (50 mL) a sample for analysis were taken every 2 hours for 10 hours. Each sample had the volume of 1.9 mL and was stabilised in 5% HCl. The samples were analysed using ICP-MS by Flinders Analytical.

To investigate what in what form the gold is found on the 50-poly(S-*r*-canola) polymer, 1 g of polymer in a cotton bag was placed in 40 mL of a 500 ppm gold solution and mixed end over end at 25 RPM for 24 hours. The gold solution was made by dissolving 153.9 mg of $AuCl_3$ in 200 mL of deionised water. The polymer was then recovered by removing it from the bag and drying it under high vacuum. SEM and EDX analysis was performed to confirm that gold had indeed hadbeen captured by the polymer.

For the ARXPS experiments the gold solution made above (500 ppm) was diluted to 1, 5, 25 and 250 ppm concentrations. A 40 mL sample of each concentration was prepared, and a 1 g 50-poly(S-*r*-canola) polymer bag was added to each solution. The solutions were then rotated end over end at 25 RPM for 24 hours. After that the polymers were recovered and vacuum dried. For ARXPS analysis each polymer sample was ground up and pressing into a molybdenum sample holder.

For the gold to mercury comparison experiment, a 5 ppm solution of Au^{3+} (from $HauCl_4$) and Hg^{2+} (from $HgCl_2$) was prepared. To three 50 mL aliquots of this solution 1 g of 50-poly(S-*r*-canola) polymer in a cotton bag was added and the samples were rotated end over end at 25 RPM. Samples for ICP-MS analysis were taken at 0, 2, 4, 6, 8 and 10 hours.

For the interfering metal experiment, the following metal salts and masses were used to make 200 mL solutions with a metal ion concentration of 5 ppm: $AuCl_3 \cdot 3H_2O$ (2.2 mg), $CuBr_2$ (3.5 mg), $FeCl_3$ (4.8 mg), $AlCl_3$ (4.9 mg), $ZnSO_4 \cdot 7H_2O$ (4.4 mg), As_2O_5 (7.7 mg), $Pb(NO_3)_2$ (8.0 mg), $Cd(NO_3)_2 \cdot 4H_2O$ (13.7 mg). The experiment was performed in triplicate. The 50-poly(S-*r*-canola) polymer bags were added to each solution and rotated end over end. Samples of 1.9 mL have been taken and stabilised in 5% HCl before testing. The samples were analysed using ICP-MS by Flinders Analytical.

Gold recovery

In order to determine if the oxidant solutions have any effect on the 50-poly(S-*r*-canola) polymer a 15 mL Ca(Ocl)$_2$ plus HCl solution was made by adding 100 mg of Ca(Ocl)$_2$, 0.138 mL of HCl and deionised water to make up a total volume of 15 mL. Also, a TCCA and NaBr solution was made by adding 108 mg of TCCA to 144 g of NaBr to deionised water to make up a total volume of 15 mL. To each solution 150 mg of polymer was added and left unagitated for 24 hours.
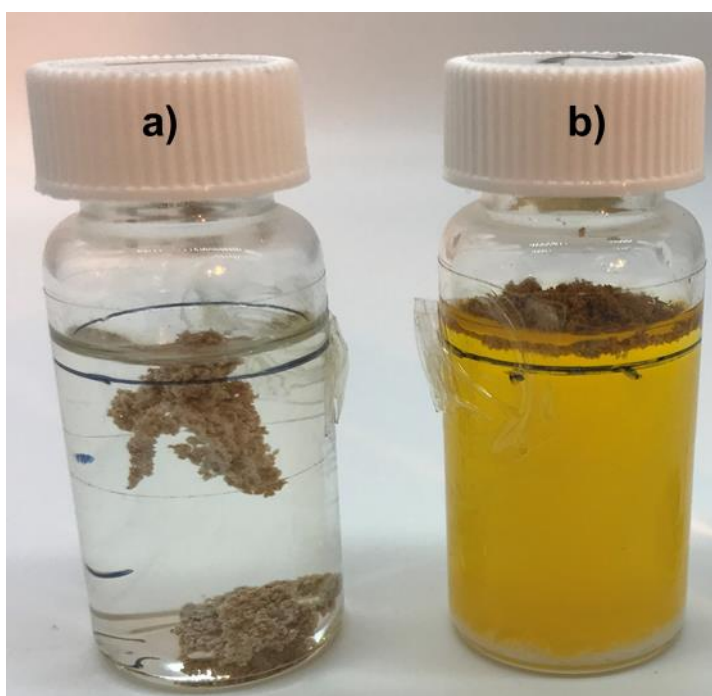
Figure 2.64: a) 150 mg of polymer in 15 mL of Ca(Ocl)$_2$ plus HCl solution and **b)** 150 mg of polymer in 15 mL of a TCCA plus NaBr solution after 24 hours.

Model gold recovery experiments

In order to determine the yield of gold recovery, three solutions containing TCCA plus NaBr and three solutions containing Ca(Ocl)$_2$ plus HCl were prepared. The TCCA plus NaBr solutions had a volume of 15 mL and contained 108 mg of TCCA and 144 mg of NaBr. The Ca(Ocl)$_2$ plus HCl solutions contained 100 mg of Ca(Ocl)$_2$ and 0.138 mL of HCl (each solution had a concentration of 186 mM of total halide, 50% halide from the pool chemical and 50% from NaBr or HCl). To each solution 50 mg of rectangular sheet gold was added.
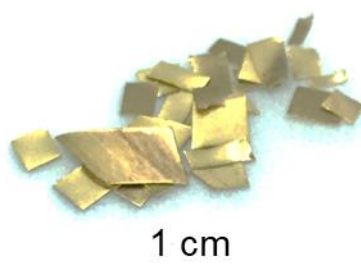
Figure 2.65: Gold sheet added to oxidising solutions.

The gold in the TCCA plus NaBr solutions had oxidised after 5 days and the gold in the Ca(Ocl)$_2$ plus HCl was oxidised after an additional 5 days. After all the gold had dissolved, 1 g of 50-poly(S-*r*-canola) polymer was added to each solution and the solutions were rotated at 20 RPM for 96 hours. Samples for ICP-MS analysis were taken before and after polymer addition and their gold concentration was determined.

Table 2.6: Gold concentration of 50 mg gold oxidation before and after 50-poly(S-*r*-canola) polymer addition as determined by ICP-OES analysis.

Solution	Oxidant	Gold concentration (ppm)		Gold removed (%)
		Before polymer	After polymer	
1	TCCA +NaBr	2860	186	93.5
2	TCCA +NaBr	2960	202	93.2
3	TCCA +NaBr	2840	192	93.2
4	Ca(OCl)$_2$ +HCl	2830	5.3	99.8
5	Ca(OCl)$_2$ +HCl	2760	3.5	99.9
6	Ca(OCl)$_2$ +HCl	2880	3.5	99.9

Then, the polymer was recovered by filtration and incinerated. Lastly, the product of incineration was weighed and characterised using SEM/EDX. From the gold concentration before and after the polymer addition the mass of gold on the polymer was calculated. This was used to determine the percentage of the recovered gold.

Table 2.7: Table of gold added to each solution and gold on polymer as well as percentage of recovered gold.

Solution	Oxidant	Gold added (mg)	Gold on polymer (mg)	Gold recovered (%)
1	TCCA + NaBr	49.4	46.1	95.4
2	TCCA + NaBr	50	47.0	93.5
3	TCCA + NaBr	49.7	46.8	94.2
4	Ca(OCl)$_2$ +HCl	49.7	49.6	99.8
5	Ca(OCl)$_2$ +HCl	50	49.9	99.89
6	Ca(OCl)$_2$ +HCl	50.2	50.1	99.9

As could be seen in the EDX elemental maps that showed mainly sodium, bromine, and calcium as contaminants. Since silver was used to coat the samples to render them conductive, silver can also be seen in the EDX elemental maps.
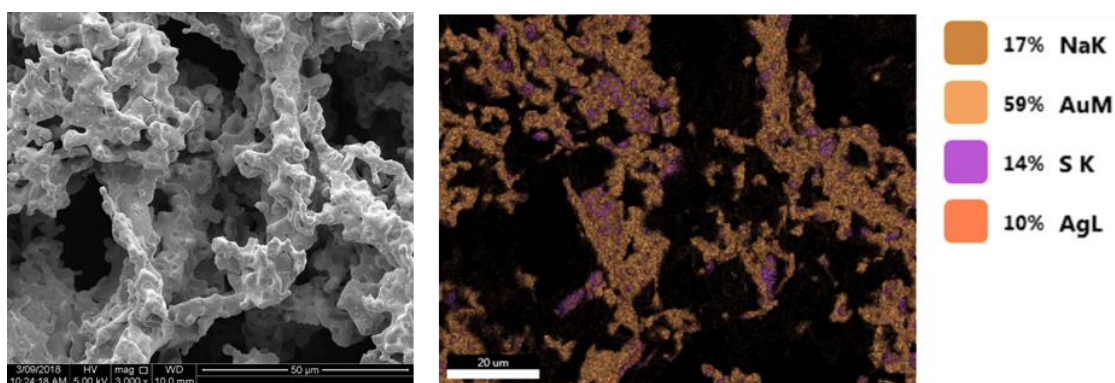
Figure 2.66: SEM micrograph and EDX elemental map of recovered gold from the first TCCA plus NaBr oxidation.
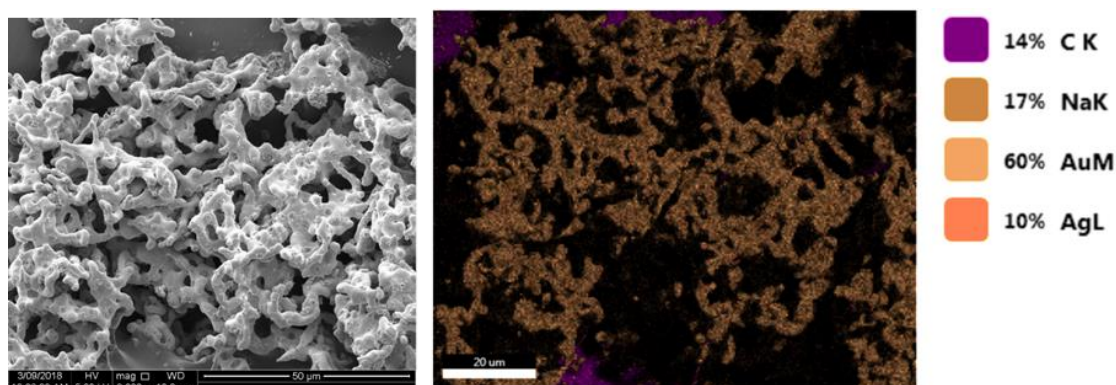
Figure 2.67: SEM micrograph and EDX elemental map of recovered gold from the second TCCA plus NaBr oxidation.
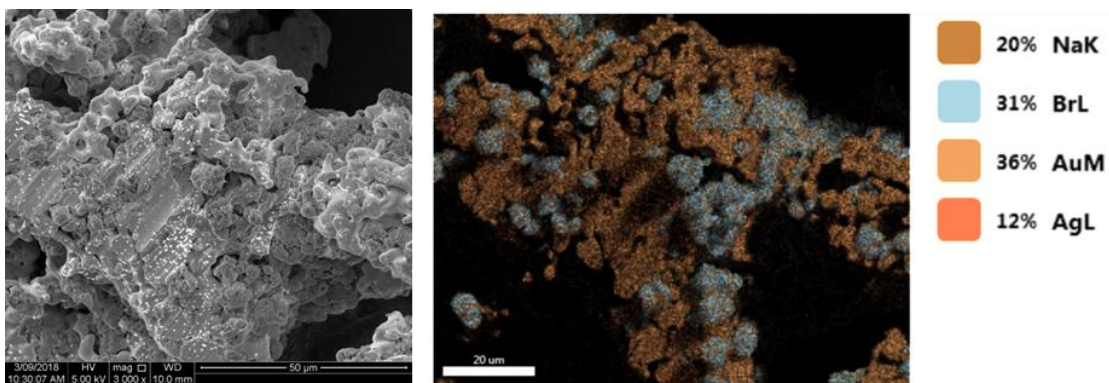
Figure 2.68: SEM micrograph and EDX elemental map of recovered gold from the third TCCA plus NaBr oxidation.
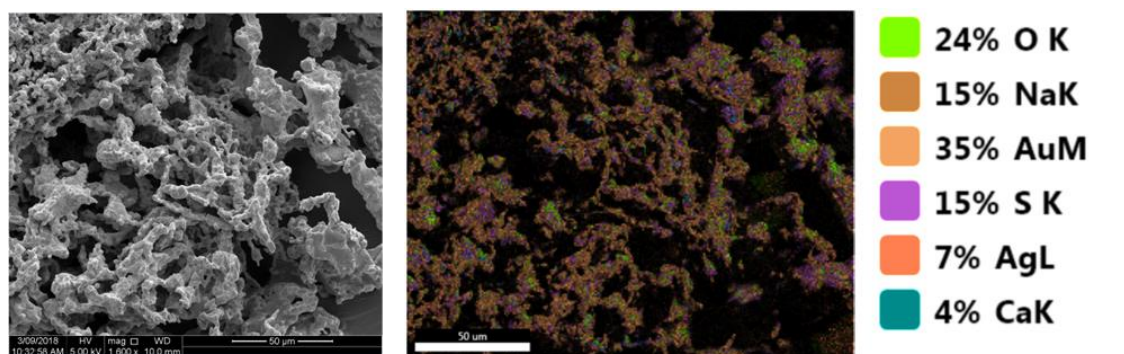
Figure 2.69: SEM micrograph and EDX elemental map of recovered gold from the first $Ca(Ocl)_2$ plus HCl oxidation.
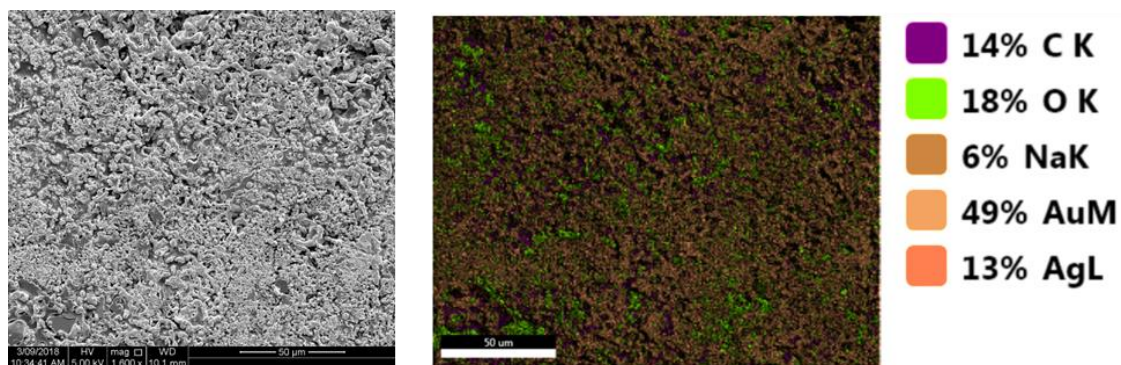
Figure 2.70: SEM micrograph and EDX elemental map of recovered gold from the second $Ca(Ocl)_2$ plus HCl oxidation.
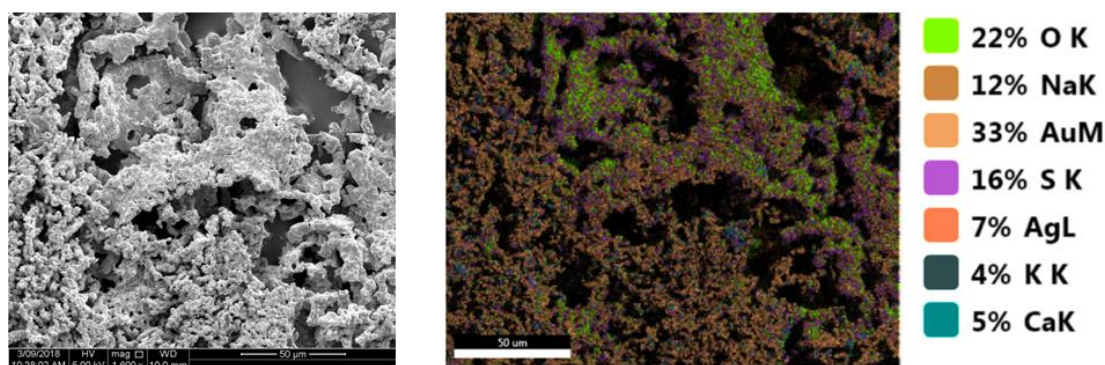
Figure 2.71: SEM micrograph and EDX elemental map of recovered gold from the third Ca(Ocl)$_2$ plus HCl oxidation.

In order the remove the contaminants, the samples were placed in 10 mL centrifuge tubes together with 10 mL of deionised water. After that the samples were sonicated for 20 minutes and finally put on and end over end rotator for 20 hours. Following that the water was removed, and the samples were dried by heating them in a crucible using a Bunsen burner. The purified gold samples were again analysed using SEM and EDX to ascertain of the contaminants were successfully removed. The purification was indeed successful since no contaminants were able to be seen. Since silver was used to coat the samples to render them conductive, silver can also be seen in the EDX elemental maps.
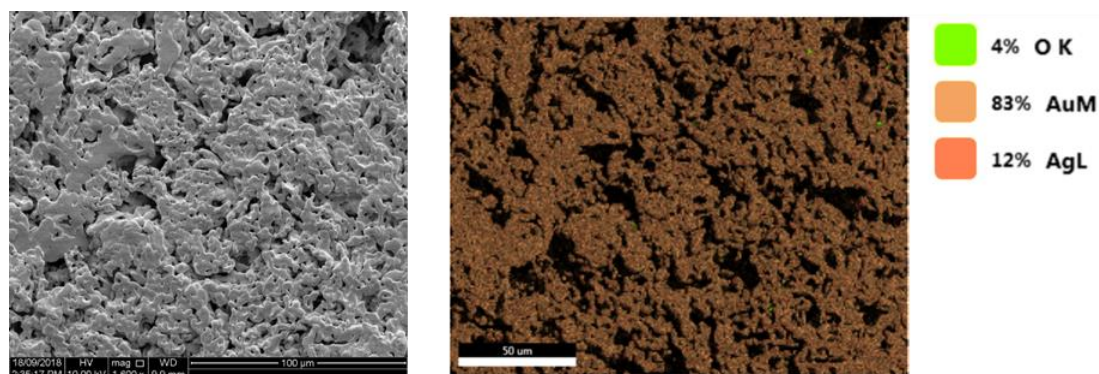
Figure 2.72: SEM micrograph and EDX elemental map of the purified gold from the first TCCA plus NaBr oxidation.

127
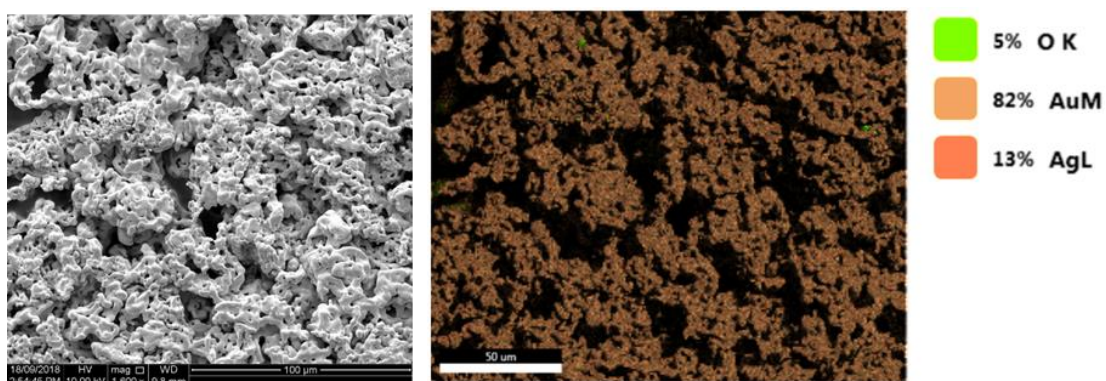
Figure 2.73: SEM micrograph and EDX elemental map of the purified gold from the second TCCA plus NaBr oxidation.
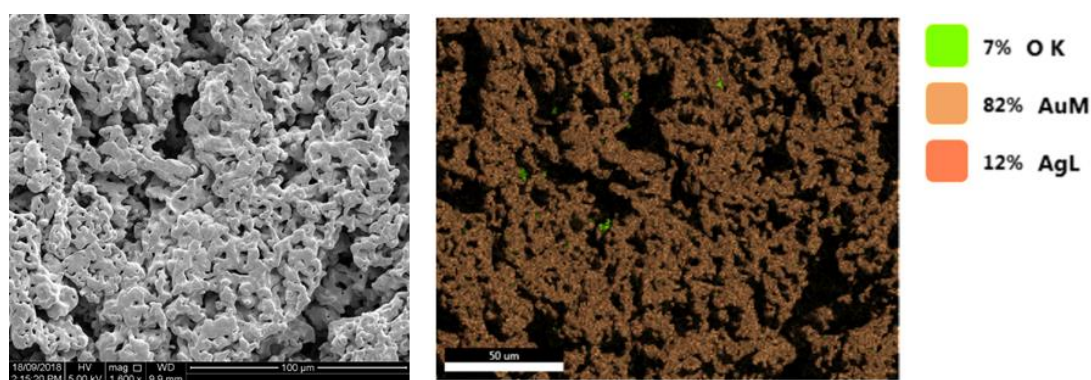
Figure 2.74: SEM micrograph and EDX elemental map of the purified gold from the third TCCA plus NaBr oxidation.
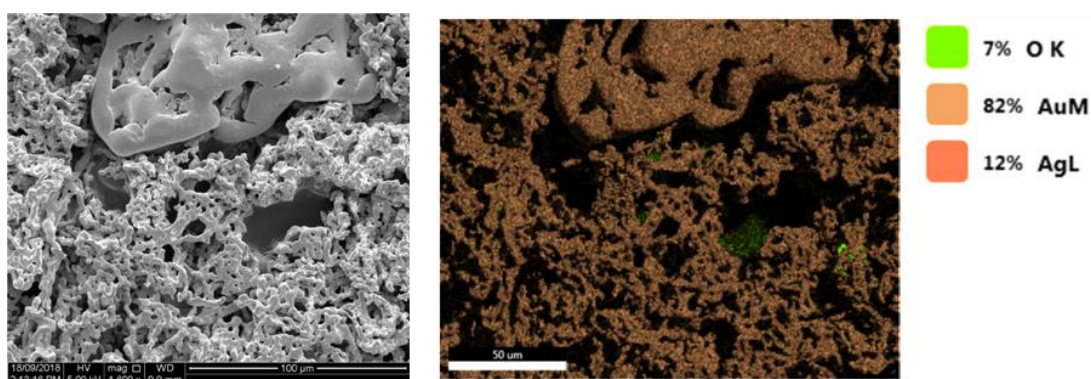
Figure 2.75: SEM micrograph and EDX elemental map of the purified gold from the first Ca(Ocl)$_2$ plus HCl oxidation.
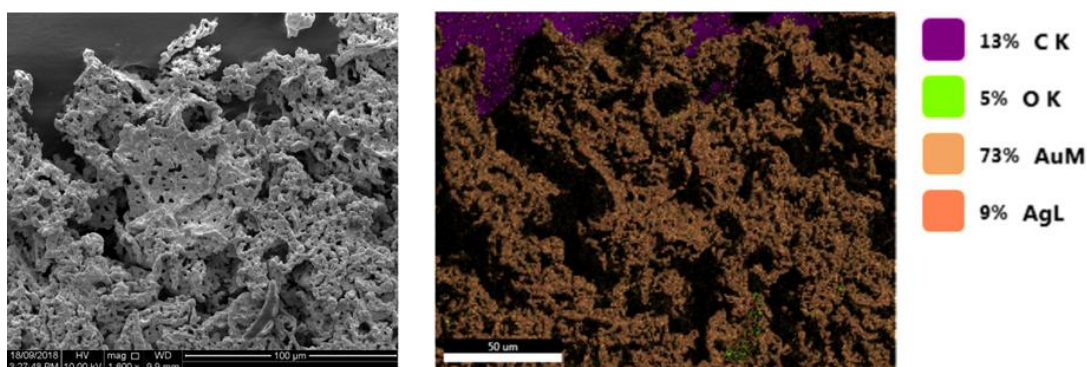
Figure 2.76: SEM micrograph and EDX elemental map of the purified gold from the second Ca(Ocl)$_2$ plus HCl oxidation.
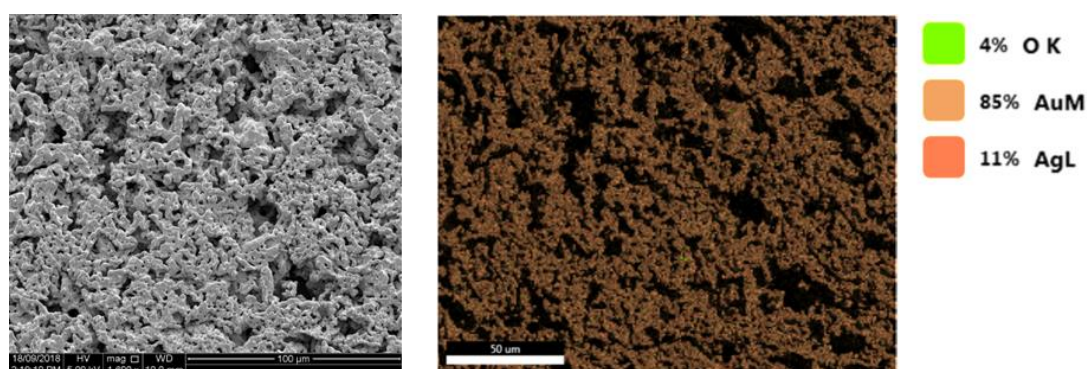
Figure 2.77: SEM micrograph and EDX elemental map of the purified gold from the third Ca(Ocl)$_2$ plus HCl oxidation.

Below is a representative sample of the purified gold.

Figure 2.78: Representative microscopy image of gold after the purification process.

To determine if the form of gold on the 50-poly(S-*r*-canola) polymer differs from when the gold is removed form a TCCA plus NaBr solution as compared to a $AuCl_3$ solution 50 mg of gold was oxidised. This was done by adding 50 mg of gold sheet to a 15 mL solution of deionised water, 108 mg of TCCA and 144 mg of NaBr. The solution was left undisturbed for 5 days after which all the gold had oxidised. Next, the solution was vacuum filtered. After that a polymer bag containing 1 g of polymer was added and rotated end over end at 25 RPM for 24 hours. After that the polymer was recovered and dried under high vacuum. Finally, the polymer was ground to a powder and pressed into a molybdenum sample holder before ARXPS analysis was performed.

Gold ore simulation

For the simulated ore experiment shale rock was collected from the university grounds and crushed using mortar and pestle to a particle size of 20 – 38 µm, which is commonly used according to a contact in the ASGM sector.
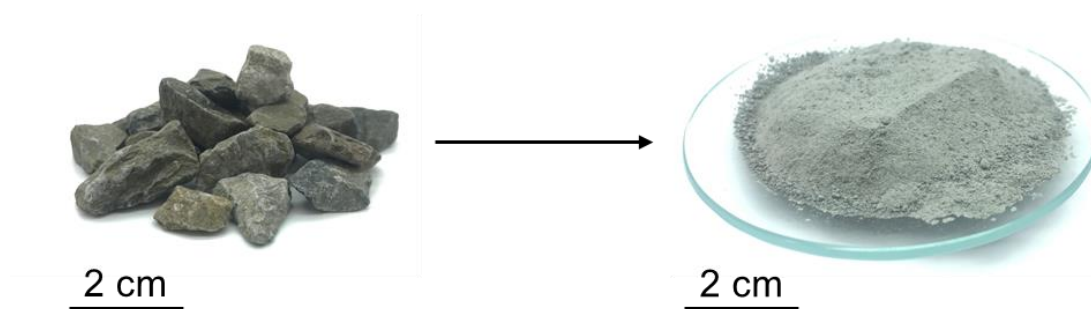
Figure 2.79: Image of shale rock that has been crushed to a particle size of 20 – 38 µm.

To test the gold oxidation of solutions containing rock and a known amount of gold, 6 solutions with a volume of 15 mL in deionised water were prepared. All solutions contained 20 mg of gold sheets and 1 g of crushed rock. Three solutions used TCCA (108 mg) plus NaBr (144 mg) as oxidant while the other three used $Ca(Ocl)_2$ (100 mg) plus HCl (0.138 mL) as oxidant. The solutions were put on end over end rotation at 20 RPM

The gold in the $Ca(Ocl)_2$ plus HCl oxidations had not been oxidised after 6 days and the pH of these solutions was found to be 5.25. Therefore, is as hypothesised that some form of carbonate might be present in the rock, reacting with the acid and neutralising it. Subsequent XRD analysis of the crushed shale rock confirmed the presence of calcium magnesium carbonate.
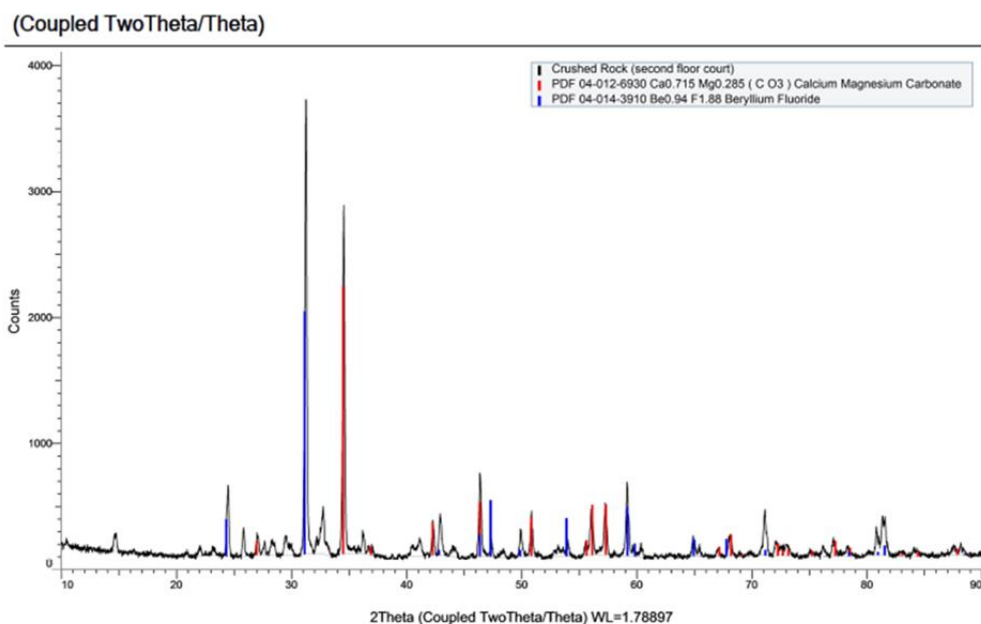
Figure 2.80: XRD spectra of the crushed shale rock matches the XRD pattern of calcium magnesium carbonate.

In order the acidify the $Ca(Ocl)_2$ plus HCl solutions another 100 mg of $Ca(Ocl)_2$ and 0.138 mL of HCl were added. Since the gold was already oxidised on the TCCA plus NaBr solutions, samples for ICO-MS were taken to determine the gold concentration. The gold concentration of these solutions was 1444 ± 25 ppm. In order to recover the gold 1 g of 50-poly(S-*r*-canola) polymer powder was added to each solution and rotated end over end at 25 RPM for 6 days. After that time the gold concentration of the solutions was 260 ± 12 ppm indicating that 82 % of gold has been removed. After that the polymers were removed by filtration and incinerated. Filtration was undertaken using a cotton cloth with a weave that would allow the rock particles to pass through while capturing most of the polymer. The masses of the incineration products were 89.2 mg, 71.3 mg and 70.3 mg. Hence, a large amount of contamination was present. This could also be seen in the incineration products which were not gold colored but had a light red color.

_1 cm_
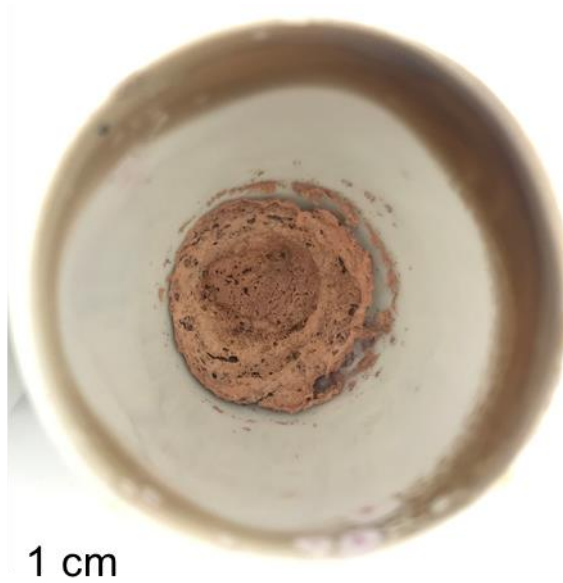
Figure 2.81: Representative sample of incinerated 50-poly(S-_r_-canola) polymer from simulated ore experiment (TCCA plus NaBr as oxidant).

SEM and EXD analysis was also performed on all the incineration samples. Since silver was used to coat the samples to render them conductive, silver can also be seen in the EDX elemental maps.

23% O K	
2% FeL	
2% NaK	
4% MgK	
8% AlK	
20% SiK	
5% AuM	
15% S K	
7% AgL	
15% CaK	
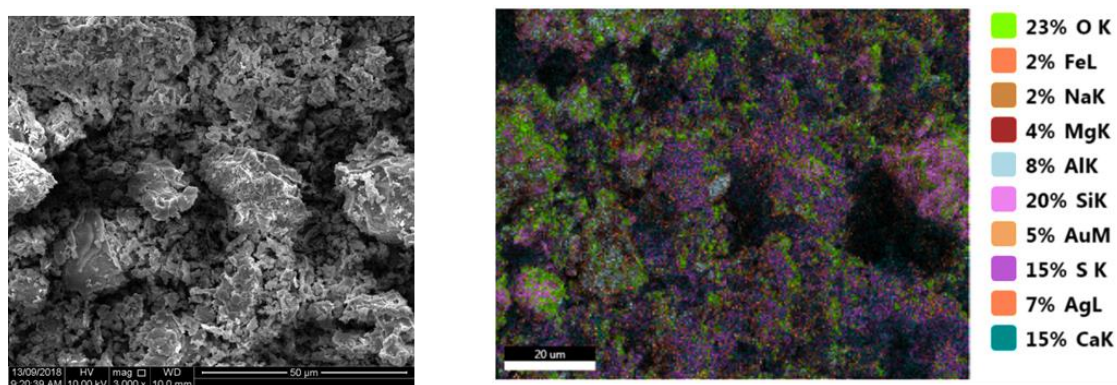
Figure 2.82: SEM micrograph and EDX elemental map of the incineration product of the first TCCA plus NaBr simulated ore oxidation

132
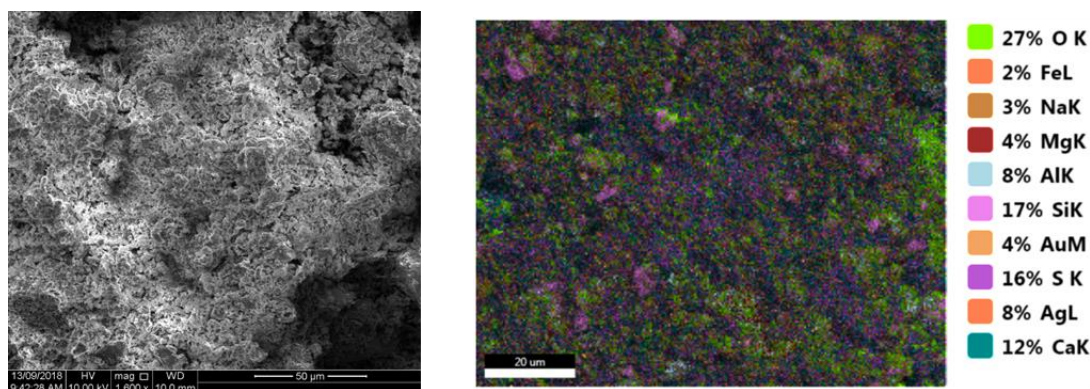
Figure 2.83: SEM micrograph and EDX elemental map of the incineration product of the second TCCA plus NaBr simulated ore oxidation.
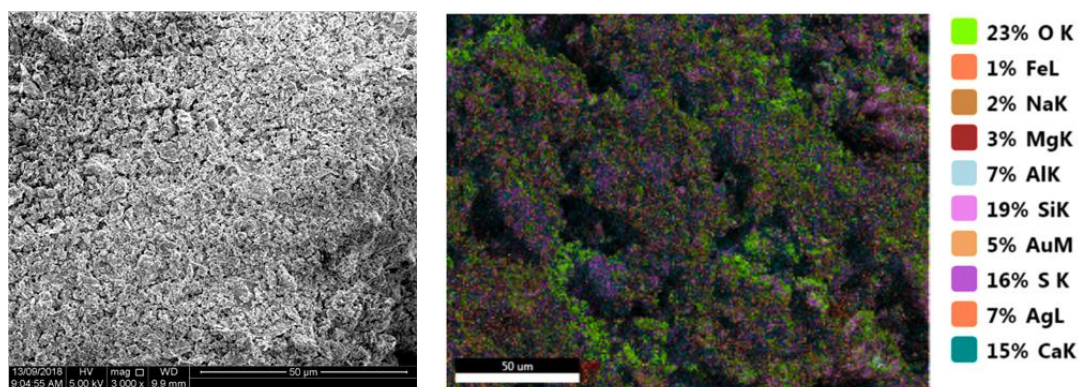
Figure 2.84: SEM micrograph and EDX elemental map of the incineration product of the third TCCA plus NaBr simulated ore oxidation.

The first $Ca(Ocl)_2$ plus HCl oxidation sample was filtered using vacuum filtration and laboratory filter paper, made up to a volume of 50 mL using deionised water before 1 g of 50-poly(S-*r*-canola) polymer as added . The sample was then rotated end over end at 25 RPM for 6 days. Samples for ICP-Ms analysis were taken at 25 hours and 6 days. The other two $Ca(Ocl)_2$ plus HCl oxidation samples were allowed to settle before 1 g of polymer sown into a cotton bag was added. The samples were left unagitated for 6 days with samples for ICP-MS analysis taken at 24 hours and 6 days.
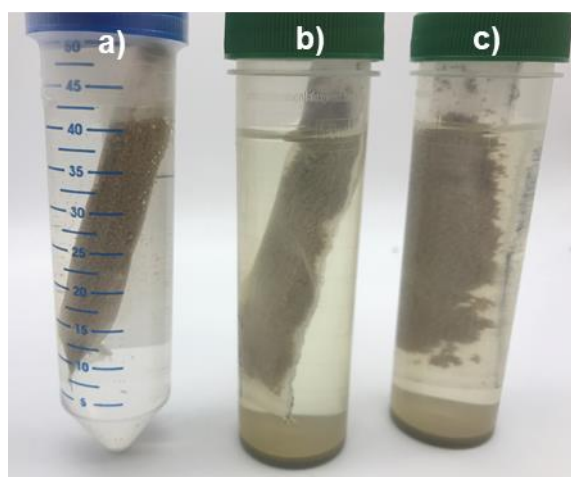
Figure 2.85: a) first Ca(Ocl)$_2$ plus HCl oxidation that was filtered after polymer addition, **b)** and **c)** second and third Ca(Ocl)$_2$ plus HCl oxidation which were unfiltered and left undisturbed after the polymer bag was added.

After that the cotton bags were removed and cut open to remove the polymer and incinerated. After the polymers were incinerated SEM and EDX analysis was performed on all of the samples. Since silver was used to coat the samples to render them conductive, silver can also be seen in the EDX elemental maps.

30% C K
9% NaK
50% AuM
12% AgL
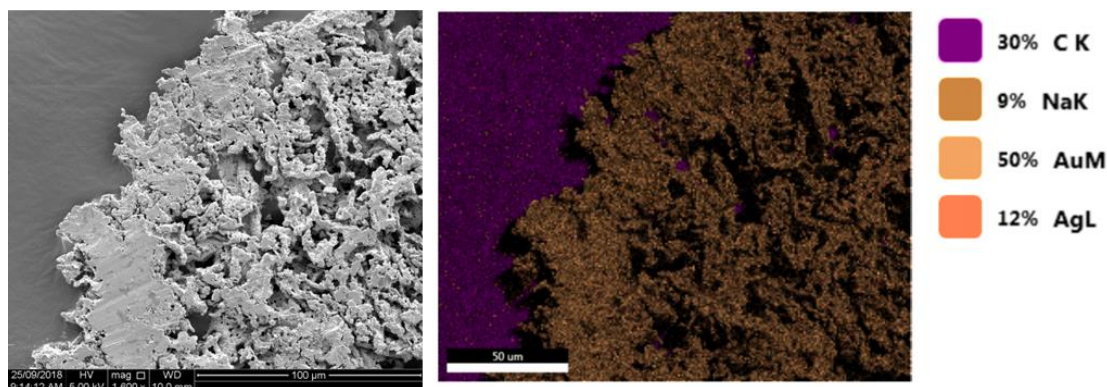
Figure 2.86: SEM micrograph and EDX elemental map of the incineration product of first Ca(Ocl)$_2$ plus HCl gold recovery which was filtered before the polymer bag was added.
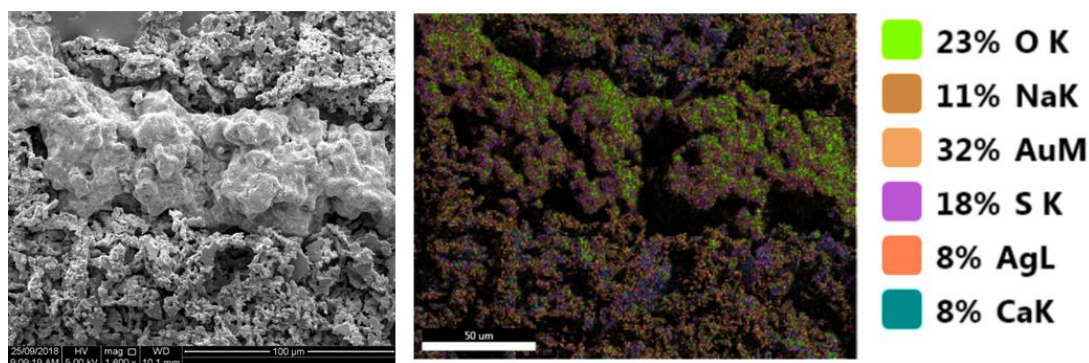
Figure 2.87: SEM micrograph and EDX elemental map of the incineration product of second Ca(Ocl)$_2$ plus HCl gold recovery which was left undisturbed after the polymer bag was added.
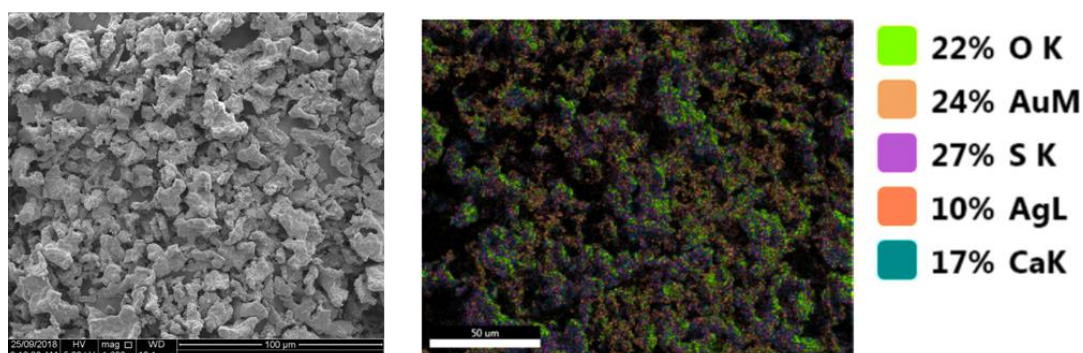
Figure 2.88: SEM micrograph and EDX elemental map of the incineration product of third Ca(Ocl)$_2$ plus HCl gold recovery which was left undisturbed after the polymer bag was added.

Small scale gold ore oxidation

Three 15 mL solutions in deionised water containing TCCA (108 mg) plus NaBr (144 mg) as well as three solutions using Ca(Ocl)$_2$ (100 mg) plus HCl (0.138 mL) as oxidant were prepared. To each solution 750 mg of crushed gold ore (20-38 μm particle size) was added. The solutions were then rotated end over end at 25 RPM for 8 days. After that the solutions were adjusted to a volume of 50 mL using deionised water.
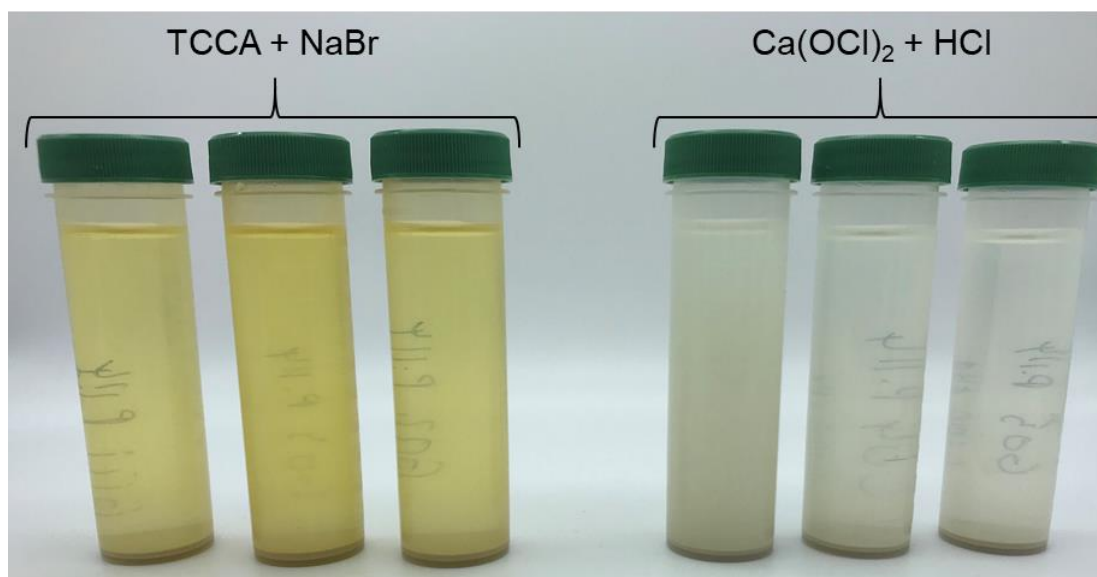
Figure 2.89: Oxidised gold ore solutions before polymer bag was added.

Next, a cotton bag containing 1 g of 50-poly(S-*r*-canola) polymer was added to each solution put on end over end rotation for 13 days. Samples for ICP-MS analysis were taken at day 0, 1, 7 and 13.

Oxidation optimisation

Oxidant concentration

In order to determine if an increased oxidant concentration also increases the rate of gold oxidations, solutions with various TCCA concentrations (16.6 mM, 83.5 mM and 166 mM) were made. All solutions were made up to a volume of 40 mL using deionised water. All solutions were made in triplicate.

Table 2.8: Oxidant concentrations and corresponding masses of TCCA and NaBr needed for a 40 mL solution.

TCCA conc.	16.6 mM	83.5 mM	166 mM
TCCA mass	0.155 g	0.775 g	1.55 g
Chloride conc.	0.05 mM	0.25 mM	0.5 mM
Chloride amount	2.00×10^{-3} moles	10.0×10^{-3} moles	20.0×10^{-3} moles
NaBr mass	0.206 g	1.02 g	2.06 g
Bromide conc.	0.05 mM	0.25 mM	0.5 mM
Bromide amount	2.00×10^{-3} moles	9.91×10^{-3} moles	20.0×10^{-3} moles
Gold Mass	5 mg	5 mg	5 mg
Gold amount	2.53×10^{-5} moles	2.53×10^{-5} moles	2.53×10^{-5} moles

All solutions were prepared in 50 mL plastic tubes. After the solutions were made, a 5 mg gold sheet was added to each solution. The solutions were left undisturbed until all the gold in the solutions was oxidised. In the 83.5 mM and 166 mM solutions the TCCA never fully dissolved.

Oxidation temperature

The next optimisation step focused on the oxidation temperature. For that purpose, two different temperatures were chosen, 45 °C and 80 °C. The same oxidant concentration as seen in Table 2.8.was used. Since the experiments were performed in triplicate a total 18 solutions with a volume of 40 mL were made in deionised water. Three samples for each oxidant concentration (16.6 mM, 83.5 mM and 166 mM) for each temperature (45 °C, 80 °C). After the solutions were made, 5 mg of gold sheet was added to each solution. The tubes were sealed and the samples for each temperature were bundled together using a rubber band. After that the samples were placed in a beaker filled with water heated to the corresponding temperature. The time by which the

gold had been fully oxidised (when gold was no longer visible) was recorded for each tube.

Figure 2.90: Samples bundled together in 45 °C water (left) and 80 °C water (right).

Table 2.9: Average oxidation time of 5 mg of gold on different oxidation concentrations and temperatures.

Temperature (°C)	TCCA conc. (mM)	Average oxidation time (hours)
	16.6	6.55
45	83.5	6.11
	166	7.5
	16.6	9
80	83.5	2.25
	166	2.25

In order to assess if sonication speeds up the oxidation process the following experiment was performed. Three solutions (45 mL) in deionised water were prepared containing 523 mg of TCCA and 695 mg of NaBr. To each solution 10 mg of gold was added. All solutions were placed in a sonicator which was preheated to 50 °C. The samples were sonicated for 8 hours by which time all the gold had been oxidised. At 1, 2, 4, 6 and 8 hour samples were taken for ICP-MS analysis.

Gas conversion of polysulfide incineration off gases

A retort was made so that the gases coming of a 50-poly(S-*r*-canola) polymer incineration can be passed through a solution of TCCA and water.
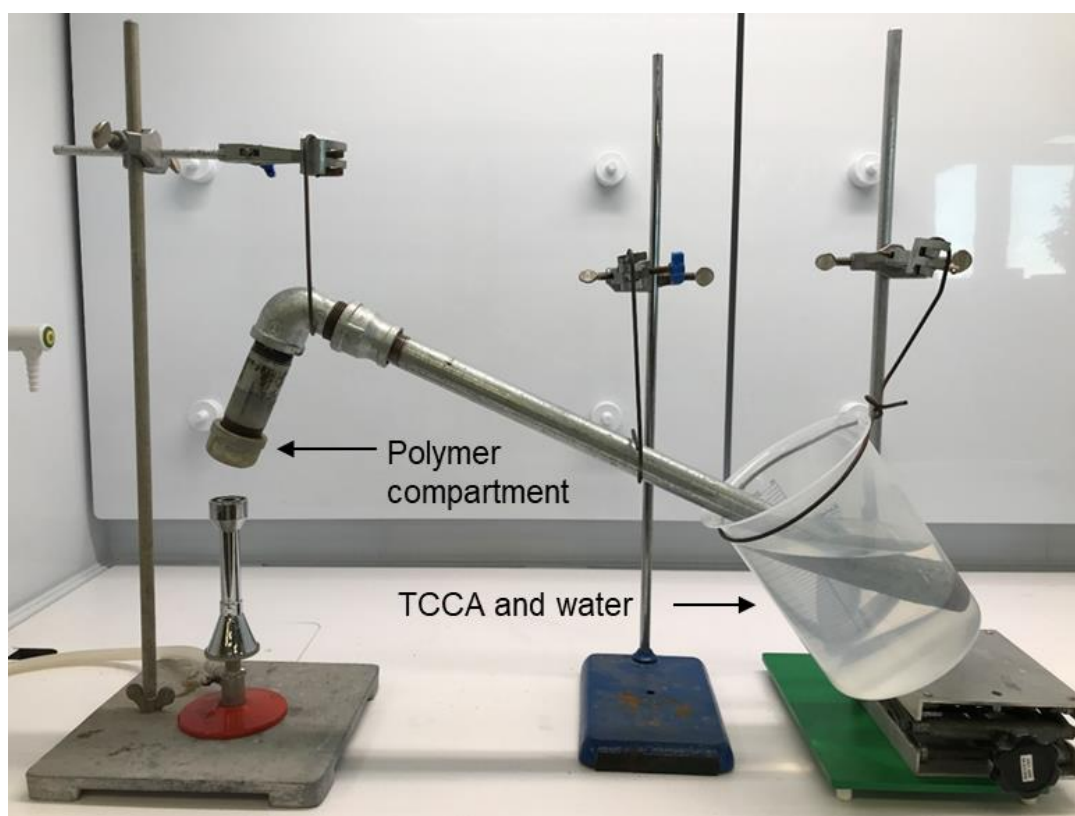
Figure 2.91: Retort set up to pass 50-poly(S-*r*-canola) polymer incineration gases through TCCA and water solution

For the experiment, 1 g of polysulfide was loaded into the polymer compartment. The mass of TCCA added to the water was calculated based on the moles of sulfur in

the polymer. To ensure enough TCCA was available to oxidise the off gases, a 5 to 1 molar ration of TCCA (89.47 g) to sulfur was chosen. The TCCA was added to deionised water and briefly stirred. After no more gas was observed, the solution was tested for sulphate using ion chromatography. The analysis was only quantitively to determine if conversion from sulfur dioxide to sulfates takes place. To do this, a standard solution containing 100 ppm of fluoride, chloride, bromide, nitrate, phosphate, and sulfate was prepared. Before the sample was run the standard solution was analysed to accurately determine the contents of the sample solution.
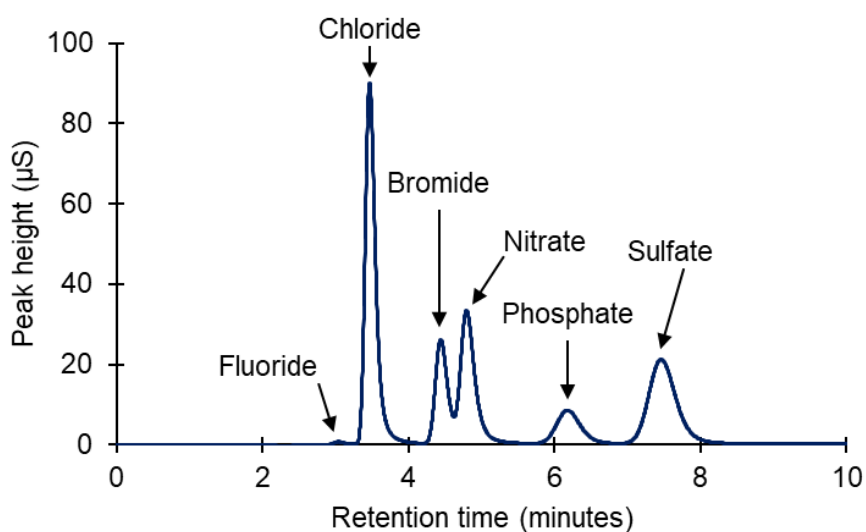
Figure 2.92: Ion chromatogram of a standard solution containing 100 ppm of fluoride, chloride, bromide, nitrite, phosphate and sulfate.

After the standard solution was run, the sample was analysed.
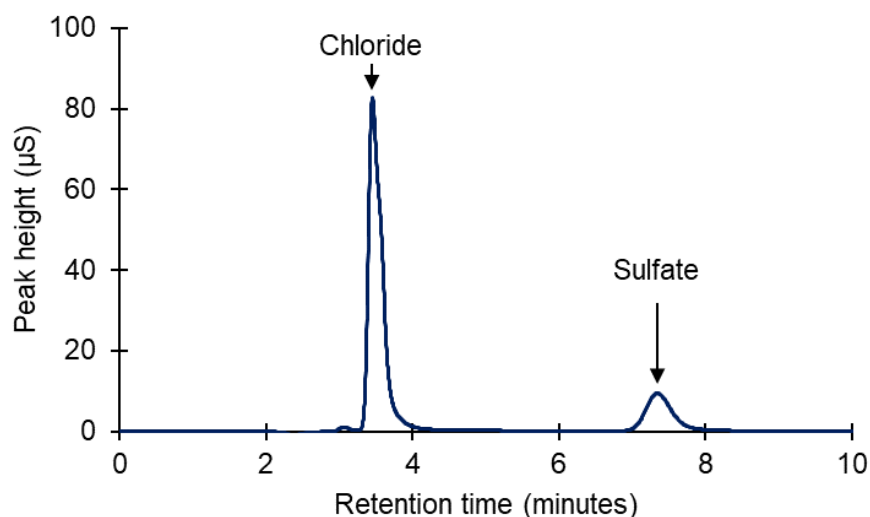
Figure 2.93: Ion chromatogram of the sample solution showing the presence of chloride and sulfate.

Battery sand oxidation and recovery

The first step was to get the ore assayed, for this an external commercial metallurgy laboratory was commissioned. This was done by firstly pulverising the sample using a ring mill so that 85 % of the sample particles are below 75 µm (P85 < 75µm). To determine the gold concentration fire assay was used. This was done by firstly adding a flux (sodium carbonate, borax, silica, lead oxide and carbon) to the sample. Next, the flux and sample mix were melted and the lead and the precious metals are collected in the slag in the form of a lead button. A furnace is than used to remove the lead to produce a metal prill. Using nitric acid, the silver is then removed from the prill leaving behind gold and platinum group metals. Following that, aqua regia is used to dissolve the remaining precious metals. Lastly, the dissolved metal solution is analysed using ICP-OES. For elements besides gold or platinum group metals a four-acid digest (hydrochloric acid, nitric acid, perchloric acid and hydrofluoric acid) or sodium peroxide fusion was used followed by ICP-OES analysis of the solution.

Table 2.10: Complete results of battery sand elemental assay.

Ag (ppm)	Al (ppm)	Au (ppm)	Ba (%)	Be (ppm)	Bi (ppm)
<2	6	1.72	0.05	<5	<10
Cr (ppm)	Cu (ppm)	Fe (%)	Hg (ppm)	K (%)	Li (ppm)
160	220	9.22	8.6	1.03	45
Pb (ppm)	S (%)	Si (%)	Sr (ppm)	Ti (%)	V (ppm)
180	1.44	26.8	108	0.69	232
Mg (%)	Mn (%)	C org (%)	Ca (%)	Cd (ppm)	Co (ppm)
2.07	0.12	0.09	2.89	5	50
Y (ppm)	Zn (ppm)	Mo (ppm)	Na (%)	Ni (ppm)	P (ppm)
15	404	<5	1.52	60	700

For the oxidation, 2L of water were added to a 5 L plastic bucket together with 200 g of ore. To remove the magnetic material from the ore, magnets were placed in plastic bags and tied to the impeller. The solution was then stirred to 5 minutes at 100 RPM. After that the magnets were removed, and the oxidants were added. To make a 0.25 M TCCA solution 120 g of TCCA was used and to make a 0.45 M NaBr solution 93 g of NaBr was used. The solution was then stirred for 24 hours at 250 RPM. After that, a sample of the solution was analysed using ICP-OES. For this analysis an external calibration was used. However strong matrix effects could be observed likely due to the high concentration of TCCA and NaBr. This matrix effect could be observed in the recovery of the internal standard used as part of the quality control of the analysis. As internal standard indium or yttrium was used. The recovery of the internal standard should be between 80%-120% to produce accurate results. However, the recovery rate dipped below 60%.
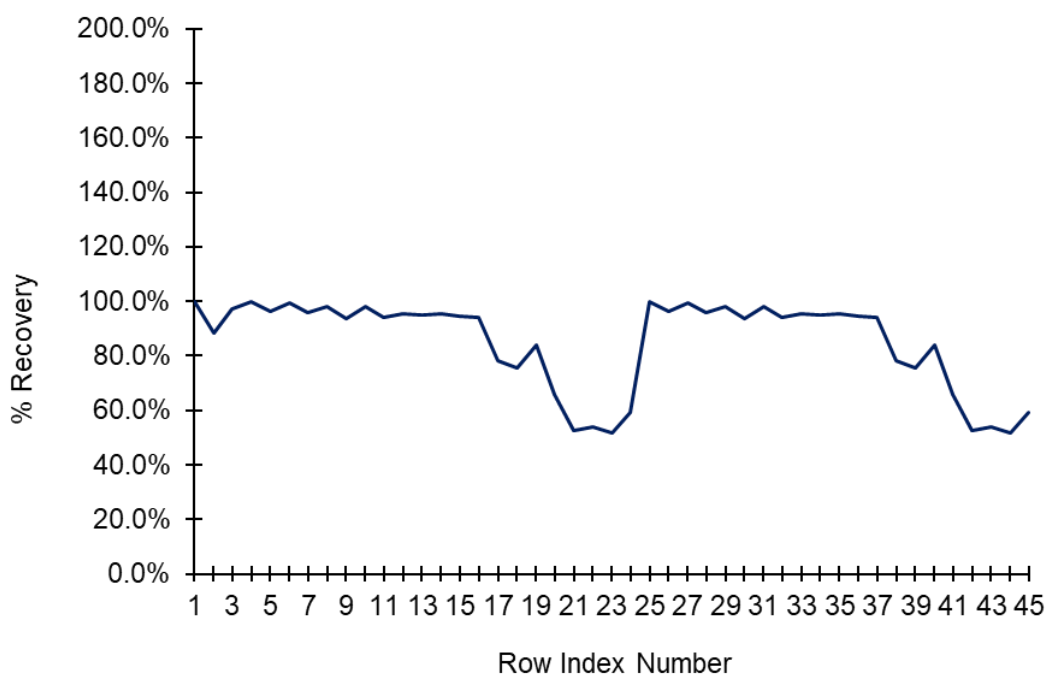
Figure 2.94: Internal standard of ICP-OES analysis of battery sand leach.

To eliminate matrix effects the standards were made in a matrix solution of TCCA and NaBr. To do this a 1L solution of 0.25 M of TCCA and 0.45 M NaBr (the same concentrations as for the leach solution) was made and left overnight. The next day the solution was filtered. The next analysis still showed matrix effects. These were likely due to too higher concentrations of TCCA and NaBr in the matrix solutions. Since some of the oxidant is lost during the leach, the concentrations of the oxidants sample solution would be lower after the leach then before. For this analysis the best results were achieved by TCCA concentration of 0.03 M and a NaBr concentration of 0.06 M in the matrix solution. Using this matrix solution, the internal standard recovery was between 100% and 79 %.
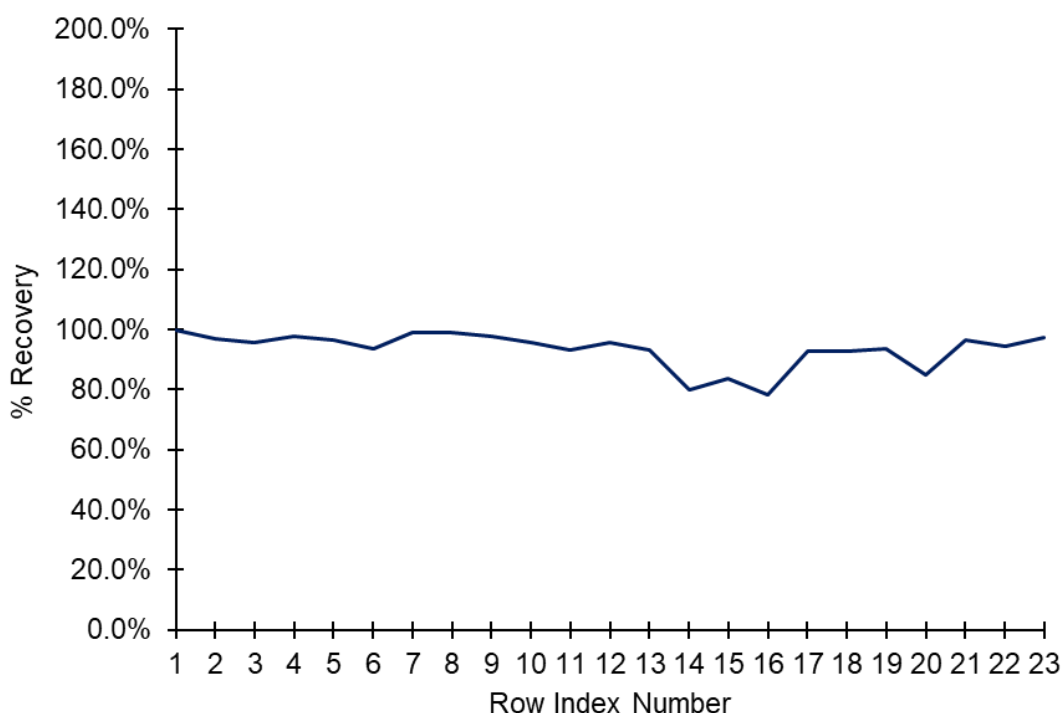
Figure 2.95: Internal standard of ICP-OES analysis of battery sand leach after using matrix solution to prepare external calibration.

However, the optimal concentration to suppress matrix effects varied from sample to sample and was adjusted for each sample accordingly. After the leach process, the battery sand samples had to be removed from the solution. This was done by first allowing the sands to settle and by decanting the solution on top of the sands. After that the sand were filtered using vacuum filtration and laboratory filter paper. During the filtration, 1.25 L of water was used to rinse the ore. Hence, the total volume of the leach solution before the polymer was added was 3.25 L. After that, 5 g of polymer was added and dispersed by briefly stirring the solution at 300 RPM. Next, the solution was stirred at 150 RPM for 24 hours. After that the polymer was left in the solution without stirring.

Gold removal from 5 ppm gold solution in oxidant matrix

In order to test if the 50-poly(S-*r*-canola) polymer is able to remove gold from solution with very low gold concentrations, the following experiment was performed. This

144

experiment was performed in triplicate. Firstly, 50 mg of gold sheet was oxidised by adding the gold together with 582 mg of TCCA (0.25 M), 1390 mg of NaBr (0.45 M) and 30 mL of deionised water to a plastic tube. After the solutions were left on end over end rotation at 25 RPM for 2 days all the gold had been dissolved. This gold solution had an estimated gold concentration of 1666 ppm based on the volume of the solution and the mass of gold used. Next three solutions with a gold concentration of 5 ppm were made. This was done by adding 90 µL of the stock gold solution to 30 mL of deionised water. Additionally, to each solution 582 mg of TCCA and 1390 mg of NaBr was added to increase their concentration to those used in the battery sand oxidation. Next, 1 g of polymer was added to each solution and the solutions were rotated end over end at 25 RPM for 6 days. Samples of all solutions for analysis by ICP-OES were taken before the polymer addition and after 6 days. The result shows over 99.9% of gold was removed from each sample.

Alternative gold recovery pathways

As alternative gold recovery pathways reduction by ascorbic acid, oxalic acid, sodium bisulfite and sodium metabisulfite was considered. Hence concentrated solutions of each were prepared.

Table 2.11: Volume and concentration of reducing agents prepared.

Reducing agent	Volume (mL)	Concentration (M)	Notes
Ascorbic acid	200	1	
Oxalic acid	200	0.7	1 M solution not possible because of limited solubility
Sodium bisulfate	200	1	
Sodium metabisulfite	200	1	

A concentrated gold solution was also prepared. This was done by adding 531.1 mg of gold sheet to a solution containing 300 mL of deionised water, 9 g of NaBr and 6 g of TCCA in a plastic bottle. The bottle was then placed in a rocker that rolled the bottle from side to side at a speed of 10 times per minute. After two days all the gold had dissolved, and the solution was gravity filtered using laboratory filter paper. The

approximate gold concentration was 1770 ppm which was calculated from the mass of gold and the volume of solution. A sufficient amount of gold solution had to be used so that any reduced gold could be clearly seen. A volume of 50 mL was used for each reaction, which amounts to approximately 88.5 mg of gold in each aliquot of solution.

Next, 50 mL of gold solution was added to each of four round bottom flasks. To each of these solutions 50 mL solution of a reducing agent was added and stirred at 250 RPM using a magnetic stirrer bar. Precipitate was only observed in the ascorbic acid reaction.

Figure 2.96: Precipitate as seen at the bottom of the ascorbic acid reaction,

The precipitate was recovered using vacuum filtration and analysed using SEM and EDX was used to analyse the precipitate of the ascorbic acid reaction.
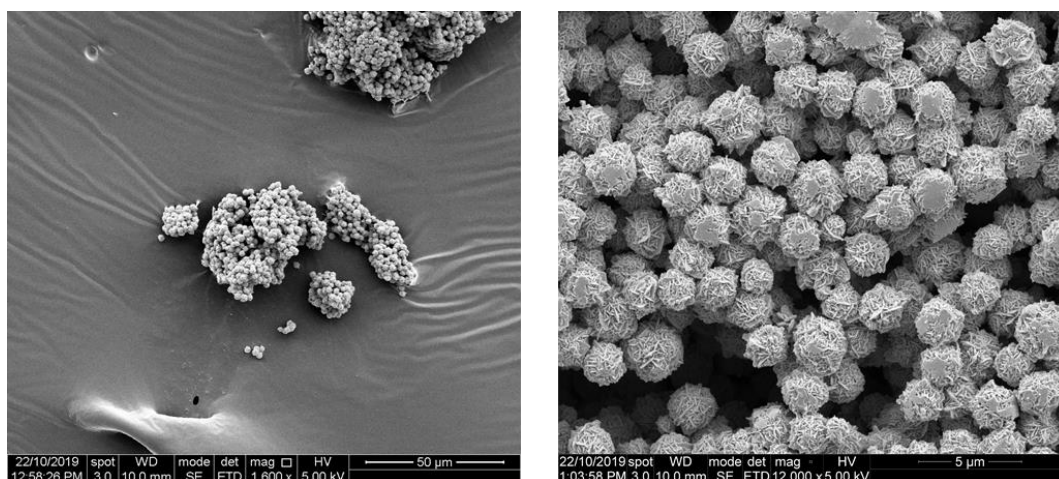
Figure 2.97: SEM images of ascorbic acid precipitate at 1600 × magnification (left) and 12000 × magnification (right).

Lastly, hydrogen as was used as a reducing agent. To do this 50 mL of gold solution was placed in a 100 mL round bottom flask and fitted with a septum. A balloon was filled with hydrogen gas and bubbled thought to gold solution with a needle. A small needle was used as an outlet to ensure gas flow. Whenever the balloon was empty it was replaced with a full one. This was done for two hours. After that time the solution turned darker, and a dark precipitate was seen. The precipitate was recovered using vacuum filtration and analysed using SEM and EDX.
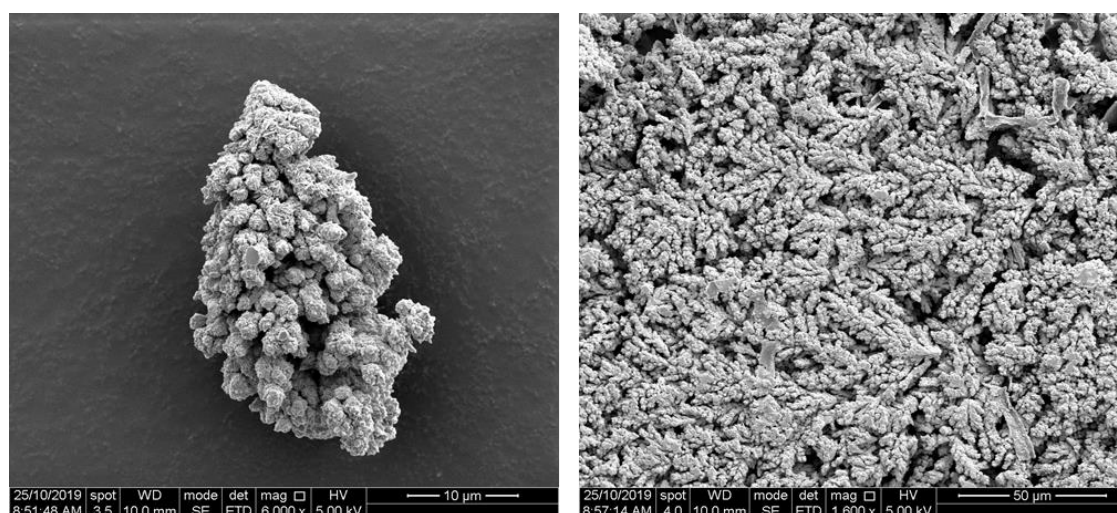
Figure 2.98: SEM micrographs of hydrogen reaction precipitate. On the left a smaller piece is seen whereas on the right a portion of a larger piece of the precipitate is shown.

147

Low grade ore concentrate oxidation and gold recovery

Firstly, a 200 g sample of the supplied ore was analysed by an external metallurgy laboratory as has been described earlies (Table 2.12).

Table 2.12: Assay of the low-grade ore concentrate.

Ag (ppm)	Al (%)	Au (ppm)	Ba (%)	Be (ppm)	Bi (ppm)
6	3.86	75.3	0.27	<5	<10
Cr (%)	Cu (ppm)	Fe (%)	Hg (ppm)	K (%)	Li (ppm)
0.11	156	19.3	3.1	0.9	15
Pb (ppm)	S (%)	Si (%)	Sr (ppm)	Ti (%)	V (ppm)
295	0.08	25.5	50	0.93	158
Mg (%)	Mn (%)	C org (%)	Ca (%)	Cd (ppm)	Co (ppm)
0.23	0.62	0.11	0.16	<5	85
Y (ppm)	Zn (ppm)	Mo (ppm)	Na (%)	Ni (ppm)	P (ppm)
155	224	10	2940	60	1200

Next, 4 kg or ore and 2 L of deionised water were placed in a 5 L bucket. To remove as much magnetic material as possible magnets were used. This was done by placing magnets in plastic bags and tying them around the stirrer bar. The stirrer bar with the magnets attached was then lowered into the water and ore mixture and mixed for 2 hours at 130 RPM. After that, the magnetic material was seen around the magnet. The magnetic material was removed, and the process repeated but with only 30 minutes of stirring.

Figure 2.99: Magnetic material stuck to the magnets attached to the stirrer bar.

After that 23.2 g of TCCA and 3.8 g of KBr were added to the solution to give a 0.05 M TCCA solution and a 0.015 M KBr solution. The sample was then stirred at 200 RPM for 4 days. The gold concentration was monitored using AAS. This was done since AAS can be used for solutions with high gold concentrations. To combat matrix effects an external calibration in a TCCA plus KBr matrix was using similar then was done for ICP-OES analysis. Since the gold concentration after 4 days was only 67 ppm out of the expected 150 ppm another 23.2 g of TCCA was added. After an additional 3 days the gold concentration had reached 156.5 ppm and the leaching process was completed. The leach solution was then filtered using vacuum filtration and laboratory filter paper. Further the ore was rinsed with a total of 1.5L deionised water. Taking this dilution into consideration the gold concentration should have been 86 ppm. The actual concentration, however, was only 79.7 ppm. This meant that 7.32% of gold have been lost during the filtration process After this process the now 3.5 L of leachate was again added to a 5 L bucked to which 10 g of 50-poly(S-*r*-canola) polymer was added. The solution was then stirred at 200 ppm. After stirring for 1 day the gold concentration had only been reduced to 77.8 ppm, a 2.38% reduction. Hence another 10 g of polymer was added. After an additional 2 days of stirring 42.5% if the gold has been removed, leaving 45.79 ppm of gold in the solution. Next, another 10 g of polymer was added and stirred for an additional 3 days. After that time the gold concentration was reduced to 27.85 ppm or 34.94% of the original concentration. An additional 10 g of polymer was added, and

the solution was stirred for 3 days. After a total of 6 days and 40 g of polymer the gold concentration was 5.5 ppm indicating that 93.1% of gold had been removed. Next, the polymer was incinerated resulting in 384.3 mg of brown powder with the expected mass of recovered gold to be 280 mg. The difference is most likely due to other metals or salts left over after the incineration. Analysis using SEM and EDX confirmed that gold and other elements are present in the incineration product.
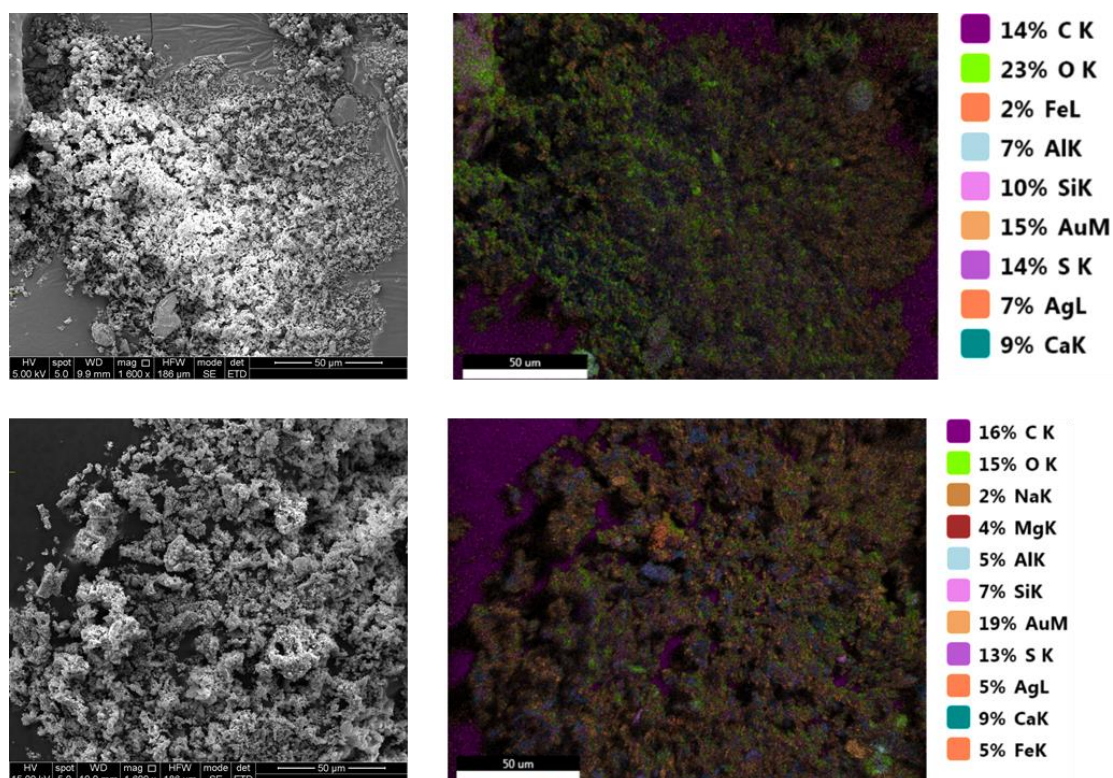
Figure 2.100: SEM micrograph (left) and corresponding elemental map (right) of incineration product.

Comparison of ore panning and ore oxidation

To determine if the panning technique is effective, 300 g of battery sands were spiked with 22.4 mg of finely cut up pure gold sheet. After panning the 300 g of sand 12.1 mg of gold was recovered which is only a 54% recovery rate. For the panning a "Garretts's gravity trap" pan was used.

Figure 2.101: Pan used for gold panning.

Hence, another 300 g of battery sands were spiked with 27 mg of gold and panned. This time 24.8 mg (91.8%) were recovered. Having established a suitable panning technique, 300 g of ore was panned. Of the 22.5 mg of estimated gold only 0.469 mg (2.08%) were recovered. The 246 g of ore left over from the panning experiment was treated with the oxidising agents TCCA plus KBr. To do that the concentrates were added to a 5 L plastic bucket together with 150 mL of deionised water. Using magnets, the magnetic material was removed. Next, 5.25 g of TCCA (0.15 M) and 0.285 g of KBr (0.015 M) was added. The solution was then stirred for 24 hours at 320 RPM. AAS analysis revealed a gold concentration of 113.48 ppm. The estimated gold concentration was 123 ppm, so an additional 1.76 g of TCCA was added and the solution (to increase the TCCA concentration by 0.05 M) was stirred for a further 24 hours. Subsequent AAS analysis put the gold concentration at 174 ppm of gold.

After the solution was vacuum filtered, 2.5 g of 50-poly(S-*r*-canola) polymer was added, and the solution was stirred at 320 RPM for 24 hours. After that time the gold concentration was 141.8 ppm. Hence, an additional 2.5 g of polymer was added and stirred for 24 hours. This was repeated until the gold recovery was satisfactory. To achieve that, a total of 9.5 g of polymer was added over 8 days, resulting in a final gold concentration of 5.4 ppm indicating that 96.9% of gold has been removed.

After that the polymer was separated by vacuum filtration and incinerated in a crucible using a Bunsen burner. SEM/EDX analysis revealed the presence of gold in the incineration product.
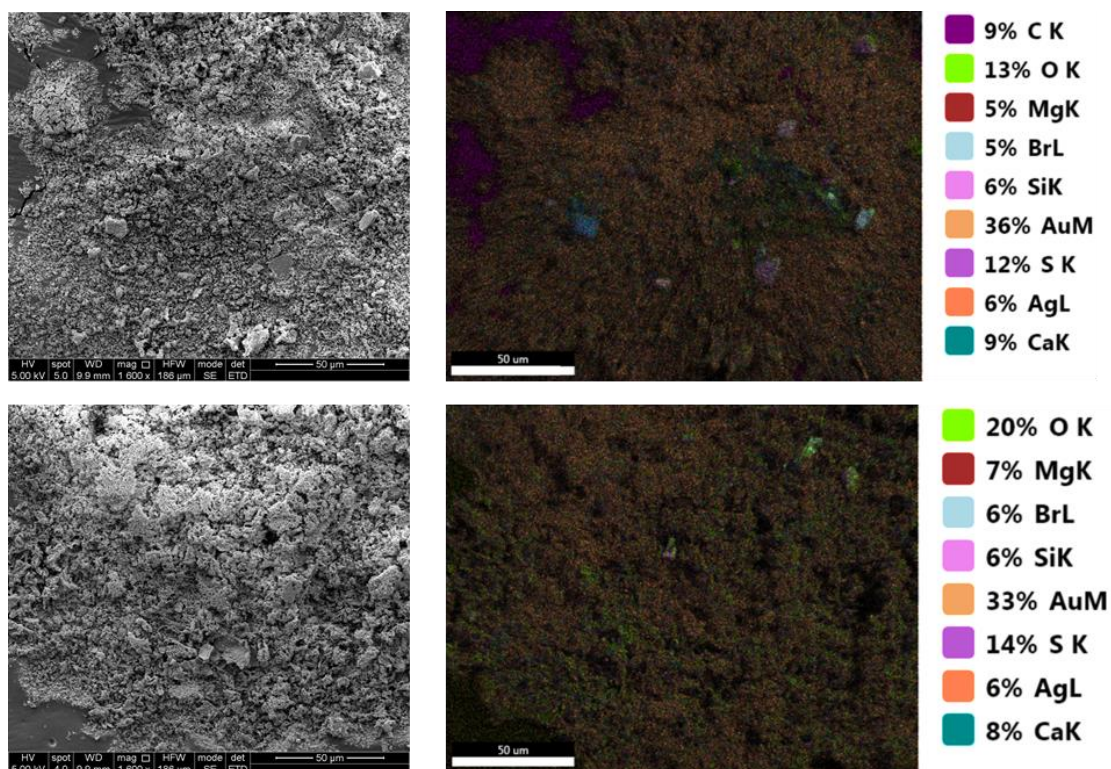
Figure 2.102: SEM micrographs (left) and EDX elemental maps (right) of the incineration product.

Determination of other leachable elements.

A 100 kg batch of ore was received and analysed by an external laboratory as described previously.

Table 2.13: Assay of 100 kg ore showing the concentration of various elements found in the ore.

Ag (ppm)	Al (%)	Au (ppm)	Ba (%)	Be (ppm)	Bi (ppm)
<2	5.87	40	425	<5	<10
Cr (ppm)	Cu (ppm)	Fe (%)	Hg (ppm)	K (%)	Li (ppm)
180	44	3.07	0.6	1.76	25
Pb (ppm)	S (%)	Si (%)	Sr (ppm)	Ti (%)	V (ppm)
70	N/A	34.5	34	0.21	76
Mg (%)	Mn (ppm)	C org (%)	Ca (%)	Cd (ppm)	Co (ppm)
0.61	460	0.28	0.28	<5	15
Y (ppm)	Zn (ppm)	Mo (ppm)	Na (ppm)	Ni (ppm)	P (ppm)
45	126	<5	5860	30	200

Since a range of elements was present in the ore, a leach with a concentrated oxidant solution was performed to assess the amount of each element leached. To do this, leach solution was made containing 400 g or ore, 800 mL of deionised water, 46.5 g of TCCA and 3.8 g of KBr. After the leach solution was prepared and the ore was added, the solution was stirred at 250 RPM using an overhead stirrer for 25 minutes before the stirring speed was reduced to 200 RPM. A lid with a cut out for the stirrer was fitted to the reaction bucked to minimise spillage and evaporation. However, at no point during the experiment was the reaction vessel sealed. After 2 days of oxidation another 46.4 g of TCCA and 3.8 g of KBr was added. Next, the solution was stirred for an additional 6 days before the solution was vacuum filtered. The filtering of the solution gave only 400 mL of liquid since the ore was still wet and retained nearly half of the original volume of solution. In order to retain the original volume, the ore was washed with deionised water until the volume of the solution was 800 mL again. A 100 mL sample was sent for external analysis.

To determine the approximate particle size of the gold ore a sample was analysed using SEM. This analysis showed very large variations of particle size within that ore sample. The largest measures particle had a length of 1444 µm and the smallest a length of 2.5 µm.
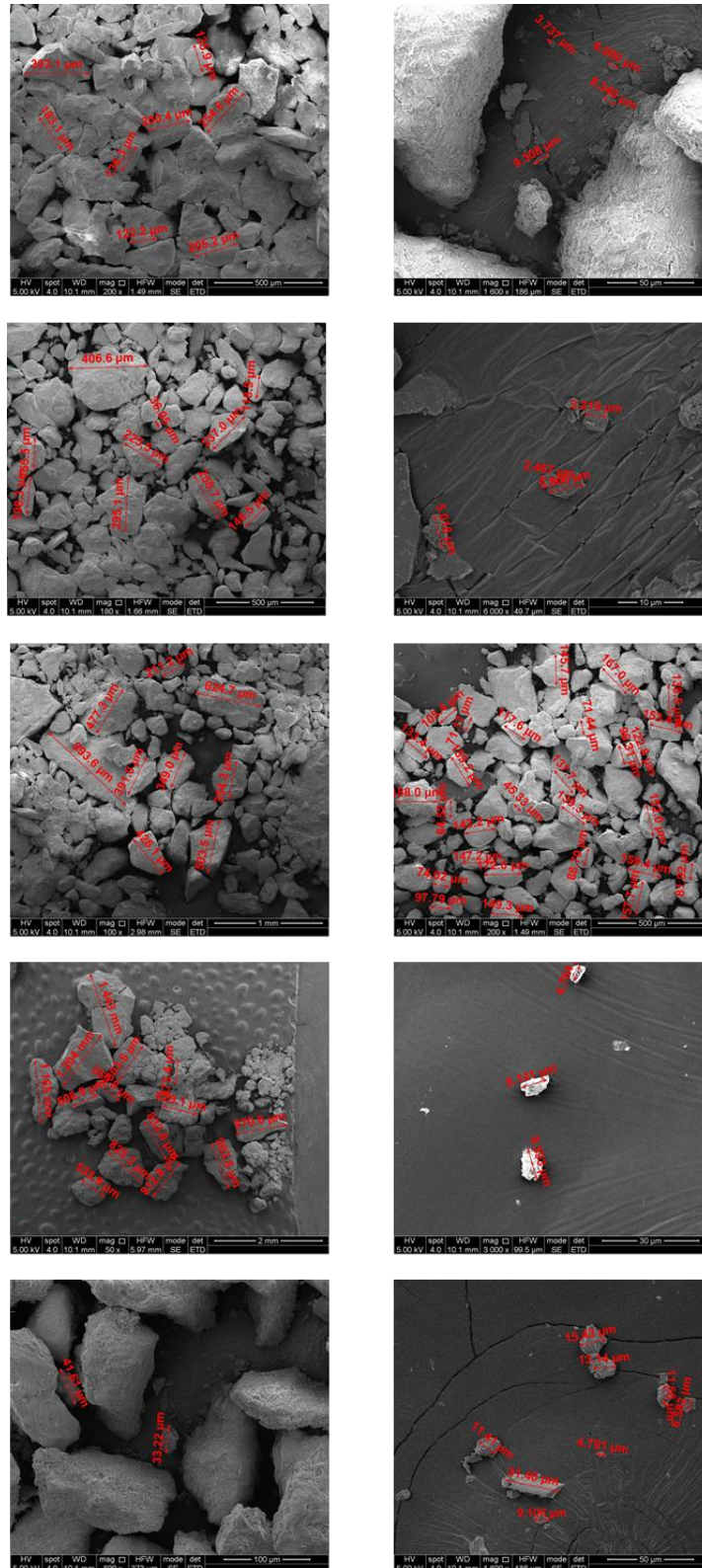
Figure 2.103: SEM micrographs of ore and particle size measurements.

Since the ore had a wide range of particle sizes, the ore needed to be homogenised. The concentrates arrived in five 20 L buckets with around 20 kg of ore in each. To ensure that the concentrates are homogenised, a layer of 4 scoops from a 435

154

mL scoop of each bucket was placed into a 100 kg bucket. After each layer the sands were mixed using a rigid plastic stirrer and another layer consisting of one scoop form each bucked was added. After all the sand was mixed in the 100 kg bucket, the sand was divided up and put in the original 20 L buckets. Then, from each bucket 25 g were taken combined and sent for elemental analysis.

At smaller particle sizes better gold liberation is achieved. To separate smaller ore particles the ore was sieved through a 90 µm laboratory test sieve. Out of approximately 100 kg of ore 4.1 kg of ≤ 90 µm ore particles were isolated. The finer particle ore was analysed by an commercial service as previously described.

Table 2.14: Assay of the ore with a particle size of ≤ 90 µm showing the concentration of various element.

Ag (ppm)	Al (%)	As (ppm)	Au (ppm)	Ba (ppm)	Be (ppm)
18	7.04	390	190	600	<5
Bi (ppm)	Cd (ppm)	Co (ppm)	Cr (ppm)	Cu (ppm)	Fe (%)
<10	<5	20	200	64	4.74
Hg (ppm)	K (%)	Li (ppm)	Mg (%)	Mn (ppm)	Mo (ppm)
0/8	1.77	30	0.8	700	<5
Na (ppm)	Ni (ppm)	P (ppm)	Pb (ppm)	Si (%)	Sr (ppm)
4120	45	<100	75	31.3	46
Ti (%)	V (ppm)	Y (ppm)	Zn (ppm)		
0.36	94	<100	166		

Small scale gold recovery from ore with a particles size of ≤ 90 µm

This experiment was performed to assess if the gold recovery process can be performed more quickly. The aim was an oxidation time of 8 hours followed by a gold uptake time of an additional 8 hours. This experiment was performed in duplicate. For each sample 25 g of ore was used together with 20 mL of deionised water, 1.98 g of TCCA and 57 mg of KBr. The water was added at a temperature of 60°C.

After the water was added the samples were put on end over end rotation at 20 RPM. The samples were briefly vented after 10 minutes, and slight pressure was observed. Samples were taken a 2, 4, 6, 8 and 24 hours. The samples were a thick slurry which made it hard to draw enough liquid for sampling. Therefore, to take a sample for testing,

a small volume (1.5 mL) of the slurry was centrifuged and the supernatant was taken to be analysed by ICP-OES.
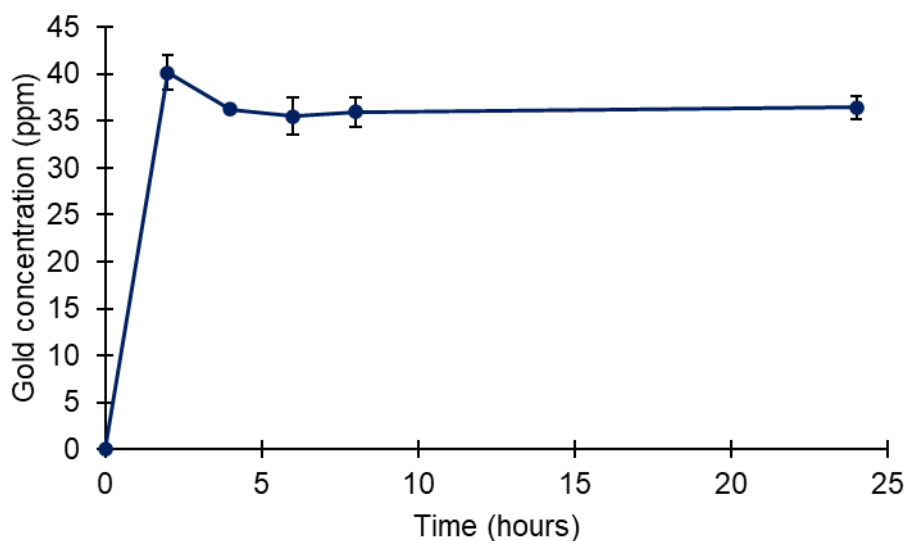
Figure 2.104: Gold concentration of oxidised ore over 24 hours.

The next experiment was performed to investigate if removing the magnetic material before oxidation or of adding more oxidants can increase the amount of gold leached. This was done by performing two experiments in duplicate. In one experiment the magnetic material was removed before the oxidation step and in the other experiment double to amount of oxidant was used.

Table 2.15: Masses of ore, TCCA, KBr and volume of water used in samples to test the effect the removal of magnetic material or doubling the amount of oxidant had.

Sample:	Ore (g)	TCCA (g)	KBr (mg)	Deionised water (mL)	Notes
1 (magnetic material removed)	25	1.98	57	20	Magnetic material removed: 33 mg
2 (magnetic material removed)	25	1.98	57	20	Magnetic material removed: 17 mg
3 (double oxidant)	25	3.96	114	20	-
4 (double oxidant)	25	3.96	114	20	-

The temperature of the water as it was added was 60°C. The samples were then rotated at 20 RPM. As the water was added slight fizzing could be seen. Samples were taken by centrifugation at 2, 4 and 6 hours. The samples were analyses by ICP-OES.

Large scale gold oxidation and recovery (5 kg ore)

Previous experiments have shown that pre-dissolving the leaching reagents by sonication and heating forces more TCCA into solution and does not affect the leach performance. Therefore, for this experiment, the reagents were pre-dissolved in two one-liter plastic bottles on the day before the leach experiment. To do that 180 g of TCCA and 7 g of KBr together with 800 mL of DI water was added to each bottle. After that the bottles were sonicated at 50 °C for 2.5 hours. After that the solution had a bright yellow color and some of the TCCA was still sitting at the bottom of the bottle. It has to be noted that after the bottles were sealed and left sitting for 3 hours, a lot of pressure built up in the bottles and were at danger of bursting. As the bottles were vented, noxious gas was released, irritating to eyes and nostrils. Therefore, it might be safer to add the oxidants directly into the ore and water mixture instead of adding a pre-made oxidant solution. On the day of the ore leach, the two bottles containing the leach solution were preheated to

50 °C and sonicated until temperature was reached. Parallel to that 2 L of DI water were also heated to 70 °C.

The ore used in this experiment was classified by ACE staff and separated in the following size ranges totaling 4759.4 g:

< 77 µm (2634.6 g)

77 µm – 91 µm (1011.3 g)

91 µm – 104 µm (1113.5 g)

Figure 2.105: Ore used for this experiment classified into three size ranges (77 µm, 77 – 91 µm, 91 – 104 µm) with a total mass of 4759.4 g

Any magnetic material was removed from the ore by pouring the ore over a strong magnet. This was done by fitting a large tubular magnet into a wooden wedge-shaped housing. As the ore was poured into the wooden housing it had to pass over the magnet which removed the magnetic material. The mass of magnetic material removed was 5.4 g. Hence 4755 g of ore were used in the leaching process.

Figure 2.106: A strong tubular magnet was used to remove magnetic material from the ore.

Next, the reagent solution (1600 mL, 65 °C), DI water (2000 mL, 70 °C) and the ore (4755 g) were added to a 20 L drum. To that drum, a PVC block (60 mm × 60 mm × 120 mm) was added to aid the mixing process. Following that, the lid was placed on the drum (the lid had a small hole drilled in the center to release and gases and to avoid the buildup of pressure inside the drum. The drum was then placed on a roller and rotated at 4.5 RPM. At the beginning of the rotation the temperature of the mixture in the drum was 40 °C.
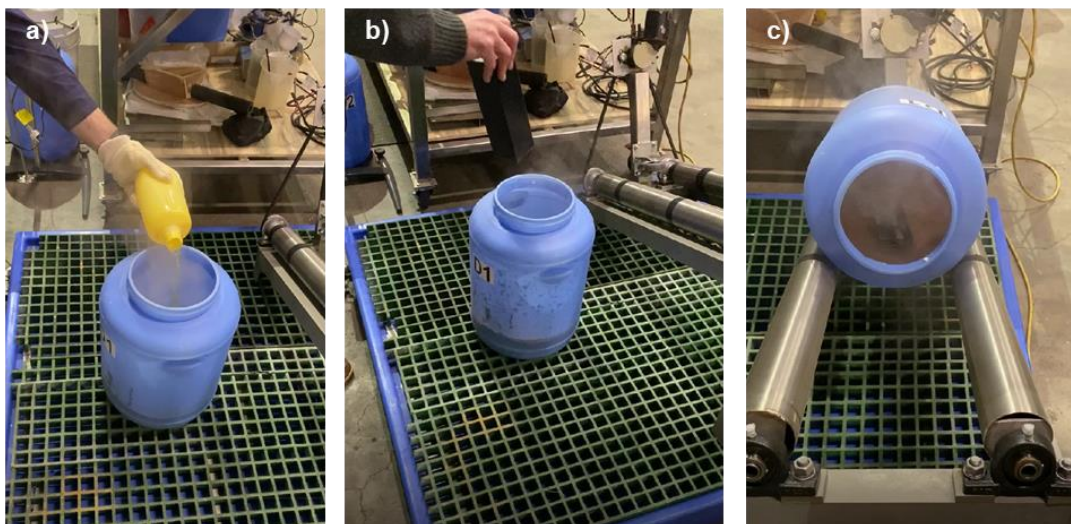
Figure 2.107: a) Pre dissolved and heated oxidant solution is added, **b)** PVC block is added to aid mixing and **c)** drum with reaction mixtures is on roller to rotate at 4.5 RPM.

A small fan heater was placed next to the drum to keep heating the drum during the leach process. After 2 hours of rotation the temperature of the mixture inside the

drum was 36.0 °C and the rotation was stopped. The lid was removed to let the mixture cool down since a lot of gas was still coming off. After 30 minutes the temperature of the mixture was 25 °C. After that the PVC block was removed.

Figure 2.108: a) reaction mixture after 2 hours, **b)** PVC block is removed prior to filtration.

To separate the leachate from the ore, the solution was filtered in two steps. The first step was to filter the solution through 50 µm nylon mesh bag. The bag was manually squeezed to remove as much liquid as possible. Further, the drum was rinsed with DI water.

Figure 2.109: a) reaction mixture is being poured into 50 µm nylon filter bag, **b)** top view of filter bag.

A total of 2697.7 g of leachate was recovered by the nylon filter bag (since the leachate was still a little cloudy, the filtrate was again filtered vacuum filtration). Next, vacuum filtration was set up to filter the remaining ore using laboratory filter paper. Additionally, the ore was washed with DI water to wash all the solubilised gold out.

Figure 2.110: Ore is being filtered using vacuum filtration.

To recover the gold, the leachate was transferred into a 20 L bucket. Two lots of 150g of finely ground 50-poly(S-*r*-canola) polymer was used in total. Firstly, 150 g of polymer was added and stirred through the leachate for 30 minutes using an overhead stirrer to quench the remaining oxidant in the leach solution. Next, another 150 g of finely ground polymer was added to the leach solution and stirred for 4 hours. Finally, the polymer was removed by filtration through a cloth.

Figure 2.111: a) filtered leach solution and 50-poly(S-*r*-canola) polymer being stirred, **b)** solution after 30 minutes stirring, **c)** filtration through cloth and **d)** recovered polymer and leach solution after gold uptake.

Once the 50-poly(S-*r*-canola) polymer was brought back to the lab, any remaining liquid was filtered out using vacuum filtration. After that, the polymer was left to dry. The following day the first 100 g of polymer were incinerated. This was done by placing 100.01 g of polymer in a large 1.1 L crucible and heating it a furnace to 1100 °C at a rate of 5 °C/minute. Once 1100 °C were reached this temperature was held for 30 minutes before the furnace cooled down naturally. Using the same protocol, portions of 100.5 g and 175.35 g were incinerated. Hence a total of 375.86 g of polymer was incinerated which is more than was originally used. However, the polymer was not completely dry, therefore the remaining water in the polymer accounts for the weight

difference After all the polymer was incinerated, 10.64 g of product was left in the form of carbon.
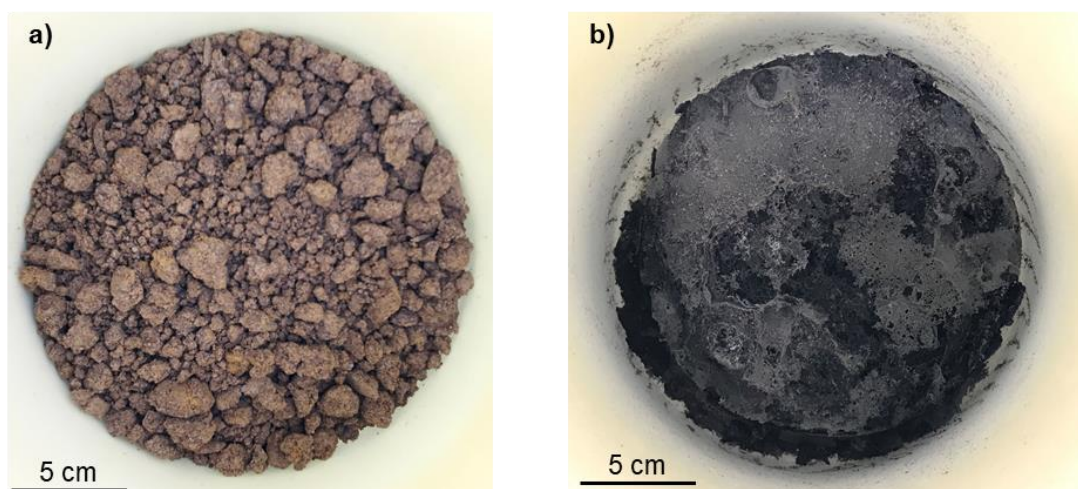
Figure 2.112: a) representative 50-poly(S-*r*-canola) polymer in crucible prior to incineration and **b)** combined product of all polymer incinerations.

To remove to remaining carbon, the product was again incinerated using the protocol as described above with the only difference that the final temperature of 1100 °C was held for 1 hour instead of 30 minutes. After that a total of 373.7 mg of product was left.
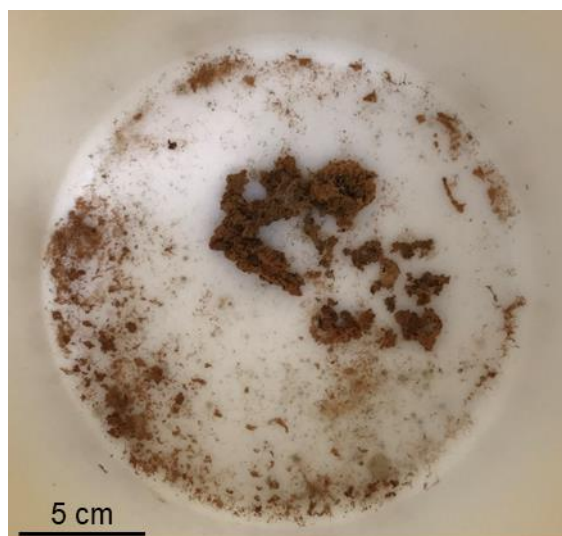
Figure 2.113: Final incineration product.

The final incineration product was characterised using SEM and EDX analysis.
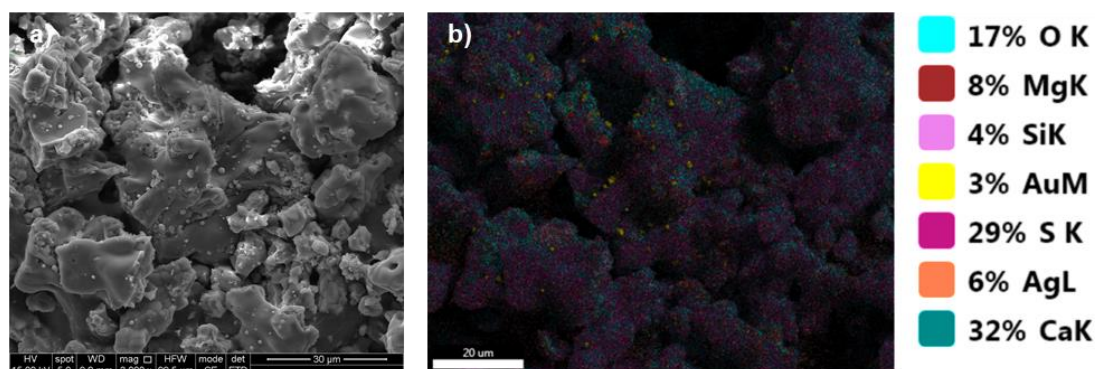
Figure 2.114: a) SEM micrograph and **b)** EXD elemental map of final incineration product.

During the gold leaching and gold uptake process the gold concentration was monitored using ICP-OES.

Electronic waste applications

To remove the gold from RAM pins, 10 RAM pins were cut in half and placed in a 500 mL oxidant solution containing TCCA (11.62 g, 0.1 M) and KBr (892.2 mg, 0.015 M) in a 1L vented plastic bottle. The container was then placed in a heated (50 °C) sonicator bath for 6 hours, during which samples for ICP-OES were taken. During this time the majority of gold visible had been oxidised.
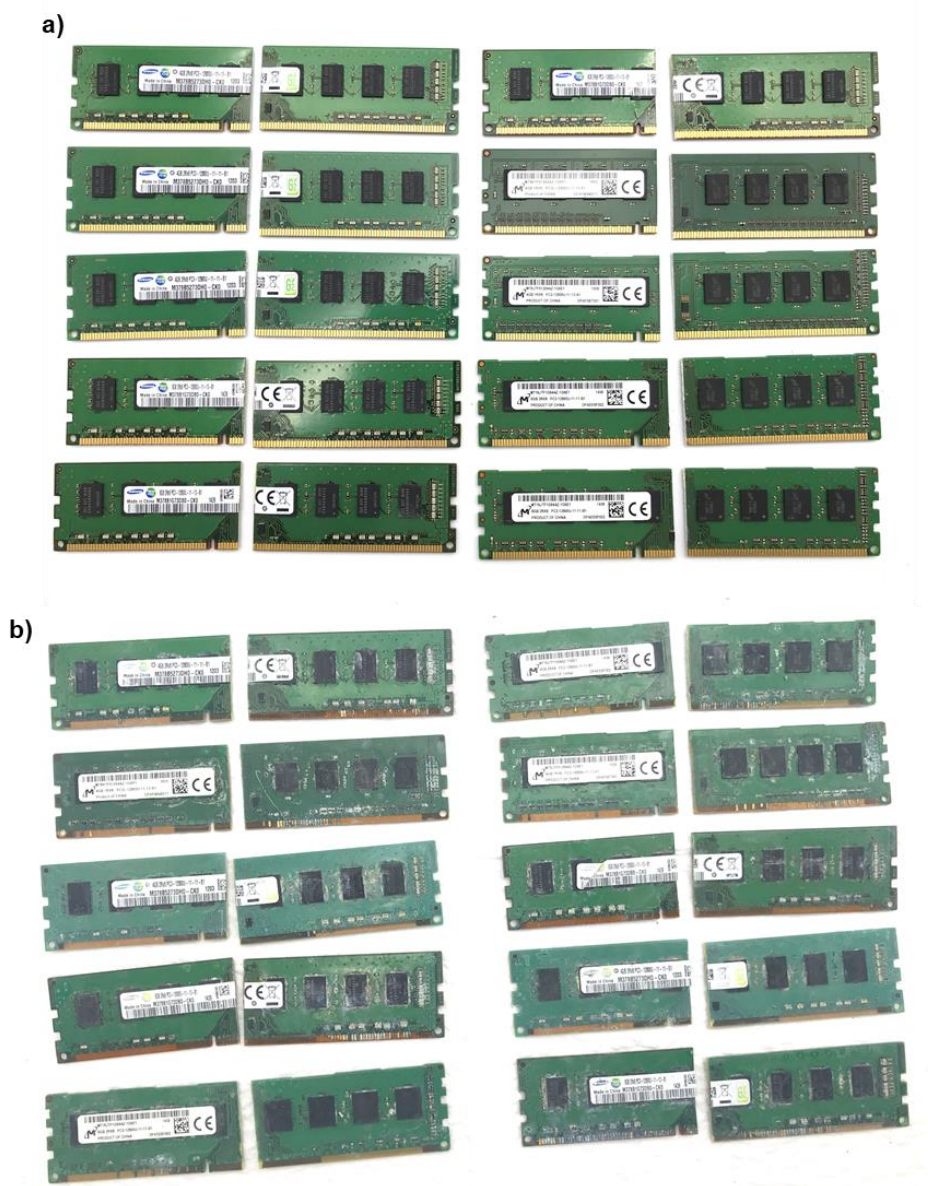
Figure 2.115: RAM modules **a)** before and **b)** after oxidation

As can be seen the reaction color turns form slightly yellow to dark green to blue in the last hour of reaction time.
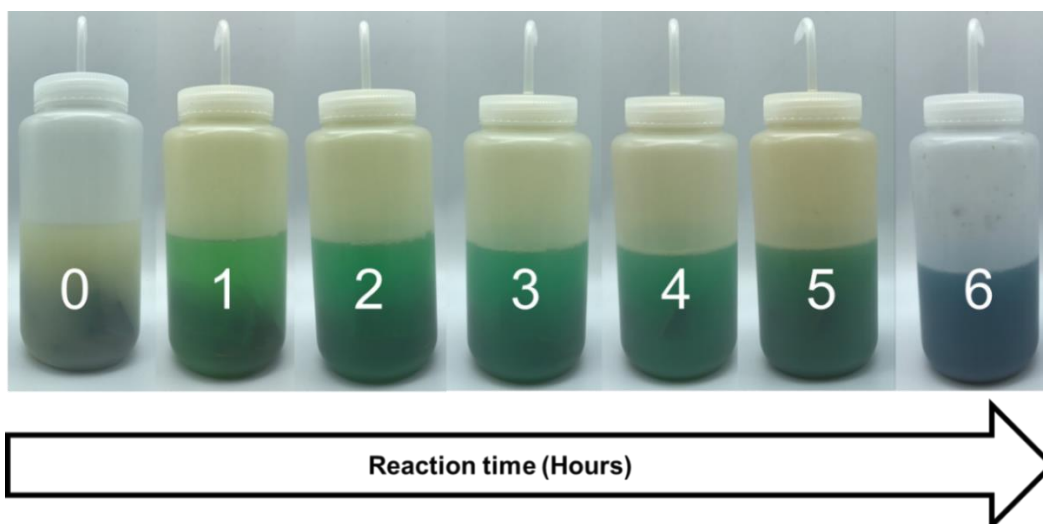
Figure 2.116: Reaction solution over the time course of 6 hours.

After the oxidation process, EDTA (50g) was added and stirred for 20 minutes to stabilise the copper that has also been leached. Following that, the solution was gravity filtered using laboratory filter paper. After the filtration the solution had a deep blue color.

Figure 2.117: Solution after EDTA addition and filtration.

To that solution, 12 g of 50-poly(S-*r*-canola) were added and stirred for 20 hours to remove the gold. During the stirring process, samples for ICP-OES were taken. The figure below shows the increase of gold concentration during the oxidation process and the subsequent gold removal by the 50-poly(S-*r*-canola).
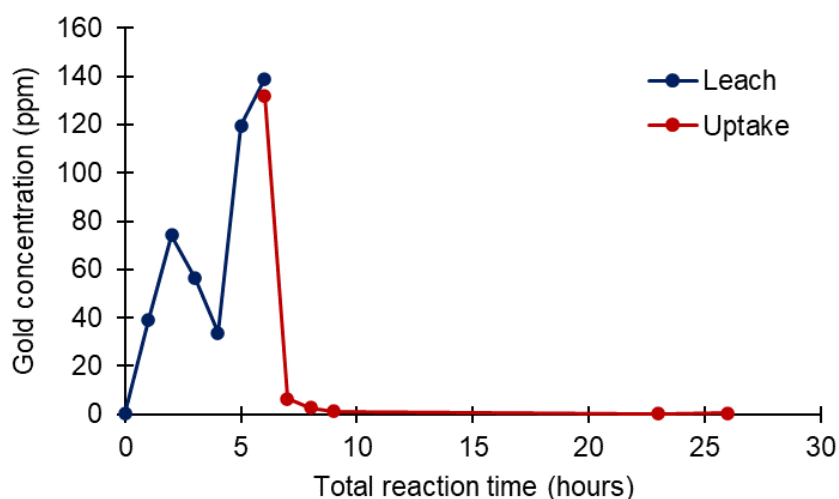
Figure 2.118: Gold concentration over the entirety of RAM module gold recovery, beginning from the leaching and continuing throughout the gold uptake stage.

Next, the 50-poly(S-*r*-canola) was recovered by gravity filtration and incinerated in a 27 mL crucible by being heated to 1100 °C with a ramp rate of 5 °C / minute and held for 30 min at 1100 °C. The weight of the recovered incineration product was 97.3 mg. The mass of gold taken up by the 50-poly(S-*r*-canola) is 65.4 mg. The identify and contamination SEM and EDX was used to analyse the incineration product.
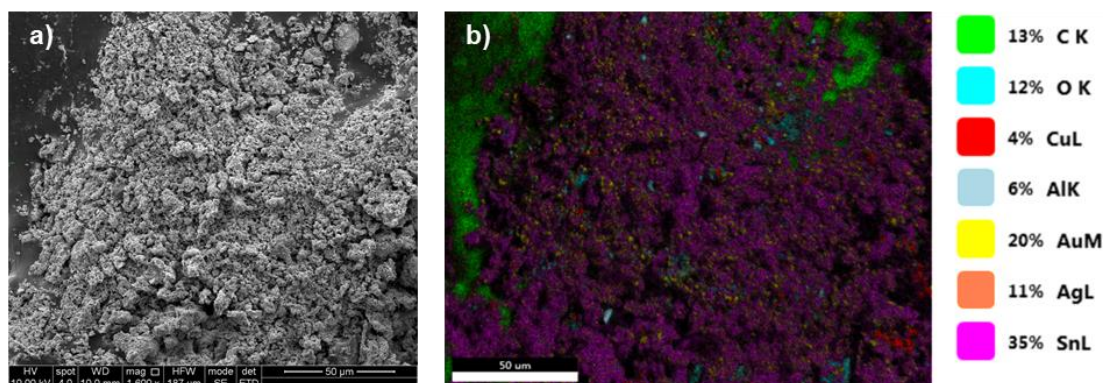
Figure 2.119: a) SEM micrograph and **b)** EDX elemental map of incineration product.

To determine how much of the 97.3 mg is gold the incineration product was microwave digested using aqua regia. To do this, the incineration product was placed in a Teflon digestion tube together with 1 mL of concentrated HNO_3 and 3 mL of concentrated HCl. After the digestion cycle was completed, the digested sample was diluted to 40 mL using deionised water and analysed using ICP-MS. The analysis revealed a gold concentration of 1032 ppm, which corresponds to a gold mass of 41.46 mg in the digested solution. Comparing that mass of gold to the mass of gold taken up by the 50-poly(S-*r*-canola) (65.3 mg) it can be said that 64 wt% of gold have been

167

recovered using the microwave digestion. Since not all of the material had dissolved during the aqua regia digestion, the remaining material was recovered by vacuum filtration, dried, and analysed .
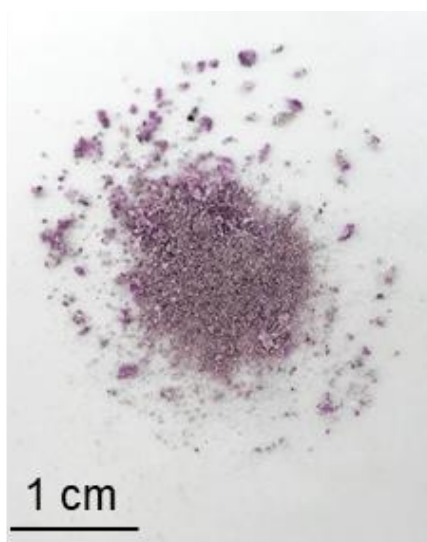
Figure 2.120: Remaining material after aqua regia digest

SEM and EDX analysis identified tin as the major element in the material.
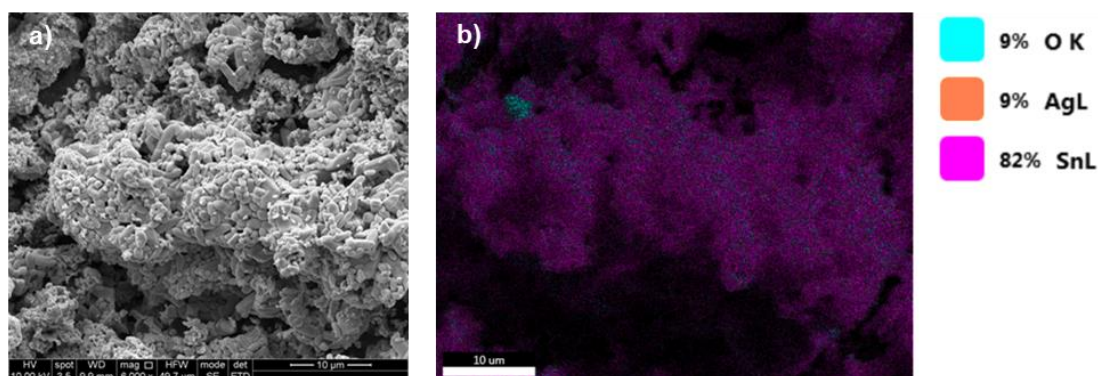
Figure 2.121: a) SEM micrograph and **b)** EDX elemental map of the remaining material after the aqua regia digestion.

Lastly, XRD analysis was performed which identified tin oxide as one constituent of the materials left over after the aqua regie digestion.
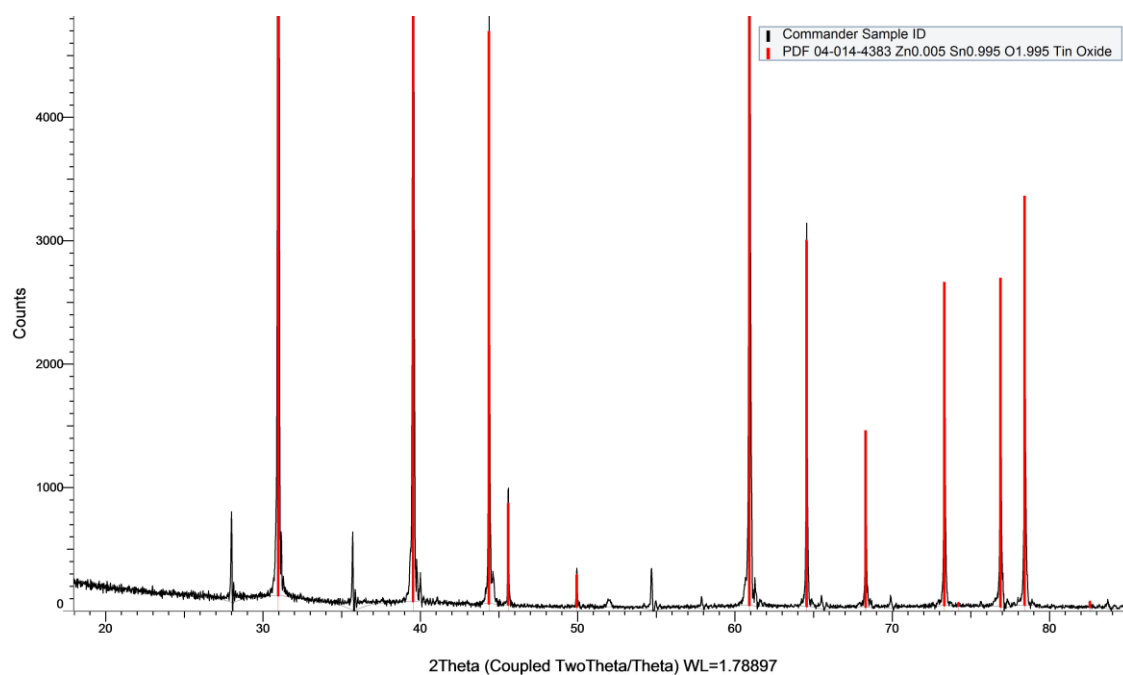
Figure 2.122: XRD of remaining material after the aqua regia digest showing a match for tin oxide

References:

1.   United States Geological Survey, How much gold has been found in the world?   https://www.usgs.gov/faqs/how-much-gold-has-been-found-world (accessed 13th of December 2021).

2.   Galbraith, C. 2019 gold output to hit new record high of 109.6 Moz. https://www.spglobal.com/marketintelligence/en/news-insights/trending/zhSggm-ztc-nJuneeXr2dQ2 (accessed 16th of April 2020).

3.   Esdaile, L. J.; Chalker, J. M., The Mercury Problem in Artisanal and Small-Scale Gold Mining. *Chem. Eur. J.* **2018,** *24*, 6905-6916.

4.   Schmidt, C. W., Quicksilver & gold: mercury pollution from artisanal and small-scale gold mining. National Institute of Environmental Health Sciences: **2012**.

5.   de Lacerda, L. D.; Salomons, W., *Mercury from Gold and Silver Mining A Chemical Time Bomb?* Springer: Berlin, **1998**.

6.   Saldarriaga-Isaza, A.; Arango, S.; Villegas-Palacio, C., A behavioral model of collective action in artisanal and small-scale gold mining. *Ecol. Econ.* **2015,** *112*, 98-109.

7.   Gonçalves, A. O.; Marshall, B. G.; Kaplan, R. J.; Moreno-Chavez, J.; Veiga, M. M., Evidence of reduced mercury loss and increased use of cyanidation at gold processing centers in southern Ecuador. *J. Clean. Prod.* **2017,** *165*, 836-845.

8.   Guimaraes, J. R. D.; Betancourt, O.; Miranda, M. R.; Barriga, R.; Cueva, E.; Betancourt, S., Long-range effect of cyanide on mercury methylation in a gold mining area in southern Ecuador. *Sci. Total Environ.* **2011,** *409* (23), 5026-5033.

9.   Velásquez-López, P. C.; Veiga, M. M.; Klein, B.; Shandro, J. A.; Hall, K., Cyanidation of mercury-rich tailings in artisanal and small-scale gold mining: identifying strategies to manage environmental risks in Southern Ecuador. *J. Clean. Prod.* **2011,** *19* (9), 1125-1133.

10.   Shandro, J. A.; Veiga, M. M.; Chouinard, R., Reducing mercury pollution from artisanal gold mining in Munhena, Mozambique. *J. Clean. Prod.* **2009,** *17* (5), 525-532.

11. Sousa, R. N.; Veiga, M. M.; Klein, B.; Telmer, K.; Gunson, A. J.; Bernaudat, L., Strategies for reducing the environmental impact of reprocessing mercury-contaminated tailings in the artisanal and small-scale gold mining sector: insights from Tapajos River Basin, Brazil. *J. Clean. Prod.* **2010,** *18* (16), 1757-1766.

12. Davies, G. R., A toxic free future: Is there a role for alternatives to mercury in small-scale gold mining? *Futures* **2014,** *62*, 113-119.

13. Manutchehr-Danai, M., Amalgam. In *Dictionary of Gems and Gemology*, Manutchehr-Danai, M., Ed. Springer Berlin Heidelberg: Berlin, Heidelberg, **2009**; pp 1-1.

14. De Miguel, E.; Clavijo, D.; Ortega, M. F.; Gómez, A., Probabilistic meta-analysis of risk from the exposure to Hg in artisanal gold mining communities in Colombia. *Chemosphere* **2014,** *108*, 183-189.

15. Rocha, J. B. T.; Aschner, M.; Dórea, J. G.; Ceccatelli, S.; Farina, M.; Silveira, L. C. L., Mercury toxicity. *J. Biomed. Biotechnol.* **2012,** *2012*, 831890-831890.

16. Park, J.-D.; Zheng, W., Human Exposure and Health Effects of Inorganic and Elemental Mercury. *J. Prev. Med. Public Health* **2012,** *45*, 344-352.

17. Rooney, J. P. K., The retention time of inorganic mercury in the brain — A systematic review of the evidence. *Toxicol. Appl. Pharmacol.* **2014,** *274* (3), 425-435.

18. Bose-O'Reilly, S.; Lettmeier, B.; Gothe, R. M.; Beinhoff, C.; Siebert, U.; Drasch, G., Mercury as a serious health hazard for children in gold mining areas. *Environ. Res.* **2008,** *107*, 89-97.

19. Cordy, P.; Veiga, M.; Crawford, B.; Garcia, O.; Gonzalez, V.; Moraga, D.; Roeser, M.; Wip, D., Characterization, mapping, and mitigation of mercury vapour emissions from artisanal mining gold shops. *Environ. Res.* **2013,** *125*, 82-91.

20. Xiao, R.; Wang, S.; Li, R.; Wang, J. J.; Zhang, Z., Soil heavy metal contamination and health risks associated with artisanal gold mining in Tongguan, Shaanxi, China. *Ecotoxicol. Environ. Saf.* **2017,** *141*, 17-24.

21. Evers, D. C.; Keane, S. E.; Basu, N.; Buck, D., Evaluating the effectiveness of the Minamata Convention on Mercury: Principles and recommendations for next steps. *Sci. Total Environ.* **2016,** *569-570*, 888-903.

22. Selin, H.; Keane, S. E.; Wang, S.; Selin, N. E.; Davis, K.; Bally, D., Linking science and policy to support the implementation of the Minamata Convention on Mercury. *Ambio* **2018,** *47* (2), 198-215.

23. Erhardt, A. J.; Rezende, C. E.; Walker, B. G.; Franceschi, D.; Downie, D., Mercury concentrations and awareness in Campos dos Goytacazes, Brazil: baseline measures for examining the efficacy of the Minamata Convention. *J. Environ. Stud. Sci.* **2015,** *5* (4), 517-525.

24. Spiegel, S. J.; Agrawal, S.; Mikha, D.; Vitamerry, K.; Le Billon, P.; Veiga, M.; Konolius, K.; Paul, B., Phasing Out Mercury? Ecological Economics and Indonesia's Small-Scale Gold Mining Sector. *Ecol. Econ.* **2018,** *144*, 1-11.

25. Veiga, M. M.; Angeloci-Santos, G.; Meech, J. A., Review of barriers to reduce mercury use in artisanal gold mining. *The Extractive Industries and Society* **2014,** *1* (2), 351-361.

26. Laitos, J. G., Cyanide, Mining, and the Environment. *Pace Envtl. L. Rev.* **2012,** (3), [i]-949.

27. Ilyas, S., *Gold Metallurgy and the Environment.* 1st ed. ed.; Milton : Taylor & Francis Group: **2018**.

28. Yannopoulos, J. C., *The extractive metallurgy of gold.* Springer Science & Business Media: **1991**.

29. Pleysier, R.; Dai, X.; Wingate, C. J.; Jeffrey, M. I., Microtomography based identification of gold adsorption mechanisms, the measurement of activated carbon activity, and the effect of frothers on gold adsorption. *Miner. Eng.* **2008,** *21* (6), 453-462.

30. Dong, K.; Xie, F.; Wang, W.; Chang, Y.; Lu, D.; Gu, X.; Chen, C., The detoxification and utilization of cyanide tailings: A critical review. *J. Clean. Prod.* **2021,** *302*, 126946.

31. Cunningham, S. A., Incident, Accident, Catastrophe: Cyanide on the Danube. *Disasters* **2005,** *29* (2), 99-128.

32. Kwaansa-Ansah, E. E.; Amenorfe, L. P.; Armah, E. K.; Opoku, F., Human health risk assessment of cyanide levels in water and tuber crops from Kenyasi, a mining community in the Brong Ahafo Region of Ghana. *Int. J. Food Contam.* **2017,** *4* (1), 16.

33. Brüger, A.; Fafilek, G.; Restrepo B, O. J.; Rojas-Mendoza, L., On the volatilisation and decomposition of cyanide contaminations from gold mining. *Sci. Total Environ.* **2018,** *627*, 1167-1173.

34. Nyanza, E. C.; Yohana, P.; Thomas, D. S. K.; Thurston, W. E.; Konje, E.; Dewey, D., Knowledge of and Adherence to the Cyanide Code Among Small-scale Gold Miners in Northern Tanzania. *J. Health Pollut.* **2017,** *7* (14), 4-14.

35. Razanamahandry, L. C.; Andrianisa, H. A.; Karoui, H.; Podgorski, J.; Yacouba, H., Prediction model for cyanide soil pollution in artisanal gold mining area by using logistic regression. *CATENA* **2018,** *162*, 40-50.

36. Sun, C.-b.; Zhang, X.-l.; Kou, J.; Xing, Y., A review of gold extraction using noncyanide lixiviants: Fundamentals, advancements, and challenges toward alkaline sulfur-containing leaching agents. *Int. J. Miner. Metall. Mater.* **2020,** *27* (4), 417-431.

37. Vieira, R., Mercury-free gold mining technologies: possibilities for adoption in the Guianas. *J. Clean. Prod.* **2006,** *14* (3), 448-454.

38. Torkaman, P.; Veiga, M. M.; de Andrade Lima, L. R. P.; Oliveira, L. A.; Motta, J. S.; Jesus, J. L.; Lavkulich, L. M., Leaching gold with cassava: An option to eliminate mercury use in artisanal gold mining. *J. Clean. Prod.* **2021,** *311*, 127531.

39. Abdelbasir, S. M.; Hassan, S. S. M.; Kamel, A. H.; El-Nasr, R. S., Status of electronic waste recycling techniques: a review. *Environ. Sci. Pollut. Res.* **2018,** *25* (17), 16533-16547.

40. Rao, M. D.; Singh, K. K.; Morrison, C. A.; Love, J. B., Challenges and opportunities in the recovery of gold from electronic waste. *RSC Adv.* **2020,** *10* (8), 4300-4309.

41. Mihai, F.-C.; Gnoni, M.-G.; Meidiana, C.; Ezeah, C.; Elia, V., Chapter 1 - Waste Electrical and Electronic Equipment (WEEE): Flows, Quantities, and Management—A Global Scenario. In *Electronic Waste Management and Treatment Technology*, Prasad, M. N. V.; Vithanage, M., Eds. Butterworth-Heinemann: **2019**; pp 1-34.

42. Cucchiella, F.; D'Adamo, I.; Lenny Koh, S. C.; Rosa, P., Recycling of WEEEs: An economic assessment of present and future e-waste streams. *Renew. Sust. Energ. Rev.* **2015,** *51*, 263-272.

43. Kim, S. S.; Xu, X.; Zhang, Y.; Zheng, X.; Liu, R.; Dietrich, K. N.; Reponen, T.; Xie, C.; Sucharew, H.; Huo, X.; Chen, A., Birth outcomes associated with maternal exposure to metals from informal electronic waste recycling in Guiyu, China. *Environ. Int.* **2020,** *137*, 105580.

44. Ding, Y.; Zhang, S.; Liu, B.; Zheng, H.; Chang, C.-c.; Ekberg, C., Recovery of precious metals from electronic waste and spent catalysts: A review. *Resour. Conserv. Recycl.* **2019,** *141*, 284-298.

45. Parajuly, K.; Fitzpatrick, C., Understanding the Impacts of Transboundary Waste Shipment Policies: The Case of Plastic and Electronic Waste. *Sustainability* **2020,** *12* (6), 2412.

46. Siringo, R.; Herdiansyah, H.; Kusumastuti, R. D., Underlying factors behind the low participation rate in electronic waste recycling. *Global J. Environ. Sci. Manage.* **2020,** *6* (2), 203-214.

47. Efthymiou, L.; Mavragani, A.; Tsagarakis, K. P., Quantifying the Effect of Macroeconomic and Social Factors on Illegal E-Waste Trade. *Int. J. Env. Res. Public Health* **2016,** *13* (8), 1-13.

48. Lee, D.; Offenhuber, D.; Duarte, F.; Biderman, A.; Ratti, C., Monitour: Tracking global routes of electronic waste. *Waste Manage.* **2018,** *72*, 362-370.

49. Rida, A.; Natasha; Shah, F.; Hashmi, M. Z.; Wahid, A.; Muhammad, A.; Mubeen, M.; Khan, N.; Muhammad Ishaq Asif, R.; Muhammadd, A.; Abbas, M.; Shahzad, K.; Ahmad, S.; Hammad, H. M.; Wajid, N., Trends of electronic waste pollution and its impact on the global environment and ecosystem. *Environ. Sci. Pollut. Res.* **2019,** *26* (17), 16923-16938.

50. Chakraborty, P.; Sampath, S.; Mukhopadhyay, M.; Selvaraj, S.; Bharat, G. K.; Nizzetto, L., Baseline investigation on plasticizers, bisphenol A, polycyclic aromatic hydrocarbons and heavy metals in the surface soil of the informal electronic waste recycling workshops and nearby open dumpsites in Indian metropolitan cities. *Environ. Pollut.* **2019,** *248*, 1036-1045.

51. Chimere May, O.; van Bodegom, P. M.; Osibanjo, O.; Xie, Q.; Chen, J.; Vijver, M. G.; Willie, J. G. M. P., Health Risks of Polybrominated Diphenyl Ethers (PBDEs) and Metals at Informal Electronic Waste Recycling Sites. *Int. J. Env. Res. Public Health* **2019,** *16* (6).

52. Zhuang, X., Chapter 14 - Chemical Hazards Associated With Treatment of Waste Electrical and Electronic Equipment. In *Electronic Waste Management and Treatment Technology*, Prasad, M. N. V.; Vithanage, M., Eds. Butterworth-Heinemann: **2019**; pp 311-334.

53. Ohajinwa, C. M.; van Bodegom, P. M.; Vijver, M. G.; Peijnenburg, W. J. G. M., Impact of informal electronic waste recycling on metal concentrations in soils and dusts. *Environ. Res.* **2018,** *164*, 385-394.

54. Kyere, V. N.; Greve, K.; Atiemo, S. M.; Amoako, D.; Aboh, I. K.; Cheabu, B. S., Contamination and health risk assessment of exposure to heavy metals in soils from informal e-waste recycling site in Ghana. *Emerg. Sci. J.* **2018,** *2* (6), 428-436.

55. Ackah, M., Informal E-waste recycling in developing countries: review of metal(loid)s pollution, environmental impacts and transport pathways. *Environ. Sci. Pollut. Res.* **2017,** *24* (31), 24092-24101.

56. Kumar, A.; Holuszko, M.; Espinosa, D. C. R., E-waste: An overview on generation, collection, legislation and recycling practices. *Resour. Conserv. Recycl.* **2017,** *122*, 32-42.

57. Quan, S.-X.; Yan, B.; Lei, C.; Yang, F.; Li, N.; Xiao, X.-M.; Fu, J.-M., Distribution of heavy metal pollution in sediments from an acid leaching site of e-waste. *Sci. Total Environ.* **2014,** *499*, 349-355.

58. Ashiq, A.; Kulkarni, J.; Vithanage, M., Chapter 10 - Hydrometallurgical Recovery of Metals From E-waste. In *Electronic Waste Management and Treatment Technology*, Prasad, M. N. V.; Vithanage, M., Eds. Butterworth-Heinemann: **2019**; pp 225-246.

59. Ma, E., Chapter 11 - Recovery of Waste Printed Circuit Boards Through Pyrometallurgy. In *Electronic Waste Management and Treatment Technology*, Prasad, M. N. V.; Vithanage, M., Eds. Butterworth-Heinemann: **2019**; pp 247-267.

60. Rene, E. R.; Sethurajan, M.; Kumar Ponnusamy, V.; Kumar, G.; Bao Dung, T. N.; Brindhadevi, K.; Pugazhendhi, A., Electronic waste generation, recycling and resource recovery: Technological perspectives and trends. *J. Hazard. Mater.* **2021,** *416*, 125664.

61. Wang, H.; Zhang, S.; Li, B.; Pan, D. a.; Wu, Y.; Zuo, T., Recovery of waste printed circuit boards through pyrometallurgical processing: A review. *Resour. Conserv. Recycl.* **2017,** *126*, 209-218.

62. Wu, Z.; Yuan, W.; Li, J.; Wang, X.; Liu, L.; Wang, J., A critical review on the recycling of copper and precious metals from waste printed circuit boards using hydrometallurgy. *Front. Environ. Sci. Eng.* **2017,** *11* (5), 8.

63. Nithya, R.; Sivasankari, C.; Thirunavukkarasu, A., Electronic waste generation, regulation and metal recovery: a review. *Environ. Chem. Lett.* **2021,** *19* (2), 1347-1368.

64. Priya, A.; Hait, S., Biometallurgical recovery of metals from waste printed circuit boards using pure and mixed strains of Acidithiobacillus ferrooxidans and Acidiphilium acidophilum. *Process Saf. Environ. Prot.* **2020,** *143*, 262-272.

65. Asibey, M. O.; Lykke, A. M.; King, R. S., Understanding the factors for increased informal electronic waste recycling in Kumasi, Ghana. *Int. J. Environ. Health Res.* **2020**, 1-16.

66. Baghalha, M., Leaching of an oxide gold ore with chloride/hypochlorite solutions. *Int. J. Miner. Process.* **2007,** *82* (4), 178-186.

67. King, S. R.; Massicot, J.; McDonagh, A. M., A straightforward route to tetrachloroauric acid from gold metal and molecular chlorine for nanoparticle synthesis. *Metals* **2015,** *5* (3), 1454-1461.

68. Nam, K. S.; Jung, B. H.; An, J. W.; Ha, T. J.; Tran, T.; Kim, M. J., Use of chloride–hypochlorite leachants to recover gold from tailing. *Int. J. Miner. Process.* **2008,** *86* (1-4), 131-140.

69. Hilson, G.; Monhemius, A. J., Alternatives to cyanide in the gold mining industry: what prospects for the future? *J. Clean. Prod.* **2006,** *14*, 1158-1167.

70. Gorguner, M.; Aslan, S.; Inandi, T.; Cakir, Z., Reactive airways dysfunction syndrome in housewives due to a bleach–hydrochloric acid mixture. *Inhalation Toxicol.* **2004,** *16* (2), 87-91.

71. Canelli, E., Chemical, bacteriological, and toxicological properties of cyanuric acid and chlorinated isocyanurates as applied to swimming pool disinfection: a review. *Am. J. Public Health* **1974,** *64* (2), 155-162.

72. Wojtowicz, J. A., Cyanuric and Isocyanuric Acids. In *Kirk-Othmer Encyclopedia of Chemical Technology*, **2000**.

73. Zwiener, C.; Richardson, S. D.; De Marini, D. M.; Grummt, T.; Glauner, T.; Frimmel, F. H., Drowning in disinfection byproducts? Assessing swimming pool water. *Environ. Sci. Technol.* **2007,** *41* (2), 363-372.

74. Chuenarrom, C.; Daosodsai, P.; Charoenphol, P., Effect of excessive trichloroisocyanuric acid in swimming pool water on tooth erosion. *Songklanakarin J. of Sci. Technol.* **2014,** *36* (4).

75. Saldick, J., Biodegradation of cyanuric acid. *Appl Microbiol* **1974,** *28* (6), 1004-1008.

76. Terman, G. L.; DeMent, J. D.; Hunt, C. M.; Cope, J. T.; Ensminger, L. E., Fertilizer Nitrogen Sources, Crop Response to Urea and Urea Pyrolysis Products. *J. Agric. Food Chem* **1964,** *12* (2), 151-154.

77. Sousa, R.; Futuro, A.; Fiúza, A.; Vila, M.; Dinis, M., Bromine leaching as an alternative method for gold dissolution. *Miner. Eng.* **2018,** *118*, 16-23.

78. Orlando, J. J.; Burkholder, J. B., Gas-phase UV/Visible absorption spectra of HOBr and Br2O. *J. Phys. Chem.* **1995,** *99* (4), 1143-1150.

79. Worthington, M. J. H.; Kucera, R. L.; Abuquerque, I. S.; Gibson, C. T.; Sibley, A.; Slattery, A. D.; Campbell, J. A.; Alboaiji, S. F. K.; Muller, K. A.; Young, J.; Adamson, N.; Gascooke, J. R.; Jampaiah, D.; Sabri, Y. M.; Bhargava, S. K.; Ippolito, S. J.; Lewis, D. A.; Quinton, J. S.; Ellis, A. V.; Johs, A.; Bernardes, G. J. L.; Chalker, J. M., Laying Waste to Mercury: Inexpensive Sorbents Made from Sulfur and Recycled Cooking Oils. *Chem. Eur. J.* **2017,** *23*, 16219-16230.

80. Mann, M.; Luo, X.; Tikoalu, A. D.; Gibson, C. T.; Yin, Y.; Al-Attabi, R.; Andersson, G. G.; Raston, C. L.; Henderson, L. C.; Pring, A.; Hasell, T.; Chalker, J. M., Carbonisation of a polymer made from sulfur and canola oil. *ChemComm* **2021,** *57* (51), 6296-6299.

81. Worthington, M. J. H.; Shearer, C. J.; Esdaile, L. J.; Campbell, J. A.; Gibson, C. T.; Legg, S. K.; Yin, Y.; Lundquist, N. A.; Gascooke, J. R.; Albuquerque, I. S.; Shapter, J. G.; Andersson, G. G.; Lewis, D. A.; Bernardes, G. J. L.; Chalker, J. M., Sustainable Polysulfides for Oil Spill Remediation: Repurposing Industrial Waste for Environmental Benefit. *Adv. Sustain. Syst.* **2018,** *2* (6), 1800024.

82. Alboaiji, S. Porous Polysulfide Polymer in Removing Perfluorooctanoic acid from Water and Extracting Gold. Flinders University, **2017**.

83. Lundquist, N. A.; Worthington, M. J. H.; Adamson, N.; Gibson, C. T.; Johnston, M. R.; Ellis, A. V.; Chalker, J. M., Polysulfides made from re-purposed waste are sustainable materials for removing iron from water. *RSC Adv.* **2018,** *8*, 1232-1236.

84. Mao, J.; Wang, Y.; Lehmann, B.; Yu, J.; Du, A.; Mei, Y.; Li, Y.; Zang, W.; Stein, H. J.; Zhou, T., Molybdenite Re–Os and albite 40Ar/39Ar dating of Cu–Au–Mo and magnetite porphyry systems in the Yangtze River valley and metallogenic implications. *Ore Geol. Rev.* **2006,** *29* (3), 307-324.

85. Huston, D. L.; Large, R. R., A chemical model for the concentration of gold in volcanogenic massive sulphide deposits. *Ore Geol. Rev.* **1989,** *4* (3), 171-200.

86.   Danilov, A. S.;   Matveeva, V. A.;   Korelskiy, D. S.;   Horttanainen, M., Backfill of a Mined-Out Gold Ore Deposit with the Cemented Rubber-Cord and Waste Rock Paste: Environmental Changes in Aqueous Media. *J. Ecol. Eng.* **2021,** *22* (7), 190-203.

87.   James, N. P.; Jones, B., *Origin of Carbonate Rocks*. John Wiley & Sons: **2015**.

88.   Rutley, A. Towards a green method of gold recovery from electronic waste. Flinders University **2020**.

89.   Yang, L.; Jiang, X.; Jiang, W.; Wang, P.; Jin, Y., Cyclic Regeneration of Pyrolusite-Modified Activated Coke by Blending Method for Flue Gas Desulfurization. *Energy Fuels* **2017,** *31* (4), 4556-4564.

90.   Song, W.; Zhou, J.; Wang, B.; Li, S.; Cheng, R., Production of SO2 Gas: New and Efficient Utilization of Flue Gas Desulfurization Gypsum and Pyrite Resources. *Ind. Eng. Chem. Res.* **2019,** *58* (44), 20450-20460.

91.   Cau, G.; Tola, V.; Bassano, C., Performance evaluation of high-sulphur coal-fired USC plant integrated with SNOX and CO2 capture sections. *Appl. Therm. Eng.* **2015,** *74*, 136-145.

92.   Srivastava, R. K.; Jozewicz, W.; Singer, C., SO2 scrubbing technologies: A review. *Environ. Prog.* **2001,** *20* (4), 219-228.

93.   Skirrow, R. G.; Huston, D. L.; Mernagh, T. P.; Thorne, J. P.; Dufler, H.; Senior, A. B. Critical commodities for a high-tech world: Australia's potential to supply global demand. https://www.ga.gov.au/data-pubs/data-and-publications-search/publications/critical-commodities-for-a-high-tech-world (accessed 17th of December 2021).

94.   Lau, S. S.; Dias, R. P.; Martin-Culet, K. R.; Race, N. A.; Schammel, M. H.; Reber, K. P.; Roberts, A. L.; Sivey, J. D., 1,3,5-Trimethoxybenzene (TMB) as a new quencher for preserving redox-labile disinfection byproducts and for quantifying free chlorine and free bromine. *Environ. Sci.: Water Res. Technol.* **2018,** *4* (7), 926-941.

95.   Riaz, A.; Khan, S.; Muhammad, S.; Shah, M. T., Mercury Contamination in Water and Sediments and the Associated Health Risk: A Case Study of Artisanal Gold-mining. *Mine Water Environ.* **2019,** *38* (4), 847-854.

96.   Ju, F.; Hu, Y., Removal of EDTA-chelated copper from aqueous solution by interior microelectrolysis. *Sep. Purif. Technol.* **2011,** *78* (1), 33-41.

Chapter 3

Carbonisation of 50-poly(S-*r*-canola) and use in mercury remediation

Introduction

Since the discover of polymers in 1920, plastics have become part of our life. The term 'plastic' includes a wide spectrum of polymers having different chemical compositions, feed stocks, mechanical characteristics and synthesis methods.[1] Polymers have a myriad of applications throughout many aspects of our lives.[2] Applications range from electronics to automobiles and planes, cutlery, medical devices and clothing.[3] Sadly concessions have been made regarding the recyclability and degradability in order to maximise their performance and durability.[4] Estimations say that 8.3 billion tons of plastic have been synthesized since the 1950's.[3] Not surprisingly, the amount of plastic produced is poised to continue to grow. In 2014, 311 million tons of plastic were produced, indeed a vast increase from only 1.65 million tons in 1950.[3] Polyolefins alone were produced at a rate of 20 kg/person per year in 2012.[5] Plastics make up around 20% of urban waste by volume[6] and only 30% of plastic products were recovered or recycled according to the 'European Strategy for Plastics in a Circular Economy'[7].These vast amounts of plastic waste pollute natural environments around the world.[8] It is estimated that between 9 and 23 million tons end up in the ocean, rivers and lakes (Figure 3.1).[8]
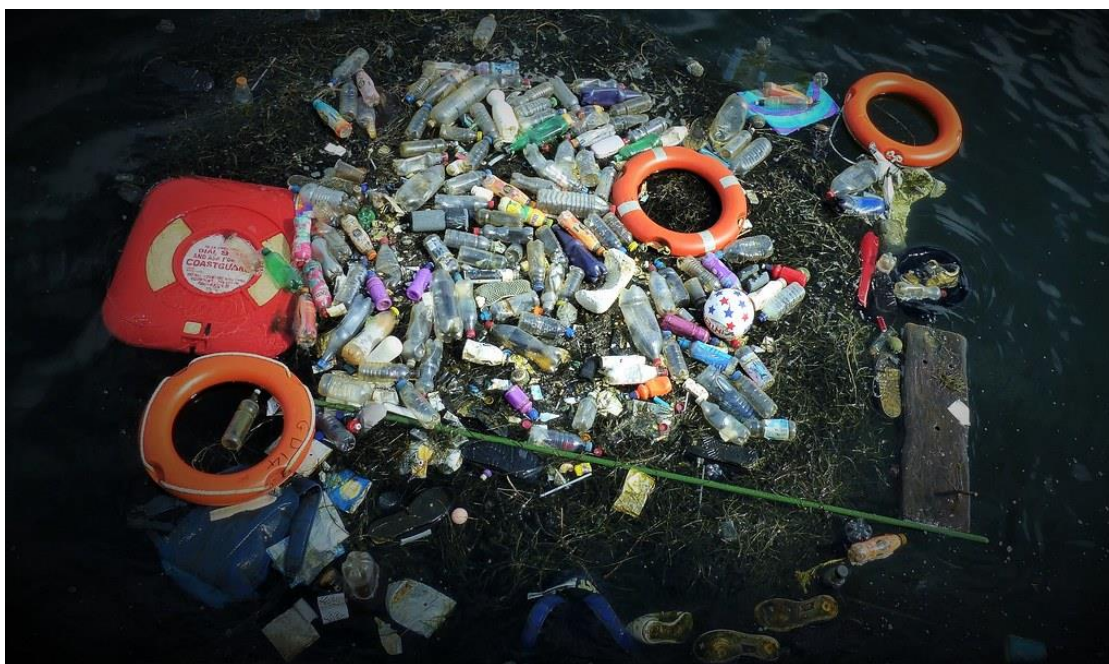
Figure 3.1: Plastic waste in the ocean. Image credit: Charos Pix, this image was reproduced under a Creative Commons Licence: CC BY-NC-SA 2.0

Clearly, end-of-life solutions for polymers as well as sustainable polymers are urgently needed.[9] Additionally, since speedy depletion of fossil fuels means supply shortages for raw materials used in the production of polymers, a need for polymers made from renewable or more abundant materials arises.[1] Some advancements regarding end-of-life solutions have been already made. For example Tondi et al. studied possible end-of-life applications for polyphenolic polymers.[10] In their report they show that tannin foams can be used as pollutant absorbent, having a high affinity for cationic dyes and anionic surfactants.[10]

In the Chalker lab the synthesis of polysulfides using renewable or low-cost precursor materials has been the focus for several years. For instance, the group pioneered the synthesis and applications of a polymer made from elemental sulfur and canola oil (50-poly-(S-*r*-canola).[11] The 50-poly-(S-*r*-canola) polymer has already shown applications in slow release fertilisers,[12] perfluorooctanoic acid (PFOA) and perfluorooctanesulfonic acid (PFOS) removal,[13] and reactive compression molding.[14] Another useful application of the 50-poly-(S-*r*-canola) is that of oil spill remediation[15]. When the polymer is added to a solution of water and oil, the polymer forms an aggregate with the oil which can be easily removed from the water. After that the oil can be separated from the polymer by simple mechanical compression. Further oil can be removed from water by filtering the solution though a 50-poly-(S-*r*-canola) filter.[15] These are just a some of the applications of the 50-poly-(S-*r*-canola) polymer. However, after

the polymer has been used for these applications the question of end-of-life solution remains. For example, after the polymer has been used to remove iron from water,[16] the polymer could be hot pressed into new products for potential use in construction such as rubber mats or bricks.[14]

However, the focus of this chapter will be the end-of-life applications of the 50-poly-(S-*r*-canola) polymer by means of carbonisation. In light of this the carbonisation of unused 50-poly-(S-*r*-canola) polymer as well as of polymer used for oil spill remediation will be explored.

Carbonaceous materials have a long history, spanning back over 5700 years when the Egyptians and Sumerians already made use of wood char for mining applications and as fuel.[17] Today, the term activated carbon can apply to various carbonised materials. Usually, these materials exhibit a high surface area and porosity as well as relatively high chemical stability.[18, 19] A wide range of precursors are used to manufacture activated carbons. These include wood biomass,[20] industrial biomass waste and agricultural waste[17] and other plant materials such as rice husks[21] or straw[22]. The synthesis pathway of activated carbon typically involves two steps. Firstly, a carbonisation procedure to lower the content of volatile matter in the material.[19] Secondly, a activation process to increase the surface area or to functionalise the surface to impart chemical reactivity.[19] Carbonisation can occur at a range of temperatures and conditions. Temperatures can vary between 300-800 °C, sometimes under an inert gas atmosphere (N_2, CO_2, Ar or mixtures).[20, 23] Li and co-workers divide the activation process into three main methods.[19] The first method is physical activation. During this type of activation, the material is treated with O_2, CO_2 or water vapor at temperatures of up to 1200 °C after the carbonisation step. During chemical activation, the second activation pathway, carbonisation and activation take place concurrently at temperatures between 450-850 °C with the addition of chemical agents.[19] These chemical agents can include Zn_2Cl, H_3PO_3, KOH, NaOH or HNO_3.[20] The third activation is physio-chemical activation.[19] As the name suggests this activation is a mix of physical and chemical activation. After chemical agents have been added to the material, physical activation follows, often with the use of an oxidising gas such as O_2.[19] Frequently, the choice of chemical activator determines the chemical and physical characteristic of the resulting activated carbon (Figure 3.2).[18, 19]
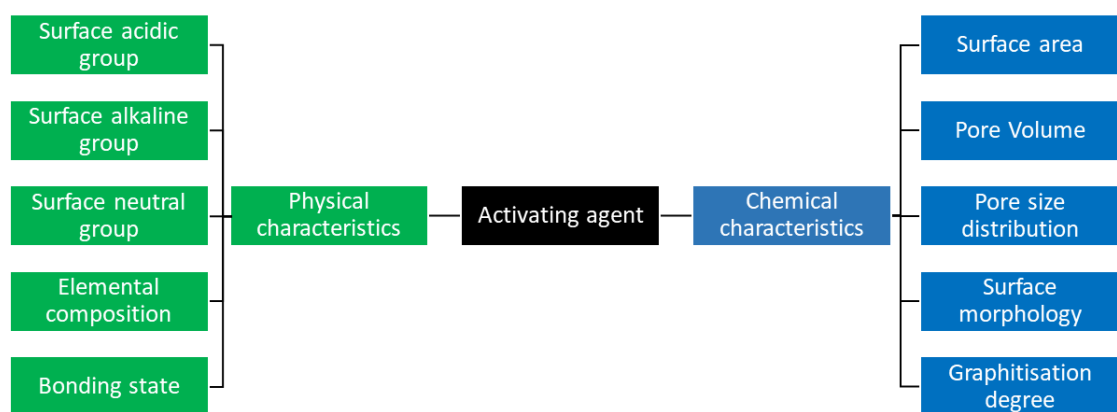
Figure 3.2: Lin et al. show the correlation between activating agent to the physical and chemical characteristics of activated carbons.[19]

There is a continuous expansion of applications for activated carbon. For example, activated carbon is used in desalination, air purification and wastewater treatment.[18, 24]. However, activated carbon also has its drawbacks. One such drawback is that the production of these carbon materials is quite energy intensive and produces a lot of chemical waste.[25] This can result in a high cost of production and regeneration.[20, 21]

Already, some efforts have been made to convert polysulfides into activated carbons.

The Hasell group reported a number of sulfur polymer carbonisations. [26, 27] In their first report they carbonised sulfur-limonene and sulfur-1,3-diisopropenyl benzene (DIB) polymers by carbonisation under inert nitrogen atmosphere at 750 °C. The resulting carbon materials showed promising results for use in gas separation.[26] In another study Hassell et al used a sulfur polymer made from sulfur and dicyclopentadiene (DCPD).[27] After synthesis, the polymer was carbonised by heating under nitrogen atmosphere. Additionally, some of the carbonised polymer was chemically activated by using KOH (Figure 3.3). Their material has been found to be of use in gas adsorption as well as gold and mercury capture.[27]
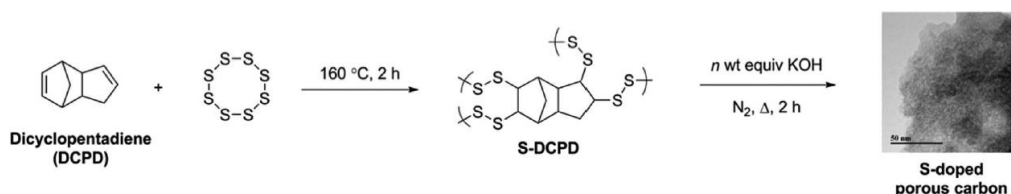
Figure 3.3: Hassell et al first synthesised a polysulfide from DCPD and sulfur before turning the polymer into activated carbon by heating under nitrogen atmosphere and KOH activation. © The Royal Society of Chemistry 2017. This image was reproduced under a Creative Commons CC BY 3.0 license.

The development of materials that can capture mercury is becoming more and more important, since there is a rising concern over global heavy metal contamination of air, water and soil.[28] Causes of heavy metal contamination range from anthropogenic sources like coal combustion, steel production, mining and waste products of industrial, agricultural or domestic origin. Heavy metal contamination also results from natural processes like geological weathering.[28, 29] Since heavy metals are persistent, bioaccumulation is a concern, contributing to contamination of the food chain, which can adversely affect human health.[30] Mercury is known to be a carcinogen, teratogen, and mutagen and readily bioaccumulates in fish species consumed by humans.[31] Heavy metals predominately accumulate in the liver, bones and kidneys causing diseases such as cancer, kidney dysfunction and vascular disease.[32] Recent research efforts in that regard have explored heavy metal remediation by means of microorganisms, functionalised carbon nanotubes and carbons.[29, 33-37]

Since sulfur is known to bind to mercury, attention has been given to sulfur rich materials such as molybdenum disulphide nanosheets, thiol functionalised porous organic polymers or sulfur functionalised polyaniline nanofiber electrodes to capture mercury.[38-41] Along with regular activated carbon, sulfur-impregnated or sulfur doped carbon has been shown to have excellent mercury capture capabilities.[27, 42] Although Hasell et al. were able to demonstrate that a sulfur-doped microporous carbon from an inverse vulcanised polymer using sulfur and DCPD outperforms activated carbon in the uptake of mercury, the upscaling of this material can prove challenging considering the potential of a runaway reaction during the polymer synthesis[27, 43].

Hence the aim of this chapter is to determine if carbonisation of 50-poly(S-r-canola) can lead to a carbonaceous material that is useful in the uptake of mercury from solution even after the polymer has already been used to remove oil from water. The synthesis of 50-poly(S-r-canola) is much safer than that of S-DCPD for example and carbonisation of 50-poly(S-r-canola) could lead to a sulfur rich carbon material.

Carbonisation of 50-poly(S-*r*-canola)

As discussed in Chapter 2, the 50-poly(S-*r*-canola) polymer can be made on multi-kg scale in the lab, and a tone scale industrially. This is of great advantage since the Chalker lab has developed many applications for this material as had been mentioned in the introduction to this chapter. To develop additional uses for this polymer we wanted to assess if a carbonised form of this polymer could be made and if it could prove useful in mercury remediation applications. Previous studies that have carbonised polysulfides usually do so under an inert gas atmosphere.[26, 27] For this study we wanted to simplify the carbonisation method as much as possible. Hence, the carbonisation was undertaken without an inert gas atmosphere. Firstly, the 50-poly(S-*r*-canola) polymer (the polymer used here was synthesised in the lab scale by the author) was thermomechanically analysed. This was done by simultaneous thermal analysis (STA) which included both thermal gravimetric analysis (TGA) and dynamic scanning calorimetry (DSC). For this type of analysis, a sample is weighed and undergoes a controlled temperature ramp. During this heating, the mass and heat flow of the sample are recorded.

STA analysis of 50-poly(S-*r*-canola) showed two characteristic mass losses (Figure 3.4). The first mass loss was starting at around 180 °C and continued to up to around 315 °C. Our lab and others have previously attributed this mass loss to a process during which the weaker S-S bonds of the sulfur rich areas of the polymer decompose into products such as sulfur dioxide.[11, 44] During the second mass loss step between 315 °C and 500 °C, remaining organic and sulfurous material decomposes (Figure 3.4).[11, 44]
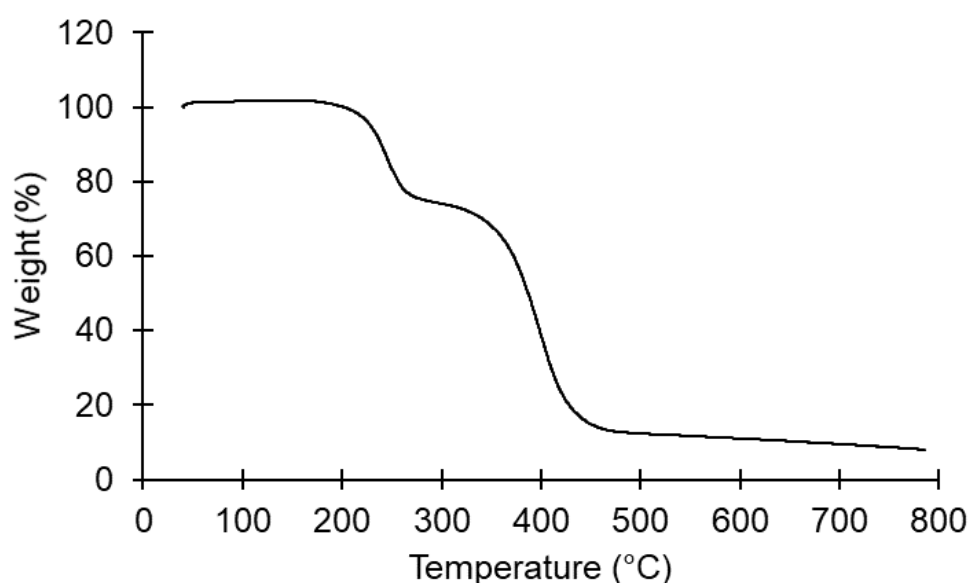
Figure 3.4: TGA of 50-poly(S-*r*-canola) polymer

After the polymer has been heated to 500 °C a total mass loss of 88% had occurred and only 4% of additional mass loss was observed between 500 °C and 800 °C. Therefore, it was reasoned that carbonisation of the polymer at 600 °C should result in an incomplete combustion while still yielding a carbonised material. For the first carbonisation 100 g of polymer was placed in a 1.1 L Al_2O_3 crucible. This crucible was then placed in a muffle furnace and the carbonisation process was started. The heating protocol for the carbonisation process was to heat the sample to 600 °C using a ramp of 5 °C per minute in an atmosphere of air. After the final temperature was reached the temperature was held for 30 minutes. Lastly, the furnace was allowed to cool down naturally. This process was performed while the furnace was in the fume hood to avoid the escape of any off gas into the laboratory. During the carbonisation process some gas was observed exiting the furnace chimney. The color of the gas turned from yellow to white to black as the heating continued. The carbonisation resulted in a black carbon material that will be called carbonised-1 from this point onward. It was observed that the volume of carbonised-1 was higher than that of 50-poly(S-*r*-canola). This can be attributed to the foam like composition of carbonised-1. As the crucible had cooled to room temperature and was removed from the furnace, a single foam like, brittle piece of carbonised-1 was observed (Figure 3.5). The weight of the first carbonisation was 12.5 g which corresponded to 12.5 % of its original mass and a mass loss of 87.5%. This matches closely with was expected when the mass loss of 88% during the TGA analysis of 50-poly(S-*r*-canola) is taken into account (Figure 3.4).
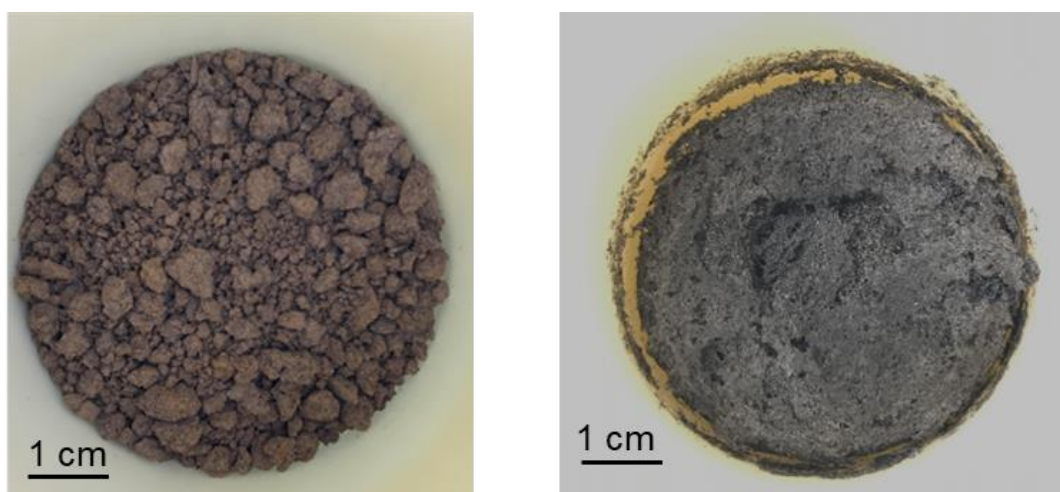
Figure 3.5: 100 g of 50-poly(S-*r*-canola) in crucible before carbonisation on the left and after carbonisation on the right. The texture of carbonised-1 was that of brittle foam. Reproduced with permission from the Royal Society of Chemistry.[45]

Next, carbonised-1 was removed from the crucible and ground using mortar and pestle and stored (Figure 3.6). A total of three carbonisations with 100 g of 50-poly(S-*r*-canola) were performed. Subsequent second and third carbonisations resulted in 13.6 g and 12.3 g of carbonised-1 respectively. The small variations in the yield are attributed to the polymer which was synthesized on a large scale and might have slight variations of composition within the batch used for the carbonisations. The total yield of three, 100 g carbonisations was 38.4 g which is 13% of the original polysulfide mass.

Figure 3.6: Carbonised-1 after grinding using mortar and pestle. Reproduced with permission from the Royal Society of Chemistry.[45]

Although no SO_2 scrubbing was performed for the small-scale carbonisations, such measures would be necessary if carbonisation is to be performed on a larger scale. However, appropriate scrubbing technologies are already available. Flue gases resulting from the combustion of sulfur-rich substances can be converted to sulfate,[46, 47] sulfuric acid[48] or sulfur.[49] The conversion of flue gases to sulfur would result in the recovery of a monomer used to synthesise 50-poly(S-*r*-canola), which then in turn can be used again in polysulfide synthesis. Next, carbonised-1 was characterised.

Characterisation of carbonised -1

The first technique used was scanning electron microscopy (SEM) in conjunction with energy dispersive X-ray spectroscopy (EDX). SEM revealed that carbonised-1 is made up of carbon sheets with a high amount of sulfur on the surface. (Figure 3.7).
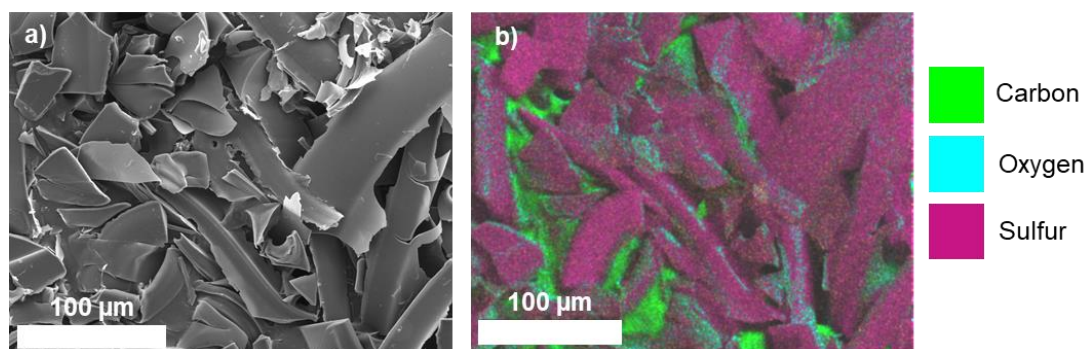
Figure 3.7: a) SEM micrograph of carbonised-1 and b) EDX elemental map of carbon, oxygen and sulfur. Reproduced with permission from the Royal Society of Chemistry.[45]

The sulfur on the surface of the carbon was intriguing and unexpected. With this discovery, the hypothesis was made that the sulfur content can potentially be beneficial for mercury removal. To gain more insight of the elemental composition, elemental analysis to determine the content of carbon, hydrogen, nitrogen, and sulfur, short CHNS analysis was performed. As expected, the majority of carbonised-1 was carbon with 65.5 wt% (Figure 3.8). Interestingly, the second most abundant element was sulfur with 16.0% and very small amounts of hydrogen (1.6%) and nitrogen (<0.3%) were observed as can be seen in Figure 3.8. The remainder of the material was made up of elements other than carbon, hydrogen, nitrogen, or sulfur. It is likely that the unknown mass is oxygen from the triglyceride component of the polymer. This is also consistent with XPS analysis, which showed evidence for C-O (Figure 3.13) and S-O (Figure 3.14) bonds in carbonised 1.
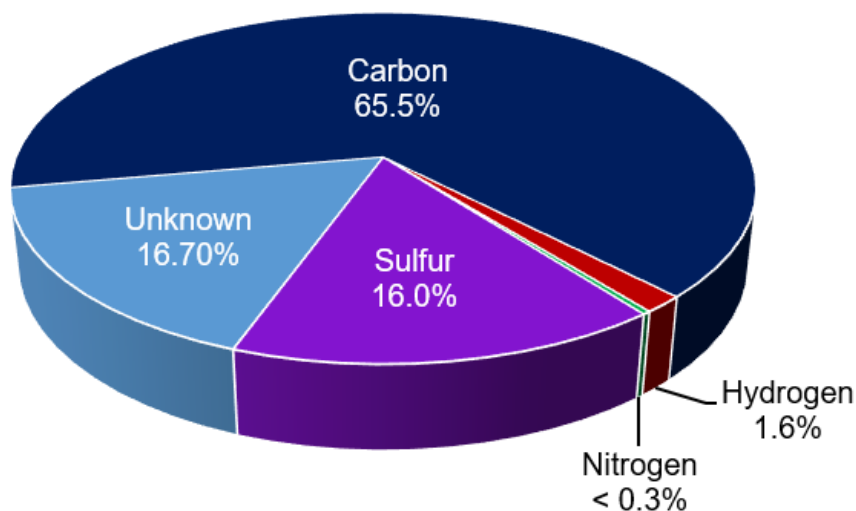
Figure 3.8: CHNS analysis of carbonised-1 showed 65.5% carbon, 16% sulfur, 1.6% hydrogen, less than 0.3% nitrogen and 16.7% unknown elements (elements other than carbon, hydrogen, nitrogen, or sulfur. Likely oxygen from the triglyceride component of the polymer.).

A sulfur content of 4% is described as high in some other reports on sulfurised carbons.[50] Hence, a sulfur content of 16% is a reasonably high level compared to other sulfur containing carbon materials. Further, previous reports mention that for carbons with a high sulfur content, the reactive sulfur on the surface of the material is crucial in mercury sorption.[42] Considering that carbonised-1 is rich in sulfur on the surface, it seemed to be an attractive candidate for mercury sorption. Next, we wanted to determine the surface area of carbonised-1 via Brunauer-Emmett-Teller (BET) analysis. This analysis proved to be quite challenging since, as can be seen in the SEM micrographs (Figure 3.7), carbonised-1 has no obvious porosity. However, for BET analysis to give satisfactory results, sufficient surface area is required for the gas to adsorb and desorb during the analysis. To that end multiple analyses were run, and an average surface area was determined. The surface area of carbonised-1 was 111 m^2/g. Knowing this, we wanted to compare our carbon to other carbons. Therefore, three additional carbons were procured: Kuraray PGW-150MP, a powdered activated carbon, powdered activated carbon (PAC) purchased from ChemSupply with a nominal particle size of 45 µm, and a granular activated carbon (GAC) purchased from Sigma-Aldrich with an 8-20 mesh particle size, corresponding to 2.38 mm to 0.84 mm particle size (Figure 3.9). BET analysis was performed on these additional carbons. The highest surface area was seen in the Kuraray PGW-150 MP with 1131 m^2/g followed by the PAC with 742 m^2/g and GAC having a surface area of 125 m^2/g. That placed carbonised-1 at the lower end of the surface areas of carbons tested. SEM and EDX analysis were performed on the

additional carbons as well to assess if any differences could be seen between them and carbonised-1.

Figure 3.9: Images carbons procured to be compared to carbonised-1 a) Kuraray PGW-150MP powdered activated carbon, b) ChemSupply powdered activated carbon (PAC) and c) Sigma-Aldrich granulated activated carbon (GAC).

As can be seen in the SEM micrographs in Figure 3.10, Kuraray's PAC presents as large particles, some around 200 µm in size, which have small pores on the surface. The material seems to have channels throughout resulting in a large surface area. And indeed, that was what was observed, as already discussed Kuraray PGW-150MP had the largest surface area with 1131 m^2/g. Since ChemSupply's PAC is a powder, smaller particle size was expected, which was confirmed during SEM analysis (Figure 3.10). Interestingly, this material does not seem as porous as the Kuraray carbon, resulting in a lower surface area (742 m^2/g) observed during BET analysis. The granulated activated carbon (Sigma-Aldrich) had a large particle size as was expected (Figure 3.10). Although the material appears very porous, the pores are very large compared the Kuraray's carbon which would explain the lower surface area of 125 m^2/g. EDX analysis of these materials showed a carbon content of over 90% in all of them. Small traces of sulfur were seen in Kuraray PGW-150MP. ChemSupply's PAC and Sigma-Aldrich's GAC showed some aluminium and silicon respectively. These impurities could be artifacts from the manufacture since it is not known how or from what these materials were made. Additionally, CHNS analysis was also performed in the commercial carbons. Sulfur, nitrogen, and hydrogen were present in negligible amount of under 1%. However, the carbon content was the highest with 91.4% in Kuraray PGW-150MP, followed by 82.4% in ChemSupply PAC and 78.6% in Sigma-Aldrich GAC. The remaining percentage was made up of unknown elements.
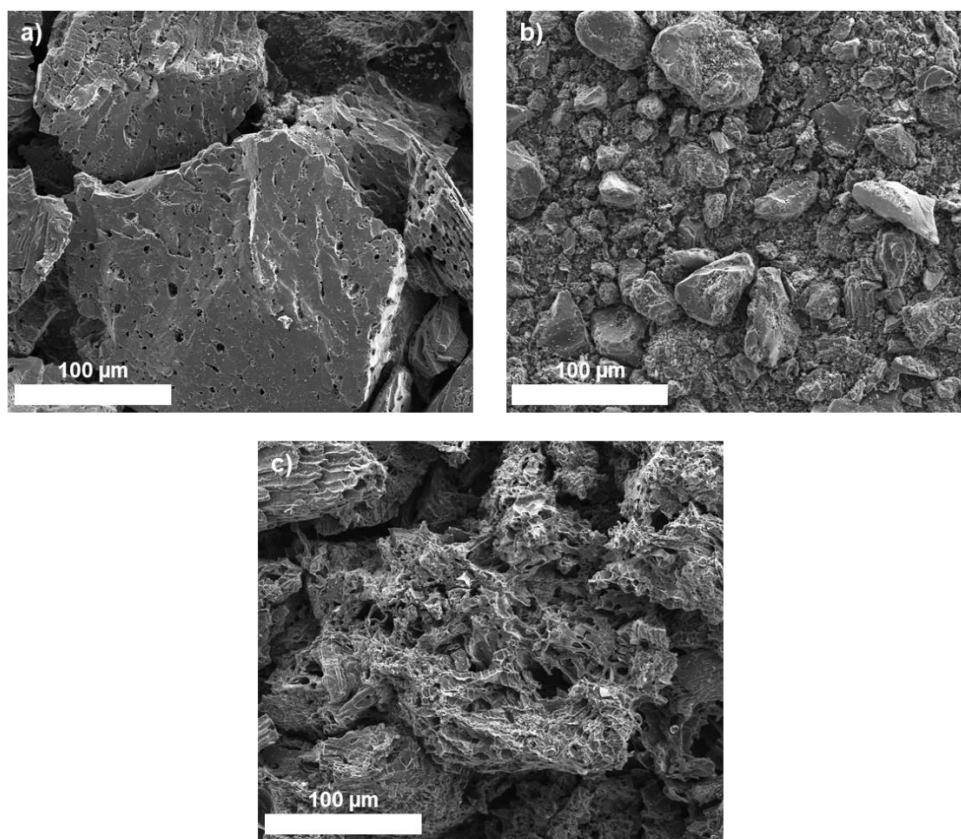
Figure 3.10: SEM micrograph of **a)** Kuraray PGW-150MP, **b)** ChemSupply PAC and **c)** Sigma-Aldrich GAC. Reproduced with permission from the Royal Society of Chemistry.[45]

To gain a better insight on the structure of carbonised-1 and the other activated carbons, Raman spectroscopy was utilised. Raman spectroscopy can prove very useful in the characterisation of activated carbon samples since the position and intensity of Raman peaks can provide an insight in the structural characteristics of the sample. Associated to the vibrational mode of the sp^2-hybridised planes in graphene is the G peak with is usually centered between 1560 to 1600 cm^{-1}. Another important peak is the D peak which can be found at 1300 to 1400 cm^{-1}. This peak arises due to defects in the material and can be an indicator for the degree of disorder in graphitic materials.[51] Therefore, is it not uncommon to use the ratio of D band to G band intensities, I_D/I_G, to probe the degree of disorder and functionalisation of various types of carbon materials.[52] The I_D/I_G for carbonised-1 was 0.85 (Figure 3.11). This was lower than for the three commercial carbons which all had an I_D/I_G value of 1.2. That the value is lower in carbonised-1 suggests a lower degree of defects and therefore functionalisation. The reason for this may well lie in the non-porous graphitic structure of carbonised-1 compared to the other carbons which had higher porosity. As Raman analysis was performed on carbonised-1, multiple areas were analysed, and hundreds of spectra were recorded for each area. It is noteworthy that no indication of S_8 was found. However,

EDX analysis revealed sulfur on the surface of carbonised-1 which is likely not in the form of S_8.
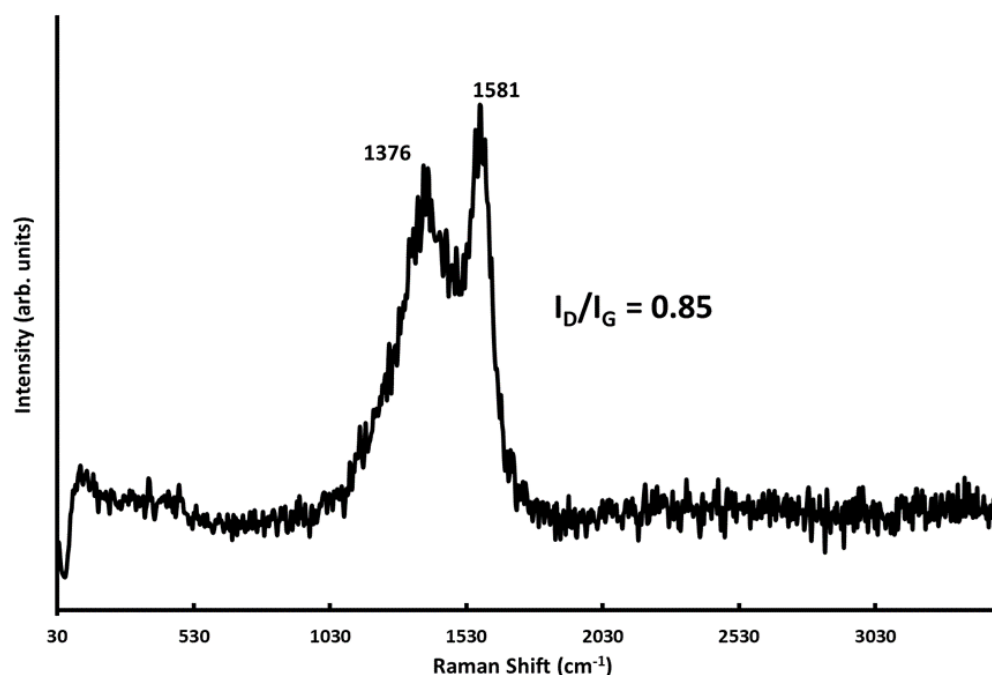
Figure 3.11: Raman spectrum of carbonised-1. Reproduced with permission from the Royal Society of Chemistry.[45]

This suggests shorter sulfur chains of sulfur which are covalently bound to the surface of the carbon. To confirm this, powder X-ray diffraction (XRD) was performed in carbonised-1. The result confirmed the absence of crystalline sulfur on the surface of carbonised-1 as can be seen in Figure 3.12, since the characteristic peaks of crystalline sulfur cannot be seen. XRD also showed that carbonised-1 had a low degree of crystallinity. Further a broad reflection at d = 3.6 Å can be seen (Figure 3.12). This peak corresponds to the van der Waals contact between graphite like sheets in carboised-1. While this reflection is also present in the commercial carbons, a further reflection at d = 2.06 Å is visible in the commercial carbons. The later reflection corresponds to the 101 reflections of graphite-2H. The absence of this reflection in carbonised-1 led to the conclusion that carbonised-1 has a highly disordered stacking of carbon sheets.
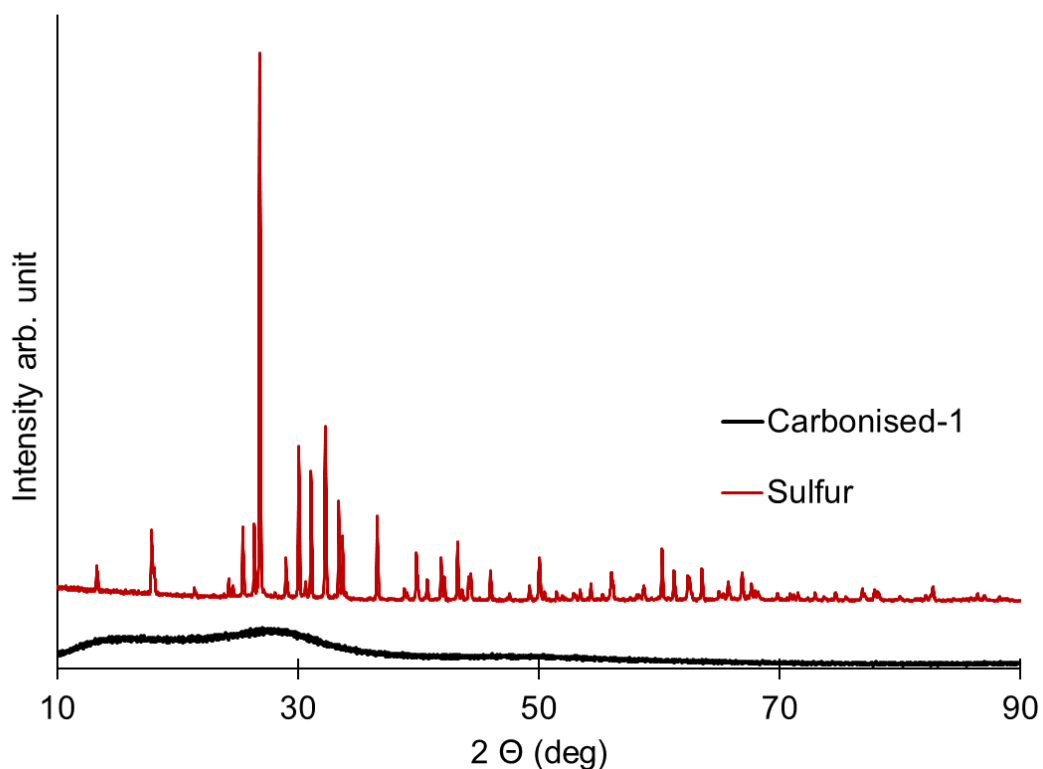
Figure 3.12: XRD spectra of carbonised-1 and sulfur. Reproduced with permission from the Royal Society of Chemistry.[45]

In an effort to gain further insight into to structure of carbonised-1, X-ray photoelectron spectroscopy (XPS) was performed. The analysis showed C=O, C-O and C-S signals (Figure 3.13).
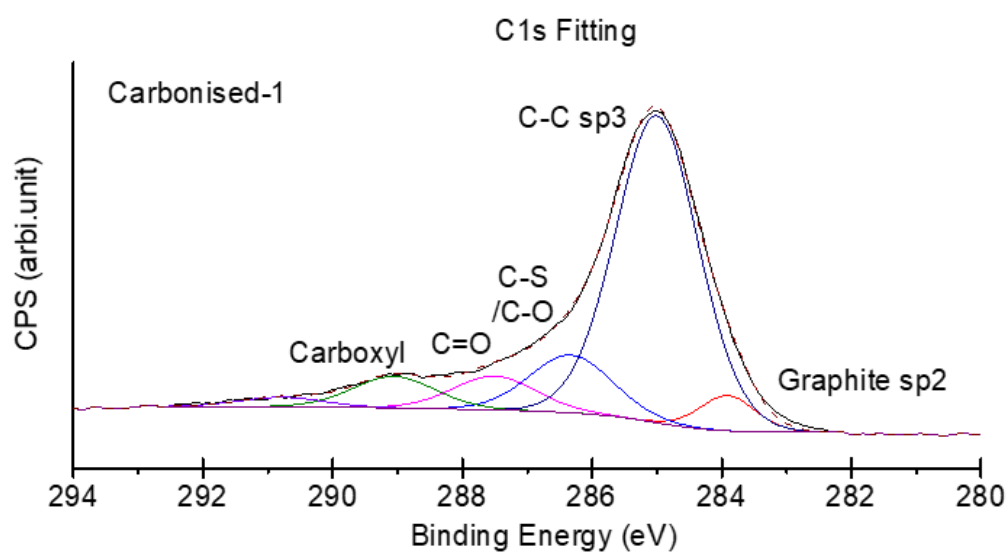
Figure 3.13: XPS analysis of carbonised-1 (carbon 1s fitting). Reproduced with permission from the Royal Society of Chemistry.[45]

192

Additionally, sulfur in high oxidation states (SO_x) were also observed, likely due to the carbonisation in air. This analysis showed evidence of C-S functionality which was consistent with the proposed structure of a sulfurised graphitic material (Figure 3.14).
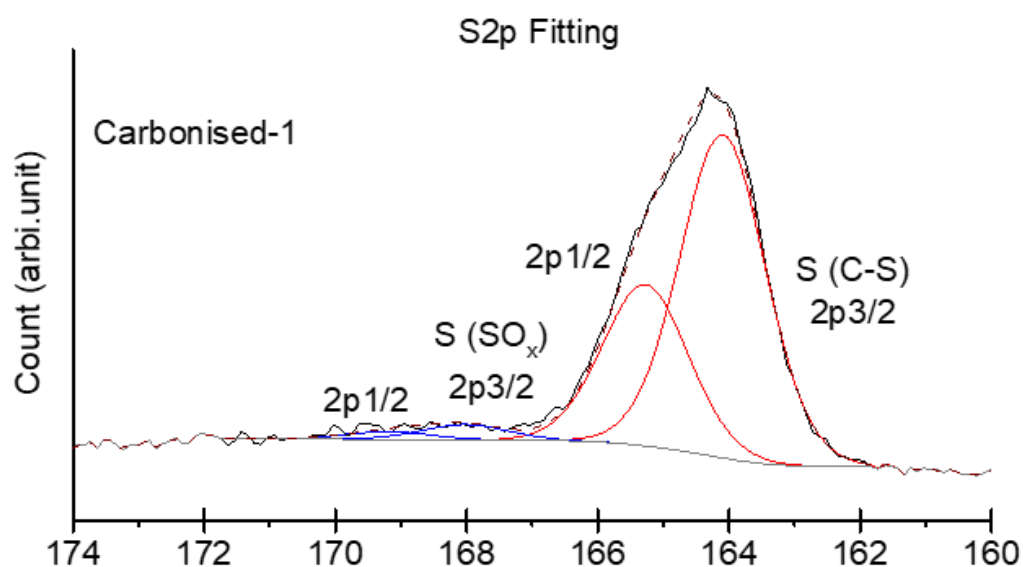
Figure 3.14: XPS analysis of carbonised-1 (sulfur 2p fitting). Reproduced with permission from the Royal Society of Chemistry.[45]

Heavy metal sorption studies

Having successfully carbonised 50-poly(S-*r*- canola) and discovered its large sulfur content, it was hypothesised that the sulfur functionality would result in a high affinity for mercury. To test this, mercury uptake experiments was performed. As source of mercury, $Hg(NO_3)_2$ was used since it is readily soluble in water. Additionally carbonised-1 was also tested as sorbent for As (As_2O_5), Cd ($Cd(NO_3)_2$), and Pb ($Pb(NO_3)_2$). A solution containing 5 ppm of each heavy metal was prepared in deionised water. Before carbonised-1 was used, it was sieved to a size of 150-500 µm. Next, 100 mg of sorbent was added to the mercury solution and rotated end-over-end at 25 RPM for 2 hours total. For comparison, the same experiment was performed for Kuraray PGW-150MP the commercial carbon with the highest surface area. As can be seen in the Figure 3.15, a negligible amount of arsenic and cadmium is removed by either carbon. Carbonised-1 was able to remove more lead from solution (18%) than PGW-150MP (5.5%). However, by far the highest uptake for both carbons were seen for mercury with over 90% removed (Figure 3.15).
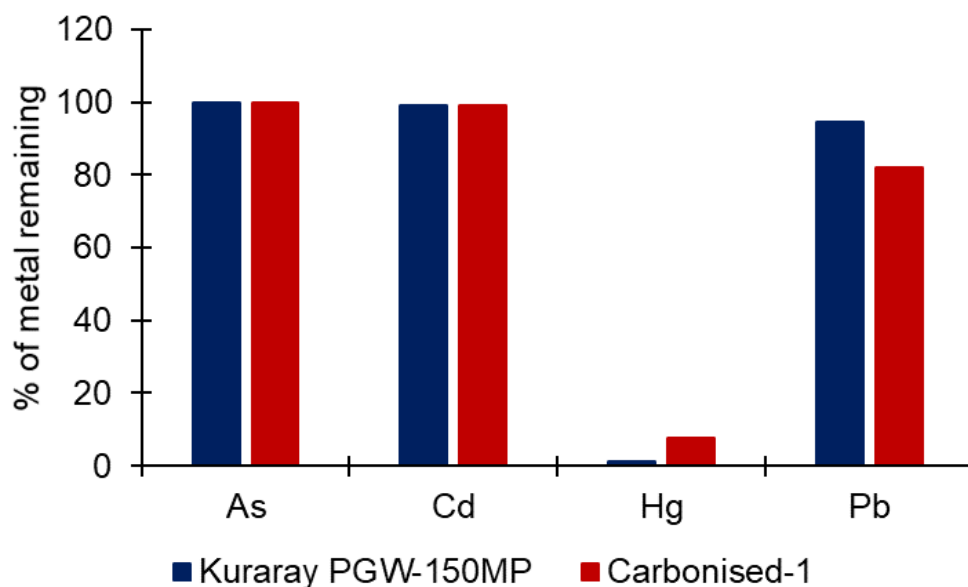
Figure 3.15: Uptake of As, Cd, Hg, and Pb from aqueous solutions using Kuraray PGW-150MP and carbonised-1. Reproduced with permission from the Royal Society of Chemistry.[45]

Since it became obvious that carbonised-1 had a higher affinity for mercury than for arsenic, cadmium or lead, subsequent sorption studies were conducted using mercury. Next, carbonised-1 was sonicated to investigate if sonication changes the mercury sorption properties of carbonised-1 by homogenising the material and by breaking down large particles. The sonicated carbonised-1 was analysed for difference in particle size using SEM. As expected, smaller more uniform particle sized were observed in the SEM micrographs (Figure 3.16).
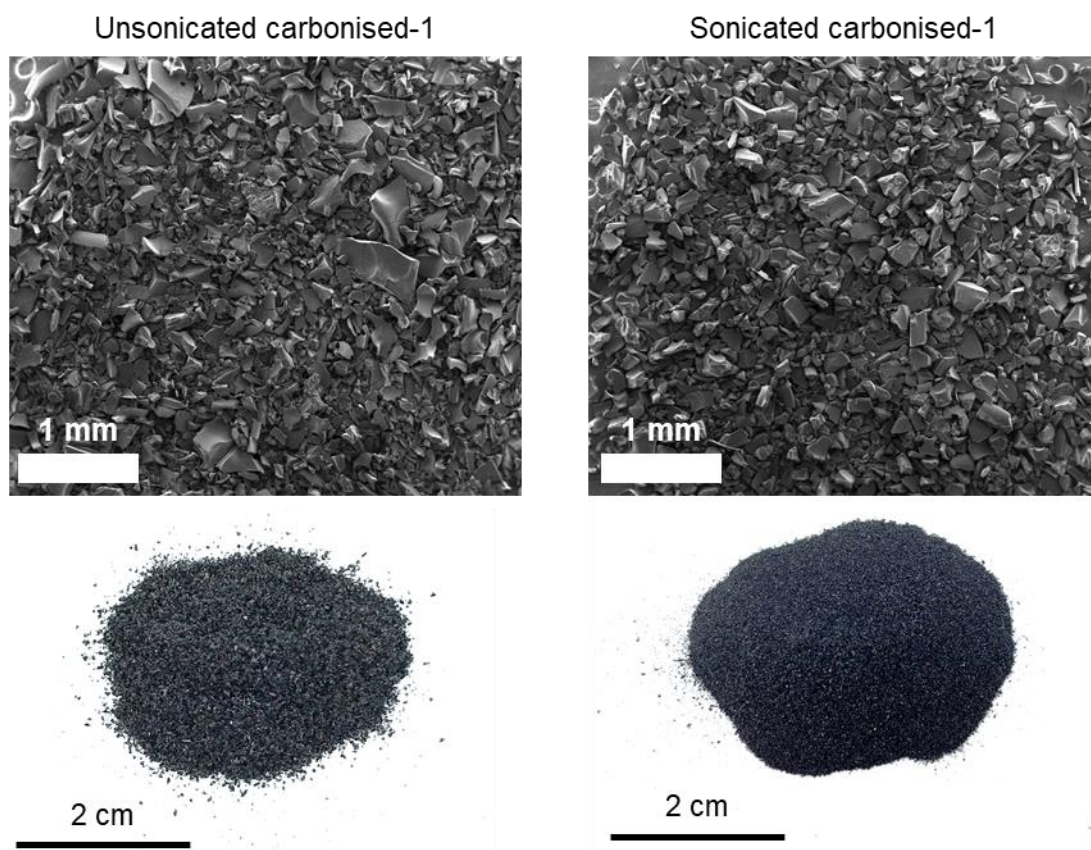
Figure 3.16: SEM micrographs and optical photographs of unsonicated and sonicated carbonised-1. Reproduced with permission from the Royal Society of Chemistry.[45]

Next, the mercury uptake of sonicated carbonised-1 was compared to the commercial carbon samples and unsonicated carbonised-1 using the same method as above. As a control to monitor mercury concentration in the stock solution, one sample of just 5 ppm Hg in deionised water was also tested. Further, the mercury uptake of the parent polymer, 50-poly(S-*r*-canola) was also tested as a comparison. The results showed that that the sonicated carbonised-1 had the highest mercury uptake of all samples tested with a total of 99% of mercury removed (Figure 3.17). This was followed by Kuraray PGW-150MP with 98% mercury removal. Interestingly, sonication seemed so improve mercury uptake since the sonicated carbonised-1 removed an additional 5% of mercury compared to the unsonicated carbonised-1. However, mercury uptake was initially faster using PGW-150MP. The other two commercial carbons removed 90% (Sigma-Aldrich GAC) and 70% (ChemSupply PAC). The parent polymer, 50-poly(S-*r*-canola) only removed 43% of mercury highlighting that carbonisation of the polymer increased rate of mercury sorption. Since carbonised-1 has a much lower surface area then Kuraray PGW-150MP we attributed the higher performance of carbonised-1 to its

high sulfur content. These sulfur rich domains serve as distinct binding sites which are lacking in the non-sulfurised carbons. The mercury uptake studies also suggested that the sulfur functionality is paramount for mercury uptake and that a high surface area is advantageous but not strictly necessarily for effective mercury removal.
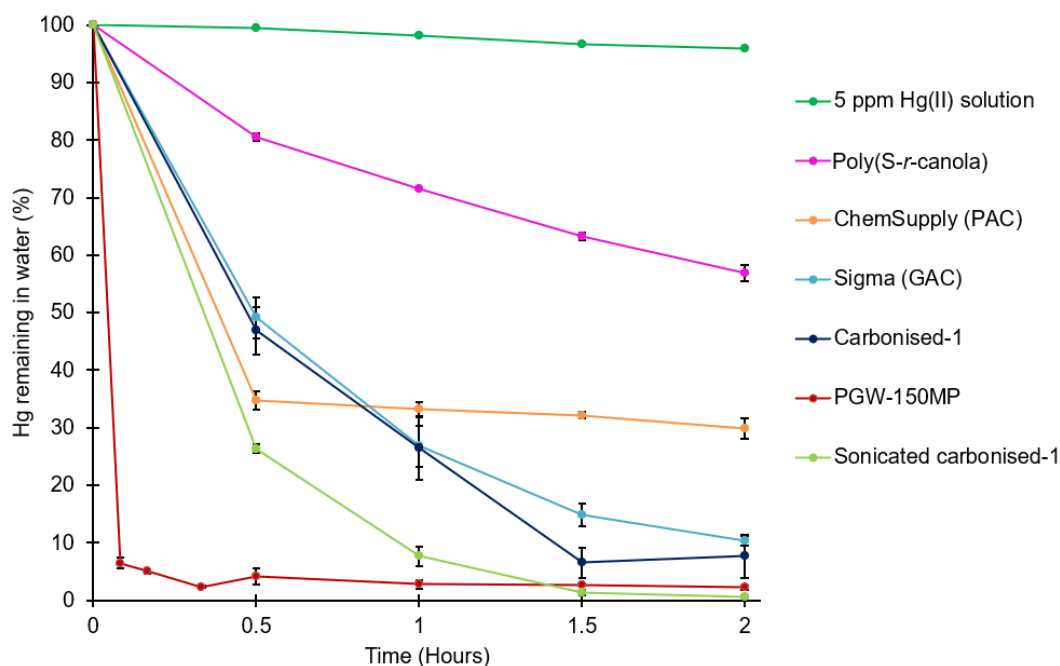
Figure 3.17: Mercury (Hg(NO₃)₂) uptake from aqueous solution using 50-poly(S-*r*-canola), ChemSupply PAC, Sigma-Aldrich GAC, carbonised-1, Kuraray PGW-150MP and sonicated carbonised-1 as sorbent. Reproduced with permission from the Royal Society of Chemistry.[45]

Kinetic analysis was performed on the mercury removal rates. To do this, the mercury removed per gram of polymer was calculated based on the concentrations of mercury removed during the sorption studies and the mass of sorbent used. Then pseudo-first and pseudo-second order kinetic models were applied to the data.[53, 54] The linear equations can be written as:

Pseudo-First Order (linear)[53]

$$\ln (q_e - q_t) = \ln q_e - k_1 t$$

Pseudo-Second Order (linear)[54]

$$\frac{t}{q_t} = \frac{1}{k_2 q_e^2} + \frac{1}{q_e}$$

These equations can then be rewritten in non-linear form as:

Pseudo-First Order (non-linearised)[53]

$$q_t = q_e\left(1 - e^{-k_1 t}\right)$$

Pseudo-Second Order (non-linearised)

$$q_t = \frac{q_e^2 kt}{1 + q_e kt}$$

q_e = mercury bound to the carbon substrate at equilibrium (mg mercury / g polymer)

q_t = mercury bound to the carbon substrate at time t (mg mercury / g polymer)

k_1 = rate constant of pseudo-first order kinetic model (hour^{-1})

k_2 = rate constant of pseudo-second order kinetic model (mg.g^{-1}.hour^{-1})

t = time (hours)

Using these equations, the rate constants for carbonised-1, sonicated carbonised-1 were determined. The calculations showed that the best fit for both sorbents was a first order model (Table 3.5 in the experimental section). For carbonised-1 the rate constant was k_1 = 1.14 h^{-1}. Sonication did increase the rate as can be seen in Figure 3.17 resulting in k_1 = 2.65 h^{-1} for sonicated carbonised-1.

Isotherms, fitted to the Langmuir model, were used to determine the mercury capacity of carbonised-1 and compared to the highest performing commercial carbon Kuraray PGW-150MP. The analysis showed that carbonised-1 had a mercury capacity of 1.1 mg/g and Kuraray PGW-150MP achieved 9.7 mg/g. However, given that the surface area of Kuraray PGW-150MP (1131 m^2/g) is nearly 10 times larger than that of carbonised-1 (125 m^2/g), these carbons show a similar capacity for mercury uptake relative to their surface areas.

Carbonisation of 50-poly(S-*r*-canola) previously used for oil sorption

Having established that 50-poly(S-*r*-canola) can be easily carbonised and is excellent in mercury removal, consideration of end-of-life solutions for the original polymer was revisited. Previously, the Chalker group has used the 50-poly(S-*r*-canola) polymer as a sorbent to clean up oil spills.[15] In this study, 50-poly(S-*r*-canola) was used to remove oil from water and then subjected to carbonization to extend the lifetime and utility of the polymer. This was done by first adding 200 mL of 2 stroke motor oil into a dish containing 1.5 L of water. To this mixture 100 g of 50-poly(S-*r*-canola) was added

and the solution was stirred. Within a couple of minutes, the oil and polymer formed an aggregate. Next, the polymer was removed using a small net, and the oil was recovered by mechanical compression. Visually, the polymer had a slight blue discoloration due to residual oil (the oil used was a blue 2-stroke motor oil) as compared to unused 50-poly(S-*r*-canola) polymer. The same carbonisation method as previously described was used on this polymer and the resulting material will be referred to as carbonised-1-O. Further, carbonised-1-O was sonicated since sonication increases mercury uptake as discussed previously. After the carbonisation process no visible difference between carbonised-1 and carbonised-1-O could be seen. As was the case with the other carbon materials, carbonised-1-O was thoroughly characterised. SEM and EDX analysis were very similar to carbonised-1. Carbonised-1-O showed no visible porosity, but large amounts of sulfur were seen on the surface (Figure 3.18). Further, the surface area of carbonised-1-O was found to be 228 m^2/g which is approximately double that of carbonised-1. This difference could possibly be due to foaming and combustion of residual oil during the carbonisation process.
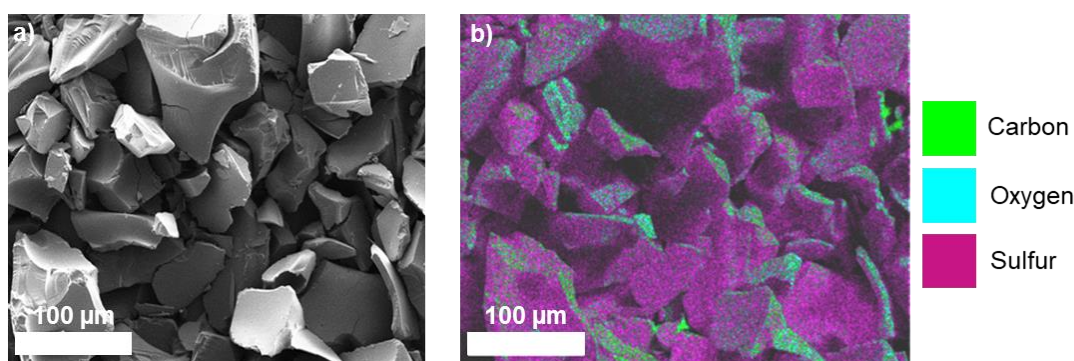
Figure 3.18: **a)** SEM micrograph of carbonised-1-O and **b)** EDX elemental map of carbon, oxygen and sulfur. Reproduced with permission from the Royal Society of Chemistry.[45]

No significant differences could be seen between the elemental CHNS analysis of carbonised-1-O compared to carbonised-1 (Figure 3.19). The carbon content was slightly higher in carbonised-1 by 2%. Nitrogen and hydrogen content were virtually the same in both materials. Sulfur content was only 0.8% lower in carbonised-1-O than it was in carbonised-1 and the number of unknown elements was 2.7% higher in carbonised-1-O. This could be due to some contamination from the oil since it was impossible to remove all the oil from the polymer before the carbonation step.
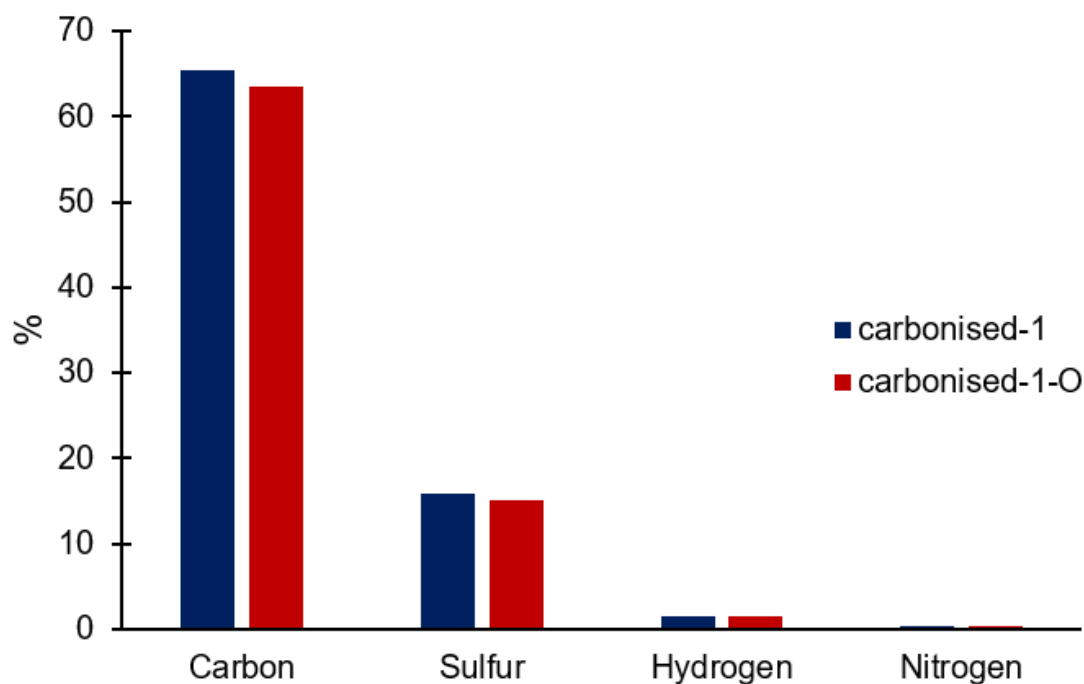
Figure 3.19: CHNS elemental analysis of carbonised-1-O compared to carbonised-1.

Raman spectroscopy of carbonised-1-O showed a I_D/I_G of 0.76 which was close to the I_D/I_G ration of 0.85 observed for carbonised-1. Further no significant difference could be seen in the XRD spectra between carbonised-1-O and carbonised-1. XPS analysis on carbonised-1-O showed no significant differences to carbonised-1. Importantly, the C-S functionality was still present in carbonised-1-O.

Mercury uptake of carbonised-1-O

Finally, mercury uptake of carbonised-1-O was assessed using the same procedure as has been used for carbonised-1 and the commercial carbons. Interestingly, the rate of mercury uptake of carbonised-1-O rivaled that of Kuraray PGW-150MP. As can be seen in Figure 3.20, carbonised-1-O removes 99% of mercury as does the sonicated carbonised-1, both of which outperform Kuraray PGW-150MP, which removed 97%. Also noteworthy is that sonicated carbonised-1 had a slower mercury uptake as compared to Kuraray PGW-150MP. However, carbonised-1-O had a similar rapid initial mercury uptake comparable to that of Kuraray PGW-150MP (Figure 3.20).
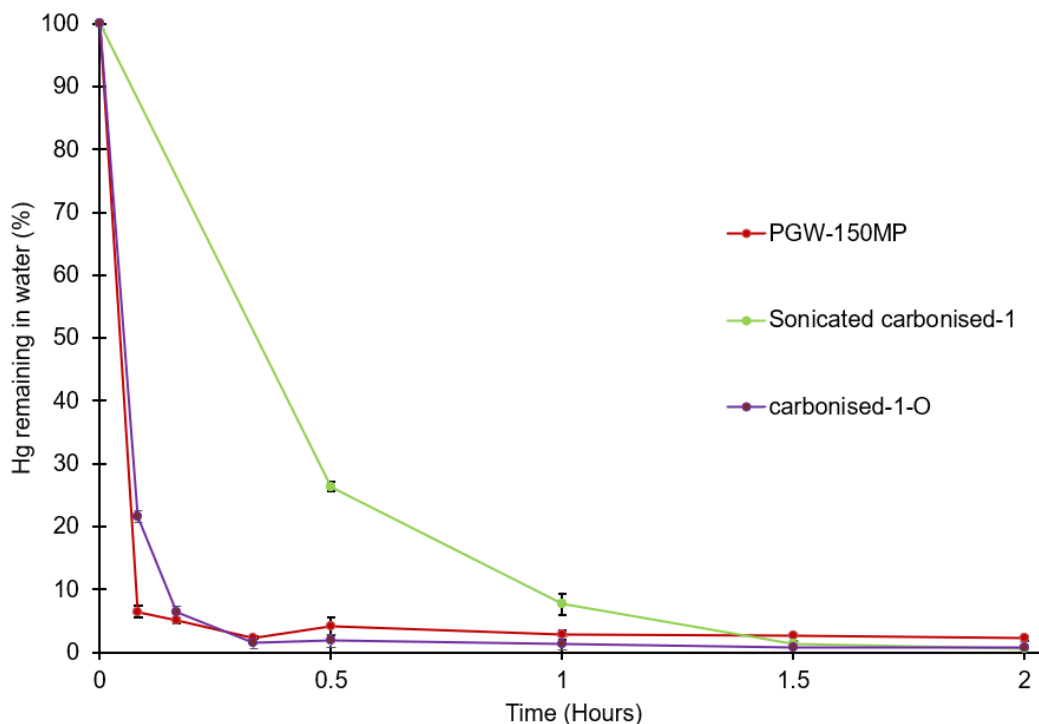
Figure 3.20: Mercury $(Hg(NO_3)_2)$ uptake from aqueous solution of PGW-150MP compared to sonicated carbonised-1 and carbonised-1-O.[55]

These experiments showed that carbonisation can be used to repurpose 50-poly(S-*r*-canola) after is already has been used as an oil sorbent. Moreover, repurposing also results in improved mercury uptake rivaling that of commercially available activated carbon.

Mercury leaching from carbonised-1 and carbonised-1-O

Throughout this project we hypothesised that carbonised-1 is able to bind mercury through its sulfur functionality, which is different from the other commercial carbons which showed no sulfur based on CHNS analysis (Figure 3.69). If this is true and mercury is bound to the commercial carbons by a physisorption process while chemically bound to the carbonised-1 and carbonised-1-O, then differences should be seen in mercury leaching for these sorbents. To test this, samples of carbonised-1, carbonised-1-O and the commercial carbons were used. Firstly, the aim was to load these samples with a large amount of mercury. This was done by placing 200 mg of each sorbent in 45 mL of a 50 ppm mercury solution $(Hg(NO_3)_2)$ stabilised in 2% HNO_3. The samples were then rotated end-over-end at a speed of 25 RPM for 2 hours to adsorb as much mercury as possible. The mercury concentration after the sorbents were removed was used to calculate the amount of mercury bound the carbons. Following

that the samples were gently washed with 50 mL of deionised water to ensure any non-bound mercury was removed. To assess the mercury leaching, the carbon samples were then placed in 45 mL of a 5% HNO_3 solution and rotated at 25 RPM for 24 hours. The leach solution was then analysed for mercury. The results showed that 32% of mercury was leached from Sigma-Aldrich GAC, 28% were leached from ChemSupply PAC and 22% form Kuraray PGW-150 MP. Remarkably, only 5% of the bound mercury leached from carbonised-1 and 9% from carbonised-1-O. These results highlighted the importance of the sulfur functionality in the binding and adhering of mercury, since only minimal leaching was observed after the sample was exposed to highly acidic water for a prolonged time of 24 hours. These results can be an advantage of carbonised-1 and carbonised-1-O compared to other non-sulfurised carbons since recovery, transport, storage, and disposal are made safer by a greatly reduced risk of mercury leaching off the spent sorbent.

Regeneration of carbonised-1 and carbonised-1-O

Next, the idea of regeneration of carbonised-1 and carbonised-1-O after mercury sorption was addressed. The premise was that heating mercury-bound carbon in a furnace would remove the mercury from it by thermal reduction and volatilisation of Hg^0. It must be noted that appropriate recovery units and retorts are available if this is done on a larger scale, to avoid mercury release into the environment. To test the concept of regeneration, 1 g of each, carbonised-1 and carbonised-1-O were exposed to a 1000 ppm mercury solution ($Hg(NO_3)_2$ in 2% HNO_3) for 24 hours while rotated at 25 RPM. The samples were then removed, washed with deionised water, and dried. Using the mercury concentration of the solution after the carbons were removed, the amount of mercury on the carbons was calculated. Carbonised-1 had 8.9 mg and carbonised-1-O had 9.7 mg of mercury bound. In order to remove the mercury from the carbon, the samples were placed in a muffle furnace and heated to 400 °C and the temperature was held for 30 min. This temperature was chosen since the boiling point of mercury is 356.5 °C.[55] To determine if this heating step removed mercury, XPS analysis of the carbons after mercury uptake was compared the that of the carbons after the heating process. XPS analysis clearly detected mercury on the surface of the mercury-rich carbonised-1 and carbonised-1-O. However, after the regeneration step no mercury could be detected (Figure 3.21). That result showed that after the carbon has been used as mercury sorbent, it can be regenerated by a simple thermal desorption protocol. Further, XPS analysis showed no discernible change in the S2p signals in the samples before and after regeneration. This indicated that the sulfur species in the carbon are the same

before and after the regeneration process. Similarly, no significant change in the carbon C1s signal could be seen between the samples before and after regeneration. Characterisation was also conducted on the regenerated carbons. CHNS combustible analysis indicated no significant difference in elemental makeup between the sorbent before and after regeneration.
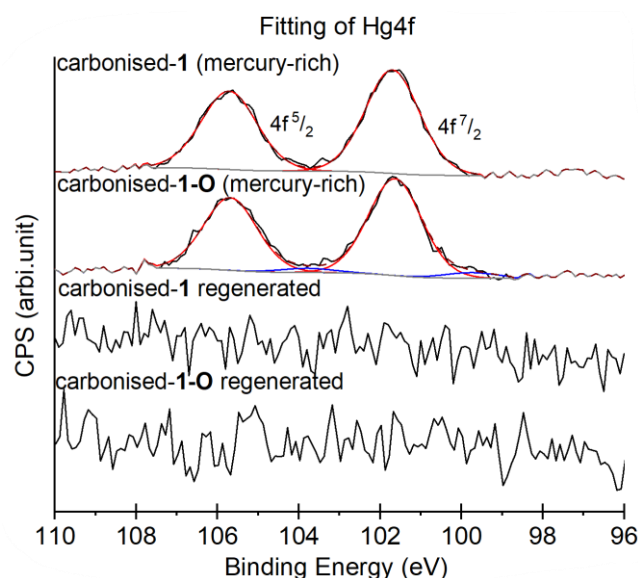
Figure 3.21: XPS analysis of mercury rich as well as regenerated carbonised-1 and carbonised-1-O. The signal for mercury at 101.6 eV ± 0.2 eV corresponds to Hg^{2+}.[56] Reproduced with permission from the Royal Society of Chemistry.[45]

Finally, the mercury sorption of regenerated carbonised-1 and carbonised-1-O was assessed. This was done in the same way as previous mercury sorption experiments. To 45 mL of a 5 ppm mercury solution (from $Hg(NO_3)_2$), 100 mg of sorbent was added. The solution was rotated on an end-over-end mixer for 2 hours at 25 RPM. Although there are some variations in the initial uptake of mercury between the samples, after the 2-hour period all samples removed over 99% of mercury from the water (Figure 3.22).
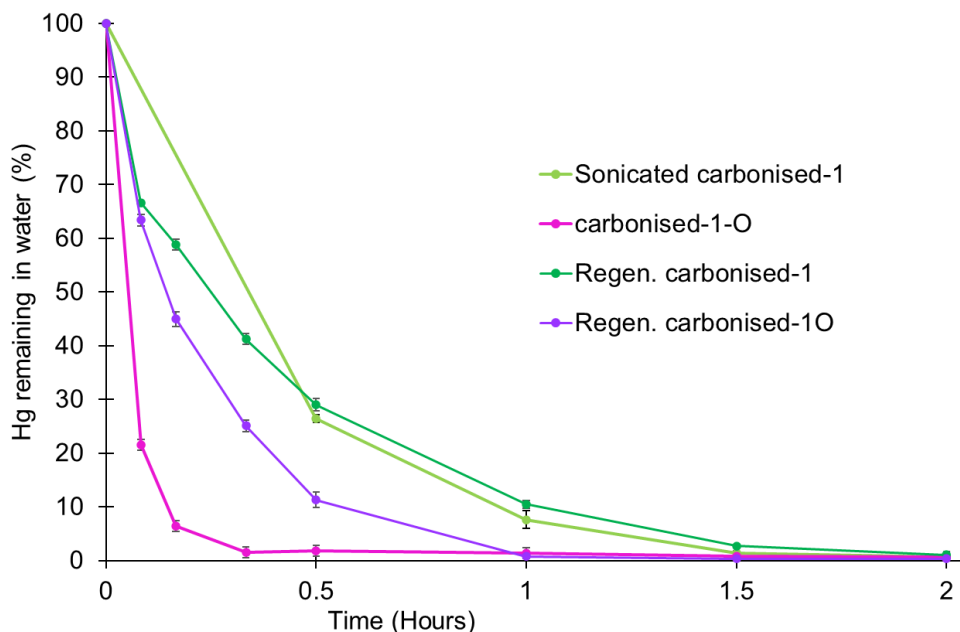
Figure 3.22: Mercury uptake of mercury rich and regenerated carbonsed-1 and carbonised-1-O.

In conclusion, a high-performance sulfurised carbon was prepared and tested for mercury sorption. A polymer made from renewable canola oil and cheap and abundant sulfur was used as the precursor for this carbon material. This polymer can now be manufactured at a ton scale and has many applications.[57] Carbonisation of this polymer resulted in a graphitic material, exhibiting sulfur functionality on the surface. Further, this carbon was made using a simple carbonisation method without the use of inert gases or additional activation steps, resulting in a less energy intensive carbonisation. Sulfur was imparted to carbonised-1 directly from the parent polymer without the need for exogenous reagents. The mercury sorption capabilities of carbonised-1 rivaled that of commercially available activated carbons. Further, is has been found that mercury leaching off carbonised-1 is minimal compared to the mercury leaching from commercial carbons. This is likely due to the sulfur-rich surface leading to chemisorption of mercury rather than the physisorption suspected to be case in the commercial carbon samples. It has also been shown that the spent carbonised-1 and carbonised-1-O sorbents can be regenerated by thermal desorption at 400 °C. While this removed the mercury bound to the materials, it does not significantly change the carbon chemical constitution. Lastly, the regenerated carbons removed mercury from water to the same extend as the fresh samples of carbonised-1 and carbonised-1-O, removing over 99% of mercury within 2 hours. Thus, this discovery had given rise to the opportunity of repurposing and extending the lifetime of the parent polymer 50-poly(S-*r*-canola).

203

Having found a way to repurpose the 50-poly(S-*r*-canola), the next chapter will consider another polysulfide system made from sulfur and dicyclopentadiene and its useful properties in mercury uptake and coating application.

Publication that resulted from the research in this chapter:

Carbonisation of a polymer made from sulfur and canola oil

Mann, M.; Luo, X.; Tikoalu, A. D.; Gibson, C. T.; Yin, Y.; Al-Attabi, R.; Andersson, G. G.; Raston, C. L.; Henderson, L. C.; Pring, A.; Hasell, T.; Chalker, J. M., Carbonisation of a polymer made from sulfur and canola oil. ChemComm **2021**, 57, 6296-6299.

Experimental

Materials: The mercury standard to prepare the mercury solution was purchased from ARC (1000 mg/L, Matrix: 2% HNO_3). The granular activated charcoal (GAC) was purchased from Sigma Aldrich (untreated, granular, 8-20 mesh) and used as revived. The powdered activated carbon (PAC) was purchased from ChemSupply and used as received. The PGW-150MP carbon was provided by Kuraray. $HgCl_2$ powder was purchased from ChemSupply. The oil for the oil removal experiment was and 'Auto-force' 2 stroke high performance motor oil

The **50-poly-(S-r-canola) polymer** used for this experiment was synthesised as previously described by our laboratory by the direct copolymerisation of equal masses of sulfur and canola oil.[11]

Carbonisation of 50-poly-(S-*r*-canola) was performed in a Carbolite Gero CWF 1200 furnace. The 50-poly-(S-*r*-canola) sample was heated to 600 °C using a 5 °C / minute heating rate. After the target temperature of 600 °C was reached the temperature was held for 30 minutes. Next, the oven was left to cool down naturally. The carbonised 50-poly-(S-*r*-canola) polymer generated is referred to as carbonised-**1**.

SEM and EDX images were obtained using a FEI Inspect F50 SEM fitted with a EDAX energy dispersive X-Ray detector. Samples were sputter coated with silver metal (20 nm thickness) before analysis.

Brunauer–Emmett–Teller (BET) surface areas were measured at 77.3 K using a Micromeritics TriStar II analyser and were determined from the N_2 adsorption isotherms. The samples were prepared by adding between 40 - 100 mg of sample into the sample tube before the samples were put under vacuum using a VacPrep061 vacuum station for at least 24 hours.

Inductively Couple Plasma – Mass Spectroscopy (ICP-MS) was performed on a Perkin Elmer NexION 350D spectrometer fitted with an EIS SC2 D *X* autosampler. This technique was used for mixed-metal analysis. The error associated with this instrument of 5% or less.

Infrared (IR) spectra were recorded (neat film or ATR) using a FTIR Perkin Elmer spectrophotometer between 4000 and 600 cm^{-1}.

Mercury analysis: CVAA was carried out by a commercial service. Briefly, aqueous samples were digested using bromine monochloride (BrCl) before Cold Vapour Atomic Absorption spectroscopic analysis using a method adapted from the following standard methods: APHA 3112 (USEPA 7471A & USEPA 1631 Rev E).

CHNS elemental analysis was performed by The Campbell Microanalytical Laboratory at the University of Otago in New Zealand.

Simultaneous Thermal Analysis (STA) was performed using a Perkin Elmer STA 8000 instrument. The sample was held at 40 °C for 4 minutes before the sample was heated to 800 °C at a rate of 10 °C / minute. This was done under nitrogen with a flow rate of 20 mL / minute.

Raman spectra were acquired using a Witec alpha300R Raman microscope at an excitation laser wavelength of 532 nm with a 40X objective (numerical aperture 0.40). Typical integration times for the Raman spectra were approximately 10 to 20 seconds. The grating used was 600 grooves / mm which gives a spectral resolution of approximately 3 to 4 wavenumbers. The current Activated carbon (AC) sample was analysed at multiple locations and hundreds of spectra were acquired not only to determine the level of disorder of the material but also to ascertain if any residual S_8 was present in the sample as the EDX indicated the element sulfur was present on the AC sheets. No S_8 was detected. For the commercial AC approximately 50 Raman spectra were collected per sample at multiple locations within each sample.

XPS (X-ray Photoelectron Spectroscopy)[58] was applied for determining the chemical elements and their bonding states on the surface. The apparatus was built by SPECS, which was operated in an ultra-high vacuum (UHV) condition at a base pressure of 10^{-10} mbar. A no-monochromatic X-ray source (12 kV - 200 W) with a magnesium anode was used for the measurements and survey. High-resolution scans were operated at a pass energy of 40eV and 10 eV respectively and recorded. Spectra were calibrated based on identifying C-C sp3 species to 285.0 eV. The relative concentration of element was calculated by normalizing the individual element intensity to its atomic sensitive factor (ASF). XPS analysis was performed by Yanting Yin.

Powder X-ray diffraction (XRD) patterns were recorded on a Bruker D8 Advance Eco diffractometer (Bragg-Brentano geometry) using Co-Kα radiation (λ = 1.78897 Å). The Bragg angle (2θ) was varied from 10 ° to 90 ° with a step size of 0.019 °, measurement time of 0.6 seconds per step and sample rotation at 10 rpm. The samples were deposited onto a sample holder well before analysis.

Inductively coupled plasma – optical emission spectroscopy (ICP-OES) was conducted using a Perkin Elmer Optima 8000 ICP-OES fitted with a Perkin Elmer S10 autosampler. For the analysis an external standard of all the target elements was used. After the calibration solutions were prepared, the samples were diluted within the calibration range (sample concentration was estimated if not known). As quality control some samples were spiked with known concentrations of the target analyte. Additionally, samples with known concentrations were made and analysed. Further an internal standard using an element not likely to be in the sample or to interfere was continually run to assess performance of the instrument. The error associated with this instrument of 5% or less.

Synthesis of 50-poly-(S-*r*-canola)

50-poly-(S-*r*-canola) was prepared as previously described in Chapter 2.

¹H NMR analysis of 50-poly-(S-*r*-canola)

To obtain ¹H NMR data of 50-poly(S-*r*-canola) polymer, a small amount was dissolved in pyridine-d5 and agitated. After no more polymer dissolved, the solution was filtered and analysed by NMR.
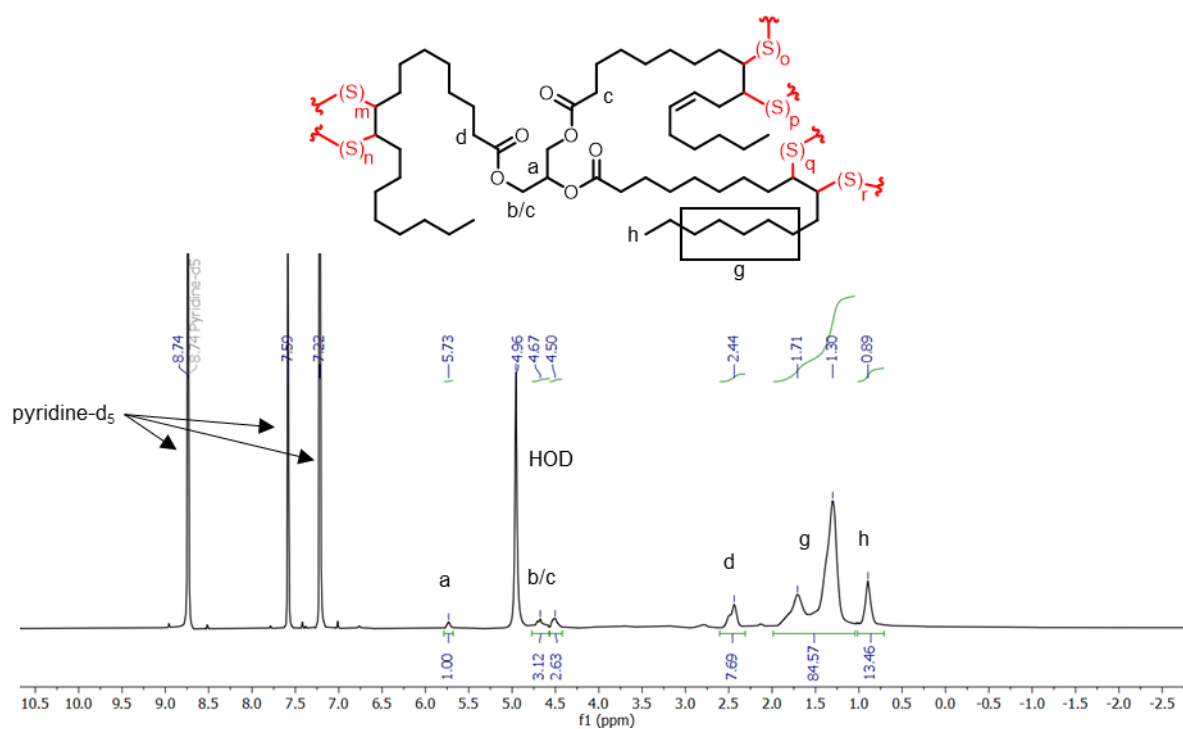
Figure 3.23: ¹H NMR of 50-poly-(S-*r*-canola) in pyridine-d5 was consistent with that previously reported.[11]

IR analysis of 50-poly-(S-*r*-canola)

      IR analysis of 50-poly-(S-*r*-canola) showed C=O stretching at 1742 cm^{-1} which corresponds to the triglyceride structure of the canola oil. These results are consistent which previously reported IR spectra of 50-poly-(S-*r*-canola).[11]
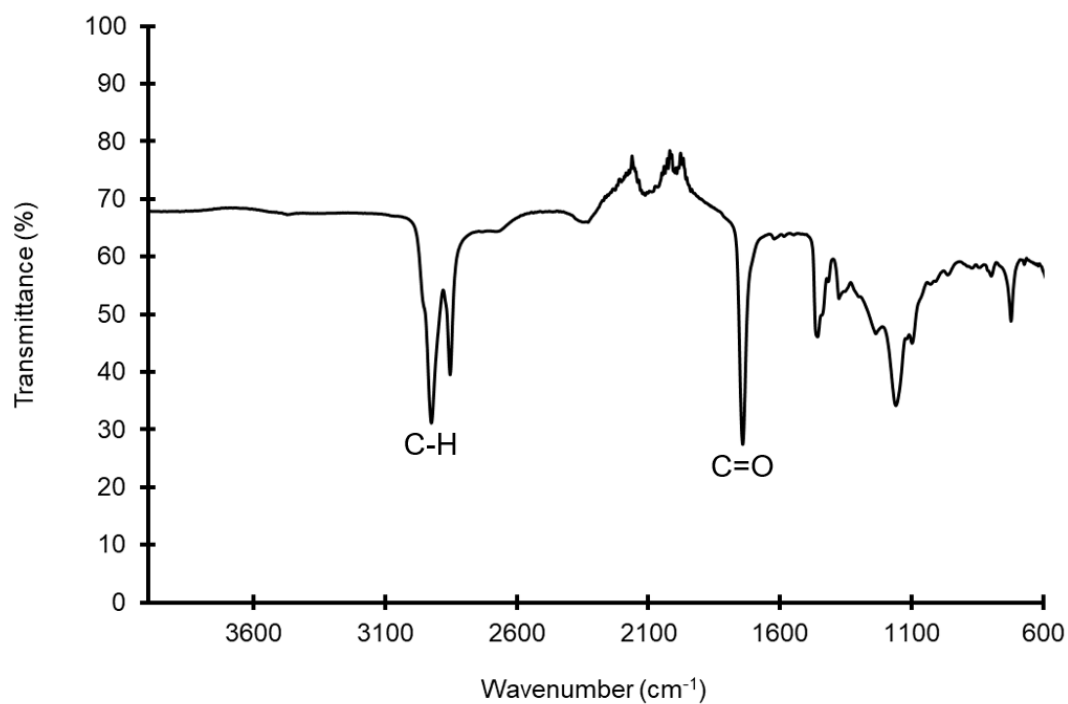
Figure 3.24: IR spectra of 50-poly-(S-*r*-canola). Reproduced with permission from the Royal Society of Chemistry.[45]

STA analysis of 50-poly-(S-*r*-canola)

The STA analysis shows that the degradation of 50-poly-(S-*r*-canola) occurs over 2 steps. The first mass loss event has an onset temperature of 180 °C and continues to around 315 °C. This is followed by a second mass loss starting at 315 °C. Most of the second mass loss is over at around 500 °C. At this stage a total mass loss of 88 % has occurred. For the remainder of the DSC protocol (500 °C – 800 °C) an additional mass loss of only 4 % was observed.
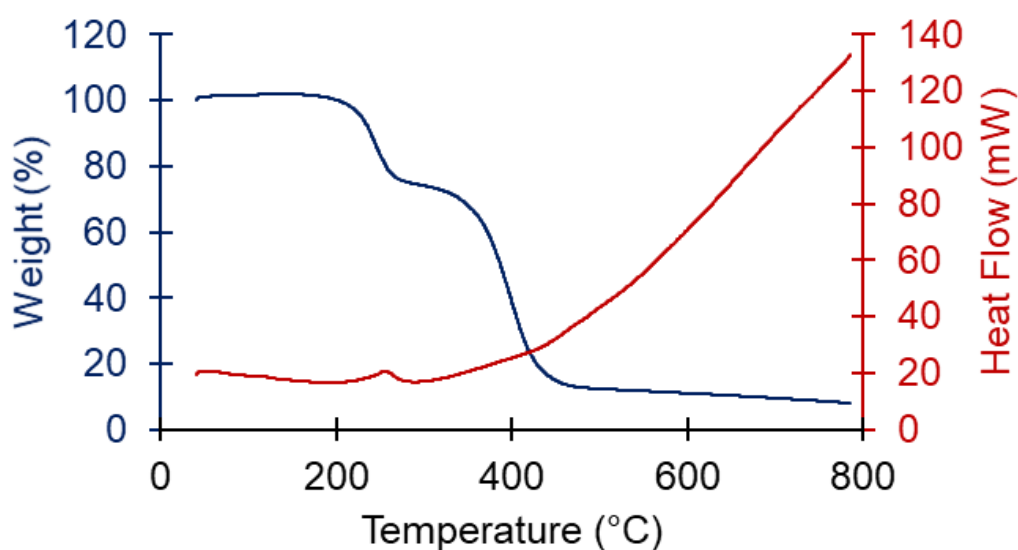
Figure 3.25: STA (DSC and TGA) of 50-poly-(S-*r*-canola). Reproduced with permission from the Royal Society of Chemistry.[45]

XRD analysis of 50-poly-(S-*r*-canola)

XRD analysis of 50-poly(S-*r*-canola) compared to sulfur showed similar peaks indicating that some free sulfur is embedded in the polymer. The broad peak in the polymer spectrum it consistent with what has been previously reported.[11]
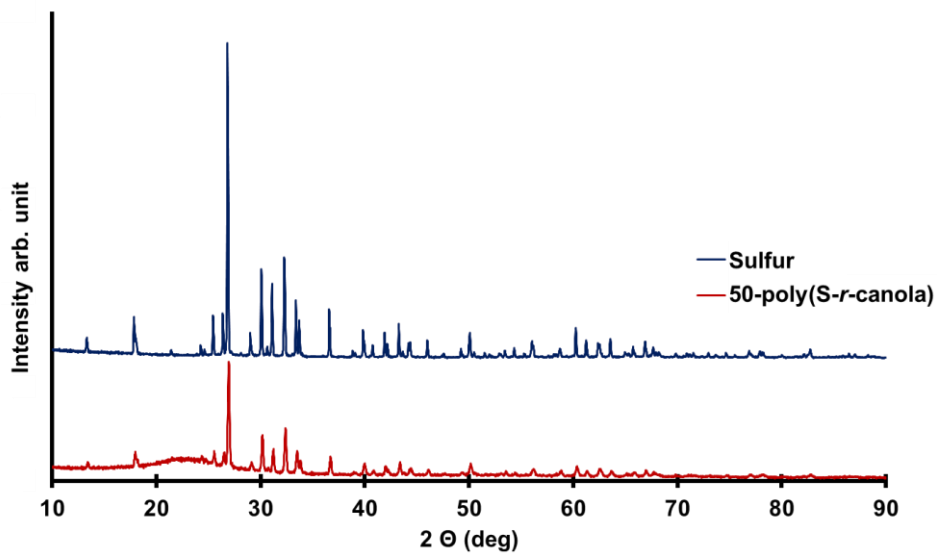
Figure 3.26: XRD spectrum of 50-poly(S-*r*-canola) and of elemental sulfur. Reproduced with permission from the Royal Society of Chemistry.[45]

CHNS combustible analysis of 50-poly-(S-*r*-canola)
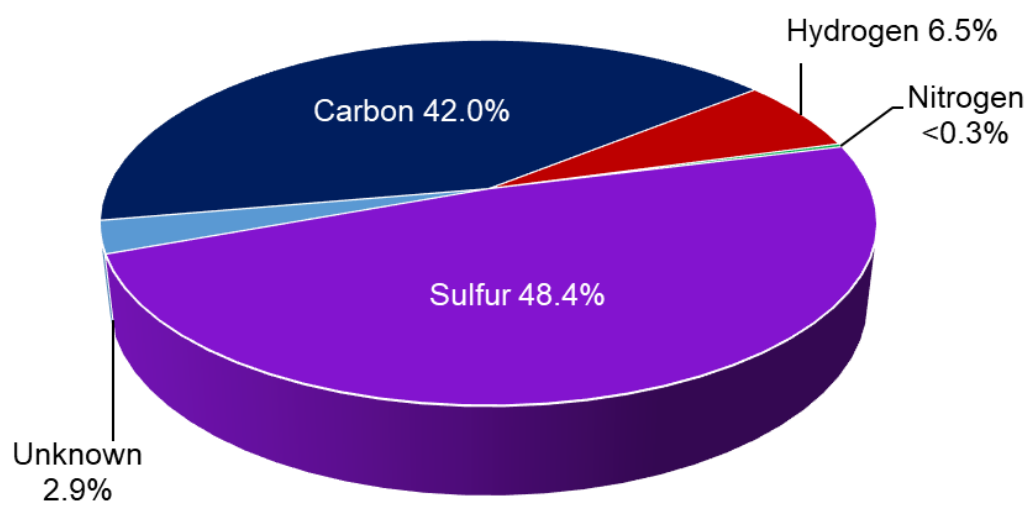
Figure 3.27: CHNS analysis of 50-poly-(S-*r*-canola)

Synthesis of carbonised-1

The 50-poly-(S-*r*-canola) sample (100 g) was placed in a crucible and heated to 600 °C using a 5 °C / minute heating rate. The heating rate was chosen as this rate was recommended by the manufacturer of the crucible. The furnace was contained in a fume hood to avoid the release of gases into the laboratory. After the target temperature of 600 °C was reached the temperature was held for 30 minutes. Next, the furnace was left to cool down naturally. The carbonised 50-poly-(S-*r*-canola) polymer generated is referred to as carbonised-1. Three carbonisation cycles with 100 g of polymer-1 each were performed. The yield from the carbonisation of 300 g of polymer was 38.4 g. After that the carbon was roughly crushed up using mortar and pestle.
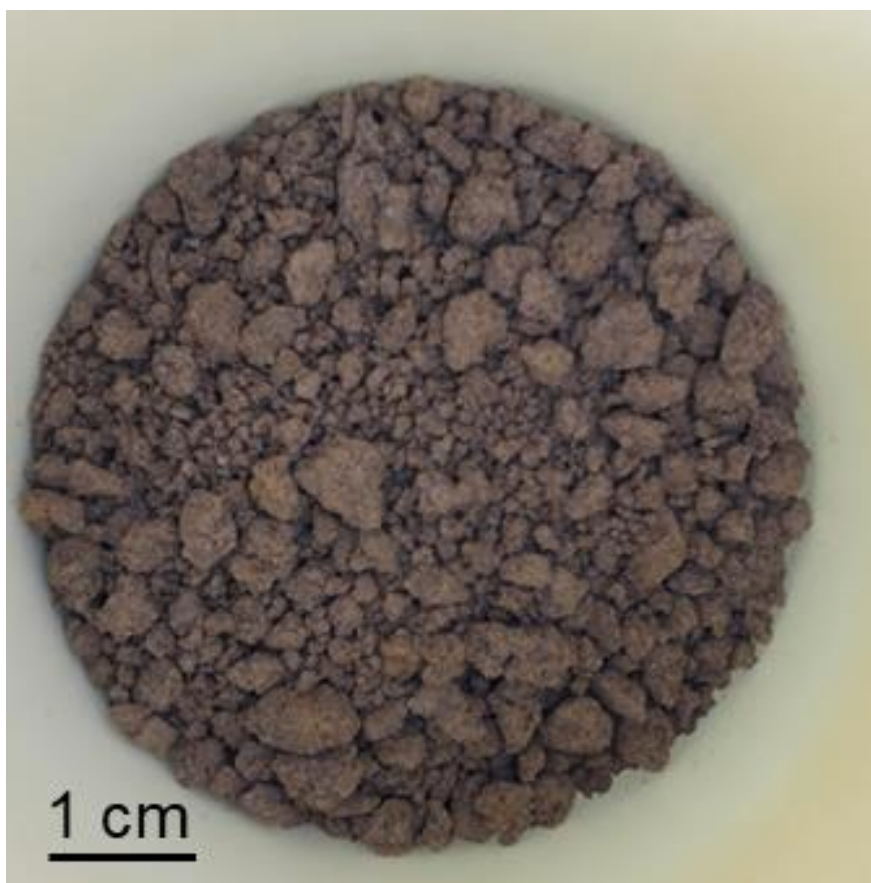
Figure 3.28: 100 g of 50-poly-(S-*r*-canola) in a 1.1 L crucible before the carbonisation process. Reproduced with permission from the Royal Society of Chemistry.[45]

Figure 3.29: Carbonised-1 in the crucible after the carbonisation. Reproduced with permission from the Royal Society of Chemistry.[45]

Figure 3.30: Carbonised-1 ground up using mortar and pestle. Reproduced with permission from the Royal Society of Chemistry.[45]

SEM analysis of carbonised-1
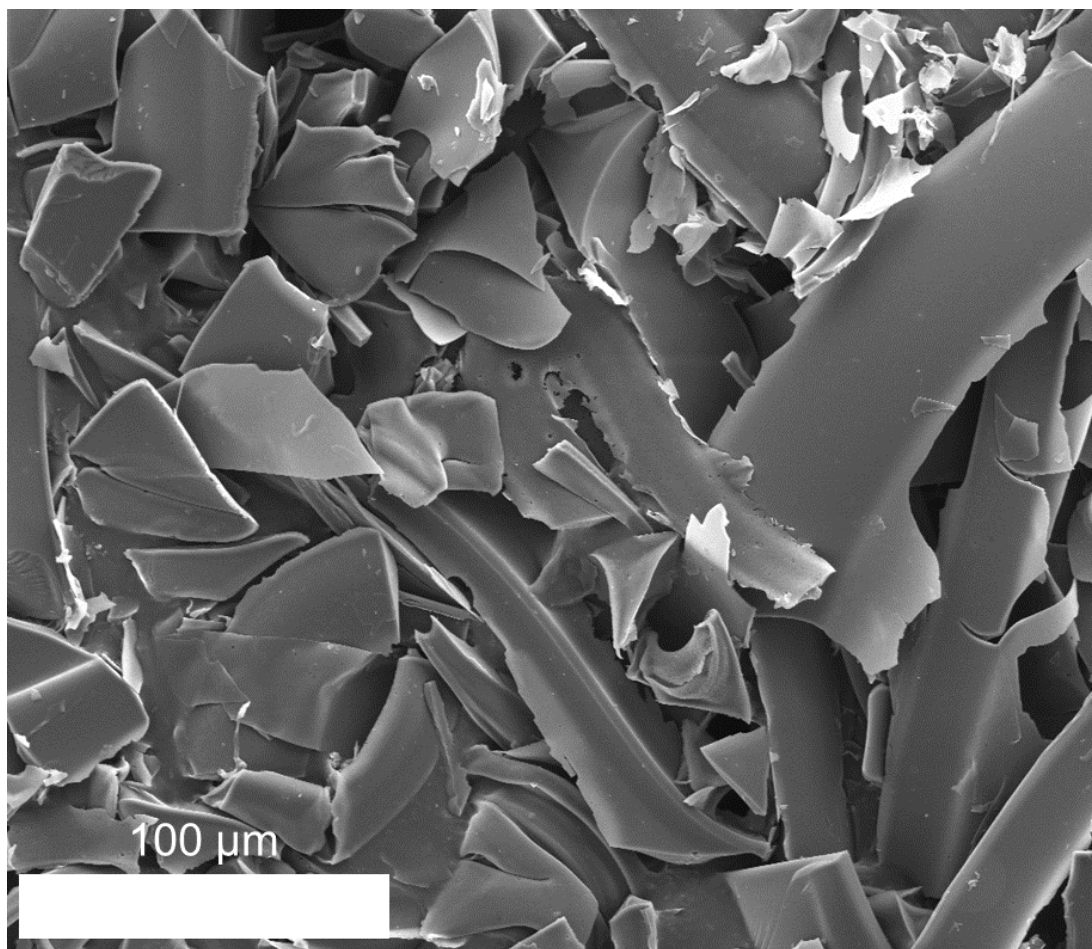
Figure 3.31: SEM micrograph at 1000 × magnification of carbonised-1 showing thin sheets of material. Reproduced with permission from the Royal Society of Chemistry.[45]
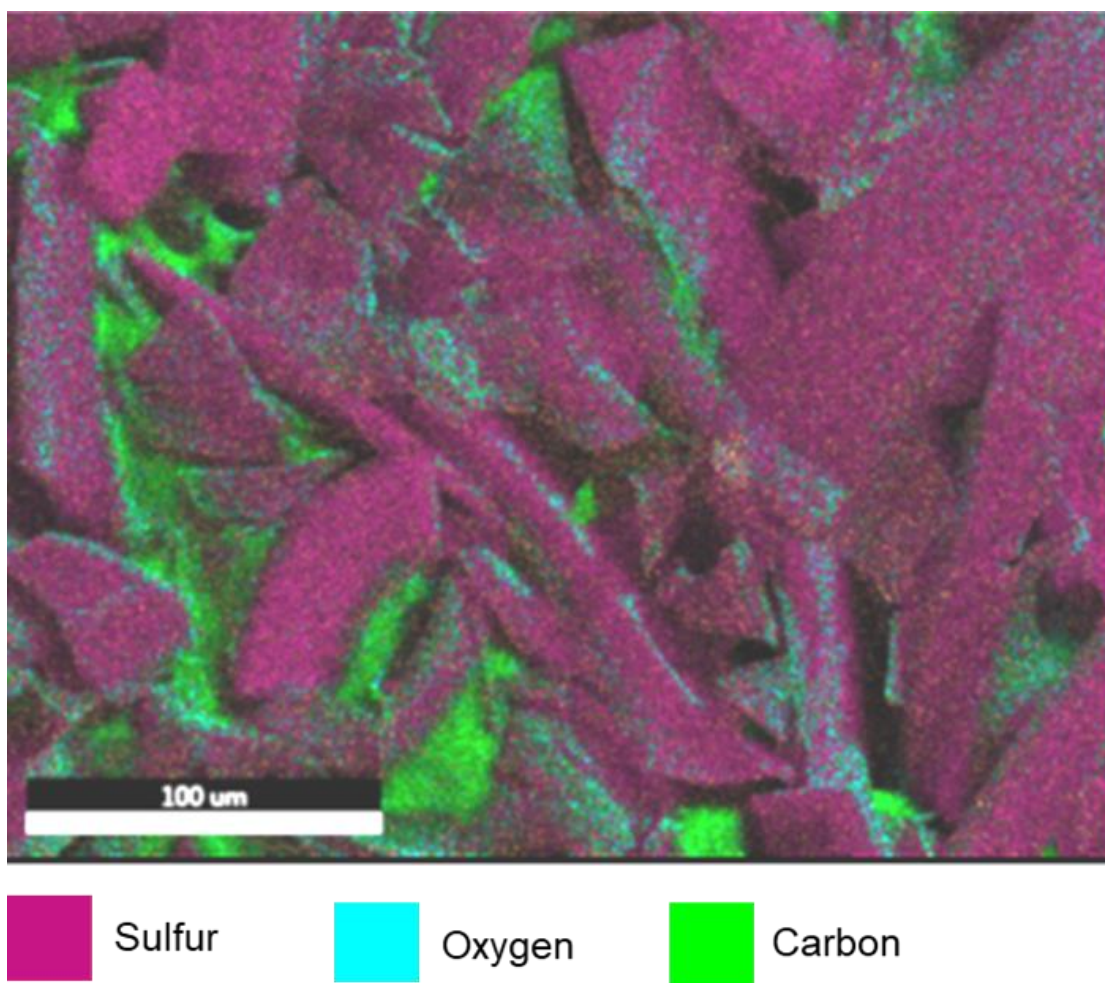
Figure 3.32: EDX elemental map of carbonised-1 showing sulfur, oxygen and carbon. Reproduced with permission from the Royal Society of Chemistry.[45]
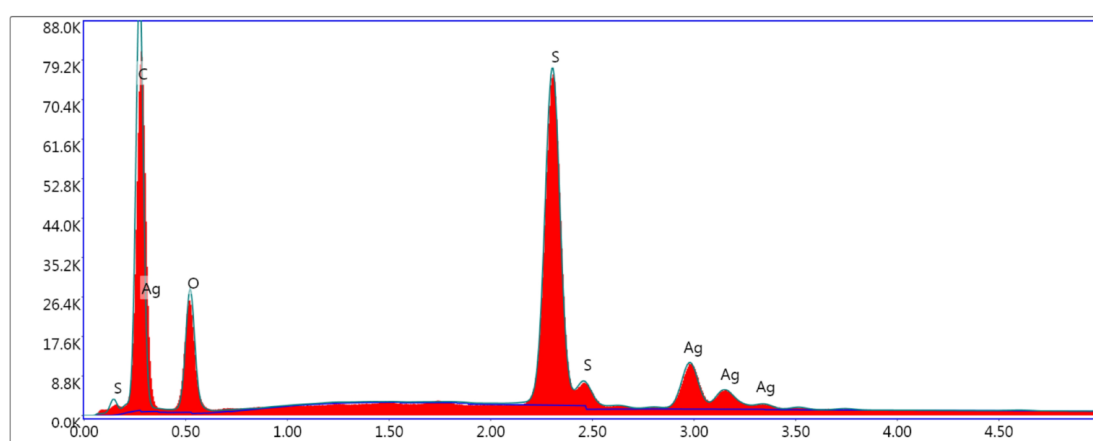
Figure 3.33: EDX sum spectrum showing sulfur, carbon, silver (from the conductive coating), and oxygen peaks.

Raman analysis of carbonised-1
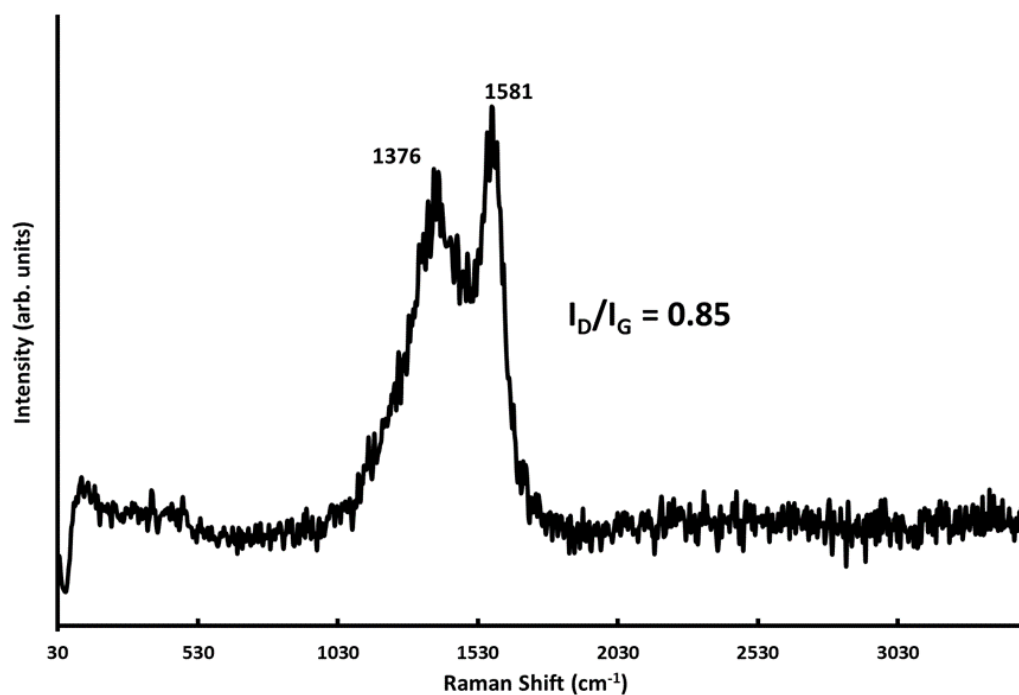
Figure 3.34: Raman spectra of carbonised-1 showing the I_D/I_G to be 0.85. Reproduced with permission from the Royal Society of Chemistry.[45]

Synthesis of carbonised-1-O

A glass dish was filled with 1.5 L of water. To that dish, 200 mL of oil (2 stroke motor oil) was added.

Figure 3.35: Motor oil on water forming layer over the whole water surface.
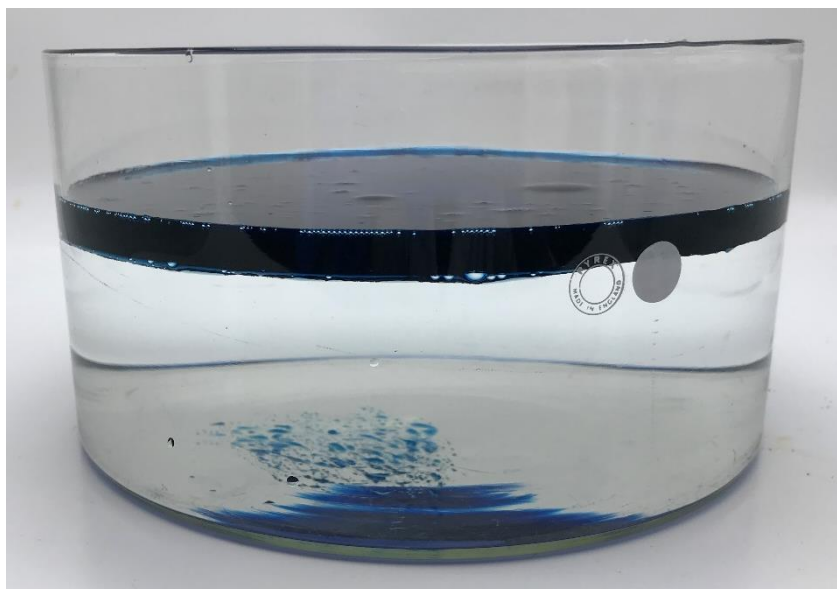
Figure 2.36: Side view of motor oil on water showing a thick layer of oil. Reproduced with permission from the Royal Society of Chemistry.[45]

Next, 100 g of polymer-1 was added to that oil/water mixture and left undisturbed for 8 minutes.
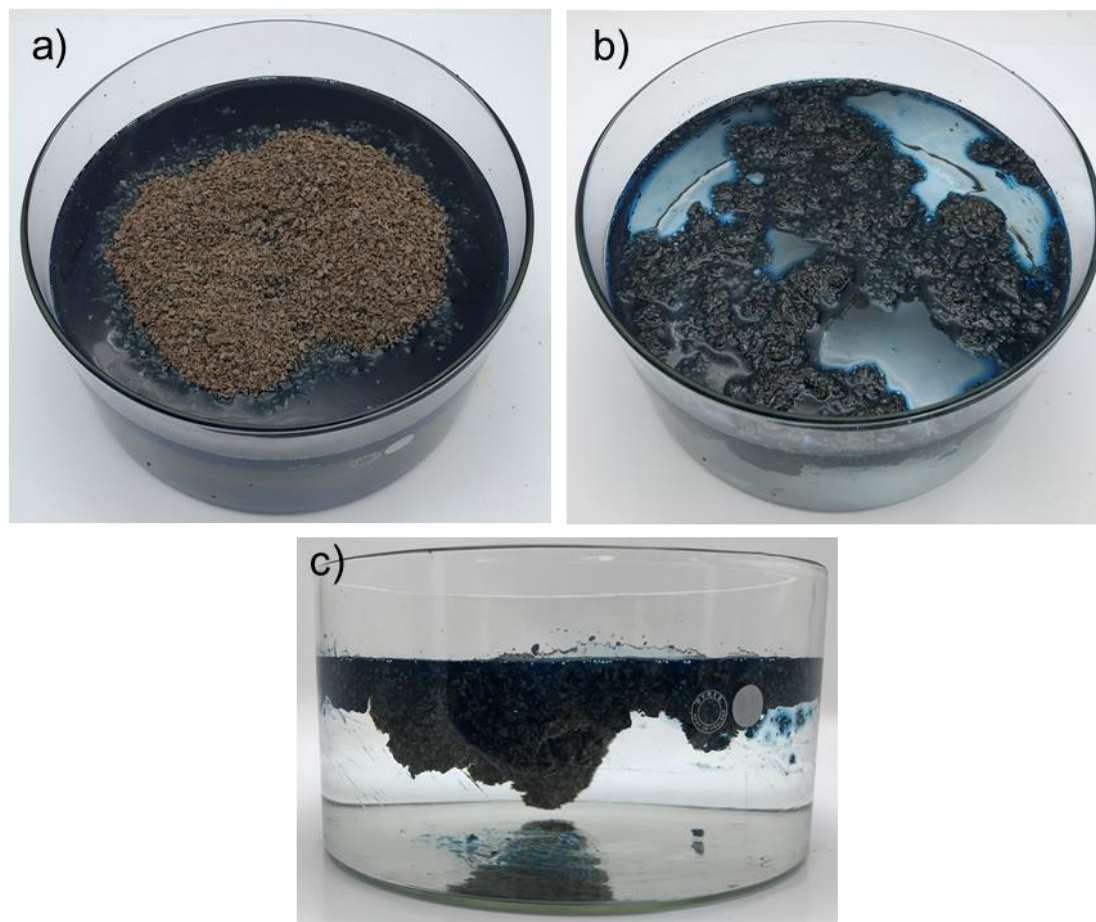
Figure 3.37: a) 100 g of 50-poly(S-*r*-canola) were added to the oil/water mixture. **b)** Top view of mixture 8 minutes after 50-poly(S-*r*-canola) was added **c)** Side view of mixture 8 minutes after 50-poly(S-*r*-canola) was added. Reproduced with permission from the Royal Society of Chemistry.[45]

Following that, the polymer was removed using a net. As previously reported, the polymer was able to remove the oil from the water.[15] Next, the 50-poly(S-*r*-canola) polymer and oil aggregate was removed using a net. Next, the oil was removed by adding some of the oil-bearing polymer into a syringe and the plunger was pressed to squeeze the oil out of the polymer. Since the process was very slow, the remaining polymer and oil mixture was placed in a press to remove the oil. After using 200 mL of oil, 160 mL were recovered. However, some of the oil has been lost during the recovery process or to the glassware and the press.

Figure 3.38: Removing the 50-poly(S-*r*-canola) polymer and oil mixture from the water using a net. Reproduced with permission from the Royal Society of Chemistry.[45]
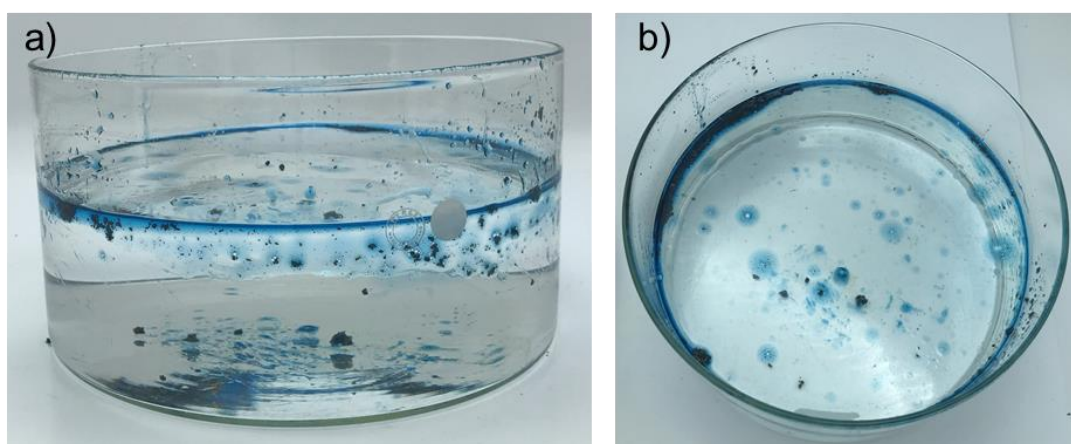
Figure 3.39: a) Side view of container after the 50-poly(S-*r*-canola) polymer and oil mixture has been removed **b)** Top view of container after the 50-poly(S-*r*-canola) polymer and oil mixture has been removed. Reproduced with permission from the Royal Society of Chemistry.[45]

Figure 3.40: Oil removal by adding the oil 50-poly(S-*r*-canola) polymer mixture into a syringe and pressing the oil out. Reproduced with permission from the Royal Society of Chemistry.[45]

After the oil was removed from the polymer, the polymer was carbonised using the same protocol as described for the synthesis of carbonised-1.

SEM and EDX characterisation of carbonised-1-O
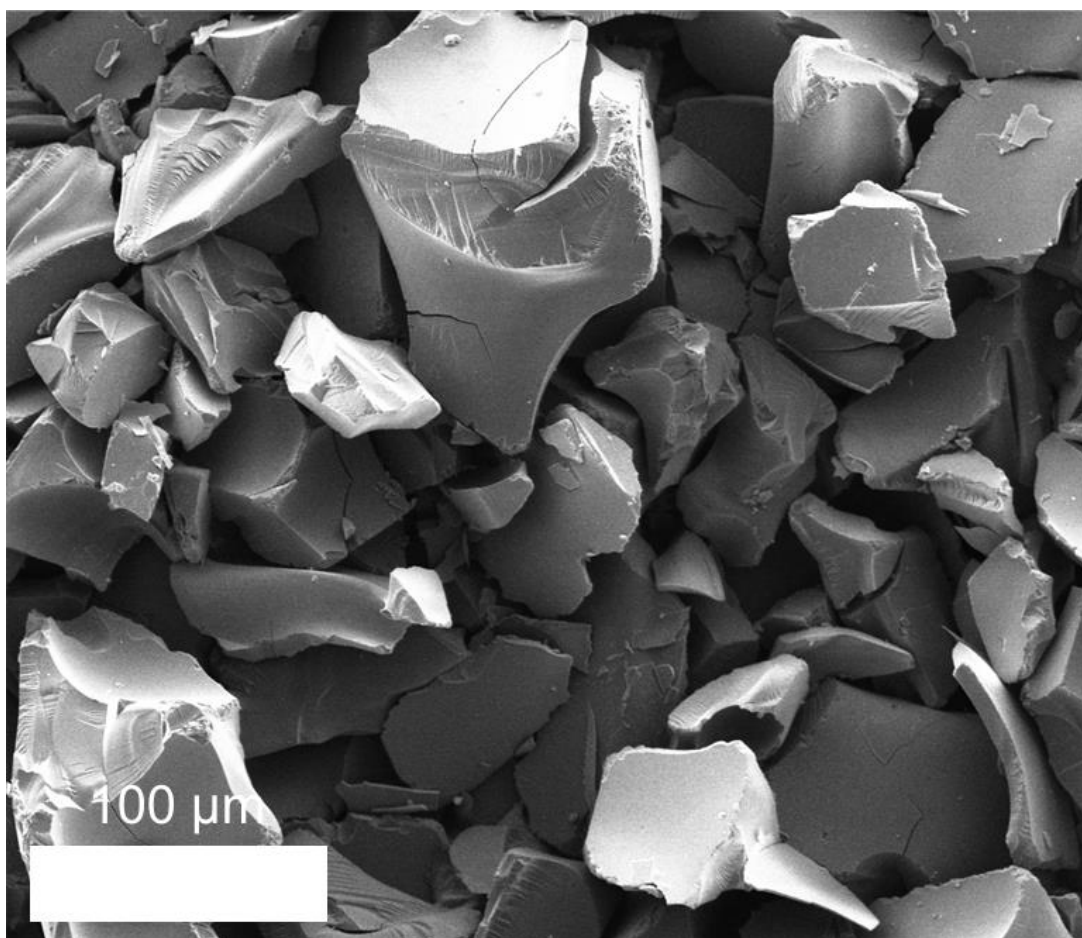
Figure 3.41: SEM micrograph of carbonised-1-O. Reproduced with permission from the Royal Society of Chemistry.[45]

Carbon   Oxygen   Sulfur
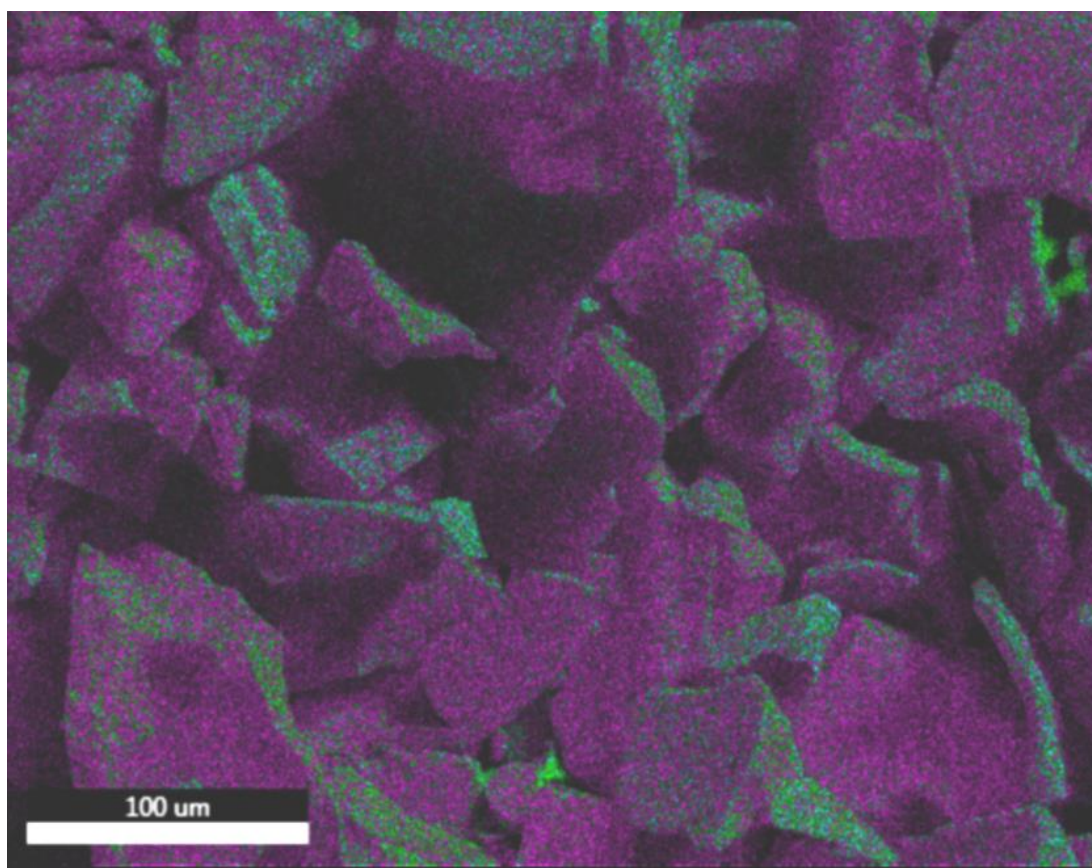
Figure 3.42: EDX elemental map of carbonised-1-O showing carbon, oxygen and sulfur. Reproduced with permission from the Royal Society of Chemistry.[45]
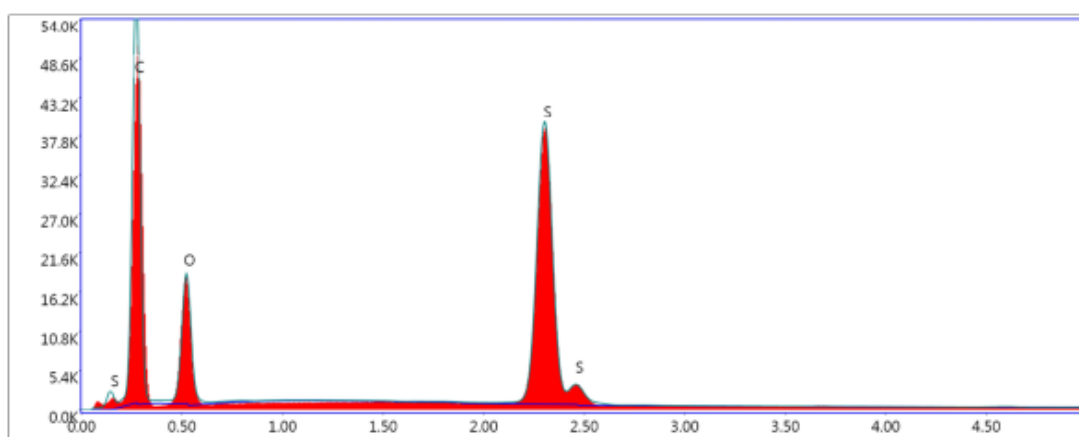
Figure 3.43: EDX sum spectrum of carbonised-1-O showing carbon, oxygen and sulfur peaks.

Raman analysis of carbonised-1-O
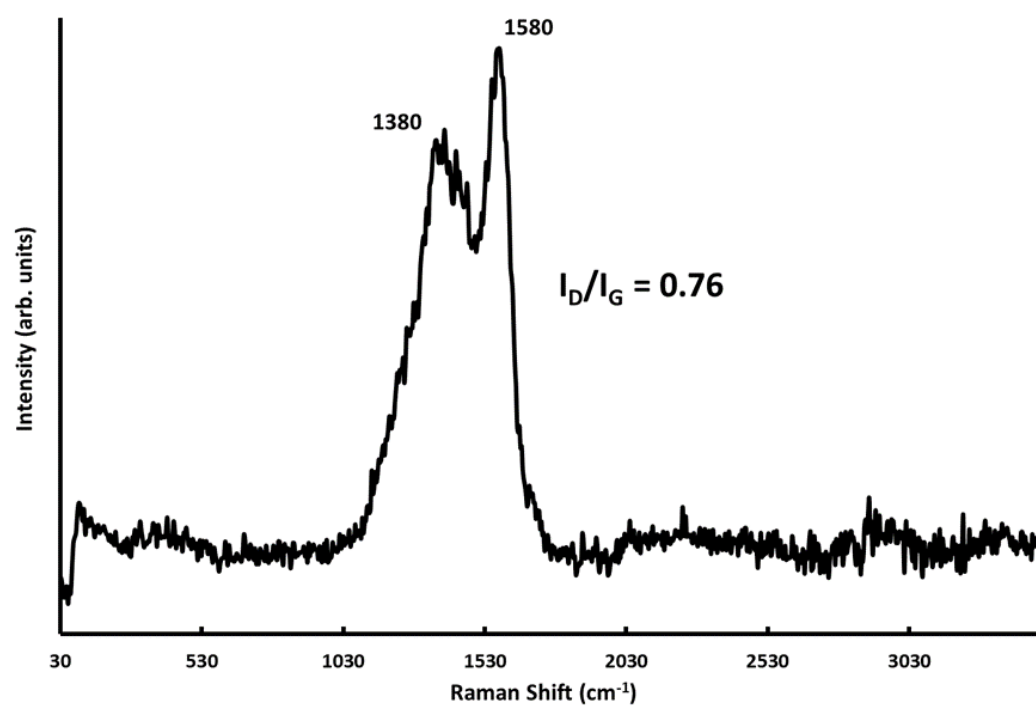
Figure 3.44: Raman spectra of carbonised-1-O showing the I_D/I_G to be 0.67. Reproduced with permission from the Royal Society of Chemistry.[45]

Brunauer-Emmett-Teller (BET) surface area analysis of all carbons

Nitrogen adsorption was measured three times for the carbonised-1 sample. The desorption cycle could not be completed despite repeated attempts, so the surface area for carbonised-1 was estimated using adsorption data only. The average surface area over four measurements was 111 m^2/g.
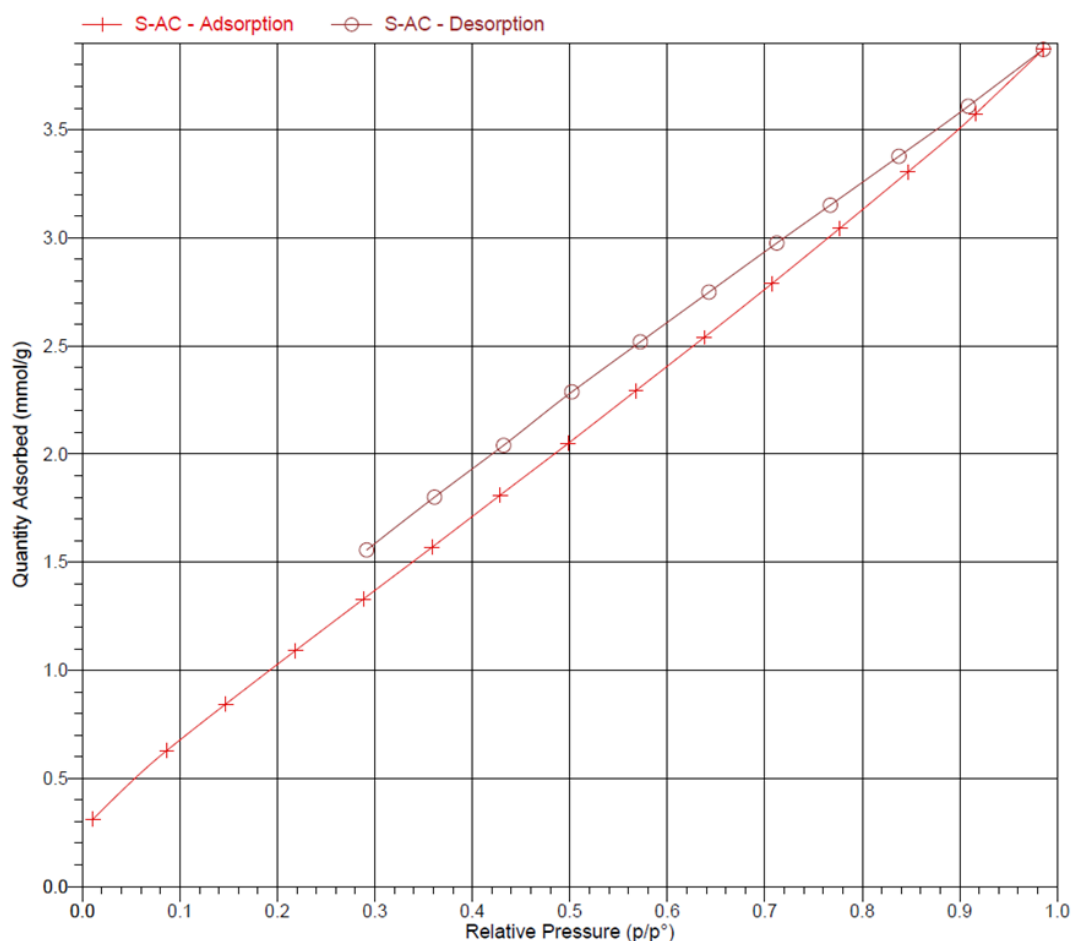
Figure 3.45: Representative isotherm plot of nitrogen adsorption and desorption carbonised-1. Reproduced with permission from the Royal Society of Chemistry.[45]
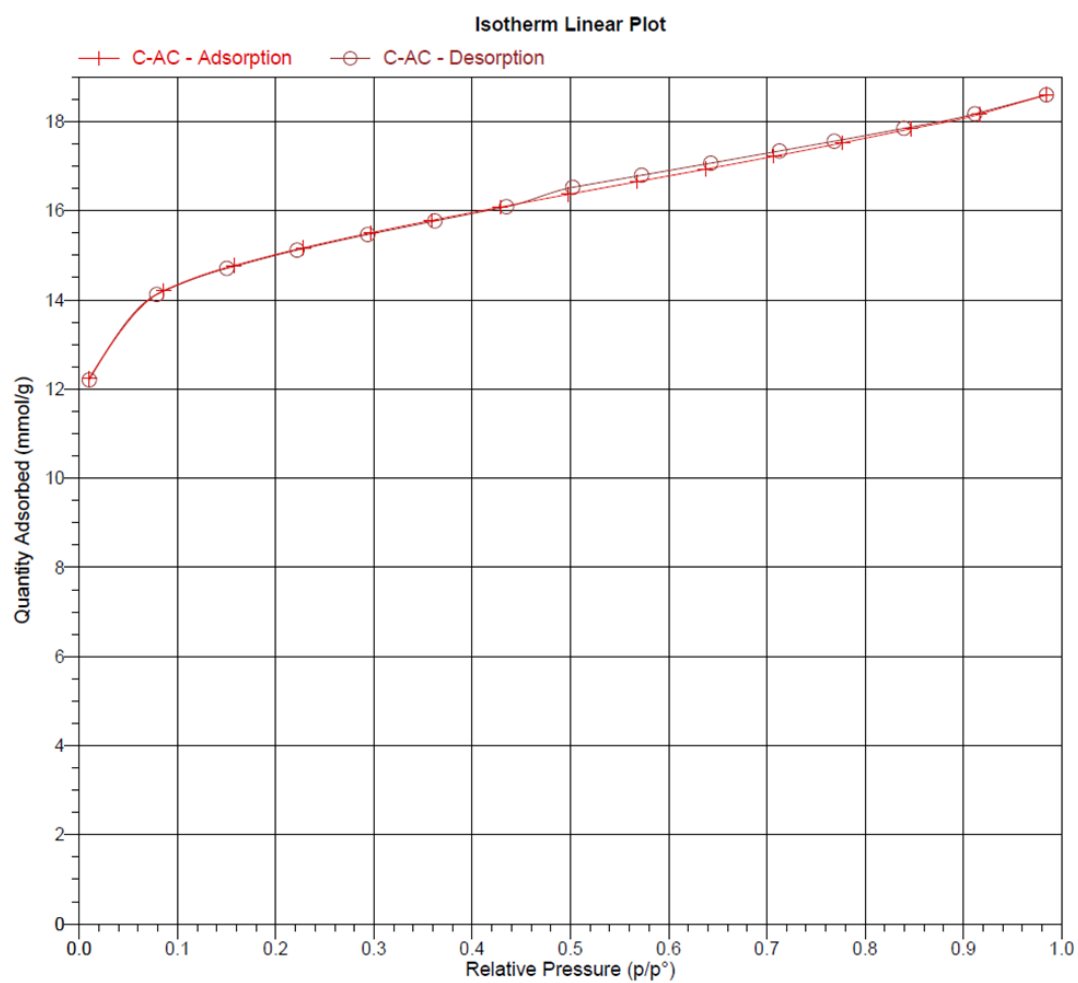
Figure 3.46: BET isotherm plot for Kuraray PGW-150MP. Reproduced with permission from the Royal Society of Chemistry.[45]
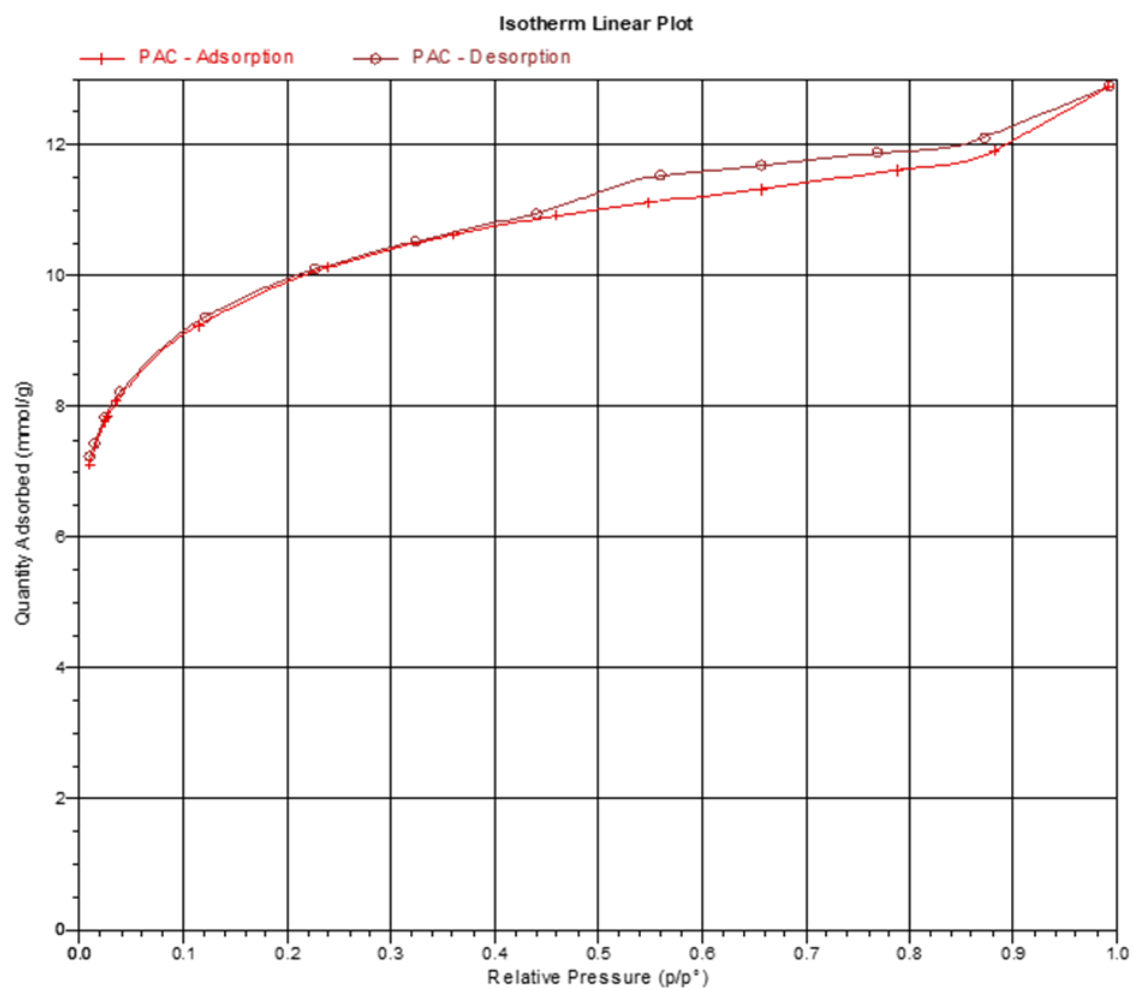
Figure 3.47: BET isotherm plot for PAC (ChemSupply). Reproduced with permission from the Royal Society of Chemistry.[45]
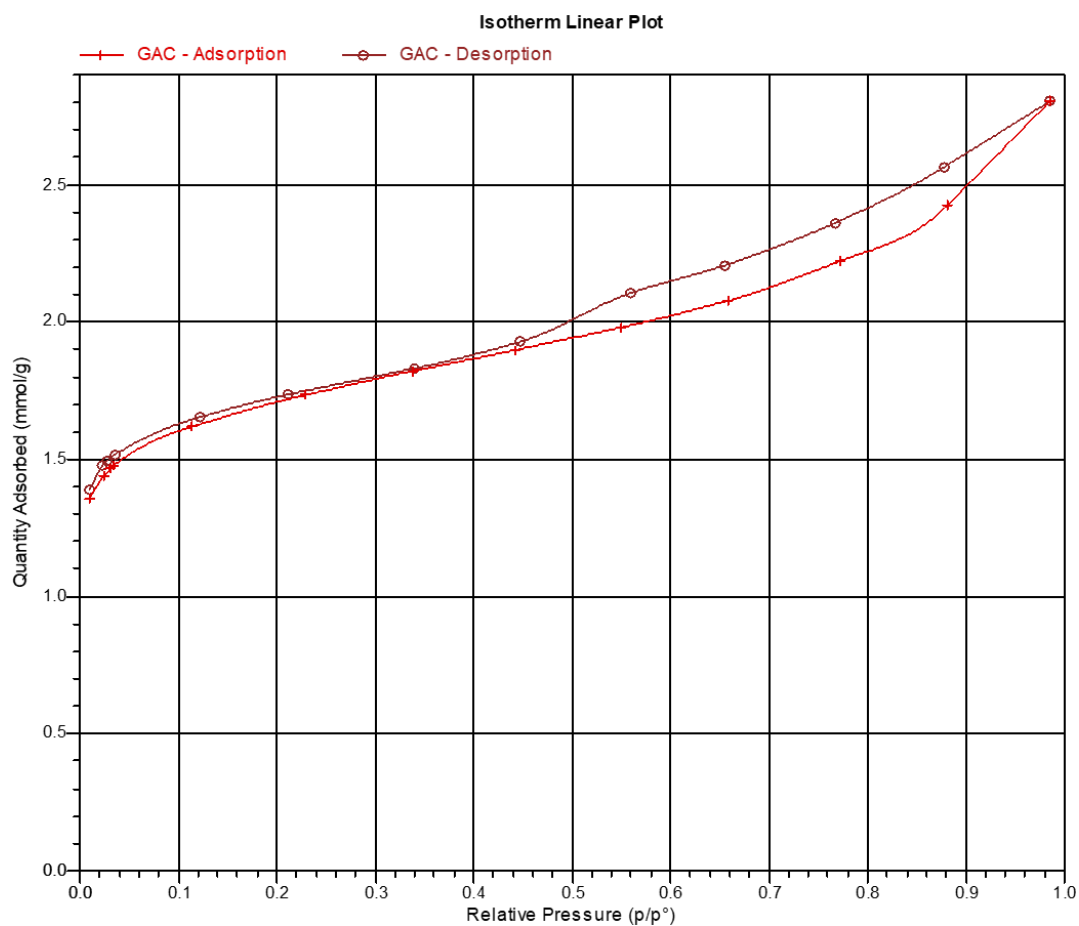
Figure 3.48: BET isotherm plot for GAC (Sigma Aldrich). Reproduced with permission from the Royal Society of Chemistry.[45]
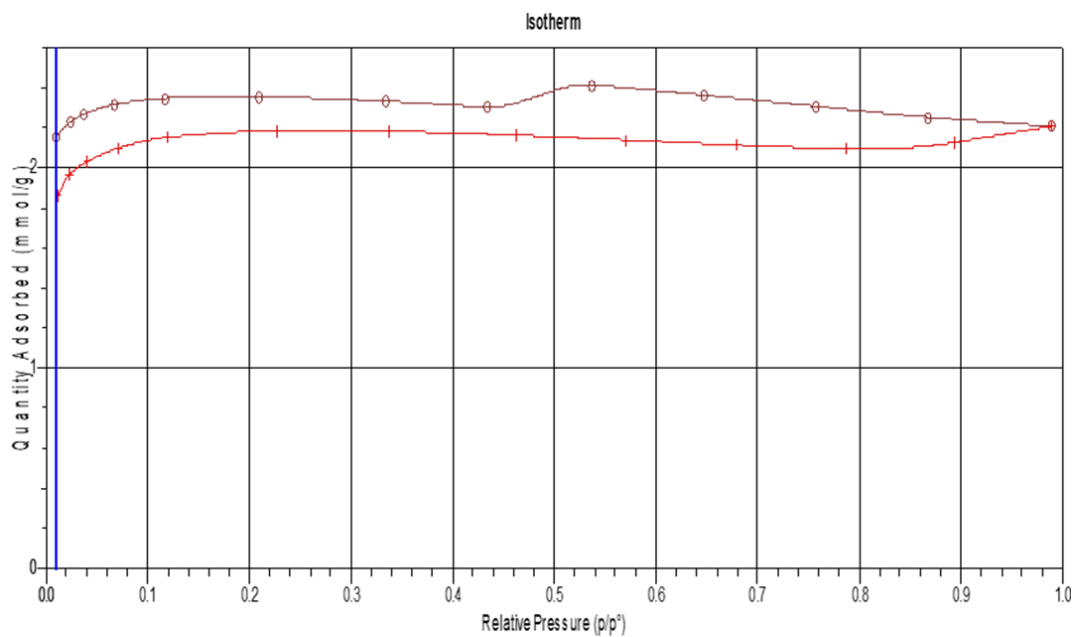
Figure 3.49: Representative isotherm plot of nitrogen adsorption and desorption carbonised-1-O. Reproduced with permission from the Royal Society of Chemistry.[45]

228

Table 3.1: Summary of BET surface areas of carbonised-1, Kuraray PGW-150MP, ChemSupply PAC and Sigma-Aldrich GAC.

Carbon	Surface Area (m^2/g)
Carbonised-**1**	111 ± 46
Carbonised-**1-O**	228 ± 45
PGW-150MP	1131 ± 136
PAC	742 ± 3
GAC	125 ± 12

SEM analysis of commercial carbons

In the SEM micrograph of Kuraray PGW-150MP a large number of pores can be seen on the surface of the caron.
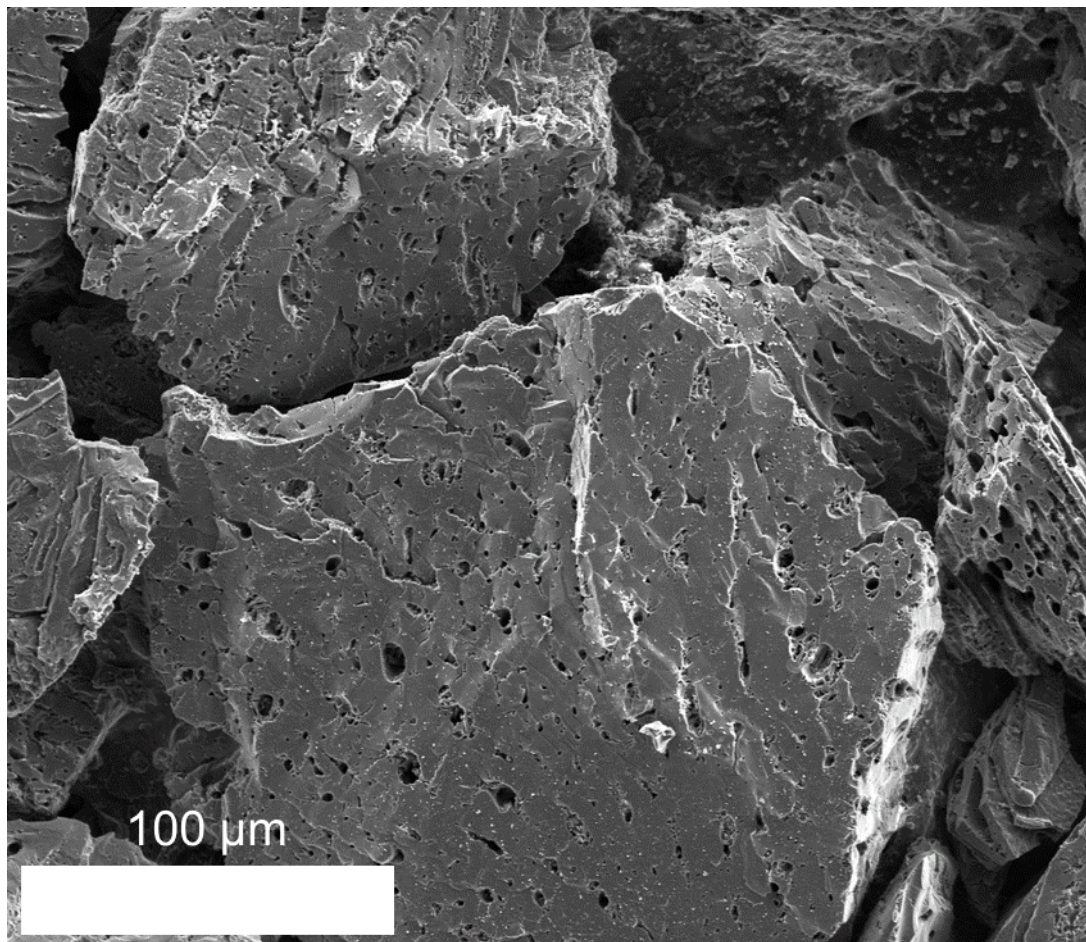
Figure 3.50: SEM micrograph of Kuraray PGW-150MP. Reproduced with permission from the Royal Society of Chemistry.[45]

EDX elemental map of Kuraray PGW-150MP only showed carbon
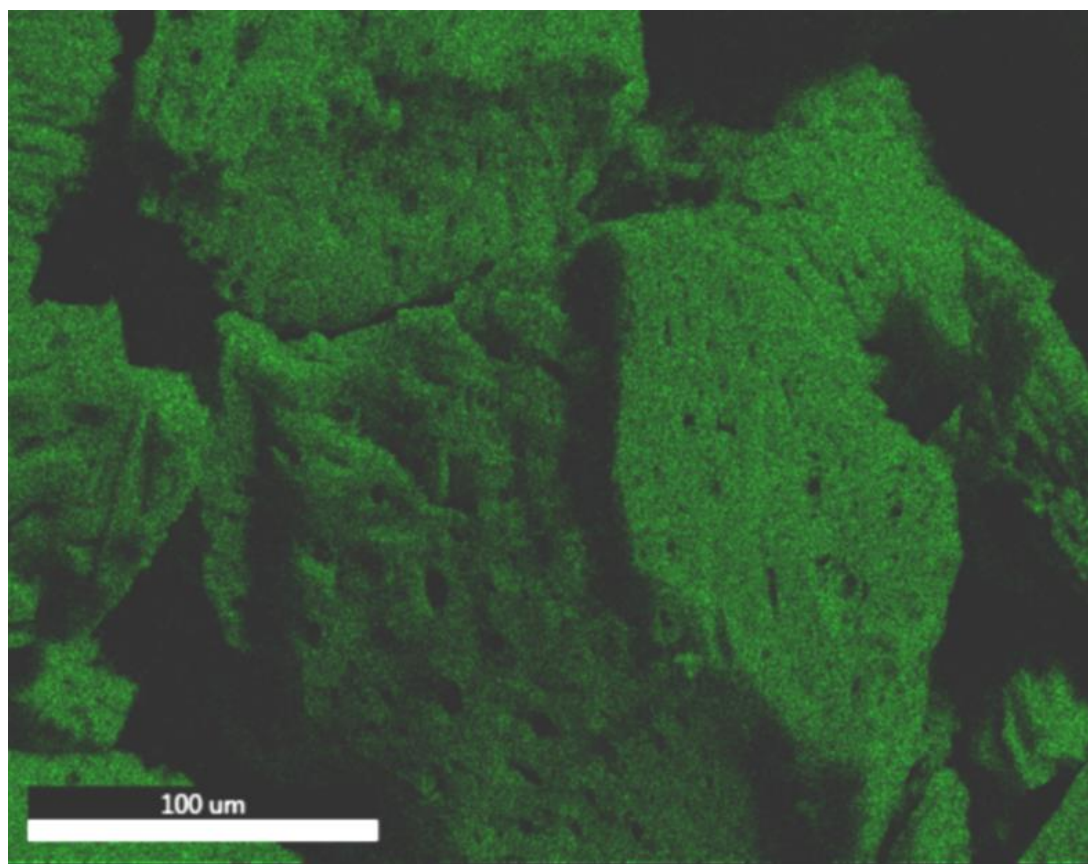
Carbon

Figure 3.51: EDX elemental map of Kuraray PGW-150MP showing only carbon. Reproduced with permission from the Royal Society of Chemistry.[45]
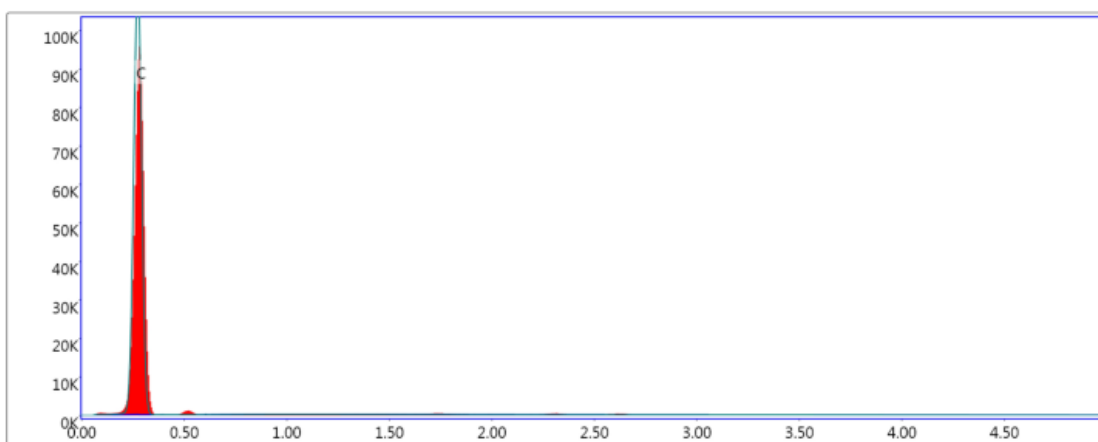
Figure 3.52: EDX sum spectrum is only showing a carbon peak.
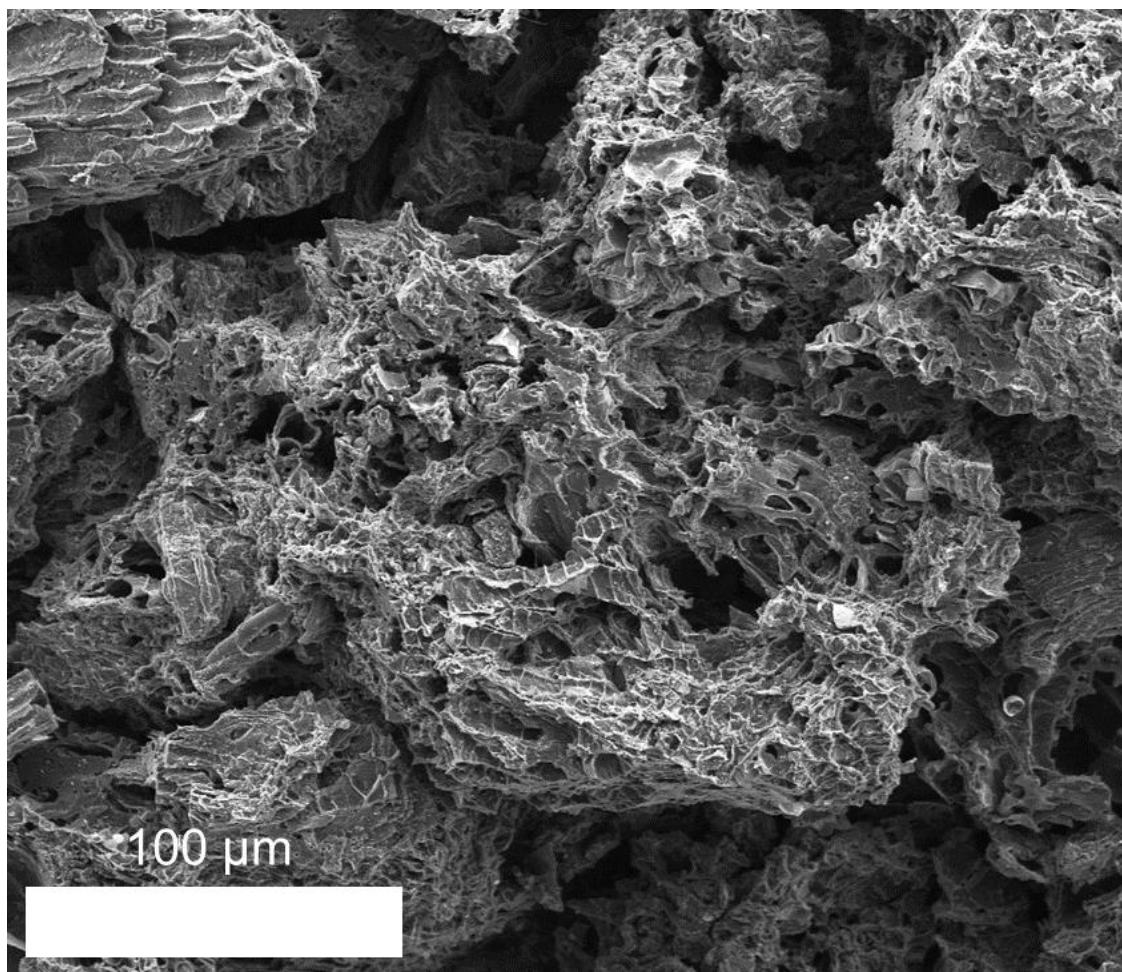
Figure 3.53: SEM micrograph of Sigma-Aldrich GAC. Reproduced with permission from the Royal Society of Chemistry.[45]
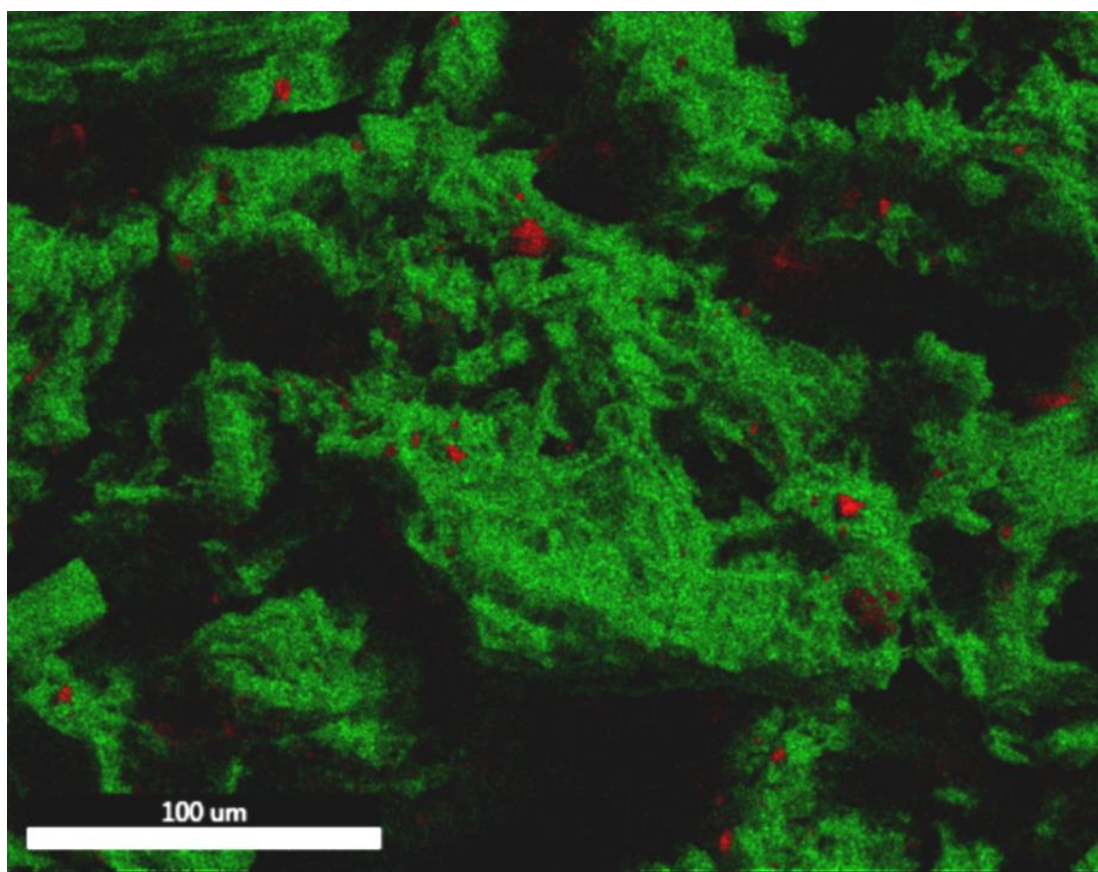
Figure 3.54: EDX elemental map of Kuraray Sigma-Aldrich GAC showing carbon and silica. Reproduced with permission from the Royal Society of Chemistry.[45]
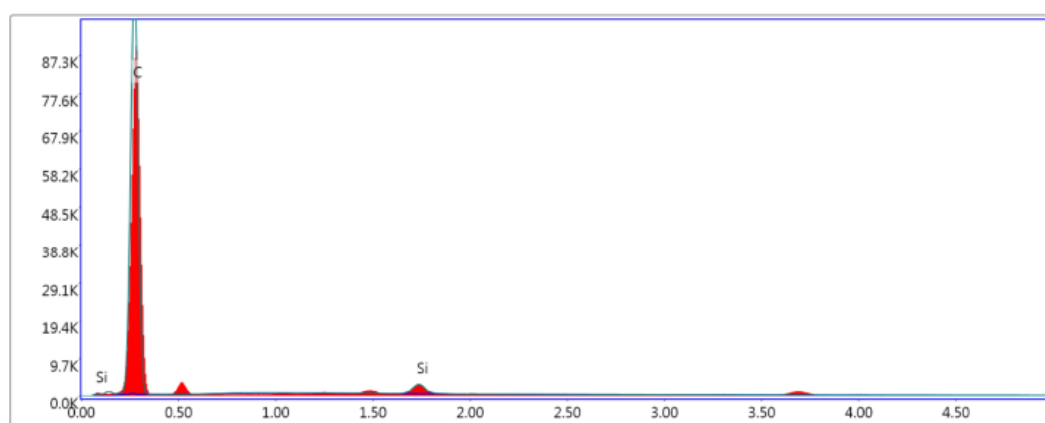
Figure 3.55: EDX sum spectrum of Sigma-Aldrich GAC showing carbon and silicon peaks.

233
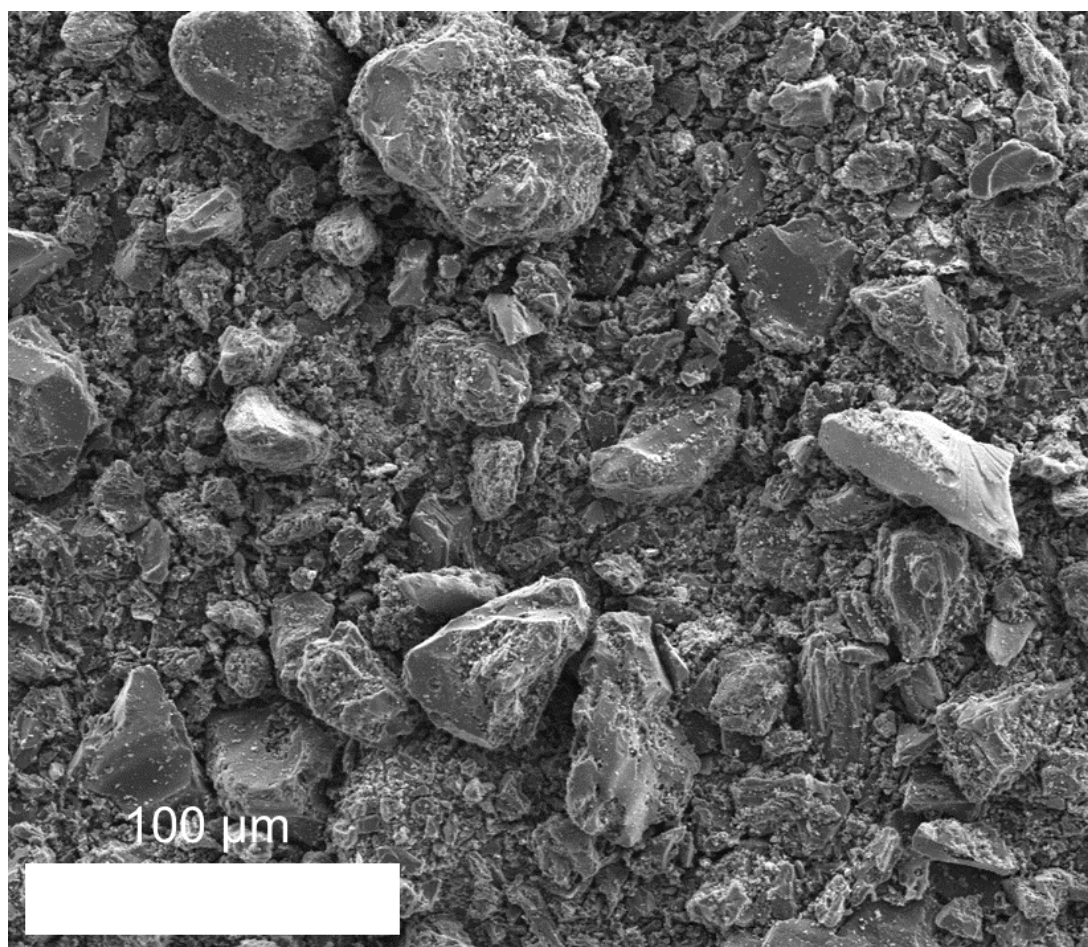
Figure 3.56: SEM micrograph of ChemSupply PAC. Reproduced with permission from the Royal Society of Chemistry.[45]

Carbon   Silicon
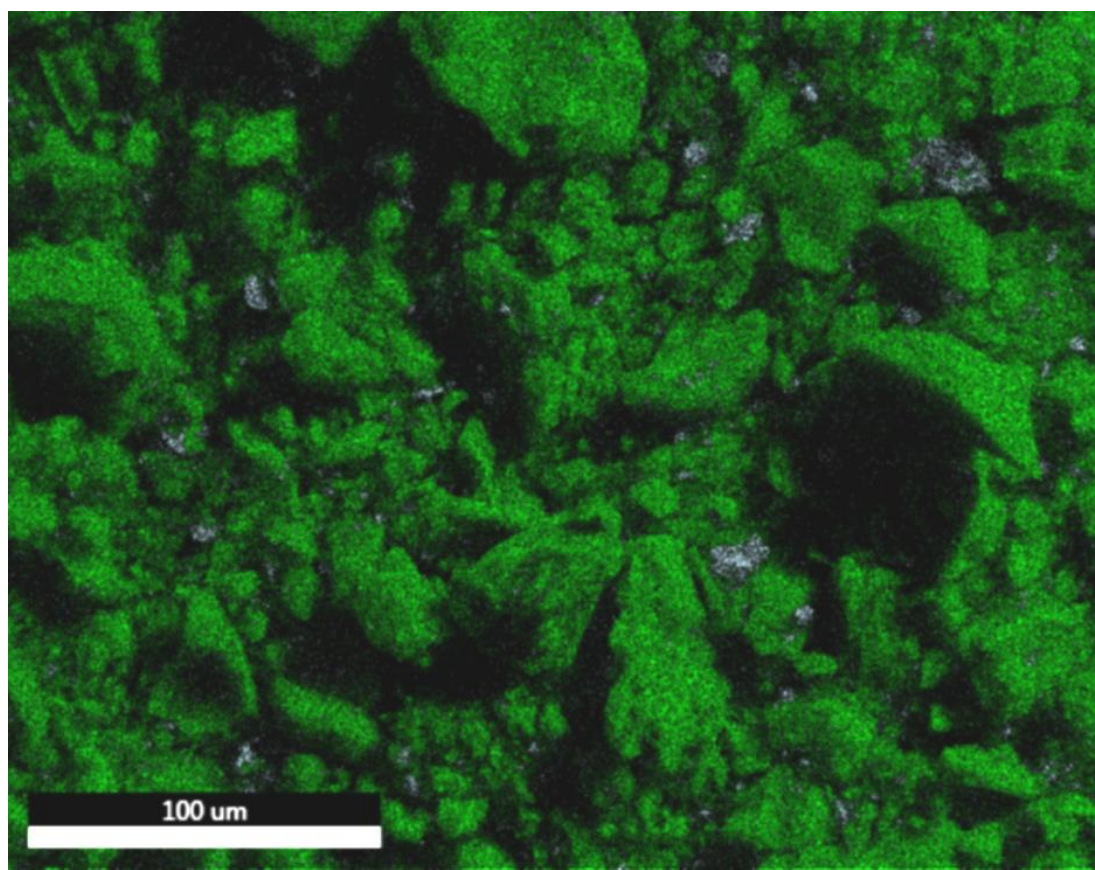
Figure 3.57: EDX elemental map of Kuraray ChemSupply PAC showing carbon and aluminium. Reproduced with permission from the Royal Society of Chemistry.[45]
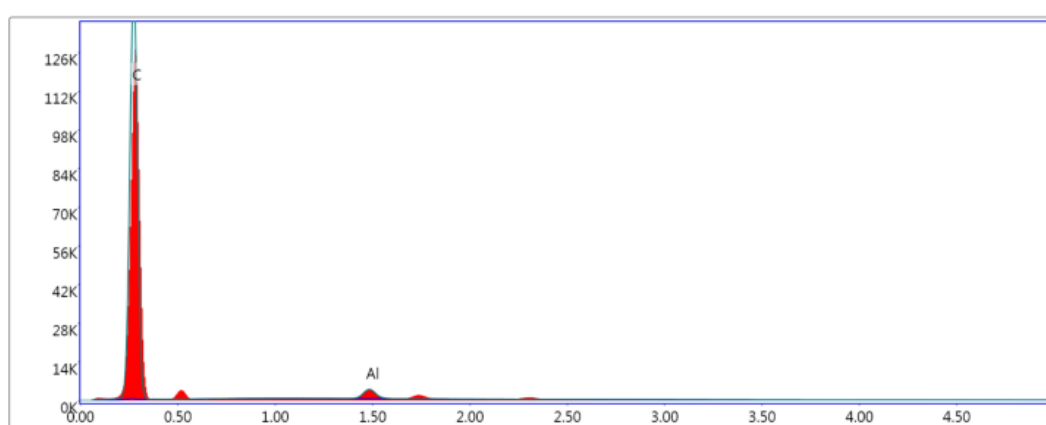
Figure 3.58: EDX sum spectrum of ChemSupply PAC showing carbon and aluminium peaks.

Raman analysis of commercial carbons
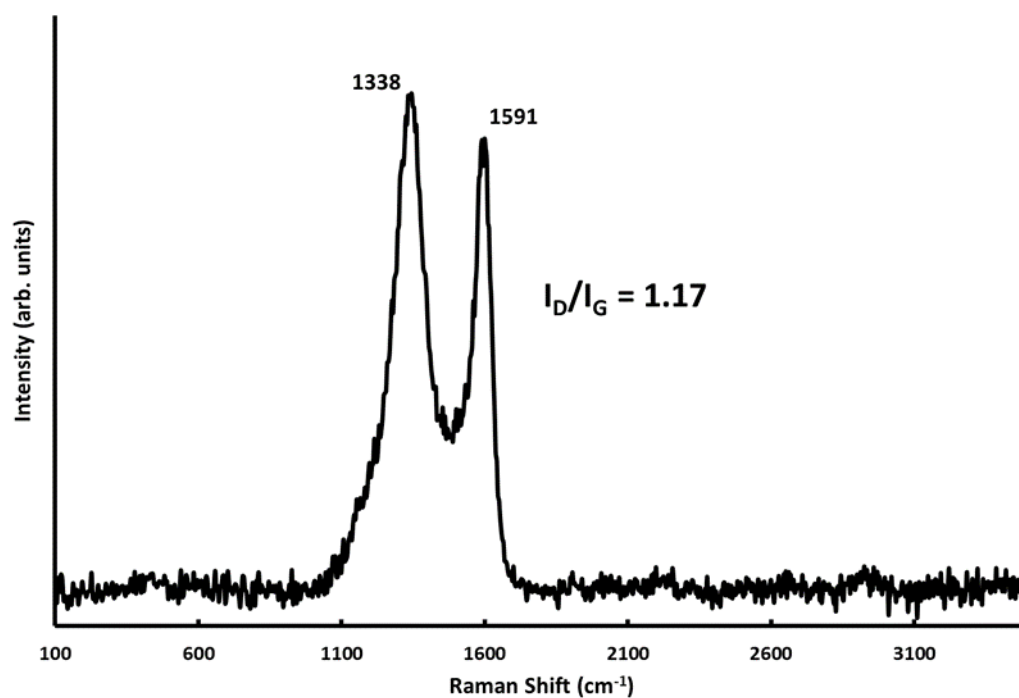
Figure 3.59: Raman spectra of Kuraray PGW-150MP showing the I_D/I_G to be 1.17. Reproduced with permission from the Royal Society of Chemistry.[45]
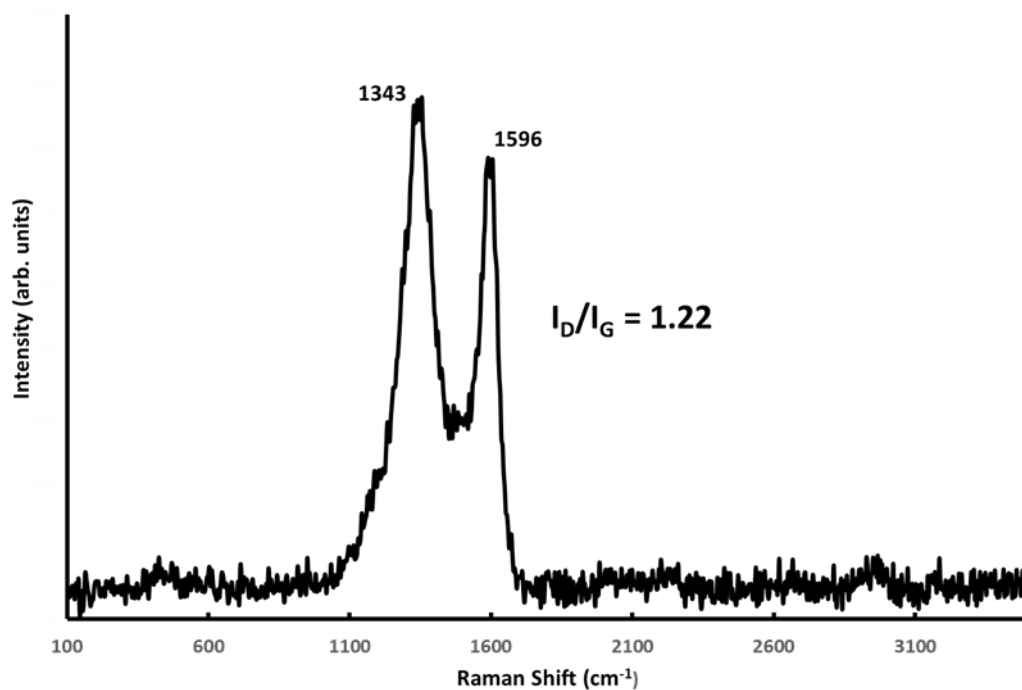
Figure 3.60: Raman spectra of Sigma-Aldrich GAC showing the I_D/I_G to be 1.22. Reproduced with permission from the Royal Society of Chemistry.[45]
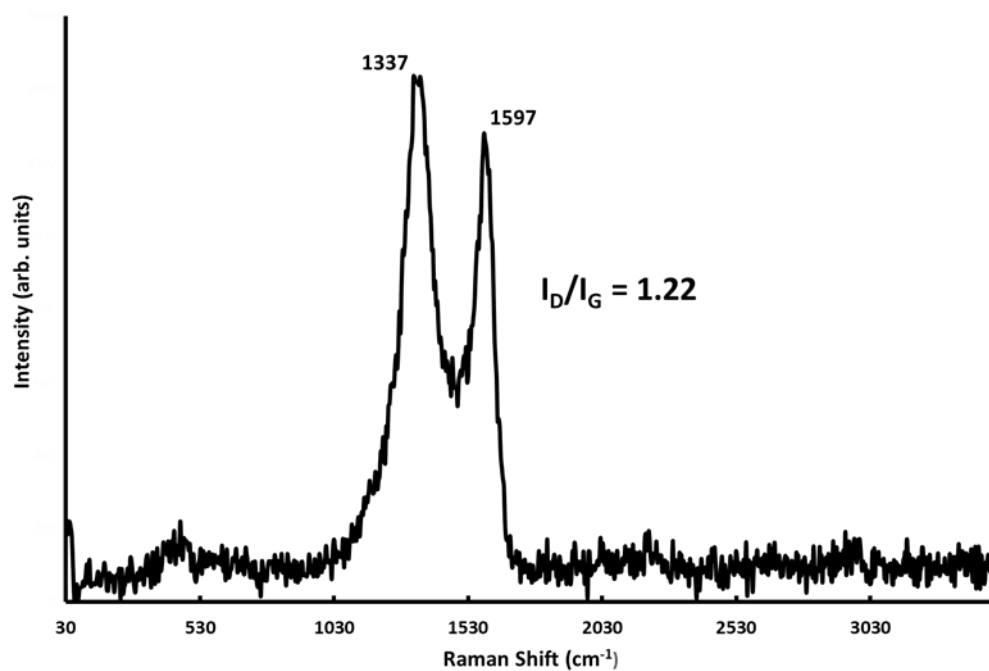
Figure 3.61: Raman spectra of ChemSupply PAC showing the I_D/I_G to be 1.22. Reproduced with permission from the Royal Society of Chemistry.[45]

Raman spectroscopy was performed on a sample of elemental sulfur to determine if any free sulfur is present in the commercial carbons and carbonised-1 or carbonised-1-O.
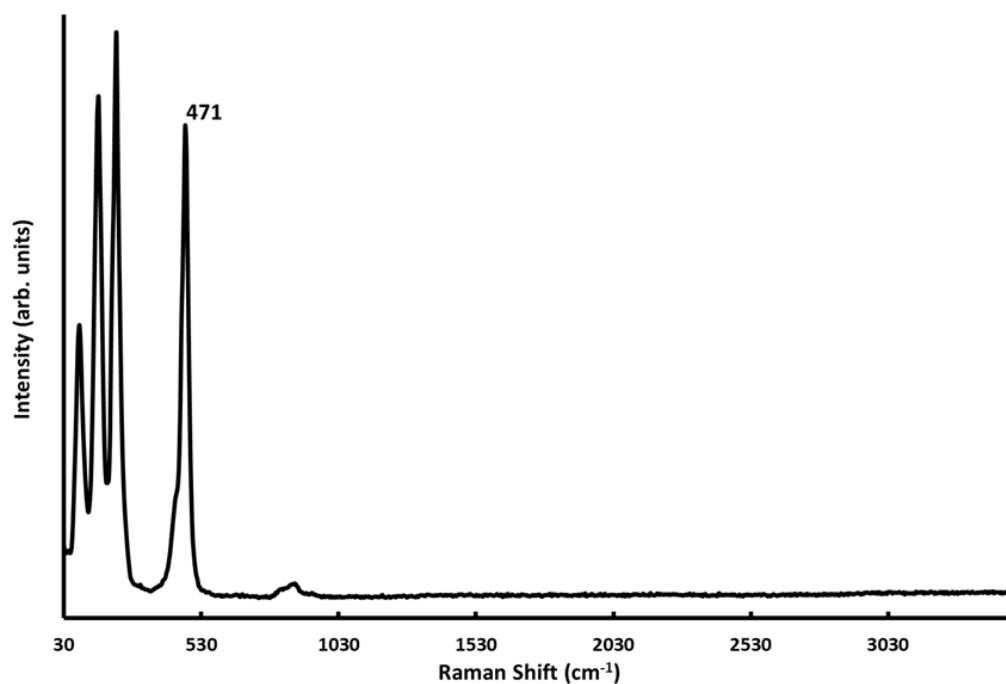
Figure 3.62: Raman spectra of elemental sulfur. Reproduced with permission from the Royal Society of Chemistry.[45]

XRD analysis of carbonised-1, carbonised-1-O and commercial carbons
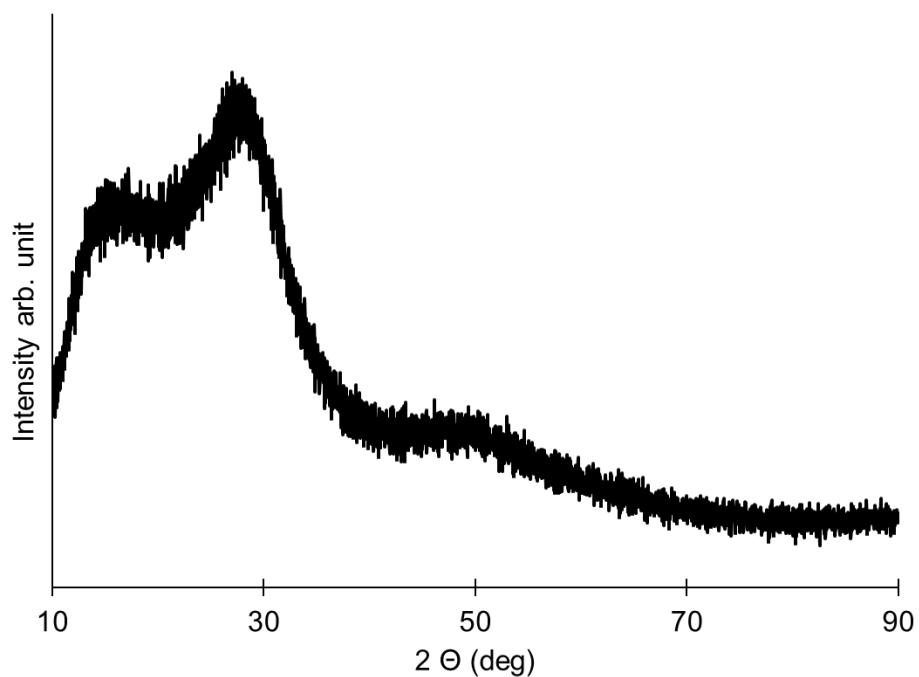
Figure 3.63: XRD spectrum of carbonised-1. Reproduced with permission from the Royal Society of Chemistry.[45]
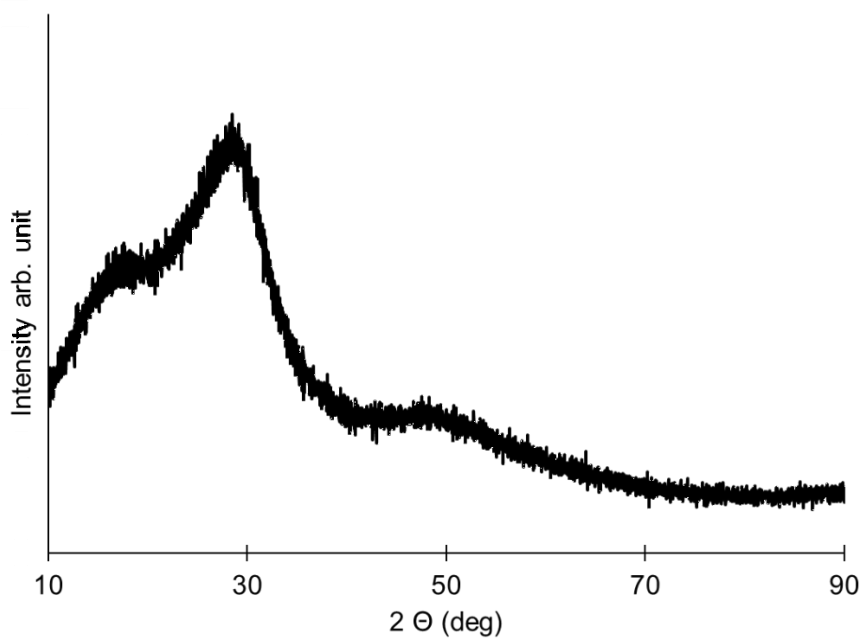
Figure 3.64: XRD spectrum of carbonised-1-O. Reproduced with permission from the Royal Society of Chemistry.[45]
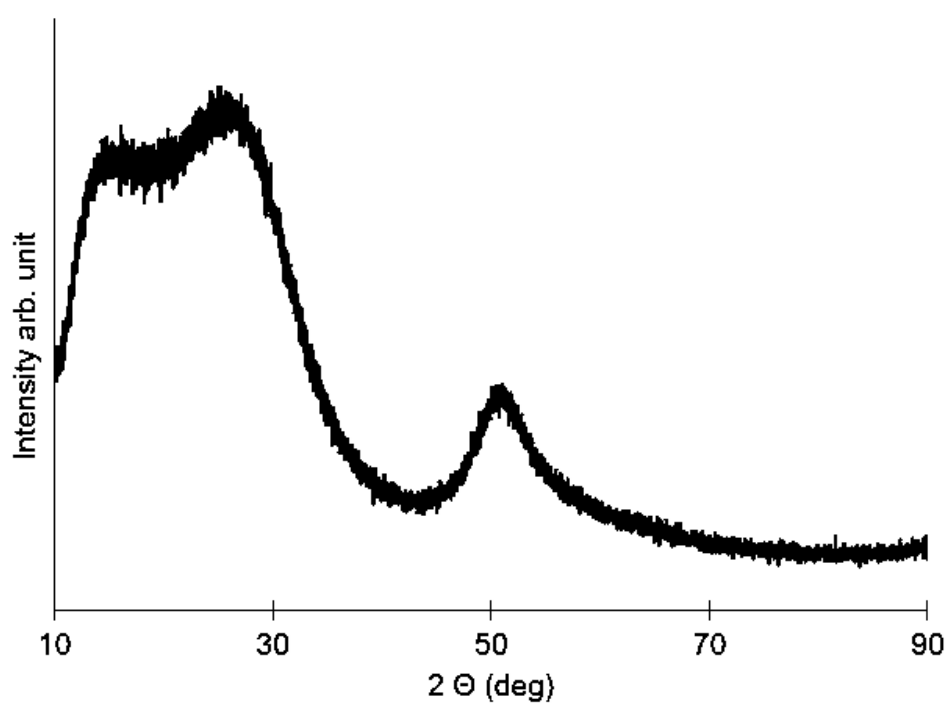
Figure 3.65: XRD spectrum of Kuraray PGW-150-MP. Reproduced with permission from the Royal Society of Chemistry.[45]
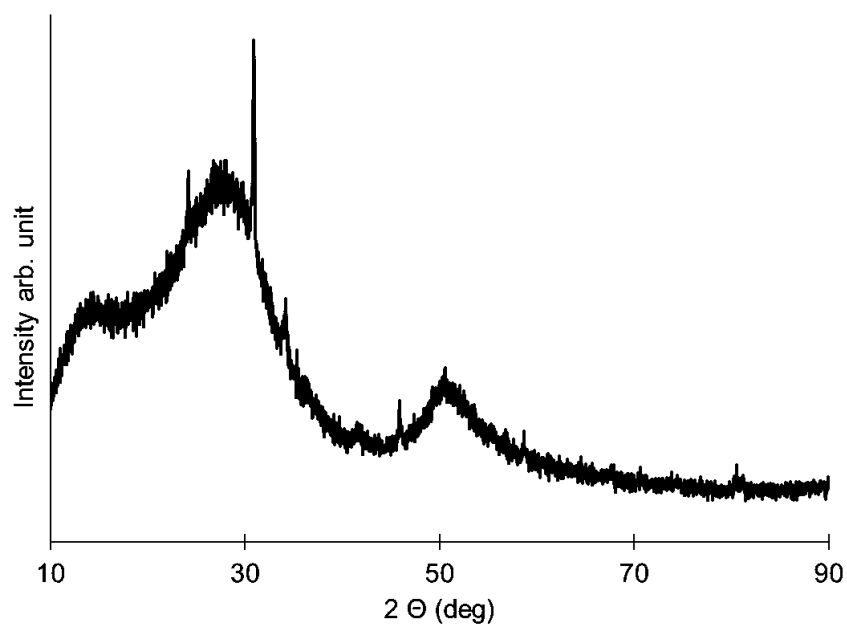
Figure 3.66: XRD spectrum of Sigma-Aldrich GAC. Reproduced with permission from the Royal Society of Chemistry.[45]
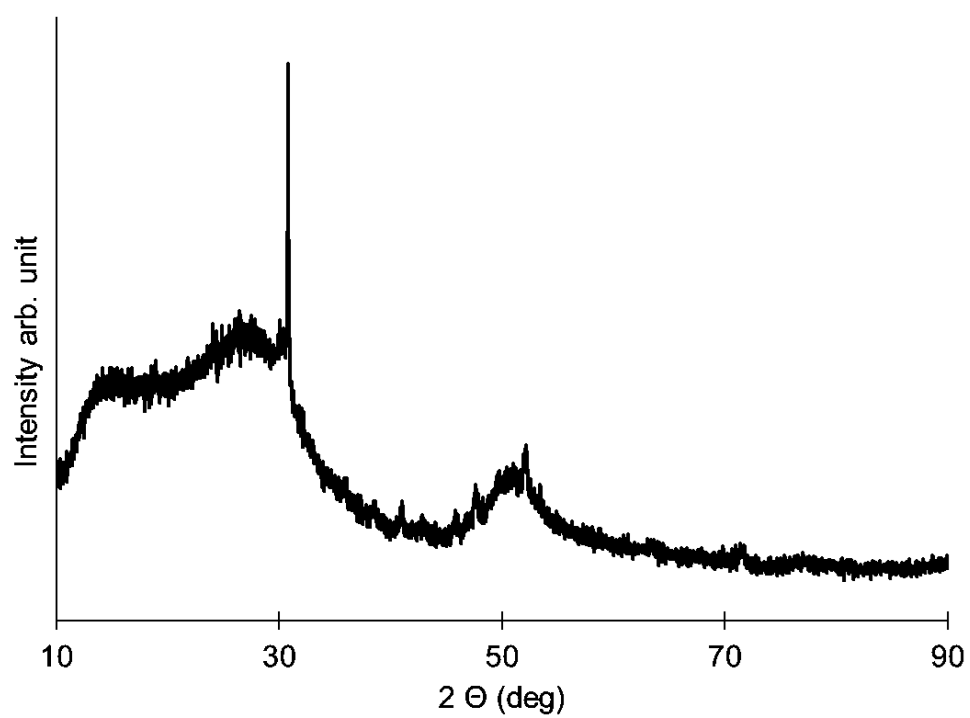
Figure 3.67: XRD spectrum of ChemSupply PAC. Reproduced with permission from the Royal Society of Chemistry.[45]

XPS analysis of carbonised-1 and carbonised-1-O

For XPS analysis, the carbonised-1 and carbonised-1-O samples were ground to a powder form and mounted on a sample holder. The high-resolution scans of C, O, S of the samples were recorded and fitted. The spectra of C and S are shown in (a) and (b) in Figure 3.68. The normalized relative concentration of element, the relative intensity of C and S species are respectively exhibited in (c), (d) and (e) in Figure 3.68.
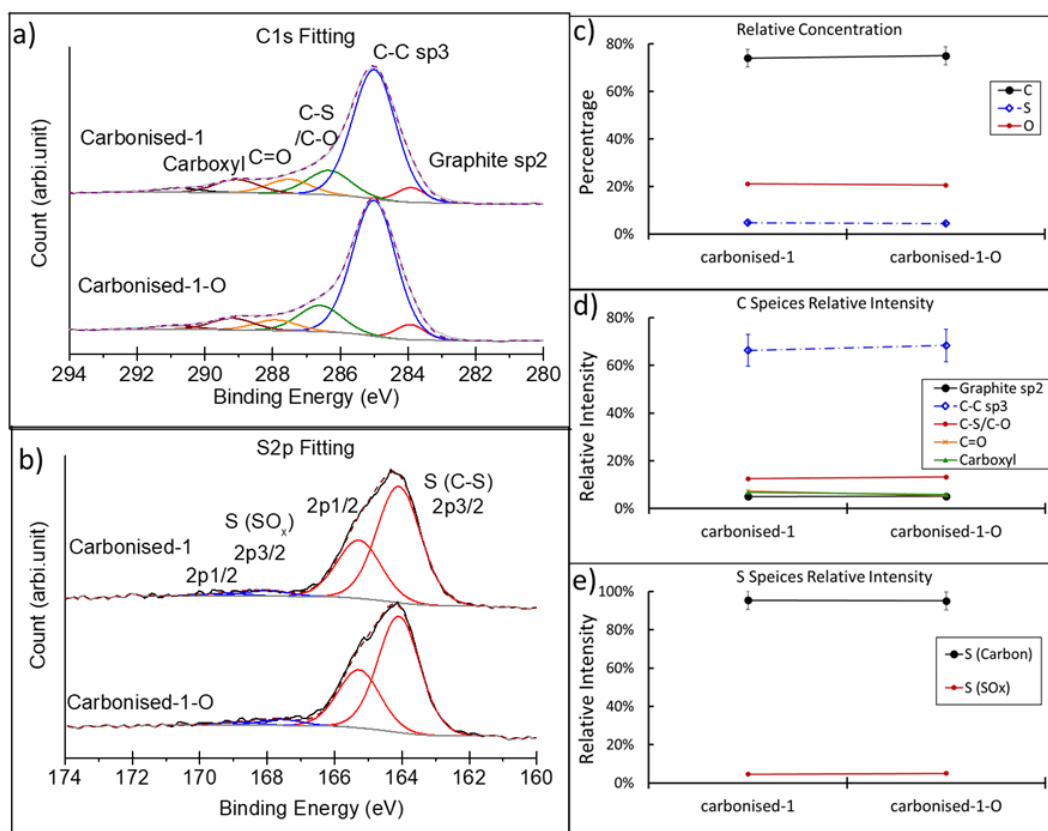
Figure 3.68: XPS analysis of carbonised-1 and carbonised-1-O. **a)** and **b)**: Fitting of C and S spectra of two samples; **c)**: relative concentration of C, O and S; **d)** and **e)**: relative intensity of C and S species of the samples. Reproduced with permission from the Royal Society of Chemistry.[45]

The fitting of C1s resulted in five individual peaks. The C-C sp3 was found and calibrated at 285.0 eV[59] and a small peak with a full width half maximum (FWHM) of 1.0 eV at 284.0 ± 0.15 eV was fitted,[60-62] indicating a fraction of sp2 graphite species. C-S and C-O peaks were fitted at 286.7 ± 0.15 eV.[59, 63] The peak levelling at 288.1 ± 0.15 eV and 289.3 ± 0.15 eV can be assigned to C=O[64] and carboxyl[65] groups. The fitting of S2p$_{3/2}$ resulted in two distinguishable components. The one fitted at 164.1 ± 0.15 eV was from C-S bonds in the carbon, while the other one fitted at 167.6 ± 0.15 eV[10,11]

241

represented the high oxidation states of sulfur SO_x, such as sulfinates or sulfonates, as a consequence of the carbonisation in air. Similar spectra and fitting were obtained for both carbonised-1 and carbonised-1-O.

The relative surface concentration from c) revealed a concentration of about 75 % of C, 20 % of O and nearly 4.6 % S in both samples (Figure 3.68). Regarding the carbon in carbonised-1 from d), about 67.3 % was C-C, 5.1% was graphite sp2 and 12.8 % was C-S/C-O, while C=O and carboxyl were 7.3 % and 6.8 %. In Figure 3.68 e), 95.4 % sulfur was bonded to carbon and 4.6 % of the sulfur was presented as a higher oxidation state. The composition was similar in sample carbonised-1-O. The chemical characterisation of the two samples indicated no noticeable difference from the perspective of elemental distribution and chemical bonds.

CHNS combustible elemental analysis of commercial carbons and carbonised-1 and carbonised-1-O

Table 3.2: CHNS combustible elemental analysis has been done for all commercial carbons as well as for carbonised-1, carbonised-1-O and 50-poly (S-*r*-canola).

Sample	Carbon (%)	Sulfur (%)	Hydrogen (%)	Nitrogen (%)
50-poly(S-*r*-canola)	42.0	48.4	6.5	<0.3
Carbonised-1	65.6	16.0	1.6	0
Carbonised-1-O	63.6	15.2	1.5	<0.3
Kuraray PGW-150MP	91.4	<0.3	0.4	<0.3
Sigma-Aldrich GAC	78.5	<0.3	<0.3	0.4
ChemSupply PAC	82.4	<0.3	<0.3	0.3
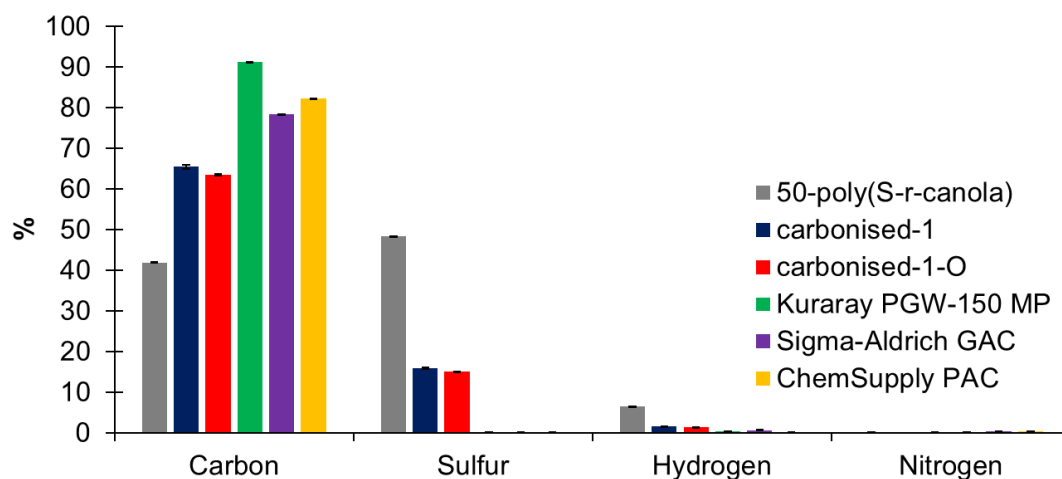
Figure 3.69: Comparison of CHNS elemental analysis of 50-poly(S-*r*-canola), carbonised-1, carbonised-1-O, Kuraray PGW150MP, Sigma-Aldrich PAC and ChemSupply PAC. Reproduced with permission from the Royal Society of Chemistry.[45]

Elemental analysis showed that carbonised-1 and carbonised-1-O had a very similar elemental composition. Further it can be seen that no commercial carbon contained a significant amount of sulfur.

Sonication of carbonised-1 and carbonised-1-O

To prepare the sonicated carbonised-1 and carbonised-1-O, 500 mg of material and 100 mL of MilliQ water were combined in a 125 mL plastic tube and then sonicated using a Bueno Biotech BEM-900A Ultrasonic Homogeniser equipped with a Φ12 probe. The settings of the ultrasonic homogeniser were set to a pulse of 2 seconds followed by a 5 second pause for a total time of 30 minutes. Further the power was set to 100 % (900 W) and the temperature was capped at 60 °C. After that the carbon was vacuum filtered and dried under high vacuum overnight.
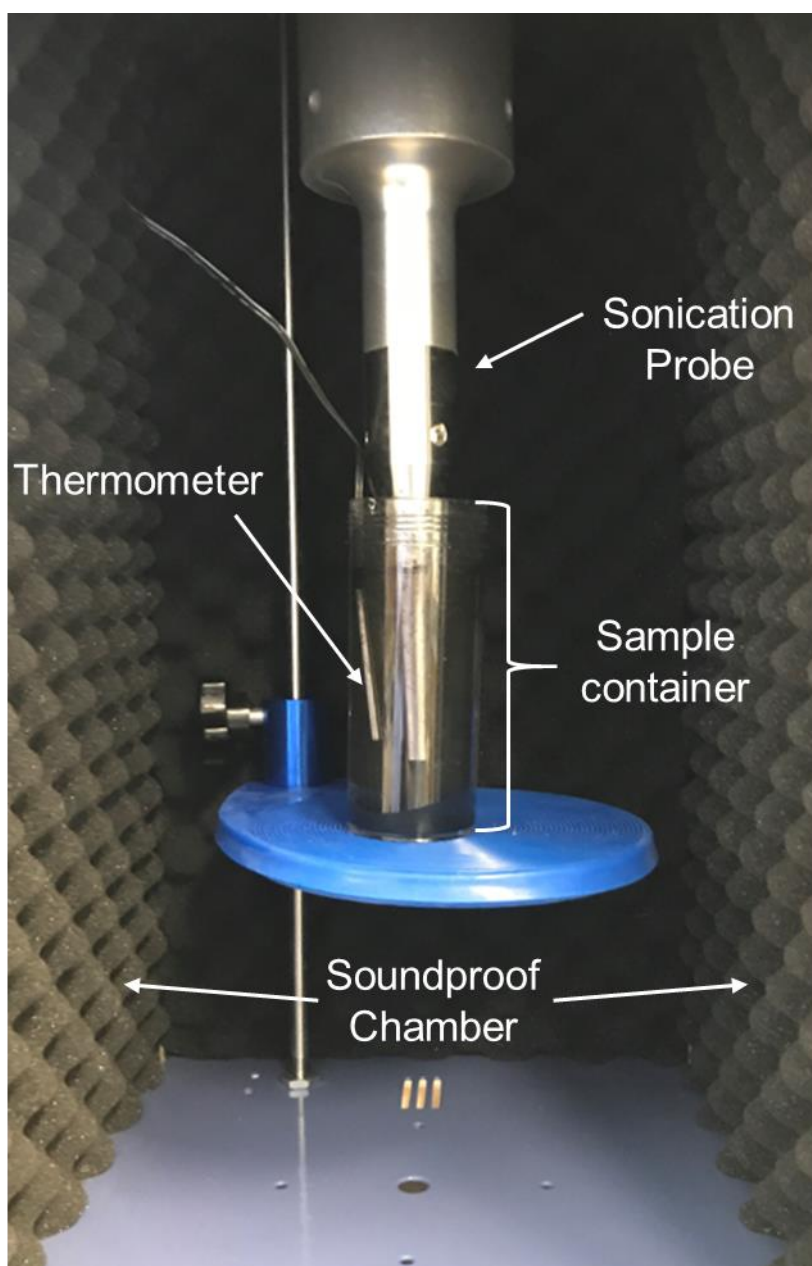
Figure 3.70: Sonication set-up used to sonicate carbonised-1 and carbonised-1-O.
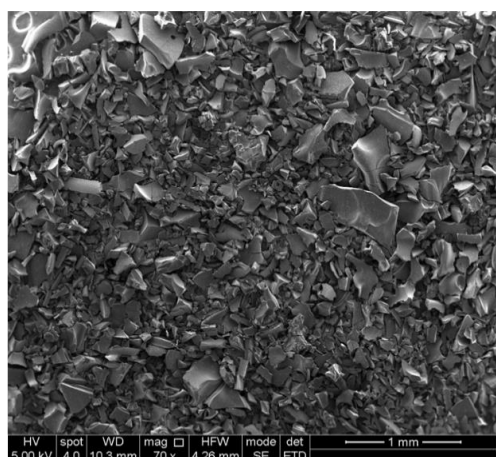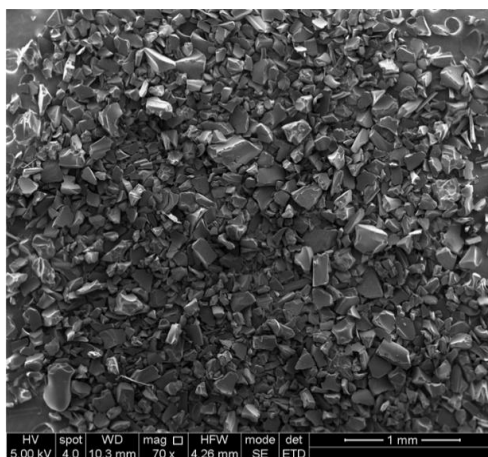
Figure 3.71: SEM micrographs of non-sonicated (left) and sonicated caronised-1 (right). Reproduced with permission from the Royal Society of Chemistry.[45]
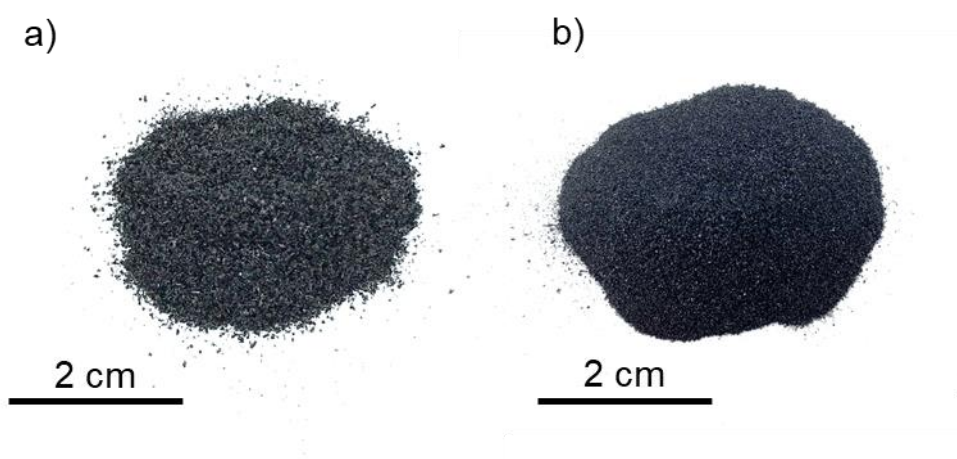
Figure 3.72: a) Non-sonicated and **b)** sonicated carbonised-1-O.

Heavy metal removal from aqueous solution (As, Cd, Hg, Pb)

This experiment was performed to assess the ability of carbonised-1 to remove heavy metals from aqueous solution. Accordingly, five solutions containing a mixture of 5 ppm each of As (As_2O_5), Cd ($Cd(NO_3)_2$), Hg ($Hg(NO_3)_2$) and Pb ($Pb(NO_3)_2$) were prepared. All standards had an original concentration of 1000 ppm and were in a matrix of 2 % HNO_3. To make solutions with a concentration of only 5 ppm of As, Cd, Hg and Pd, 250 µL of each standard was added to a 50 mL plastic tube and diluted to 45 mL using deionised water. PGW-150MP had a particle size range from 150 µm to 500 µm. To have similar particle sizes for the S-activated carbon, the crushed carbon was sieved through a 500 µm sieve. To three 5 ppm heavy metal solutions, 100 mg of the sieved carbonised-1 was added whereas 100 mg of the PGW-150MP carbon was added to another 3 heavy metal solutions. To the last solution no activated carbon was added as this solution acted as a control to monitor the metal concentration over time. After the activated carbon was added to the 6 sample solutions, the samples were put on head over tail rotation at 25 RPM. Samples for ICP-MS were taken at 0, 0.5, 1, 1.5 and 2 hours after carbon addition. The samples were analysed using ICP-OES.

Table 3.3: Percentage of metals removed after 2 hours using Kuraray PGW-150MP or carbonised-1.

Sorbent	Heavy metal and removed percentage			
	As	Cd	Hg	Pb
Kuraray PGW-150 MP	0 %	1 %	97.9 %	5.5 %
Carbonised-1	0 %	1 %	92.3 %	18 %

Since it can be clearly seen that the carbons are excellent in mercury uptake but not in the uptake of arsenic, cadmium and lead, any subsequent heavy metal uptake studies will be conducted using mercury only.

Mercury removal from water (Poly-50(S-*r*-canola), ChemSupply PAC, Sigma-Aldrich GAC, carbonised-1, Kuraray PGW-150MP, sonicated carbonised-1, carbonised-1-O)

Since it has been previously discovered that carbonsed-1 is excellent in removing mercury, the mercury sorption capabilities of all other commercial carbons as well as carbonised-1-O will be assessed.

The protocol used was the same as for the arsenic, cadmium, mercury, and lead uptake studies. Mercury analysis was carried out using cold vapour atomic absorption spectroscopy (CVAA).

Table 3.4: Percentage of metals removed using commercial and synthesised carbons.

Sorbent	Hg removed after 2 hours (%)	Sorbent	Hg removed after 2 hours (%)
Poly-50(S-r-canola)	43.1	Kuraray PGW-150MP	97.8
ChemSupply PAC	70.1	Sonicated carbonised-1	99.3
Sigma-Aldrich GAC	89.6	Carbonised-1-O	99.3
Carbonised-1	92.3		

Kinetic analysis of mercury removal

To perform the kinetic analysis, the mass of mercury removed per gram of polymer was calculated using the concentrations of the heavy metal removal analysis of the carbon materials and their masses used. In order to fit the kinetic model to the dataset, pseudo-first order and pseudo second order kinetic models were used.[53, 54]

The linear equations of these kinetic models can be written as:

Pseudo-First Order (linear)[53]

$$\ln(q_e - q_t) = \ln q_e - k_1 t$$

Pseudo-Second Order (linear)[54]

$$\frac{t}{q_t} = \frac{1}{k_2 q_e^2} + \frac{1}{q_e}$$

The pseudo-first order kinetic model equation can be rewritten in non-linearised form as:

Pseudo-First Order (non-linearised)[53]

$$q_t = q_e\left(1 - e^{-k_1 t}\right)$$

Pseudo-Second Order (non-linearised)

$$q_t = \frac{q_e^2 k t}{1 + q_e k t}$$

q_e = mercury bound to the carbon substrate at equilibrium (mg mercury / g polymer)

q_t = mercury bound to the carbon substrate at time t (mg mercury / g polymer)

k_1 = rate constant of pseudo-first order kinetic model (hour^{-1})

k_2 = rate constant of pseudo-second order kinetic model (mg.g^{-1}.hour^{-1})

t = time (hours)
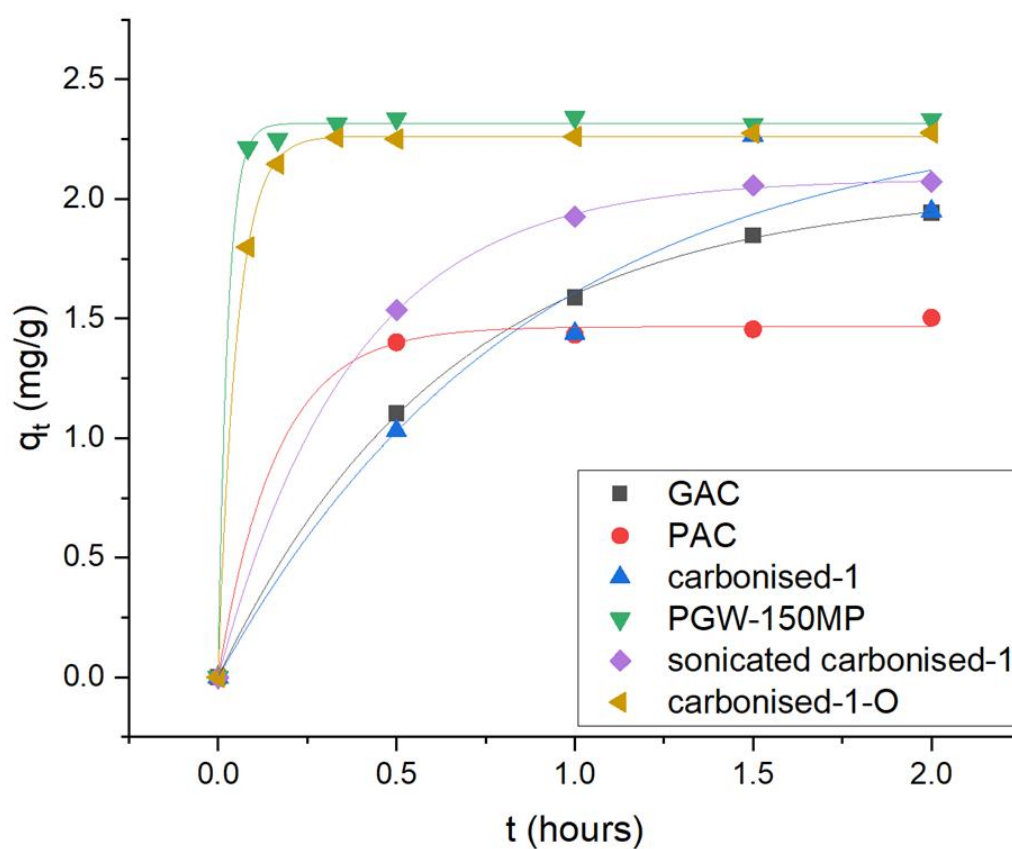
Figure 3.73: Pseudo-first order non-linear plot of q_t vs time for Sigma-Aldrich GAC, ChemSupply PAC, carbonised-1, Kuraray PGW-150MP, sonicated carbonised-1 and carbonised-1-O. Reproduced with permission from the Royal Society of Chemistry.[45]
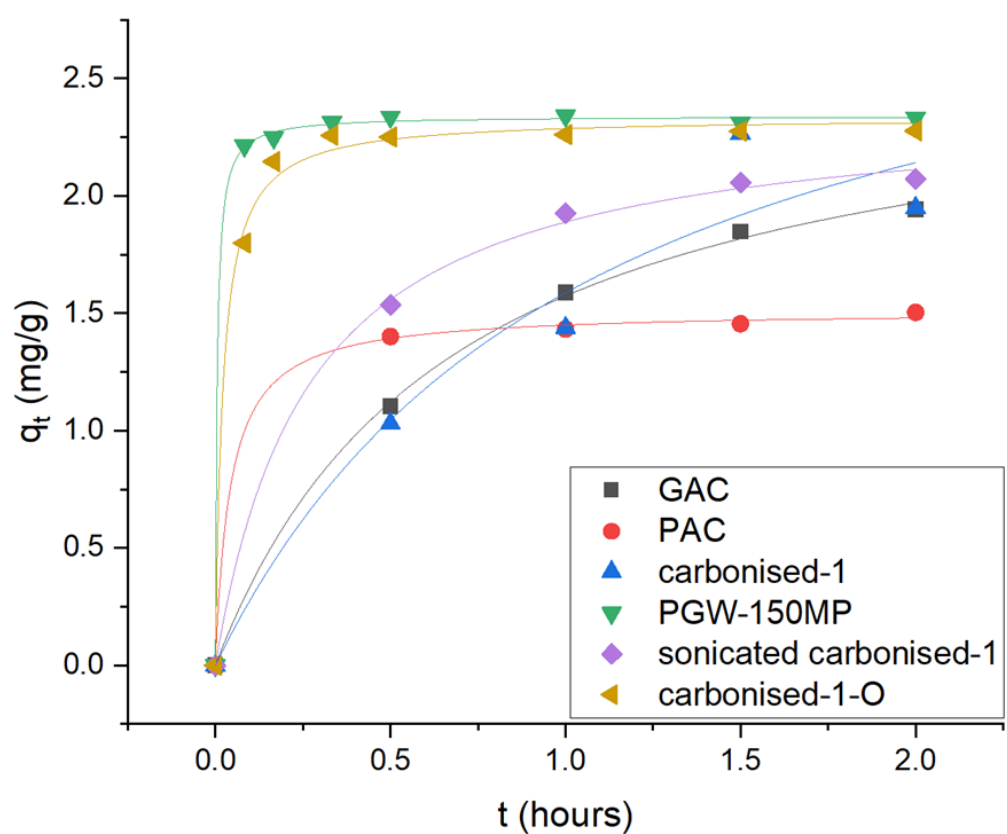
Figure 3.74: Pseudo-second order non-linear plot q_t vs time for for Sigma-Aldrich GAC, ChemSupply PAC, carbonised-1, Kuraray PGW-150MP, sonicated carbonised-1 and carbonised-1-O. Reproduced with permission from the Royal Society of Chemistry.[45]

Table 3.5: Kinetic rate parameters of mercury sorption of the carbon substrates using non-linear models.

Carbon Substrate	Rate constant (k)	q_e (expt.) (mg/g)	q_e (calc.) (mg/g)	r^2
GAC	$k_1 = 1.54 \pm 0.03$ h^{-1}	1.94	2.04 ± 0.01	1.000
	$k_2 = 0.562 \pm 0.6$ mg.g^{-1}.h^{-1}		2.64 ± 0.08	0.999
PAC	$k_1 = 6.14 \pm 0.99$ h^{-1}	1.50	1.47 ± 0.02	0.998
	$k_2 = 15.4 \pm 4.92$ mg.g^{-1}.h^{-1}		1.51 ± 0.02	1.000
Carbonised-1	$k_1 = 1.14 \pm 0.53$ h^{-1}	1.95	2.36 ± 0.46	0.927
	$k_2 = 0.283 \pm 0.289$ mg.g^{-1}.h^{-1}		3.29 ± 1.05	0.923
PGW-150MP	$k_1 = 36.8 \pm 3.61$ h^{-1}	2.33	2.32 ± 0.01	0.999
	$k_2 = 84.7 \pm 12.9$ mg.g^{-1}.h^{-1}		2.34 ± 0.01	1.000
Sonicated carbonised-1	$k_1 = 2.65 \pm 0.04$ h^{-1}	2.07	2.09 ± 0.01	1.000
	$k_2 = 1.55 \pm 0.23$ mg.g^{-1}.h^{-1}		2.40 ± 0.06	0.998
carbonised-1-O	$k_1 = 18.8 \pm 0.32$ h^{-1}	2.28	2.26 ± 0.01	1.000
	$k_2 = 20.2 \pm 3.26$ mg.g^{-1}.h^{-1}		2.34 ± 0.03	0.996

The best fit for each substrate was determined by comparing the experimental and calculated q_e. The kinetic model with the closest calculated q_e compared to the experimental value was chosen.

Isotherm adsorption of carbonised-1 and PGW-150MP

Isotherms of the carbonised-1 and PGW-15-MP were performed. Firstly, a 1000 ppm Hg solution was made by dissolving 676.7 mg of HgCl$_2$ in a 500 mL volumetric flask in MilliQ water. For the isotherm of the carbonised-1, 5 samples with different Hg concentrations (50 ppm, 100 ppm, 150 ppm, 200 ppm, 250 ppm) and volumes of 20 mL were prepared in triplicate in plastic tubes. To each sample 100 µg of carbonised-1 was added. After that the samples were rotated at 25 RPM for 7 hours. Following that an aliquot of each sample was filtered using a 0.45 µm nylon syringe filter and sent for analysis. For the PGW-150MP isotherm, 5 samples with different Hg concentrations (50 ppm, 100 ppm, 200 ppm, 300 ppm, 400 ppm) and volumes of 20 mL were prepared in triplicate in plastic tubes. To each sample 20 mg of PGW-150MP was added. Following that the samples were rotated at 25 RPM for 7 hours. After that an aliquot of the samples were filtered using a 0.45 µm nylon syringe filter and sent for analysis.

For the isotherm fitting the Langmuir model was used.

$$q_{eq} = \frac{Q_{max}K_L C_{eq}}{1 + K_L C_{eq}}$$
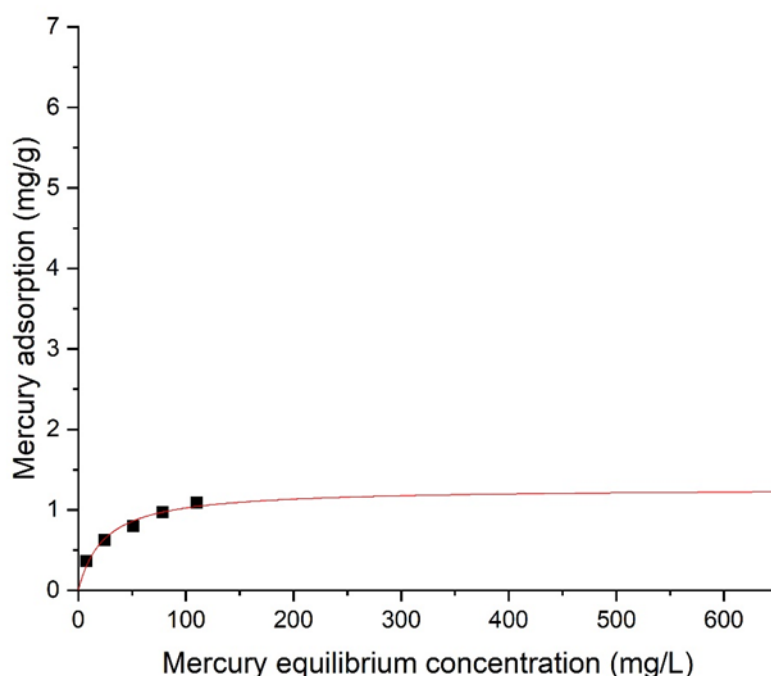
Figure 3.75: Adsorption isotherm of mercury onto samples of carbonised-**1** using Langmuir isotherm fitting (red line). Reproduced with permission from the Royal Society of Chemistry.[45]

Adsorption isotherm of mercury onto samples of PGW-150MP using Langmuir
isotherm fitting (red line)
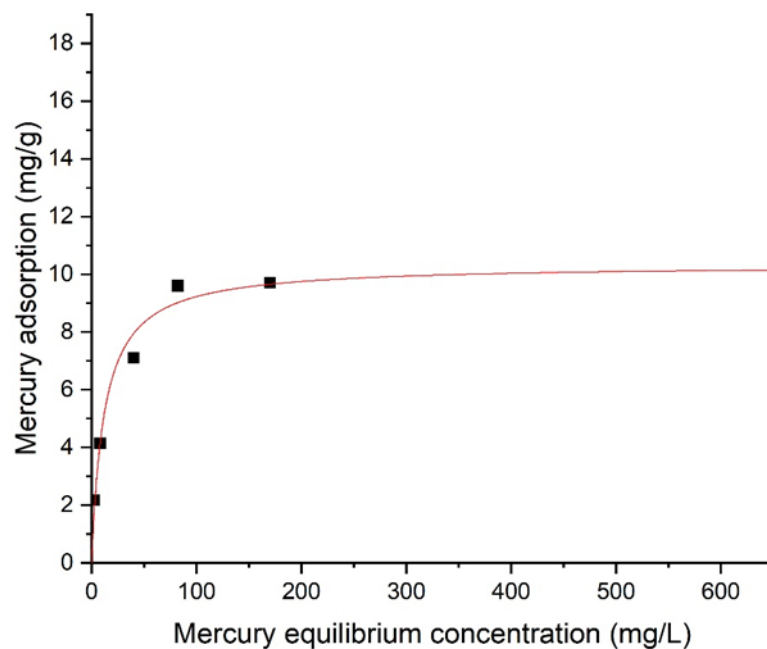
Figure 3.76: Adsorption isotherm of mercury onto samples of PGW-150MP using Langmuir
isotherm fitting (red line). Reproduced with permission from the Royal Society of Chemistry.[45]

Hg leaching from carbons

The following experiment was performed to investigate if Hg that was captured by carbonised-1 or carbonised-1-O is leached off again when exposed to acidic conditions. In this experiment all the available carbons were tested (carbonised-1, carbonised-1-O, PGW-150MP, GAC, PAC). All experiments were performed in triplicate.

Firstly, 200 mg of each carbon was placed in separate 45 mL mercury solution (50 ppm) made from a 1000 ppm mercury standard in 2% HNO_3. After that all the samples were rotated at 25 RPM for 2 hours. After that, each sample was recovered by vacuum filtration and washed with 50 mL MilliQ water. Then, the samples were placed in 45 mL of a 5% HNO_3 solution and rotated at 25 RPM for 24 hours. Samples for Hg analysis were taken of each solution before adding the carbon and then after 2 hours Hg exposure in order to calculate the amount of mercury on the carbon sorbent. Samples were also taken immediately after adding the carbon to the nitric acid solution, and after the samples have been in the nitric acid solution for 24 hours. Samples were taken by centrifuging 1 mL for 1 minute to separate the carbon from the solution and diluting 0.7 mL of sample to 7 mL, stabilised in 5% nitric acid. The samples were analysed by CVAAS. The results are summarised below.

Table 3.6: Hg leached from mercury rich carbonised-1, carbonised-1-O, Kuraray PGW-150MP, Sigma-Aldrich GAC and ChemSupply PAC.

Sample	Hg leached (%)
Carbonised-1	5
Carbonised-1-O	9
Kuraray PGW-150MP	22
Sigma-Aldrich GAC	32
ChemSupply PAC	28

Regeneration of carbonised-1 and carbonised-1-O after mercury sorption

First, spent sorbents were prepared with mercury bound to the carbon. All experiments were carried out in triplicate. To generate the spent sorbent, 1.000 g of either carbonised-1 or carbonised-1-O was placed in a 45 mL solution of 250 ppm $Hg(NO_3)_2$ and rotated for 24 hours. Following this time, the carbon samples were recovered by filtration and washed with 50 mL water and dried under vacuum. The concentration of the mercury solution after the incubation with carbon was measured by CVAA and used to determine the amount of mercury bound to each carbon sample.

Table 3.7: Mercury on carbonised-1 and carbonised-1-O after mercury uptake for carbon regeneration experiment.

Sample	Hg on carbon (mg)
Carbonised -1	8.9 ± 0.8
Carbonised-1-O	9.7 ± 1.1

To regenerate the carbons, the spent sorbents (prepared above, bound to mercury) were placed in an open crucible and heated at a rate of 5 °C per minute to 400 °C in a muffle furnace. The temperature was held at 400 °C for 30 minutes. The furnace was contained in a fume hood to avoid the release of any off gases. For larger scale, a mercury scrubber or retort is required for safe regeneration and capture of mercury.

XPS analysis of carbonised-1 and carbonised-1-O before and after regeneration
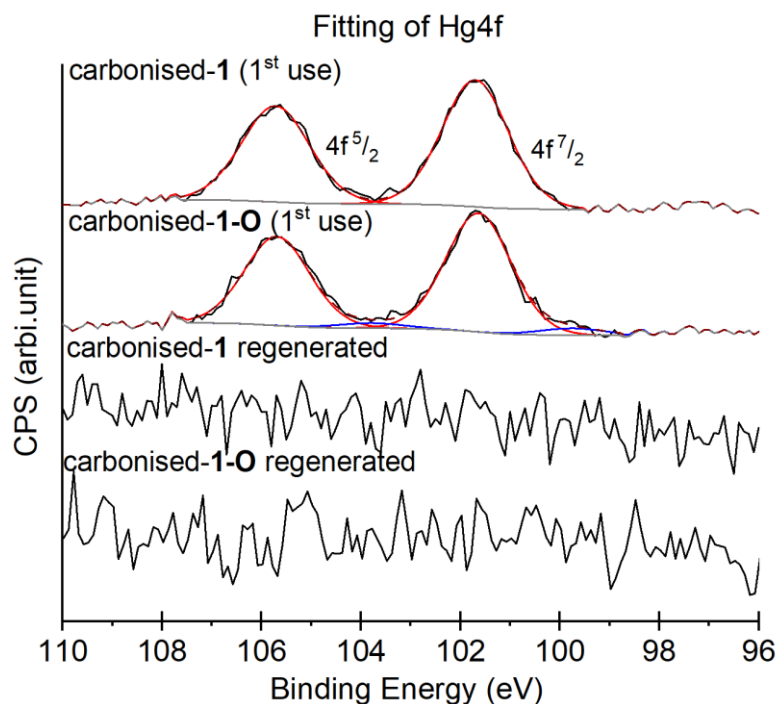
Figure 3.77: XPS analysis was used to clearly detect mercury on the surface of spent carbonised-1 and spent carbonised-1-O. After the regeneration procedure (400 ºC, 30 minutes), no mercury could be detected by XPS. Reproduced with permission from the Royal Society of Chemistry.[45]

Note that the signal for mercury at 101.6 eV +/- 0.2 eV corresponds to Hg^{2+}.[56]
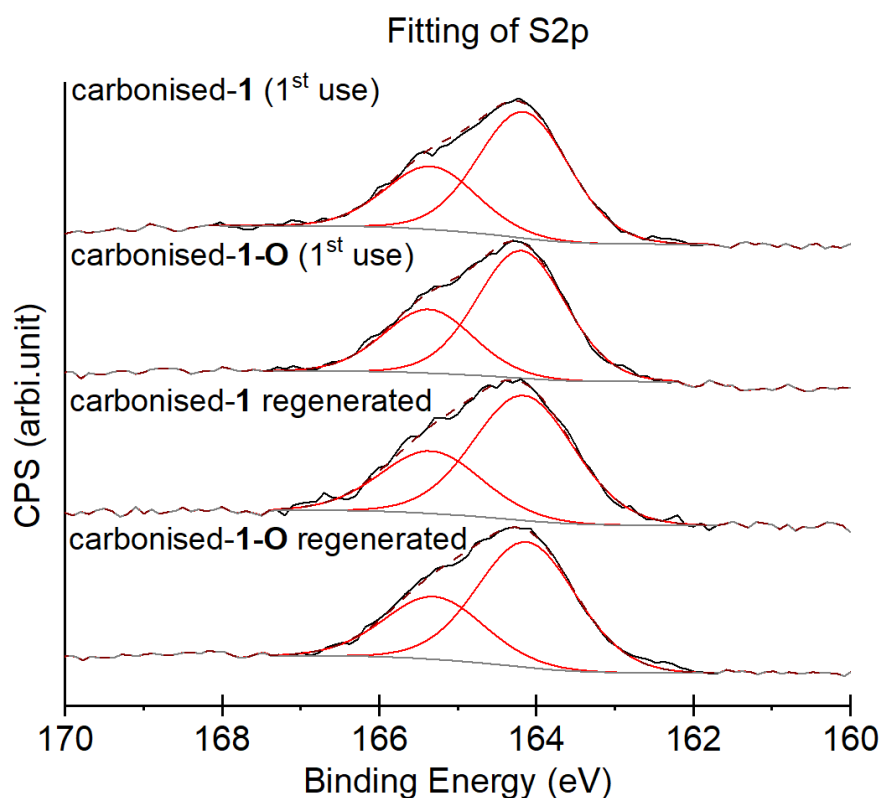
Figure 3.78: XPS analysis of the spent carbonised-1 and spent carbonised-1-O indicated that there is no discernible change in the sulfur S2p signals after regeneration. These signals are the same observed for freshly prepared carbonised-1 and carbonised-1-O (Figure 3.68). These results indicate the sulfur species in the carbon are consistent throughout the mercury binding and regeneration process. Reproduced with permission from the Royal Society of Chemistry.[45]
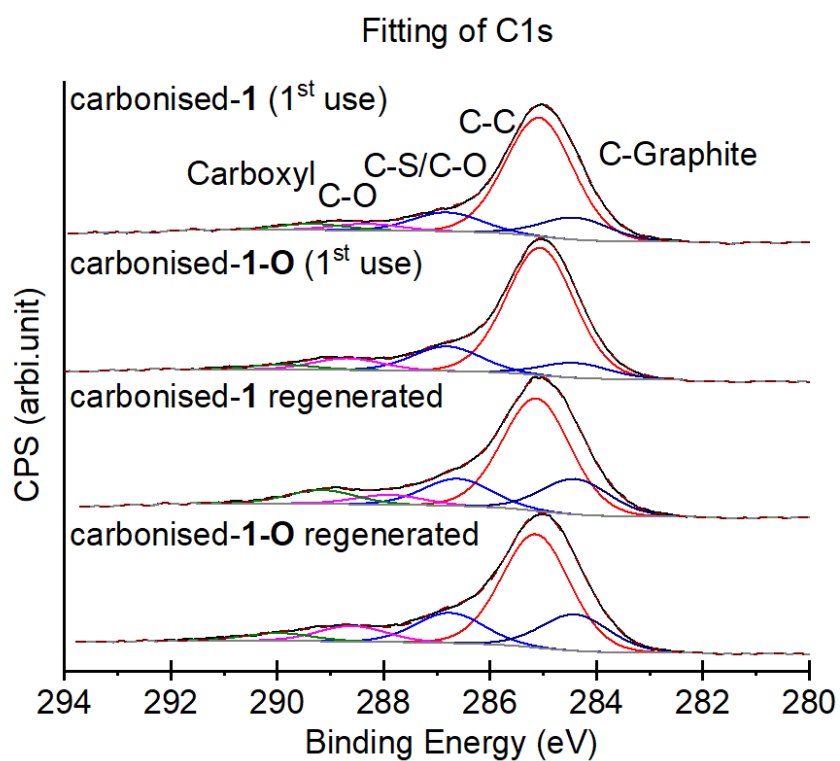
Figure 3.79: XPS analysis of the spent carbonised-1 and spent carbonised-1-O indicated there is no discernible change in the carbon C1s signal after the regeneration process compared to before the regeneration process. Reproduced with permission from the Royal Society of Chemistry.[45]
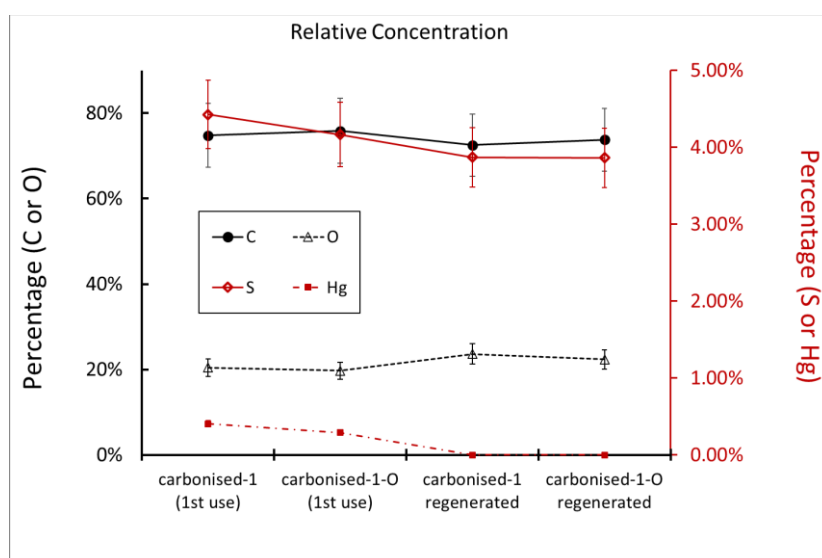
Figure 3.80: XPS analysis of the spent carbonised-1 and spent carbonised-1-O and the regenerated carbon samples indicate minor changes in the relative amount of carbon, oxygen, and sulfur before and after regeneration. Mercury was removed during the regeneration. Reproduced with permission from the Royal Society of Chemistry.[45]
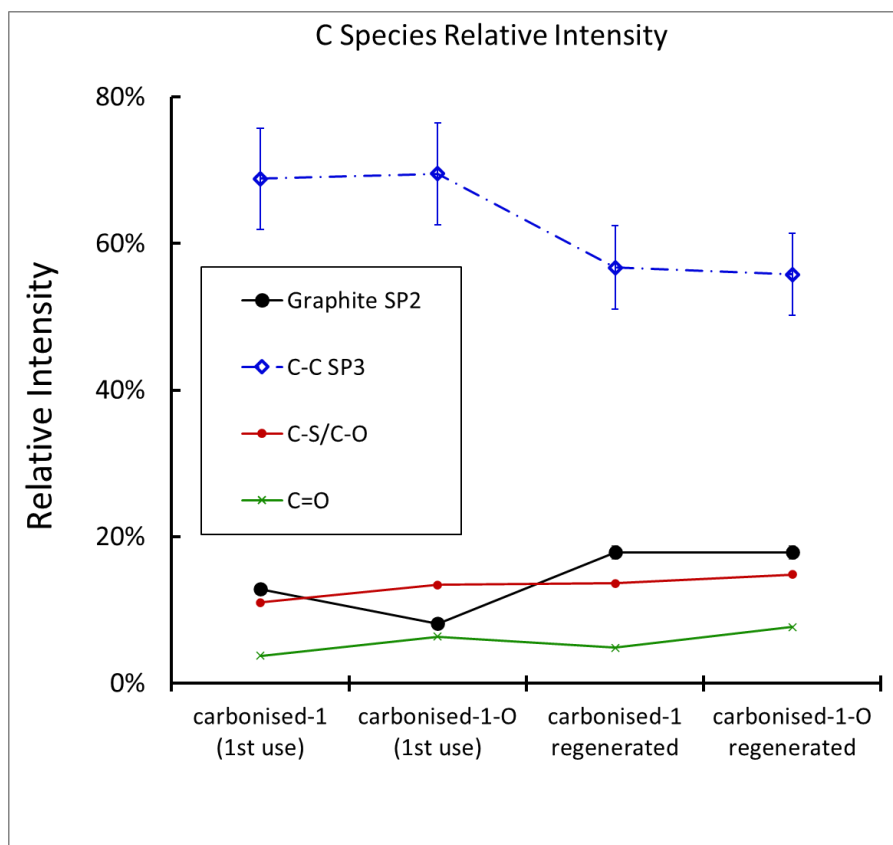
Figure 3.81: XPS analysis of the spent carbonised-1 and spent carbonised-1-O indicated the regenerated carbon samples undergo relatively minor changes in the carbon speciation after regeneration. Reproduced with permission from the Royal Society of Chemistry.[45]

Combustible analysis of carbonised-1 and carbonised-1-O

The elemental composition of freshly prepared carbonised-1 and carbonised-1-O are also provided for comparison. These results indicate the regeneration procedure does not substantially alter the elemental composition of the carbon.

Table 3.8: Elemental analysis of carbonised-1 and carbonised-1-O as well as of regenerated carbonised-1 and regenerated carbonised-1-O.

Material	C (%)	S (%)	H (%)
Carbonised-1	65.5	16.0	1.6
Carbonised-1 regenerated	64.5	16.1	1.1
Carbonised-1-O	63.6	15.2	1.5
Carbonised-1-O regenerated	65.0	15.2	1.3

Mercury sorption of carbonised-1 and carbonised-1-O after regeneration

100 mg of sorbent was added to a 45 mL sample of 5 ppm $Hg(NO_3)_2$. The sample was mixed using an end-over-end mixer, sampling the solution over a 2-hour period. The mercury concentration in the water was measured by CVAA. Triplicate measurements were made for each timepoint. The results are plotted below for carbonised-1 (freshly prepared), regenerated carbonised-1, carbonised-1-O (freshly prepared), and regenerated carbonised-1-O. While there are subtle variations in initial rate of mercury uptake for these samples, the mercury concentration at the end of the 2-hour period was essentially the same for all samples, with > 99 % of mercury removed.
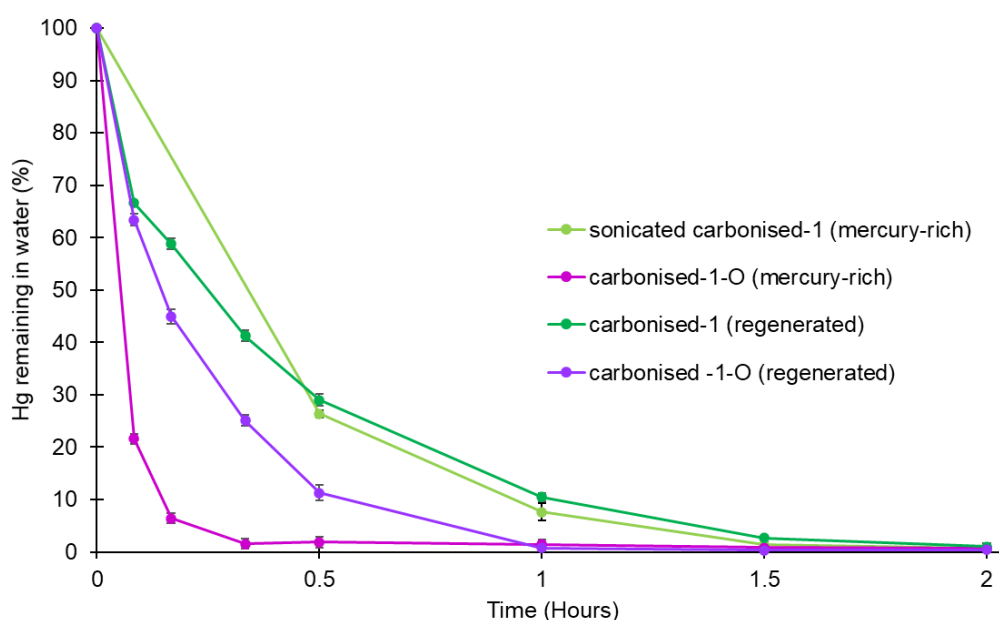
Figure 3.82: Mercury uptake of mercury rich and regenerated carbonsed-1 and carbonised-1-O.

References:

1.   Walker, S.; Rothman, R., Life cycle assessment of bio-based and fossil-based plastic: A review. *J. Clean. Prod.* **2020,** *261*, 121158.

2.   Ramesh, P.; Vinodh, S., State of art review on Life Cycle Assessment of polymers. *Int. J. Sustain. Eng.* **2020,** *13* (6), 411-422.

3.   Zhang, X.; Fevre, M.; Jones, G. O.; Waymouth, R. M., Catalysis as an Enabling Science for Sustainable Polymers. *Chem. Rev.* **2018,** *118* (2), 839-885.

4.   Hong, M.; Chen, E. Y. X., Chemically recyclable polymers: a circular economy approach to sustainability. *Green Chem.* **2017,** *19* (16), 3692-3706.

5.   Lu, X.-B.; Liu, Y.; Zhou, H., Learning Nature: Recyclable Monomers and Polymers. *Chem. Eur. J.* **2018,** *24* (44), 11255-11266.

6.   Badia, J. D.; Gil-Castell, O.; Ribes-Greus, A., Long-term properties and end-of-life of polymers from renewable resources. *Polym. Degrad. Stab.* **2017,** *137*, 35-57.

7.   Romani, A.; Mantelli, A.; Suriano, R.; Levi, M.; Turri, S., Additive Re-Manufacturing of Mechanically Recycled End-of-Life Glass Fiber-Reinforced Polymers for Value-Added Circular Design. *Materials* **2020,** *13* (16), 3545.

8.   MacLeod, M.; Arp, H. P. H.; Tekman, M. B.; Jahnke, A., The global threat from plastic pollution. *Science* **2021,** *373* (6550), 61-65.

9.   Loos, K.; Zhang, R.; Pereira, I.; Agostinho, B.; Hu, H.; Maniar, D.; Sbirrazzuoli, N.; Silvestre, A. J. D.; Guigo, N.; Sousa, A. F., A Perspective on PEF Synthesis, Properties, and End-Life. *Front. Chem.* **2020,** *8* (585).

10.   Sepperer, T.; Neubauer, J.; Eckardt, J.; Schnabel, T.; Petutschnigg, A.; Tondi, G., Pollutant Absorption as a Possible End-Of-Life Solution for Polyphenolic Polymers. *Polymers* **2019,** *11* (5), 911.

11.   Worthington, M. J. H.; Kucera, R. L.; Abuquerque, I. S.; Gibson, C. T.; Sibley, A.; Slattery, A. D.; Campbell, J. A.; Alboaiji, S. F. K.; Muller, K. A.; Young, J.; Adamson, N.; Gascooke, J. R.; Jampaiah, D.; Sabri, Y. M.; Bhargava, S. K.; Ippolito, S. J.; Lewis, D. A.; Quinton, J. S.; Ellis, A. V.; Johs, A.; Bernardes, G. J. L.; Chalker, J. M., Laying Waste to Mercury: Inexpensive Sorbents Made from Sulfur and Recycled Cooking Oils. *Chem. Eur. J.* **2017,** *23*, 16219-16230.

12.   Mann, M.; Kruger, J. E.; Andari, F.; McErlean, J.; Gascooke, J. R.; Smith, J. A.; Worthington, M. J. H.; McKinley, C. C. C.; Campbell, J. A.; Lewis, D. A.; Hasell, T.; Perkins, M. V.; Chalker, J. M., Sulfur polymer composites as controlled-release fertilisers. *Org. Biomol. Chem* **2018**.

13. Lundquist, N. A.; Sweetman, M. J.; Scroggie, K. R.; Worthington, M. J. H.; Esdaile, L. J.; Alboaiji, S. F. K.; Plush, S. E.; Hayball, J. D.; Chalker, J. M., Polymer Supported Carbon for Safe and Effective Remediation of PFOA- and PFOS-Contaminated Water. *ACS Sustain. Chem. Eng.* **2019,** *7* (13), 11044-11049.

14. Lundquist, N. A.; Tikoalu, A. D.; Worthington, M. J. H.; Shapter, R.; Tonkin, S. J.; Stojcevski, F.; Mann, M.; Gibson, C. T.; Gascooke, J. R.; Karton, A.; Henderson, L. C.; Esdaile, L. J.; Chalker, J. M., Reactive Compression Molding Post-Inverse Vulcanization: A Method to Assemble, Recycle, and Repurpose Sulfur Polymers and Composites. *Chem. Eur. J.* **2020,** *26* (44), 10035-10044.

15. Worthington, M. J. H.; Shearer, C. J.; Esdaile, L. J.; Campbell, J. A.; Gibson, C. T.; Legg, S. K.; Yin, Y.; Lundquist, N. A.; Gascooke, J. R.; Albuquerque, I. S.; Shapter, J. G.; Andersson, G. G.; Lewis, D. A.; Bernardes, G. J. L.; Chalker, J. M., Sustainable Polysulfides for Oil Spill Remediation: Repurposing Industrial Waste for Environmental Benefit. *Adv. Sustain. Syst.* **2018,** *2* (6), 1800024.

16. Lundquist, N. A.; Worthington, M. J. H.; Adamson, N.; Gibson, C. T.; Johnston, M. R.; Ellis, A. V.; Chalker, J. M., Polysulfides made from re-purposed waste are sustainable materials for removing iron from water. *RSC Adv.* **2018,** *8,* 1232-1236.

17. González-García, P., Activated carbon from lignocellulosics precursors: A review of the synthesis methods, characterization techniques and applications. *Renew. Sust. Energ. Rev.* **2018,** *82,* 1393-1414.

18. Heidarinejad, Z.; Dehghani, M. H.; Heidari, M.; Javedan, G.; Ali, I.; Sillanpää, M., Methods for preparation and activation of activated carbon: a review. *Environ. Chem. Lett.* **2020,** *18* (2), 393-415.

19. Gao, Y.; Yue, Q.; Gao, B.; Li, A., Insight into activated carbon from different kinds of chemical activating agents: A review. *Sci. Total Environ.* **2020,** *746,* 141094.

20. Danish, M.; Ahmad, T., A review on utilization of wood biomass as a sustainable precursor for activated carbon production and application. *Renew. Sust. Energ. Rev.* **2018,** *87,* 1-21.

21. Menya, E.; Olupot, P. W.; Storz, H.; Lubwama, M.; Kiros, Y., Production and performance of activated carbon from rice husks for removal of natural organic matter from water: A review. *Chem. Eng. Res. Des.* **2018,** *129,* 271-296.

22. Wang, H.; Xu, J.; Liu, X.; Sheng, L., Preparation of straw activated carbon and its application in wastewater treatment: A review. *J. Clean. Prod.* **2021,** *283,* 124671.

23. Maciá-Agulló, J. A.; Moore, B. C.; Cazorla-Amorós, D.; Linares-Solano, A., Activation of coal tar pitch carbon fibres: Physical activation vs. chemical activation. *Carbon* **2004,** *42* (7), 1367-1370.

24.   Kosheleva, R. I.; Mitropoulos, A. C.; Kyzas, G. Z., Synthesis of activated carbon from food waste. *Environ. Chem. Lett.* **2019,** *17* (1), 429-438.

25.   Ahmed, M. B.; Hasan Johir, M. A.; Zhou, J. L.; Ngo, H. H.; Nghiem, L. D.; Richardson, C.; Moni, M. A.; Bryant, M. R., Activated carbon preparation from biomass feedstock: Clean production and carbon dioxide adsorption. *J. Clean. Prod.* **2019,** *225*, 405-413.

26.   Bear, J. C.; McGettrick, J. D.; Parkin, I. P.; Dunnill, C. W.; Hasell, T., Porous carbons from inverse vulcanised polymers. *Microporous Mesoporous Mater.* **2016,** *232*, 189-195.

27.   Lee, J.-Sing M.; Parker, D. J.; Cooper, A. I.; Hasell, T., High surface area sulfur-doped microporous carbons from inverse vulcanised polymers. *J. Mater. Chem. A* **2017,** *5* (35), 18603-18609.

28.   Kumar, V.; Parihar, R. D.; Sharma, A.; Bakshi, P.; Singh Sidhu, G. P.; Bali, A. S.; Karaouzas, I.; Bhardwaj, R.; Thukral, A. K.; Gyasi-Agyei, Y.; Rodrigo-Comino, J., Global evaluation of heavy metal content in surface water bodies: A meta-analysis using heavy metal pollution indices and multivariate statistical analyses. *Chemosphere* **2019,** *236*, 124364.

29.   Yin, K.; Wang, Q.; Lv, M.; Chen, L., Microorganism remediation strategies towards heavy metals. *Chem. Eng. J.* **2019,** *360*, 1553-1563.

30.   Vareda, J. P.; Valente, A. J. M.; Durães, L., Assessment of heavy metal pollution from anthropogenic activities and remediation strategies: A review. *J. Environ. Manage.* **2019,** *246*, 101-118.

31.   Zhang, D.; Crini, G.; Lichtfouse, E.; Rhimi, B.; Wang, C., Removal of Mercury Ions from Aqueous Solutions by Crosslinked Chitosan-based Adsorbents: A Mini Review. *Chem. Rec.* **2020,** *20* (10), 1220-1234.

32.   Wu, W.; Wu, P.; Yang, F.; Sun, D.-l.; Zhang, D.-X.; Zhou, Y.-K., Assessment of heavy metal pollution and human health risks in urban soils around an electronics manufacturing facility. *Sci. Total Environ.* **2018,** *630*, 53-61.

33.   AlOmar, M. K.; Alsaadi, M. A.; Hayyan, M.; Akib, S.; Ibrahim, M.; Hashim, M. A., Allyl triphenyl phosphonium bromide based DES-functionalized carbon nanotubes for the removal of mercury from water. *Chemosphere* **2017,** *167*, 44-52.

34.   Jang, H.-N.; Back, S.-K.; Sung, J.-H.; Kang, Y.-S.; Jurng, J.; Seo, Y.-C., The simultaneous capture of mercury and fine particles by hybrid filter with powder activated carbon injection. *Environ. Pollut.* **2018,** *237*, 531-540.

35.   Liu, D.; Lu, C.; Wu, J., Gaseous Mercury Capture by Copper-Activated Nanoporous Carbon Nitride. *Energy Fuels* **2018,** *32* (8), 8287-8295.

36. Lu, C.; Wu, J.; Liu, D., Graphitic carbon nitride for elemental mercury capture. *Mater. Lett.* **2018,** *227*, 308-310.

37. Zhang, C.; Song, W.; Zhang, X.; Li, R.; Zhao, S.; Fan, C., Synthesis, characterization and evaluation of resin-based carbon spheres modified by oxygen functional groups for gaseous elemental mercury capture. *J. Mater. Sci.* **2018,** *53* (13), 9429-9448.

38. Ai, K.; Ruan, C.; Shen, M.; Lu, L., MoS2 Nanosheets with Widened Interlayer Spacing for High-Efficiency Removal of Mercury in Aquatic Systems. *Adv. Funct. Mater.* **2016,** *26* (30), 5542-5549.

39. Aguila, B.; Sun, Q.; Perman, J. A.; Earl, L. D.; Abney, C. W.; Elzein, R.; Schlaf, R.; Ma, S., Efficient Mercury Capture Using Functionalized Porous Organic Polymer. *Adv. Mater.* **2017,** *29* (31), 1700665.

40. Kim, Y.; Lin, Z.; Jeon, I.; Van Voorhis, T.; Swager, T. M., Polyaniline Nanofiber Electrodes for Reversible Capture and Release of Mercury(II) from Water. *J. Am. Chem. Soc.* **2018,** *140* (43), 14413-14420.

41. Hasell, T.; Parker, D. J.; Jones, H. A.; McAllister, T.; Howdle, S. M., Porous inverse vulcanised polymers for mercury capture. *ChemComm* **2016,** *52* (31), 5383-5386.

42. Gai, K.; Avellan, A.; Hoelen, T. P.; Lopez-Linares, F.; Hatakeyama, E. S.; Lowry, G. V., Impact of mercury speciation on its removal from water by activated carbon and organoclay. *Water Res.* **2019,** *157*, 600-609.

43. Wu, X.; Smith, J. A.; Petcher, S.; Zhang, B.; Parker, D. J.; Griffin, J. M.; Hasell, T., Catalytic inverse vulcanization. *Nat. Commun.* **2019,** *10* (1), 647.

44. Hoefling, A.; Lee, Y. J.; Theato, P., Sulfur-Based Polymer Composites from Vegetable Oils and Elemental Sulfur: A Sustainable Active Material for Li–S Batteries. *Macromol. Chem. Phys.* **2017,** *218*, 1600303.

45. Mann, M.; Luo, X.; Tikoalu, A. D.; Gibson, C. T.; Yin, Y.; Al-Attabi, R.; Andersson, G. G.; Raston, C. L.; Henderson, L. C.; Pring, A.; Hasell, T.; Chalker, J. M., Carbonisation of a polymer made from sulfur and canola oil. *ChemComm* **2021,** *57* (51), 6296-6299.

46. Yang, L.; Jiang, X.; Jiang, W.; Wang, P.; Jin, Y., Cyclic Regeneration of Pyrolusite-Modified Activated Coke by Blending Method for Flue Gas Desulfurization. *Energy Fuels* **2017,** *31* (4), 4556-4564.

47. Song, W.; Zhou, J.; Wang, B.; Li, S.; Cheng, R., Production of SO2 Gas: New and Efficient Utilization of Flue Gas Desulfurization Gypsum and Pyrite Resources. *Ind. Eng. Chem. Res.* **2019,** *58* (44), 20450-20460.

48. Cau, G.; Tola, V.; Bassano, C., Performance evaluation of high-sulphur coal-fired USC plant integrated with SNOX and CO2 capture sections. *Appl. Therm. Eng.* **2015,** *74*, 136-145.

49. Srivastava, R. K.; Jozewicz, W.; Singer, C., SO2 scrubbing technologies: A review. *Environ. Prog.* **2001,** *20* (4), 219-228.

50. Chen, Y.; Li, J.; Mei, T.; Hu, X. g.; Liu, D.; Wang, J.; Hao, M.; Li, J.; Wang, J.; Wang, X., Low-temperature and one-pot synthesis of sulfurized graphene nanosheets via in situ doping and their superior electrocatalytic activity for oxygen reduction reaction. *J. Mater. Chem. A* **2014,** *2* (48), 20714-20722.

51. Ghazinejad, M.; Holmberg, S.; Pilloni, O.; Oropeza-Ramos, L.; Madou, M., Graphitizing Non-graphitizable Carbons by Stress-induced Routes. *Sci. Rep.* **2017,** *7* (1), 16551.

52. Bissett, M. A.; Köper, I.; Quinton, J. S.; Shapter, J. G., Dendron growth from vertically aligned single-walled carbon nanotube thin layer arrays for photovoltaic devices. *Phys. Chem. Chem. Phys.* **2011,** *13* (13), 6059-6064.

53. Wong, Y. C.; Szeto, Y. S.; Cheung, W. H.; McKay, G., Pseudo-first-order kinetic studies of the sorption of acid dyes onto chitosan. *J. Appl. Polym. Sci.* **2004,** *92* (3), 1633-1645.

54. Ho, Y.-S., Second-order kinetic model for the sorption of cadmium onto tree fern: A comparison of linear and non-linear methods. *Water Res.* **2006,** *40* (1), 119-125.

55. Beattie, J. A.; Blaisdell, B. E.; Kaminsky, J., An Experimental Study of the Absolute Temperature Scale. IV. The Reproducibility of the Mercury Boiling Point. The Effect of Pressure on the Mercury Boiling Point. *Proc. Am. Acad. Arts Sci.* **1937,** *71* (6/8), 375-385.

56. Seals, R. D.; Alexander, R.; Taylor, L. T.; Dillard, J. G., Core electron binding energy study of group IIb-VIIa compounds. *Inorg. Chem.* **1973,** *12* (10), 2485-2487.

57. Chalker, J. M.; Mann, M.; Worthington, M. J. H.; Esdaile, L. J., Polymers Made by Inverse Vulcanization for Use as Mercury Sorbents. *Organic Materials* **2021,** *03* (02), 362-373.

58. Yin, Y.; Sibley, A.; Quinton, J. S.; Lewis, D. A.; Andersson, G. G., Dipole Formation at the MoO3/Conjugated Polymer Interface. *Adv. Funct. Mater.* **2018,** *28* (46), 1802825.

59. Liu, C.-Y.; Lai, C.-H.; Lin, C.-C.; Yang, C.-P., Insertion of a Graphene Oxide Layer into a Cu/SiO2/Pt Structure to Overcome Performance Degradation in a Vaporless Environment. *Appl. Sci* **2019,** *9* (7), 1432.

60. Jackson, S. T.; Nuzzo, R. G., Determining hybridization differences for amorphous carbon from the XPS C 1s envelope. *Appl. Surf. Sci.* **1995,** *90* (2), 195-203.

61. Díaz, J.; Paolicelli, G.; Ferrer, S.; Comin, F., Separation of the sp^3 and sp^2 components in the C1s photoemission spectra of amorphous carbon films. *Phys. Rev. B* **1996,** *54* (11), 8064-8069.

62. De Barros Bouchet, M. I.; Martin, J. M.; Avila, J.; Kano, M.; Yoshida, K.; Tsuruda, T.; Bai, S.; Higuchi, Y.; Ozawa, N.; Kubo, M.; Asensio, M. C., Diamond-like carbon coating under oleic acid lubrication: Evidence for graphene oxide formation in superlow friction. *Sci. Rep.* **2017,** *7* (1), 46394.

63. Dolgov, A.; Lopaev, D.; Lee, C. J.; Zoethout, E.; Medvedev, V.; Yakushev, O.; Bijkerk, F., Characterization of carbon contamination under ion and hot atom bombardment in a tin-plasma extreme ultraviolet light source. *Appl. Surf. Sci.* **2015,** *353*, 708-713.

64. Elmas, S.; Skipper, K.; Salehifar, N.; Jamieson, T.; Andersson, G. G.; Nydén, M.; Leterme, S. C.; Andersson, M. R., Cyclic Copper Uptake and Release from Natural Seawater—A Fully Sustainable Antifouling Technique to Prevent Marine Growth. *Environ. Sci. Technol.* **2021,** *55* (1), 757-766.

65. Bywalez, R.; Karacuban, H.; Nienhaus, H.; Schulz, C.; Wiggers, H., Stabilization of mid-sized silicon nanoparticles by functionalization with acrylic acid. *Nanoscale Res. Lett.* **2012,** *7* (1), 76.

Chapter 4

A copolymer made from sulfur and dicyclopentadiene:

Synthesis, properties, and applications

Acknowledgements

Christopher Gibson for AFM analysis

Zhongfan Jia and Max Worthington for help and training regarding GPC analysis

Samuel Tonkin for help with GC-MS

Introduction

As mentioned in previous chapters of this thesis, there is a large excess of sulfur around the world. It is estimated that over 78 million tons were produced in 2018 alone.[1] Therefore the discovery of inverse vulcanisation opened the way to produce polymers with a high sulfur content hence taking advantage of the huge sulfur stockpiles.[2] These new inverse vulcanised polymers show strong potential for a multitude of applications ranging from cathode materials for LiS batteries to oil spill and heavy metal remediation, optical materials, fertilisers and more.[3] However, in many cases it remains difficult to control the properties of the polymers and some polymers are prone to unintended runaway reactions.[4, 5] For example Jenkins et al point out that the method by with inverse vulcanised polymers are made can vary significantly.[5] This includes the reaction type (1-step, 2-step, curing, temperature ramp), reaction scale (0.5 g – 2 g) and reaction time (0.5 hr – 6 hr). For example, when the synthesis of a copolymer made with equal masses of sulfur and divinylbenzene (poly(S50%-DVB50%)) is performed in a 1-step reaction (monomer and sulfur heated simultaneously) the solubility is 26% (in dichloromethane) whereas when the same reaction is performed as a 2-step reaction (sulfur heated first to initiate radical formation followed by monomer addition), the solubility is only 16% in dichloromethane. Alongside different solubilities, Jenkins et al also noted differences in molecular weight depending on reaction type, scale and time.[5]

Nevertheless, efforts are being made to control the properties and processability of inverse vulcanised polymers. For instance, Hasell et al reported that the tensile, hardness, flexural and compression properties of selected polymers can be tailored by combining different organic comonomers.[6] In their work the authors use a triglyceride (for example linseed oil), terpinolene, limonene, ethylene glycol dimethylacrylate (EGDMA), 1,3-diisopropenylbenzene (DIB) and dicyclopentadiene (DCPD) (Figure 4.1).

Alterations in the feed ratio can result in different properties of the polymers as can be seen in the example of a S-limonene-DCPD polymer. As the ratio of DCPD was increased (sulfur ratio was kept constant) the glass transition temperature of the material increased linearly (Figure 4.1).[6] Further, Hasell and co-workers have shown that the feed ratio of crosslinkers influences the flexural modulus (Figure 4.1).[6] Additionally, reaction temperatures and times can be altered with the use of catalysts or accelerators like zinc-, iron-, cobalt-, copper-, nickel-, or sodium-diethyldithiocarbamate.[4] However, many of these polymers, behave like crosslinked, thermoset materials that are hard to process.[7]
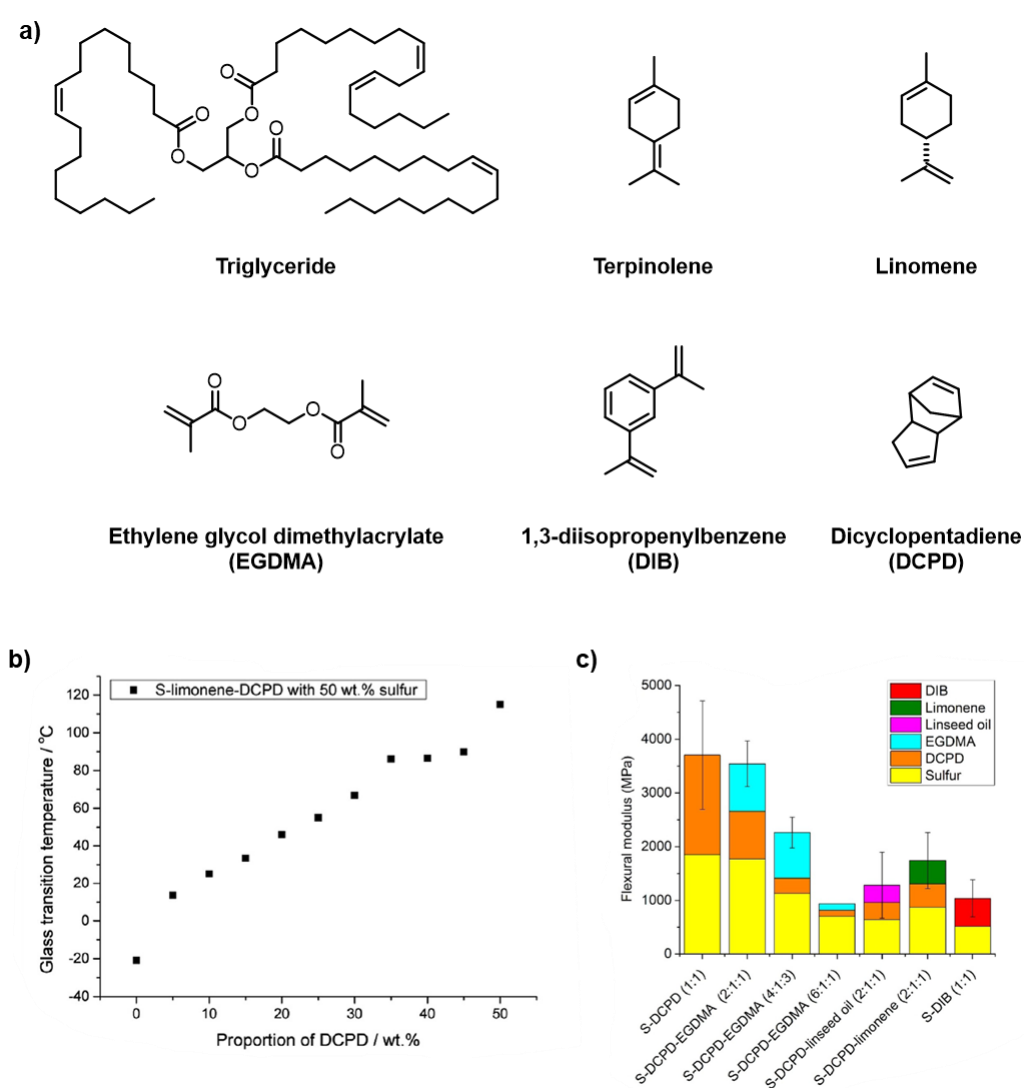
Figure 4.1: a) Range of crosslinkers used in a report by Hasell et al.[6] **b)** Effect ratio of DCPD in a S-limonene-DCPC (50 wt% sulfur) polymer has on the glass transition temperature. **c)** Effect the ratio of crosslinkers had on the flexural modulus of polysulfide polymers. © 2019 Wiley-VCH Verlag GmbH & Co. KGaA, Weinheim. Images preproduced under a RightsLink license.[6]

The ability to process polymers is paramount to their usefulness. In the case of thermoplastics, extrusion, post-die processing, foaming and injection moulding are widely used.[8] Of these processes, extrusion is the most commonly used method to process thermoplastics.[8] However, the crosslinked nature of many of the polysulfide polymers makes these processing techniques difficult to implement.[9] Polymer processing techniques like spin coating, spray coating, solvent, drop or film casting as well as dip coating rely on the polymers to be soluble.[8, 10] Unfortunately, many sulfur polymers possess limited or poor solubility in common organic solvents.[6, 7, 11] Nevertheless, advances have been made to improve the processability of sulfur polymers. For example, Pyun et al. used melt processing on a poly(S-*r*-1,3-diisopropenylbenzene) polymer to form a patterned film (Figure 4.2).[2]

Micropatterned PDMS mould → Drop cast S-DIB copolymer → Curing at 200 °C → Released from mould → Free-standing micropatterned S-DIB copolymer
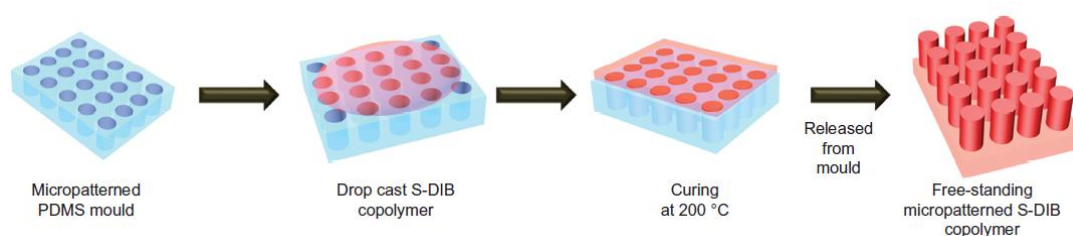
Figure 4.2: Pyun et al have used melt processing of a S-DIB polymer to form a micropatterned film. © 2013 Macmillan Publishers Limited. The images were preproduced under a RightsLink license.[2]

The same group also used a thermal annealing process at 100 °C to repair a poly(S-*r*-DIB$_{30}$) lens.[12] Hasell et al. have also shown that sulfur-perillyl alcohol and sulfur-squalene polymers can be crushed up and reprocessed by melting.[13] However, not all polysulfides lend themselves to this processing technique. For example polymers made from sulfur-canola oil or sulfur-DCPD do not melt when heated.[14] Notably, some low molecular weight polymers like sulfur-limonene are soluble and could have a use in processing methods such as spin or spray coating.[4, 15] Regrettably though, sulfur limonene is not a durable material. Alternatively, some polymers like a sulfur-canola oil polysulfide can be reprocessed by reactive compression moulding, a process in which a ground up polymer is pressed together under high pressure and heat to form a rubber like material (Figure 4.3).[14] However, a soft material is needed for the reactive compression moulding process to work.[14]

Figure 4.3: A sulfur-canola oil polymer is processed by active compression moulding which results in flexible polymer mats. © 2020 Wiley-VCH Verlag GmbH & Co. KGaA, Weinheim. Images reproduced under a RightsLink license.[14]

Another strategy deployed to process sulfur polymers is that of using a prepolymer. Hasell et al. showed that a prepolymer consisting of sulfur, DCPD and EGDMA can be synthesised first, before being processed and cured at a later stage.[16] Similarly, Theato et al. recently demonstrated the synthesis of a sulfur-styrylethyltrimethoxysilane polymer that is initially soluble in THF but can be rendered insoluble by subsequent acid-catalysed polycondensation of the siloxane groups.[17]

For nearly 50 years, the reaction between sulfur and DCPD has been investigated, resulting in a processable form of sulfur for use in composites and the construction industry.[18-22] A solution of low molecular weight polysulfide with a low DCPD content (25% or less by mass) is used in these applications. The sulfur in these solutions is primarily unreacted, dissolved elemental sulfur.[18-22] These mixtures can be used as reinforcement for glass and plastic fibres,[20] as mortar in concrete construction work,[19] or as sealant for tailing ponds.[19] However, in these applications the sulfur was used as a coating, knowing that the majority of the material will be sulfur.[18-23] These developments also coincide with the need to use sulfur accumulated from the desulfurisation of coal gas and oil.[19] Recently the reaction of sulfur and DCPD has been of interest again and it has been shown that the feed ratio of the starting materials can be adjusted to tailor the mechanical and thermal properties of the resulting materials.[6, 24] In contrast to the early studies mentioned previously, which resulted in sulfur plasticisation, the recent studies fully incorporated sulfur into a polymeric material. Useful properties such as solvent resistance, and high modulus and hardness, were observed in the fully crosslinked polymers.[6, 24] The properties of these copolymers from sulfur and DCDP would be beneficial for coating applications, however their insolubility presents a challenge in processing these materials.

Although previous studies have explored pre-polymer resins based on sulfur which can be thermally[16] or chemically[17] cured at a later stage, this has not been done with the simplest sulfur-DPCD system.

Therefore, the aim of this project was to develop a safe and reliable synthesis protocol produce a pre-polymer through the reaction of sulfur and DCPD. Further, curing at a later stage to produce an insoluble material was explored. Along with a thorough characterisation of the material, the focus was also on finding useful application of this polymer system.

S-DCPD synthesis optimisation

First, the goal was to establish a safe and reliable process to synthesise a pre-polymer through the reaction of sulfur and DCPD. Ideally, this pre-polymer should be easily soluble and shelf stable. In order the avoid the risk of auto acceleration, as has been known to occur with this reaction at temperature between 160 to 185 °C,[16, 24] the reaction temperature was lowered. At the temperatures usually used for this reaction (160 to 185 °C), DCPD can undergo a retro Diels-Alder reaction, resulting in the generation of cyclopentadiene (Scheme 4.1).

dicyclopentadiene   cyclopentadiene
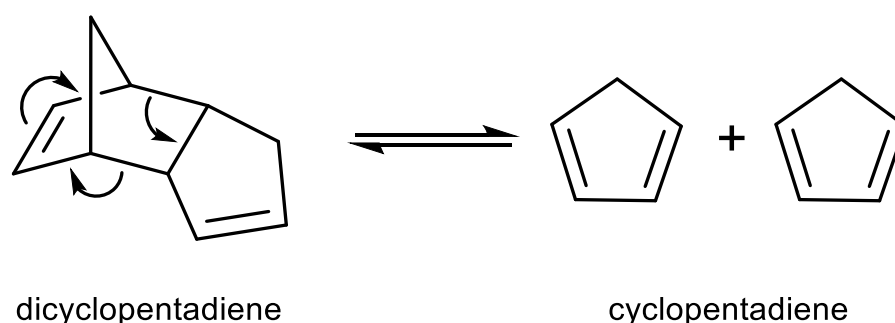
Scheme 4.1: Mechanism of the retro Diels-Alder reaction of dicyclopentadiene to form two equivalents of cyclopentadiene.

This was observed in initial experiments that were conducted to determine the cyclopentadiene formation from DCPD. Heating DCPD for 2 hours at 160 °C clearly showed the formation of cyclopentadiene (12%) upon ^{1}H NMR analysis (Figure 4.4). The formation of cyclopentadiene can create dangerous conditions by doubling the amount of alkenes in the reaction system leading to a rapid and uncontrolled increase of the exothermic reaction between sulfur and an alkene.[19] At these temperatures (160 to 185 °C) the formed cyclopentadiene is also in a gas state which can lead to changes in pressure and reagent loss to the atmosphere. All these factors play a role in the unsafe, runaway reactions which are known to occur in high temperature reactions of sulfur and DCPD.[4, 19, 24] Efforts have been made to overcome these issues thought the use of

catalysts and accelerators which enabled a lower reaction temperature.[4] However, these additives will remain in the polymer after the synthesis. Therefore, we investigated the synthesis of a catalyst-free sulfur-dicyclopentadiene (S-DCPD) polymer at lower temperatures. As shown already, heating DCPD to 160 °C resulted in the formation of a substantial amount of 12% cyclopentadiene (Figure 4.4).
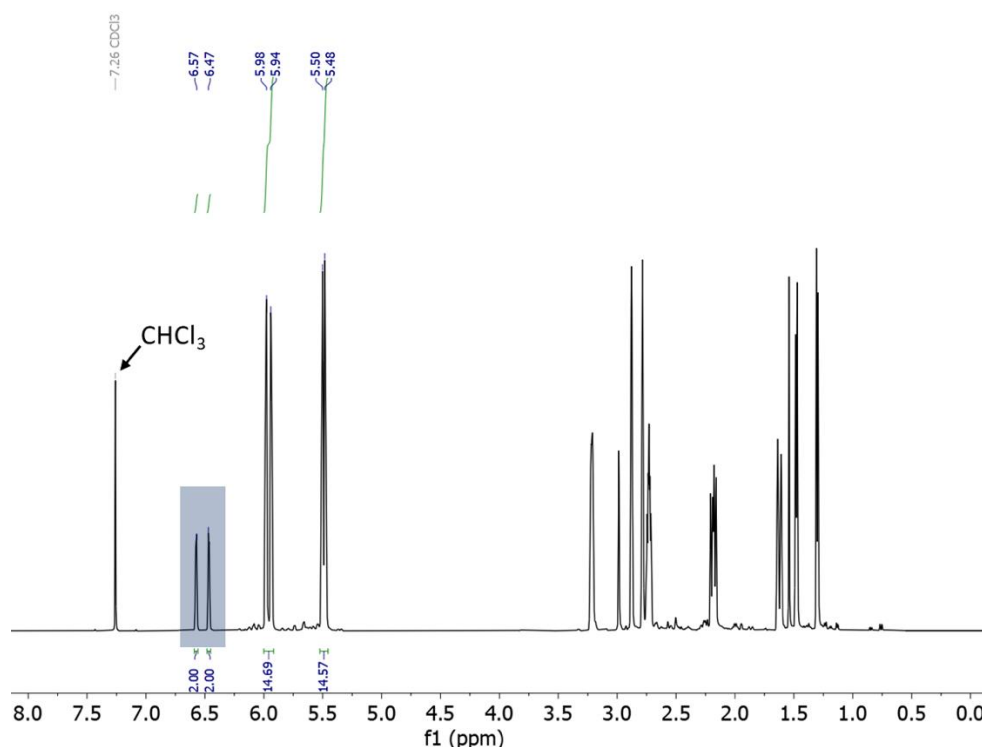
Figure 4.4: ^{1}H NMR spectrum of DCPD after heating at 160 °C for 2 hours. The peaks at $\delta = 6.57$ and 6.47 ppm are due to the vinylic protons of cyclopentadiene and the peaks between $\delta = 5.98$ and 5.48 correspond to the vinylic protons of DCPD. Reproduced with permission from the Royal Society of Chemistry.[25]

However, heating the reaction to only 140 °C resulted in only 3 % of cyclopentadiene generation. Based on this we wanted to investigate 140 °C as reaction temperature. It has to be noted that the reaction mechanism of a reaction at this temperature could be potentially different to that of other inverse vulcanisations[5, 11, 26] since at 140 °C ring opening polymerisation of sulfur does not occur.[23] Nevertheless, a reaction between sulfur and DCPD does occur at 140 °C by first forming cyclic polysulfides across the alkene of the norbornene (Figure 4.5) and subsequent oligomerisation during further heating (presumably by ring-opening polymerisation).[20-22]
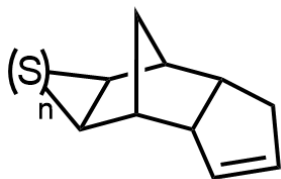
Figure 4.5: Cyclic polysulfides are formed first in the reaction between sulfur and DCPD which oligomerise during further heating.

Importantly, the reactions in these previous studies typically had a far higher sulfur content then reported here. This led to large amounts of free sulfur in the synthesised material which crystallises resulting in products that were brittle.[18-22]

To investigate different conditions, the first set of reactions was performed in a 140 °C oven. For that, equal masses (3 g each) of sulfur and DCPD (>95% endo) in a 20 mL glass vial were placed uncapped in the oven without any stirring. The average sulfur rank, the number of sulfur atoms per alkene, was 2 at this chosen feed ratio of sulfur and DCPD. A sulfur rank of two should result in a material that exhibits greater chemical and thermal stability then polymers with longer sulfur crosslinks due to the more stable nature of shorter sulfur chains. [6, 14, 27].

Figure 4.6 below, shows the reactions directly after they have been removed from the oven. It is obvious that no polymer has been formed within a 2-hour reaction time (Figure 4.6). However, after 2 hours, although phase separation can be observed, the color of the reaction changed significantly from yellow to dark brown (Figure 4.6).
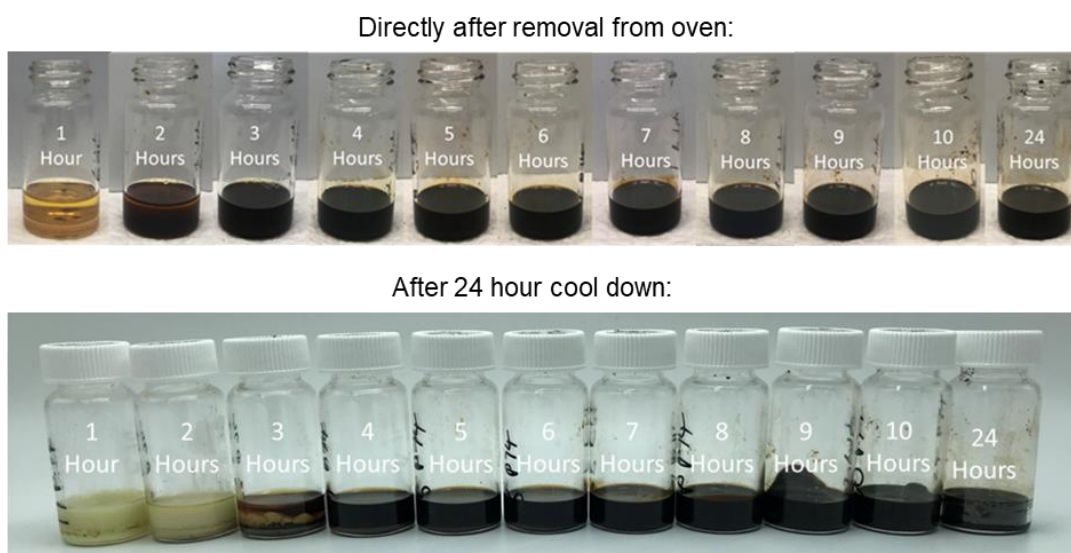
Figure 4.6: Reaction of DCPD and sulfur (3 g each) in an oven at 140 °C for 1-24 hours directly after the have been removed from the oven and after 24 hours. Reproduced with permission from the Royal Society of Chemistry.[25]

At reaction times of 3-24 hours the product presented as a homogenous dark material (Figure 4.6). However, after the samples have been left to cool for 24 hours, phase separation was observed in the samples with reaction times of up to 7 hours (Figure 4.6). Further, samples that were reacted for 3-6 hours showed low viscosity and would flow like oil whereas samples reacted longer would have a higher viscosity and did not flow. Next the solubility in chloroform of the samples reacted from 4 hour onwards was tested. Reaction times of under 7 and over 10 hours resulted in a substantial amount of insoluble material, which was not desired since the aim of the synthesis was a fully soluble S-DCPD polymer. However, ^{1}H NMR analysis of the materials gave interesting insights into the reaction. As Figure 4.7 below shows, the alkenes of the norbornene are consumed within 8 hours of reactions time. After that the remaining alkenes are consumed at a slower rate up to the 24 hours of reaction time (Figure 4.7).
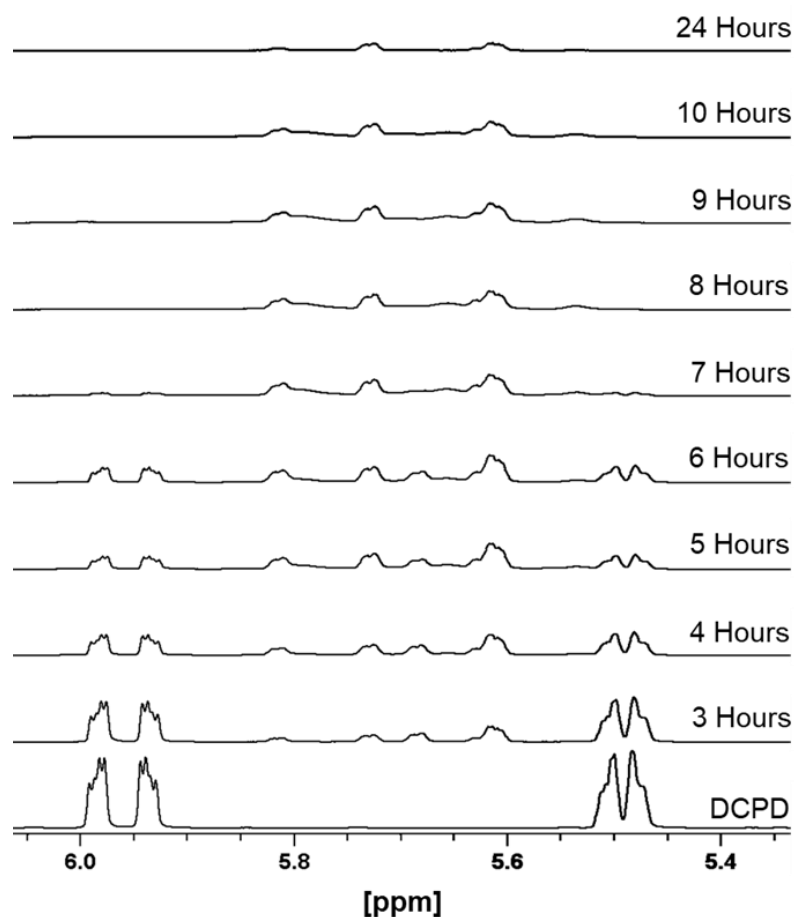
Figure 4.7: ^{1}H NMR spectra of sulfur and DCPD (3 g each) at reaction time of 3-24 hours. Reproduced with permission from the Royal Society of Chemistry.[25]

Samples that showed no phase separation and were fully soluble after they have been allowed to cool (8-10 hours), showed a linear increase in glass transition temperature (T_g) which is consistent with increased crosslinking and the increased viscosities of the materials (Figure 4.8).
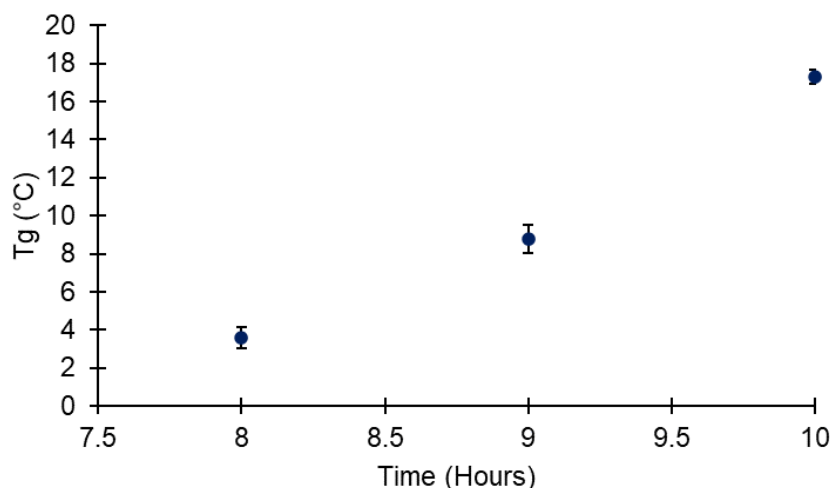
Figure 4.8: T_g temperatures of materials with reaction times of 8-10 hours. Reproduced with permission from the Royal Society of Chemistry.[25]

Starting with a T_g of 3.6 °C for the material reacted for 8 hours the T_g of the material reacted for 10 hours increased to 17.3 °C. Crucially, reacting sulfur and DCPD at 140 °C, even for 24 hours, did never cause a runaway reaction. However, the long reaction time was not ideal and needed to be reduced.

Therefore, in an effort to reduce the reaction time and increase mass transfer to avoid phase separation, the reaction was next run at 140 °C in an aluminium hot block with magnetic stirring. Firstly, a reaction was run for 7 hours, since at that time the reaction in the oven produced a fully soluble polymer. However, the resulting product was very hard and insoluble. This led to the conclusion that stirring increased the mass transfer and the reaction rate significantly. Therefore, subsequent reaction times had to be reduced. Thus, a total of 8 reactions were run next starting with 15 minutes reaction time up to 2 hours. From that experiment it became clear that at least 1 hour of reaction time is needed to form a polymer (Figure 4.9). At times less than that the product would solidify into a yellow brittle material (Figure 4.9).
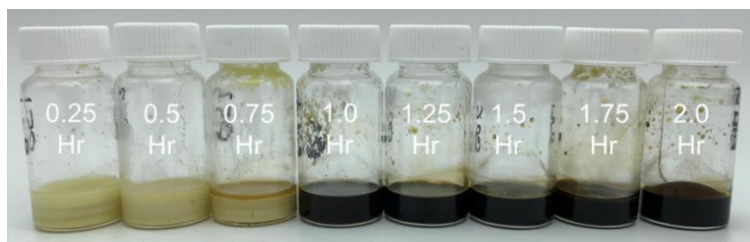
Figure 4.9: S-DPCD synthesis with reaction times of 0.25, 0.5, 0.75, 1.0, 1.25, 1.5, 1.75 and 2 hours at 140 °C on a hot block while magnetically stirred after cooldown. Reproduced with permission from the Royal Society of Chemistry.[25]

Since the samples with reaction times of over 1 hour looked promising, solubility studies were performed next. As solvents chloroform, THF and DCM were chosen. Surprisingly, none of the samples were fully soluble in any of the used solvents while samples reacted in the oven without stirring were. While stirring is indeed critical for mass transfer of the reagents to ensure a reliable reaction it was hypothesised that agitation might also result in a greater exposure to oxygen which could potentially influence the reaction.

To test this, two reactions of 3 g of sulfur and 3 g of DCPD were performed in parallel. Both reactions took place at 140 °C in a hot block while being stirred. However, one reaction was performed under a nitrogen atmosphere while the other reaction was open to air. Visually, both polymers had the same dark brown appearance, yet distinct differences were observed in their solubility. The polymer synthesised under a nitrogen atmosphere was fully soluble while the polymer synthesised while open to air was not with only 36% of its mass insoluble in chloroform. (Figure 4.10).
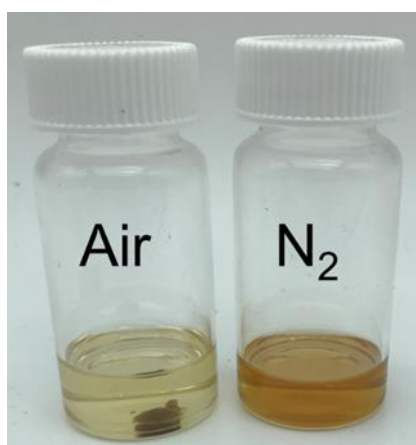
Figure 4.10: Solubility of polymers synthesised while open to air or under nitrogen atmosphere in chloroform.

IR analysis performed on the insoluble material, showed a broad C-H alkane stretch and a small C=C-H alkene stretch, indicating that not all the alkenes of DCPD had reacted (Figure 4.11).
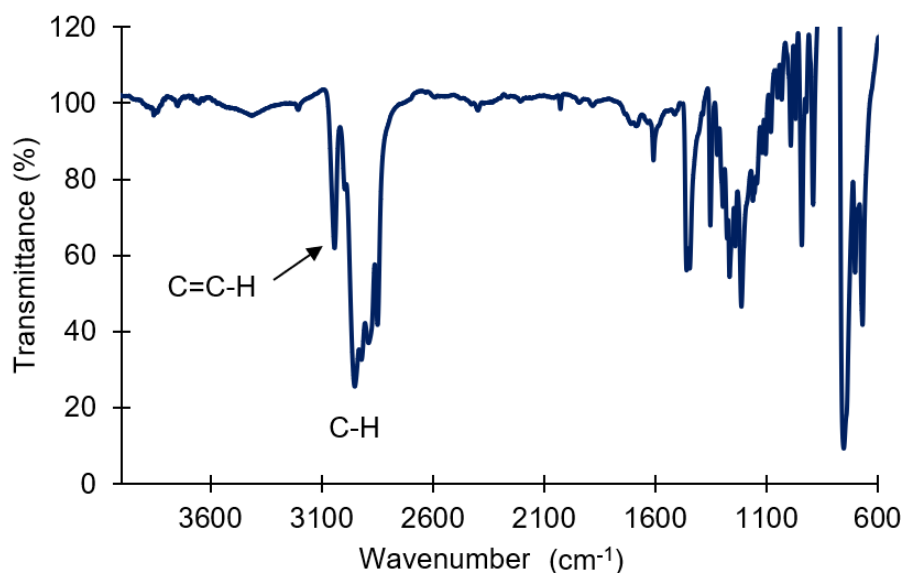
Figure 4.11: IR analysis of insoluble fraction of polymer synthesised in an open atmosphere. Reproduced with permission from the Royal Society of Chemistry.[25]

This was an encouraging result and a step towards the synthesis of a fully soluble S-DCPD polymer using a simple and save method. Control experiments were also conducted to investigate if water could result in insoluble material by interfering with the reaction. To do that, two reactions were run under a nitrogen atmosphere while a small amount of water was added to one of these reactions. The results showed that water can interfere with the reaction since 18% of the material synthesised with the addition water was not soluble in chloroform (Figure 4.12).
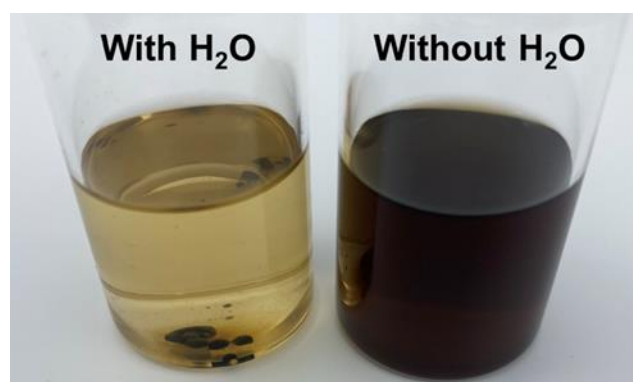
Figure 4.12: Solubility of polymers synthesised under a nitrogen atmosphere with or without the addition of water. Reproduced with permission from the Royal Society of Chemistry.[25]

This highlighted the importance to run the reaction under nitrogen and under dry conditions. Hence, a protocol to synthesise a S-DCPD polymer that is safe, without the risk of runaway reaction and results in a fully soluble material was established. The preferred protocol was to react equal masses of sulfur and DCPD for 2 hours at 140°C while stirring vigorously under an atmosphere of nitrogen und under dry conditions (Figure 4.13).
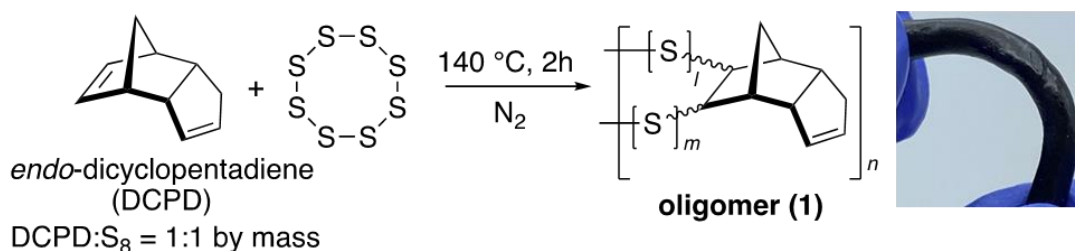
Figure 4.13: Synthesis scheme of oligomer 1 and showing its flexibility at room temperature. Reproduced with permission from the Royal Society of Chemistry.[25]

The product of this reaction will subsequently referred to as oligomer 1.

Characterisation of oligomer 1

Oligomer 1 was a malleable, wax-like solid at room temperature, fully soluble in chloroform as well as stable for more than 10 months and no elemental sulfur crystallised over this period (Figure 4.13). ^{1}H NMR analysis of oligomer 1 revealed partial consumption of DCPD alkenes. Further, CHS groups were detected as seen by peaks at 3.5-4.0 ppm (Figure 4.14).
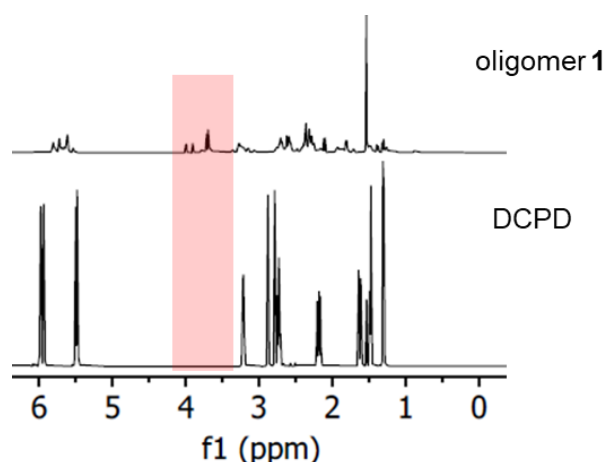
Figure 4.14: ^{1}H NMR of oligomer 1 and DCPD (red box shows peaks corresponding the CHS groups between 3.5-4.0 ppm). Reproduced with permission from the Royal Society of Chemistry.[25]

Additionally, ^{13}C NMR analysis showed signals between 60-75 ppm which corelate to the formation of C-S bonds (Figure 4.15).
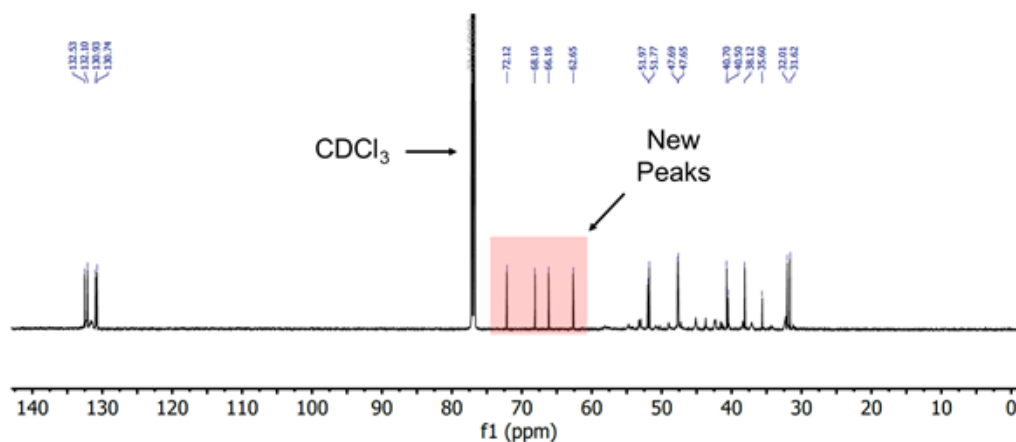
Figure 4.15: ^{13}C NMR analysis of oligomer 1 (red box shows formation of new peaks at 60-75 ppm corresponding the C-S bonds). Reproduced with permission from the Royal Society of Chemistry.[25]

X-ray diffraction (XRD) analysis was used to determine if any unreacted, elemental sulfur was still present in oligomer 1. Figure 4.16 shows the XRD diffraction pattern of oligomer 1 and elemental sulfur. As can be seen no elemental sulfur could be detected, hence no elemental sulfur is present in oligomer 1. This has also been confirmed by differential scanning calorimetry (DCS) analysis which did not reveal the melting transition of sulfur.
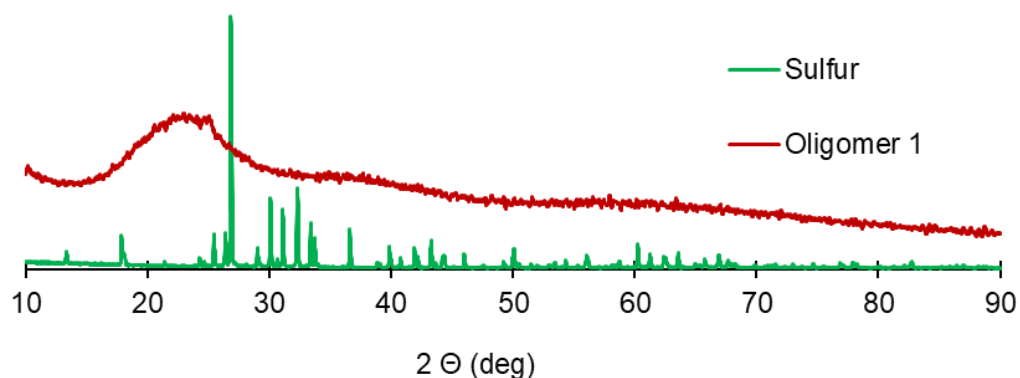
Figure 4.16: XRD diffraction pattern of elemental sulfur and oligomer 1. Reproduced with permission from the Royal Society of Chemistry.[25]

DSC analysis of oligomer one revealed a T_g of 3 °C which is consistent with the malleable nature of the material at room temperature. Thermogravimetric analysis (TGA) was used to determine the mass loss of the material upon heating. Figure 4.17 shows that two mass loss events took place. The first mass loss had an onset of 160 °C and the second mass loss occurred after 250 °C leaving a remaining mass of 40% after being heated to 800 °C (Figure 4.17). Previously, the Chalker group and others have contributed that two stage mass loss to a process where the weaker S-S bonds in the material decompose first which is then followed by the decomposition of the remaining sulfur and other organic material during the second mass loss.[28, 29]
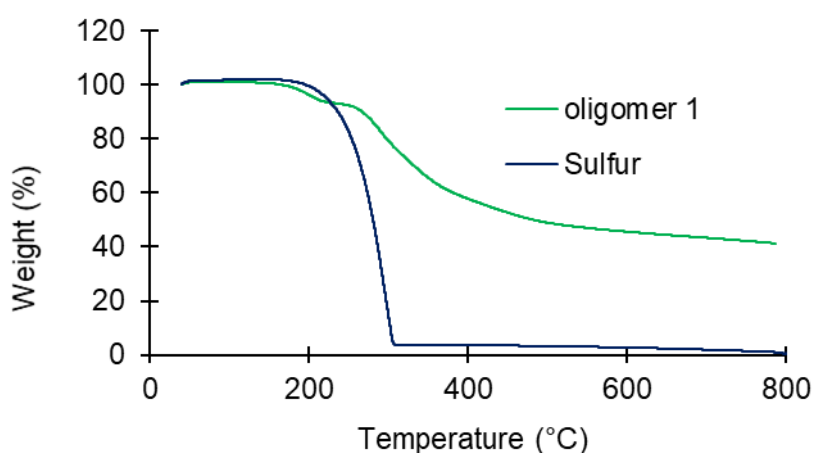
Figure 4.17: TGA of oligomer 1 and elemental sulfur. Reproduced with permission from the Royal Society of Chemistry.[25]

Laser desorption mass spectroscopy (LD-MS) was also used to characterise oligomer 1. This analysis revealed a mixture of species between m/z 500 and 1000. Interestingly, each species was separated by 32 mass units which is consistent with the polysulfide structure of oligomer 1. In an effort to determine the molecular weight of oligomer 1 gel permeation chromatography (GPC) was used. To do that a solution of oligomer 1 with the concentration of 2 mg / mL was prepared and ran against a polystyrene standard. The results showed a molecular weight of 1100 g/mol and a dispersity of 1.8. Next, the molecular weight of the polymer during the rection was monitored by taking a sample every 30 minutes. After 30 minutes reaction time no polymer could be detected. However, at reaction times of 60 minutes or more, the formation of the oligomer could be observed. Samples taken after 60, 90 and 120 minutes had a very similar molecular weights between 950-970 Da. This Mw is different from the one mentioned above, since the results are from difference batches, indicating that there is some variability between different reactions. However, the product was

always soluble in chloroform. This indicated that the majority of polymer is formed after 60 minutes of reaction time. Further the peaks broadened with longer reaction times indicating an increase of high molecular weight fractions. (Figure 4.18).
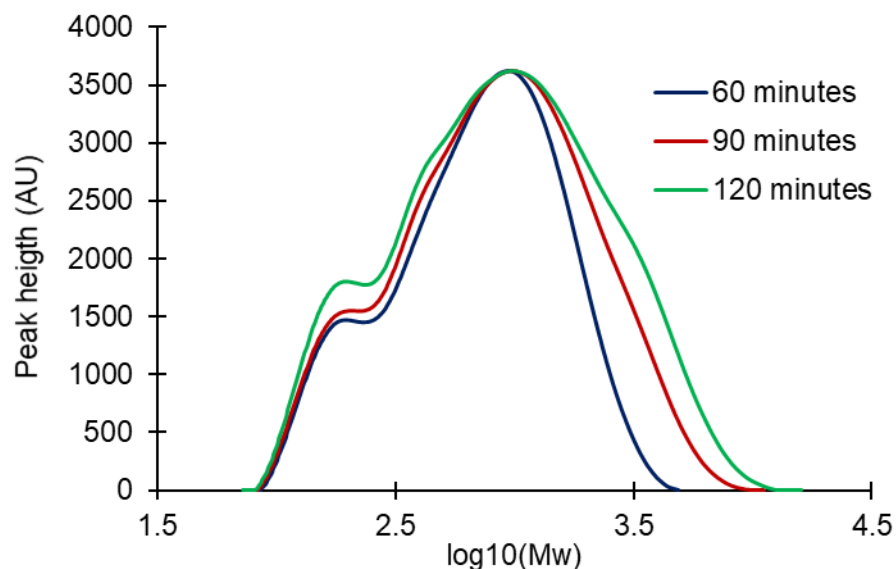
Figure 4.18: GPC analysis of the reaction mixture after 60, 90 and 120 minutes (DCPD was run and excluded as source of the peak at the left shoulder of the main peak, hence the peak in the shoulder is likely due to an additional low-molecular weight species forming during the synthesis of oligomer 1). Reproduced with permission from the Royal Society of Chemistry.[25]

To further elucidate the structure of oligomer 1 the material was reduced with LiAlH$_4$ and analysed using GC-MS. This showed 4 major products and an interesting minor product.

The first major product was DCPD. Since ^{1}H NMR analysis indicated that complete consumption of DCPD takes place during the formation of oligomer, it is proposed that the highly basic LiAlH$_4$ is able to convert oligomer 1 to DCPD during the reduction via an elimination reaction. The next two major products eluted very close to each other and had the same m/z of 166.1.

It is proposed that these two products are the thiols seen in Figure 4.19. These molecules can arise from the breaking of C-S bonds induced by the hydride, resulting in the desulfurised product.
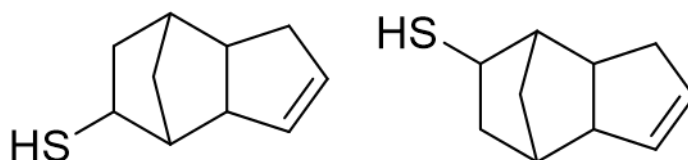
Figure 4.19: Products of oligomer 1 reduction with a molecular weight of 166 identified using GC-MS (only one potential regioisomer is shown for each product).

The next major product had a m/z of 198.1. This matches the dithiol product (Figure 4.20) which is expected to be formed during the reduction of the S-S bonds in oligomer 1.
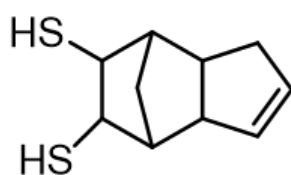
Figure 4.20: Product of oligomer 1 reduction with a molecular weight of 198 identified using GC-MS. This product is expected to from during the reduction of the S-S bonds in oligomer 1.

The last major product seen had a m/z of 228, which matches the trisulfide seen in Figure 4.21.
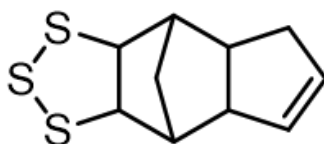
Figure 4.21: Product of oligomer 1 reduction with a molecular weight of 228 identified using GC-MS.

This product (Figure 4.21) is likely to form via intramolecular cyclisation during the reduction reaction. Additionally, this product could be further reduced to yield the molecule seen in Figure 4.20. A proposed pathway for the formation of the trisulfide and subsequent additional reduction to the dithiol product can be seen in Scheme 4.2 below.
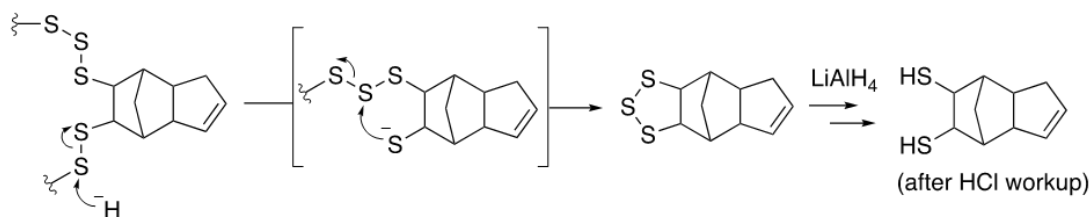
Scheme 4.2: Proposed reaction pathway of oligomer 1 reduction, leaking to trisulfide and finally dithiol products. Reproduced with permission from the Royal Society of Chemistry.[25]

The relative ratios of the thiol, dithiol and trisulfides are 18:22:1. This indicated that the dithiol was the most abundant species which was to be expected of the polymerisation occurred at the alkene or the norbornene.

After oligomer 1 had been characterised, the focus was put on a thermal curing process for oligomer 1 with the aim of further polymerising and crosslinking the oligomer into an insoluble material (Scheme 4.3). For this, curing for 24 hours in a 140 °C oven was chosen. The hypothesis was that this prolonged heating would induce a reaction of the intermediate thiyl-radicals with unreacted alkenes as well as a S-S metathesis reactions.
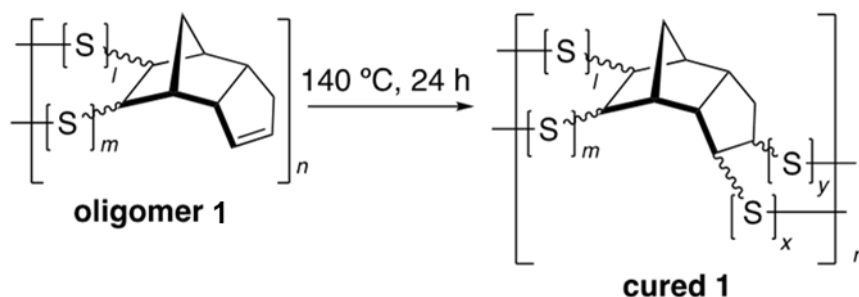
Scheme 4.3: Curing process of oligomer 1 and proposed structure of cured 1. Reproduced with permission from the Royal Society of Chemistry.[25]

Characterisation of cured 1

Curing oligomer 1 at these conditions did indeed result in changes in the material (cured oligomer 1 will be called cured 1 from now on). The T_g of cured 1 had increased to   106 °C as compared to oligomer 1 with 3°C. Further the material was no longer malleable but hard and brittle. Next, the solubility of cured 1 was tested. To do that, small amounts of cured 1 were placed in 3 mL of 9 commonly used solvents (DMF, THF, NMP, chloroform, ethyl acetate, acetone, methanol, isopropanol, and water). After 24 hours

cured 1 was removed, washed, and dried and weight to determine if any weight loss had occurred due to solvation of cured 1. No weight loss was recorded for all the cured 1 samples used, indicating that curing oligomer 1 did indeed result in an insoluble product (cured 1). The surface of cured 1 looked very flat and smooth. To attain some information about the surface of cured 1, atomic force microscopy (AFM) analysis was undertaken (Figure 4.22). This analysis showed an average surface roughness (R_a) of 0.37 ± 0.07 nm and a root mean square roughness of 0.92 ± 0.36 nm. These values are low compared to other polymers analysed preciously. For example a terpolymer made from sulfur, canola oil and DCPC had an average surface roughness of 8.8 nm[27] and a polydopamine polymer made by Ellis et al through the self-polymerisation of dopamine showed an average surface roughness of 1-4 nm.[30] However, some imperfections with an average height of 16 nm were observed on the surface of cured 1 which are likely particles that were deposited during the curing process or dust that had settled on the surface before the analysis (Figure 4.22).
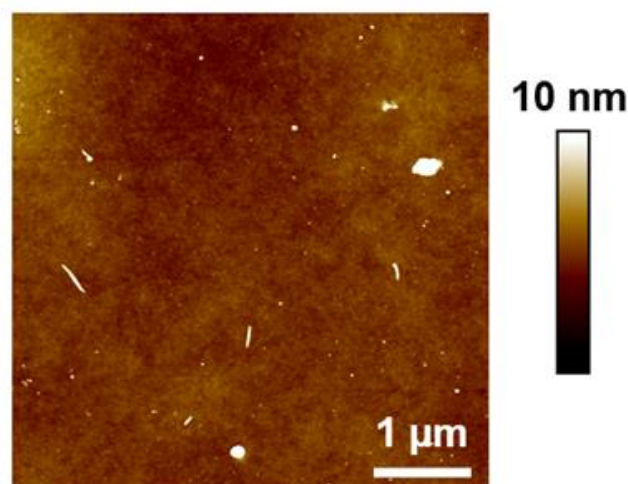
Figure 4.22: AFM image of the surface of cured 1. Reproduced with permission from the Royal Society of Chemistry.[25]

To determine additional properties of cured 1 nano-indentation measurements using AFM were performed. The resulting indentation curves were calibrated as described by Sader at al[31] and Kontomaris et al.[32] This analysis can shed light on the mechanical properties of cured 1 which is important if the material was to be used as a coating. Further, data from nanoindentation can also provide useful information on the bulk material.[33] This analysis resulted in elastic modulus of 1.49 ± 0.36 GPa which is comparable to nylon, PVC and polycarbonate.[34] Further a surface area hardness of 0.25

± 0.09 GPa and a Vickers hardness of 25.9 ± 9.6 GPa was calculated, which is similar to that of nylon, PMMA and polystyrene.[34, 35]

TGA analysis of cured 1 showed distinct differences to oligomer 1. Cured 1 showed only one weight loss starting at 250 °C whereas oligomer 2 displayed two mass losses (Figure 4.23). The difference may be attributed to stronger S-S bonds and a lower sulfur rank of cured 1 after curing.[14, 27, 28] The mass loss of cured 1 is very similar, only 3.5% more mass is retained compared to oligomer 1 (Figure 4.23).
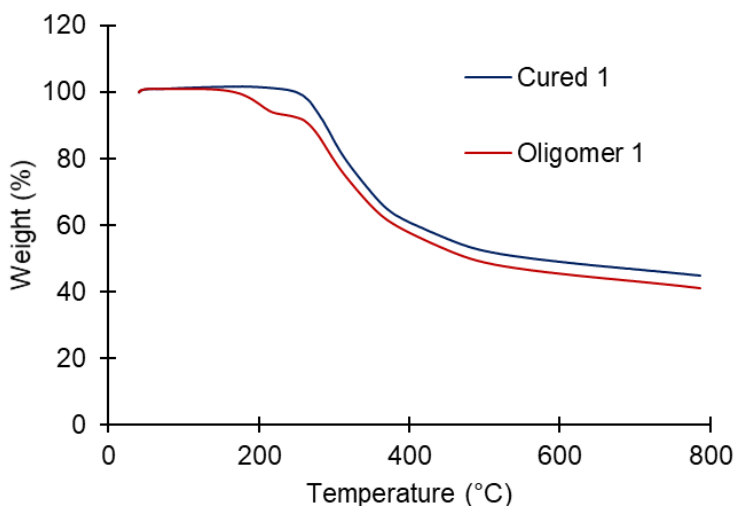
Figure 4.23: TGA of cured 1 compared to oligomer 1. Reproduced with permission from the Royal Society of Chemistry.[25]

Next, cured 1 was reduced using LiAlH$_4$ or NaBH$_4$. GC-MS analysis of the reduction products revealed a complex mixture of compounds. However, the products were consistent with S-S metathesis as well as addition of the polysulfide to the unreacted alkene of DCPD. DCPD was one on the products of the reduction. As was previously explained, it is proposed that the highly basic LiAlH$_4$ or NaBH$_4$ is able to convert oligomer 1 to DCPD during the reduction via an elimination reaction. Further, the same products as seen in Figure 4.19 – Figure 4.21 were detected. However, additional species were also seen. The proposed product seen in Figure 4.24 is consistent with addition of sulfur groups to the unreacted alkene during the curing process.
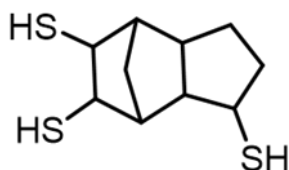
Figure 4.24: Proposed product of cured 1 reduction with molecular weight of 232 identified using GC-MS (Only one potential regio- and diasteroisomer is shown).

The odd number of sulfur atoms in the putative structure may be due to C-S bond cleavage by the hydride (Scheme 4.4).
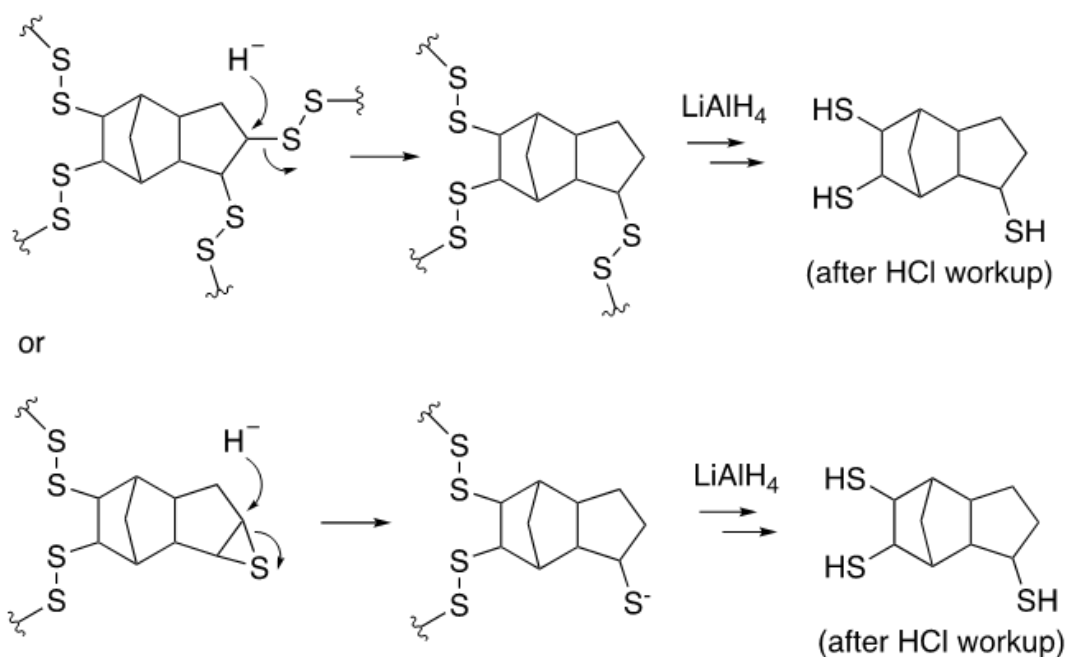
Scheme 4.4: Proposed pathways to trithiol product. Reproduced with permission from the Royal Society of Chemistry.[25]

The last newly detected compound was given the tentative structure seen in Figure 4.25 below. If the proposed structure is indeed correct, it is not clear if the episulfide is formed during the reduction or curing process.
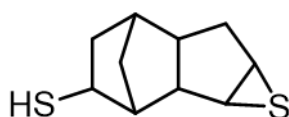
Figure 4.25: Proposed product of cured 1 reduction with molecular weight of 198 identified using GC-MS.

Overall, it can be said that these results indicated that curing oligomer 1 results in a chemically and thermally more resilient material.

Recycling of cured 1

Next, it was explored if the reduction process could be part of a recycling method for this polymer system. The hypothesis was to reduce cured 1 into a small oligomer (or a mixture of oligomers) and then re-cure that material to convert it back to cured 1 or a similar material. To do that, 4.4 g of cured 1 was reduced using NaBH₄, extracted with dry THF and was then cured again at 140 °C for 24 hours. GC-MS analysis of the reduction product of cured 1 matched that of previous reductions of cured 1 which were already discussed earlier. Interestingly, the re-cured material displayed the same physical characteristics by being hard and brittle as did cured 1. TGA analysis was performed on cured 1 and the re-cured reduction of cured 1. This analysis showed differences (Figure 4.26). While only one mass loss can be seen in the re-cured material similar to cured 1, the onset of the mass loss differs between the two samples. The re-cured materials mass loss begins at 225 °C which is 25 °C lower than the mass loss onset of cured 1. Further, after heating to 800 °C the re-cured material lost 13% more of its mass as cured 1.
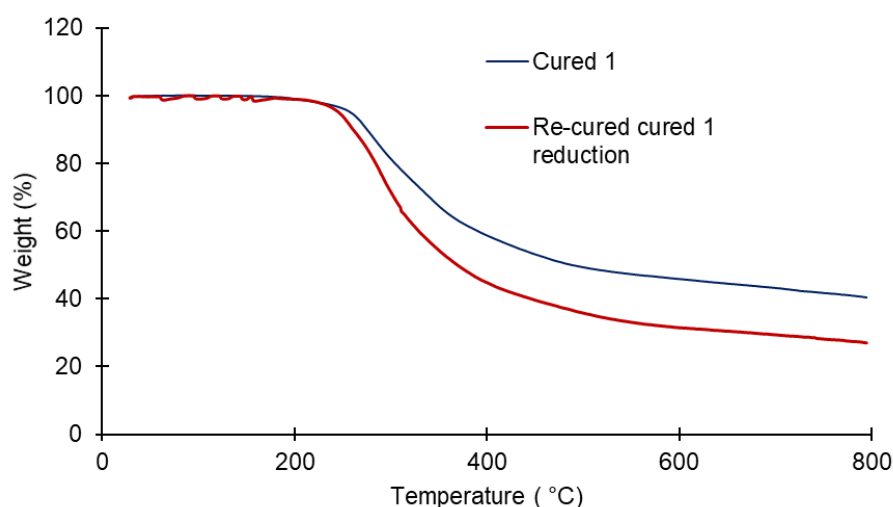
Figure 4.26: TGA of cured 1 compared to the re-cured cured1 reduction. Reproduced with permission from the Royal Society of Chemistry.[25]

Elemental analysis also revealed differences between the re-cured material and cured 1. The sulfur content was lower and the carbon content higher in the re-cured material (Figure 4.27). This difference could be due to the formation of sodium sulfide during the reduction which is then lost on workup.
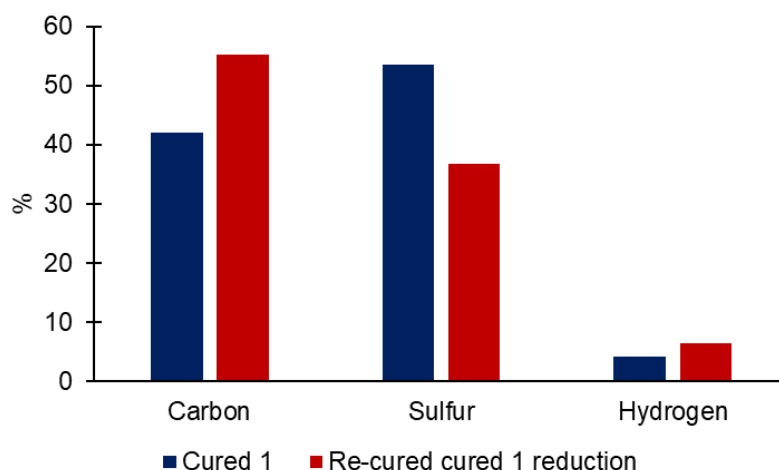
Figure 4.27: Elemental analysis of cured 1 compared to the re-cured cured 1 reduction. Reproduced with permission from the Royal Society of Chemistry.[25]

Next, the solubility of the re-cured material was investigated. For this the same solvents were used as for the solubility studies for cured 1 (DMF, THF, NMP, chloroform, ethyl acetate, acetone, methanol, isopropanol, and water). The re-cured material started to dissolve almost immediately after it was added to NMP, chloroform and THF. All material had dissolved in chloroform and THF after 30 minutes. After a further 30 minutes all material had fully dissolved in NMP The material added to DMF started to dissolve after 60 minutes and 60% of its weight had dissolved after 24 hours. Only very slight solvation was seen from the material in acetone (1.4% by mass).

Although the re-cured material had a similar appearance as cured 1, there are distinct differences in the solubility, elemental composition, and thermal properties. This presents limitations in using the re-cured material in acid or solvent resistant coating applications. However, these results illustrate the ability to use reduction to break down polysulfides and the potential of repolymerisation to gain access to new materials. Further, it has been shown that cured 1, a solvent and acid resistant polymer can be degraded using reducing agents. This could prove useful in the removal of coatings made from cured 1.

Coating applications

Coating applications using the sulfur-DCPD polymer were investigated next. The first application was coating silica gel with oligomer 1. This was done by dissolving 1.66 g of oligomer 1 in 150 mL of THF. Next, 16.6 g of silica gel (46-63 μm particles, 60 Å pore size) was added and the solution was thoroughly stirred. After that the solvent was

removed via rotary evaporation. The result was a free-flowing polymer coated powder (Figure 4.28). After that the polymer on the silica gel was cured by placing the material in a 140 °C oven for 24 hours. Curing darkened the color of the silica gel polymer coating as can be seen in Figure 4.28. However, even after curing the material was still a free-flowing powder.
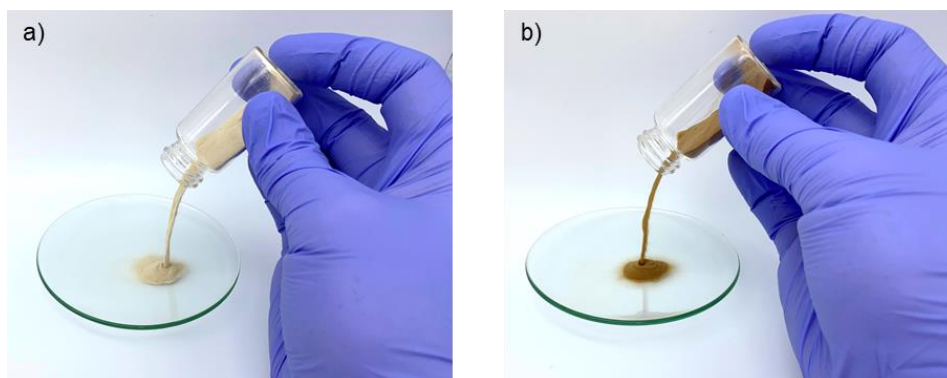
Figure 4.28: a) silica gel coated with oligomer 1 before curing and b) cured polymer coated silica gel. Reproduced with permission from the Royal Society of Chemistry.[25]

Next the solubility of the polymer on the silica gel before and after curing was investigated. As a solvent chloroform was used. As can be seen in Figure 4.29 below, using chloroform to wash (6 × 15 mL) the uncured material resulted in the polymer being dissolved off the silica gel, whereas washing the cured material with chloroform (8 × 15 mL) did not remove polymer from the silica gel. This was also confirmed using scanning electron microscopy (SEM) and energy dispersive X-ray analysis (EDX) analysis. Figure 4.29 shows elemental silica and sulfur maps of the uncured coated silica gel that was unwashed as well as material that was washed with chloroform. Washing the uncured polymer coated silica gel with chloroform resulted in no sulfur being detected, confirming that the polymer had been completely dissolved off the silica gel (Figure 4.29). On the other hand, the same chloroform treatment of the cured coated silica gel did not remove the coating since sulfur was still detected using EDX after the chloroform wash (Figure 4.29).
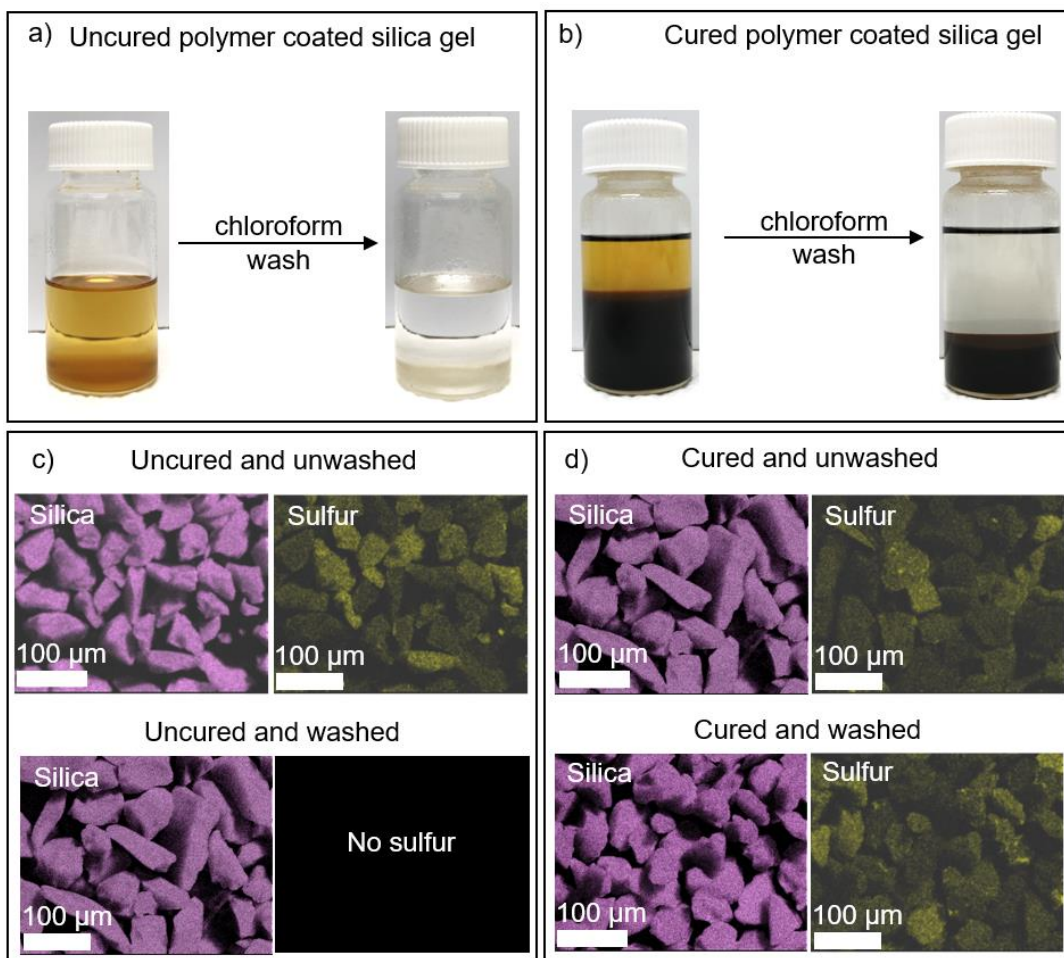
Figure 4.29: a) uncured and **b)** cured polymer coated silica gel after chloroform wash. **c)** EDX and SEM analysis on uncured polymer coated silica gel before and after chloroform wash and **d)** EDX and SEM analysis of cured polymer coated silica gel before and after chloroform wash. Reproduced with permission from the Royal Society of Chemistry.[25]

Mercury removal using polymer coated silica gel (from aqueous solution)

The next step was to assess the mercury removal capabilities of the coated silica gel. Since mercury pollution is of great global concern, the Minamata convention entered into force in 2017 with the goal to govern and control the use of this harmful metal.[36] Therefore, it has become all the more important to remove mercury from the environment, particularly from water. Although a number of mercury sorbents already exist,[37-40] the need for low-cost sorbents still persists. In light of this it comes as no surprise that polysulfides made by inverse vulcanisation have been investigated as useful materials for mercury remediation in recent reports.[15, 17, 24, 41] However, there seems to be a lack of studies of mercury sorbents that show a general solvent resistivity. Such a material would have viable industrial applications. For example, a sorbent that is

effective in removing mercury from a mixture of hydrocarbons and water can prove useful in the oil and gas sector.[42] Therefore, the silica gel coated with the solvent resistant S-DCPD polymer could possibly be useful in that context.

Mercury removal from an aqueous solution was tested first. This was done by adding 100 mg of sorbent to a 45 mL, 5ppm mercury solution made from $HgCl_2$. The samples were then agitated using an end-over-end mixer set to 25 RPM. Uncoated silica gel was used as a control. During the reaction, samples were taken and analysed using cold vapor atomic absorption spectroscopy (CVVAS). Further, the experiment was run in triplicate. The mercury stock solution was tested before and after the experiment to ensure that the mercury concentration did not drop by adhering to the glass vial, for instance. Besides the uncoated silica gel, 3 additional sorbents were tested: silica gel coated with oligomer 1, silica gel coated with oligomer 1 with subsequent curing, and silica gel coated with oligomer 1 with curing and then an extensive wash with chloroform. The results show that the uncoated silica gel only removed only 14% of mercury (Figure 4.30). In contrast, the polymer coated silica gels indicated excellent mercury sorption. The uncured coated silica gel was able to remove over 99% of mercury within 2 hours, while both cured samples (unwashed and washed with chloroform) removed at least 92% of mercury over the sample time period (Figure 4.30). As can be seen from these results, curing the polymer on the silica gel slightly reduces the effectiveness of mercury uptake. However, the cured coated silica gel is solvent resistant, which is a useful property in different settings, like when the mercury is in a solution containing hydrocarbons.

	Sample	Mercury removed after 2 hours
a) —	5 ppm Hg^{2+} solution (no sorbent)	0%
b) —	Uncoated Silica Gel	14%
c) —	Silica coated with oligomer 1, uncured (unwashed)	> 99%
d) —	Silica coated with oligomer 1, cured (unwashed)	92%
e) —	Silica coated with oligomer 1, cured (washed with chloroform)	93%

Figure 4.30: Mercury uptake from aqueous solution using **b)** uncoated silica gel, **c)** silica gel coated with oligomer 1, **d)** silica gel coated with oligomer 1 and cured and **e)** silica gel coated with oligomer 1 cured and washed. Reproduced with permission from the Royal Society of Chemistry.[25]

Next, an isotherm was performed to determine the maximum mercury capacity of the material. The data collected was fitted using the Langmuir model. This analysis found that the mercury capacity for the cured coated silica gel is 5 mg / g (Figure 4.31). However, it must be taken into consideration that only 10% of the sorbent is polymer by mass and that the remaining 90% is silica gel. Hence, the polymer component of the sorbent had a capacity of 50 mg of mercury per gram of polymer coating.
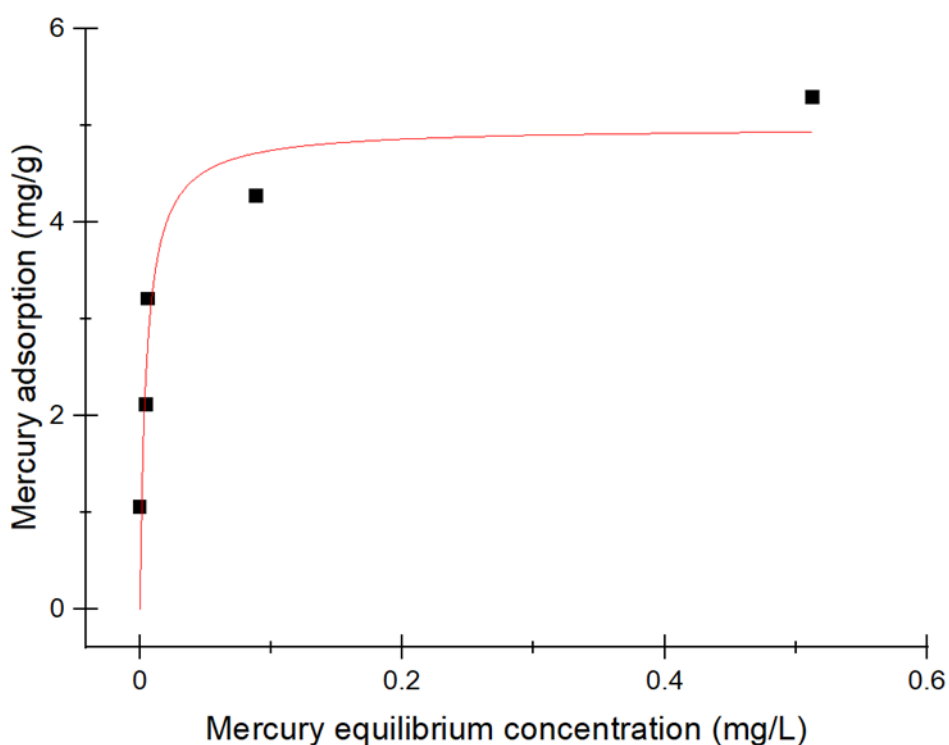
Figure 4.31: Adsorption isotherm of mercury onto sample of silica gel coated with cured **1** using Langmuir isotherm fitting (red line). Reproduced with permission from the Royal Society of Chemistry.[25]

Mercury removal using polymer coated silica gel (from mixture of water and diesel)

As mentioned before, the insolubility of the polymer coating after curing has the possibility in applications in which mercury is found in solutions containing hydrocarbons. To test the mercury uptake in such a scenario, the cured coated silica gel was used to remove mercury from a diesel-water mixture. Equal volumes of diesel fuel and water were spiked with $HgCl_2$ resulting in a mercury concentration of 5 ppm. To 45 mL of this solution 100 mg of cured coated silica gel was added. The samples were then rotated, end-over-end for 2 hours. During the experiment the mercury concentration in the aqueous layer was monitored taking a sample every 30 minutes, separating the organic and aqueous layer via centrifugation and analysing the aqueous layer using CVAAS. As the samples were rotated the diesel and water layers formed an emulsion ensuring contact of the coated silica gel with both phases.

After 2 hours the cured coated silica gel removed 92% of the mercury from the solution (Figure 4.32). This indicated that the diesel did not interfere with the mercury uptake, nor did it dissolve the polymer coating on the silica gel. Hence it can be said that the cured polymer coating on the silica gel is tolerant to these hydrocarbon mixtures.
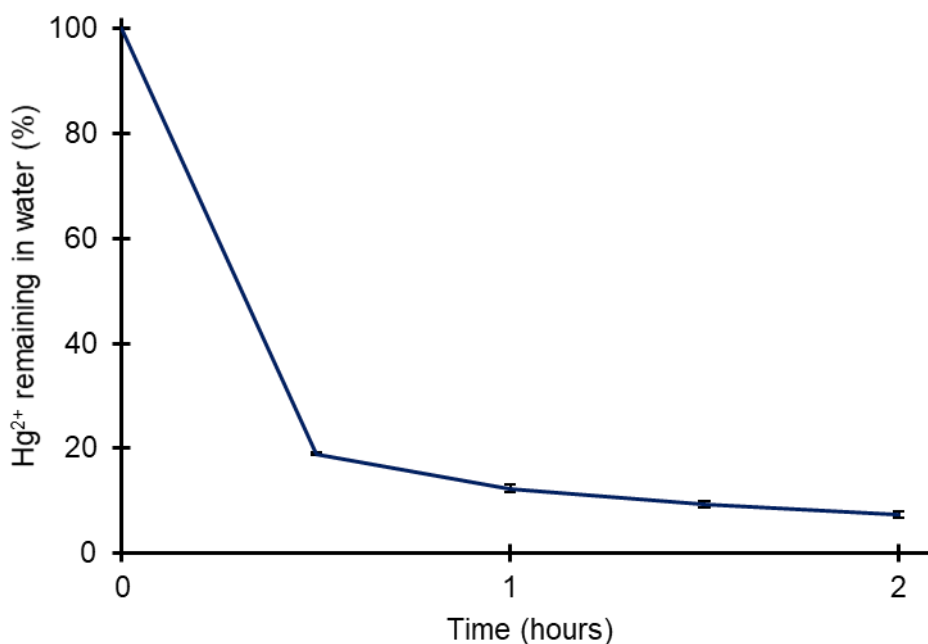
Figure 4.32: Mercury uptake from diesel / water mixture using cured coated silica gel. Reproduced with permission from the Royal Society of Chemistry.[25]

Applications as protective coating for metal and cement

Finally, applications of oligomer 1 as a protective coating were explored. While other studies have shown that sulfur polymers are resistant to acid,[43, 44] there is still a need for solvent processable prepolymers for the development of coating applications. Therefore, it was investigated if oligomer 1 could fill this need. To test the acid resistivity of cured 1, small amounts (57-77 mg) of the material were added to 3 mL of acid (to HCl, H_2SO_4, HNO_3, TFA, H_3PO_4, and acetic acid). After 24 hours the polymers were removed, rinsed with water, dried and weighed. The effect an acid had on the polymer was determined if a mass loss due to the acid exposure was recorded. Only 2 acids affected the polymer. Nitric acid dissolved 6% in 24 hours and sulfuric acid dissolved 3% in 24 hours (Figure 4.33). This result was encouraging since is showed that the polymer is only minimally affected by a variety of acids, even highly oxidising acids such as nitric and sulfuric acid.
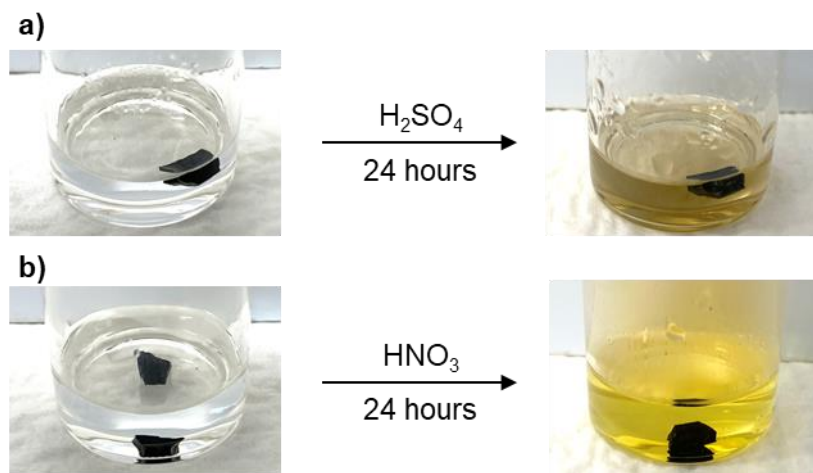
Figure 4.33: a) Cured 1 before and after 24-hour exposure to H_2SO_4 and b) HNO_3. Reproduced with permission from the Royal Society of Chemistry.[25]

Next, the polymer was tested as a protective coating on aluminium. Coatings to protect metals form corrosion are important to protect To prepare the coating, 1 g of oligomer 1 was dissolved in 2 mL of chloroform. Then, 0.1 mL of that solution was placed on the surface of an aluminium wafer with a surface area of 1 cm^2. The solvent was allowed to evaporate before the coated aluminium was cured for 24 hours in a 140 °C oven. After the curing process, the final coating had a mass of 30 mg. The cured polymer coating was black and had a very smooth surface. Further it adhered to the aluminium wafer. The acid resistance was tested by placing a drop of hydrochloric acid (37%, 5 µL) on the surface of the polymer coating for 3 hours. After that the acid was washed away with water. As can be seen in Figure 4.34, no apparent corrosion or reaction was observed on the cured polymer surface. In contrast, clear corrosion was observed on the uncoated aluminium after it was exposed to HCl for 3 hours.
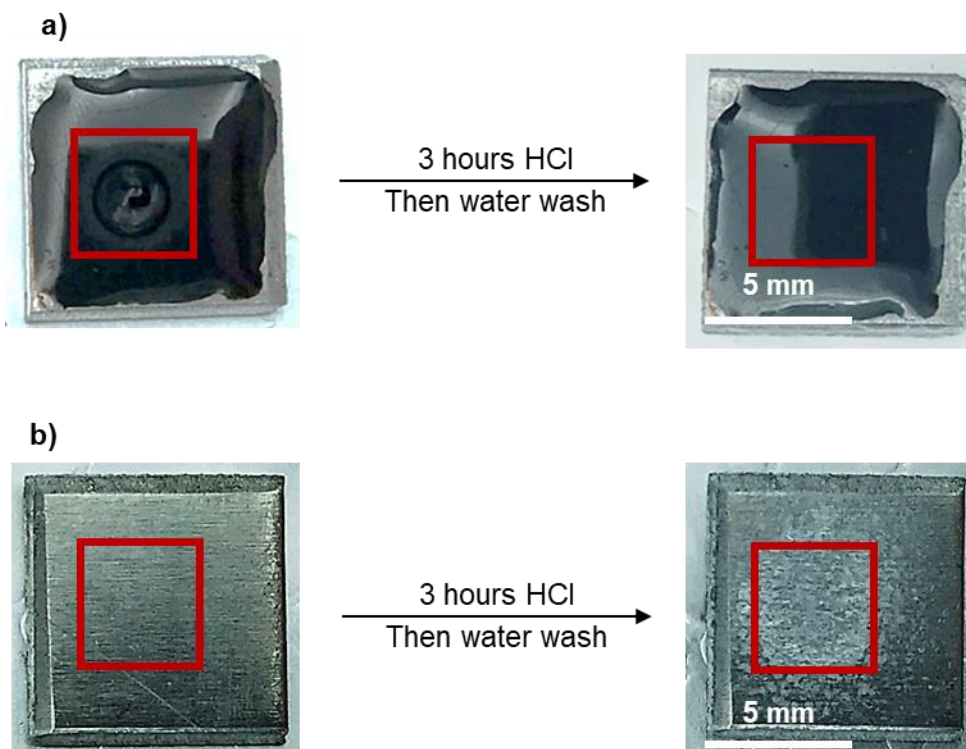
Figure 4.34: a) aluminium coated with oligomer 1 and cured with HCl on the surface for 3 hours and after the acid was washed away with water and b) uncoated aluminium with HCl on the surface for 3 hours and after the acid was washed away with water. Reproduced with permission from the Royal Society of Chemistry.[25]

Next, further protective coating applications for cured **1** were explored. For this the coating of cement was investigated. Cement is a widely used construction material that can degrade when exposed to acids.[45] The first step was to dissolve 1.0 g of oligomer **1** in 2 mL of chloroform. Next, a 100 μL aliquot of this solution was placed on the surface of a thin cement sheet (1 cm × 1.5 cm) and the solvent was allowed to evaporate. To ensure an even polymer coating, this procedure was repeated twice more (300 μL of polymer solution in total). After that, the coated cement sheet was cured at 140 °C for 24 hours. The resultant polymer coating had a mass of 80 mg. Acid resistivity of the cured polymer coating was assessed next by adding 25 μL of HCl (37%) to the surface of the polymer as was done to a piece of uncoated cement. Moreover, 25 μL of water were placed on another uncoated cement sheet. As the acid was placed on the uncoated cement sheet foaming was observed, indicative to the corrosive reaction between the acid and the cement (Figure 4.35). However, no foaming was observed on the polymer coated cement, confirming acid resistivity. Interestingly, after 2 hours had passed, the water and HCl had penetrated the uncoated cement. On the cured **1** coated

297

sample no penetration of the acid into the sample was observed, indicating that cured 1 protected the cement from acid and water (Figure 4.35).
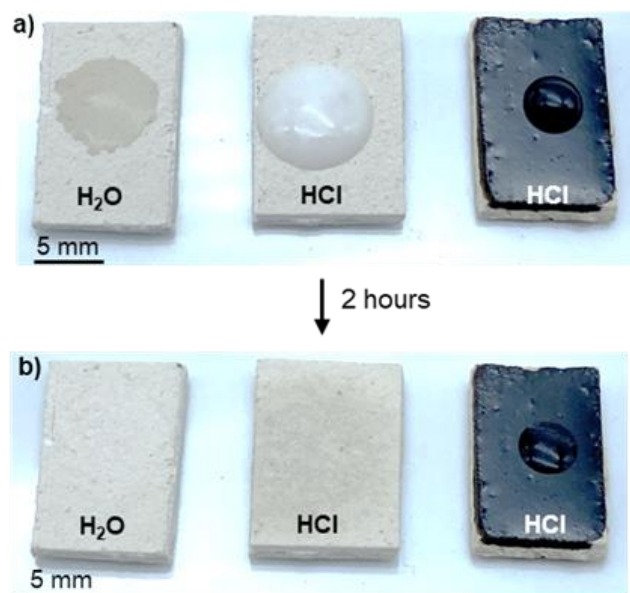
Figure 4.35: a) Water and acid were added to the surface of uncoated cement sheets. The acid on the uncoated cement sample resulted on immediate foaming. No reaction was observed when the acid was added to the cured 1 coated cement sheet. **b)** After 2 hours the coated cement was still unaffected by the acid whereas the acid and water had penetrated the uncoated samples. Reproduced with permission from the Royal Society of Chemistry.[25]

Since the prevention of chemical degradation of cement is an important component of preserving cement in the build environment, the finding that cured 1 can prevent acid degradation was an important result. It is also important to protect cement from water penetration since this can lead to cracking when the concrete is objected to repeated freeze-thaw cycles.[46]

As has already been discussed, cured 1 was also insoluble in common solvents like water, DMF, NMP, THF, methanol, chloroform, ethyl acetate, isopropanol, and acetone. This property of cured 1 was further explored by lining a PVC pipe with oligomer 1 and curing it to result in a protective coating of the pipe. To coat the pipe, no solvents were required. Because of the malleable nature of oligomer 1, oligomer 1 was rolled flat and wrapped around a silicon insert in the shape of a cylinder (Figure 4.36). The polymer wrapped silicon cylinder was then placed inside a PVC pipe (Figure 4.36). The diameter of the silicon insert was chosen so that the gap between the insert and the pipe was filled by oligomer 1. Another advantage of this method is that the thickness of the coating can

be determined by the dimensions of the silicon insert. The PVC pipe containing the polymer and silicon insert were then placed into a cylindrical aluminium mould to prevent deformation of the PVC pipe during the curing process at 140 °C, which is above the T_g of the PVC pipe (Figure 4.36). After curing at 140 °C for 24 hours the silicone insert was removed, and the inside of the pipe was evenly coated with cured 1 (Figure 4.37).
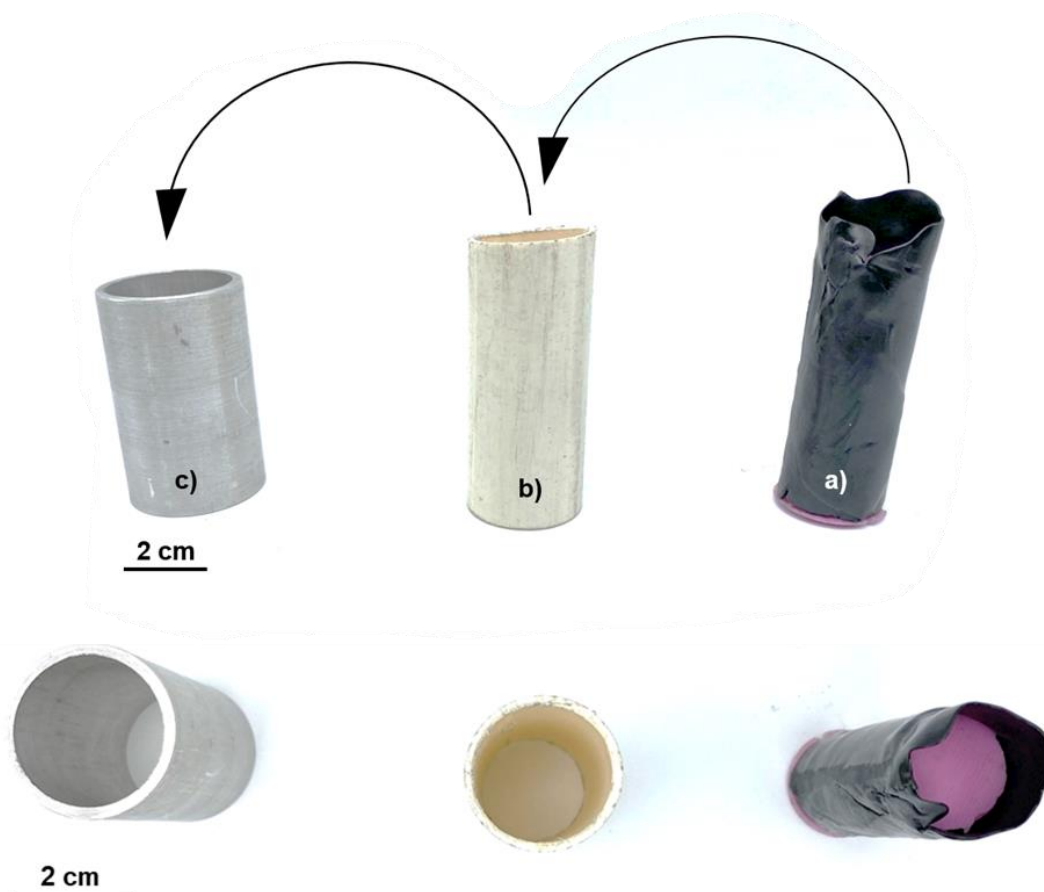
Figure 4.36: a) Oligomer 1 wrapped silicon insert. **b)** The oligomer 1 and silicon insert was placed into a PVC pipe. **c)** The PVC pipe containing the silicone/polymer insert was added to an aluminium mould. Reproduced with permission from the Royal Society of Chemistry.[25]

To show the solvent resistance of the coating, THF was passed through the coated pipe for 2 hours at a flow rate of 5 mL/minute (600 mL total). The same was also done with a piece of uncoated PVC pipe (Figure 4.37). After the THF exposure for 2 hours, the uncoated pipe showed significant signs of damage and the solvent that had passed through the pipe had a cloudy appearance due to the dissolved PVC (Figure 4.37). In contrast no damage was observed for the pipe lined with cured 1 and the solvent remained clear. (Figure 4.37)
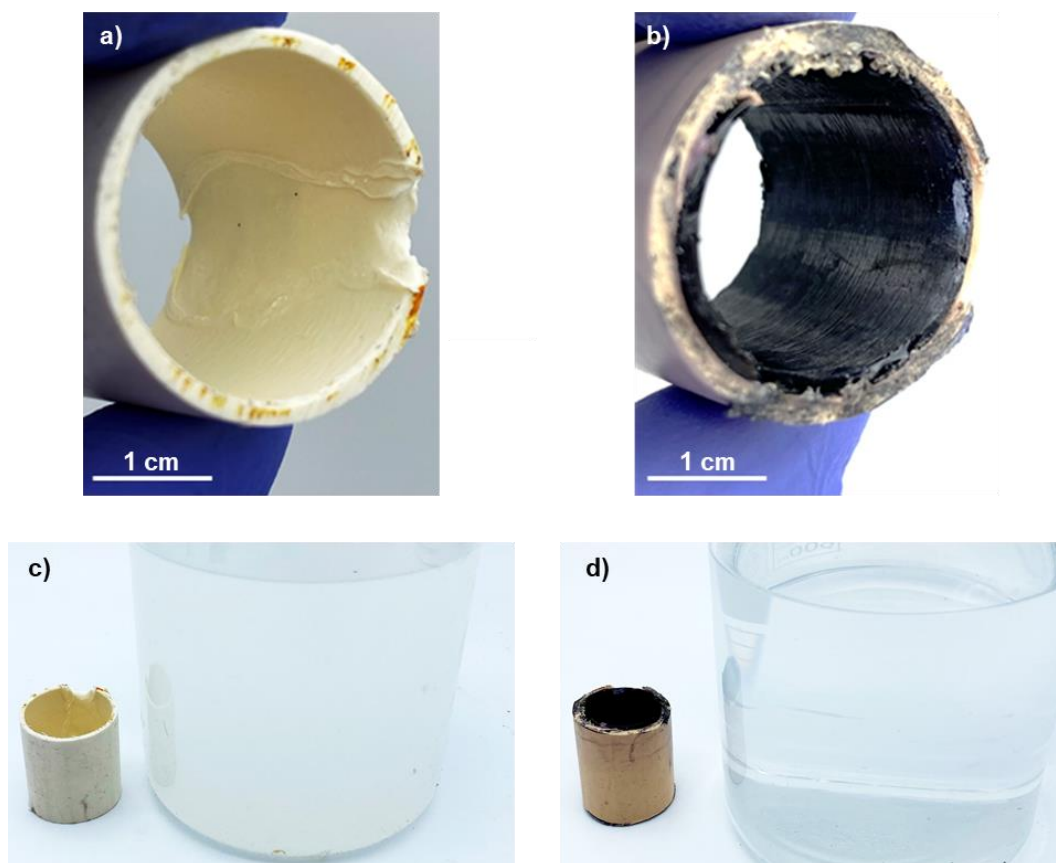
Figure 4.37: a) Unlined PVC pipe after 600 mL of THF were passed through showed dissolution. **b)** Cured 1 lined PVC pipe showed no signs of damage after feeding thought 600 mL of THF. **c)** The THF passed thought the unlocated pipe was opaque due to the dissolved PVC. **d)** The THF passed thought he cured 1 coated pipe remained clear Reproduced with permission from the Royal Society of Chemistry.[25]

It is known that networks of polymers containing polysulfide crosslinks have S-S bonds that, with the addition of heat[12-14] or a nucleophilic catalyst,[27] can be broken and reformed. Although cured 1 is a crosslinked polymer the possibility of thermal repair of a damaged polymer was investigated. This would make the coating a smart coating. Smart coatings are coatings that can dynamically adapt through external influences.[47] One class of smart coatings are self-healing polymer coatings by shape recover, which is achieved by light or heat.[47] To investigate if the S-DCPD coating can be classed as a smart coating, small scratches were made on the surface of the cured 1 square (1 cm × 1 cm). The polymer was then heated to 240 °C using a heat gun. Using a thermal imaging camera, the temperature of the polymer surface was monitored. After heating the polymer for 15 minutes the shallow scratches were repaired and only some "scarring" remained from the deeper scratches (Figure 4.38). Although it can be challenging to accurately control the temperature using a heat gun, this method of heating had the

advantage of being portable and can be applied to coated materials which are fixed in position and cannot be heated in an oven.
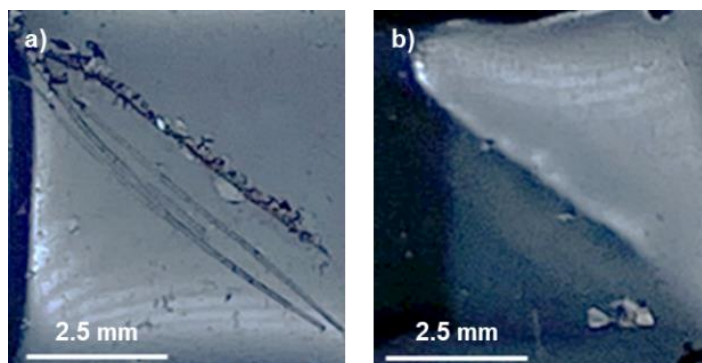
Figure 4.38: a) Scratched on the surface of cured 1 before heating. **b)** Scratched area of cured 1 after thermal treatment using a heat gun at 240 °C for 15 minutes. Reproduced with permission from the Royal Society of Chemistry.[25]

Conclusion

In conclusion, a safe, robust, and reliable method was developed to synthesise a sulfur-DCPD copolymer. This method resulted in a solvent processable pre-polymer that was used as an active coating to coat silica gel for mercury removal. This pre-polymer can be rendered solvent and acid resistant through a simple curing process in an oven at 140°C for 24 hours. This polymer has been used as an active coating to coat silica gel which displayed excellent mercury removal capabilities from aqueous solution, a protective coating for aluminium, cement, and PVC to provide acid and solvent resistivity and as and dynamic material capable to be thermally repaired. Additionally, the cured coated silica gel was able to remove mercury form a mixture of diesel and water. This chapter highlights the use of an additional polysulfide polymer system following the exploration of end of life used of a polysulfide polymer system discussed in the previous chapter.

Future work in this polymer system should aim to probe more into the recycling aspect of the cured polymer to explore if the polymer can be broken down and re-formed while retaining its properties. Additionally, the premise of synthesising a trisulfide (as was seen in the reduction of the polymer as seen in Figure 4.21) as a monomer which can be polymerised and converted back to a monomer could be explored. Further, future work can include the electrochemical reduction of cured 1 as supposed to the hydride reduction discussed in this chapter. This would render the reduction safer since the hydrides used here a toxic.

301

Publication that resulted from the research in this chapter:

Processes for coating surfaces with a copolymer made from sulfur and dicyclopentadiene.

Mann, M.; Zhang, B.; Tonkin, S. J.; Gibson, C. T.; Jia, Z.; Hasell, T.; Chalker, J. M., Processes for coating surfaces with a copolymer made from sulfur and dicyclopentadiene. *Polym. Chem.* **2021**, in press. DOI: 10.1039/D1PY01416A.

Experimental details

General considerations

Materials: Dicyclopentadiene (DCPD) was purchased from Sigma-Aldrich. Sulfur was purchased from Sigma-Aldrich (reagent grade, powder, purified by refining, 100 mesh particle size). Silica gel was purchased from Sigma-Aldrich (technical grade, pore size 60Å, 230-400 mesh particle size, 40-63 µm particle size).

Simultaneous thermal analysis (STA) was performed using a Perkin Elmer STA 8000. Between 5-10 mg of sample were held at 40 °C for 4 minutes before the temperature was increased by 10 °C/minute to 800 °C. This was done under a 20 mL/min nitrogen flow.

Differential scanning calorimetry (DSC) was performed using a Perkin Elmer DSC 8000. Between 5-10 mg of sample was cooled to -80 °C and held for 4 minutes. After that the temperature was increased to 80 °C by 10 °C/minute and held for 4 minutes. Next, the sample was again cooled to -80 °C by 10 °C/minute and held for 4 minutes at that temperature. Finally, the sample was heated to 250 °C by 10 °C/minute. This was under a 20 mL/minute nitrogen flow.

^{1}H NMR spectra were recorded on a 600 MHz Bruker spectrometer with $CDCl_3$ as solvent. Spectra were referenced to residual solvent peaks (δ_H = 7.26 for $CDCl_3$).

^{13}C NMR spectra were recorded on a 600 MHz Bruker spectrometer with $CDCl_3$ as solvent. Spectra were referenced to residual solvent peaks (δ_C =77.36 for $CDCl_3$).

Infrared (IR) spectra were recorded using a FTIR Perkin Elmer Frontier spectrometer between 4000 and 500 cm^{-1}. This was done by using the ATR samples technique or a KBr disk. An KBr disk was fashioned by adding a small amount of sample (10-50 mg) to 200 mg of dry KBr. The sample was thoroughly mixed using mortar and pestle before being pressing onto a disk using pressures of around 10 tons.

Scanning electron microscopy (SEM) and energy dispersive X-ray analysis (EDX) images were obtained using a FEI Inspect F50 SEM fitted with a EDAX energy dispersive X-Ray detector. Samples were sputter coated with silver metal (20 nm thickness) before analysis.

Cold vapour atomic absorption spectroscopy (CVAA) was carried out by a commercial service. Briefly, aqueous samples were digested using bromine monochloride (BrCl) before Cold Vapour Atomic Absorption spectroscopic analysis

using a method adapted from the following standard methods: APHA 3112 (USEPA 7471A & USEPA 1631 Rev E).

CHNS elemental analysis was performed by The Campbell Microanalytical Laboratory at the University of Otago in New Zealand.

Gel permeation chromatography (GPC) was performed using a Shimadzu Prominence UPLC fitted with a Phenomenex Linear (2) column with matching guard column and a refractive index detector. The analysis was performed with a mobile phase of HPLC grade chloroform with 1% ethanol and an oven temperature of 40 °C. The flow rate was set to 1.00 mL/min. Polystyrene standards were used for calibration.

Laser desorption mass spectroscopy (LD-MS) was performed using a Bruker Autoflex III Smartbeam instrument. To collect the data a nitrogen laser with a wavelength of 355 nm was used and the instrument was set to reflectron mode.

Gas chromatography – mass spectrometry (GC-MS) was performed using an Agilent 7890A GC system fitted with an Agilent 5975C inert XL EI/CL MSD with triple-axis detector and Agilent 7693 autosampler. The column used was an Agilent J&W HP-4ms GC Column, 30 m, 0.25 mm, 0.25 µw, 7-inch cage (19091S-433). The initial temperature of 30 °C was held for 3 minutes before ramping by 20 °C / min to 200 °C. The gas flow rate (helium) was 1.2 mL / min. The injection volume was 1 µL with a 60:1 split ratio. The total run time was 21.5 minutes.

Atomic force microscopy (AFM) (performed by Christopher Gibson) images were acquired using a Bruker Multimode 9 AFM with a Nanoscope V controller using tapping mode in air, with all parameters including set-point, scan rate and feedback gains adjusted to optimize image quality. In order to minimize tapping force amplitude, set-points during scanning, were kept at 80 to 90% of the cantilever free amplitude. As a result, no image or adhesion artefacts were observed in the AFM images indicating no tip contamination occurred due to the polymer surface.[48, 49] The AFM probes used for all measurements were Mikromasch HQ: NSC15 Si probes with a nominal spring constant of 40 Nm^{-1} and a nominal tip diameter of 16 nm. For the measurement of mechanical properties (elastic modulus and hardness) of the polymer the cantilever sensitivity and spring constant were calibrated using procedures outlined in Sader et al.[31] The spring constant for cantilevers calibrated ranged between 23.8 to 34.6 N/m. The scanner was calibrated in x, y and z directions using a silicon calibration grid (Bruker model number VGRP: 10 µm pitch, 180 nm depth PG: 1 µm pitch, 110 nm depth, Mikromasch model TGZ01: 3 µm pitch, 18 nm depth). Roughness analysis of AFM images was performed using Nanoscope analysis software version 2.0 and elastic modulus and hardness

measurements were analysed using a combination of Nanoscope Analysis version 2.0 and the data analysis software Gwyddion version 2.59. Samples for AFM were prepared by placing flat pieces of oligomer **1** in silicon wafers and curing them in an oven at 140 °C for 24 hours. Before AFM analysis each sample was gently rinsed with ethanol and dried with nitrogen gas.

Powder X-ray diffraction (XRD) patterns were recorded on a Bruker D8 Advance Eco diffractometer (Bragg-Brentano geometry) using Co-Kα radiation (λ = 1.78897 Å). The Bragg angle (2θ) was varied from 10° to 90° with a step size of 0.019°, measurement time of 0.6 s per step and sample rotation at 10 rpm. The samples were deposited onto a sample holder well before analysis

S-DCPD synthesis optimisation

This experiment was performed to assess if cyclopentadiene is formed when dicyclopentadiene (DCPD) is heated to 160 °C and if less CPD is formed during lower temperatures (140 °C). To do this 5.00 g of DCPD was added into a 100 mL round bottom flask fitted with a condenser. Then, the DCPD was heated to 140 °C or 160 °C respectively while being magnetically stirred for 2 hours before analysis by ^{1}H NMR (600 MHz, CDCl$_3$). Freshly cracked and distilled cyclopentadiene was also analysed by ^{1}H NMR for comparison:
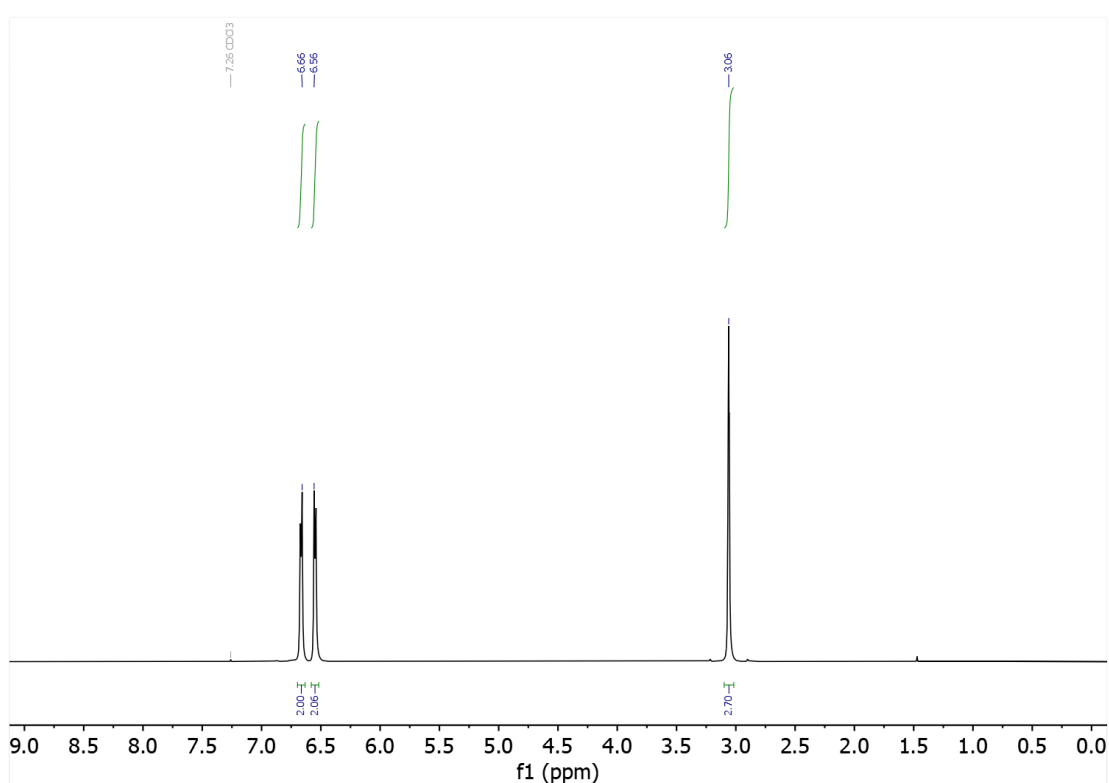
Figure 4.39: ^{1}H NMR spectrum of freshly cracked and distilled cyclopentadiene (CDCl$_3$, control spectrum). Reproduced with permission from the Royal Society of Chemistry.[25]
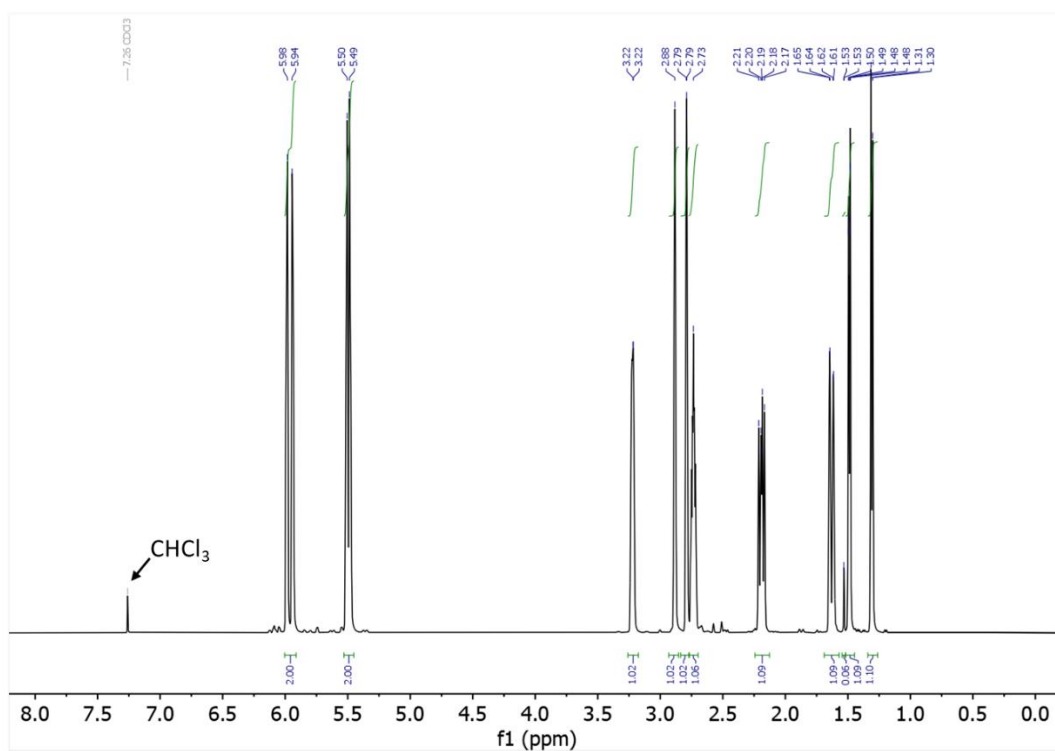
Figure 4.40: ^{1}H NMR spectrum of DCPD (CDCl$_3$, 600 MHz, control, no heating). Reproduced with permission from the Royal Society of Chemistry.[25]
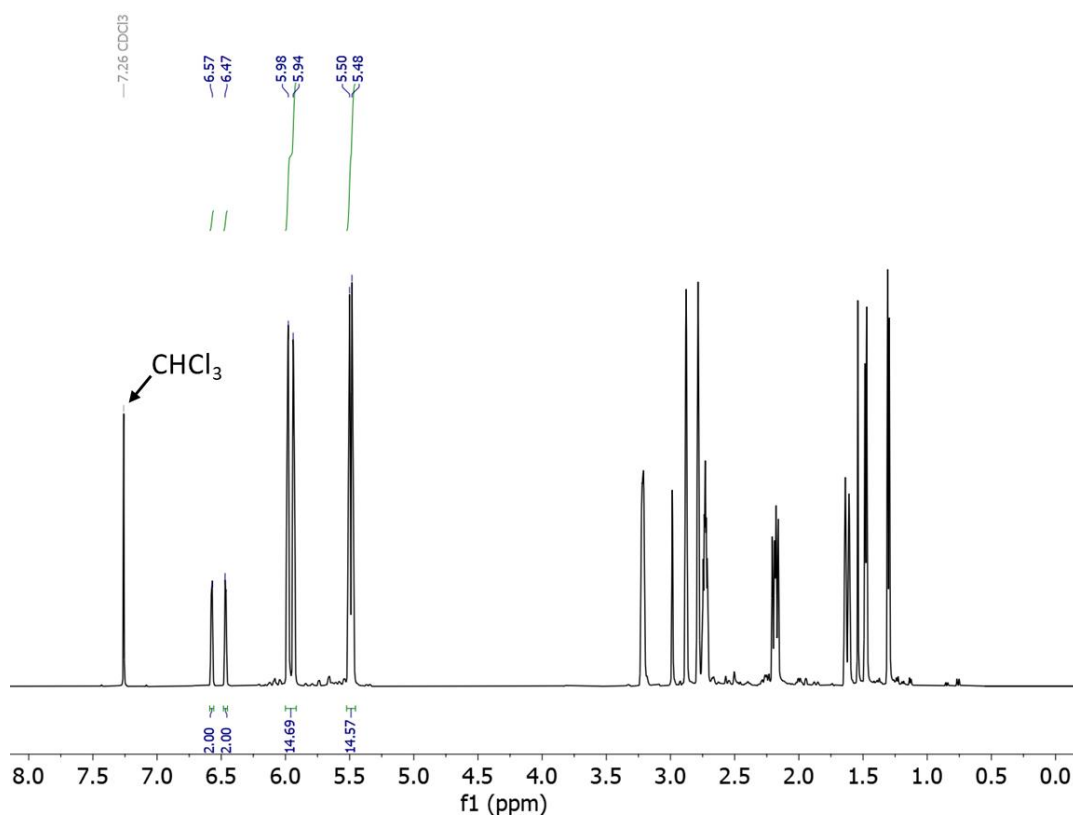
Figure 4.41: ^{1}H NMR spectrum of DCPD after heating at 160 °C for 2 hours. The peaks at δ = 6.57 and 6.47 ppm are due to the vinylic protons of cyclopentadiene and the peaks between δ = 5.98 and 5.48 correspond to the vinylic protons of DCPD. Reproduced with permission from the Royal Society of Chemistry.[25]

Result: 12% cyclopentadiene and 88% DCPD
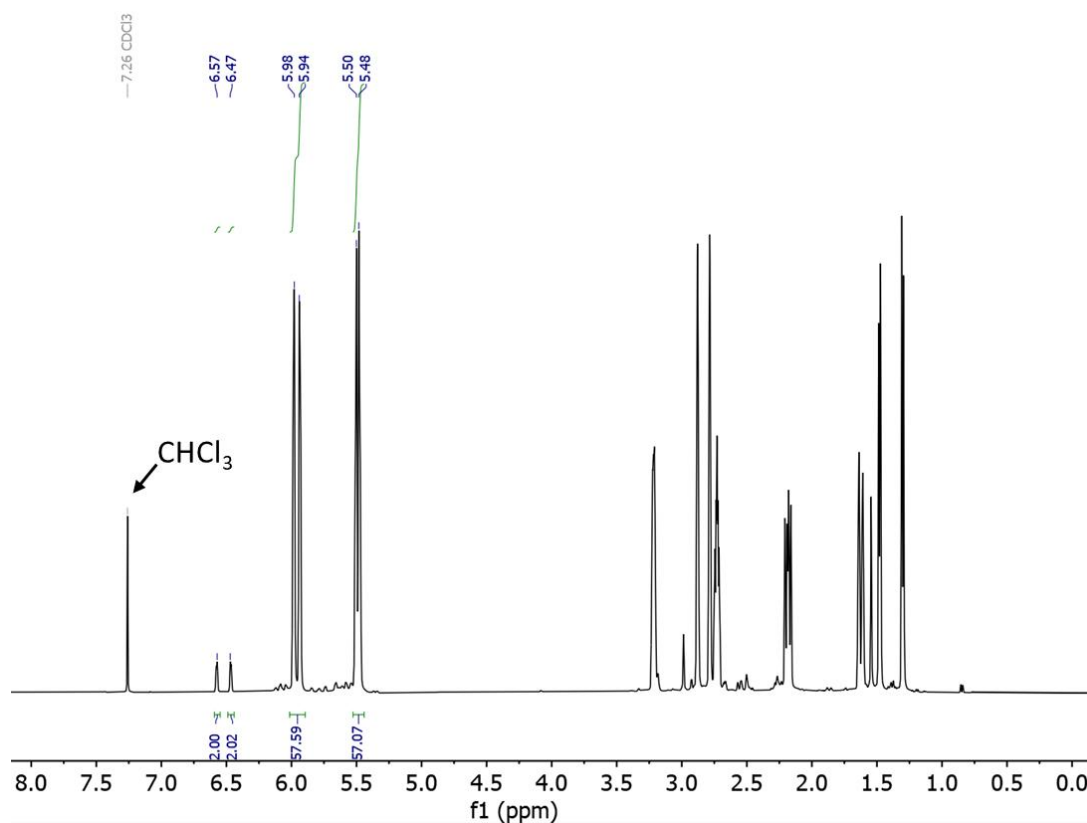
Figure 4.42: ^{1}H NMR spectrum of DCPD after heating at 140 °C for 2 hours. The peaks at $\delta = 6.57$ and 6.47 ppm are due to the vinylic protons of cyclopentadiene and the peaks between $\delta = 5.98$ and 5.48 correspond to the vinylic protons of DCPD. Reproduced with permission from the Royal Society of Chemistry.[25]

Result: 3% cyclopentadiene and 97% DCPD

To investigate if the polymer could be synthesised in a 140 °C oven, uncapped and without stirring, 11 glass vials (20 mL) each containing 3.00 g of sulfur and 3.00 g of DCPD were prepared. These vials were placed in a 140 °C oven (uncapped) for 1, 2, 3, 4, 5, 6, 7, 8, 9, 10 and 24 hours.
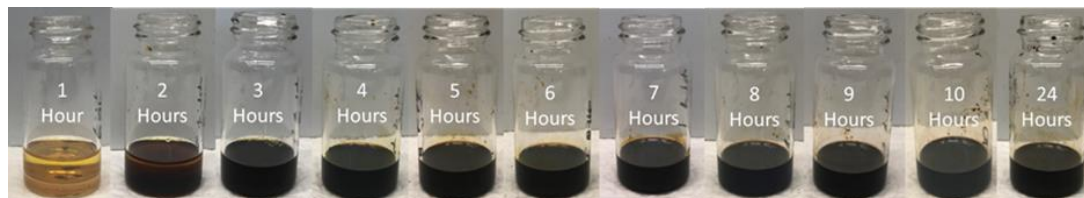
Figure 4.43: Reaction of 3.00 g DCPD and 3.00 g sulfur at 140 °C in an oven for 1-24 hours directly after they have been removed from oven. Phase separation was observed for the 1- and 2-hour samples. Reproduced with permission from the Royal Society of Chemistry.[25]

Figure 4.44: Reaction of 3.00 g DCPD and 3.00 g sulfur synthesised at 140 °C in an oven 24 hours. The image shows all samples after the final sample of 24 h reaction time was removed from the oven. Reproduced with permission from the Royal Society of Chemistry.[25]

In order to determine the T_g of the materials with a reaction time of 8, 9 and 10 hours DSC analysis was performed. If possible, to T_g was calculated for each cooling and heating cycle.
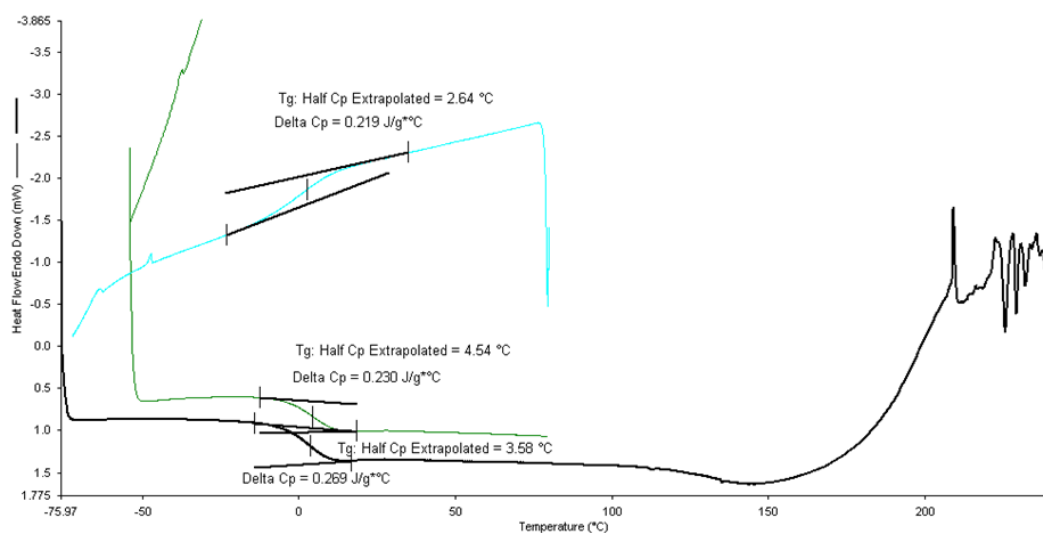
Figure 4.45: DSC of material reacted uncapped for 8 hours in a 140°C oven.
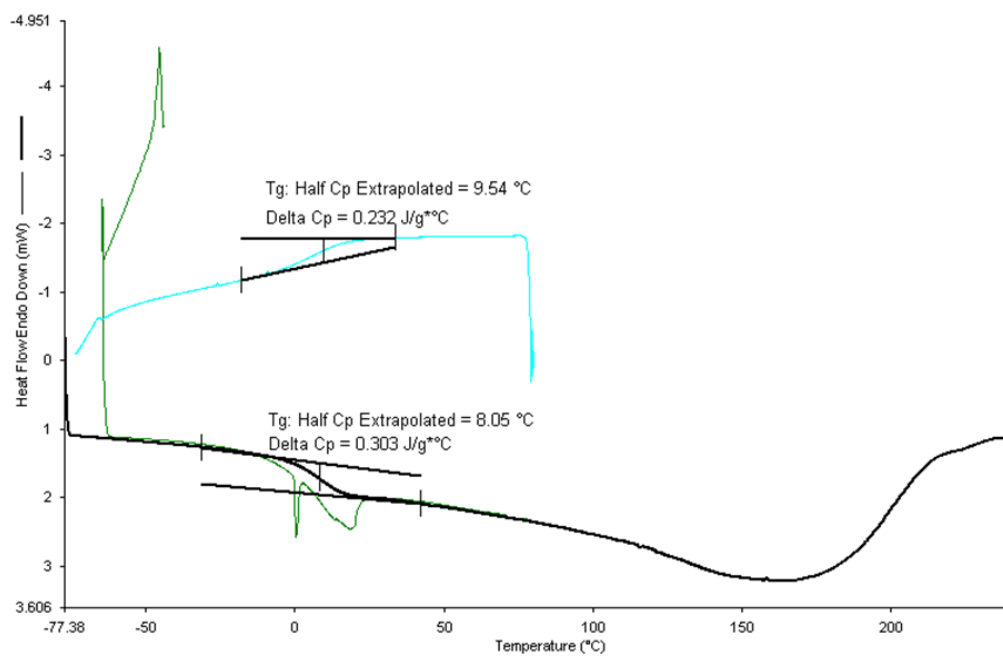
Figure 4.46: DSC of material reacted uncapped for 9 hours in a 140°C oven.
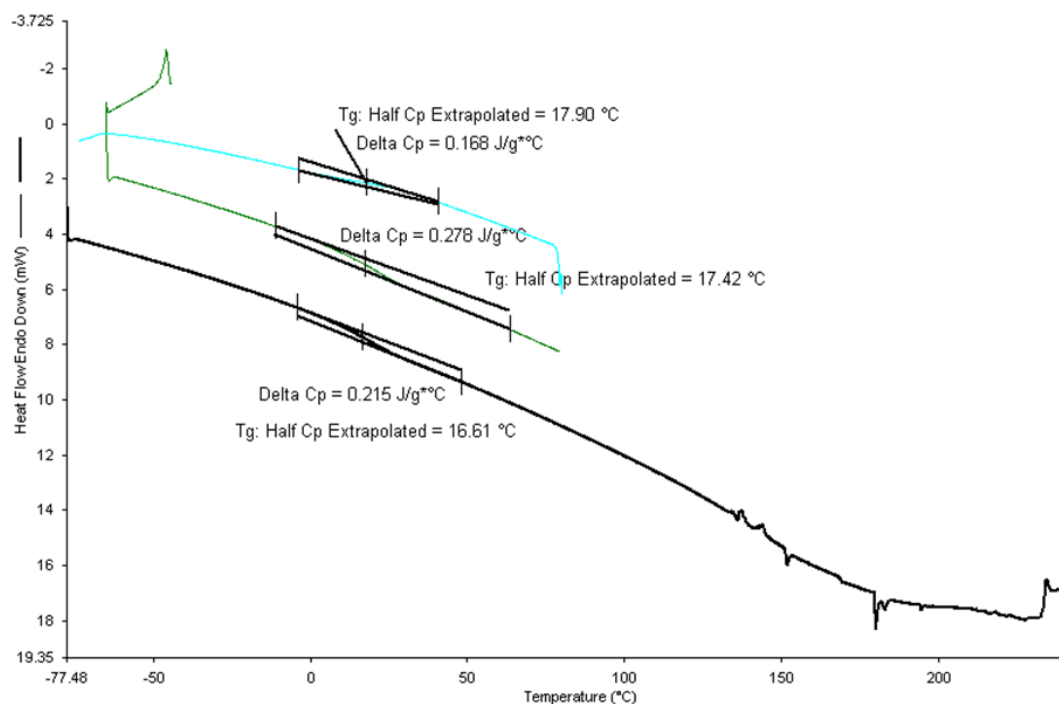
Figure 4.47: DSC of material reacted uncapped for 10 hours in an 140°C oven.

To determine if increased mass transfer through stirring can increase the reaction rate, 3 of sulfur and 3 g of DCPD were placed in a 20 mL glass vial and added to a 140°C aluminium hot plate and magnetically stirred at 500 RPM for 7 hours. The resulting material was hard and insoluble in chloroform.

For the reactions with a reduced reaction time 3 g of sulfur and 3 g of DCDP were placed in a 20 mL glass vial and added to a 140°C aluminium hot plate and magnetically stirred at 500 RPM. In total 8 individual reaction were performed with reaction times of 0.25, 0.5, 0.75. 10. 1.25, 1.5, 1.75 and 2 hours.
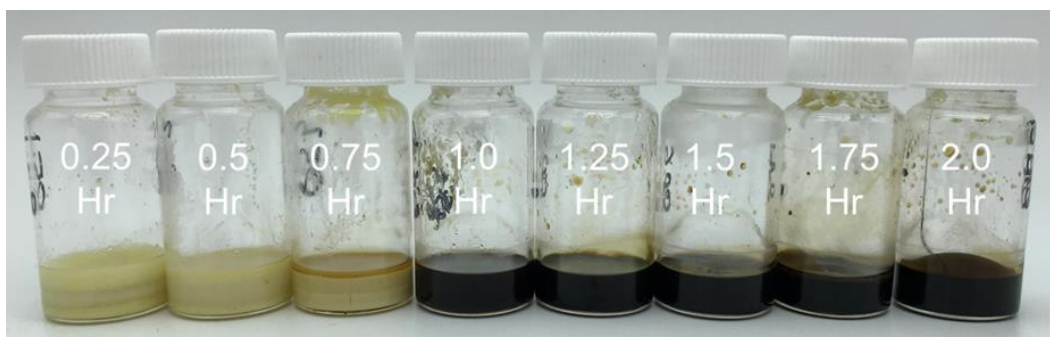
Figure 4.48: S-DPCD synthesis with reaction times of 0.25, 0.5, 0.75, 1.0, 1.25, 1.5, 1.75 and 2 hours at 140 °C while magnetically stirred after having cooled down to room temperature. Reproduced with permission from the Royal Society of Chemistry.[25]

To determine the solubility of the polymers, a small amount was added to 10 mL of chloroform, THF or DCM.
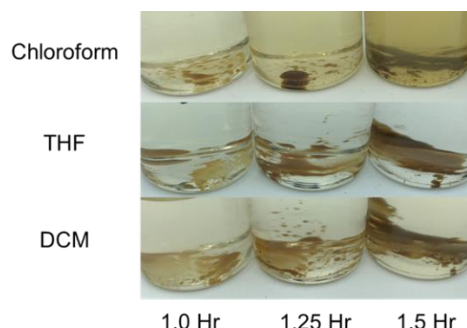
Figure 4.49: Polymer synthesised at 140 °C while magnetically stirred for 1.0, 1.25 and 1.5 hours in chloroform, THF and DCM.

For the reactions run parallel under an atmosphere of nitrogen or open to air, 3 g of sulfur and 3 g of DCPD were placed in a 20 mL glass vial and added to a 140°C aluminium hot plate and magnetically stirred at 500 RPM for 2 hours. The reaction under nitrogen was first purged for 20 minutes with nitrogen before the reaction was started.

For the control experiment to determine the effect water has on the reaction when performed under a nitrogen atmosphere, 3 of sulfur and 3 g of DCPD were placed in a 20 mL glass vial, to one of the vials, 400 µL of deionised water was added. The vials were then purged with nitrogen for 20 minutes, and then placed under 1 atm of nitrogen for the reaction (balloon). Following that, both reactions were stirred and heated to 140 °C for 2 hours. After this time, the reactions were cooled under nitrogen.
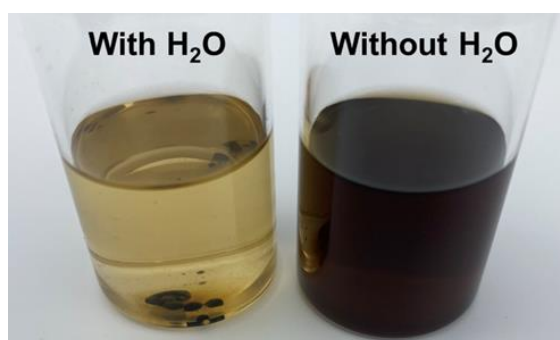
Figure 4.50: 55 mg of the products obtained above were mixed with 10 mL of chloroform. An insoluble fraction can be seen in the solution containing the product synthesised in the presence of water. The polymer synthesised under dry conditions was fully soluble in chloroform. Reproduced with permission from the Royal Society of Chemistry.[25]

To assess solubility of S-DCDP-A (polymer made under same conditions as oligomer 1 but open to air) and S-DCPD-H2O, 500 mg of each polymer was placed in 15 mL of chloroform. After 1 hour the solvent was removed and replaced with another lot of 15 mL of chloroform. This process was repeated after an additional 100 hours and 200 hours. After the solvent had been removed the samples were dried under high vacuum for 24 hours. Of the S-DCDP-A polymer 36% of its mass was not soluble under these conditions.18% of the mass of the S-DCPD-H2O polymer was insoluble under these conditions. We attribute this insolubility to the interference of water in the reaction. Since the reaction is likely of ionic nature, water can attack a cation adding a OH group to the polymer. This in turn will render the polymer less soluble in organic solvent like chloroform. When the polymer is formed under dry, conditions and an inert atmosphere, the product polymer is fully soluble in chloroform.
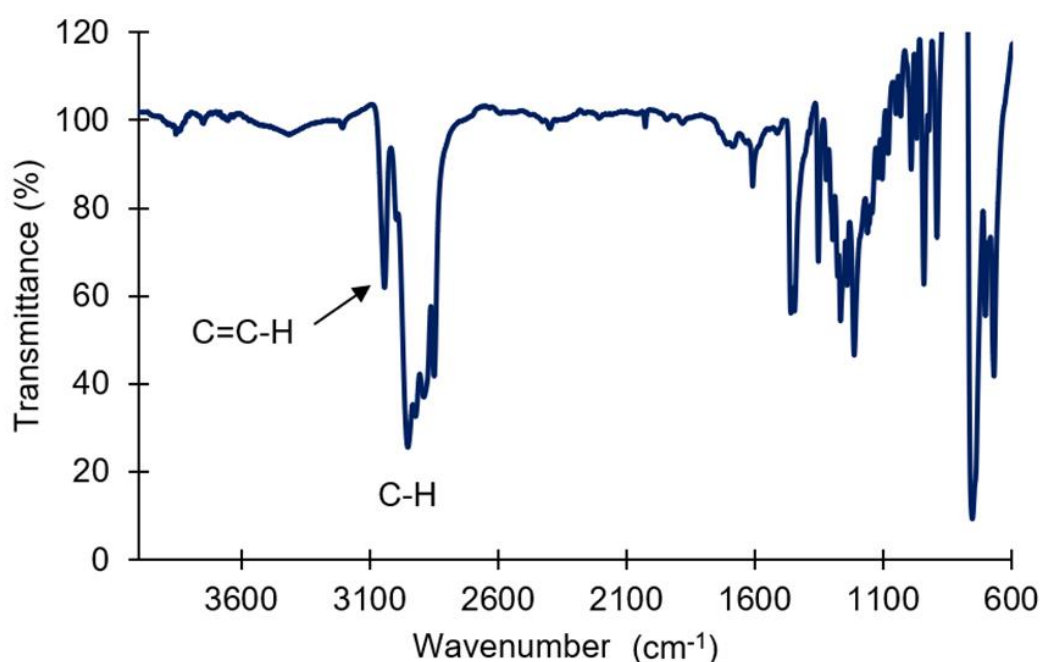
Figure 4.51: IR spectrum of insoluble material from a reaction open to air after 2 hours showing a broad C-H alkane stretch and a small C=H alkene stretch. Reproduced with permission from the Royal Society of Chemistry.[25]

Characterisation of oligomer 1
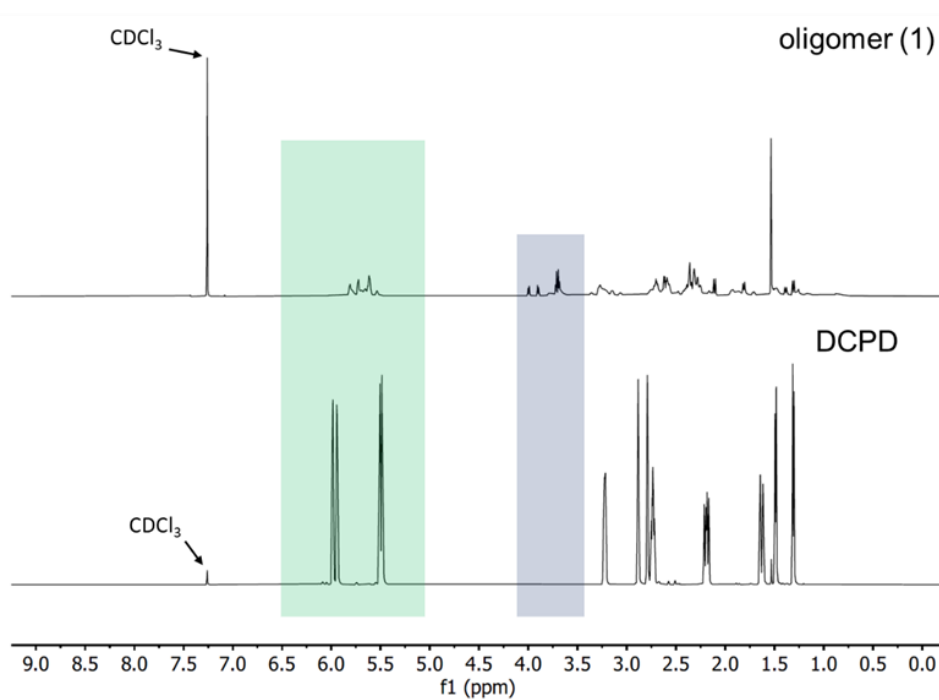
Figure 4.52: ^{1}HNMR of DCPD and oligomer **1** indicating partial consumption of alkenes between 5.5-6.5 ppm and the formation of C<u>H</u>S groups between 3.5-4.0 ppm. Reproduced with permission from the Royal Society of Chemistry.[25]
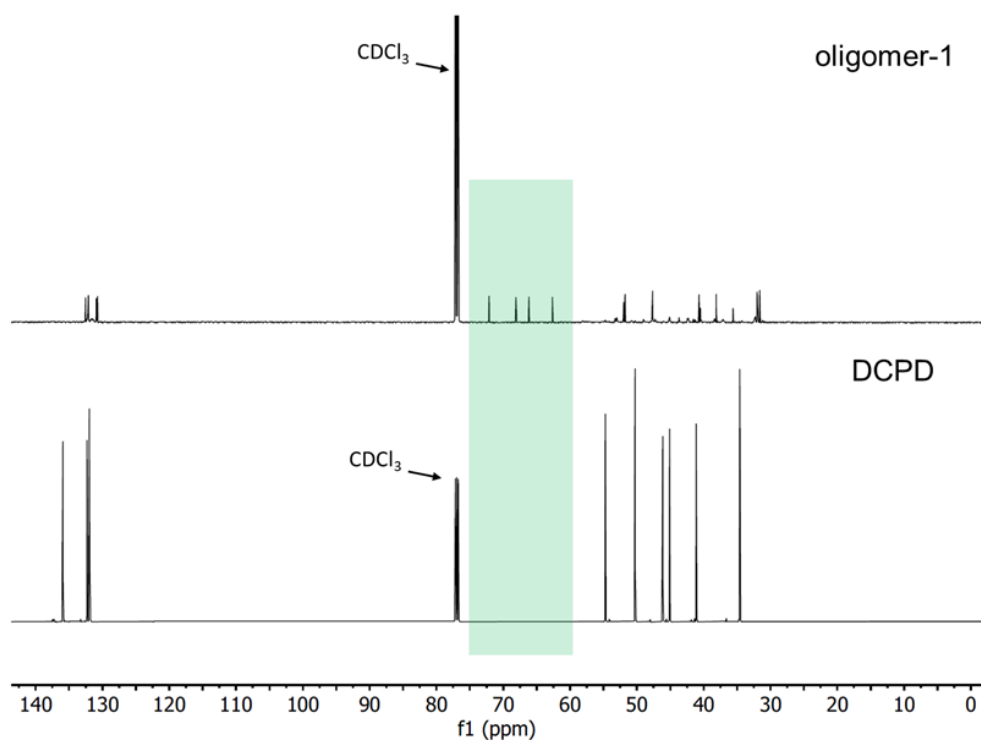
Figure 4.53: ^{13}CNMR of DCPD and oligomer **1** showing the formation of new peaks due to C-S bond formation. Reproduced with permission from the Royal Society of Chemistry.[25]
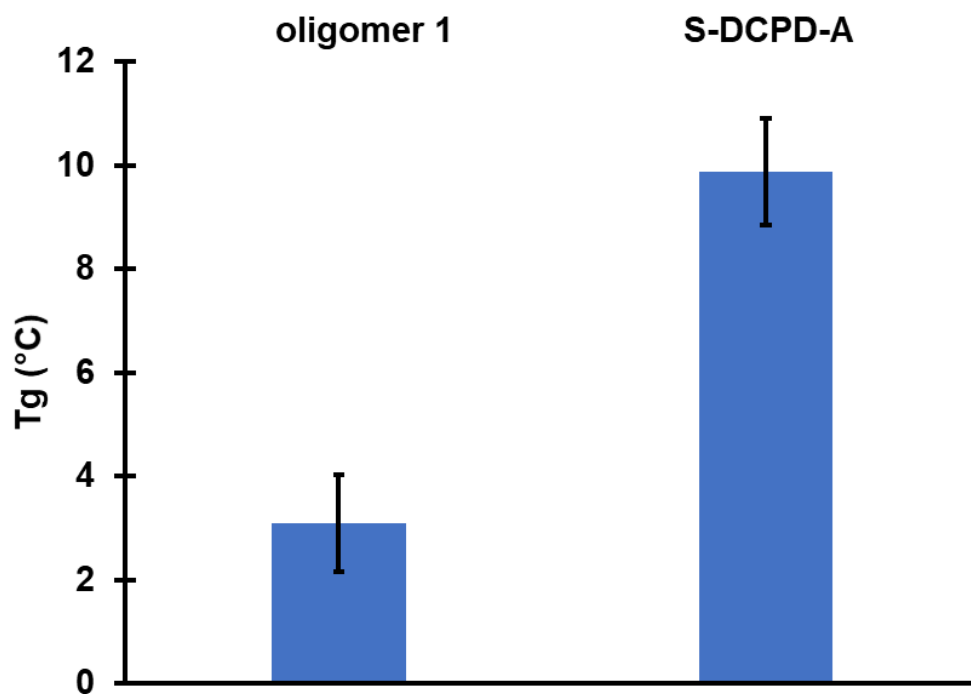
Figure 4.54: DSC analysis revealed a T_g of 3 ± 1 °C for oligomer **1** a T_g of 10 ± 1 °C for the polymer synthesised under an open to air atmosphere. Reproduced with permission from the Royal Society of Chemistry.[25]
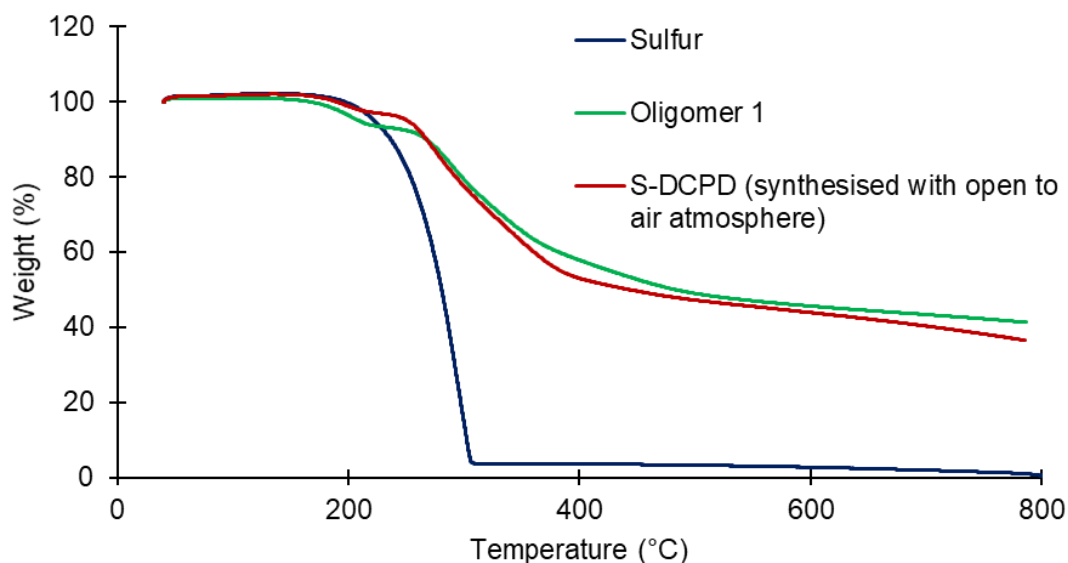
Figure 4.55: TGA analysis of elemental sulfur oligomer 1 and S-DCPD synthesised under an atmosphere open to air. Oligomer 1 revealed two mass losses. The first one starting at around 160 °C. The second mass loss occurs above 250 °C. The polymer synthesised under an atmosphere open to air showed two mass losses also. However, the onset of these mass losses was at slightly higher temperature then for oligomer 1. Further a total of 63.5 % of mass loss was recorded for the polymer synthesised under an atmosphere open to air compared to a mass loss of 63.5% for oligomer 1. Reproduced with permission from the Royal Society of Chemistry.[25]

XRD analysis of oligomer 1 was performed finely griding a small amount of material and placing it on a sample holder, the sample was then analysed according to the instrument settings outlined in the general considerations section.

For the LD-MS analysis a small amount of oligomer 1 was ground up using a mortar and pestle and suspended in 2 mL of methanol. Aliquots of 2 µL of suspension were placed on the LD-MS target plate until a layer of oligomer 1 had built up.
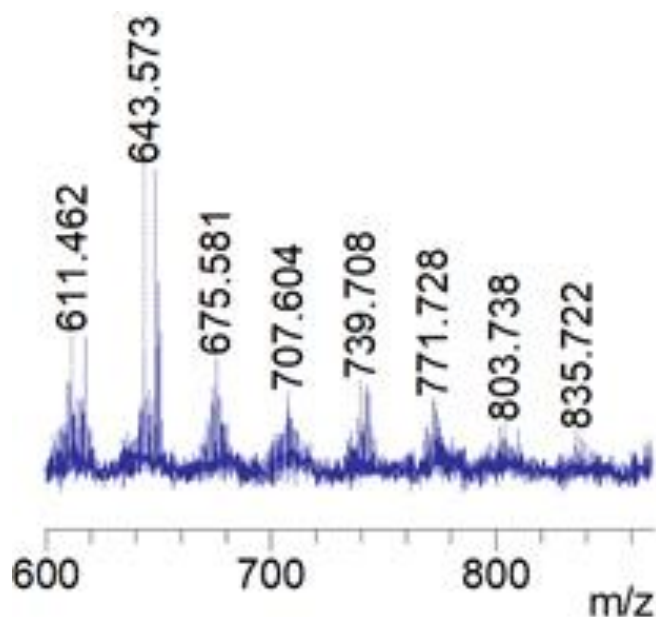
Figure 4.56: Laser desorption mass spectrometry (LD-MS) showing a distribution of species with a mass range spanning ~500-1000 Da. Peak separation of 32 mass units is consistent with a mixture of polysulfides. Reproduced with permission from the Royal Society of Chemistry.[25]

For GPC analysis of oligomer 1 a solution with a concentration of 2 mg/mL was prepared in HPLC grade chloroform. To calibrate the instrument a polystyrene standard was used.
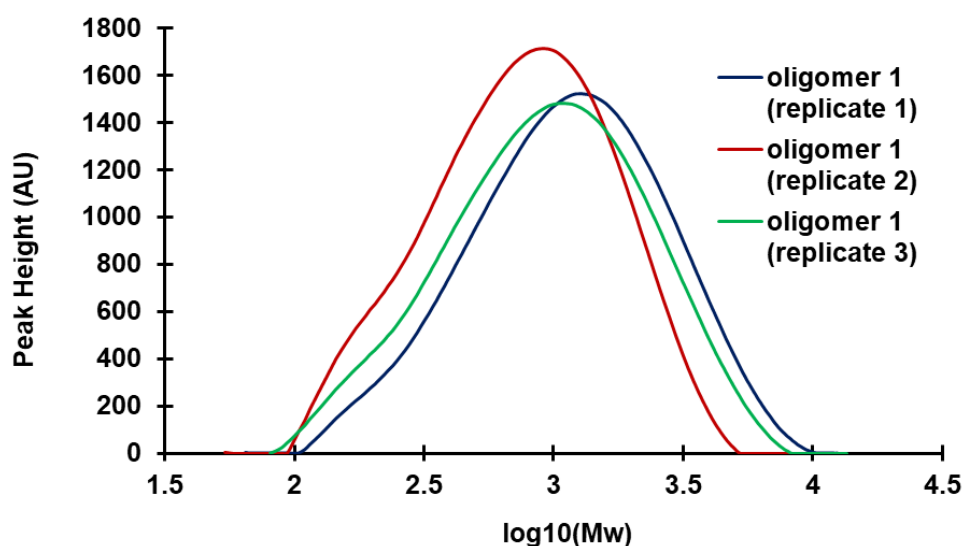
Figure 4.57: GPC analysis of oligomer **1** indicated an average M_w = 1099 ± 104 g mol^{-1} and Đ of 1.8. The analysis was run for three independently synthesised samples. (This analysis was based on a polystyrene calibration). Reproduced with permission from the Royal Society of Chemistry.[25]

To monitor the molecular weight of oligomer 1 during the synthesis, 3 g of DCPD and 3 g of sulfur were placed in a 20 mL glass vial together with a stirrer bar. Next, the vial was purged with nitrogen for 20 minutes. Following that the vial was placed in a pre-heated 140 °C hot block for 2 hours while being magnetically stirred at 500 RPM and kept under nitrogen atmosphere. After 30, 60, 90 and 120 minutes a sample was taking using a syringe. The samples were diluted to a concentration of 2 mg/mL in HPLC grade chloroform and analysed using GPC.
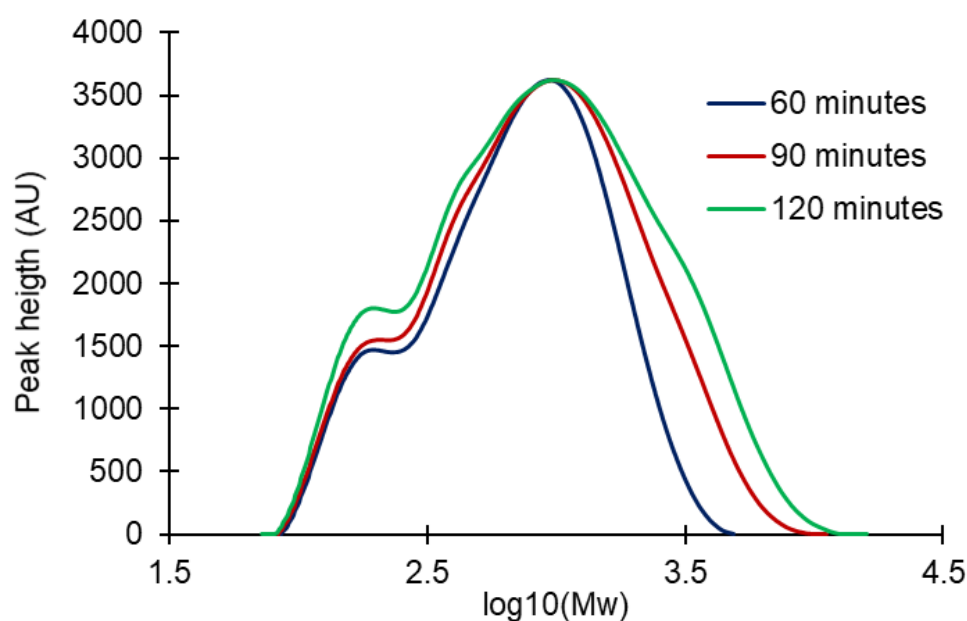
Figure 4.58: GPC analysis of the reaction mixture taken 60, 90 and 120 minutes reaction time showed polymer with similar Mw. The Mw after 60 minutes was 950, after 90 minutes 979 and after 120 minutes 979. (This analysis was based on a polystyrene calibration). Reproduced with permission from the Royal Society of Chemistry.[25]

The small peak at the left shoulder of the main peak was thought to be residue DCPD, yet, after a sample of DCPD was run no peak was observed at the Mw the shoulder can be seen. Therefore, it can be said that the shoulder is not DCPC but possible an additional oligomer produced during the polymer synthesis.

For the LiAlH$_4$ reduction, 41 mg of oligomer **1** was used. First, the sample and magnetic stirrer bars were added to a flame dried 25 mL round bottom flask. After that the reaction was purged with nitrogen for 20 minutes. A LiAlH$_4$ solution (approximately 1M) was prepared by weighing 377 mg of LiAlH$_4$ while maintaining a nitrogen atmosphere in a 20 mL glass vial. Next, 10 mL of anhydrous THF was carefully added

while under nitrogen. The solution was stirred for 10 minutes. Next, 2.5 mL of the LiAlH$_4$ solution was added to the reaction vessel using a glass syringe while maintaining a nitrogen atmosphere. Following that, the reaction was stirred for 24 hours.

After this time, the reaction was quenched using 5 mL of 1 M HCl. The acid was added slowly to accommodate the formation of hydrogen gas. After the reaction was quenched, 5 mL of cyclohexane was added to extract the organic material. Following the cyclohexane addition, the reaction was stirred for 1 hour.

Lastly, the organic fraction was separated using a 100 mL separating funnel and collected for analysis by GC-MS.
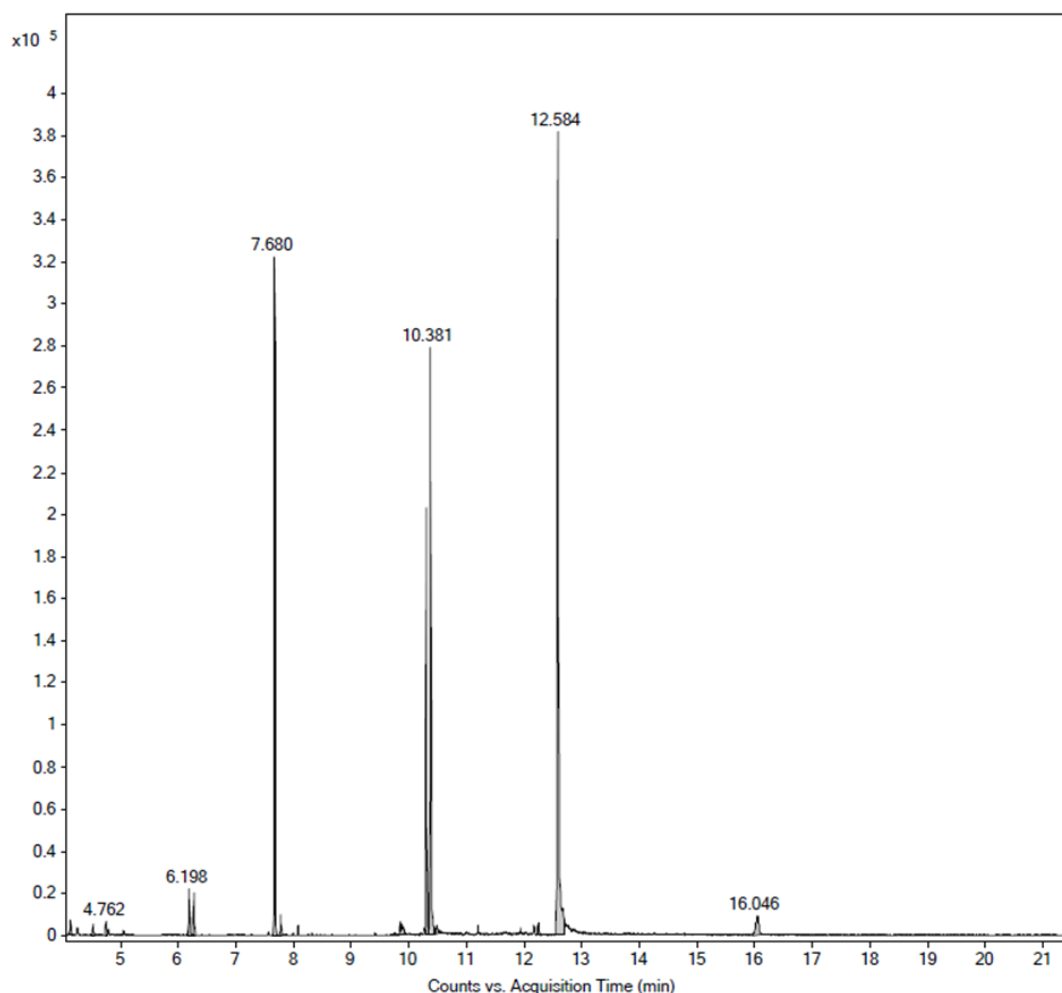
Figure 4.59: Gas chromatograph of the LiAlH$_4$ reduction of oligomer 1, showing four major products at retention times of 7.68, 10.31, 10.38, and 12.58 minutes. Reproduced with permission from the Royal Society of Chemistry.[25]

320
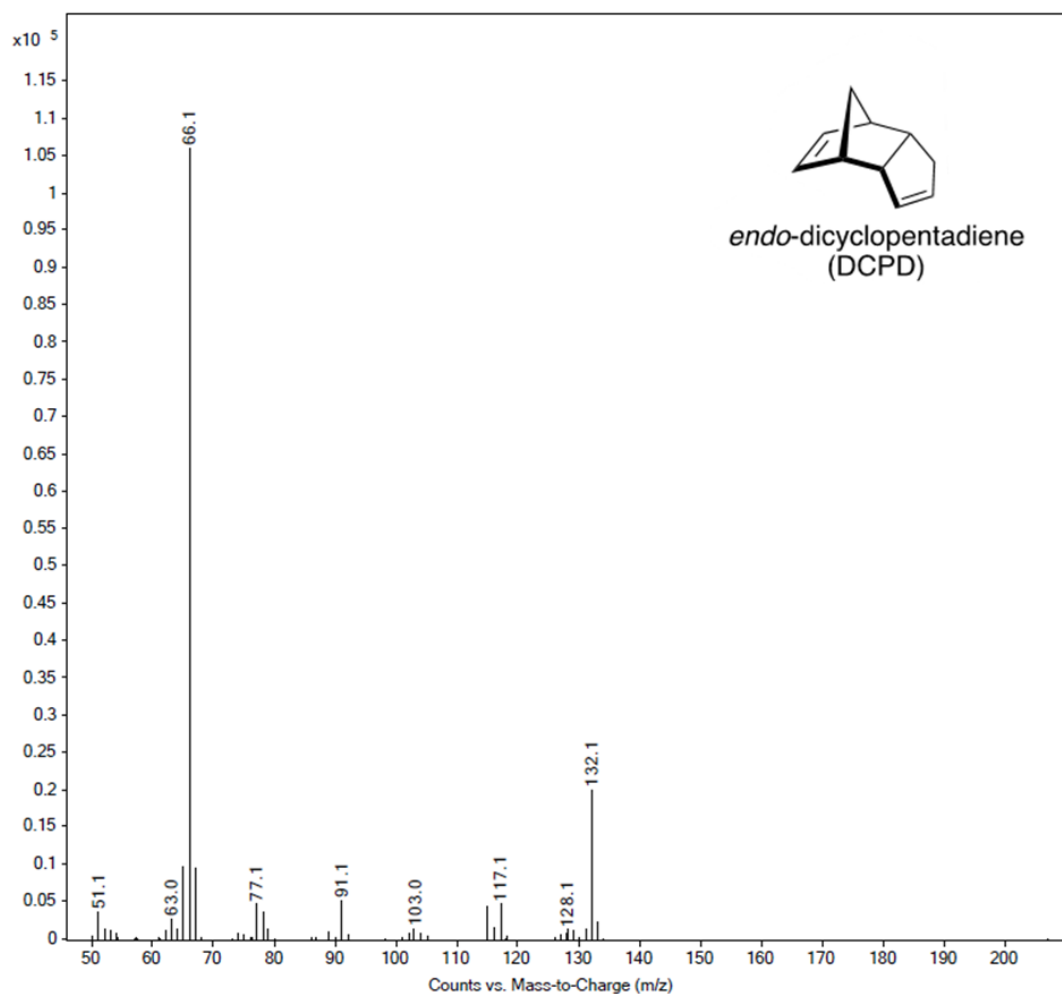
Figure 4.60: Mass spectrum of the peak at 7.68 minutes is consistent with that of DCPD. Since ^{1}H NMR indicated complete consumption of DCPD in the formation of oligomer 1, we propose that highly basic LiAlH[4] can convert oligomer 1 to DCPD via an elimination reaction. Reproduced with permission from the Royal Society of Chemistry.[25]
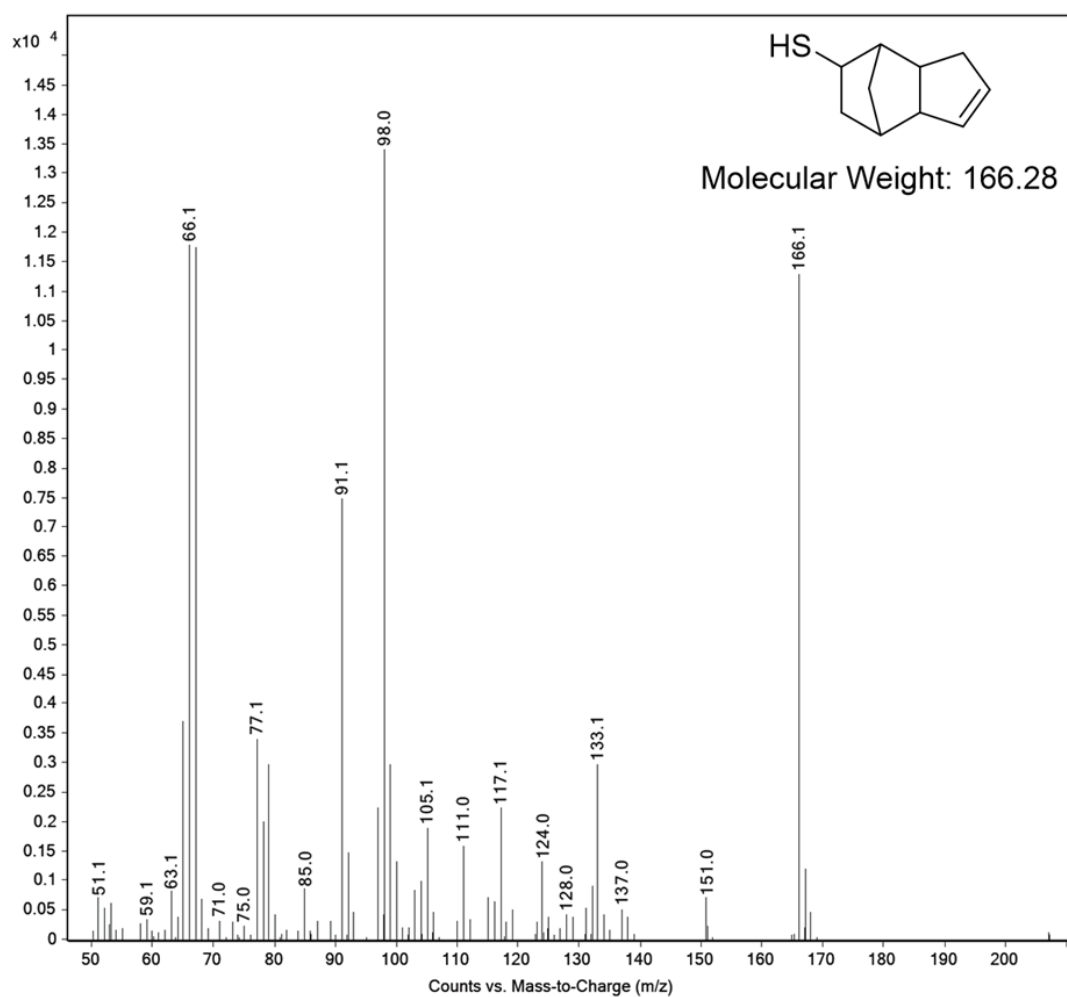
Figure 4.61: Mass spectrum of the peak at 10.31 minutes of the LiAlH₄ reduction of oligomer 1. We propose that the hydride can break C-S bonds, resulting in the desulfurised product. Note only one possible regioisomer of the thiol is shown. Reproduced with permission from the Royal Society of Chemistry.[25]
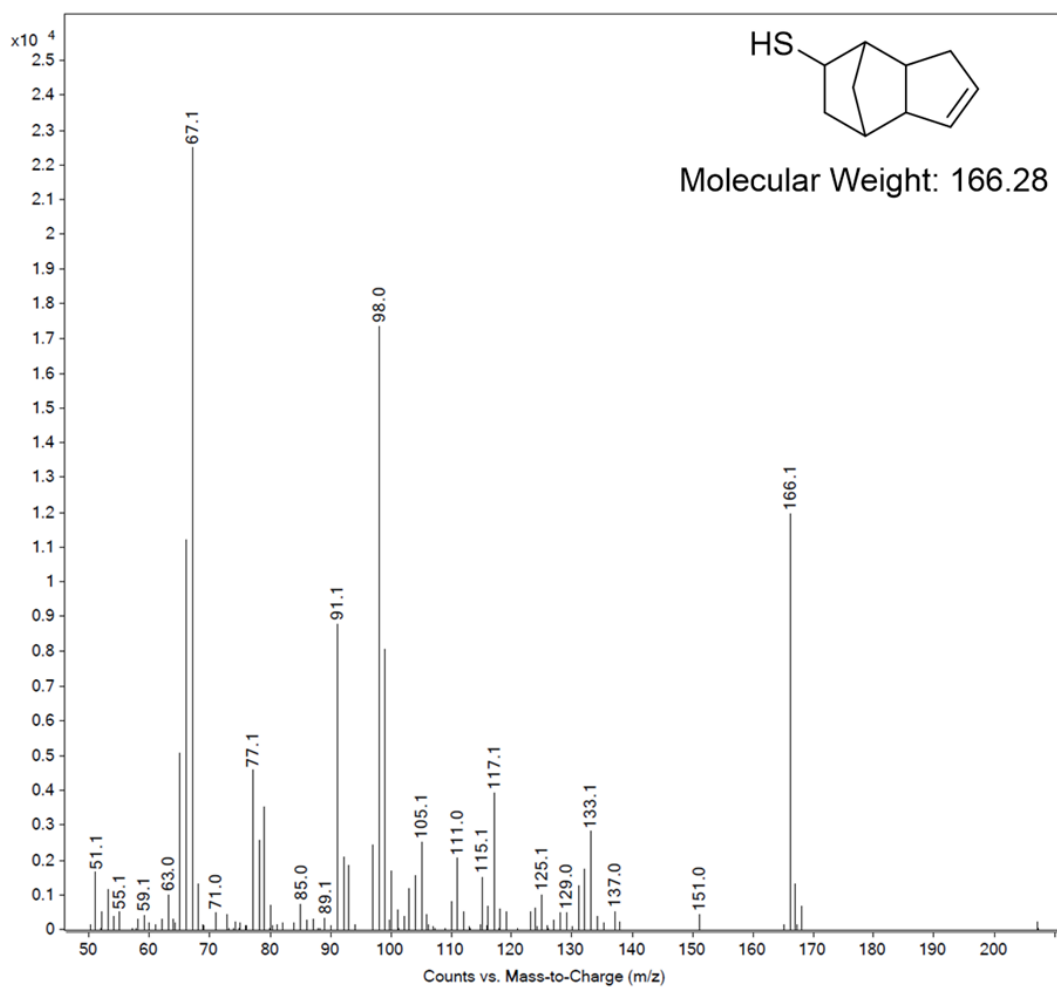
Figure 4.62: Mass spectrum of the peak at 10.38 minutes of the LiAlH$_4$ reduction of oligomer **1**. The proposed product could be a regio- or diastereoisomer of the compound associated with the peak at 10.31 minutes. (Only one potential regioisomer is shown). Reproduced with permission from the Royal Society of Chemistry.[25]

323
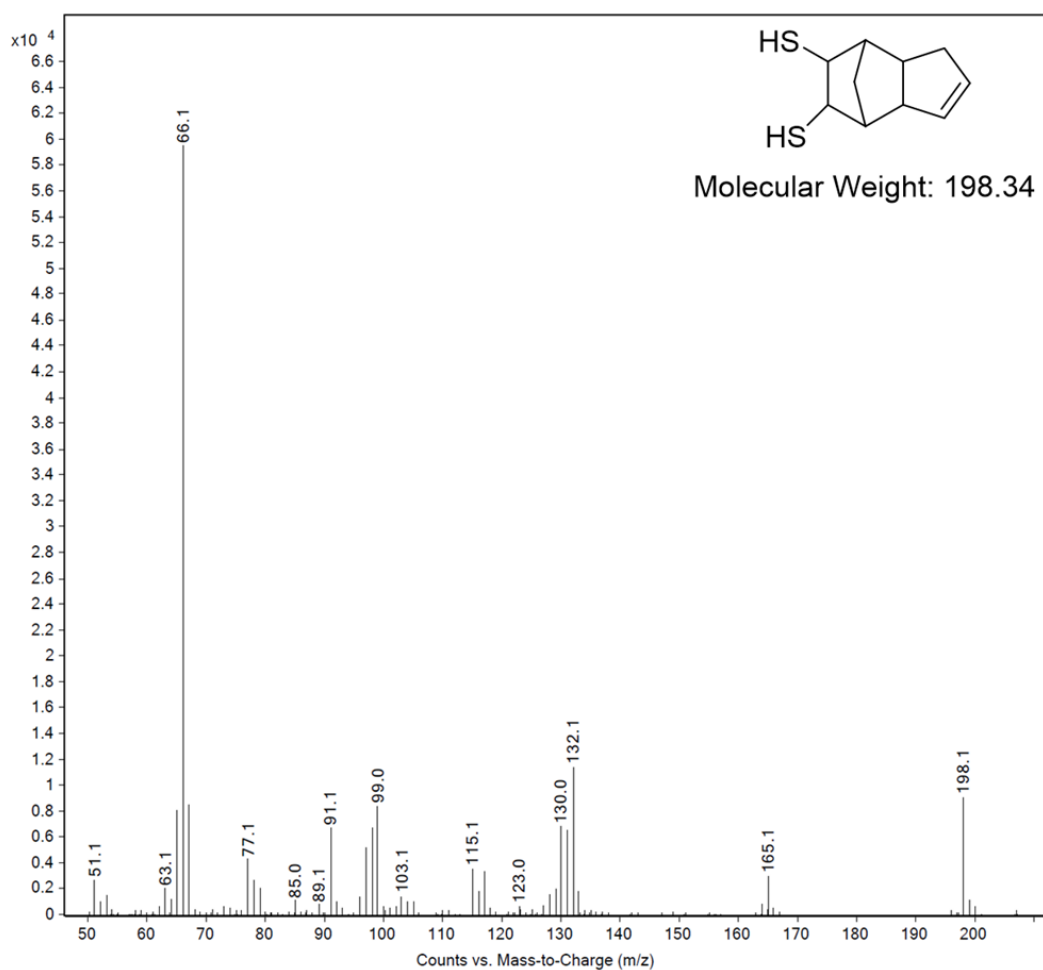
Figure 4.63: Mass spectrum of the peak at 12.58 minutes of the LiAlH$_4$ reduction of oligomer 1. This is the major product and the one expected to be formed upon reduction of the S-S bonds in oligomer 1. Reproduced with permission from the Royal Society of Chemistry.[25]
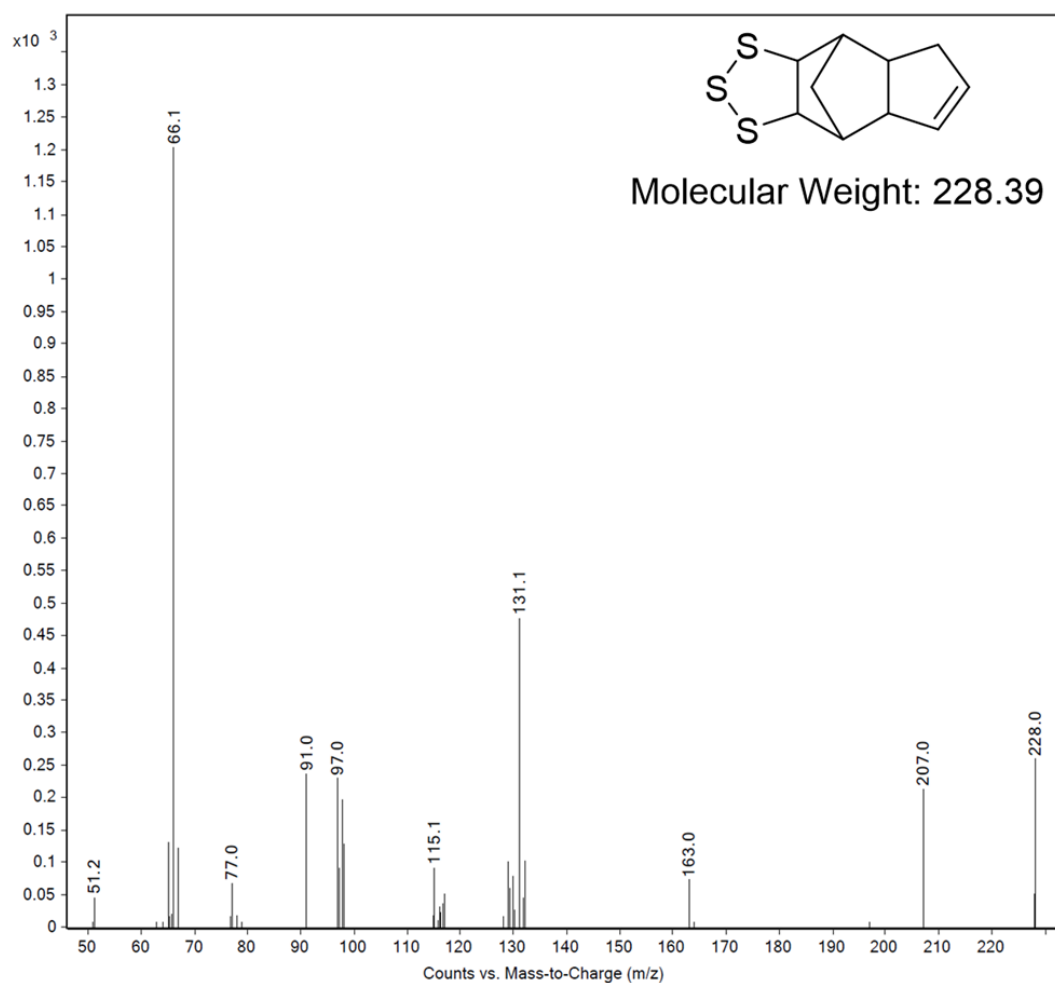
Figure 4.64: Mass spectrum of the of the peak at 16.1 minutes of the LiAlH₄ reduction of oligomer 1. This cyclic product could form via intramolecular cyclisation during the reduction. Reproduced with permission from the Royal Society of Chemistry.[25]

Characterisation of cured 1
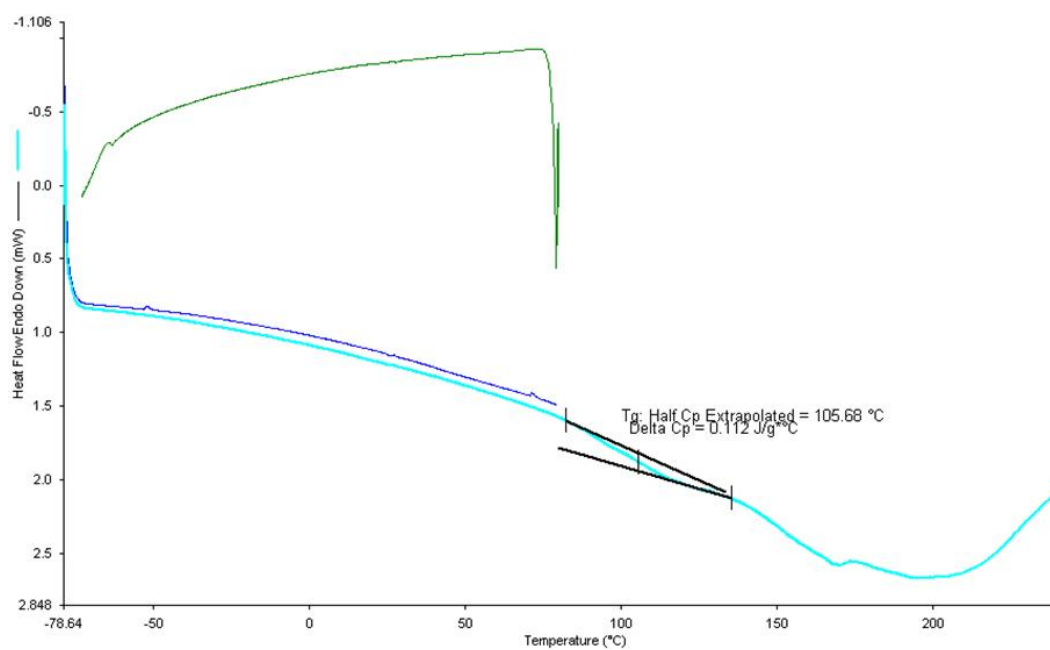
Figure 4.65: DSC of cured 1.

To assess its solubility 100 mg of cured **1** was added to 3 mL of solvent. The following solvents were used: DMF, THF, NMP, chloroform, ethyl acetate, acetone, methanol, isopropanol, and water. After 24 hours the polymers were removed from the solvents, rinsed with acetone, and dried under high vacuum overnight. The weight of the polymers before and after their exposure to the solvents was recorded. Since no weight loss was recorded for the cured 1 sample exposed to solvent, cured 1 has shown solvent resistance to all solvents used here.
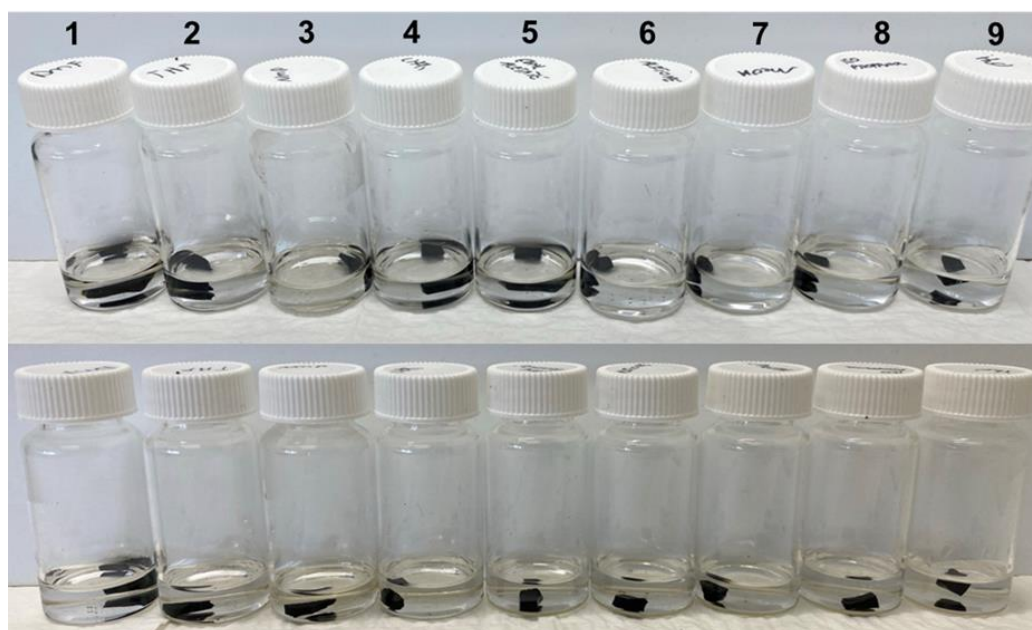
Figure 4.66: Cured 1 in solvents at 0 hours (top) and after 24 hours solvent exposure (bottom). Solvents: 1) DMF, 2) THF, 3) NMP, 4) Chloroform, 5) Ethyl acetate, 6) Acetone, 7) Methanol, 8) Isopropanol, 9) Water. Reproduced with permission from the Royal Society of Chemistry.[25]

AFM analysis (performed by Christopher Gibson)

Small pieces of oligomer **1** were placed on a silicon wafer and placed in an oven at 140 °C to cure for 24 hours. Thirteen 5 × 5 μm images were acquired on the polymer sample at separate locations. Average surface roughness (R_a), and root mean square (RMS), R_q, roughness analysis was performed on each AFM image. R_a and R_q roughness are standard analysis methods to report surface roughness using AFM. They differ in their mathematical description of roughness. Where R_q is the root mean square average of the height deviations taken from the mean image data line and R_a is the arithmetic average of the absolute values of the surface height deviations measured from the mean plane. In many instances they give different answers but do often follow the same trends between images as we observed in our case. It can be infered from examination of their definitions and formulas, that a single large peak or flaw within the microscopic surface texture will affect (raise) the R_q value more than the R_a value. The case of cured 1, although we saw differences between the absolute values for the R_a and R_q roughness for each AFM image the overall trends for both types of roughness analysis were similar. For the AFM images acquired the average roughness R_a = 0.37±0.07 nm and the RMS roughness R_q = 0.92±0.36 nm. The image in Figure 4.67 below is an example of one of the AFM images acquired of cured 1. While the roughness for the polymer over the regions examined is low compared to other polymers studied using AFM (for example R_a = 8.84 nm for a polymer made by Chalker et al[27] or R_a = 1-4 nm for a polymer made by Ellis et al[30]) Some imperfections are present on the surface, in some images, some particles or imperfections range from 6 to 46 nm and have an average height of 16 ± 14 nm. These are indicated on the AFM image by red arrows.
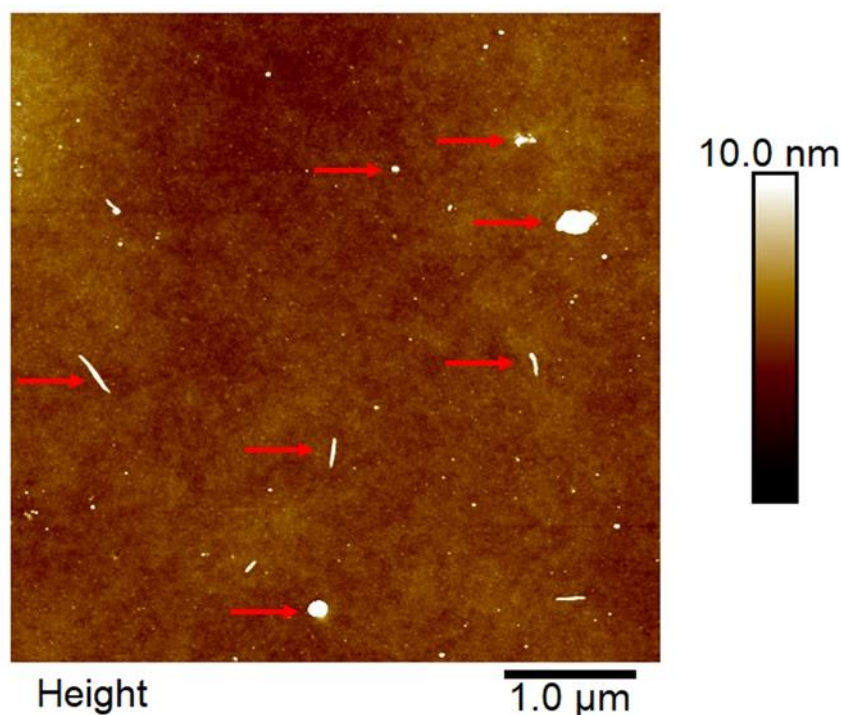
Figure 4.67: Representative AFM image of the surface of cured **1**. Red arrows indicate small particles on the surface. Reproduced with permission from the Royal Society of Chemistry.[25]

<u>Elastic modulus</u>

For all surface mechanical measurements, the force spectroscopy section of the Nanoscope software was used for analysis. Approximately 25 force curves were acquired at several locations across the polymer surface. The force curves were converted to indentation curves and the Hertz model was used to determine the elastic modulus. The Hertz model approximates the AFM tip as a sphere contacting an elastic surface which serves as a good model for the tip-surface interaction in our measurements. The equation for the Hertz model is given below[50]

$$F = E \left[(4/3)R^{1/2}\delta^{3/2}(1-v)^{-1} \right]$$

(1)

Where E is the elastic modulus, F is the applied force determined by the calibration of the cantilever sensitivity and spring constant[31] and extracted from the indentation curve, R is the AFM tip radius which is the nominal value provided by the manufacturer of 8 nm, δ is the indentation of the surface produced from the applied Force, F, and v is the Poission ratio which is approximated as 0.3 which is a value typical for polymers.[51] The Nanoscope software fits a curve, using the Hertz model, to the indentation curve and from this the elastic modulus is determined as a fit parameter. Only loading curves were

analysed to determine the elastic modulus as outlined in Kontomaris et al.[32] It was found that for applied forces less than 100 nN plastic deformation of the sample was minimized. This analysis resulted in a measured elastic modulus of 1.49 ± 0.36 GPa with the error in the measurement representing one standard deviation in the data. The elastic modulus is comparable to value reported for nylon, PVC and polycarbonate.[34]
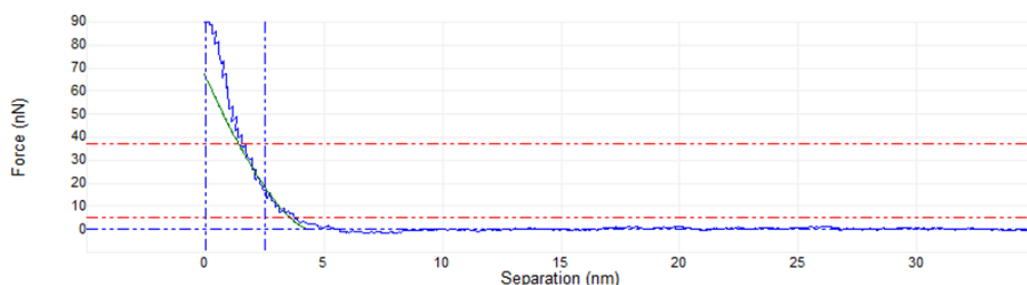
Figure 4.68: Example indentation curve (blue) acquired on the polymer surface. The green curve is the Hertz model fit which, for this particular curve, yielded an elastic modulus of 1.74 GPa. Reproduced with permission from the Royal Society of Chemistry.[25]

Hardness

For surface area hardness measurements, the maximum applied force and the area of the indent made by the AFM tip must be determined. The equation for determining hardness is below[50]

$$H = F_{max}/A_{indent}$$

(2)

Where H is the surface area hardness, F_{max} is the maximum applied force extracted from the force curve and A_{indent} is the area of the indentation produced by F_{max}. Approximately 25 force curves were acquired at several locations across the polymer surface with the maximum applied force ~ 2-2.5 µN. When the force curves were completed, typically over a 2x2 µm scan size, the areas were reimaged in tapping mode to produce the AFM images of the resulting indents. The area of the indents, A_{indent}, was determined using the specialised indentation section of the online analysis software Gwyddion version 2.59 and was, on average, ~ 10,000 nm^2. This analysis resulted in a measured hardness of 0.25 ± 0.09 GPa and 25.9 ± 9.6 for the surface area hardness and Vickers hardness, respectively. The error in each measurement represents one standard deviation in the data. This is comparable to hardness values reported for various polymers such as nylon, PMMA and polystyrene.[34, 35]
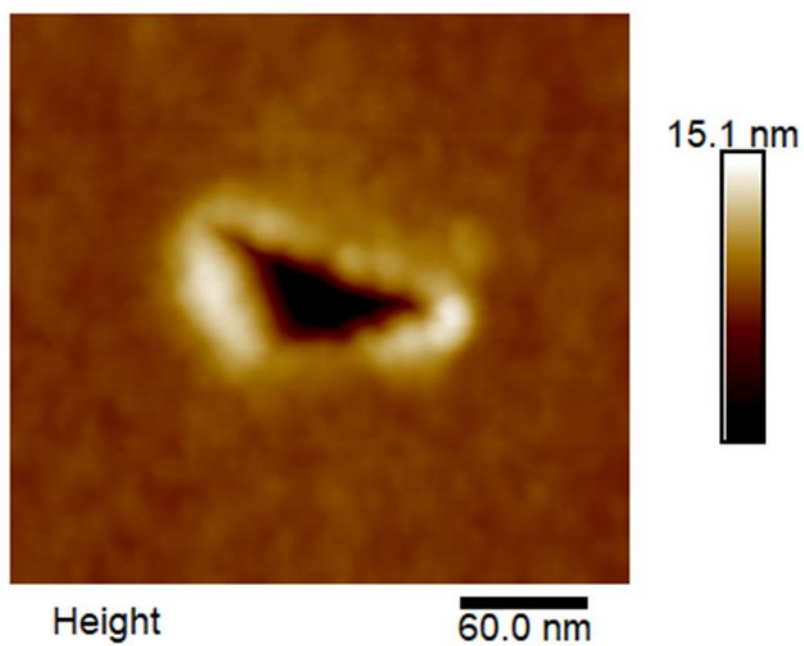
Figure 4.69: AFM image of an indentation acquired in tapping mode of cured 1. Reproduced with permission from the Royal Society of Chemistry.[25]

TGA analysis of cured 1
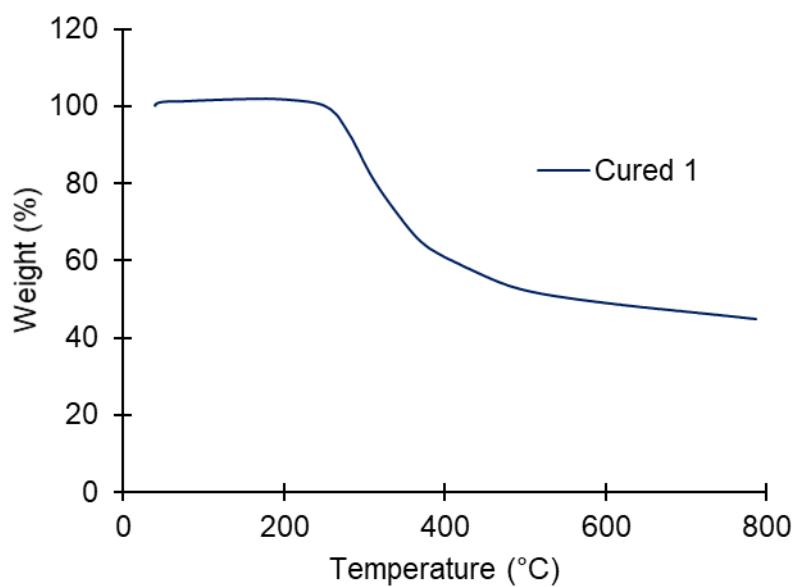
Figure 4.70: TGA of cured 1. Only one mass loss was seen with an onset at 250 °C. After heating the sample to 800 °C, 55.2% if the original mass was lost. Reproduced with permission from the Royal Society of Chemistry.[25]

The reduction of cured 1 was performed using the same method as for oligomer 1 already described previously.
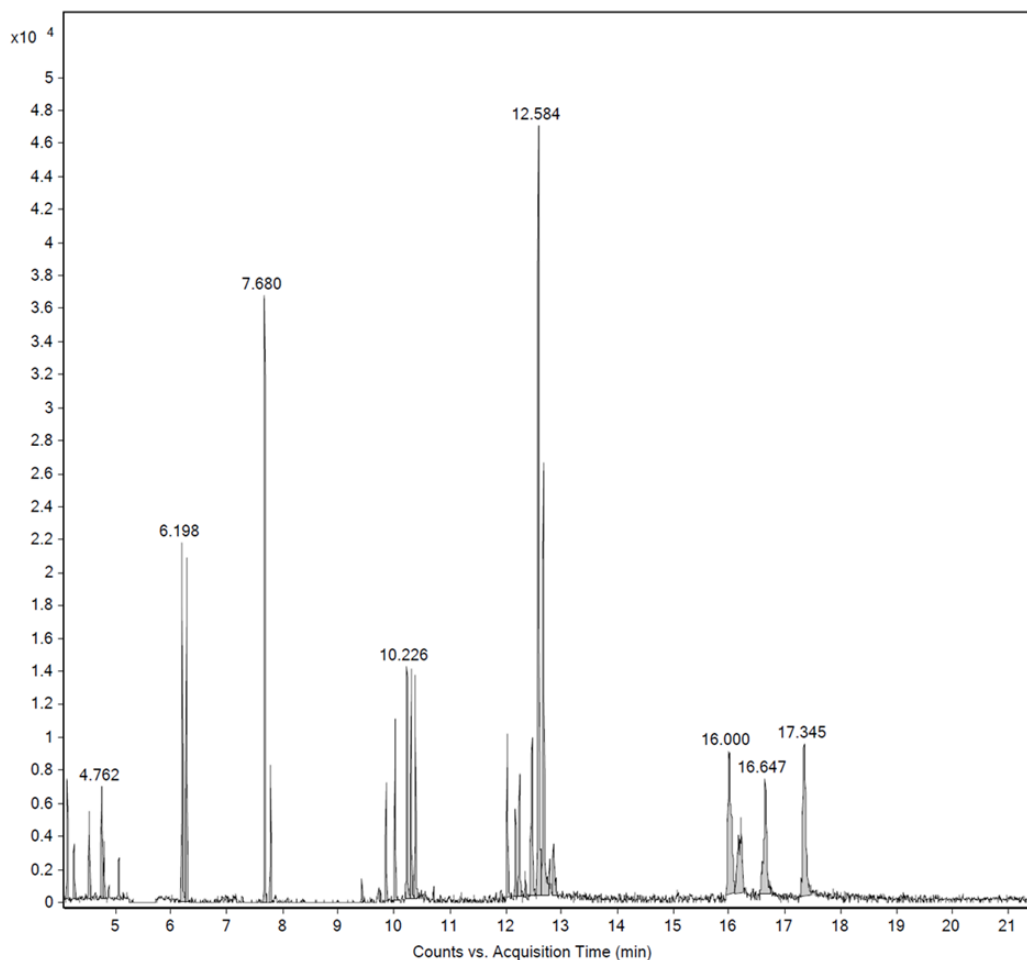
Figure 4.71: Gas chromatogram of the LiAlH$_4$ reduction of cured **1**. The product distribution is more complicated than for the reduction of oligomer **1**. We attribute this difference to additional crosslinking reactions via S-S metathesis of the polysulfide groups and also the reaction of the polysulfide with the unreacted alkenes in oligomer **1**. MS and proposed structures are provided for selected peaks on the subsequent pages. Reproduced with permission from the Royal Society of Chemistry.[25]
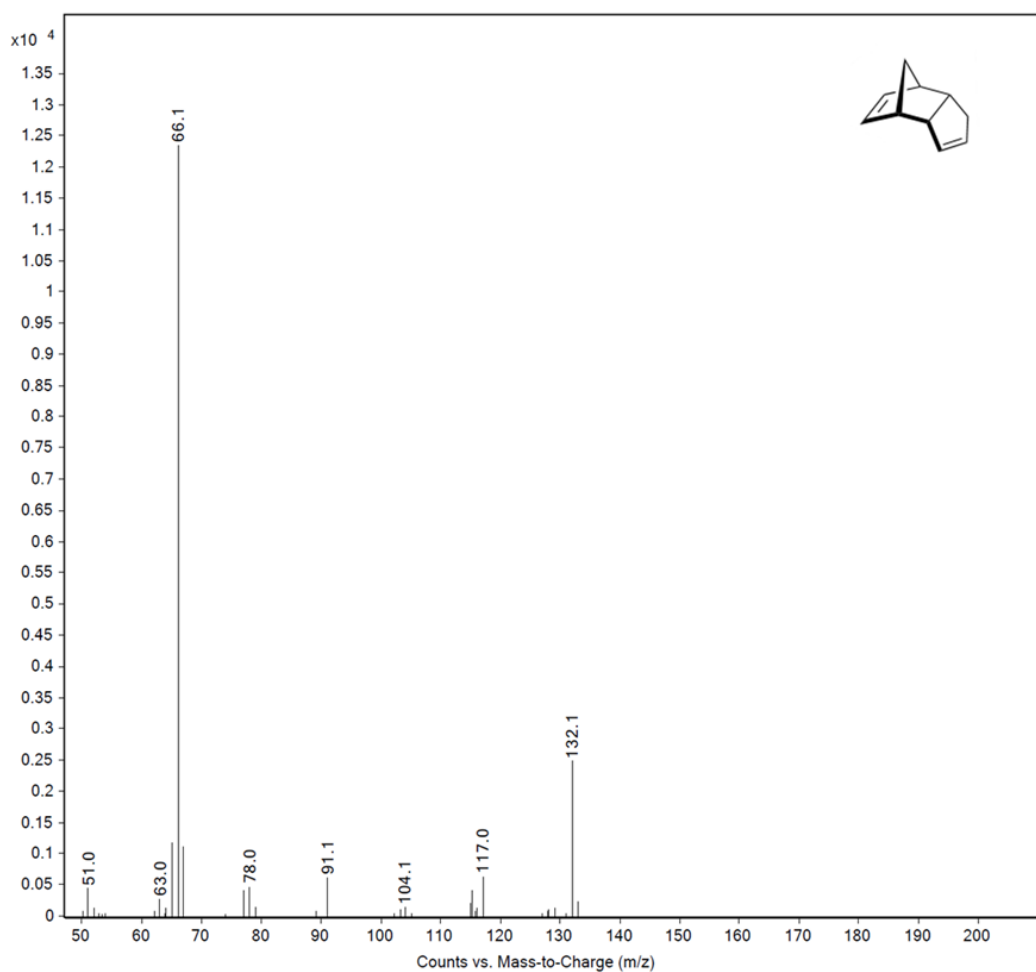
Figure 4.72: Mass spectrum of the peak at 7.68 minutes of the LiAlH$_4$ reduction of cured **1**. We propose that highly basic LiAlH$_4$ can convert cured **1** to DCPD via elimination reactions. Reproduced with permission from the Royal Society of Chemistry.[25]
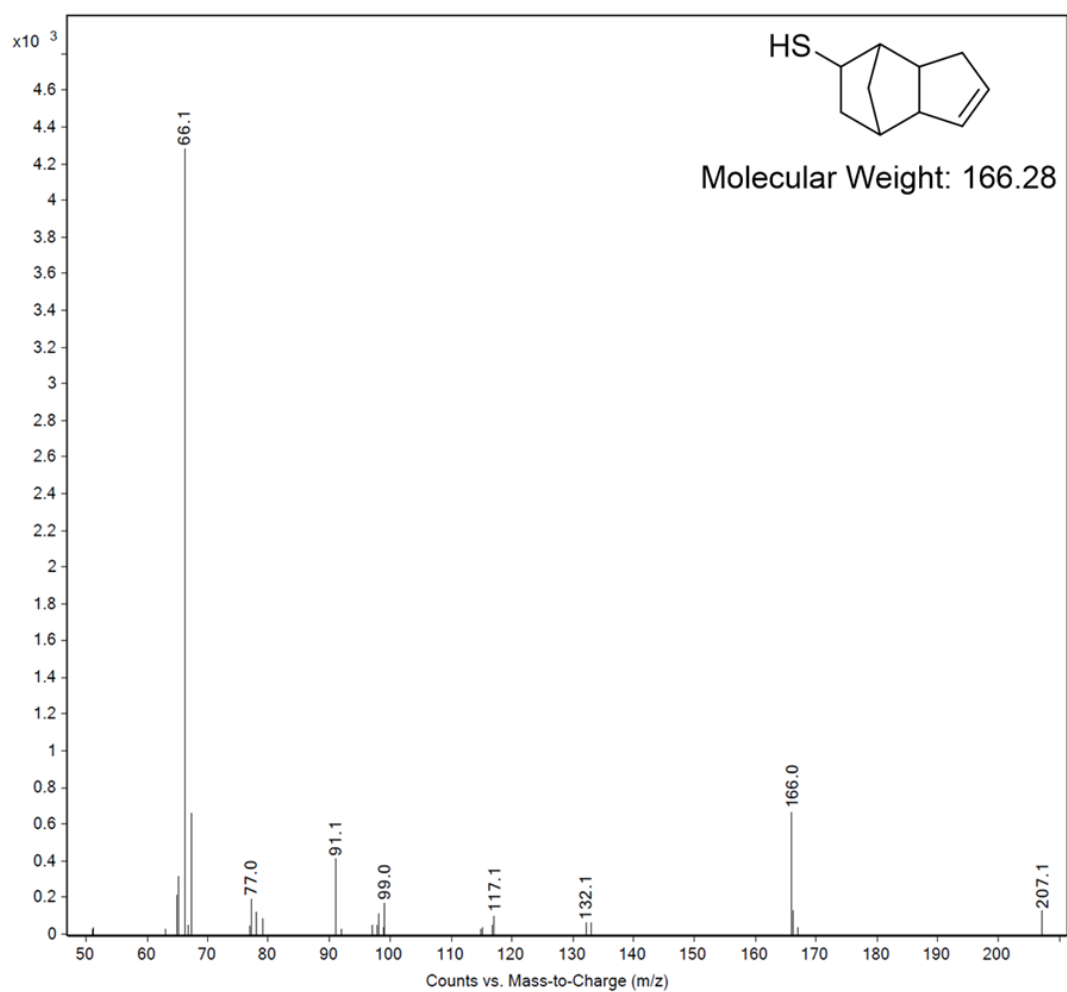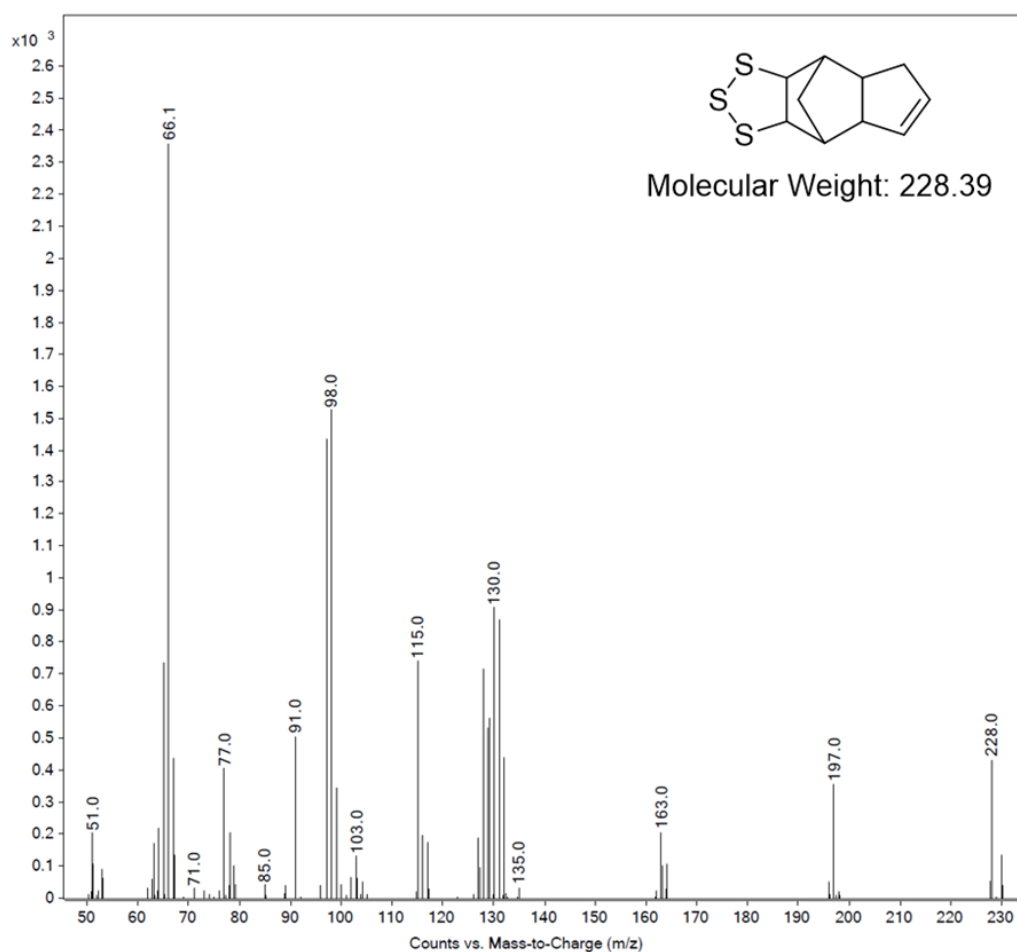
Figure 4.73: Mass spectrum of the of the peak at 10.23 minutes of the LiAlH$_4$ reduction of cured **1**. C-S bond cleavage by the hydride is proposed to account for the putative structure. Reproduced with permission from the Royal Society of Chemistry.[25]
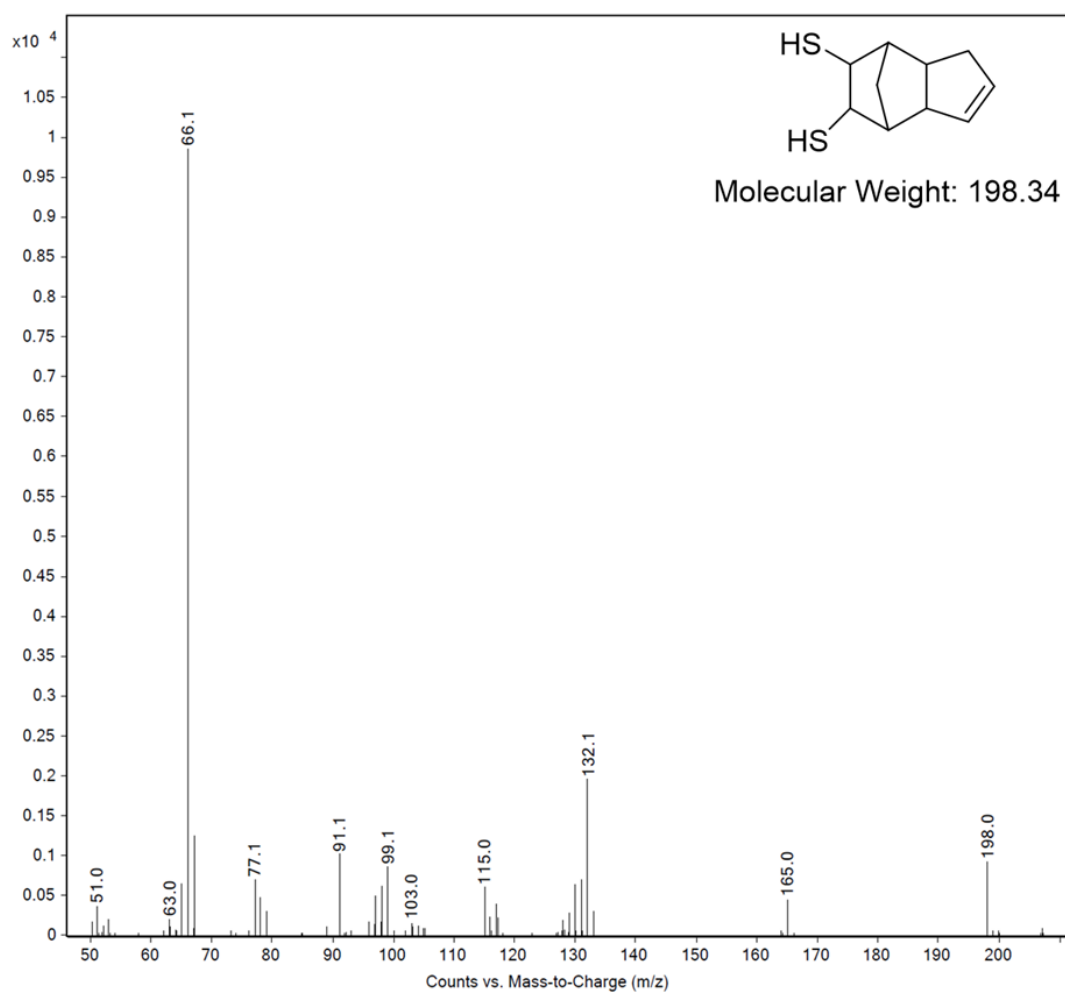
Figure 4.74: Mass spectrum of the peak at 12.58 minutes of the LiAlH₄ reduction of cured 1. The alkene of the putative structure may be from unreacted alkene after curing or the alkene could be formed via an elimination reaction. Reproduced with permission from the Royal Society of Chemistry.[25]
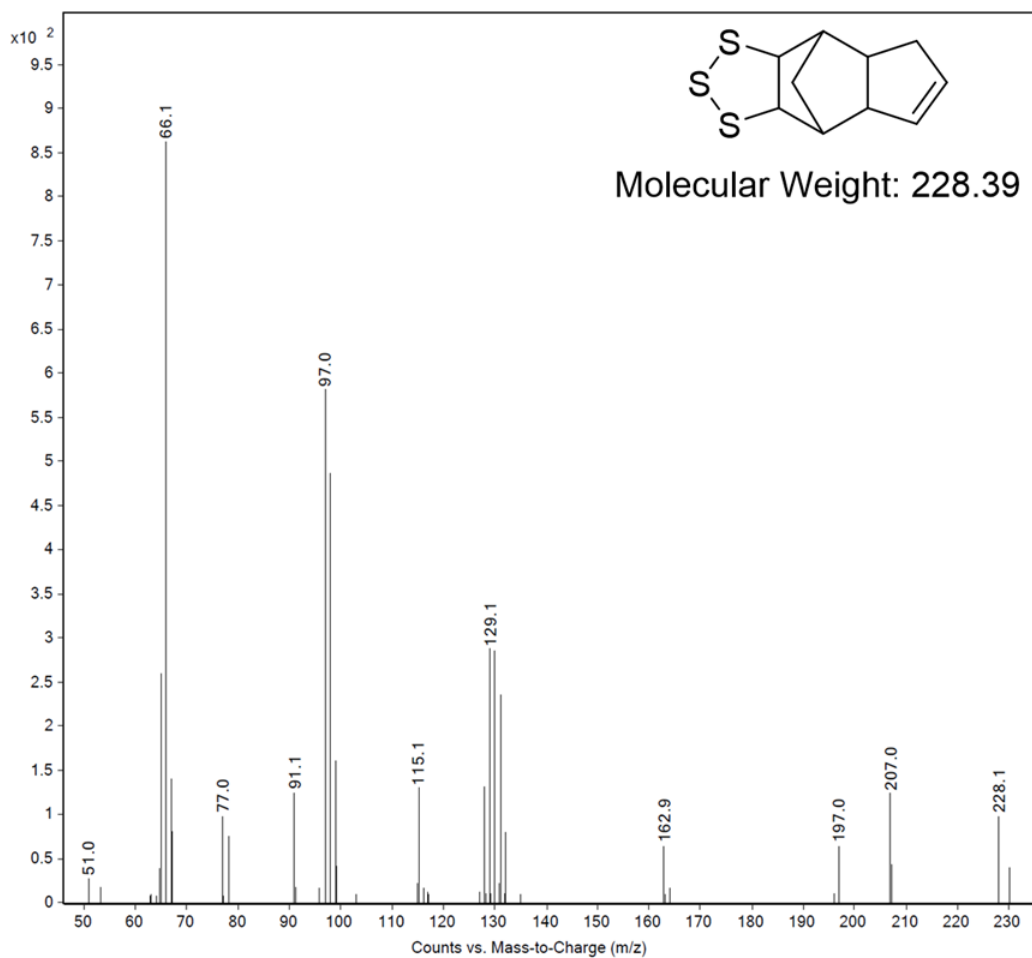
Figure 4.75: Mass spectrum of the of the peak at 16.0 minutes of the LiAlH$_4$ reduction of cured 1. Reproduced with permission from the Royal Society of Chemistry.[25]
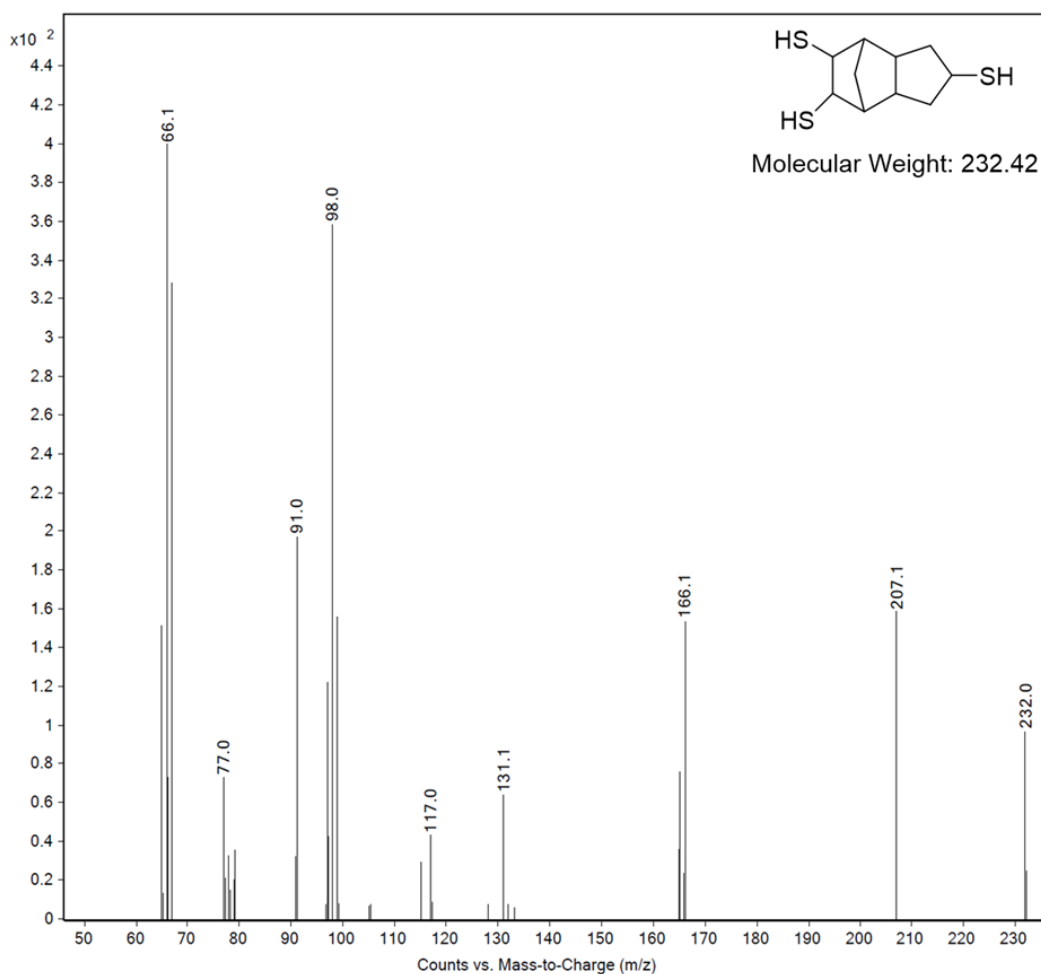
Figure 4.76: Mass spectrum of the peak at 16.21 minutes of the LiAlH$_4$ reduction of cured 1. Reproduced with permission from the Royal Society of Chemistry.[25]

The proposed structure is consistent with addition of sulfur groups to the unreacted alkene during curing process. C-S bond cleavage by the hydride is proposed to account for the odd number of sulfur atoms in the putative structure. Only one potential regio- and diastereoisomer is shown. For instance:

338
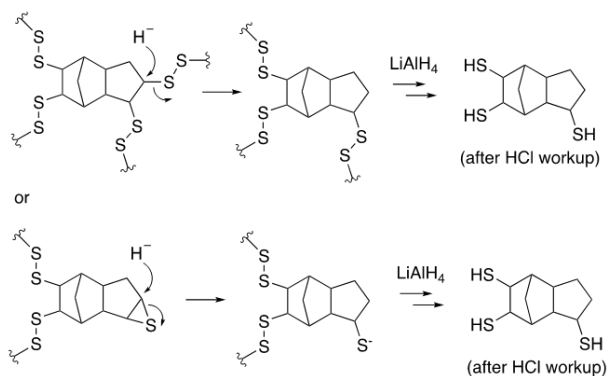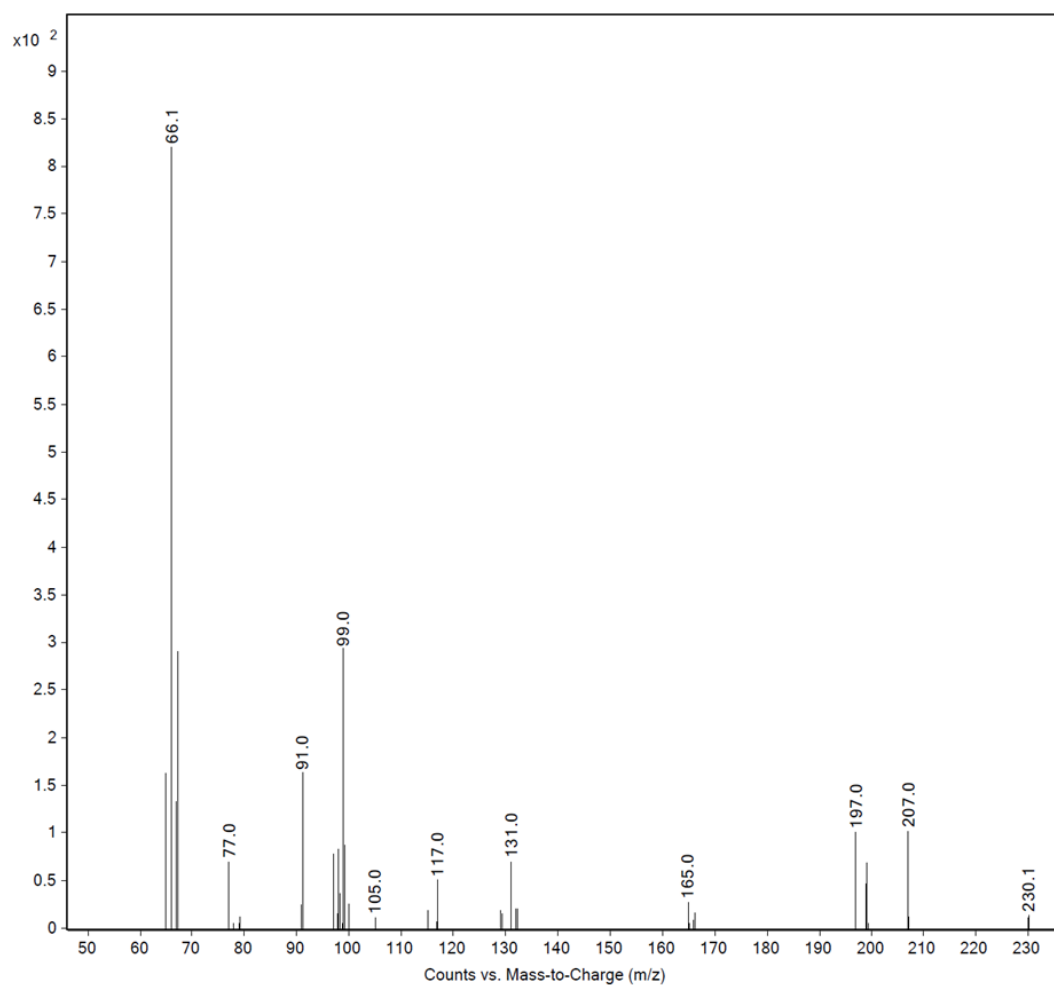
Figure 4.77: Mass spectrum of the peak at 16.65 minutes of the LiAlH$_4$ reduction of cured 1. The structure proposed is tentative. It is not clear if the episulfide, if present, is formed during the curing process or in the reduction with LiAlH$_4$. Reproduced with permission from the Royal Society of Chemistry.[25]
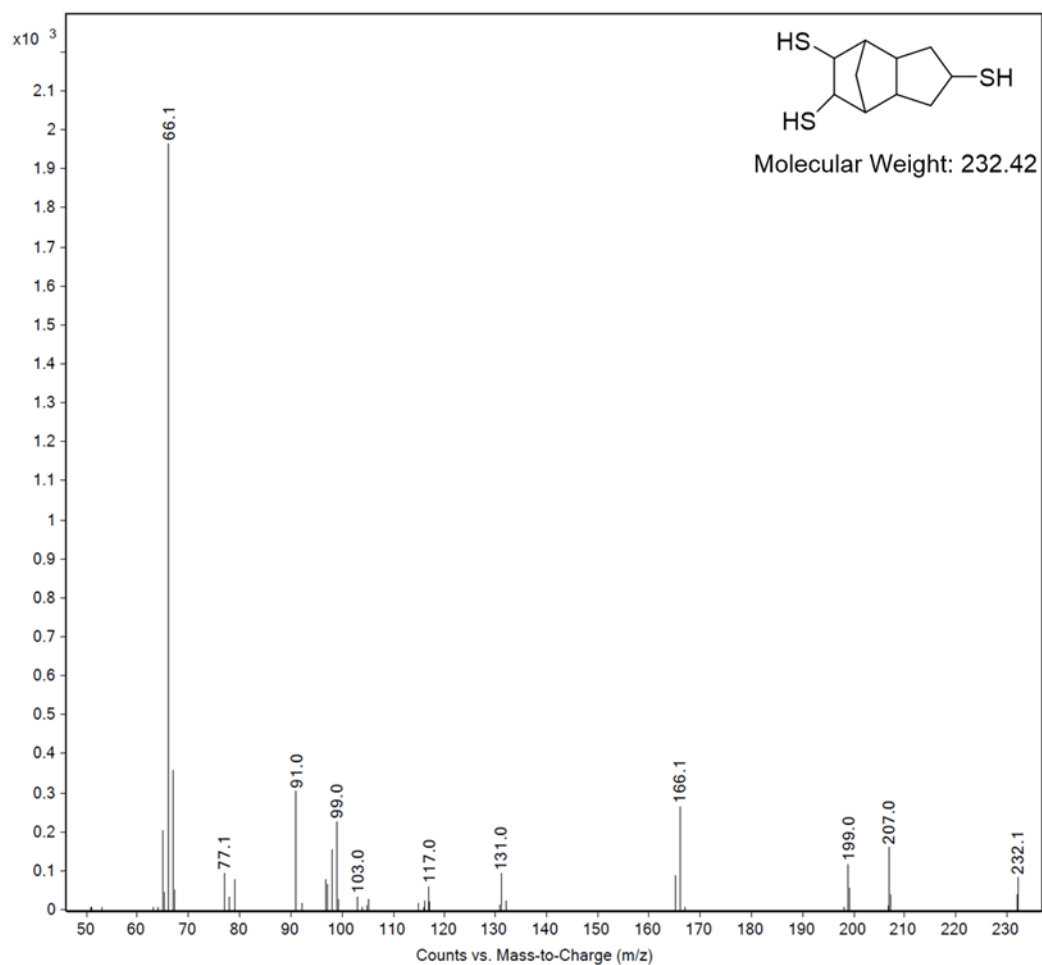
Figure 4.78: Mass spectrum of the peak at 17.35 minutes of the LiAlH$_4$ reduction of cured 1. Note that this product could be a structural or diastereoisomer of the compound detected at 16.21 minutes (only one possible isomer is shown). Reproduced with permission from the Royal Society of Chemistry.[25]

Recycling of cured 1

Cured **1** (4.4 g), NaBH$_4$ (9.68g) and a stirrer bar were added to a flame dried 1000 mL round bottom flask and purged with nitrogen for 20 minutes. After that dry THF (250 mL) was carefully added while under nitrogen. The flask was equipped with a condenser and then stirred at 50 °C for 24 hours while a nitrogen atmosphere was maintained. After this time, the reaction placed in an ice-bath and quenched with 1 M HCl. The acid was added very carefully and slowly so that the off gases generated could exit the flask. After the reaction was quenched, 150 mL of hexane were added to extract the organic material. Following the hexane addition, the mixture was stirred for 1 hour. Lastly, the organic fractions of both reactions were separated using a 1000 mL separating funnel and collected for GC-MS analysis.
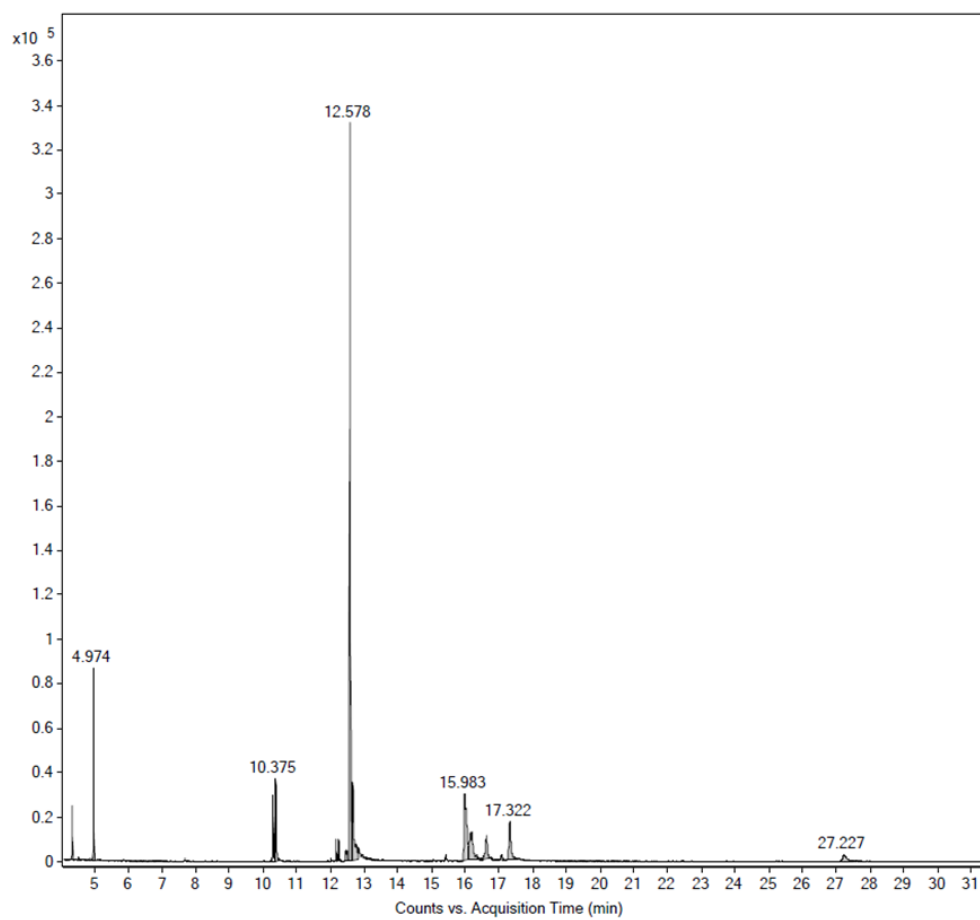
Figure 4.79: Gas chromatogram of the NaBH$_4$ reduction of cured 1. Reproduced with permission from the Royal Society of Chemistry.[25]
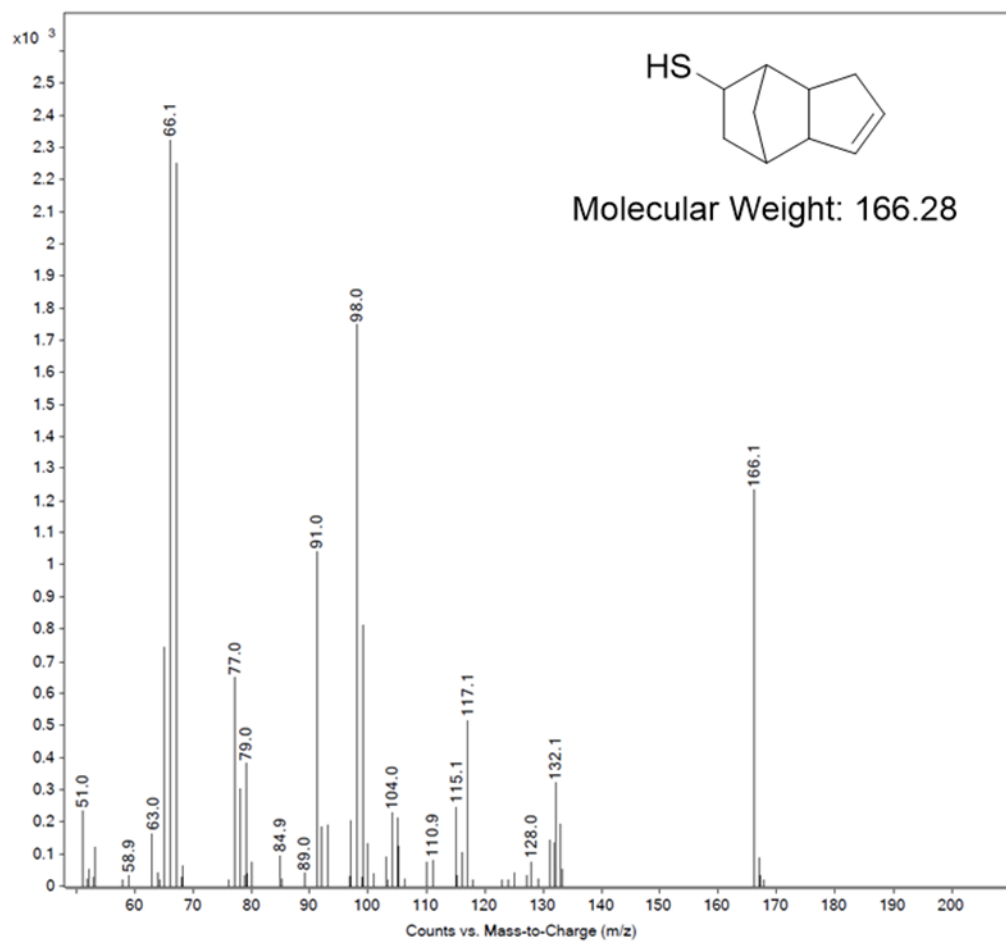
Figure 4.80: Mass spectrum of the of the peak at 10.38 minutes of the NaBH₄ reduction of cured **1**. C-S bond cleavage by the hydride is proposed to account for the putative structure. Reproduced with permission from the Royal Society of Chemistry.[25]
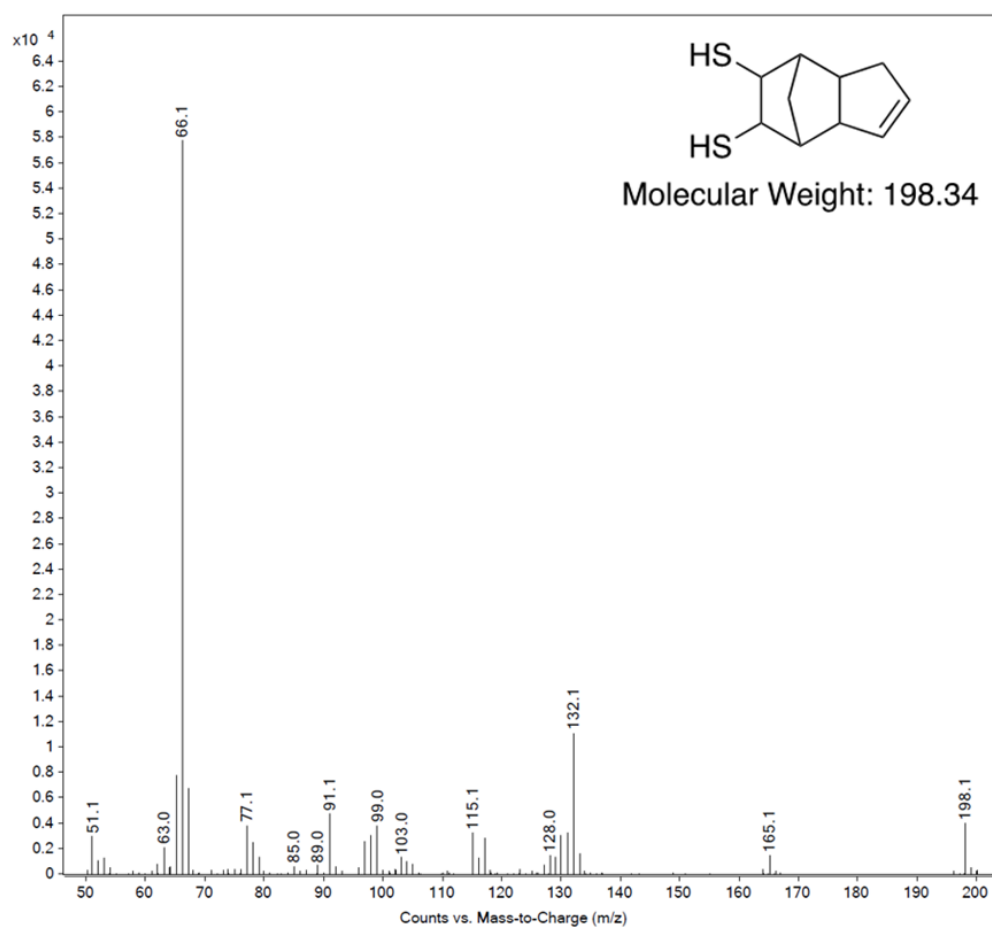
Figure 4.81: Mass spectrum of the peak at 12.58 minutes of the NaBH$_4$ reduction of cured 1. The alkene of the putative structure may be from unreacted alkene after curing or the alkene could be formed via an elimination reaction. Reproduced with permission from the Royal Society of Chemistry.[25]

Figure 4.82: Mass spectrum of the of the gas chromatogram peak at 15.98 minutes of the NaBH₄ reduction of oligomer 1. Reproduced with permission from the Royal Society of Chemistry.[25]

This is the major product of the reduction under these conditions. The cyclic trisulfide is proposed to form during the reduction:
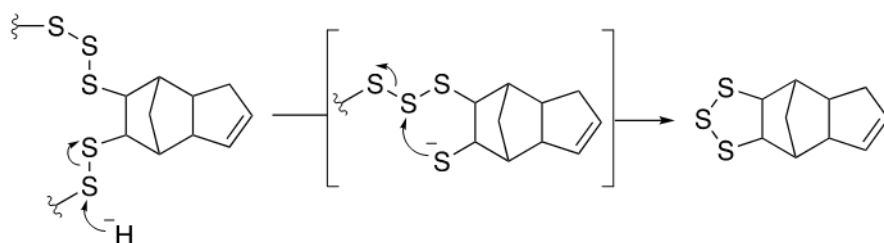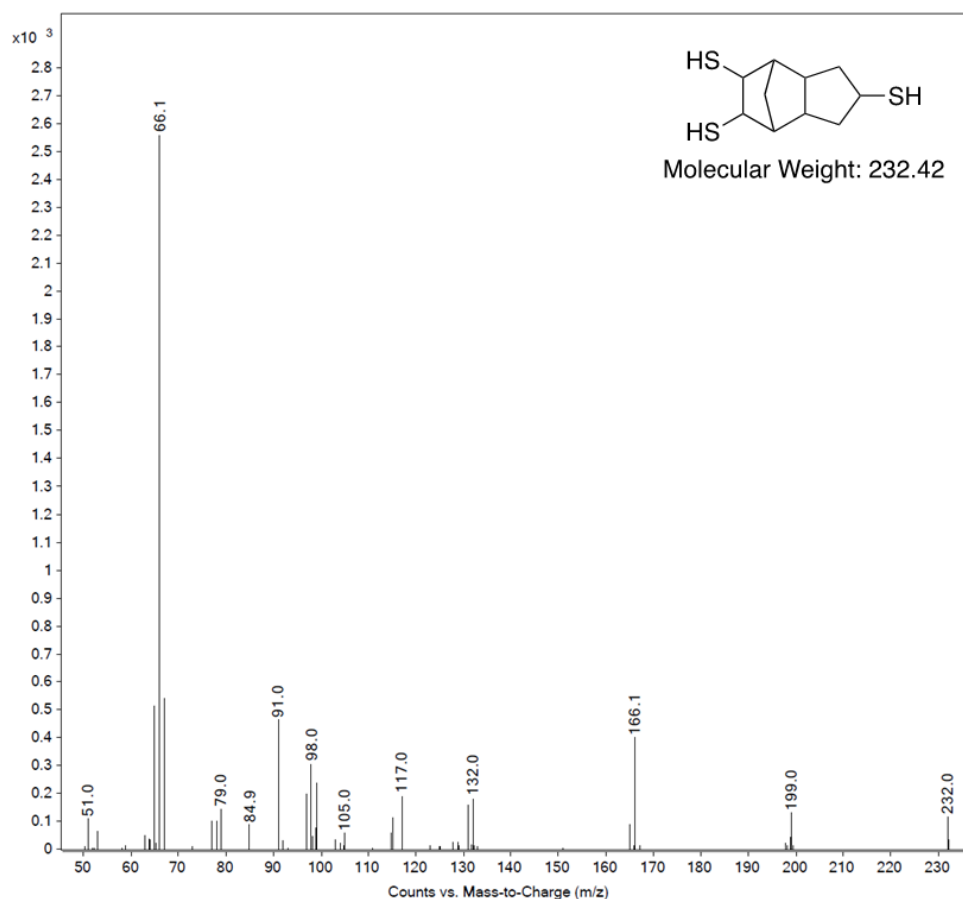
Figure 4.83: Mass spectrum of the peak at 17.32 minutes of the NaBH₄ reduction of cured 1. Reproduced with permission from the Royal Society of Chemistry.[25]

After the organic material was extracted, the hexane was removed using a rotary evaporator. Next some of the sample was transferred into a silicon mould and dried under high vacuum overnight. After the sample was dried under vacuum, the sample was cured for 24 hours in a 140 °C oven. Before the curing process the sample had a waxy consistency. After the during process, the sample was hard and brittle.
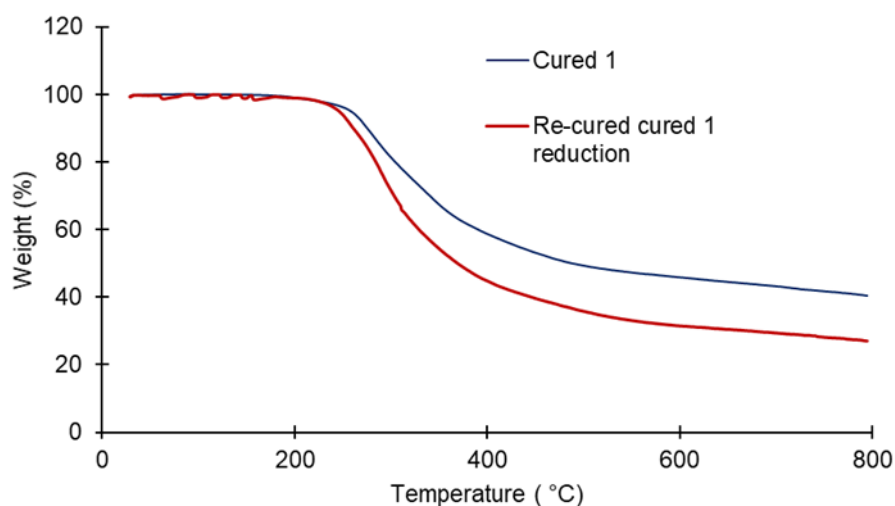
Figure 4.84: STA analysis of cured **1** and cured **1** after reduction and subsequent curing. The first mass loss of cured **1** is around 250 °C whereas the reduced and again cured sample has a mass loss at lower temperatures at around 225 °C. Further, after heating to 800 °C the reduced and cured sample lost a total of 72% of its mass which is 13% more than cured 1 which only lost 59% of its mass. Reproduced with permission from the Royal Society of Chemistry.[25]
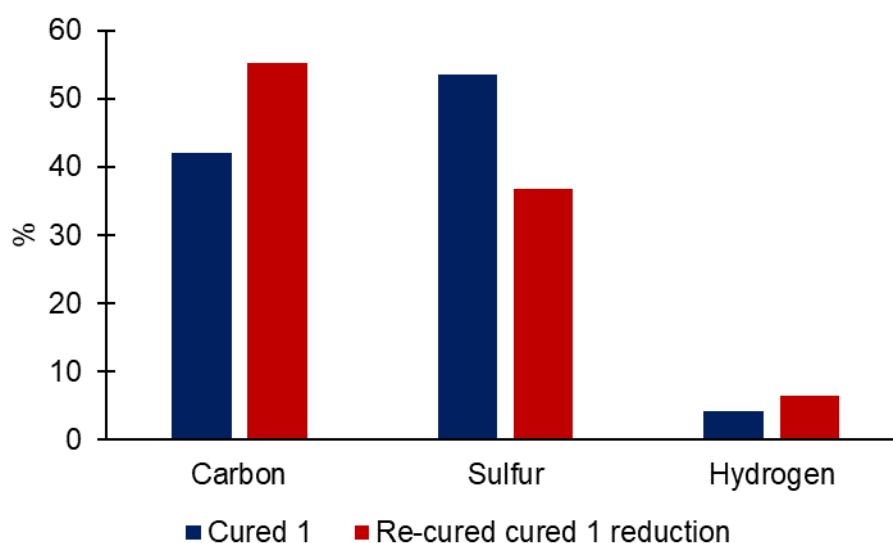
Figure 4.85: Elemental analysis of cured 1 and the cured reduction products of cured 1. While there is only minimal difference in the hydrogen content, the sulfur and carbon content show differences. Cured 1 had higher sulfur content and lower carbon content compared to the reduced and cured product. On the other had the cured produced of the cured 1 reduction shows a lower sulfur and higher carbon content. Reproduced with permission from the Royal Society of Chemistry.[25]

To conduct the solubility studies approximately 100 mg of cured **1** was added to 3 mL of solvent. The following solvents were used: DMF, THF, NMP, chloroform, ethyl acetate, acetone, methanol, isopropanol, and water. Immediately after the polymer was added to the solvents the polymer started to dissolve in THF, NPM and chloroform. After 30 minutes all the polymer had dissolved in THF and chloroform. At 60 minutes the polymer had dissolved in NMP. The polymer in DMF began do dissolve after around 1 hour and after 24 hours 60% by weight had dissolved. Very slight solvation (1.4 % by mass) was observed in acetone. No solvation was observed in ethyl acetone, methanol, isopropanol, or water.
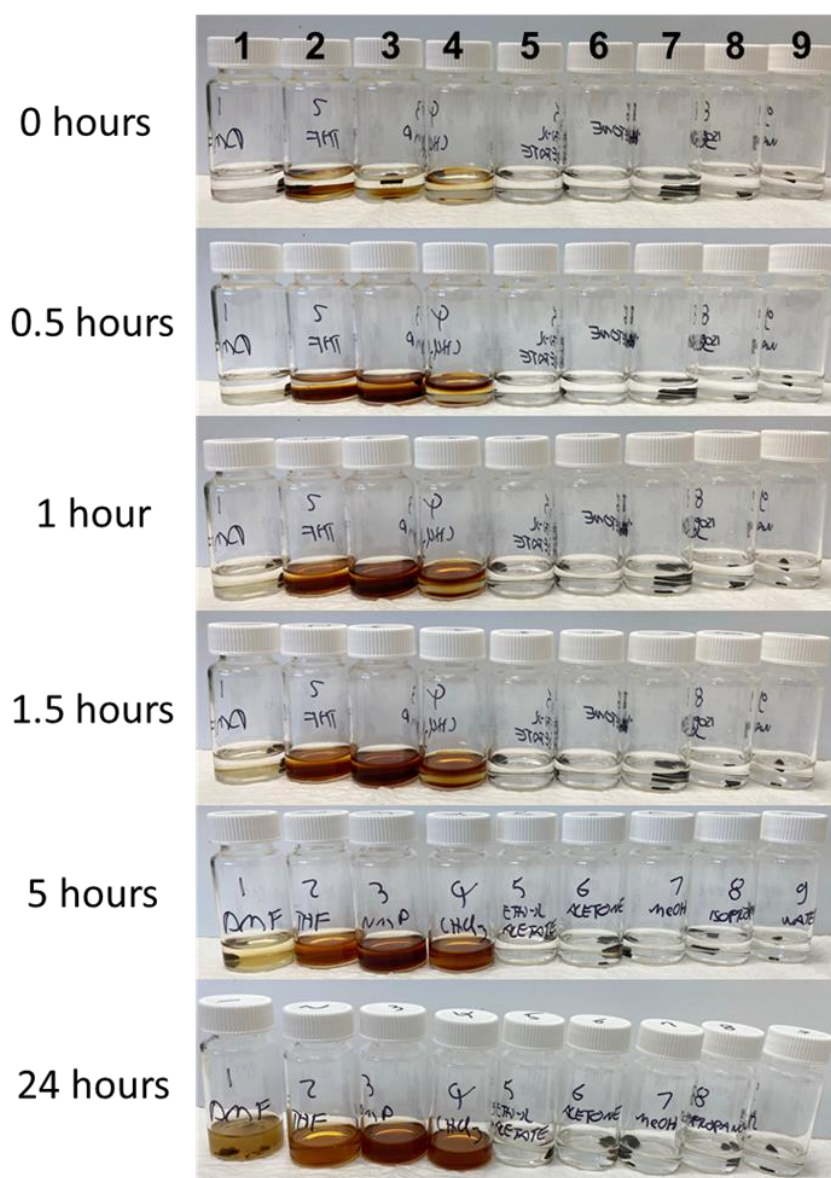
Figure 4.86: Images of cured **1** in solvents at 0 hours (top) and after 24 hours solvent exposure (bottom). Solvents: 1) DMF, 2) THF, 3) NMP, 4) Chloroform, 5) Ethyl acetate, 6) Acetone, 7) Methanol, 8) Isopropanol, 9) Water. Reproduced with permission from the Royal Society of Chemistry.[25]

Coating applications

To coat silica gel, 1.66 g of oligomer **1** was dissolved in 150 mL of chloroform in a 250 mL round bottom flask before 16.6 g of silica gel was added. After stirring the solution for 20 minutes the solvent was removed by rotary evaporation. To cure oligomer **1** on the silica gel, the coated silica gel was placed in a 140 °C oven for 24 hours. To wash the cured coated silica gel, 15 mL of chloroform were added to 2 g of coated and cured silica gel. The washing process involved filtering the silica gel using vacuum filtration, recovering the silica gel, and placing it back in the glass vial before the next 15 mL of chloroform were added. Then, the mixture was briefly stirred, and the filtration process was repeated. The washing process was performed 8 times. An image of the coated silica and the chloroform is shown below for each wash:
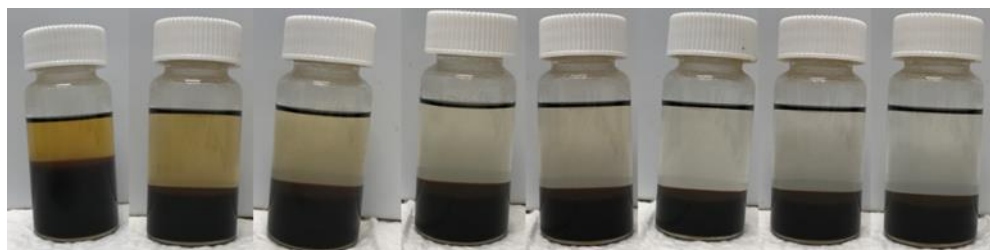
Figure 4.87: Consecutive washing of cured coated silica gel with 15 mL aliquots of chloroform. Reproduced with permission from the Royal Society of Chemistry.[25]

The washing was done 8 times with 15 mL of chloroform in each wash, showing that the curing process rendered the polymer coating insoluble. It should be noted in the first three washes there is some trace soluble material (indicated by the darker liquid phase), but the remaining cured polymer was not removed from the silica after repeated washing. The final coated silica gel was recovered by filtration, air dried, and then evaluated in mercury sorption.

Mercury removal using polymer coated silica gel (from aqueous solution)

In order to test the mercury uptake, silica gel was coated with oligomer **1** as previously described. A 14 g portion of the coated silica gel was cured in an oven at 140

°C for 24 hours. Following that, 2 g of the cured oligomer **1** coated silica gel was washed with 7 aliquots of 15 mL chloroform as described above. Next, 45 mL of a 5 ppm aqueous solution of $HgCl_2$ was added to each of 13 separate 50 mL plastic tubes. One of these solutions served as control with no silica gel added to monitor the Hg concentration. The following experimental samples were then prepared in triplicate:

a) 100 mg of uncoated silica gel was added to 45 mL aqueous $HgCl_2$ (5 ppm)

b) 100 mg of the silica gel coated with uncured oligomer **1** was added to 45 mL aqueous $HgCl_2$ (5 ppm)

c) 100 mg of the silica gel coated with cured **1** (not washed with $CHCl_3$) was added to 45 mL aqueous $HgCl_2$ (5 ppm)

d) 100 mg of the silica gel coated with cured **1** (washed with $CHCl_3$) was added to 45 mL aqueous $HgCl_2$ (5 ppm)

After the silica gel was added the samples were rotated at 25 RPM for 2 hours. Samples for analysis were taken before the silica gel addition and at 0.5, 1.0, 1.5 and 2 hours. Samples were taken by removing 1 mL of solution and centrifuging the sample to separate the silica gel from the sample. Then, 0.7 mL of sample was stabilised in 5 % HCl and made up to a volume of 7 mL. The samples were analysed using CVAAS.

	Sample	Mercury removed after 2 hours
a) —	5 ppm Hg^{2+} solution (no sorbent)	0%
b) —	Uncoated Silica Gel	14%
c) —	Silica coated with oligomer 1, uncured (unwashed)	> 99%
d) —	Silica coated with oligomer 1, cured (unwashed)	92%
e) —	Silica coated with oligomer 1, cured (washed with chloroform)	93%
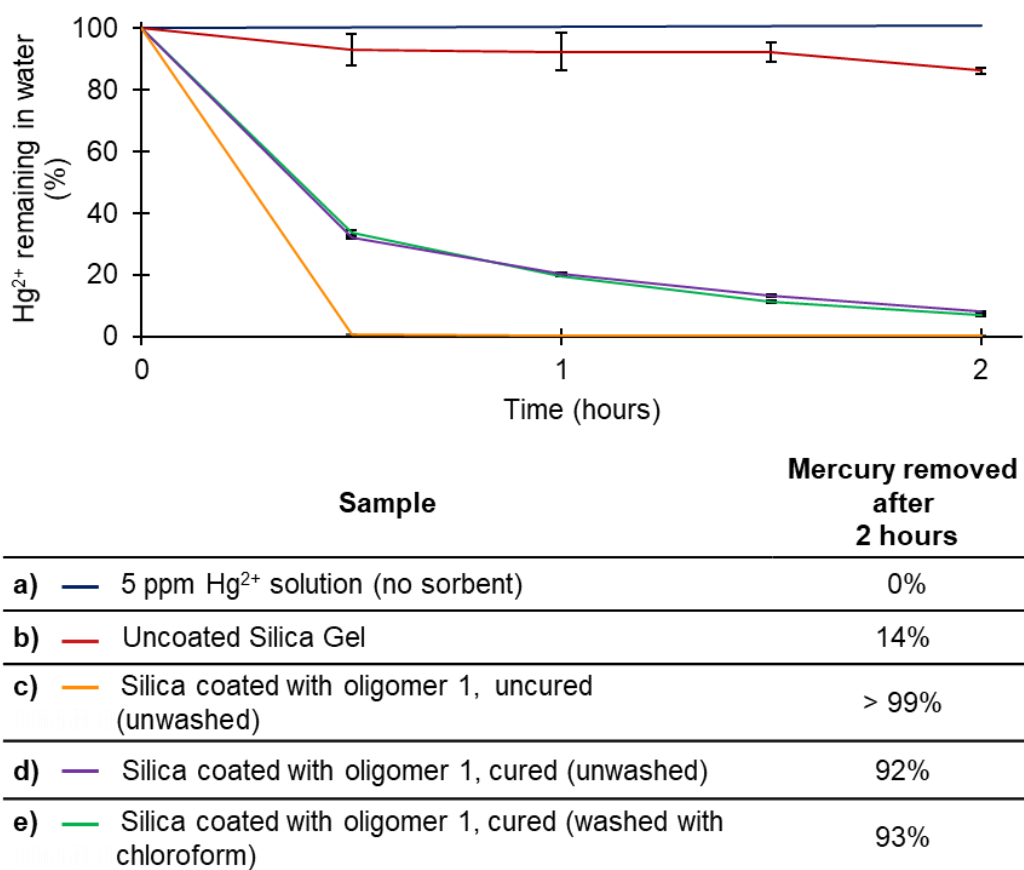
Figure 4.88: a) stable mercury solution without added sorbent. **b)** 14% of mercury was removed by only silica gel. **c)** over 99% of mercury was removed by the unwashed and uncured oligomer 1 coated silica gel. **d)** cured and unwashed oligomer 1 coated silica gel removed 92% of mercury. **e)** Oligomer 1 coated silica gel that was cured and washed with chloroform removed 93% of mercury. Reproduced with permission from the Royal Society of Chemistry.[25]

Isotherms of silica gel coated with cured **1** were performed. Firstly a 1000 ppm Hg solution was made by dissolving 136.4 mg of HgCl$_2$ in a 100 mL volumetric flask in deionised water. For the isotherm, 5 samples with different Hg concentrations (4 ppm, 8 ppm, 12 ppm, 16 ppm and 20 ppm,) and volumes of 50 mL were prepared in triplicate in plastic tubes. To each sample 200 mg of silica gel coated with cured **1** was added. After that the samples were rotated at 25 RPM for 7 hours. Following that an aliquot of each sample was filtered using a 0.45 µm nylon syringe filter and sent for analysis.

For the isotherm fitting the Langmuir model was used.

$$q_{eq} = \frac{Q_{max} K_L C_{eq}}{1 + K_L C_{eq}}$$
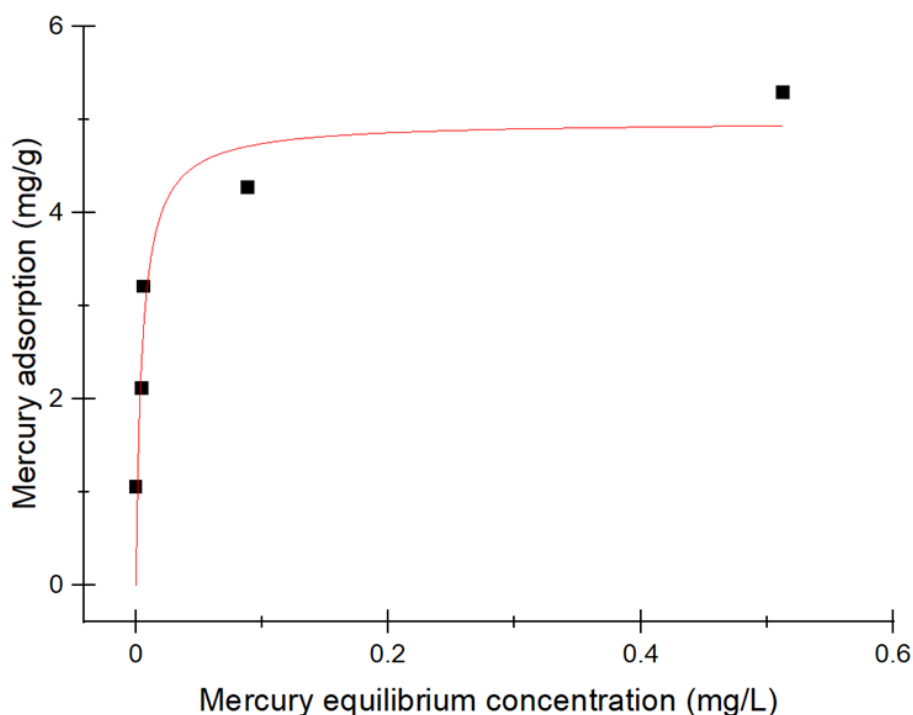
Figure 4.89: Adsorption isotherm of mercury onto sample of silica gel coated with cured **1** using Langmuir isotherm fitting (red line). The maximum mercury capacity was 5 mg/g of sorbent.

Mercury removal using polymer coated silica gel (from mixture of water and diesel)

Firstly, a 384 ppm Hg solution was made by dissolving 52 mg of $HgCl_2$ in a 100 mL volumetric flask and diluting to the mark with deionised water. Next, three 45 mL samples with a Hg concentration of 5 ppm were prepared in 50 mL plastic tubes. This was done by adding 586 µL of the 384 ppm mercury solution, 22.5 mL of deionised water and 22.5 mL of diesel fuel. Following that, 100 mg of the coated silica gel was added (coated with **1** and cured, as previously described, 10:1 mass ratio of silica to polymer). Then, the samples were shaken for 20 seconds to mix the contents before they were rotated at 25 RPM for 2 hours. Samples were taken at 0, 0.5, 1, 1.5 and 2 hours by removing 1 mL the aqueous phase and centrifuging the sample to ensure separation from the diesel. Finally, 0.7 mL of the aqueous samples were diluted to 7 mL in 5 % HCl and then analysed by CVAAS.

Before mixing   After mixing

Figure 4.90: Mixture of equal volumes of diesel fuel and water before and after end-over-end mixing, illustrating the emulsion that forms. Reproduced with permission from the Royal Society of Chemistry.[25]
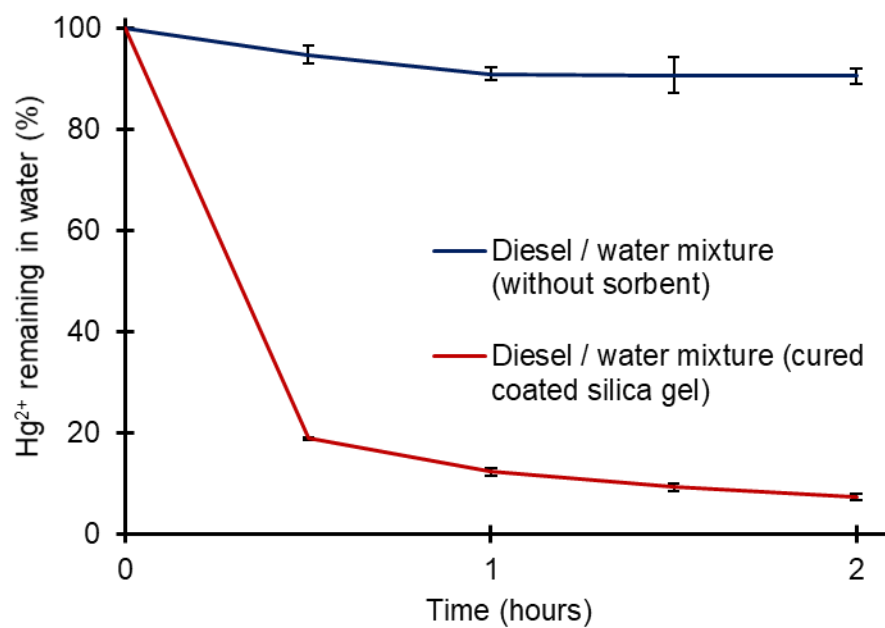
Figure 4.91: Hg uptake from a diesel/water mixture containing 5 ppm of Hg using silica gel coated with cured oligomer 1. Over 92 % of mercury was removed within 2 hours.

Applications as protective coating for metal

To conduct the acid resistivity studies, 57 – 77 mg of cured **1** was added to 3 ml of undiluted acid. The following acids were used: HCl, H_2SO_4, HNO_3, TFA, H_3PO_4, and acetic acid. After 24 hours the polymers were removed from the acids, rinsed with deionised water, and dried under high vacuum overnight. The weight of the polymers before and after their exposure to the solvents was recorded. Only two acids showed any effect on the polymer. Sulfuric acid dissolved 3% of cured-1 in 24 hours and nitric acid dissolved 6% in 24 hours. This could also be seen in the discoloration of the acids 24 hours after the polymer as added.
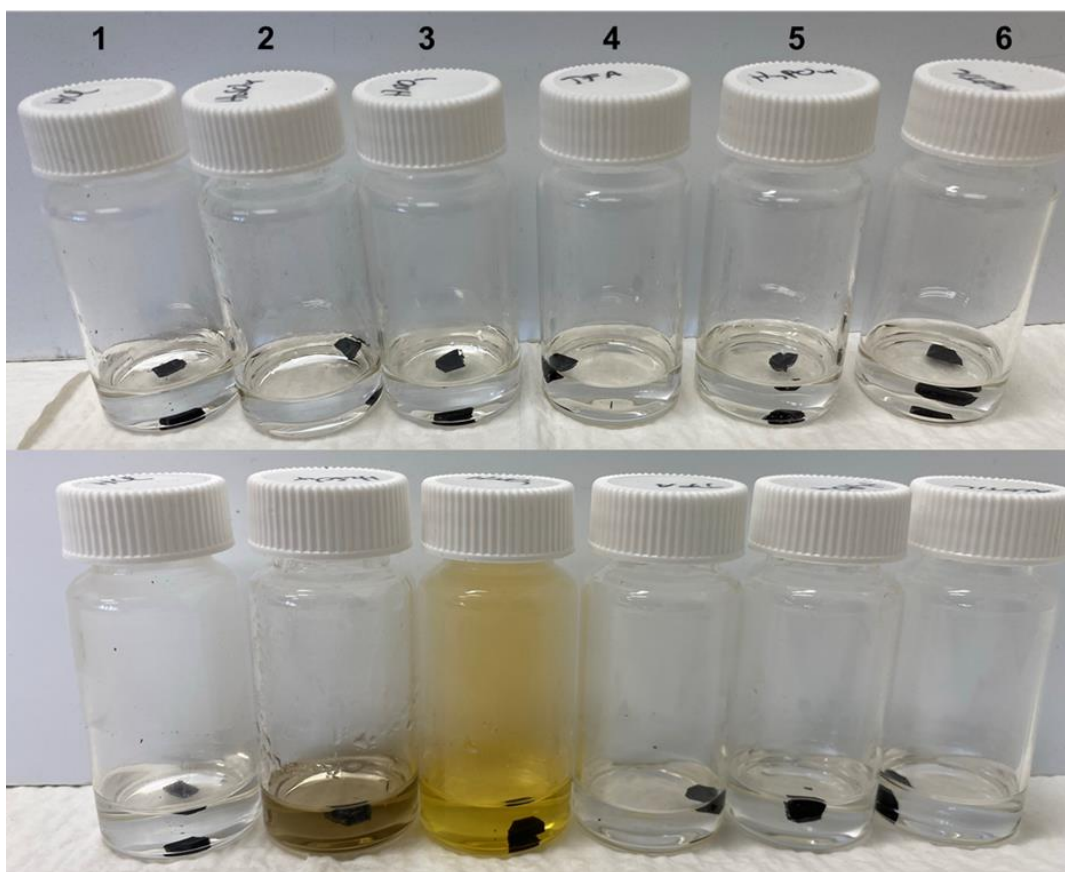
Figure 4.92: Images of polymer in acids at 0 hours (top) and after 24 hours solvent exposure (bottom). Acids: 1) HCl, 2) H_2SO_4, 3) HNO_3, 4) TFA, 5) H_3PO_4, 6) Acetic acid. Reproduced with permission from the Royal Society of Chemistry.[25]

In order to test if cured **1** coated into aluminium is able to protect the metal from acid corrosion the following experiment was performed. Firstly, 1.0 g of oligomer **1** was dissolved in 2 mL of chloroform, with stirring for 1 hour to ensure complete dissolution. Next, the surface of four 1cm x 1cm aluminium pieces were covered with the oligomer **1** solution. The samples were left overnight in order to allow the majority of the solvent to evaporate. The samples were then placed in an oven pre-heated to 140 °C, followed by curing for 24 h. After that time, the oven was turned off so that the samples could cool down slowly. The aluminium pieces were weighed before the addition of the polymer solution and after the curing process to determine the weight of the polymer coating. The average polymer coating mass was 29.8 ± 0.7 mg.

Next, 5 µL of HCl (37%) were added to the surface of cured coating and left for 3 hours. After this time, the acid was washed off with water and the sample was gently dried with a paper towel. In addition, a chip of cured **1** was added to vial containing 5 mL of HCl and left for 24 hours. As a control, 5 µL of acid were place on a piece of aluminium to document the corrosion after 3 hours.
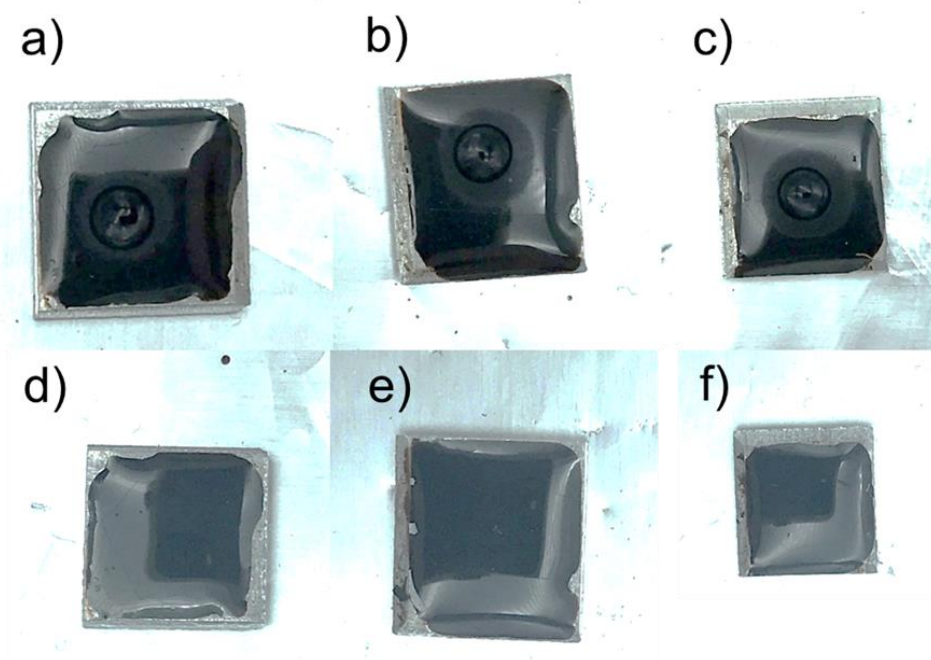
Figure 4.93: a, b, c) Aluminium pieces coated with cured **1** and 5 µL of HCl on the surface. **d, e, f)** Aluminium pieces coated with cured **1** after acid has been washed off. No damage or reaction was observed. Reproduced with permission from the Royal Society of Chemistry.[25]
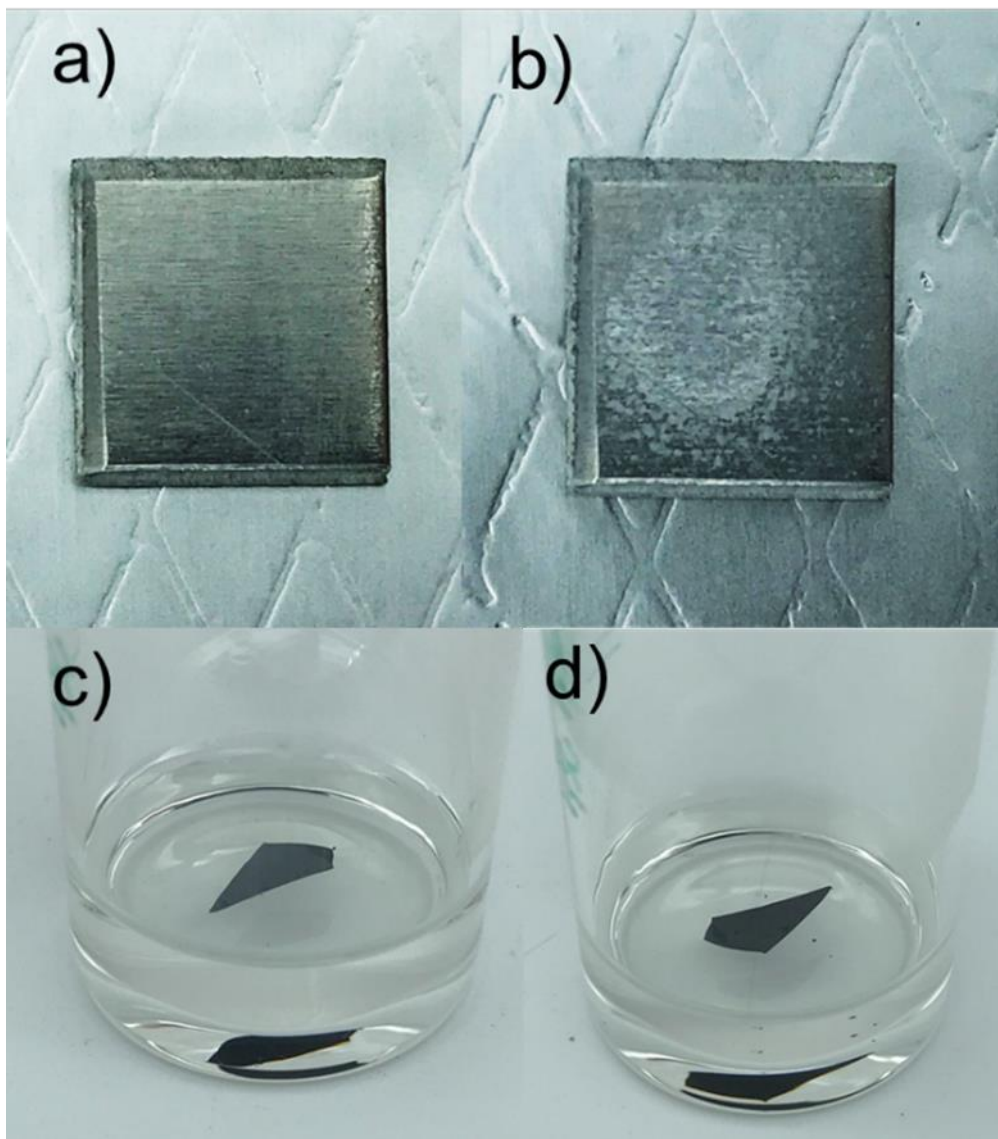
Figure 4.94: a) Aluminium piece before 5 µL of HCl (37%) were added on top. **b)** Aluminium piece after 3 hours of HCl exposure, indicating significant corrosion. **c)** 8 mg of cured **1** submerged in 5 mL of HCl (37%) **d)** 8 mg of cured **1** after 24 hours in 5 mL of HCl (37%). No degradation or reaction of cured **1** was observed. Reproduced with permission from the Royal Society of Chemistry.[25]

Coating cement with cured 1

Gyprock™ Cornice Cement was mixed with water as per instructions and poured into an 8.5 cm long, 5.5 cm wide and 1.0 mm deep mould. After the cement had dried for 24 hours it was removed from the mould and cut into 1.5 cm long and 1.0 cm wide pieces resulting in a surface area of 1.5 cm^2. Next, a polymer solution was prepared by dissolving 1.0 g of oligomer **1** in 2 mL of chloroform. A 100 µL aliquot of that polymer solution was placed on the surface of a cement sheet and the solvent was allowed to evaporate. This procedure was repeated twice more (3 × 100 µL polymer solution in total) to ensure an even and complete coating of oligomer **1** on the cement surface. The coated cement sheet was then cured for 24 hours at 140 °C. To test acid resistance after curing, 25 µL of HCl (37%) was placed on the cement sheet coated with cured **1**. As a control the same was done to an uncoated cement sheet. Additionally, a 25 µL aliquot of water was placed on a third cement sheet.
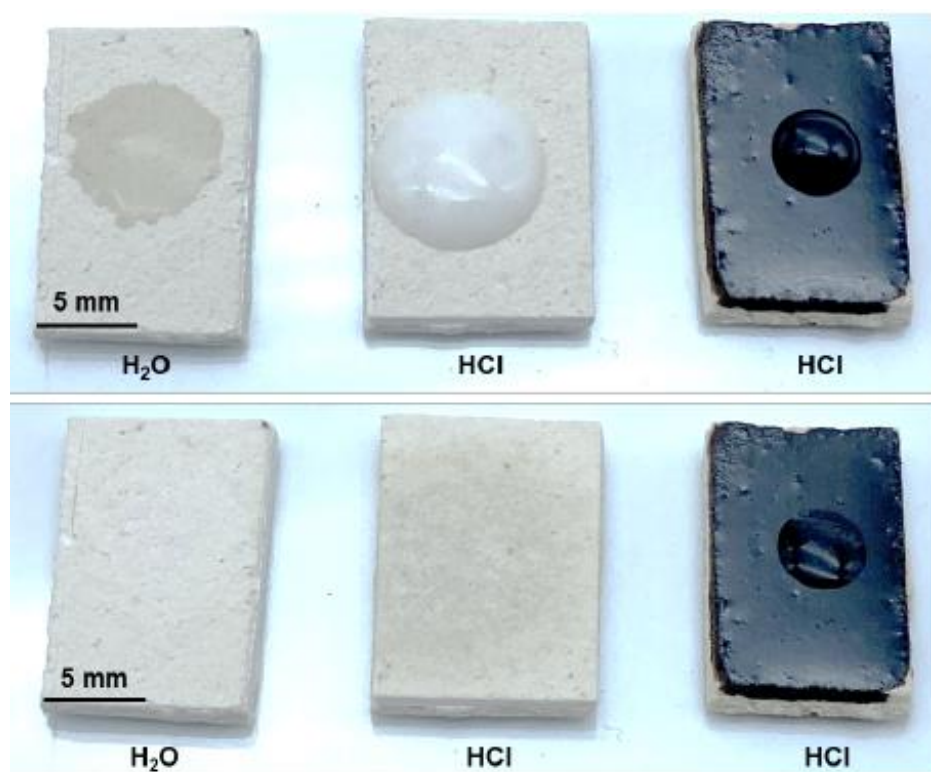
Figure 4.95: Top: Cement sheets straight after water or HCl (37%) was added. Foaming on the uncoated cement sheet indicated a chemical reaction. No reaction was observed on the coated cement sheet that was treated with acid. **Bottom:** Same cement sheets after 2 hour treatment of water or HCl. The water or HCl was absorbed into the uncured sheets whereas no absorption of damage was seen on the coated sheet. Reproduced with permission from the Royal Society of Chemistry.[25]

Lining PVC pipe with cured 1 for solvent resistance

To coat the inside of a PVC pipe, 6.0 g of oligomer **1** was placed on baking paper on top of a hotplate. Upon warming (approximately 40 ºC), oligomer **1** softens and can be rolled flat with a metal rolling pin. A sample approximately 7 x 7.5 cm was prepared by this method. The polymer film was then rolled around a cylindrical silicone insert (7 cm tall, 2.1 cm diameter). The silicon cylinder with the polymer wrapped around it was then placed into the PVC pipe (2.4 cm internal diameter, 6.5 cm length). The polymer filled the gap between the silicone insert and the PVC pipe; the polymer was in direct contact with the PVC. The PVC pipe, polymer film, and silicone insert were then secured in an aluminium mould to help maintain the shape of the PVC pipe. The full assembly was cured in an over at 140 ºC for 24 hours.
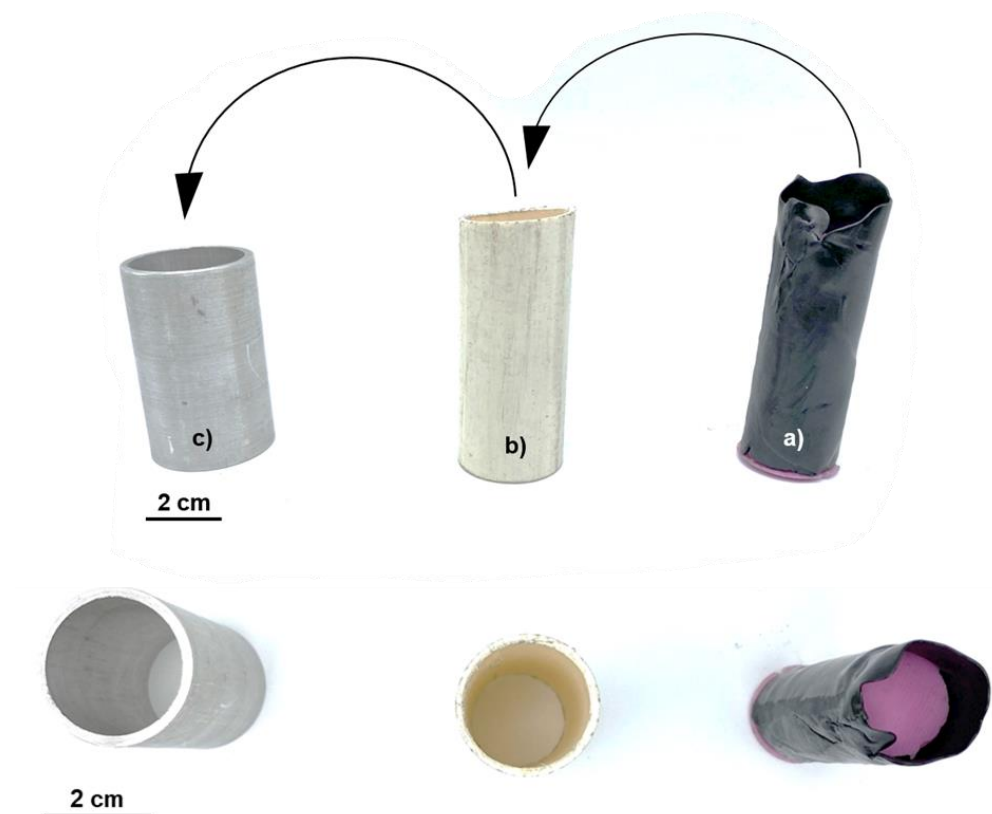
Figure 4.96: a) A polymer mat was rolled around a cylinder made out of silicon and placed into a PVC pipe **(b)**. **c)**The assembly of the PVC and the polymer around the silicon cylinder was placed into a aluminium mould and cured. Reproduced with permission from the Royal Society of Chemistry.[25]

After the curing was completed, the assembly was removed from the oven and allowed to cool to room temperature. Next, the silicon cylinder was removed using pliers. The coated PVC pipe was then cut to a length of 3 cm. This was done by first heating the blade of a hacksaw with a Bunsen burner. Using the hot blade, the pipe was carefully cut so as to not damage the polymer coating.

To test solvent resistance, a separatory funnel was set up so that a steady flow of 5 mL/min of THF was able to pass through the pipe. Using this set up a total of 600 mL of THF was passed though both the uncoated and cured **1** coated PVC pipe over 2 hours.

Figure 4.97: A separator funnel was set up so that a steady flow of 5 mL/min of THF could pass though the uncoated PVC pipe. Reproduced with permission from the Royal Society of Chemistry.[25]
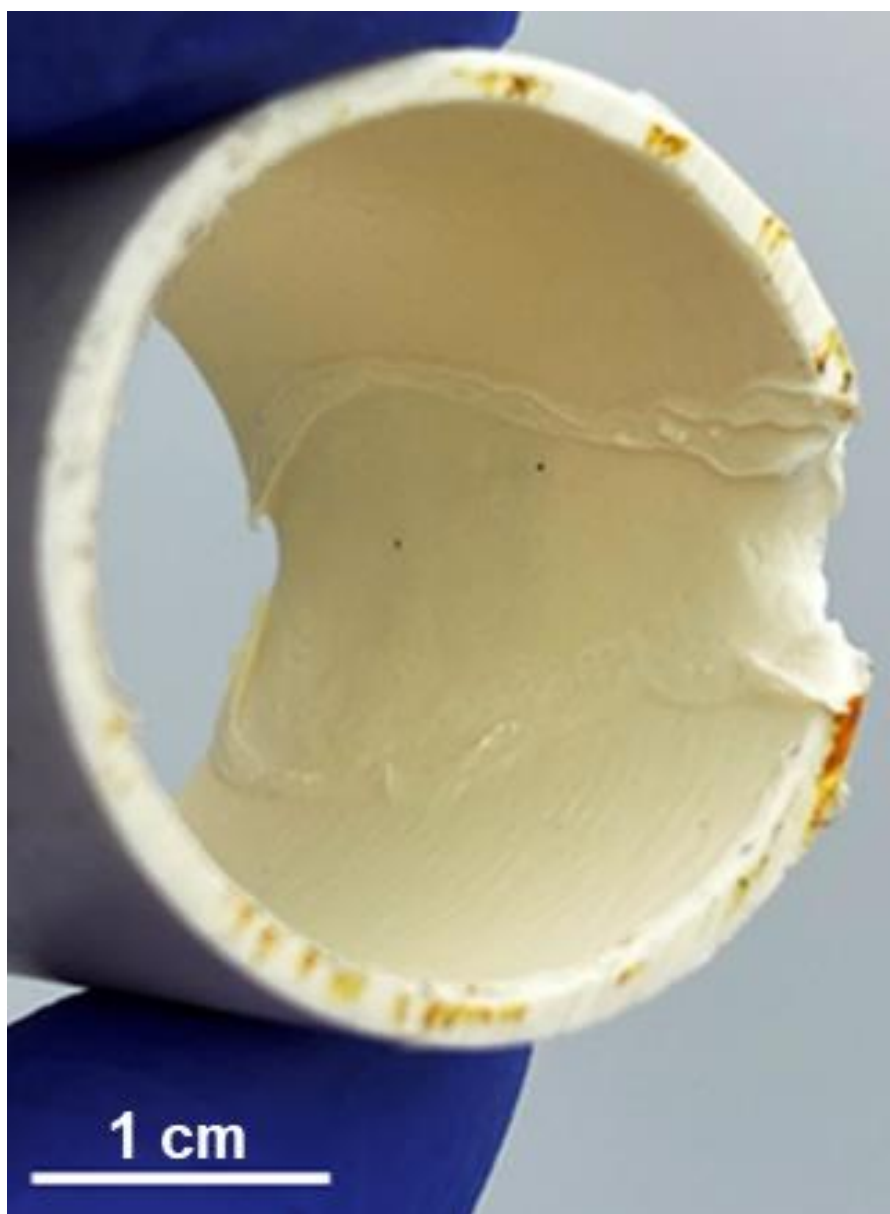
Figure 4.98: Uncoated PVC pipe after 600 mL of THF were passed through showed substantial damage. Reproduced with permission from the Royal Society of Chemistry.[25]
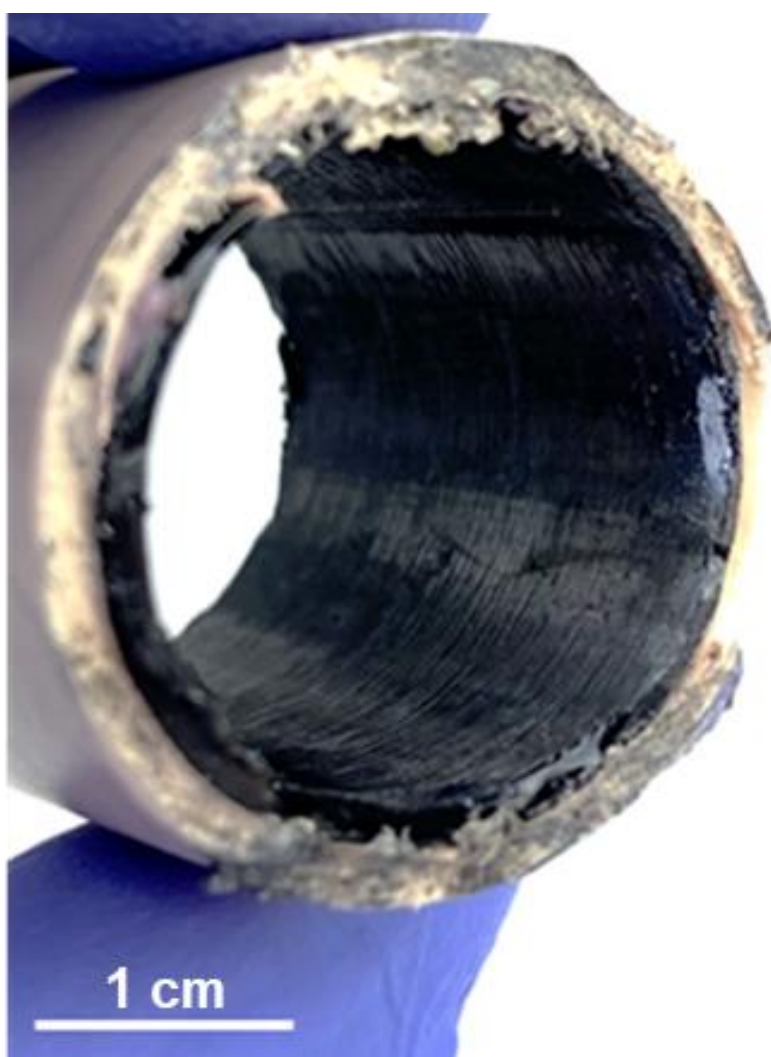
Figure 4:99: Cured 1 coated PVC pipe showed no damage after 600 mL of THF were passed through. Reproduced with permission from the Royal Society of Chemistry.[25]

References:

1. Brown, T.; Idoine, N.; Raycraft, E.; Shaw, R.; Hobbs, S.; Everett, P.; Deady, E.; Bide, T. *World Mineral Production 2014-20118*; British Geological Survey: Nottingham, **2020**.

2. Chung, W. J.; Griebel, J. J.; Kim, E. T.; Yoon, H.; Simmonds, A. G.; Ji, H. J.; Dirlam, P. T.; Glass, R. S.; Wie, J. J.; Nguyen, N. A.; Guralnick, B. W.; Park, J.; Somogyi, Á.; Theato, P.; Mackay, M. E.; Sung, Y.-E.; Char, K.; Pyun, J., The use of elemental sulfur as an alternative feedstock for polymeric materials. *Nat. Chem.* **2013,** *5*, 518-524.

3. Chalker, J. M.; Worthington, M. J. H.; Lundquist, N. A.; Esdaile, L. J., Synthesis and Applications of Polymers Made by Inverse Vulcanization. *Top. Curr. Chem.* **2019,** *377* (3), 16.

4. Wu, X.; Smith, J. A.; Petcher, S.; Zhang, B.; Parker, D. J.; Griffin, J. M.; Hasell, T., Catalytic inverse vulcanization. *Nat. Commun.* **2019,** *10* (1), 647.

5. Orme, K.; Fistrovich, A. H.; Jenkins, C. L., Tailoring Polysulfide Properties through Variations of Inverse Vulcanization. *Macromolecules* **2020,** *53* (21), 9353-9361.

6. Smith, J. A.; Green, S. J.; Petcher, S.; Parker, D. J.; Zhang, B.; Worthington, M. J. H.; Wu, X.; Kelly, C. A.; Baker, T.; Gibson, C. T.; Campbell, J. A.; Lewis, D. A.; Jenkins, M. J.; Willcock, H.; Chalker, J. M.; Hasell, T., Crosslinker Copolymerization for Property Control in Inverse Vulcanization. *Chem. Eur. J.* **2019,** *25* (44), 10433-10440.

7. Smith, J. A.; Wu, X.; Berry, N. G.; Hasell, T., High sulfur content polymers: The effect of crosslinker structure on inverse vulcanization. *J. Polym. Sci., Part A: Polym. Chem.* **2018,** *56* (16), 1777-1781.

8. Baird, D. G.; Collias, D. I., *Polymer Processing : Principles and Design*. John Wiley & Sons, Incorporated: Somerset, UNITED STATES, **2014**.

9. Diez, S.; Hoefling, A.; Theato, P.; Pauer, W., Mechanical and Electrical Properties of Sulfur-Containing Polymeric Materials Prepared via Inverse Vulcanization. *Polymers* **2017,** *9* (12), 59.

10. Rangappa, S. M.; Parameswaranpillai, J.; Siengchin, S., *Polymer Coatings: Technologies and Applications*. Taylor & Francis Group: Milton, UNITED KINGDOM, **2020**.

11. Zhang, Y.; Glass, R. S.; Char, K.; Pyun, J., Recent advances in the polymerization of elemental sulphur, inverse vulcanization and methods to obtain functional Chalcogenide Hybrid Inorganic/Organic Polymers (CHIPs). *Polym. Chem.* **2019,** *10* (30), 4078-4105.

12.	Griebel, J. J.; Nguyen, N. A.; Namnabat, S.; Anderson, L. E.; Glass, R. S.; Norwood, R. A.; Mackay, M. E.; Char, K.; Pyun, J., Dynamic Covalent Polymers via Inverse Vulcanization of Elemental Sulfur for Healable Infrared Optical Materials. *ACS Macro Lett.* **2015,** *4* (9), 862-866.

13.	Parker, D. J.; Chong, S. T.; Hasell, T., Sustainable inverse-vulcanised sulfur polymers. *RSC Adv.* **2018,** *8* (49), 27892-27899.

14.	Lundquist, N. A.; Tikoalu, A. D.; Worthington, M. J. H.; Shapter, R.; Tonkin, S. J.; Stojcevski, F.; Mann, M.; Gibson, C. T.; Gascooke, J. R.; Karton, A.; Henderson, L. C.; Esdaile, L. J.; Chalker, J. M., Reactive Compression Molding Post-Inverse Vulcanization: A Method to Assemble, Recycle, and Repurpose Sulfur Polymers and Composites. *Chem. Eur. J.* **2020,** *26* (44), 10035-10044.

15.	Crockett, M. P.; Evans, A. M.; Worthington, M. J. H.; Albuquerque, I. S.; Slattery, A. D.; Gibson, C. T.; Campbell, J. A.; Lewis, D. A.; Bernardes, G. J. L.; Chalker, J. M., Sulfur-Limonene Polysulfide: A Material Synthesized Entirely from Industrial By-Products and Its Use in Removing Toxic Metals from Water and Soil. *Angew. Chem. Int. Ed.* **2016,** *55*, 1714-1718.

16.	Zhang, B.; Petcher, S.; Hasell, T., A ternary system for delayed curing inverse vulcanisation. *ChemComm* **2019,** *55* (72), 10681-10684.

17.	Scheiger, J. M.; Direksilp, C.; Falkenstein, P.; Welle, A.; Koenig, M.; Heissler, S.; Matysik, J.; Levkin, P. A.; Theato, P., Inverse Vulcanization of Styrylethyltrimethoxysilane–Coated Surfaces, Particles, and Crosslinked Materials. *Angew. Chem. Int. Ed.* **2020,** *59* (42), 18639-18645.

18.	Currell, B. R.; Williams, A. J.; Mooney, A. J.; Nash, B. J., Plasticization of Sulfur. In *New Uses of Sulfur*, West, J., Ed. American Chemical Society: **1975**; Vol. 140, pp 1-17.

19.	Sullivan, T. A.; McBee, W. C.; Blue, D. D., Sulfur in Coatings and Structural Materials. In *New Uses of Sulfur*, AMERICAN CHEMICAL SOCIETY: **1975**; Vol. 140, pp 55-74.

20.	Blight, L.; Currell, B. R.; Nash, B. J.; Scott, R. A. M.; Stillo, C., Preparation and Properties of Modified Sulfur Systems. In *New Uses of Sulfur—II*, AMERICAN CHEMICAL SOCIETY: **1978**; Vol. 165, pp 13-30.

21.	Bordoloi, B. K.; Pearce, E. M., Plastic Sulfur Stabilization by Copolymerization of Sulfur with Dicyclopentadiene. In *New Uses of Sulfur—II*, AMERICAN CHEMICAL SOCIETY: 1978; Vol. 165, pp 31-53.

22.	Blight, L. B.; Currell, B. R.; Nash, B. J.; Scott, R. T. M.; Stillo, C., Chemistry of the modification of sulphur by the use of dicyclopentadiene and of styrene. *Br. Polym. J.* **1980,** *12* (1), 5-11.

23.	Meyer, B., Elemental sulfur. *Chem. Rev.* **1976,** *76* (3), 367-388.

24. Parker, D. J.; Jones, H. A.; Petcher, S.; Cervini, L.; Griffin, J. M.; Akhtar, R.; Hasell, T., Low cost and renewable sulfur-polymers by inverse vulcanisation, and their potential for mercury capture. *J. Mater. Chem. A* **2017,** *5* (23), 11682-11692.

25. Mann, M.; Zhang, B.; Tonkin, S. J.; Gibson, C. T.; Jia, Z.; Hasell, T.; Chalker, J. M., Processes for coating surfaces with a copolymer made from sulfur and dicyclopentadiene. *Polym. Chem.* **2022**.

26. Worthington, M. J. H.; Kucera, R. L.; Chalker, J. M., Green chemistry and polymers made from sulfur. *Green Chem.* **2017,** *19*, 2748-2761.

27. Tonkin, S. J.; Gibson, C. T.; Campbell, J. A.; Lewis, D. A.; Karton, A.; Hasell, T.; Chalker, J. M., Chemically induced repair, adhesion, and recycling of polymers made by inverse vulcanization. *Chem Sci* **2020,** *11* (21), 5537-5546.

28. Worthington, M. J. H.; Kucera, R. L.; Abuquerque, I. S.; Gibson, C. T.; Sibley, A.; Slattery, A. D.; Campbell, J. A.; Alboaiji, S. F. K.; Muller, K. A.; Young, J.; Adamson, N.; Gascooke, J. R.; Jampaiah, D.; Sabri, Y. M.; Bhargava, S. K.; Ippolito, S. J.; Lewis, D. A.; Quinton, J. S.; Ellis, A. V.; Johs, A.; Bernardes, G. J. L.; Chalker, J. M., Laying Waste to Mercury: Inexpensive Sorbents Made from Sulfur and Recycled Cooking Oils. *Chem. Eur. J.* **2017,** *23*, 16219-16230.

29. Hoefling, A.; Lee, Y. J.; Theato, P., Sulfur-Based Polymer Composites from Vegetable Oils and Elemental Sulfur: A Sustainable Active Material for Li–S Batteries. *Macromol. Chem. Phys.* **2017,** *218*, 1600303.

30. Gibson, C. T.; Ridings, C. R.; Blok, A. J.; Shearer, C. J.; Andersson, G. G.; Ellis, A. V., Morphological changes of sintered polydopamine coatings. *Surf. Topogr.: Metrol. Prop.* **2019,** *7* (1), 015016.

31. Sader, J. E.; Borgani, R.; Gibson, C. T.; Haviland, D. B.; Higgins, M. J.; Kilpatrick, J. I.; Lu, J.; Mulvaney, P.; Shearer, C. J.; Slattery, A. D.; Thorén, P.-A.; Tran, J.; Zhang, H.; Zhang, H.; Zheng, T., A virtual instrument to standardise the calibration of atomic force microscope cantilevers. *Rev. Sci. Instrum.* **2016,** *87* (9), 093711.

32. Kontomaris, S. V.; Malamou, A., Hertz model or Oliver & Pharr analysis? Tutorial regarding AFM nanoindentation experiments on biological samples. *Mater. Res. Express* **2020,** *7* (3), 033001.

33. Ferencz, R.; Sanchez, J.; Blümich, B.; Herrmann, W., AFM nanoindentation to determine Young's modulus for different EPDM elastomers. *Polym. Test.* **2012,** *31* (3), 425-432.

34. Jee, A.-Y.; Lee, M., Comparative analysis on the nanoindentation of polymers using atomic force microscopy. *Polym. Test.* **2010,** *29* (1), 95-99.

35. Baltá Calleja, F. J., Microhardness relating to crystalline polymers. In *Characterization of Polymers in the Solid State I: Part A: NMR and Other Spectroscopic Methods Part B: Mechanical Methods*, Springer Berlin Heidelberg: **1985**; pp 117-148.

36. United Nations Environment Programme, Minamata Convention on Mercury. https://www.mercuryconvention.org/sites/default/files/documents/information_document/Minamata-Convention-booklet-Sep2019-EN.pdf (accessed 12th of October 2021).

37. Brião, G. d. V.; de Andrade, J. R.; da Silva, M. G. C.; Vieira, M. G. A., Removal of toxic metals from water using chitosan-based magnetic adsorbents. A review. *Environ. Chem. Lett.* **2020,** *18* (4), 1145-1168.

38. Ochedi, F. O.; Liu, Y.; Hussain, A., A review on coal fly ash-based adsorbents for mercury and arsenic removal. *J. Clean. Prod.* **2020,** *267*, 122143.

39. Raj, D.; Maiti, S. K., Sources, toxicity, and remediation of mercury: an essence review. *Environ. Monit. Assess.* **2019,** *191* (9), 566.

40. Wang, L.; Hou, D.; Cao, Y.; Ok, Y. S.; Tack, F. M. G.; Rinklebe, J.; O'Connor, D., Remediation of mercury contaminated soil, water, and air: A review of emerging materials and innovative technologies. *Environ. Int.* **2020,** *134*, 105281.

41. Chalker, J. M.; Mann, M.; Worthington, M. J. H.; Esdaile, L. J., Polymers Made by Inverse Vulcanization for Use as Mercury Sorbents. *Organic Materials* **2021,** *03* (02), 362-373.

42. Wilhelm, S. M., Mercury in petroleum and natural gas: estimation of emissions from production, processing, and combustion. *U.S. Environmental Protection Agency, Washington, DC, EPA/600/R-01/066 (NTIS PB2001-109026)* **2001**.

43. Thiounn, T.; Tennyson, A. G.; Smith, R. C., Durable, acid-resistant copolymers from industrial by-product sulfur and microbially-produced tyrosine. *RSC Adv.* **2019,** *9* (54), 31460-31465.

44. Lopez, C. V.; Karunarathna, M. S.; Lauer, M. K.; Maladeniya, C. P.; Thiounn, T.; Ackley, E. D.; Smith, R. C., High strength, acid-resistant composites from canola, sunflower, or linseed oils: Influence of triglyceride unsaturation on material properties. *J. Polym. Sci.* **2020,** *58* (16), 2259-2266.

45. Alexander, M.; Bertron, A.; De Belie, N., *Performance of cement-based materials in aggressive aqueous environments.* Springer: **2013**; Vol. 10.

46. Zhang, W.; Pi, Y.; Kong, W.; Zhang, Y.; Wu, P.; Zeng, W.; Yang, F., Influence of damage degree on the degradation of concrete under freezing-thawing cycles. *Constr. Build. Mater.* **2020,** *260*, 119903.

47.   Nazeer, A. A.; Madkour, M., Potential use of smart coatings for corrosion protection of metals and alloys: A review. *J. Mol. Liq.* **2018,** *253*, 11-22.

48.   Kuttner, C.; Tebbe, M.; Schlaad, H.; Burgert, I.; Fery, A., Photochemical Synthesis of Polymeric Fiber Coatings and Their Embedding in Matrix Material: Morphology and Nanomechanical Properties at the Fiber–Matrix Interface. *ACS Appl. Mater. Interfaces* **2012,** *4* (7), 3484-3492.

49.   Nikfarjam, M.; López-Guerra, E. A.; Solares, S. D.; Eslami, B., Imaging of viscoelastic soft matter with small indentation using higher eigenmodes in single-eigenmode amplitude-modulation atomic force microscopy. *Beilstein J. Nanotechnol.* **2018,** *9* (1), 1116-1122.

50.   Caron, A., Quantitative Hardness Measurement by Instrumented AFM-indentation. *J Vis Exp* **2016,** (117).

51.   Rosato, D. V., *Plastics engineered product design*. Elsevier: **2003**.

Chapter 5

Sulfur polymers and their evaluation as latent adhesives and structural composites

Introduction

The construction industry remains one of the world's largest consumer of raw materials using 40% of natural materials.[1, 2] Further, the construction industry alone contributes 5% to the global energy consumption and is responsible for 10% of global CO_2 emissions (Figure 5.1).[3]
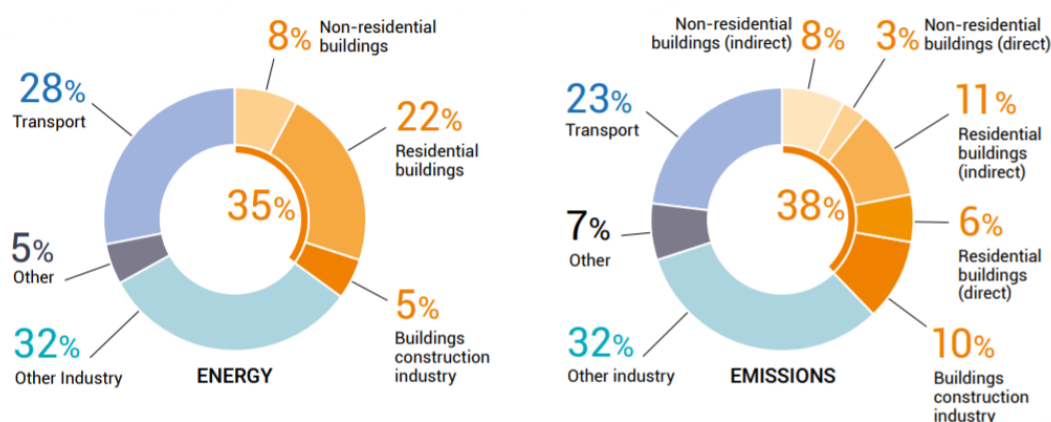
Figure 5.1: Global contribution to energy consumption and emissions of the construction industry in 2019. © United Nations Environment Programme, 2020. The image may be reproduced for non-profit purposes without special permission.[3]

Besides the construction of buildings, the construction of roads using asphalt consumes vast amounts of raw materials and energy, contributing the release of greenhouse gases into the environment.[4, 5] Taking into account the current threat of climate change, energy production and fossil fuel depletion, it comes as no surprise that more sustainability and reduced energy consumption in the building sector are pressing issues.[6] Key areas in which the pressure on the natural environment by the building

industry can be lessened is by researching and implementing the use of materials made from sustainable resources resulting in reduced water, raw materials and energy consumption.[1, 7] Recently, increasing attention was given to the research of materials that can be beneficial for the building industry in reducing its environmental impact.[2] In an effort to produce building materials made from renewable sources, polymer composites have been a prevalent topic in the field of material science.[7] Encouraging reports from using natural fibres to produce a toughened bio epoxy blend indicate research that may mitigate some of the sustainability problems with construction (Figure 5.2).[7] Additionally, studies into repurposing waste show promise as composite materials. For example, our own research team has combined wool, coconut coir, PVC shavings or sand with a polysulfide made from cheap and abundant resources to make composites with tuneable mechanic properties (Figure 5.2).[8, 9]

Natural and waste materials investigated in polymer composites

Natural fibers   PVC shavings   Sand

Figure 5.2: A range of natural fibres (sisal fibres[7], coconut coir[9] and wool[8]), PVC shavings[9] and sand[9] have been evaluated as parts of polymer composites. Image credits: Fibres: Scratching post by Andrew Malone under a CC BY 2.0 licence. PVC by pepperberryfarm under a CC BY-NC-ND 2.0 licence. Sand: Sand patters by PK under a CC BY 2.0 licence.

Since the introduction of inverse vulcanised polysulfides by Pyun et al,[10] a large library of these classes of polymers have been synthesised and researched.[11] Not only is sulfur abundant but it is also inexpensive[12] making it an ideal feedstock for inverse vulcanised polymers with applications in the construction sector. The use of sulfur in construction has a long history. As early as the 1930's, research into the properties of sulfur mortar was published, and during the 1960's the emphasis was on making construction materials such as concrete which contained sulfur.[13] As sulfur concrete utilises some of the stockpiles of sulfur it provides a low cost and chemical resistant building material.[14] Further, the mechanical properties of these materials can be enhanced by various additives such as dipentene, dicyclopentadiene or oleic acid.[15, 16] However, sulfur is brittle and offers less resistance to water, as does traditional Portland cement concrete.[16] While traditional concrete is still widely used, it releases vast

amounts of emissions contributing to global warming with many of these emissions coming from the cement production, a main part of concrete.[17]

More recently, efforts have been made to produce polysulfide composites for use in construction. For instance, Smith et al have produced polysulfide composites using cellulose,[18] terpenoids[19] or lignin.[20] Alhassan et al showed the synthesis of sulfur-nylon,[21] sulfur-polypropylene composites.[22] Further, the Chalker lab has recently developed composites containing a polysulfide and coconut coir, PVC, sand[9] or wool.[8]

While many building composites are joined together using fasteners like rivets or welding, adhesives also play an important role.[23] While bonded joints are inexpensive, light, and resistant to damage, additional advantages are their fatigue strength and low structural weight.[23] In light of this, it is important to research adhesives that can be synthesised and used with minimal energy consumption.

The Chalker laboratory recently reported a room temperature method to catalyse S-S bond metathesis of polymers made from sulfur, canola oil and dicyclopentadiene (DCPD). The study shows that recycling, adhesion and chemically induced repair of inverse vulcanised polymer is possible at room temperature with the use of a highly nucleophilic catalyst like tributylphosphine, pyridine or triethylamine (Et_3N).

While previous studies showed preliminary results regarding the catalysts use as an adhesive, the research in this chapter aims to evaluate the catalytic adhesion as a tool for use in the construction industry. The advantage of such a system is that the building material is the bulk material and the latent adhesive, which can be activated by an amine catalyst like Et_3N. Hence, no welding, adhesives or mortar is required to join two pieces together.

In this chapter the use of Et_3N as a catalyst for the adhesion of S-Canola-DCPD polymers was investigated (Figure 5.3).
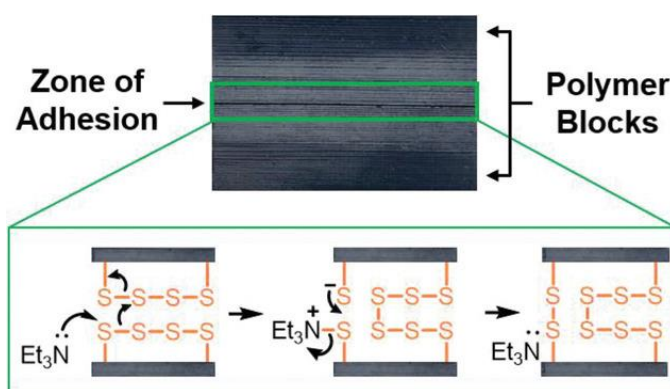
Figure 5.3: Catalytic adhesion of polysulfide polymers catalysed by triethylamine through S-S bond metathesis resulting in chemical bonding at the polymer interface. © 2021Wiley-VCH GmbH. Image was reproduced under a RightsLink license.[24]

The aim of this chapter was to quantify the bond strength as well as to develop ways to reinforce the polymer to imply more structural integrity.

All materials used to synthesise this polymer are all in high abundance, or either derived from waste streams or renewable low-cost sources. Sulfur is produced on a multimillion tone scale every year as a co-product of petroleum refining,[10] DCPD is also a coproduct form the petroleum industry, generated during ethylene production through naphtha cracking[25] and canola oil is a unsaturated triglyceride derived from plants which is of interest as a sustainable and renewable monomer.[9, 26-29] All these factors increase the potential of the polymer described here as a sustainable building material or for related applications. Additionally, it has been shown that the polymer can be moulded into various architectures in its soft pre-polymer stage. We also report the first vigorous quantitative mechanical testing of this polymer and the catalytic adhesion.

In recent years, carbon materials such as graphene, carbon nanotubes or carbon fibres have been vigorously investigated as mechanical reinforcements in the engineering of materials.[30] This is due to the outstanding wear resistance, modulus and tensile strength of these carbon materials.[31-33] Polymers that have been reinforced with carbon fibre demonstrate remarkable mechanical properties and low densities.[31] These carbon fibre reinforced polymers owe their strength to very thin carbon fibres (1-5 μm) which are embedded into the polymer matrix.[34] Another carbon material routinely used as reinforcement are carbon nanotubes.[35] Like carbon fibre these hollow cylinder shaped carbon structures in the form of hexagonal unit cells, exhibit remarkable stiffness and strength while having a low density.[32] In light of this, the mechanical strength of the bulk S-Canola-DCPD polymer was improved by adding carbon fibre or carbon nanotubes.

Synthesis and characterisation of the polysulfide terpolymer

The key polymer of this chapter was synthesised by adapting a protocol from a different study conducted in the Chalker laboratory.[36, 37] In the previous study, the S-S metathesis chemistry was established on polymers with a mass under 1 g which had poor mechanical properties and were not evaluated as a potential construction material.[36] However, in this study polymers with a mass of 30 g were used to assess these materials for potential use in construction or structural applications. Further, the mechanical properties (shear and tensile strength) of the amine-catalysed adhesion were evaluated together with strategies to increase the mechanical strength of the polymers.

Firstly, the procedure was optimised from the previous study.[36] In the optimised procedure, 3.5 g of canola oil and 1.5 g of DCPD were preheated on a 170 °C aluminium hot block for 30 seconds before being added to 5 g of molten sulfur in a 20 mL glass vial at 170 °C in a aluminium hot block. This mixture was then stirred for 9.5 minutes before being removed from the heat source. These conditions were chosen as to avoid potential runway reactions which can occur in reactions that contain DCPD as was discussed in Chapter 4 of this thesis. At this stage the mixture was still liquid and was poured in a silicone mould and transferred to a 130 °C oven for a 24-hour curing process (Figure 5.4).
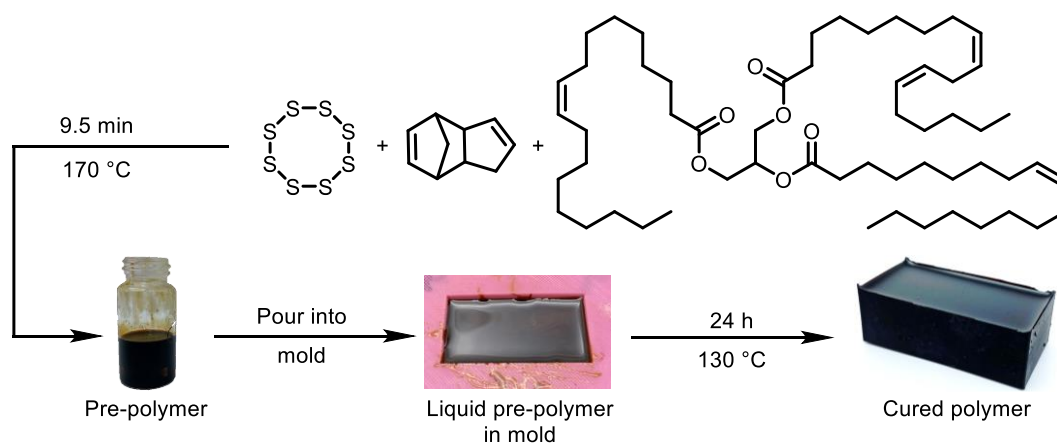
Figure 5.4: Reaction scheme of the polymer synthesis. Canola oil and DCPD are briefly pre-heated before being added to molten sulfur and reacted for 9.5 minutes. After that the liquid mixture in poured into a polymer mould and cured for 24 hours in a 130°C oven. © 2021 Wiley-VCH GmbH. Image was reproduced under a RightsLink license.[24]

The feed ratio of 50 wt% sulfur, 35 wt% canola oil, and 15% DCPD was chosen based on a previous study, as mentioned earlier.[36] At this feed ratio the sulfur rank, the average amount of sulfur atoms in the crosslinks, is 4. Further, the glass transition temperature of the polymer with these feed ratios is suitable for S-S metathesis using amines.[36] For the polymer block in this study, three batches of 10 g polymer reactions were run in parallel and poured onto the mould to yield a 30 g polymer block. After the curing process, a phase separation was observed in the polymer block: a soft top phase and a hard and brittle bottom phase (Figure 5.5). This was not observed in the previous study and was a surprising result.
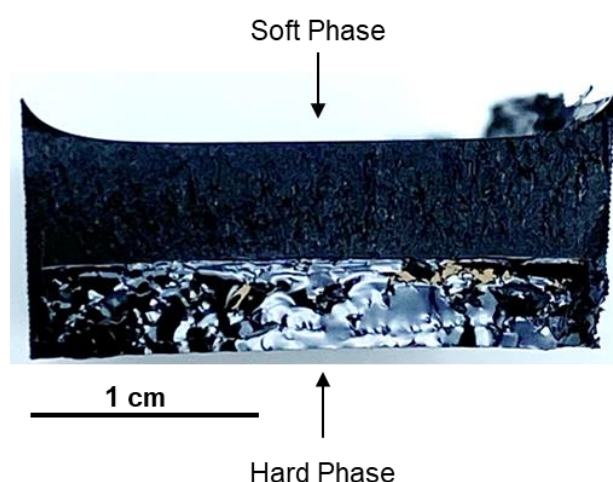
Figure 5.5: The soft phase on the top of the polymer and the hard phase on the bottom of the polymer can be clearly seen after curing. © 2021 Wiley-VCH GmbH. Image was reproduced under a RightsLink license.[24]

In previous studies, the polymers cured had an approximate mass of <1.0 g,[36] compared to the 30 g polymer blocks prepared here. The likely reason for the phase separation observed here, is that the monomers and oligomers separate during the curing process since this curing takes place without agitation. Simultaneous thermal analysis (STA) was used to shed light on the characteristics of the two phases (Figure 5.6). Only one mass lost could be observed in the hard phase of the 15% DCPD polymer. The onset of this mass loss was at 180 °C and 82% of the weight of the hard phase was lost upon reaching 800 °C (Figure 5.6).
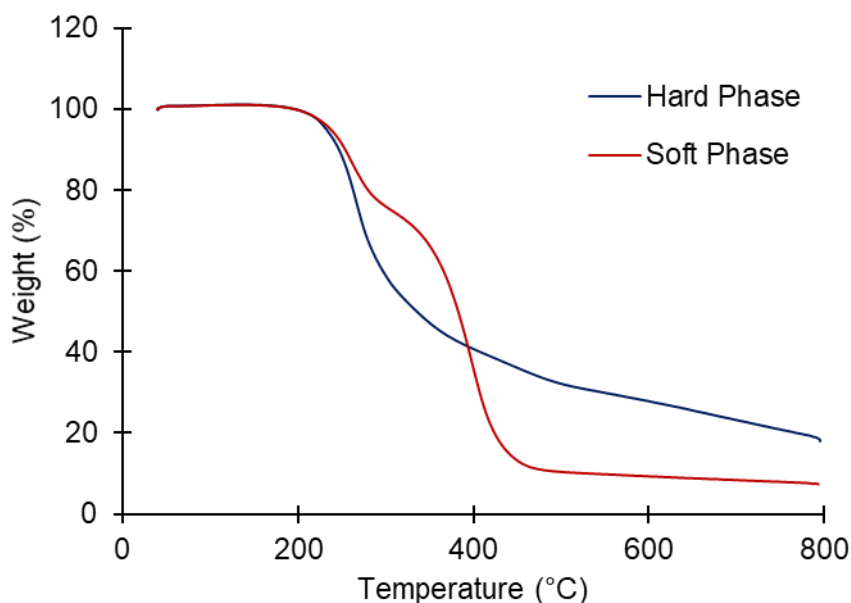
Figure 5.6: STA of soft and hard phase of 15% DCDP polysulfide. © 2021 Wiley-VCH GmbH. Image was reproduced under a RightsLink license.[24]

The soft phase displayed a two-stage mass loss. The first mass loss took place between 180 °C and 320 °C resulting in a weight loss of approximately 30%. During the second mass loss which took place between 320 °C and 500 °C an additional 60% of weight was lost. This two stage mass loss has been previously seen and has been attributed to a process in which the weaker S-S bonds in the polysulfide decompose first, followed by a decomposition of the remaining sulfur and organic material during the second mass loss.[27, 38] Differential scanning calorimetry (DSC) was employed to determine the glass transition temperature (T_g) of the two different phases. This analysis showed a T_g of 41 °C for the hard phase and a T_g of -26 °C for the soft phase. These results correspond to the physical appearance of the phases, with the soft phase being soft and rubbery while the hard phase was hard and brittle. A higher amount of DCPD might be present in the hard phase giving rise to a harder material and a higher T_g. This agrees with previous studies of similar terpolymers, that indicated a linear relationship between the feed ratio of DCPD and the T_g of terpolymers with a wide range of sulfur content.[37] To gain more insight into the composition of the two phases, elemental analysis was performed. A lower carbon content (19%) was observed in the hard phase compared to the carbon content of the soft phase (55%). However, the sulfur content was much higher (79%) in the hard phase then the sulfur content in the soft phase (36% Figure 5.7). This is since DCPD is more reactive it reacts with sulfur first and forms a dense hard bottom phase with a higher T_g (this is consistent with the T_g measurements

(T_g of 41 °C) and elemental analysis (Figure 5.7)). On the other hand, the soft phase contains more canola oil (higher carbon content (Figure 5.7)) is softer and has as a lower T_g (-26 °C).
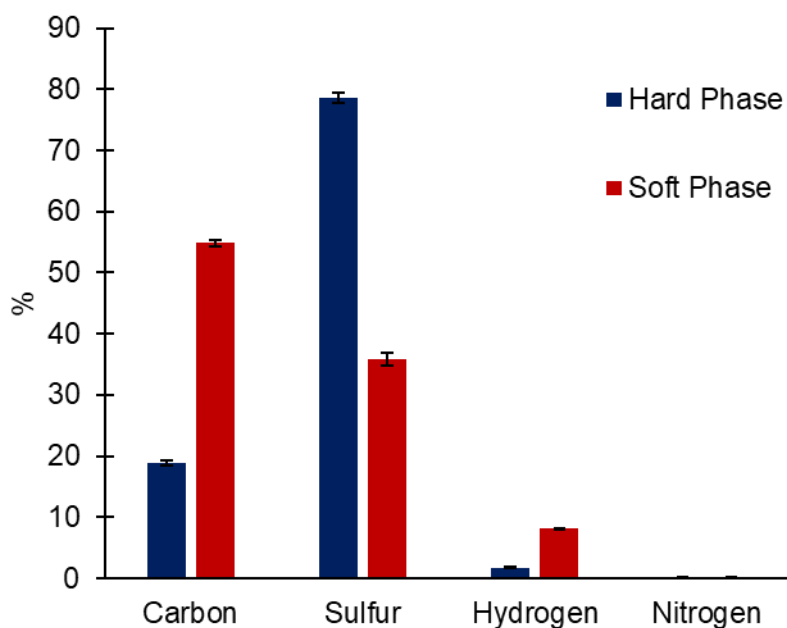
Figure 5.7: Elemental analysis of soft and hard phases of the 15% DCPD polymer. © 2021 Wiley-VCH GmbH. Image was reproduced under a RightsLink license.[24]

To determine if elemental sulfur was present in the bulk material, powder X-ray diffraction (XRD) analysis was performed. As can be seen in Figure 5.8, no crystalline sulfur was detected. This was further confirmed by the absence a melting transition of elemental sulfur during DSC analysis.
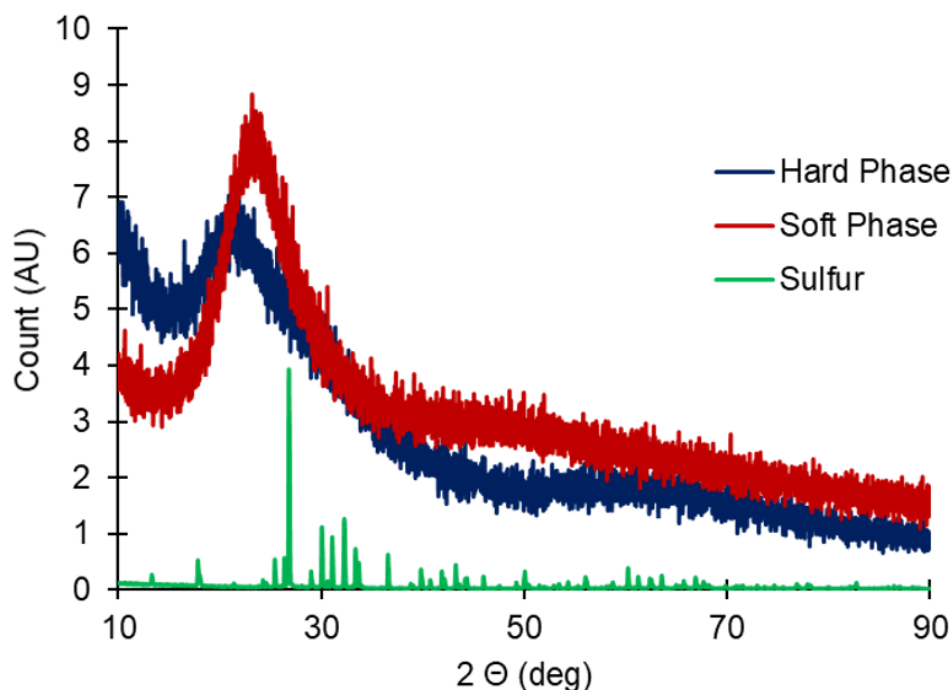
Figure 5.8: XRD analysis of hard and soft phase of 15% DCPD polymer compared the elemental sulfur. © 2021 Wiley-VCH GmbH. Image was reproduced under a RightsLink license.[24]

The XRD results indicated complete consumption of sulfur during the polymerisations. However, two days after curing, a patchy grey layer developed on the surface of the hard phase of the material. This was attributed so-called "sulfur blooming", a process during which elemental sulfur is regenerated by the depolymerisation of the polymer or polymeric sulfur and which has been previously observed on other cured inverse vulcanised polymer systems.[9, 39-41] In this case here, elemental sulfur was only observed on the surface of the polymer. To analyse the grey layer, SEM and EDX analysis was used. SEM analysis showed particles with various sizes ranging from sub-micron to over 20 microns (Figure 5.9). Using EDX analysis it was confirmed that these particles are indeed sulfur (Figure 5.9). This free sulfur on the surface on the polymer could potentially interfere with the adhesion experiments. Therefore, ways to remove the sulfur layer were investigated. The simplest was to treat the surface by hand using sandpaper (P80 grade). EDX analysis after sandpaper treatment of the surface showed no more large sulfur particles (Figure 5.9).
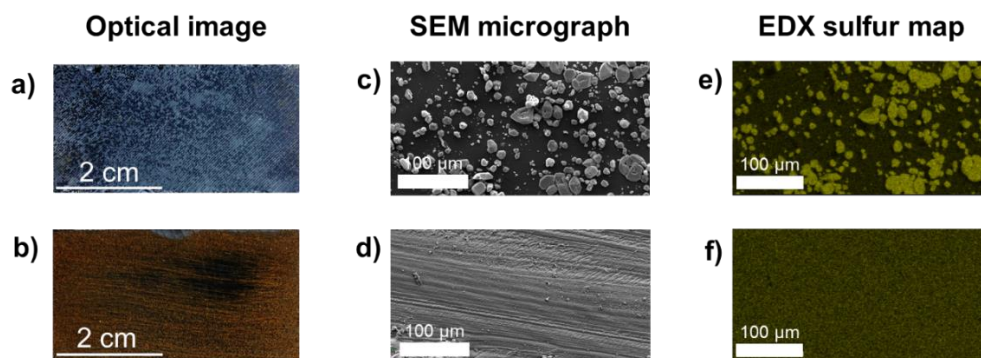
Figure 5.9: a) Image of polymer with gray sulfur layer after 2 days of curing. **b)** Image of polymer that had grey layer removed by hand using sandpaper. **c)** SEM micrograph of surface of polymer with gray layer showing particles on the surface. **d)** SEM micrograph of surface of polymer that was treated with sandpaper showing no particles left on the surface. **e)** EDX analysis showed that the particles on the surface are indeed sulfur. **f)** EDX analysis of the surface treated with sulfur showed no large sulfur particles on surface. © 2021 Wiley-VCH GmbH. Image was reproduced under a RightsLink license.[24]

Synthesis and characterisation of 50 wt% sulfur, 45 wt% canola oil, and 5% DCPD polysulfide

After the characterisation of the composite containing 15% of DCPD was completed, the phase separation observed was revisited. To investigate if the feed ratios of monomers had an impact on the phase separation, polymers with different feed ratios were made. The first new polymer had a feed ratio of 50 wt% sulfur, 45 wt% canola oil, and 5 wt% DCPD to determine if a higher canola oil content has an impact. For the synthesis total mass of 10 g for each reaction as well as the protocol was kept the same as for the previously described syntheses of the 15% DCDP polymer. After the 5% DCPD polymer was cured, it had a physical appearance which was very similar to the 15% DCPD polymer also showing phase separation (Figure 5.10).
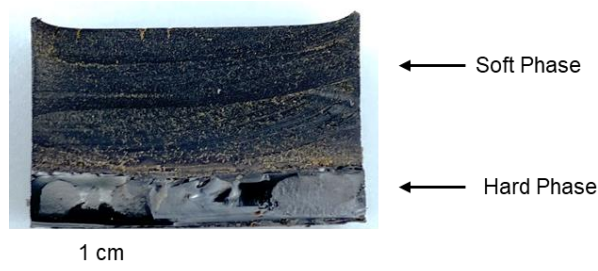
Figure 5.10: 5% DCPD polymer showing a soft and a hard phase.

DSC analysis of the soft phase showed a T_g of -30 °C, which is lower than the T_g of -26 °C that was recorded for the 15% DCPD polymer. This also matched with the physical characteristics of the soft phase of the 5% DCPD polymer, since it was softer to the touch compared to the soft phase of the 15% DCPD polymer. Interestingly, no T_g was observed for the hard phase of the 5% DCPD polymer. This means that the hard phase of the 5% DCPD polymer had no crystalline portion or the T_g is over the set instrument temperature of 250°C. Both phases were also analysed using STA. This showed a rapid mass loss in the hard phase between 170 °C and 350 °C (Figure 5.11). The mass loss continued after that, however at a much slower rate, until only 1% of its original mass was left at 800 °C (Figure 5.11). This is less mass retained compared to the hard phase of the 15% DCPD polymer which retained 18%. Two mass losses were seen in the soft phase of the 5% DCPD polymer, which is similar than the mass loss of the soft phase of the 15% DCPD polymer, however the mass losses of the 5% DCPD polymer are less pronounced. The first mass loss occurred between 190 °C and 300 °C and the second between 300 °C and 450 °C with 92% of its mass lost (Figure 5.11). However, after that the mass continued to decrease as a slower rate until all the mass was lost at 714 °C (Figure 5.11). This was a higher mass lost as was seen in the soft phase of the 15% DCPD polymer which still retained a mass of 7% at 800 °C.
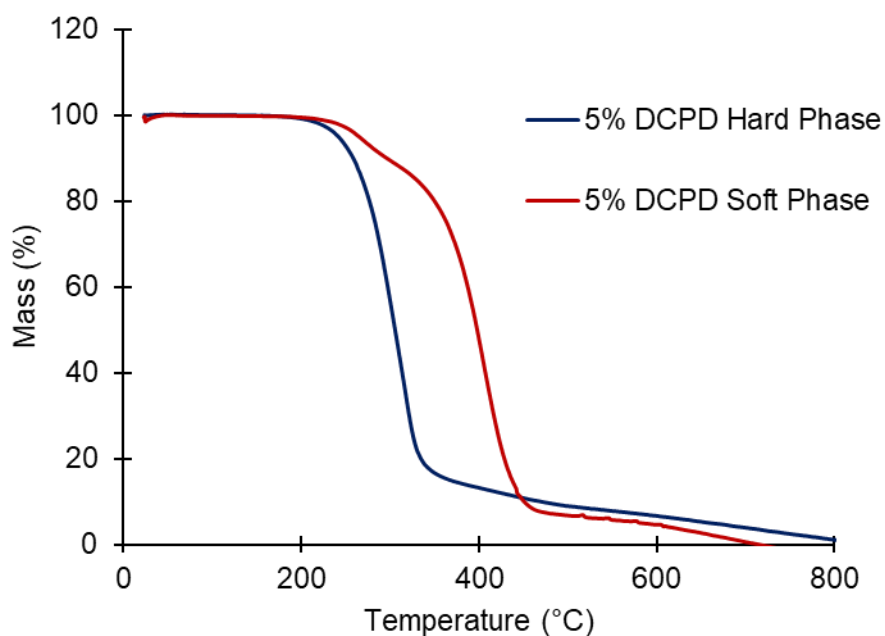
Figure 5.11: STA of soft and hard phase of 5% DCDP polymer.

Elemental analysis was also performed on the soft and hard phases of the 5% DCPD polymer. A similar trend was observed as has been seen in the 15% DCPD polymer. the hard phase showed a much higher sulfur content (93%) as did the soft phase (18%). On the other hand, the softer phase had a much higher carbon content (64%) as the hard phase (6%).

Synthesis and characterisation of 50 wt% sulfur, 25 wt% canola oil, and 25% DCPD polysulfide

It could be seen that the monomer feed ration had an impact on the characteristics of the material. Therefore, to probe more into the impact of feed ratios, attempts were made to synthesise a 50 wt% sulfur, 25 wt% canola oil, and 25% DCPD polymer since the polymer with a federation 50 wt% sulfur, 45 wt% canola oil, and 15% DCPD still showed phase separation. The same reaction protocol was used as for the other polymerisation. However, 6.5 minutes after the canola oil and DCPD were added into the molten sulfur, the reaction contents turned black and started to rise out of the reaction vessel indicating that a runaway reaction had occurred (Figure 5.12). This has been observed in other inverse vulcanisations with sulfur and DCPD.[39, 42, 43] As has been previously discussed in this thesis, this is likely due to DCPD undergoing a retro Diels-Alder reaction which results in the generation of cyclopentadiene, which in turn increases the alkene concentration in the reaction. This can lead to an uncontrolled increase of reaction rate (which was discussed in chapter 4 of this thesis).[42]

Figure 5.12: 25% DCPD reaction at 170 °C, 6.5 minutes after the canola oil and DCPD was added to the molten sulfur. © 2021 Wiley-VCH GmbH. Image was reproduced under a RightsLink license.[24]

In order to avoid further runaway reaction, the same reaction was performed again but at a lower temperature of 140 °C (this was in line with the strategy used in chapter 4 of this thesis and was done to avoid a runaway reaction). After the standard reaction of 9.5 minutes after the canola oil and DCPD addition the reaction mixture had still two phases and it was obvious that no polymer had formed yet (Figure 5.13). Regardless, the reaction mixture was poured into a mould and cured at 130 °C for 24 hours. Another reaction like this was run, this time however, the reaction was allowed to continue until the reaction contents presented as one phase. After a reaction time of 65 minutes this as the case and the reaction was a homogenous black liquid (Figure 5.13). Next, reaction contents were also poured into a mould and cured for 24 hours as 130 °C.
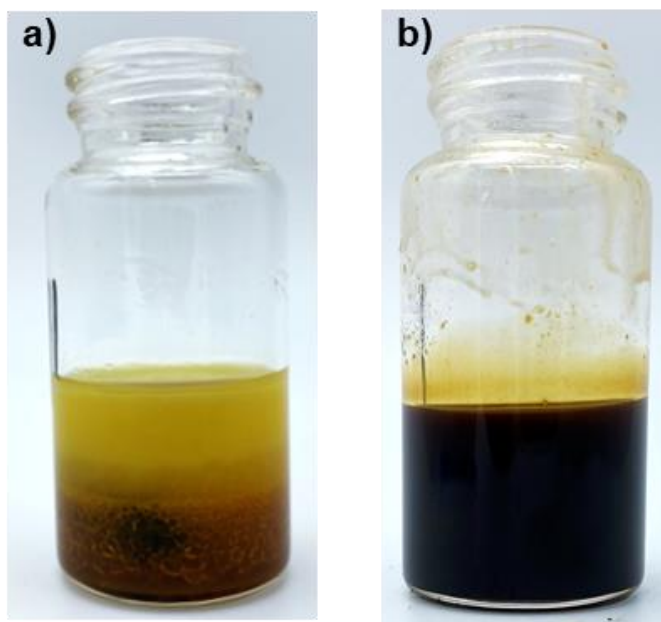
Figure 5.13: a) 25% DCPD reaction at a lower temperature of 130 °C after the normal reaction time of 9.5 minutes. **b)** 25% DCPD reaction at a lower temperature of 140 °C after a reaction time of 65 minutes.

After the curing process, the samples were removed from the oven and allowed to cool to room temperature. Both samples had a liquid top layer with the top layer of the sample with the longer reaction time being more viscous (Figure 5.14).
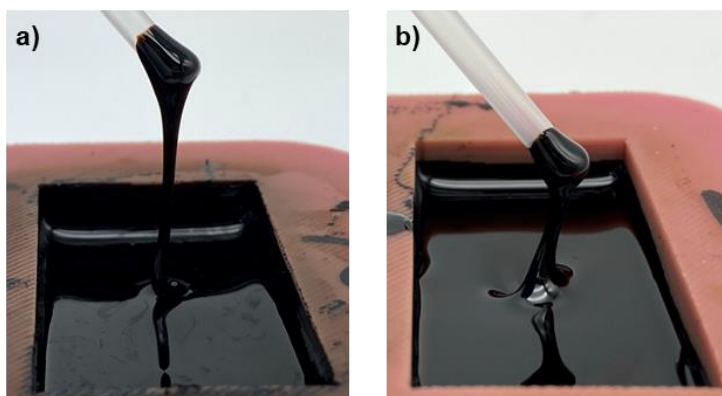
Figure 5.14: a) Short (9.5 minutes) and **b)** long (65 minutes) reaction time 25% DCPD low temperature reactions showing a liquid layer on top after the curing process.

However, under the liquid layer both samples had a harder layer. The hard layer of the long reaction time sample was as hard as the hard layer of the 15% DCPD polymer. However, the hard layer of the short reaction time 25% DCPD polymer was softer than that of the long reaction time sample. Following that, both phases of both samples were analysed using DSC and STA. No T_g was observed in either material. This could possibly be due to only low molecular weight species being present. STA analysis of the liquid phases of the short and long reaction time samples showed similar results. At first a rapid two stage mass loss was observed between 180 °C and 470 °C (Figure 5.15). This was then followed by a more gradual mass loss up to 800 at which temperature the liquid phase of the short reaction time sample retained a mass of 3% while all the mass was lost from the long reaction time sample (Figure 5.15). STA analysis of the hard phases of both reactions showed differences. While both materials showed a rapid single mass loss followed by a gradual mass loss, the hard phase of the short reaction lost around 75% of its mass by that point which is around 25% more mass loss as was seen in the hard phase of the long reaction time sample (Figure 5.15). Further, as the final temperate of 800 had been reached the hard phase of the long reaction retained 22% of its weight compared to a 6% mass retention of the hard phase of the short reaction time reaction (Figure 5.15). These results indicate that clear differences existed between the two different phases within the different reaction times. Further, differences between the long and short reaction times have been observed. This is also reflected in the elemental analysis (Figure 5.16).
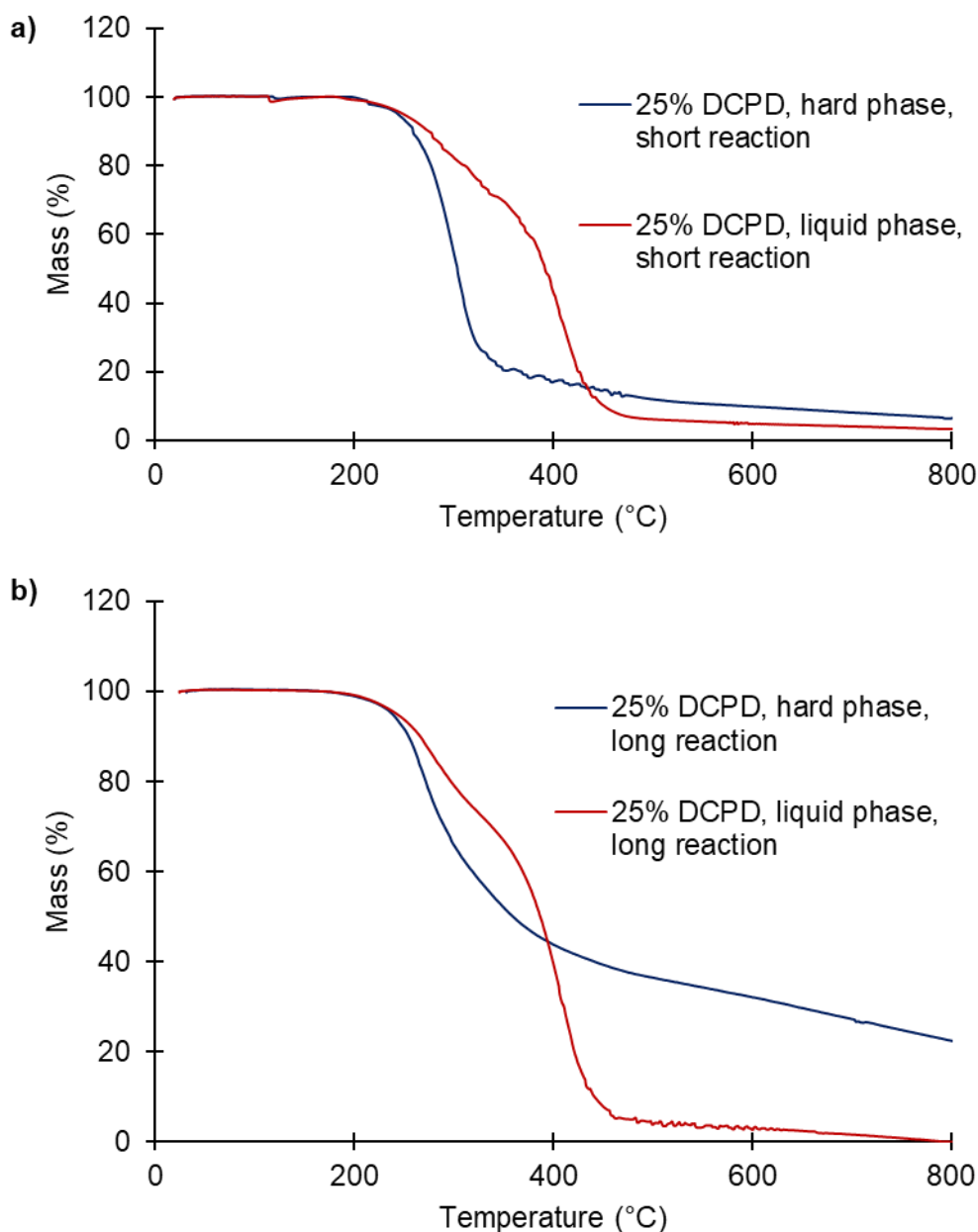
Figure 5.15: STA analysis of **a)** 25% DCPD long reaction time (65 minutes) sample and **b)** of the 25% DCPD short reaction time (9.5 minutes) sample.

Elemental analysis of the liquid and soft phases of the short (9.5 minutes) and long (65 minutes) reaction time, low temperature 25% DCPD reactions followed the same trend as was seen for the 15% and 5% DCPD polymers. The sulfur content in both reactions was much higher in the hard phase (91% in the short reaction and 75% in the long reaction) as compared to the liquid phase (19% in the short reaction and 20% in the long reaction). In contrast the carbon content was much higher in the liquid phase

(66% in the short reaction and 63% in the long reaction) as it was on the hard phase (8% in the short reaction and 23% in the long reaction).
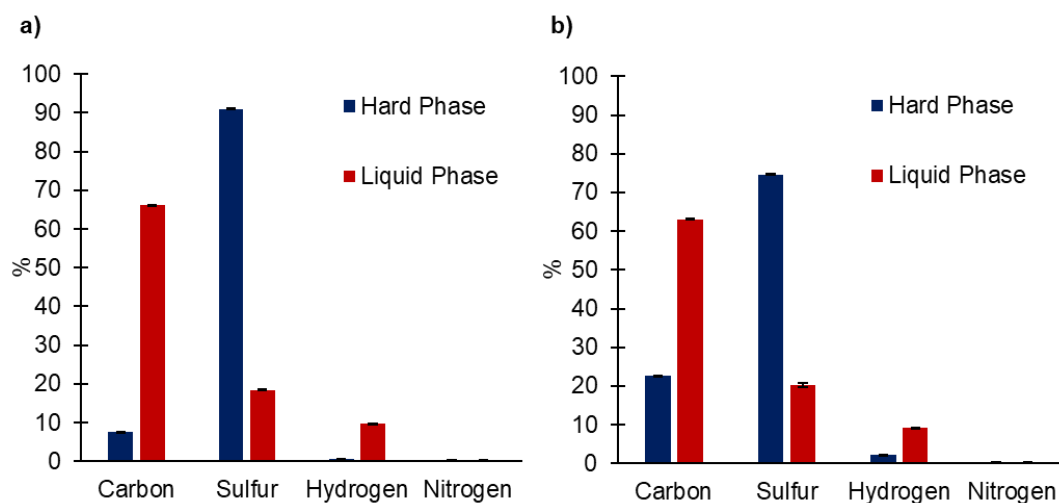
Figure 5.16: Elemental analysis of **a)** the short (9.5 minutes) 25% DCPC low temperature reaction and **b)** long (65 minutes) 25% DPCD low temperature reaction.

The liquid phases of both, the short and long reaction time samples were soluble in chloroform, making it possible to perform ^{1}H NMR analysis. The NMR spectra of the liquid phases of both samples did not show any significant differences (Figure 5.17). Therefore, only the spectrum of the liquid phase of the long reaction phase was compared to ^{1}H NMR spectra of DCPD and canola oil.
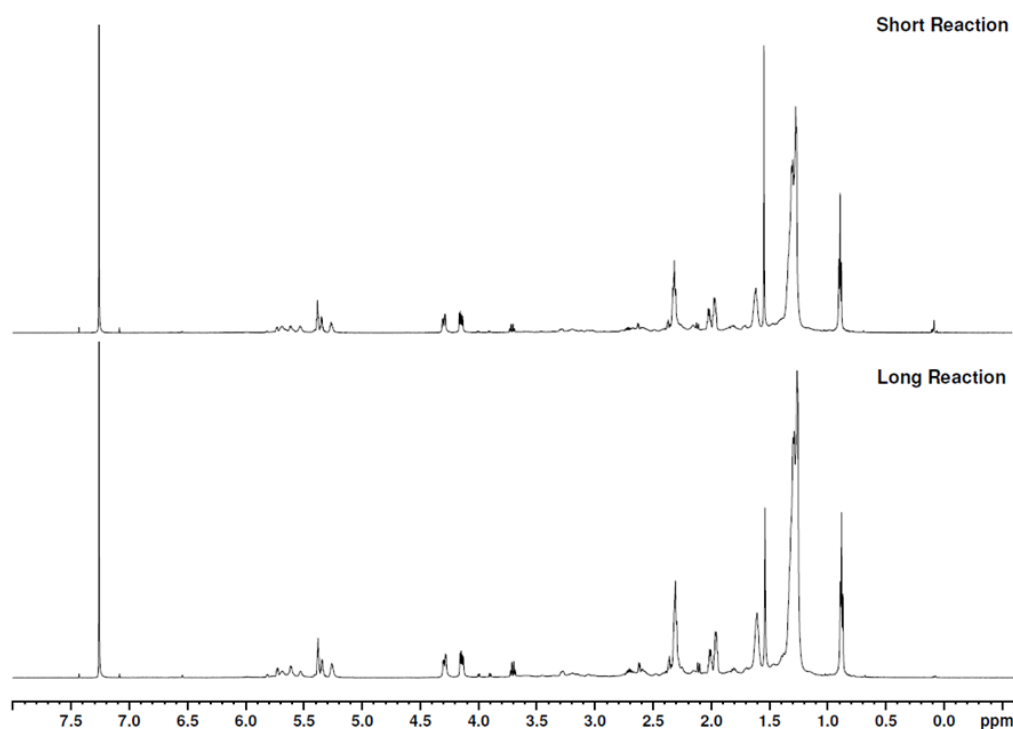
Figure 5.17: Comparison of the ^{1}H NMR spectra of the liquid phase of the short and long reaction time samples.

As can be seen in Figure 5.18, no unreacted DCPD has been observed, which can be concluded from the absence of their characteristic peaks between 6.0-5.5 ppm. The DCPD had reacted and is in this soft phase, or it is mostly in the hard phase since it is the more reactive alkene. Peaks between 3.5-4 ppm seen in the liquid phase spectra of the long reaction time product indicate the presence of CHS groups which have been formed during the reaction since they cannot be seen in the DCPC or canola oil spectra (Figure 5.18). However, some alkenes are still present in the liquid phase of the long reaction time product as the peaks between 5.7-5.5 ppm indicate. Since the signals from the canola oil alkenes (5.3-5.2 ppm) are still visible in the spectra of the liquid some of the alkenes between 5.7-5.5 ppm are likely from unreacted canola oil (Figure 5.18). The reason that some of the canola oil had not reacted might be the lower temperature of 140 °C at which the reaction was performed. It is possible the canola oil alkenes only react at higher temperatures. Although the liquid phase still contained mostly canola oil, some had sulfurised as indicated by the sulfur content of the liquid phase in the elemental analysis above (Figure 5.16) However, the alkenes of DCPD readily reacted at 140 °C.
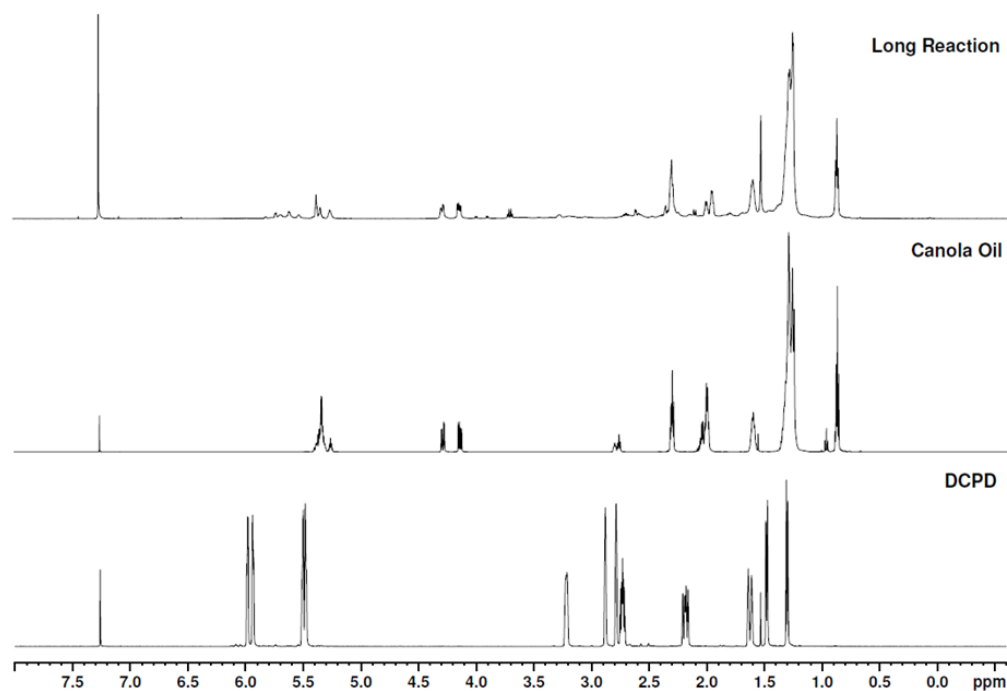
Figure 5.18: ^{1}H NMR spectra of DCPD, canola oil and the liquid phase of the long reaction.

Therefore, for this terpolymer to form, higher temperatures are needed in order for both, the canola oil and the DCPD to react. Even when higher temperatures and vigorous stirring are used during the synthesis, phase separation still occurs. Additionally, the syntheses of the 5% DCPD polymer and the 25% DCDP polymer showed that the original composition of 50 wt% sulfur, 35 wt% canola oil, and 15% DCPD was ideal. When a composition of 50 wt% sulfur, 45 wt% canola oil, and 5% DCPD is used the polymer is softer than the original polymer which can influence the stability and strength of the material. If a higher content of DCPD is used (50 wt% sulfur, 25 wt% canola oil, and 25% DCPD) a dangerous runaway reaction can occur. Further, it has been shown that increasing the reaction time while decreasing the reaction temperature leads to a liquid top phase which renders the material unusable. For subsequent experiments the 50 wt% sulfur, 35 wt% canola oil, and 15% DCPD polymer was used.

Chemically induced adhesion and mechanical testing of the 50 wt% sulfur, 35 wt% canola oil, and 15% DCPD polymer

Since the synthesis and upscaling of the key polymer resulted in solid polymer blocks, the chemical adhesion using an amine catalyst and the strength of this adhesion was explored next. In previous studies the Chalker lab had reported that the amine-catalysed S-S metathesis was most effective when it was performed above the T_g of the polymer.[36] If bonding is carried out above the T_g of the polymer, the polymer chains are mobile enough to facilitate bonding after the cleavage of the S-S crosslinks. Therefore, the soft phase with the lower T_g of the 15% DCPD polymer was chosen as surface for S-S metathesis, leaving the hard phase with a higher T_g as a rigid base. This way advantage could be taken of the phase separation, with using the hard phase as a base whereas the soft phase served as the bonding surface. First tests showed that the bond was significantly stronger if the grey sulfur layer was removed before hand using sandpaper. The treatment of the bonding surface would not only remove the sulfur layer but would also provide a rougher interface with greater surface area for bonding. Since triethylamine was the most efficient catalyst that has been screened in previous studies, proving its ability to restore cut dog bone specimens of the same polymer to their original strength,[36] it was evaluated as catalyst for S-S metathesis for this study. The first step of the bonding protocol was to remove the sulfur layer and roughen the surface of the soft phase of two polymers with sandpaper (4 cm^2 surface area for each polymer block). Next, 100 μL of triethylamine (this volume was chosen to that the bonding surface was covered with the catalyst) was added to the surface of one block. Another polymer block was then placed on top of the block with the catalyst on its surface. A 10 kg weight was added on top of the polymer for a total of 3 hours to ensure efficient surface contact and bonding. In order to determine and triethylamine could be detected after the bonding, the bonded polymers were cut in half and a cross section was analysed using scanning electron microscopy (SEM) and energy dispersive X-ray analysis (EDX). This analysis did not detect any nitrogen, therefore indicating that triethylamine was not incorporated into the polymer (Figure 5.19). Also, a drop of triethylamine was deposited on the surface of the polymer and left for 24 hours. SEM and EDX analysis of the surface of this polymer also showed no nitrogen (Figure 5.19). This led to the conclusion that the S-S metathesis using triethylamine is effectively traceless.

Cross-section of Et₃N adhesion

Surface Et₃N
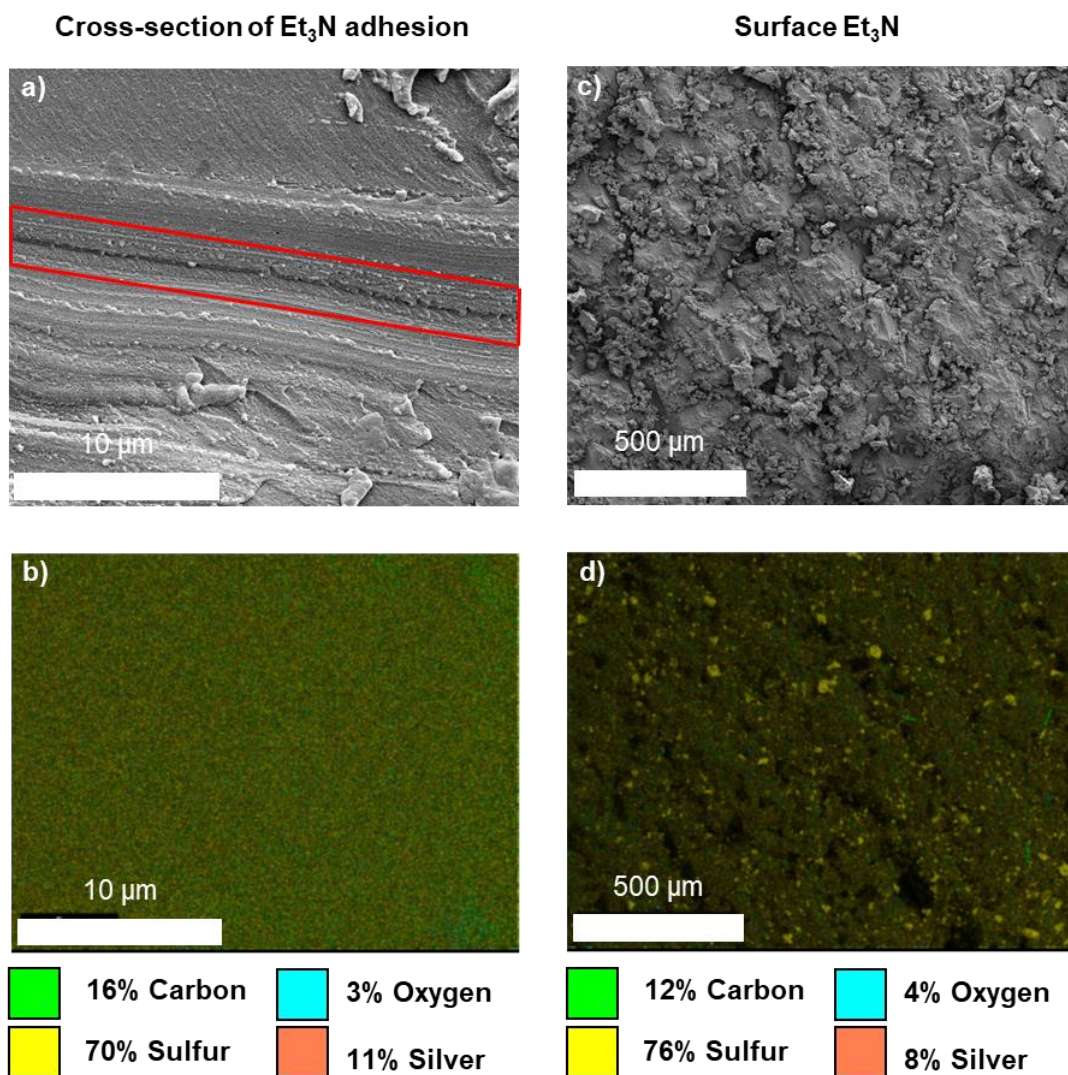
Figure 5.19: a) SEM micrograph of cross section of polymer interface. The adhesion zone of the two polymers after the adhesion took place is highlighted in red. **b)** EDX elemental map of adhesion zone. **c)** SEM micrograph of surface of polymer on which 5 µL of triethylamine were deposited 24 hours ago and **d)** EDX elemental map of the area on which the triethylamine was placed. Silver signal is due to conductive coating. © 2021 Wiley-VCH GmbH. Image was reproduced under a RightsLink license.[24]

Next, the strength of the bonded polymer surface was tested. In the first instance, a metal plate attached to bolts was embedded into the polymer by first synthesising the polymer, pouring it into the mould around the metal framework and finally curing the polymer at 130 °C for 24 hours. The metal plate had the dimensions of 5 cm × 2 cm and was suspended approximately 5 mm above the bottom of the mould (Figure 5.20). This resulted in a polymer bock with the with a length of 6 cm a width of 2.5 cm and a height of 1.5 cm with threaded metal rod protruding out of the material (Figure 5.20). Using this

set-up, two samples were prepared. Next, the samples were bonded together by adding 300 μL of triethylamine (enough to cover the surface from which the grey sulfur layer was removed) to the surface of one polymer block before the other polymer block was placed on top and a 5 kg weight was used to ensure contact between the surfaces. A total of 5 hours was allowed for the adhesion to take place (Figure 5.20).
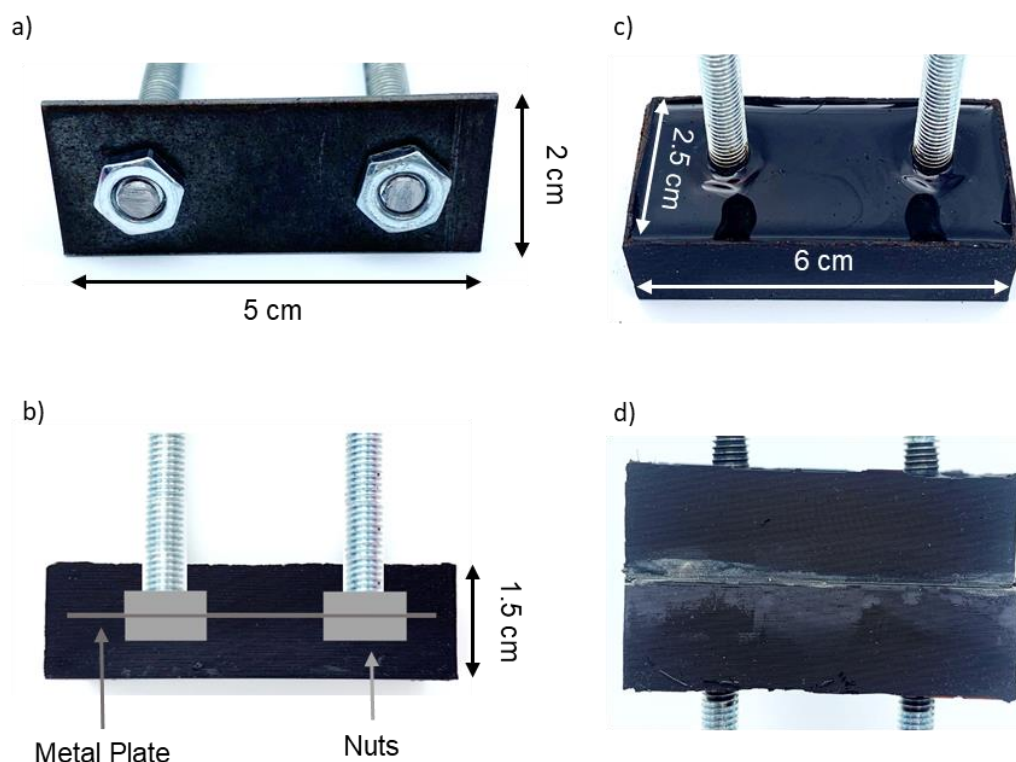
Figure 5.20: a) metal scaffold for the polymer made out of a metal plate (5 cm × 2 cm) fastened to two threaded rods using nuts. **b)** Position of metal plate in cured polymer. **c)** Cured polymer containing metal plate. **d)** Two polymer samples bonded together using triethylamine. © 2021 Wiley-VCH GmbH. Image was reproduced under a RightsLink license.[24]

It should be noted that this setup resulted in the hard phases being bonded since the soft phase had the rod protruding out of it hence it was not known if the adhesion would be successful. However, the polymers did bond together and were tested for shear strength next (Figure 5.21). The sample failed at a load of 6.2 kg after a displacement of 2.5 mm (Figure 5.24). The failure of the material occurred in the bulk polymer, around the metal plate and at the adhesion site. While it was encouraging that adhesion took place, this result showed that the set-up of this test could not give representative results

for the adhesion of the polymer interface since the failure showed a weak spot around the metal plate, which acted as a stress concentrator.
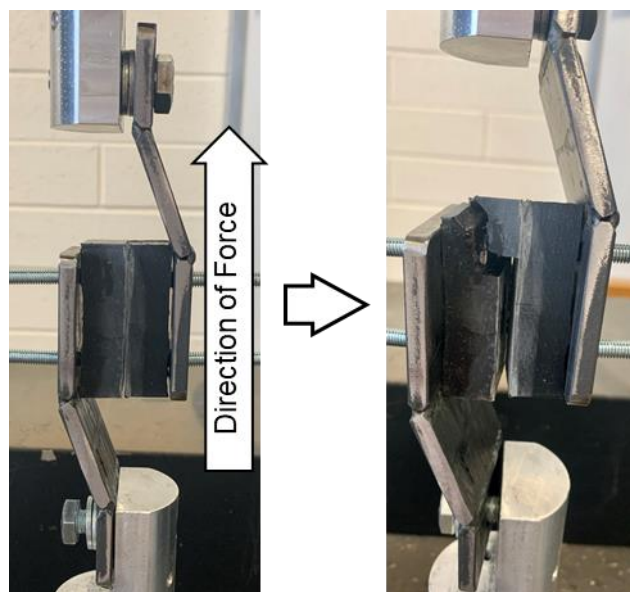
Figure 5.21: Shear test set-up. A force was applied to the polymer and the material failed at the adhesion site as well as at the bulk material and the embedded metal plate. © 2021 Wiley-VCH GmbH. Image was reproduced under a RightsLink license.[24]

Therefore, a new sample holder was developed. The aim was to make a sample holder that was able to hold bonded polymer blocks and test the strength of the bond without having any internal metal components that could act as stress concentrators. Figure 5.22 shows the new sample holder.

Figure 5.22: New sample holder. © 2021 Wiley-VCH GmbH. Image was reproduced under a RightsLink license.[24]

This new sample holder also allowed the polymers to be bonded together at the softer phase with a lower T_g as the hard phase. The dimensions of the polymer needed for the new sample holder was a width of 2.5 cm, a height of 1.7 cm and a length of 5.00 cm. The surfaces of the cured polymer samples were prepared for bonding by removing any surface sulfur by a treatment with sandpaper and to ensure a flat and roughened surface for better surface contact. For the adhesion, 300 µL of triethylamine was added to the surface of one polymer block and another bock was added on top. Then, a 10 kg weight was applied for 3 hours. The adhesion was tested using the same protocol as for the samples with the metal plate bonded at the hard phase. For comparison, polymers were bonded together at the soft phase using commercially available superglue (Bostik Super Glue Industrial Strength). This was done by treating the polymer surfaces with sandpaper before enough super glue was added to cover the surface of one polymer block. After that, a second polymer was placed on top, and a 10 kg weight was added for 3 hours. On all samples shear tests were carried out. Figure 5.23 shows the setup for these tests as well as the polymer blocks used, and a representative sample of polymer blocks bonded together using triethylamine after shear testing.
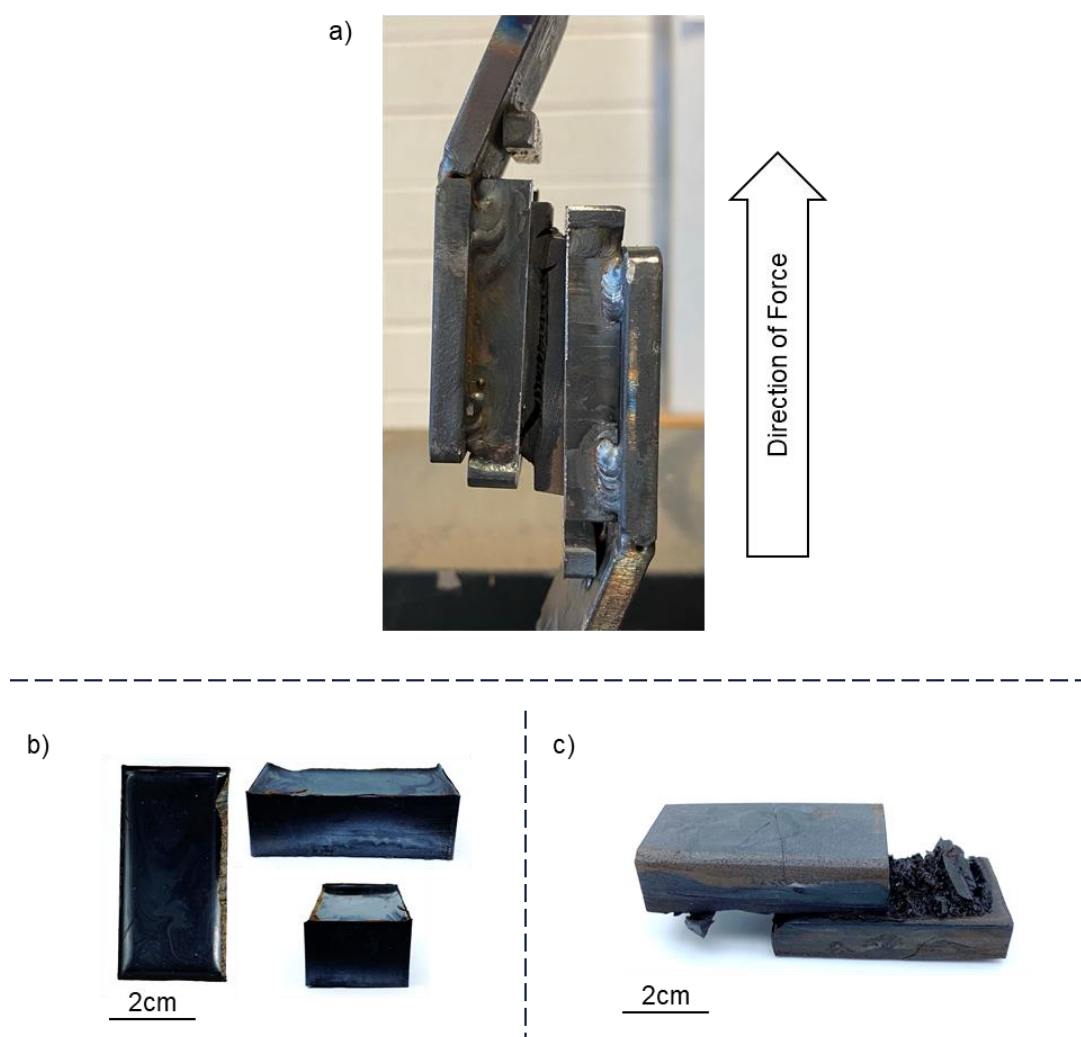
Figure 5.23: a) Sample during shear test with modified sample holder. **b)** Top, side and front view of polymer block after curing ready for adhesion. **c)** Representative sample of polymer blocks bonded together using triethylamine after shear testing. © 2021 Wiley-VCH GmbH. Image was reproduced under a RightsLink license.[24]

The best performing sample was that bonded together with triethylamine with a maximum load of 25 kg at a displacement of 8.7 cm (Figure 5.24). In contrast, when the polymers were bonded at the hard phase the bond failed at a much lower load of 2.46 kg at a displacement of 1.6 mm (Figure 5.24). The superglue adhesion demonstrated a relatively high load of 20 kg (at a displacement of 4.75 mm) (Figure 5.24). However, in this case the adhesion failed close to the surface of the polymers. This is in contrast to the samples that were bonded by triethylamine at the soft phase which failed at the bulk polymer and not at the adhered surface.
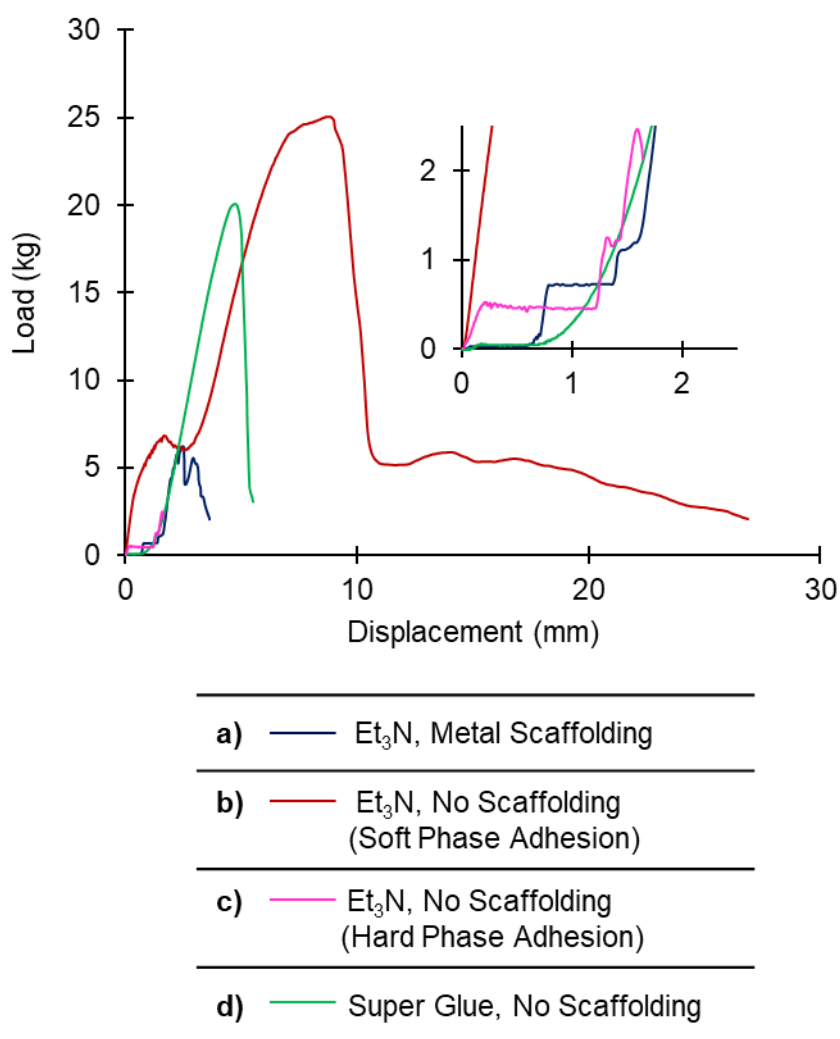
Figure 5.24: Shear tests of polymer bonded with **a)** triethylamine containing the metal scaffolding (maximum load of 6.24 kg at a displacement of 2.48 mm), **b)** triethylamine without scaffolding, adhered to the soft phase (maximum load of 25.01 kg at a displacement of 8.7 mm), **c)** triethylamine without scaffolding adhered to at the hard phase (maximum load of 2.48 kg at a displacement of 1.6 mm) and **d)** superglue without scaffolding at the soft phase (maximum load of 20.05 kg at a displacement of 4.75 mm). © 2021 Wiley-VCH GmbH. Image was reproduced under a RightsLink license.[24]

Next, bonding at the soft phase without sandpaper treatment was tried. However, as the polymer is poured into the mould and cured, the surface of the polymer blocks is not flat. Ridges can be seen towards the edges. An attempt was made to trim the edges before the bonding procedure, but the strength of the adhesion was not as strong as seen in bonding experiments for which the polymer surfaces were treated with sandpaper. This could be because of the bonding surfaces not being flat enough to ensure maximum contact between the two polymers. To ensure an even, flat surface it

would have been necessary to remove a whole layer form the surface of each polymer. Doing that would have resulted in more lost material then is lost during the sandpaper treatment. This emphasise that the strongest bond is achieved when the polymer blocks are bonded at the soft phase after the surface has been treated with sandpaper.

These results showed that the triethylamine induced S-S metathesis results in a strong bond at the soft interface of the polymers and that adhesion at the hard phase is the site of failure. Further, the failing of the samples bonded with superglue at the interface indicated that the S-S metathesis is a superior method of bonding the polymers bocks together.

Structural strength improvement of the polymer material

With the testing of the shear strength of the triethylamine complete attempts were made to improve the structural strength of the polymer. This was done by adding carbon materials to the polymer before the curing process since they are known the increase the mechanical of materials as was discussed in the introduction of this chapter. The structural strength of the polymers was determined using three point bent testing (Figure 2.25).
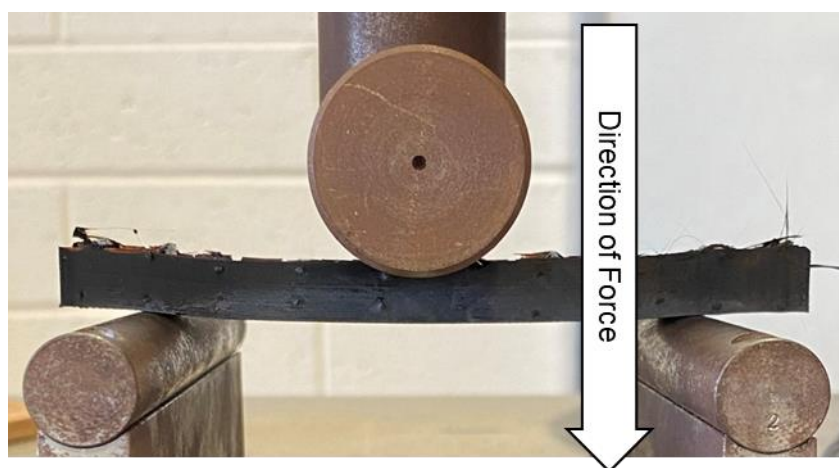
Figure 5.25: Set-up of three-point bend testing. © 2021 Wiley-VCH GmbH. Image was reproduced under a RightsLink license.[24]

The carbon materials chosen were carbon fibre (Filaments 12K, Tensile strength: 3530 MPa, Tensile modulus: 230 GPa, Elongation: 1.5%, Density: 1.76 g/cm^3) and carbon nanotubes (outside diameter: 48-78 nm, length: 10-30 μm). These were chosen

to test two different forms of carbon material, long carbon fibres and short carbon nanotubes. To assess the effect these carbon materials have on the structural strength of the polymer, three-point bend testing was used. A total of five samples with the dimensions of 12 × 2 × 1 cm were prepared. The synthesis protocol of the polymers used for three-point bend testing was the same as for the polymers made for the shear tests (three 10 g reactions simultaneously run). The liquid polymers were then poured into a different mould to produce polymer block with the above mentioned dimensions and cured at 130 °C for 24 hours (Figure 5.26).

Figure 5.26: Mould for pouring polymers for three point bend testing. © 2021 Wiley-VCH GmbH. Image was reproduced under a RightsLink license.[24]

The first sample made did not contain any reinforcement do determine the strength of the pure polymer. The next two samples were reinforced with approximately 0.5 g of carbon fibre. To one sample the carbon fibre strands were added loosely to the liquid polymer after it was poured into the mould. Care was taken that the fibres were evenly distributed throughout the polymer before the mould was placed into the oven to cure the polymer (Figure 5.27). The next sample was reinforced by threading 0.5 g of carbon fibres though the mould. This insured alignment as well as even distribution of the fibres (Figure 5.27).
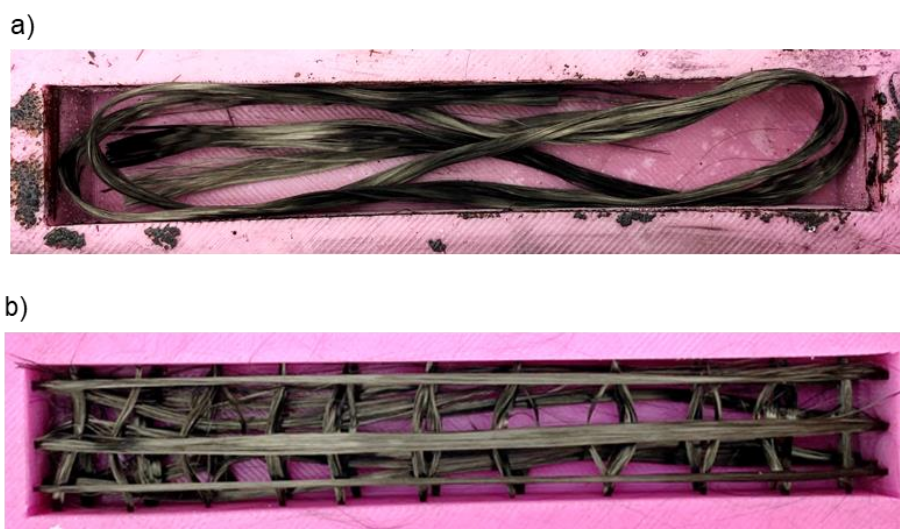
Figure 5.27: a) 0.5 g of loose and **b)** threaded carbon fibre in mould. © 2021 Wiley-VCH GmbH. Image was reproduced under a RightsLink license.[24]

For the last two samples carbon nanorods were used to reinforce the samples. To one sample 0.5 g of nanotubes were added and to the other samples 1.0 g of nanotubes were added. This corresponded to a carbon weigh % of 1.88 and 3.86 respectively. The nanotubes were added to the liquid polymer after it was poured into the mould. To ensure even distribution the mixture was stirred suing a spatula. It has to be noted that after adding 1.0 g of nanotubes, the consistency of the polymer was that of a thick paste and that it would have been difficult to ensure even distribution if more nanotubes were to be added. After the samples were cured the polymer blocks were a hard material. The paste-like consistency of the polymers before the curing process might prove useful as putty or mortar before curing, since unlike the liquid polymer the polymer-nanorod past does adhere to surfaces without running off. Next, three-point bend tests were performed on all the polymer samples (Figure 5.28).
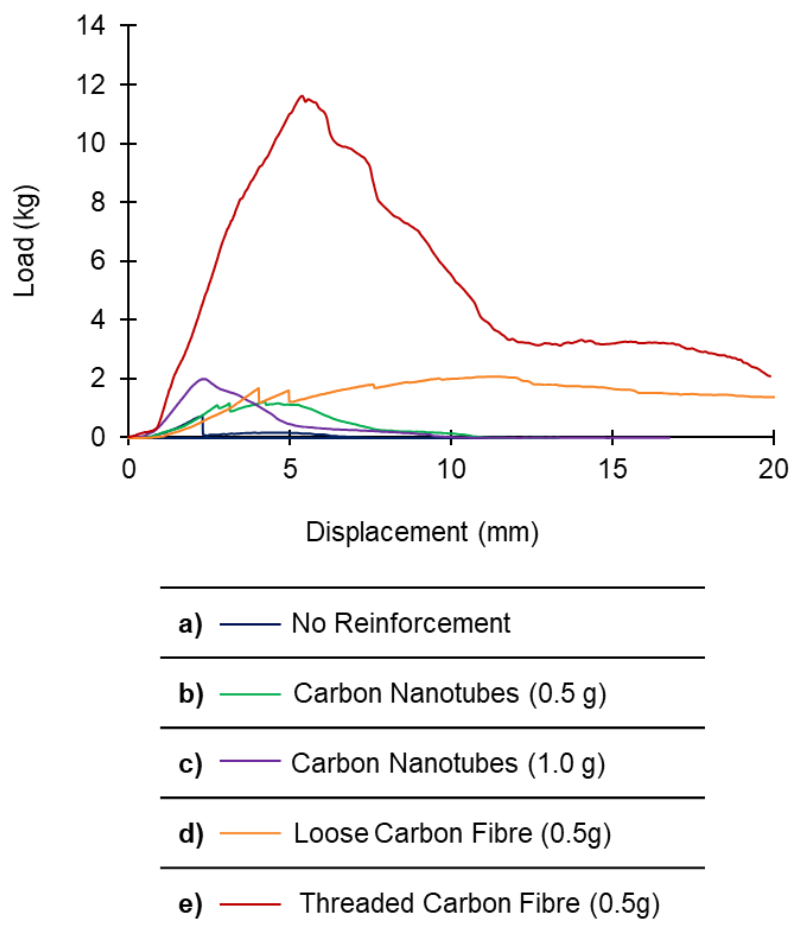
Figure 5.28: Three-point bend tests of polymers **a)** without reinforcement (max. load: 0.73 kg), **b)** reinforced with 0.5 g of carbon nanotubes (max, load: 1.21 kg) or **c)** 1.0 g of carbon nanotubes (max. load: 1.99 kg), **d)** reinforced with 0.5 g of loose carbon fibre (max. load: 2.02 kg) and **e)** reinforced with 0.5 g of threaded carbon fibre (max. load: 11.61 kg). © 2021 Wiley-VCH GmbH. Image was reproduced under a RightsLink license.[24]

By far the weakest material was the polymer without any reinforcement, failing at a load of 0.73 kg (Figure 5.28). Adding carbon nanotubes to the polymers slightly improved the maximum loads. The polymer reinforced with 0.5 g of nanotubes returned a maximum load of 1.21 kg whereas adding 1.0 g of nanotubes gave a maximum load of 1.99 kg (Figure 5.28). Adding 1.0 g of loose carbon fibre resulted in a maximum load of 2.05 kg which was similar to the sample which had 1.0 g of nanotubes added (Figure 5.28). However, the highest load was seen in the polymer that was reinforced by threading aligned carbon fibre (0.5 g) through the mould. The way of reinforcement resulted in a maximum load of 11.61 kg (Figure 5.28).

Besides adding to the structural strengh of the polymers, reinforement also affected the stiffness of the materials. Polymer samples reinforces with 0.5 g of carbon

nanotubes oar loose carbon fibre had a similar stiffness to the pure polymer samlple (modulus of elastitity of 54.0 MPa, 45.9 MPa and 41.6 MPa, respectively). This showed that the polymer itself is the main contributor to the stiffness of the samples. In contrast, reinforcing the sample with 1.0 of carbon nanotubes increased the stiffness significantly to 121.3 MPa. The highest stiffness was seen in the sample that was reinforced with threaded carbon fibre with a modulus of elasticity of 256.2 MPa. This emphasised that the orientation of the fibres is critical to the maximum load and stiffness of the sample. Additionally, all the samples that were reinforces failed at a greater displacement as the pure polymer sample, especially the samples containing carbon fibre. These samples (loose and threaded carbon fibre) reached displacement of over 20 mm while still displaying a load (Figure 5.28). For the samples containing carbon nanotubes, their stiffness increased with increasing nanotube content. Attempts were made to adhere two carbon reinforced polymer blocks to each other, however the bond failed before the instrument registered any force. We attribute that to the large number of carbon fibre present at the bonding interface of the polymer pieces. The present of carbon would reduce the amount of sulfur that is necessary to facilitate the adhesion.

Conclusion

In conclusion, a polymer made from canola oil, DCPD and elemental sulfur was successfully synthesised and shaped into polymer blocks by pouring the liquid pre-polymer into mould followed by curing at 130 °C for 24 hours. Phase separation into a soft top phase and a hard bottom phase was observed. However, it has been found that the soft phase with a lower T_g is better suited for the adhesion chemistry using triethylamine then the hard phase with a higher T_g. The strength of the adhesion was quantified using shear testing and has been found to be stronger than the adhesion of commercial superglue. Efforts to increase the flexural strength of the bulk polymer by adding carbon materials were also successful. This study is a step toward using polysulfide polymer as the bulk material and to bond them covalently at their interface without the use of adhesives but only using catalytic amounts of an amine like triethylamine. Future research has to focus on further improving the mechanical properties of these terpolymers and upscaling their synthesis for commercial uses such as in construction.

The last experimental chapter of this theses will investigate yet another polysulfide polymer system. Namely the catalytic adhesion of a polymer made from sulfur, canola oil and dicyclopentadiene using triethylamine.

Publication that resulted from the research in this chapter:

Chemically Activated S-S Metathesis for Adhesive-Free Bonding of Polysulfide Surfaces

Mann, M.; Pauling, P. J.; Tonkin, S. J.; Campbell, J. A.; Chalker, J. M., Chemically Activated S-S Metathesis for Adhesive-Free Bonding of Polysulfide Surfaces. *Macromol. Chem. Phys.* **2021,** 2100333.

Experimental details

General considerations

Materials

Dicyclopentadiene (DCPD) was purchased from Sigma-Aldrich and used as received. Sulfur was purchased from Sigma-Aldrich (reagent grade, powder, purified by refining, -100 mesh particle size). The carbon fiber tow (fiber type: T300, Filaments 12K, Tensile strength (MPa): 3530, Tensile modulus (Gpa): 230, Elongation (%): 1.5, Density (g/cm^3): 1.76) was purchased from Carbon Fiber Australia. Carbon nanotubes were purchased from Nanografi Nanotechnology (Industrial grade MWCNT, purity: >92%, outside diameter: 48-78 nm, length: 10-30 µm). Canola oil was purchased from Just Fry Oil Australia. Triethylamine (Et$_3$N, ≥99.0%) was purchased from Sigma-Aldrich.

Simultaneous thermal analysis (STA) was performed using a Perkin Elmer STA 8000. Between 5-10 mg of sample were held at 40 °C for 4 minutes before the temperature was increased by 10 °C/minute to 800 °C. This was done under a 20 mL/min nitrogen flow.

Differential scanning calorimetry (DSC) was performed using a Perkin Elmer DSC 8000. Between 5-10 mg of sample was cooled to -80 °C and held for 4 minutes. After that the temperature was increased to 80 °C by 10 °C/minute and held for 4 minutes. Next, the sample was again cooled to -80 °C by 10 °C/minute and held for 4 minutes at that temperature. Finally, the sample was heated to 250 °C by 10 °C/minute. This was under a 20 mL/minute nitrogen flow.

CHNS elemental analysis was performed by The Campbell Microanalytical Laboratory at the University of Otago in New Zealand.

Scanning electron microscopy (SEM) and energy dispersive X-Ray (EDX) analysis were obtained using a FEI Inspect F50 SEM fitted with a EDAX energy dispersive X-Ray detector. Samples were sputter coated with silver metal (20 nm thickness) before analysis.

Powder X-ray diffraction (XRD) was carried out on a Bruker D8 Advance Eco diffractometer (Bragg-Brentano geometry) using Co-Kα radiation (λ = 1.78897 Å). The Bragg angle (2θ) was varied from 10° to 90° with a step size of 0.019°, measurement time of 0.6 s per step and sample rotation at 10 rpm. The samples were deposited onto a sample holder well before analysis.

Mechanical testing: Shear testing and three-point bend testing was performed using an Intron Series XI Materials Testing System fitted with a 5 kN static load cell. For the shear test the samples were mounted in the custom-made sample holder and the cross head was driven up (tension/shear) at a speed of 1.3 mm / minute. For the three-point bend test, the sample was placed on the instrument sample holder and the cross head was driven down (flexure) at a speed of 10 mm / minute.

1H NMR spectra were recorded on a 600 MHz Bruker spectrometer with $CDCl_3$ as solvent.

Spectra were referenced to residual solvent peaks ($\delta H = 7.26$ for $CDCl_3$).

Polymer synthesis and characterisation

After the polymer was synthesised, the liquid mixture was poured into a silicon mould. After the curing process, the material presented as solid polymer block.

Figure 5.29: Silicon mould into which the liquid polymer is poured prior to curing and cured polymer block. © 2021 Wiley-VCH GmbH. Image was reproduced under a RightsLink license.[24]

STA analysis of the hard bottom part and the soft top parts of the polymers were done in triplicate.
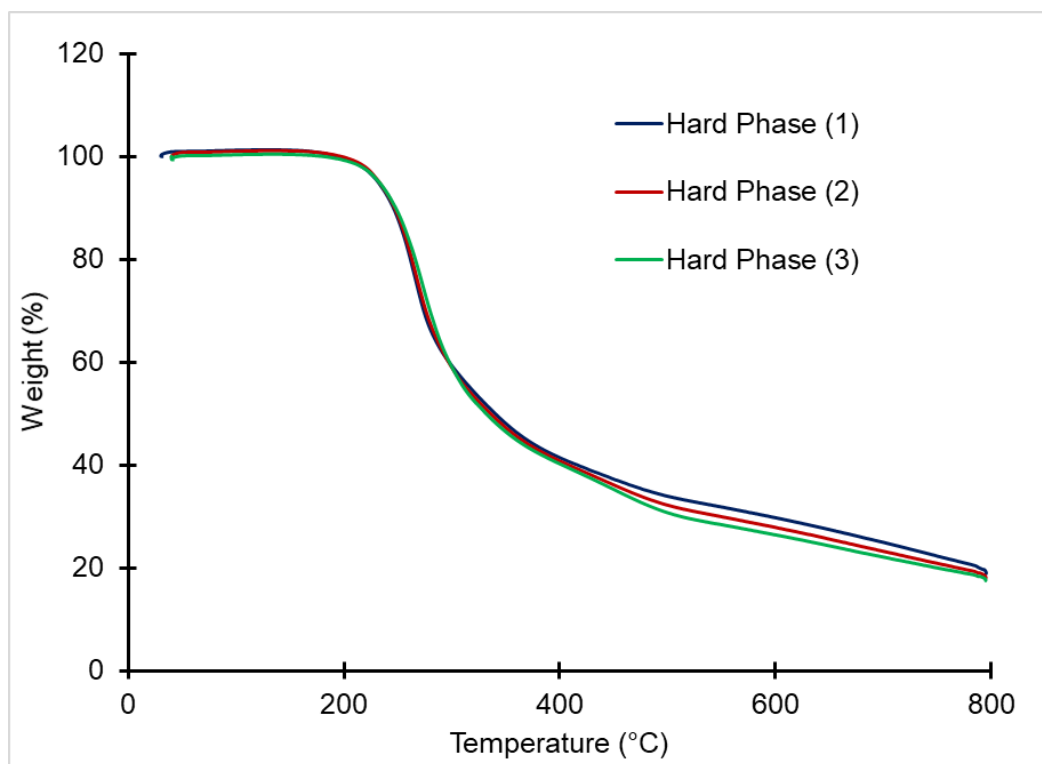
Figure 5.30: STA of the hard phase of the 15% DCPD polymer indicating a continuous weight loss starting at 180 °C. After the samples have been heated to 800 °C, only 18 % of their mass remains. © 2021 Wiley-VCH GmbH. Image was reproduced under a RightsLink license.[24]
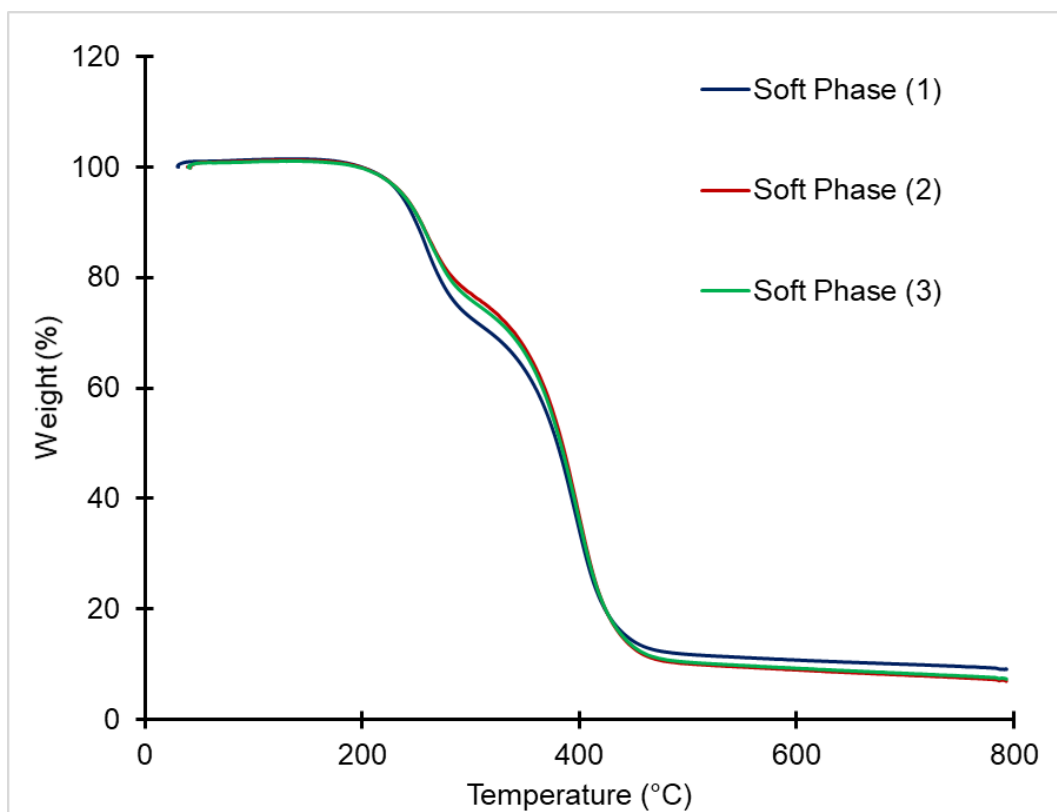
Figure 5.31: STA of the hard phase of the 15% DCPD polymer indicates a first mass loss between 180 and 315 °C and a second mass loss between 315 and 470 °C. At this temperature the remaining mass was 10 %. Between 470 and 800 °C only a small mass loss an additional 3 % was observed. © 2021 Wiley-VCH GmbH. Image was reproduced under a RightsLink license.[24]
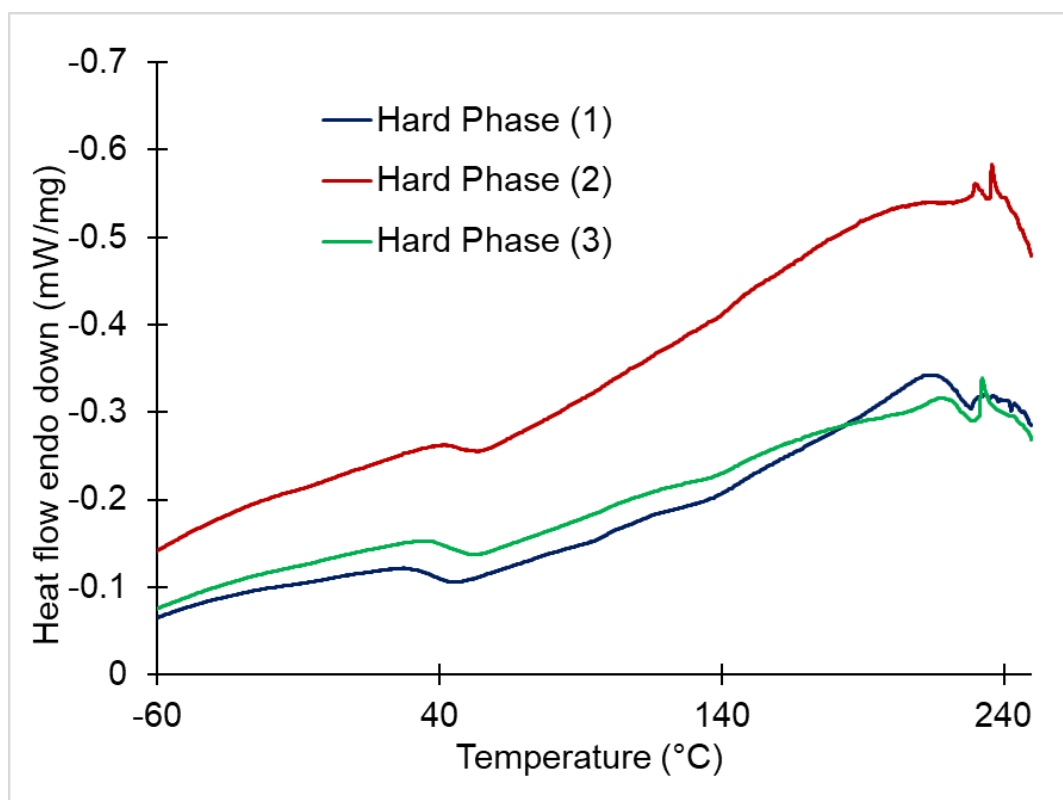
Figure 5.32: DSC analysis of the hard phase of the 15% DCPD polymer revealed a T_g of 41 ± 2°C. © 2021 Wiley-VCH GmbH. Image was reproduced under a RightsLink license.[24]
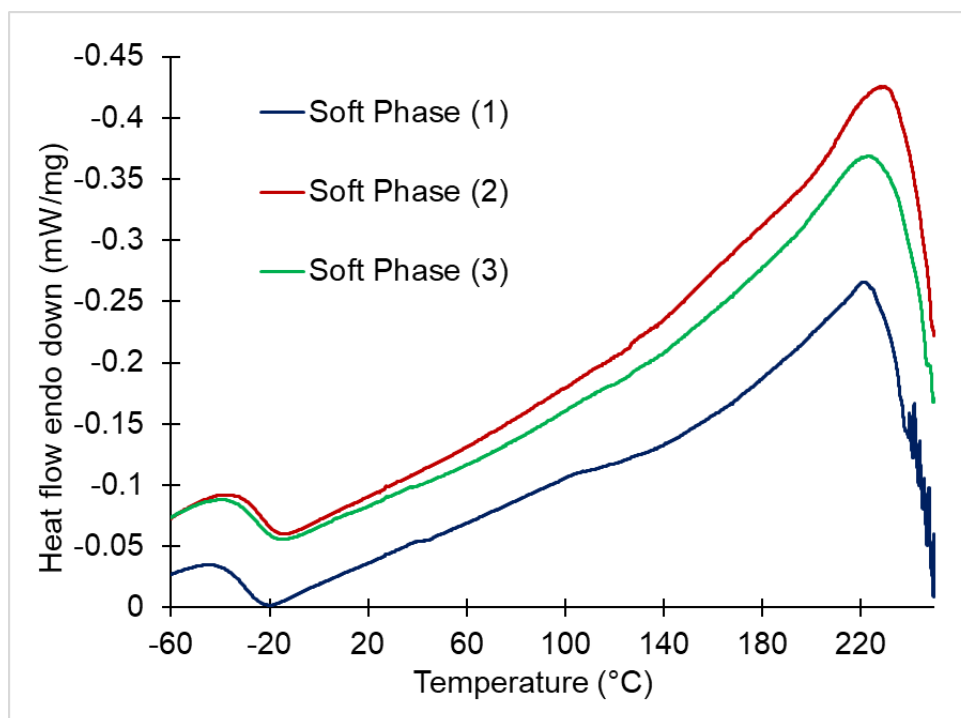
Figure 5.33: DSC of the soft phase of the polymer revealed a T_g of -26 ± 1 °C. © 2021 Wiley-VCH GmbH. Image was reproduced under a RightsLink license.[24]

Synthesis and characterisation of 50 wt% sulfur, 45 wt% canola oil, and 5% DCPD polysulfide

For the synthesis of this polymer the same total mass of reagents as before was used, however the feed ratios were changed to have a DCPD content of 5%. Therefore, 5 g of sulfur, 4.5 g of canola oil and 0.5 g of DCPD was used for his reaction. The reaction protocol was the same as for the 15% DCPD polymer.
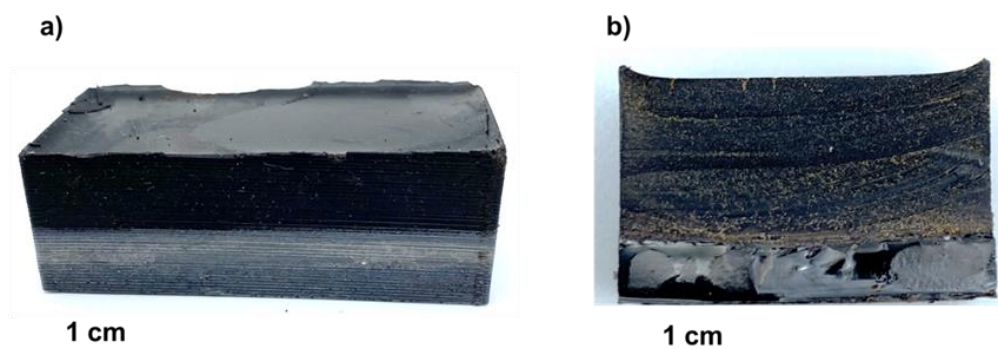
Figure 5.34: a) 5% DCPD polymer. **b)** Cross section of 5% DCPD polymer.
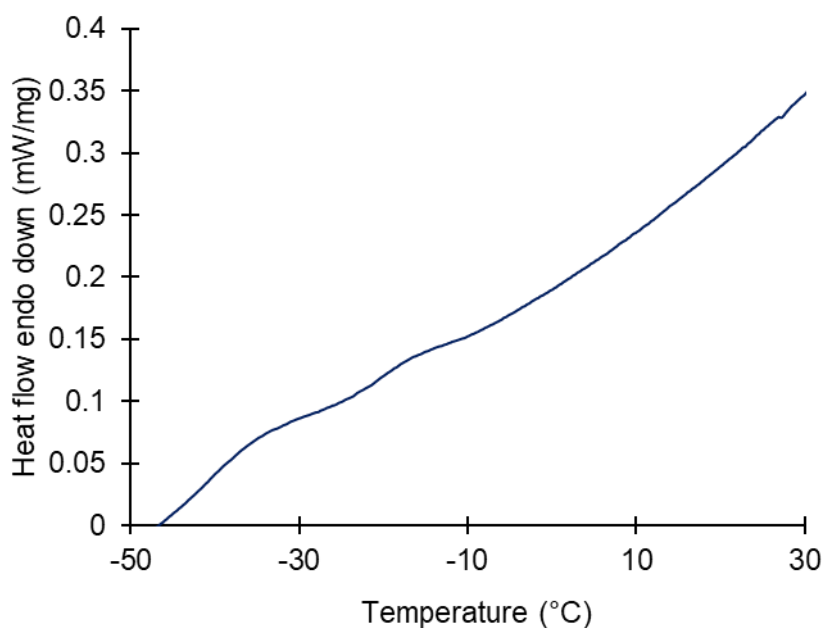
Figure 5.35: DSC of soft phase of 5% DCPD sample showed a T_g of -30 °C. © 2021 Wiley-VCH GmbH. Image was reproduced under a RightsLink license.[24]
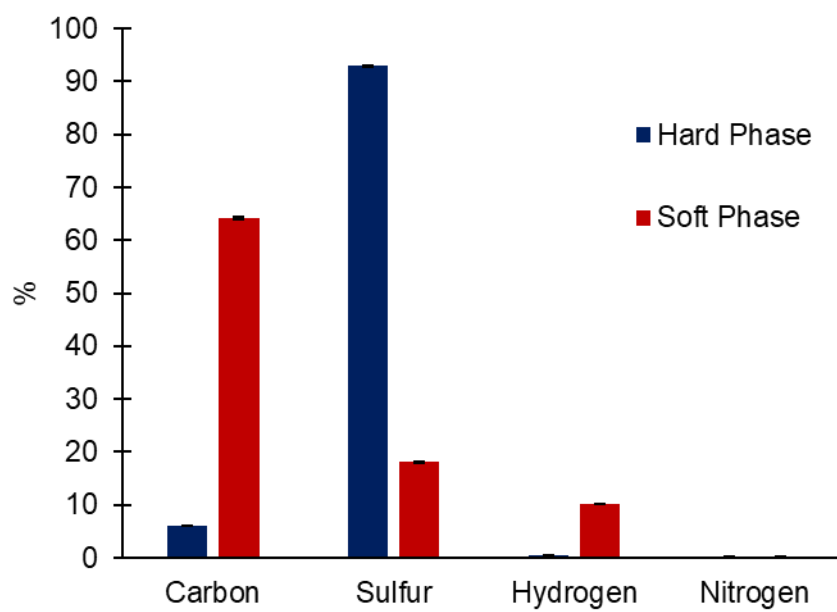
Figure 5.36: Elemental analysis of the 5% DCPD polysulfide.

Synthesis and characterisation of 50 wt% sulfur, 25 wt% canola oil, and 25% DCPD polysulfide

For the synthesis of this polymer the same total mass of reagents as before was used, however the feed ratios were changed to have a DCPD content of 5%. Therefore, 5 g of sulfur, 2.5 g of canola oil and 2.5 g of DCPD was used for his reaction. Since the reaction at 170 °C resulted in a runaway reaction, the reaction temperature was decreased to 140 °C.
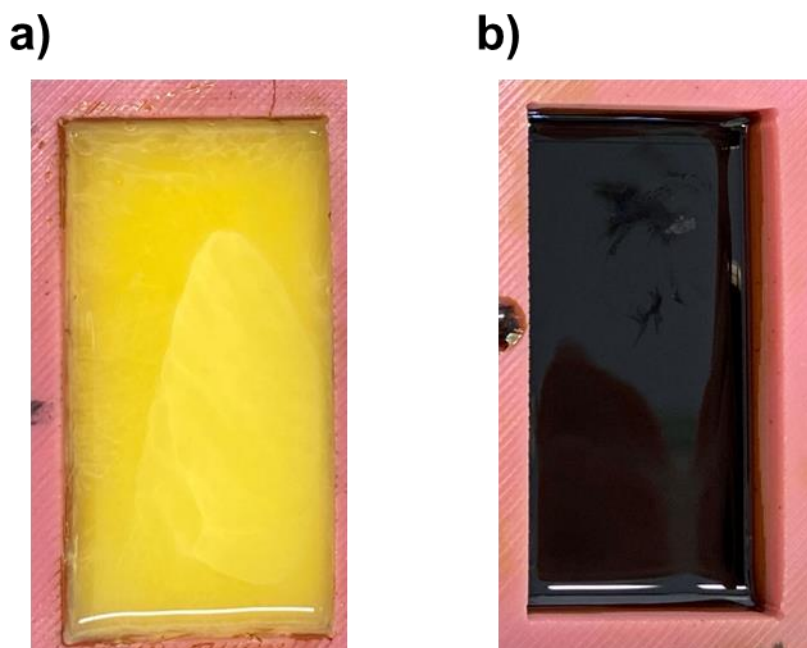
Figure 5.37: a) Short reaction time (9.5 minutes), low temperature (140°C) 25% DCPD reaction and **b)** long reaction time (65 minutes), low temperature (140°C) 25% DCDP reaction time immediately after being poured into mould.

¹H NMR analysis was performed by dissolving a small amount of sample on CDCl₃ and analysing the sample using a 600 MHz NMR spectrometer
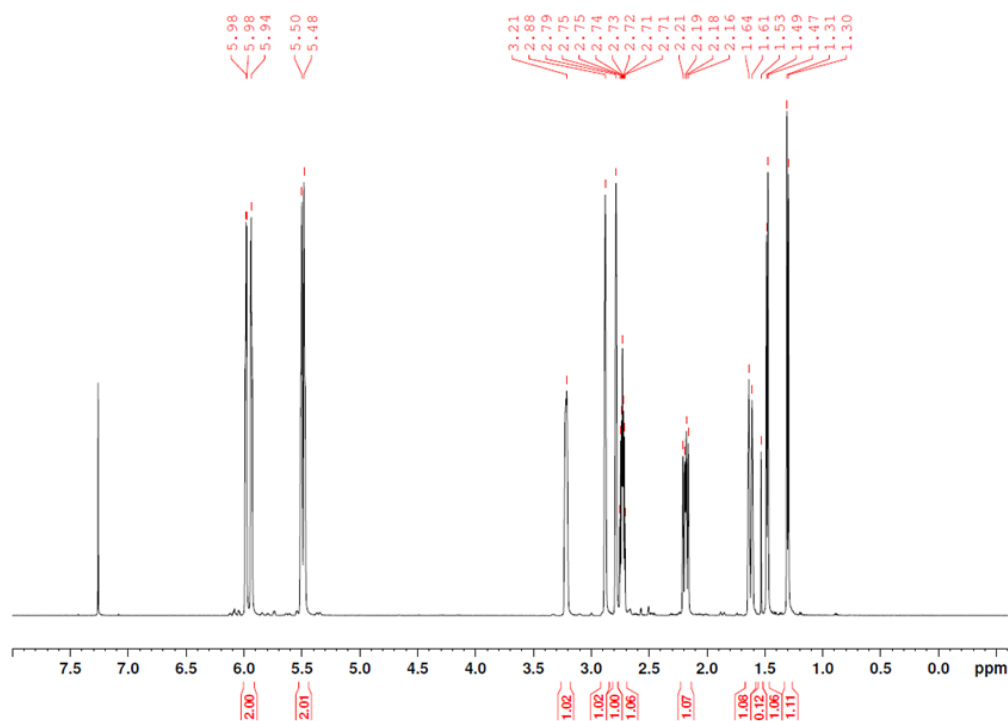
Figure 5.38: ¹H NMR of DCDP.
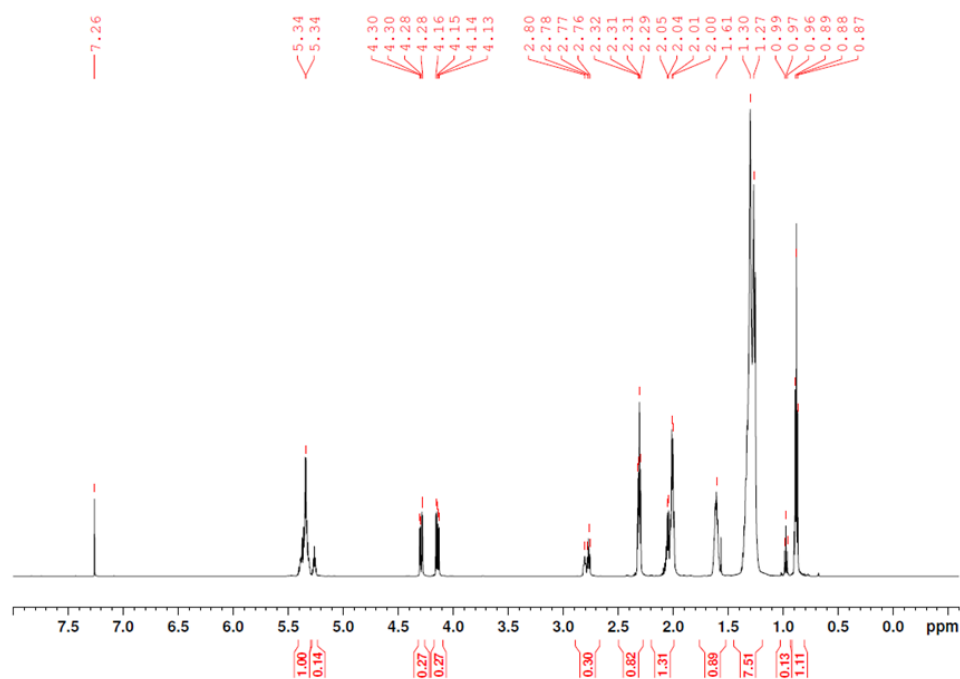
Figure 5.39: ¹H NMR of canola oil.
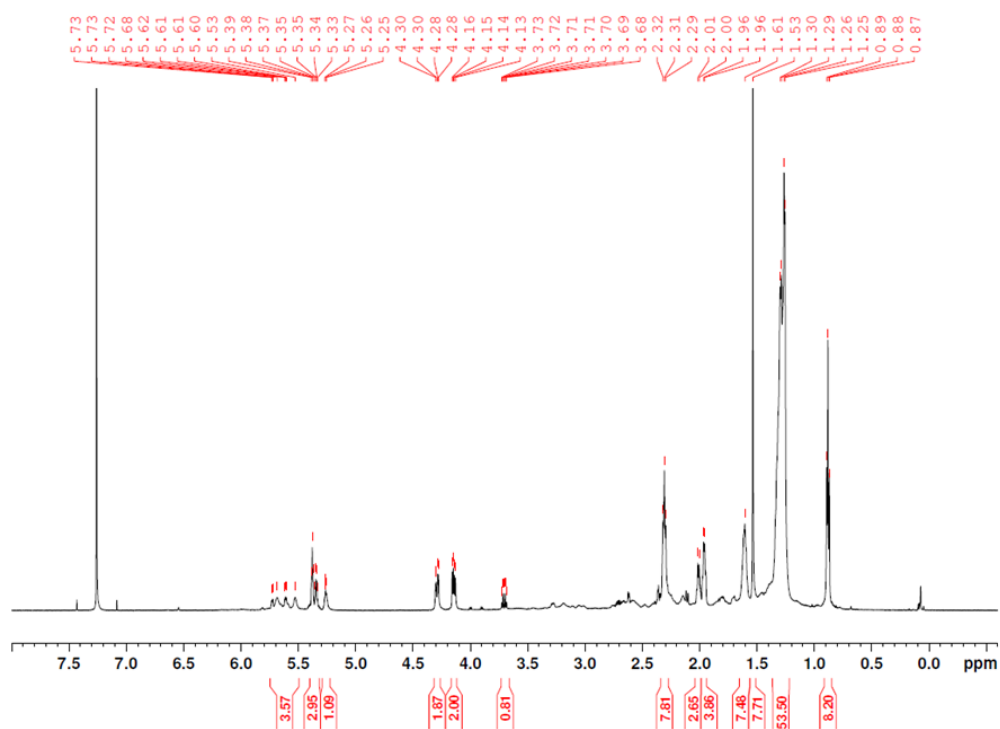
Figure 5.40: ^{1}H NMR of the liquid phase of the short 25% DCPD reaction.
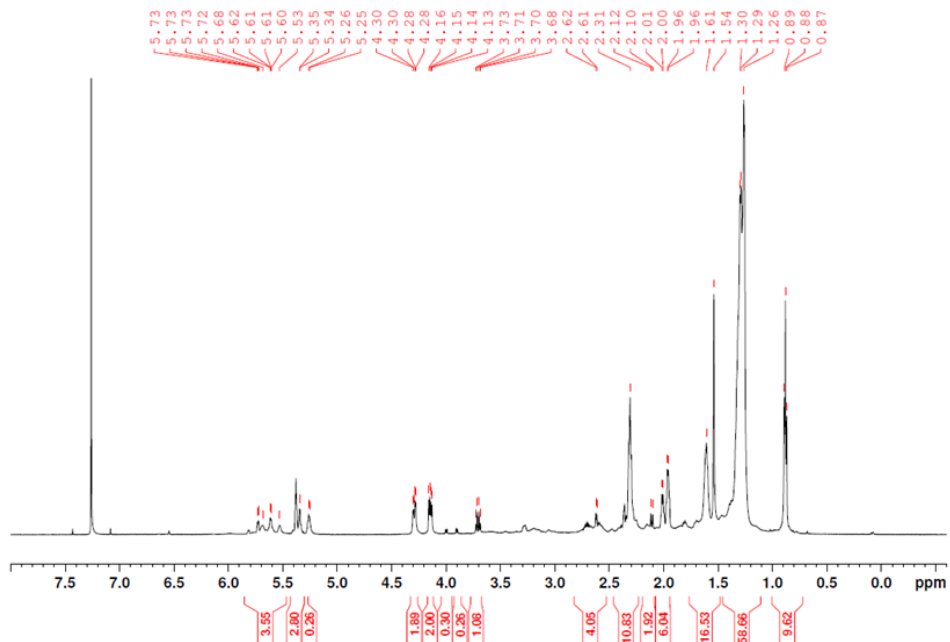
Figure 5.41: ^{1}H NMR of the liquid phase of the long 25% DCPD reaction.

Chemically-induced adhesion and mechanical testing

In order to test the force needed to break the bond formed between the two polymer pieces by an amine-catalyst, a meal scaffolding supporting the polymer was fabricated. Metal plates that were 5 cm long and 2 cm wide with 2 holes in the centre were made. A thread and nuts were used to fix the metal plate in position.
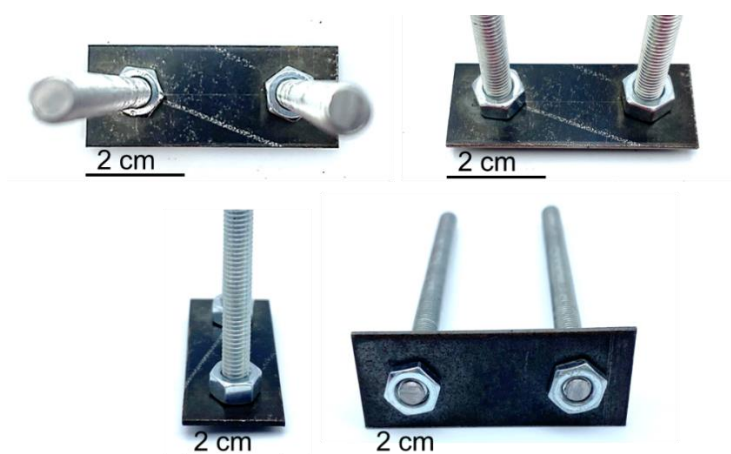
Figure 5.42: Metal scaffolding to support the polymer made from metal plates (5 cm x 2 cm) fixed with thread and nuts. © 2021 Wiley-VCH GmbH. Image was reproduced under a RightsLink license.[24]

Next, to pour polymer around the metal scaffold, a silicon mould was fabricated. In the mould were two channels with the dimensions of L10 cm x W2.5 cm x D2.0 cm. In order to fill the mould with polymer, 6 reactions with 10 g reaction volume carried out. However, to minimise the amount of polymer needed, a silicon block with the dimensions of L4 cm x W2.5 cm x D2.0 cm was made and placed in the mould to lower the volume needed for each polymer pour.

Figure 5.43: Silicon mould for polymer pouring with the dimensions of L10 cm x W2.5 cm x D2.0 cm and with a silicon block (L4 cm x W2.5 cm x D2.0 cm) fitted to minimise the volume of polymer needed to fill the mould. © 2021 Wiley-VCH GmbH. Image was reproduced under a RightsLink license.[24]

To pour the polymer, three 10 g reactions were set up according to the synthesis protocol. These were then poured onto the mould in which the metal scaffolding was placed. Following that the mould was placed in a 130 °C oven for 24 hours to cure. The result of these pours was the metal scaffold imbedded in polymer.
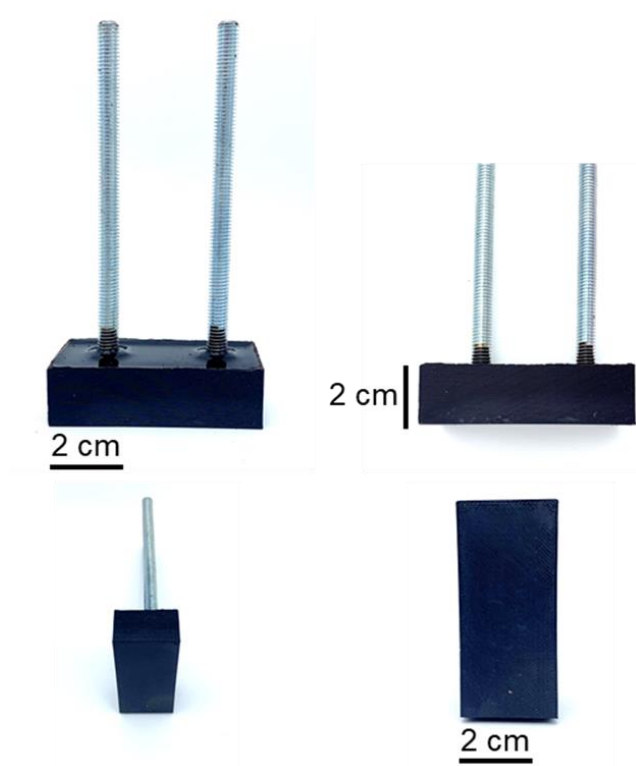

Figure 5.44: Polymer after curing, including metal scaffold with the dimensions of 6 x 2.5 x 2 cm. © 2021 Wiley-VCH GmbH. Image was reproduced under a RightsLink license.[24]
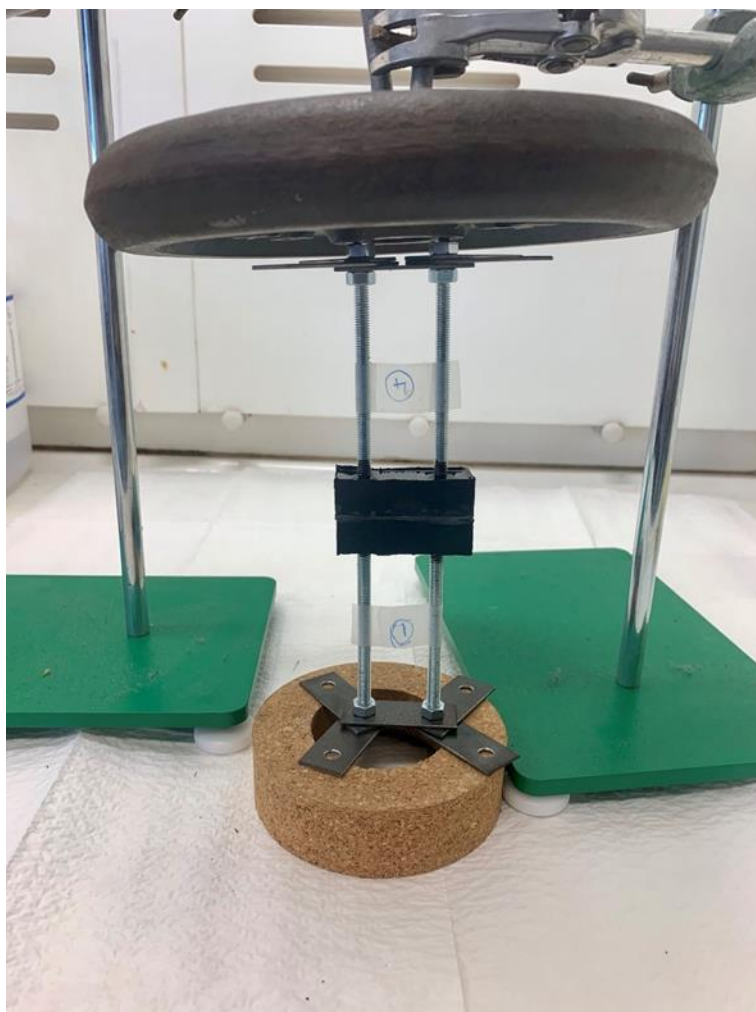
Figure 5.45: Polymer adhesion induced by 300 μL of triethylamine, 5 kg weight, 5 hours. © 2021 Wiley-VCH GmbH. Image was reproduced under a RightsLink license.[24]

In order to assess the bond strength of the bulk material without any metal scaffold the following sample holder was made.
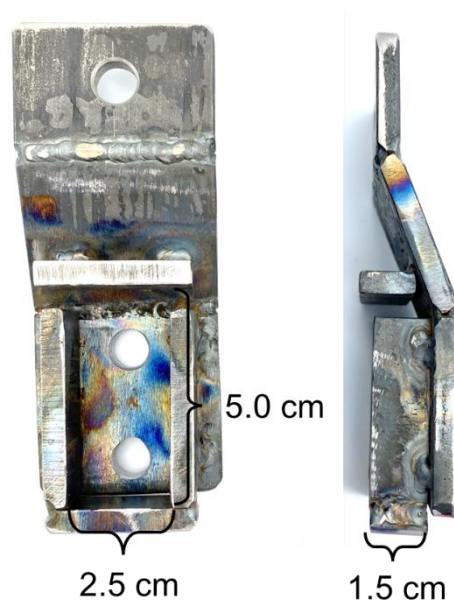
Figure 5.46: Modified sample holder allowing samples with a size of 5.0 cm × 2.5 cm × 1.5 cm (or higher) to be tested. © 2021 Wiley-VCH GmbH. Image was reproduced under a RightsLink license.[24]
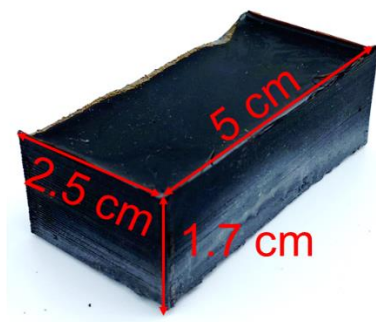
Figure 5.47: Representative cured polymer used for shear strength testing. © 2021 Wiley-VCH GmbH. Image was reproduced under a RightsLink license.[24]

Figure 5.48: Polymer pieces with sandpaper treated surface ready for adhesion using triethylamine. © 2021 Wiley-VCH GmbH. Image was reproduced under a RightsLink license.[24]

Figure 5.49: 10 kg weight on polymer samples after triethylamine adhesion was started. © 2021 Wiley-VCH GmbH. Image was reproduced under a RightsLink license.[24]
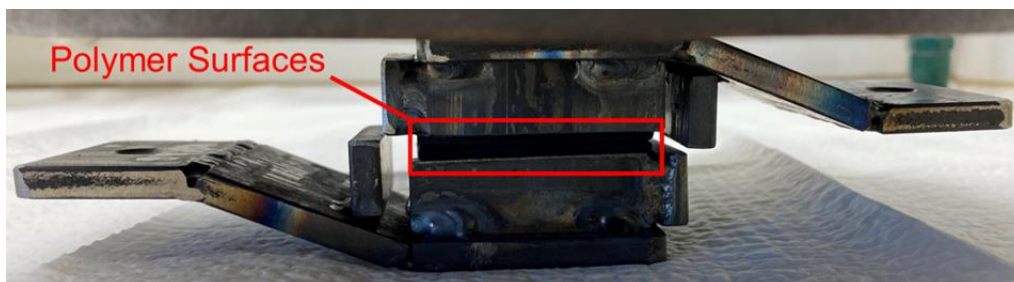
Figure 5.50: Image of the polymer surfaces during the adhesion process under 10 kg of pressure. © 2021 Wiley-VCH GmbH. Image was reproduced under a RightsLink license.[24]

To evaluate of bonding the soft phase surfaced without sandpaper treatment would result in strong bonding two polymers were bonded using triethylamine and the same protocol as for the other samples.
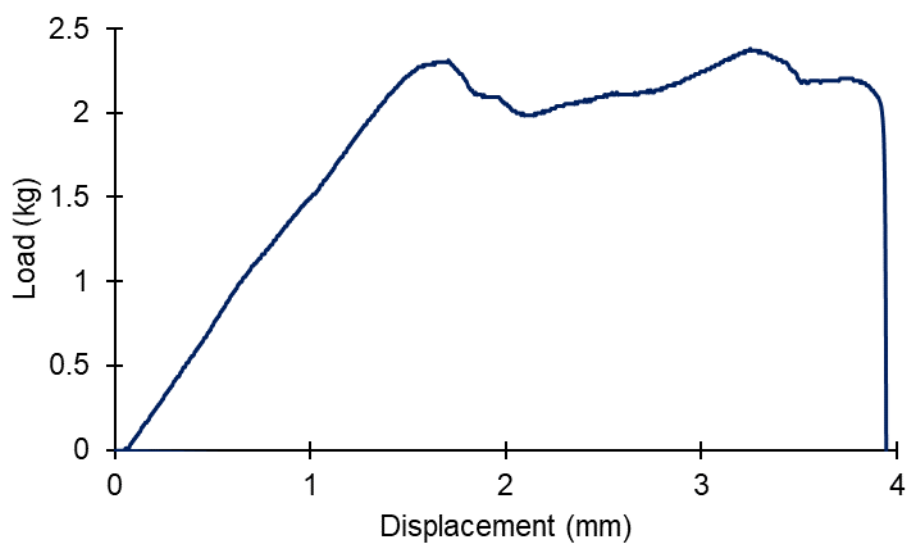
Figure 5.51: Load vs displacement curve of polymer bonded as soft surface without sandpaper treatment showing a maximum load of 2.4 kg at a displacement of 3.2 mm.

Structural strength improvement of the polymer material

Figure 5.52: Cured polymer with no reinforcement.

Figure 5.53: Cured polymer with no reinforcement after three-point bend test showing site of structural failure.

Figure 5.54: Cured polymer with loose carbon fibre (0.5 g) reinforcement.

Figure 5.55: Cured polymer with loose carbon fibre (0.5 g) reinforcement after three point bent test showing site of structural failure.

Figure 5.56: Cured polymer with threaded carbon fibre (0.5 g) reinforcement.

Figure 5.57: Cured polymer reinforced with carbon fibre (0.5 g) after three point bent test showing site of structural failure.

Figure 5.58: Cured polymer with carbon nanotube (0.5 g) reinforcement. © 2021 Wiley-VCH GmbH. Image was reproduced under a RightsLink license.[24]

Figure 5.59: Cured polymer reinforced with carbon nanotubes (0.5 g) after three point bent test showing site of structural failure.

Figure 5.60: Cured polymer with carbon nanotube (1.0g) reinforcement. © 2021 Wiley-VCH GmbH. Image was reproduced under a RightsLink license.[24]

Figure 5.61: Cured polymer reinforced with carbon nanotubes (1.0 g) after three point bent test showing site of structural failure.

References:

1.   Pomponi, F.; Moncaster, A., Circular economy for the built environment: A research framework. *J. Clean. Prod.* **2017,** *143*, 710-718.

2.   Robati, M.; Daly, D.; Kokogiannakis, G., A method of uncertainty analysis for whole-life embodied carbon emissions (CO2-e) of building materials of a net-zero energy building in Australia. *J. Clean. Prod.* **2019,** *225*, 541-553.

3.   United Nations Environment Programme, 2020 Global Status Report for Buildings and Construction: Towards a Zero-emission, Efficient and Resilient Buildings and Construction Sector. **2020**.

4.   Almeida-Costa, A.; Benta, A., Economic and environmental impact study of warm mix asphalt compared to hot mix asphalt. *J. Clean. Prod.* **2016,** *112*, 2308-2317.

5.   T. Calabi-Floody, A.; A. Valdés-Vidal, G.; Sanchez-Alonso, E.; A. Mardones-Parra, L., Evaluation of Gas Emissions, Energy Consumption and Production Costs of Warm Mix Asphalt (WMA) Involving Natural Zeolite and Reclaimed Asphalt Pavement (RAP). *Sustainability* **2020,** *12* (16), 6410.

6.   Soares, N.; Bastos, J.; Pereira, L. D.; Soares, A.; Amaral, A. R.; Asadi, E.; Rodrigues, E.; Lamas, F. B.; Monteiro, H.; Lopes, M. A. R.; Gaspar, A. R., A review on current advances in the energy and environmental performance of buildings towards a more sustainable built environment. *Renew. Sust. Energ. Rev.* **2017,** *77*, 845-860.

7.   Rangappa, S. M.; Parameswaranpillai, J.; Yorseng, K.; Pulikkalparambil, H.; Siengchin, S., Toughened bioepoxy blends and composites based on poly(ethylene glycol)-block-poly(propylene glycol)-block-poly(ethylene glycol) triblock copolymer and sisal fiber fabrics: A new approach. *Constr. Build. Mater.* **2021,** *271*, 121843.

8.   Bu Najmah, I.; Lundquist, N. A.; Stanfield, M. K.; Stojcevski, F.; Campbell, J. A.; Esdaile, L. J.; Gibson, C. T.; Lewis, D. A.; Henderson, L. C.; Hasell, T.; Chalker, J. M., Insulating Composites Made from Sulfur, Canola Oil, and Wool. *ChemSusChem* **2021,** *14* (11), 2352-2359.

9.   Lundquist, N. A.; Tikoalu, A. D.; Worthington, M. J. H.; Shapter, R.; Tonkin, S. J.; Stojcevski, F.; Mann, M.; Gibson, C. T.; Gascooke, J. R.; Karton, A.; Henderson, L. C.; Esdaile, L. J.; Chalker, J. M., Reactive Compression Molding Post-Inverse Vulcanization: A Method to Assemble, Recycle, and Repurpose Sulfur Polymers and Composites. *Chem. Eur. J.* **2020,** *26* (44), 10035-10044.

10.   Chung, W. J.; Griebel, J. J.; Kim, E. T.; Yoon, H.; Simmonds, A. G.; Ji, H. J.; Dirlam, P. T.; Glass, R. S.; Wie, J. J.; Nguyen, N. A.; Guralnick, B. W.; Park, J.; Somogyi, Á.; Theato, P.; Mackay, M. E.; Sung, Y.-E.; Char, K.; Pyun, J., The use of elemental sulfur as an alternative feedstock for polymeric materials. *Nat. Chem.* **2013,** *5*, 518-524.

11. Zhang, Y.; Glass, R. S.; Char, K.; Pyun, J., Recent advances in the polymerization of elemental sulphur, inverse vulcanization and methods to obtain functional Chalcogenide Hybrid Inorganic/Organic Polymers (CHIPs). *Polym. Chem.* **2019,** *10* (30), 4078-4105.

12. Worthington, M. J.; Kucera, R. L.; Chalker, J. M., Green chemistry and polymers made from sulfur. *Green Chem.* **2017,** *19* (12), 2748-2761.

13. Gregor, R.; Hackl, A., A New Approach to Sulfur Concrete. Washington, DC: American Chemical Society: Washington, DC, **1978**.

14. El Gamal, M.; El-Sawy, K.; Mohamed, A.-M. O., Integrated mixing machine for sulfur concrete production. *Case Stud. Constr. Mater.* **2021,** *14,* e00495.

15. Smith, A. D.; Smith, R. C.; Tennyson, A. G., Polymer cements by copolymerization of waste sulfur, oleic acid, and pozzolan cements. *Sustain. Chem. Pharm.* **2020,** *16,* 100249.

16. Dugarte, M.; Martinez-Arguelles, G.; Torres, J., Experimental Evaluation of Modified Sulfur Concrete for Achieving Sustainability in Industry Applications. *Sustainability* **2019,** *11* (1), 70.

17. Gulzar, M. A.; Rahim, A.; Ali, B.; Khan, A. H., An investigation on recycling potential of sulfur concrete. *J. Build. Eng.* **2021,** *38,* 102175.

18. Lauer, M. K.; Estrada-Mendoza, T. A.; McMillen, C. D.; Chumanov, G.; Tennyson, A. G.; Smith, R. C., Durable Cellulose–Sulfur Composites Derived from Agricultural and Petrochemical Waste. *Adv. Sustain. Syst.* **2019,** *3* (10), 1900062.

19. Maladeniya, C. P.; Karunarathna, M. S.; Lauer, M. K.; Lopez, C. V.; Thiounn, T.; Smith, R. C., A role for terpenoid cyclization in the atom economical polymerization of terpenoids with sulfur to yield durable composites. *Mater. Adv.* **2020,** *1* (6), 1665-1674.

20. Karunarathna, M. S.; Lauer, M. K.; Thiounn, T.; Smith, R. C.; Tennyson, A. G., Valorisation of waste to yield recyclable composites of elemental sulfur and lignin. *J. Mater. Chem. A* **2019,** *7* (26), 15683-15690.

21. Wadi, V. S.; Jena, K. K.; Halique, K.; Alhassan, S. M., Linear Sulfur–Nylon Composites: Structure, Morphology, and Antibacterial Activity. *ACS Appl. Poly, Mater.* **2020,** *2* (2), 198-208.

22. Wadi, V. S.; Halique, K.; Alhassan, S. M., Polypropylene–Elemental Sulfur (S8) Composites: Effect of Sulfur on Morphological, Thermal, and Mechanical Properties. *Ind. Eng. Chem. Res.* **2020,** *59* (29), 13079-13087.

23. Jeevi, G.; Nayak, S. K.; Abdul Kader, M., Review on adhesive joints and their application in hybrid composite structures. *J. Adhes. Sci. Technol.* **2019,** *33* (14), 1497-1520.

24. Mann, M.; Pauling, P. J.; Tonkin, S. J.; Campbell, J. A.; Chalker, J. M., Chemically Activated S-S Metathesis for Adhesive-Free Bonding of Polysulfide Surfaces. *Macromol. Chem. Phys.* **2021**, 2100333.

25. Hsu, H.-C.; Wang, S.-J.; Ou, J. D.-Y.; Wong, D. S. H., Simplification and Intensification of a C5 Separation Process. *Ind. Eng. Chem. Res.* **2015,** *54* (40), 9798-9804.

26. Montero de Espinosa, L.; Meier, M. A. R., Plant oils: The perfect renewable resource for polymer science?! *Eur. Polym. J.* **2011,** *47* (5), 837-852.

27. Worthington, M. J. H.; Kucera, R. L.; Abuquerque, I. S.; Gibson, C. T.; Sibley, A.; Slattery, A. D.; Campbell, J. A.; Alboaiji, S. F. K.; Muller, K. A.; Young, J.; Adamson, N.; Gascooke, J. R.; Jampaiah, D.; Sabri, Y. M.; Bhargava, S. K.; Ippolito, S. J.; Lewis, D. A.; Quinton, J. S.; Ellis, A. V.; Johs, A.; Bernardes, G. J. L.; Chalker, J. M., Laying Waste to Mercury: Inexpensive Sorbents Made from Sulfur and Recycled Cooking Oils. *Chem. Eur. J.* **2017,** *23*, 16219-16230.

28. Tikoalu, A. D.; Lundquist, N. A.; Chalker, J. M., Mercury Sorbents Made By Inverse Vulcanization of Sustainable Triglycerides: The Plant Oil Structure Influences the Rate of Mercury Removal from Water. *Adv. Sustain. Syst.* **2020,** *4* (3), 1900111.

29. Lundquist, N. A.; Chalker, J. M., Confining a spent lead sorbent in a polymer made by inverse vulcanization prevents leaching. *SM&T* **2020,** *26*, e00222.

30. Papageorgiou, D. G.; Li, Z.; Liu, M.; Kinloch, I. A.; Young, R. J., Mechanisms of mechanical reinforcement by graphene and carbon nanotubes in polymer nanocomposites. *Nanoscale* **2020,** *12* (4), 2228-2267.

31. Yao, S.-S.; Jin, F.-L.; Rhee, K. Y.; Hui, D.; Park, S.-J., Recent advances in carbon-fiber-reinforced thermoplastic composites: A review. *Compos. B. Eng.* **2018,** *142*, 241-250.

32. Imani Yengejeh, S.; Kazemi, S. A.; Öchsner, A., Carbon nanotubes as reinforcement in composites: A review of the analytical, numerical and experimental approaches. *Comput. Mater. Sci.* **2017,** *136*, 85-101.

33. Gao, B.; Zhang, R.; He, M.; Sun, L.; Wang, C.; Liu, L.; Zhao, L.; Cui, H.; Cao, A., Effect of a multiscale reinforcement by carbon fiber surface treatment with graphene oxide/carbon nanotubes on the mechanical properties of reinforced carbon/carbon composites. *Compos. Part A Appl. Sci. Manuf.* **2016,** *90*, 433-440.

34. Pramanik, A.; Basak, A. K.; Dong, Y.; Sarker, P. K.; Uddin, M. S.; Littlefair, G.; Dixit, A. R.; Chattopadhyaya, S., Joining of carbon fibre reinforced polymer (CFRP) composites and aluminium alloys – A review. *Compos. Part A Appl. Sci. Manuf.* **2017,** *101*, 1-29.

35. Mittal, G.; Dhand, V.; Rhee, K. Y.; Park, S.-J.; Lee, W. R., A review on carbon nanotubes and graphene as fillers in reinforced polymer nanocomposites. *J. Ind. Eng. Chem.* **2015,** *21*, 11-25.

36. Tonkin, S. J.; Gibson, C. T.; Campbell, J. A.; Lewis, D. A.; Karton, A.; Hasell, T.; Chalker, J. M., Chemically induced repair, adhesion, and recycling of polymers made by inverse vulcanization. *Chem Sci* **2020,** *11* (21), 5537-5546.

37. Smith, J. A.; Green, S. J.; Petcher, S.; Parker, D. J.; Zhang, B.; Worthington, M. J. H.; Wu, X.; Kelly, C. A.; Baker, T.; Gibson, C. T.; Campbell, J. A.; Lewis, D. A.; Jenkins, M. J.; Willcock, H.; Chalker, J. M.; Hasell, T., Crosslinker Copolymerization for Property Control in Inverse Vulcanization. *Chem. Eur. J.* **2019,** *25* (44), 10433-10440.

38. Hoefling, A.; Lee, Y. J.; Theato, P., Sulfur-Based Polymer Composites from Vegetable Oils and Elemental Sulfur: A Sustainable Active Material for Li–S Batteries. *Macromol. Chem. Phys.* **2017,** *218*, 1600303.

39. Parker, D. J.; Jones, H. A.; Petcher, S.; Cervini, L.; Griffin, J. M.; Akhtar, R.; Hasell, T., Low cost and renewable sulfur-polymers by inverse vulcanisation, and their potential for mercury capture. *J. Mater. Chem. A* **2017,** *5* (23), 11682-11692.

40. Smith, J. A.; Wu, X.; Berry, N. G.; Hasell, T., High sulfur content polymers: The effect of crosslinker structure on inverse vulcanization. *J. Polym. Sci., Part A: Polym. Chem.* **2018,** *56* (16), 1777-1781.

41. Wręczycki, J.; Bieliński, D. M.; Anyszka, R., Sulfur/Organic Copolymers as Curing Agents for Rubber. *Polymers* **2018,** *10* (8), 870.

42. Sullivan, T. A.; McBee, W. C.; Blue, D. D., Sulfur in Coatings and Structural Materials. In *New Uses of Sulfur*, AMERICAN CHEMICAL SOCIETY: **1975**; Vol. 140, pp 55-74.

43. Wu, X.; Smith, J. A.; Petcher, S.; Zhang, B.; Parker, D. J.; Griffin, J. M.; Hasell, T., Catalytic inverse vulcanization. *Nat. Commun.* **2019,** *10* (1), 647.

Chapter 6
Summary of achievements and future work

The main focus of this thesis was to explore more uses and applications of sulfur polymers as functional materials and understand more of the mechanistic aspects of inverse vulcanisation. This was done by investigating multiple polysulfide polymer systems and investigation potential used for each of these systems. The following provides a summary of each of these chapters.

Chapter 2 focused on a novel gold oxidation method that can be implemented in the artisanal and small-scale gold mining sector (ASGM) as well as the informal electronic waste (e-waste) space. To do that a new gold oxidation method was developed. This new method uses trichloroisocyanuric acid (TCCA) and NaBr or KBr, both benign, low-cost chemicals to oxidise gold. Using TCCA and NaBr/KBr to oxidise gold proved to be very robust (no pH adjustments needed) and simple to perform. The method was successfully tested on gold ore tailings from a mine in Western Australia that have been previously treated with mercury to remove gold, gold ore concentrates from an additional mine site in Western Australia as well as on e-waste. To recover the leached gold a polysulfide made from sulfur and canola oil (50-poly(S-*r*-canola)) was used. It has been shown that the polymer is able to remove aqueous gold from solution with high selectivity for gold even in the presence of other metal ions commonly found in mining applications. This polymer was also able to remove oxidised gold from the gold or tailings, gold ore concentrates and e-waste samples. Since e-waste contains orders of magnitude more copper than gold, gold uptake by the polymer can be hindered by the large amount of copper present. To counteract that, EDTA was successfully used to first complex the copper before using the polymer to remove the leached gold. In order the recover the gold from the polymer, the polymer was incinerated. Incineration of the polymer resulted in successful gold recovery. Further, work was undertaken to upscale to polymer to a multi-kg scale in a laboratory setting. These experiments have been crucial in the further upscaling of the (50-poly(S-*r*-canola). A proprietary plant built by an engineering company used the results from this thesis to produce the polymer at a 500 kg scale. Additionally, the gold oxidation method has since been patented and assigned to a mining company. Currently efforts are underway to design and build a pilot plant to use the novel leach method and the 50-poly(S-*r*-canola) polymer to recover gold from e-waste on a multi-tone scale. Further, the engineering company is working on a small pilot plant that addresses the filtration problems and aims to have modular and

containerised plant design suitable for use in ASGM, as well as small and medium formal mines.

Future work regarding this project involves around further optimising the gold oxidation and tailor the method to different types of ore and e-waste. In addition, work should be undertaken to explore ways to remove the copper in the e-waste leach solutions electrochemically before the gold is removed using the polymer. Also, the final contents of the leach solution after the gold has been removed needs to be determined. Knowing this, ways to safely dispose the leach solution (for example by removing contaminants first through filtration) or recycle the leach solution (for example be using the solution as leach solution again after filtration) can be explored.

Chapter 3 described the carbonisation of a 50-poly(S-*r*-canola) polymer, therefore offering an end-of-life solution for this material. While previous studies carbonised sulfur polymers under inert atmosphere followed by an additional activation step, the carbonisation described in this thesis was not undertaken under inert atmosphere and without additional activation of the carbon product. The resulting carbon showed a higher sulfur content that other sulfur doped carbons. This new product (carbonised-1) was used to remove mercury from aqueous solution and was compared to other commercially available carbons. Carbonised-1 showed excellent mercury sorption that rivaled that of the commercial carbons. To further demonstrate the end-of-life applications for the 50-poly(S-*r*-canola) polymer by means of carbonisation, 50-poly(S-*r*-canola) was used to remove oil from water before subsequent carbonisation (carbonised-1-O). This carbon also displayed excellent mercury uptake capabilities. While the commercial carbons leached mercury once exposed to an acidic solution, significantly less mercury leached from carbonised-1 or carbonised-1-O. This highlighted that the sulfur functionality is vital in binding and adhering the mercury to the carbon. To further highlight the versatility of the new carbon materials it has been shown that the bound mercury can be removed by heating the carbons in a furnace. After this regeneration the carbon still removed mercury successfully from an aqueous solution. This work has given rise to the opportunity to repurpose and extend the lifetime of the parent polymer 50-poly(S-*r*-canola) as well as of the resulting carbon materials.

Future work in this field can include the carbonisation of different sulfur polymers and investigating their use in mercury remediation. Further, the use of carbonised-1 or carbonised-1-O as filter for water to remove general contaminants could be investigated.

In **Chapter 4** a safe and robust synthesis protocol was developed to obtain sulfur-DCPD polymers. Earliest studies using this polymer reported runaway reactions at elevated temperatures. To avoid these dangerous outcomes, the new protocol performs the reaction at lower temperatures an under an inert nitrogen atmosphere. This led to a

shelf stable, malleable, and solvent processable pre-polymer (oligomer 1). This polymer was rendered insoluble and rigid upon curing in an oven (cured 1). Advantage was taken of the malleable and solvent processable pre-polymer in various coating applications. Firstly, silica gel was coated with the prepolymer, cured, and used to remove aqueous mercury from solution. Since the cured polymer was solvent resistant, the cured polymer coated silica gel was successfully used to remove mercury from a mixture of water and diesel fuel, thus demonstrating that the cured polymer coating is tolerant to hydrocarbon mixtures. Additionally, aluminium was coated with oligomer 1 and cured. The resulting coating was resistant to HCl and protected the metal from acid corrosion. To expand on the coating applications, cement was coated with cured 1. The cured 1 coating was acid resistant and successfully protected the cement from acid corrosion. As a final coating application, the inside of a PVC pipe was coated with cured 1 using a solvent free process. Exposure of the uncoated PVC pipe THF resulted in damage of the pipe through solvation whereas no damage could be seen on the pipe, lined with cured 1. It has also been shown that a scratched coating of cured 1 can be repaired using thermal treatment. Attempts were made to recycle the polymer. This was done by reducing oligomer 1 or cured 1 using a hydride reduction, isolating the reduced product, and recuring it. Although the resulting material had the physical appearance of the original polymer, the recycled product lacked solvent resistance.

Future work with this polymer system should include further investigation into the recycling aspect. Although initial attempts to recycle the material were imperfect, attempts to improve the properties of the recycled material can lead to a polymer system that can be broken down to small molecule monomers and re-cured to access new materials.

Chapter 5 explored a terpolymer made from canola oil, dicyclopentadiene and elemental sulfur as a bulk structural material. This was done by bonding polymer blocks by means of an amine catalysed S-S metathesis using triethylamine. Although earlier studies described the S-S metathesis, the work within this thesis is the first quantitative evaluation of the strength of this bonding. It has been found that the triethylamine bond is stronger than that of commercial super glue. Further efforts have been made to reinforce the polymer using carbon fibers and carbon nanotubes. Reinforcement with aligned carbon fibers increased the flexural strength nearly 16-fold as compared to the unreinforced polymer.

Future work might include the reinforcement of this polymer using other materials as carbon fibers or carbon nanotubes such as natural fibers. It would also be beneficial to explore the use of the amine catalysed S-S metathesis on different polymer systems. Further, degradability studies of the canola oil, dicyclopentadiene and sulfur polymer as

well as of the amine catalysed bond should be conducted further evaluate their use as a structural material for the building industry.

7
Rights and Permissions

Rights and permissions Chapter 1

Inverse Vulcanization of Styrylethyltrimethoxysilane–Coated Surfaces, Particles, and Crosslinked Materials

Author: Patrick Theato, Pavel A. Levkin, Jörg Matysik, et al
Publication: Angewandte Chemie International Edition
Publisher: John Wiley and Sons
Date: Oct 5, 2020

Optical Properties of a Sulfur-Rich Organically Modified Chalcogenide Polymer Synthesized via Inverse Vulcanization and Containing an Organometallic Comonomer

Author: Darryl A. Boyd, Vinh Q. Nguyen, Collin C. McClain, et al
Publication: ACS Macro Letters
Publisher: American Chemical Society
Date: Feb 1, 2019

BACK

CLOSE WINDOW

428

CCC Marketplace™

Order Confirmation

Thank you, your order has been placed. An email confirmation has been sent to you. Your order license details and printable licenses will be available within 24 hours. Please access Manage Account for final order details.

This is not an invoice. Please go to manage account to access your order history and invoices.

CUSTOMER INFORMATION

Payment by invoice: You can cancel your order until the invoice is generated by contacting customer service.

Billing Address

Mr. Maximilian Mann
Biological Science Road
Bedford Park, SA 5042
Australia

+61 (4)48106964
max.mann@flinders.edu.au

Customer Location

Mr. Maximilian Mann
Biological Science Road
Bedford Park, SA 5042
Australia

PO Number (optional)

N/A

Payment options

Invoice

PENDING ORDER CONFIRMATION

Confirmation Number: Pending

Order Date: 06-Dec-2021

---

1. Polymer chemistry   0.00 AUD

Article: Phosphazene Based Star-Branched Polymeric Cathode Materials via Inverse Vulcanization of Sulfur for Lithium–Sulfur Batteries

Order License ID	Pending	Publisher	Royal Society of Chemistry
ISSN	1759-9962		
Type of Use	Republish in a thesis/dissertation	Portion	Chart/graph/table/figure

LICENSED CONTENT

Publication Title	Polymer chemistry	Publication Type	e-Journal
		Start Page	4124
		End Page	4132
		Issue	25

Article Title	Phosphazene Based Star-Branched Polymeric Cathode Materials via Inverse Vulcanization of Sulfur for Lithium–Sulfur Batteries	**Volume**	11
		URL	http://www.rsc.org/Publishing/Journals/PY/Index.asp
Author/Editor	Royal Society of Chemistry (Great Britain)		
Date	01/01/2010		
Language	English		
Country	United Kingdom of Great Britain and Northern Ireland		
Rightsholder	Royal Society of Chemistry		

REQUEST DETAILS

Portion Type	Chart/graph/table/figure	**Distribution**	Worldwide
Number of charts / graphs / tables / figures requested	2	**Translation**	Original language of publication
		Copies for the disabled?	No
Format (select all that apply)	Electronic	**Minor editing privileges?**	Yes
Who will republish the content?	Academic institution	**Incidental promotional use?**	No
Duration of Use	Current edition and up to 15 years	**Currency**	AUD
Lifetime Unit Quantity	Up to 499		
Rights Requested	Main product		

NEW WORK DETAILS

Title	Sulfur copolymers for coatings, composites and mining applications	**Institution name**	Flinders University
		Expected presentation date	2022-02-04
Instructor name	Maximilian Mann		

ADDITIONAL DETAILS

Order reference number	N/A	**The requesting person / organization to appear on the license**	Maximilian Mann (Flinders University Thesis)

REUSE CONTENT DETAILS

Title, description or numeric reference of the portion(s)	Scheme 1, Figure 4	**Title of the article/chapter the portion is from**	Phosphazene Based Star-Branched Polymeric Cathode Materials via Inverse Vulcanization of Sulfur for Lithium–Sulfur Batteries
Editor of portion(s)	Yeşilot, Serkan; Kucukkoylu, Sedat; Demir, Emrah; Demir-Cakan, Rezan		
		Author of portion(s)	Yeşilot, Serkan; Kucukkoylu, Sedat; Demir, Emrah; Demir-Cakan, Rezan
Volume of serial or monograph	11		

430

| Page or page range of portion | 4124-4132 | Issue, if republishing an article from a serial | 25 |
| | | Publication date of portion | 2020-01-01 |

Total Items: 1   **Total Due: 0.00 AUD**

Accepted: All Publisher and CCC Terms and Conditions

431

JOHN WILEY AND SONS LICENSE
TERMS AND CONDITIONS

Nov 30, 2021

This Agreement between Mr. Maximilian Mann ("You") and John Wiley and Sons ("John Wiley and Sons") consists of your license details and the terms and conditions provided by John Wiley and Sons and Copyright Clearance Center.

License Number	5198991245605
License date	Nov 30, 2021
Licensed Content Publisher	John Wiley and Sons
Licensed Content Publication	Chemistry - A European Journal
Licensed Content Title	Reactive Compression Molding Post-Inverse Vulcanization: A Method to Assemble, Recycle, and Repurpose Sulfur Polymers and Composites
Licensed Content Author	Nicholas A. Lundquist, Alfrets D. Tikoalu, Max J. H. Worthington, et al
Licensed Content Date	Jun 18, 2020
Licensed Content Volume	26
Licensed Content Issue	44
Licensed Content Pages	10

432

Type of use	Dissertation/Thesis
Requestor type	University/Academic
Format	Electronic
Portion	Figure/table
Number of figures/tables	1
Will you be translating?	No
Title	Porous carbons from inverse vulcanised polymers
Institution name	Flinders University
Expected presentation date	Feb 2022
Portions	Figure 6 page 10042
Requestor Location	Mr. Maximilian Mann Biological Science Road Bedford Park, SA 5042 Australia Attn: Flinders University
Publisher Tax ID	EU826007151
Total	0.00 USD

Terms and Conditions

TERMS AND CONDITIONS

433

JOHN WILEY AND SONS LICENSE
TERMS AND CONDITIONS

Dec 06, 2021

This Agreement between Mr. Maximilian Mann ("You") and John Wiley and Sons ("John Wiley and Sons") consists of your license details and the terms and conditions provided by John Wiley and Sons and Copyright Clearance Center.

License Number	5202910255084
License date	Dec 06, 2021
Licensed Content Publisher	John Wiley and Sons
Licensed Content Publication	ChemSusChem
Licensed Content Title	Insulating Composites Made from Sulfur, Canola Oil, and Wool**
Licensed Content Author	Justin M. Chalker, Tom Hasell, Luke C. Henderson, et al
Licensed Content Date	Mar 10, 2021
Licensed Content Volume	14
Licensed Content Issue	11
Licensed Content Pages	8
Type of use	Dissertation/Thesis
Requestor type	University/Academic
Format	Electronic
Portion	Figure/table

434

Number of figures/tables	1
Will you be translating?	No
Title	Sulfur copolymers for coatings, composites and mining applications
Institution name	Flinders University
Expected presentation date	Feb 2022
Portions	figure 1
Requestor Location	Mr. Maximilian Mann Biological Science Road Bedford Park, SA 5042 Australia Attn: Flinders University
Publisher Tax ID	EU826007151
Total	0.00 USD

CCC Marketplace™

Order Confirmation

Thank you, your order has been placed. An email confirmation has been sent to you. Your order license details and printable licenses will be available within 24 hours. Please access Manage Account for final order details.

This is not an invoice. Please go to manage account to access your order history and invoices.

CUSTOMER INFORMATION

Payment by invoice: You can cancel your order until the invoice is generated by contacting customer service.

Billing Address

Mr. Maximilian Mann
Biological Science Road
Bedford Park, SA 5042
Australia

+61 (4)48106964
max.mann@flinders.edu.au

Customer Location

Mr. Maximilian Mann
Biological Science Road
Bedford Park, SA 5042
Australia

PO Number (optional)

N/A

Payment options

Invoice

PENDING ORDER CONFIRMATION

Confirmation Number: Pending

Order Date: 06-Dec-2021

---

1. Organic & biomolecular chemistry   0.00 AUD

Article: Sulfur polymer composites as controlled-release fertilisers.

Order License ID	Pending	Publisher	ROYAL SOCIETY OF CHEMISTRY
ISSN	1477-0539		
Type of Use	Republish in a thesis/dissertation	Portion	Chart/graph/table/figure

LICENSED CONTENT

Publication Title	Organic & biomolecular chemistry	Publication Type	e-Journal
		Start Page	1929
		End Page	1936
		Issue	7

Article Title	Sulfur polymer composites as controlled-release fertilisers.	Volume	17
		URL	http://www.rsc.org/is/journals/current/obc/obcpub.htm
Author/Editor	Royal Society of Chemistry (Great Britain)		
Date	01/01/2003		
Language	English		
Country	United Kingdom of Great Britain and Northern Ireland		
Rightsholder	Royal Society of Chemistry		

REQUEST DETAILS

Portion Type	Chart/graph/table/figure	Distribution	Worldwide
Number of charts / graphs / tables / figures requested	1	Translation	Original language of publication
		Copies for the disabled?	No
Format (select all that apply)	Electronic	Minor editing privileges?	Yes
Who will republish the content?	Academic institution	Incidental promotional use?	No
Duration of Use	Current edition and up to 15 years	Currency	AUD
Lifetime Unit Quantity	Up to 499		
Rights Requested	Main product		

NEW WORK DETAILS

Title	Sulfur copolymers for coatings, composites and mining applications	Institution name	Flinders University
		Expected presentation date	2022-02-04
Instructor name	Maximilian Mann		

ADDITIONAL DETAILS

| Order reference number | N/A | The requesting person / organization to appear on the license | Maximilian Mann (Flinders University Thesis) |

REUSE CONTENT DETAILS

| Title, description or numeric reference of the portion(s) | Figure 1a | Title of the article/chapter the portion is from | Sulfur polymer composites as controlled-release fertilisers. |

437

Editor of portion(s)	Andari, Firas; Campbell, Jonathan A.; Chalker, Justin M.; Gascooke, Jason R.; Hasell, Tom; Kruger, Jessica E.; Lewis, David A.; Mann, Maximilian; McErlean, Joshua; McKinley, Cheylan C. C.; Perkins, Michael V.; Smith, Jessica A.; Worthington, Max J. H.	Author of portion(s)	Andari, Firas; Campbell, Jonathan A.; Chalker, Justin M.; Gascooke, Jason R.; Hasell, Tom; Kruger, Jessica E.; Lewis, David A.; Mann, Maximilian; McErlean, Joshua; McKinley, Cheylan C. C.; Perkins, Michael V.; Smith, Jessica A.; Worthington, Max J. H.
Volume of serial or monograph	17	Issue, if republishing an article from a serial	7
Page or page range of portion	1929-1936	Publication date of portion	2019-02-13

Total Items: 1   Total Due: 0.00 AUD

438

JOHN WILEY AND SONS LICENSE
TERMS AND CONDITIONS

Dec 06, 2021

This Agreement between Mr. Maximilian Mann ("You") and John Wiley and Sons ("John Wiley and Sons") consists of your license details and the terms and conditions provided by John Wiley and Sons and Copyright Clearance Center.

License Number	5202900714674
License date	Dec 06, 2021
Licensed Content Publisher	John Wiley and Sons
Licensed Content Publication	Journal of Polymer Science Part A: Polymer Chemistry
Licensed Content Title	Combining agriculture and energy industry waste products to yield recyclable, thermally healable copolymers of elemental sulfur and oleic acid
Licensed Content Author	Ashlyn D. Smith, Timmy Thiounn, Elliott W. Lyles, et al
Licensed Content Date	Jul 12, 2019
Licensed Content Volume	57
Licensed Content Issue	15
Licensed Content Pages	7

439

Type of use	Dissertation/Thesis

Requestor type	University/Academic

Format	Electronic

Portion	Figure/table

Number of figures/tables	1

Will you be translating?	No

Title	Sulfur copolymers for coatings, composites and mining applications

Institution name	Flinders University

Expected presentation date	Feb 2022

Portions	Figure 3

Requestor Location	Mr. Maximilian Mann Biological Science Road Bedford Park, SA 5042 Australia Attn: Flinders University

Publisher Tax ID	EU826007151

Total	0.00 AUD

Terms and Conditions

TERMS AND CONDITIONS

440

ELSEVIER LICENSE
TERMS AND CONDITIONS

Nov 30, 2021

This Agreement between Mr. Maximilian Mann ("You") and Elsevier ("Elsevier") consists of your license details and the terms and conditions provided by Elsevier and Copyright Clearance Center.

License Number	5198630901726
License date	Nov 30, 2021
Licensed Content Publisher	Elsevier
Licensed Content Publication	Microporous and Mesoporous Materials
Licensed Content Title	Porous carbons from inverse vulcanised polymers
Licensed Content Author	Joseph C. Bear,James D. McGettrick,Ivan P. Parkin,Charles W. Dunnill,Tom Hasell
Licensed Content Date	Sep 15, 2016
Licensed Content Volume	232
Licensed Content Issue	n/a
Licensed Content Pages	7
Start Page	189
End Page	195
Type of Use	reuse in a thesis/dissertation
Portion	figures/tables/illustrations

441

Number of figures/tables/illustrations	1
Format	electronic
Are you the author of this Elsevier article?	No
Will you be translating?	No
Title	Porous carbons from inverse vulcanised polymers
Institution name	Flinders University
Expected presentation date	Feb 2022
Portions	Scheme 1
Requestor Location	Mr. Maximilian Mann Biological Science Road Bedford Park, SA 5042 Australia Attn: Flinders University
Publisher Tax ID	GB 494 6272 12
Total	0.00 USD

Terms and Conditions

INTRODUCTION

1. The publisher for this copyrighted material is Elsevier. By clicking "accept" in connection with completing this licensing transaction, you agree that the following terms and conditions apply to this transaction (along with the Billing and Payment terms and conditions established by Copyright Clearance Center, Inc. ("CCC"), at the time that you opened your Rightslink account and that are available at any time at http://myaccount.copyright.com).

GENERAL TERMS

2. Elsevier hereby grants you permission to reproduce the aforementioned material subject to the terms and conditions indicated.

442

Rights and permissions Chapter 2

Understanding the factors for increased informal electronic waste recycling in Kumasi, Ghana

Author: Michael Osei Asibey, , Anne Mette Lykke, et al
Publication: International Journal of Environmental Health Research
Publisher: Taylor & Francis
Date: May 12, 2020

Rights managed by Taylor & Francis

Thesis/Dissertation Reuse Request

Taylor & Francis is pleased to offer reuses of its content for a thesis or dissertation free of charge contingent on resubmission of permission request if work is published.

BACK

CLOSE

SPRINGER NATURE LICENSE
TERMS AND CONDITIONS

Dec 15, 2021

This Agreement between Mr. Maximilian Mann ("You") and Springer Nature ("Springer Nature") consists of your license details and the terms and conditions provided by Springer Nature and Copyright Clearance Center.

License Number	5210410287208
License date	Dec 15, 2021
Licensed Content Publisher	Springer Nature
Licensed Content Publication	Springer eBook
Licensed Content Title	Cyanidation of Gold Ores
Licensed Content Author	J. C. Yannopoulos
Licensed Content Date	Jan 1, 1991
Type of Use	Thesis/Dissertation
Requestor type	academic/university or research institute
Format	electronic
Portion	figures/tables/illustrations
Number of figures/tables/illustrations	1
Will you be translating?	no

Circulation/distribution	1 – 29
Author of this Springer Nature content	no
Title	Sulfur copolymers for coatings, composites and mining applications
Institution name	Flinders University
Expected presentation date	Feb 2022
Portions	Page 145 Figure 8-1
Requestor Location	Mr. Maximilian Mann Biological Science Road Bedford Park, SA 5042 Australia Attn: Flinders University
Total	0.00 AUD

Terms and Conditions

SPRINGER NATURE LICENSE
TERMS AND CONDITIONS

Dec 14, 2021

This Agreement between Mr. Maximilian Mann ("You") and Springer Nature ("Springer Nature") consists of your license details and the terms and conditions provided by Springer Nature and Copyright Clearance Center.

License Number	5207900898181
License date	Dec 14, 2021
Licensed Content Publisher	Springer Nature
Licensed Content Publication	Frontiers of Environmental Science & Engineering
Licensed Content Title	A critical review on the recycling of copper and precious metals from waste printed circuit boards using hydrometallurgy
Licensed Content Author	Zebing Wu et al
Licensed Content Date	Oct 23, 2017
Type of Use	Thesis/Dissertation
Requestor type	academic/university or research institute
Format	electronic
Portion	Abstract
Will you be translating?	no
Circulation/distribution	1 - 29

445

Author of this Springer Nature content	no
Title	Sulfur copolymers for coatings, composites and mining applications
Institution name	Flinders University
Expected presentation date	Feb 2022
Requestor Location	Mr. Maximilian Mann Biological Science Road Bedford Park, SA 5042 Australia Attn: Flinders University
Total	0.00 AUD

Terms and Conditions

Springer Nature Customer Service Centre GmbH
Terms and Conditions

This agreement sets out the terms and conditions of the licence (the **Licence**) between you and **Springer Nature Customer Service Centre GmbH** (the **Licensor**). By clicking 'accept' and completing the transaction for the material (**Licensed Material**), you also confirm your acceptance of these terms and conditions.

1. Grant of License

1. 1. The Licensor grants you a personal, non-exclusive, non-transferable, world-wide licence to reproduce the Licensed Material for the purpose specified in your order only. Licences are granted for the specific use requested in the order and for no other use, subject to the conditions below.

1. 2. The Licensor warrants that it has, to the best of its knowledge, the rights to license reuse of the Licensed Material. However, you should ensure that the material you are requesting is original to the Licensor and does not carry the copyright of another entity (as credited in the published version).

1. 3. If the credit line on any part of the material you have requested indicates that it was reprinted or adapted with permission from another source, then you should also seek permission from that source to reuse the material.

2. Scope of Licence

JOHN WILEY AND SONS LICENSE
TERMS AND CONDITIONS

Dec 15, 2021

This Agreement between Mr. Maximilian Mann ("You") and John Wiley and Sons ("John Wiley and Sons") consists of your license details and the terms and conditions provided by John Wiley and Sons and Copyright Clearance Center.

License Number	5210060568008
License date	Dec 15, 2021
Licensed Content Publisher	John Wiley and Sons
Licensed Content Publication	Chemistry - A European Journal
Licensed Content Title	The Mercury Problem in Artisanal and Small–Scale Gold Mining
Licensed Content Author	Louisa J. Esdaile, Justin M. Chalker
Licensed Content Date	Feb 5, 2018
Licensed Content Volume	24
Licensed Content Issue	27
Licensed Content Pages	12
Type of use	Dissertation/Thesis
Requestor type	University/Academic

447

Format	Electronic
Portion	Figure/table
Number of figures/tables	1
Will you be translating?	No
Title	Sulfur copolymers for coatings, composites and mining applications
Institution name	Flinders University
Expected presentation date	Feb 2022
Portions	figure 1
Requestor Location	Mr. Maximilian Mann Biological Science Road Bedford Park, SA 5042 Australia Attn: Flinders University
Publisher Tax ID	EU826007151
Total	0.00 AUD

Terms and Conditions

TERMS AND CONDITIONS

ELSEVIER LICENSE
TERMS AND CONDITIONS

Dec 15, 2021

_____

This Agreement between Mr. Maximilian Mann ("You") and Elsevier ("Elsevier") consists of your license details and the terms and conditions provided by Elsevier and Copyright Clearance Center.

License Number	5210051171001
License date	Dec 15, 2021
Licensed Content Publisher	Elsevier
Licensed Content Publication	Elsevier Books
Licensed Content Title	Electronic Waste Management and Treatment Technology
Licensed Content Author	Florin-Constantin Mihai,Maria-Grazie Gnoni,Christia Meidiana,Chukwunonye Ezeah,Valerio Elia
Licensed Content Date	Jan 1, 2019
Licensed Content Pages	34
Start Page	1
End Page	34
Type of Use	reuse in a thesis/dissertation
Portion	figures/tables/illustrations

Number of figures/tables/illustrations	1
Format	electronic
Are you the author of this Elsevier chapter?	No
Will you be translating?	No
Title	Sulfur copolymers for coatings, composites and mining applications
Institution name	Flinders University
Expected presentation date	Feb 2022
Portions	Figure 4
Requestor Location	Mr. Maximilian Mann Biological Science Road Bedford Park, SA 5042 Australia Attn: Flinders University
Publisher Tax ID	GB 494 6272 12
Total	0.00 AUD

Terms and Conditions

INTRODUCTION

1. The publisher for this copyrighted material is Elsevier. By clicking "accept" in connection with completing this licensing transaction, you agree that the following terms and conditions apply to this transaction (along with the Billing and Payment terms and conditions established by Copyright Clearance Center, Inc. ("CCC"), at the time that you opened your Rightslink account and that are available at any time at http://myaccount.copyright.com).

GENERAL TERMS

450

ELSEVIER LICENSE
TERMS AND CONDITIONS

Dec 15, 2021

This Agreement between Mr. Maximilian Mann ("You") and Elsevier ("Elsevier") consists of your license details and the terms and conditions provided by Elsevier and Copyright Clearance Center.

License Number	5210041007754
License date	Dec 15, 2021
Licensed Content Publisher	Elsevier
Licensed Content Publication	Elsevier Books
Licensed Content Title	Electronic Waste Management and Treatment Technology
Licensed Content Author	Xuning Zhuang
Licensed Content Date	Jan 1, 2019
Licensed Content Pages	24
Start Page	311
End Page	334
Type of Use	reuse in a thesis/dissertation
Portion	figures/tables/illustrations
Number of	1

451

figures/tables/illustrations

Format	electronic
Are you the author of this Elsevier chapter?	No
Will you be translating?	No
Title	Sulfur copolymers for coatings, composites and mining applications
Institution name	Flinders University
Expected presentation date	Feb 2022
Portions	figure 1
Requestor Location	Mr. Maximilian Mann Biological Science Road Bedford Park, SA 5042 Australia Attn: Flinders University
Publisher Tax ID	GB 494 6272 12
Total	0.00 AUD

Terms and Conditions

INTRODUCTION

1. The publisher for this copyrighted material is Elsevier. By clicking "accept" in connection with completing this licensing transaction, you agree that the following terms and conditions apply to this transaction (along with the Billing and Payment terms and conditions established by Copyright Clearance Center, Inc. ("CCC"), at the time that you opened your Rightslink account and that are available at any time at http://myaccount.copyright.com).

GENERAL TERMS

452

Rights and permission Chapter 3

ELSEVIER LICENSE
TERMS AND CONDITIONS

Dec 07, 2021

This Agreement between Mr. Maximilian Mann ("You") and Elsevier ("Elsevier") consists of your license details and the terms and conditions provided by Elsevier and Copyright Clearance Center.

License Number	5203460819364
License date	Dec 07, 2021
Licensed Content Publisher	Elsevier
Licensed Content Publication	Science of The Total Environment
Licensed Content Title	Insight into activated carbon from different kinds of chemical activating agents: A review
Licensed Content Author	Yuan Gao,Qinyan Yue,Baoyu Gao,Aimin Li
Licensed Content Date	Dec 1, 2020
Licensed Content Volume	746
Licensed Content Issue	n/a
Licensed Content Pages	1
Start Page	141094
End Page	0
Type of Use	reuse in a thesis/dissertation
Portion	figures/tables/illustrations

453

Number of figures/tables/illustrations	1

Format	electronic

Are you the author of this Elsevier article?	No

Will you be translating?	No

Title	Sulfur copolymers for coatings, composites and mining applications

Institution name	Flinders University

Expected presentation date	Feb 2022

Portions	Figure 9

Requestor Location	Mr. Maximilian Mann Biological Science Road Bedford Park, SA 5042 Australia Attn: Flinders University

Publisher Tax ID	GB 494 6272 12

Total	0.00 AUD

Terms and Conditions

INTRODUCTION

1. The publisher for this copyrighted material is Elsevier. By clicking "accept" in connection with completing this licensing transaction, you agree that the following terms and conditions apply to this transaction (along with the Billing and Payment terms and conditions established by Copyright Clearance Center, Inc. ("CCC"), at the time that you opened your Rightslink account and that are available at any time at http://myaccount.copyright.com).

GENERAL TERMS

2. Elsevier hereby grants you permission to reproduce the aforementioned material subject to the terms and conditions indicated.

454

Rights and permissions Chapter 4

JOHN WILEY AND SONS LICENSE
TERMS AND CONDITIONS

Dec 09, 2021

This Agreement between Mr. Maximilian Mann ("You") and John Wiley and Sons ("John Wiley and Sons") consists of your license details and the terms and conditions provided by John Wiley and Sons and Copyright Clearance Center.

License Number	5205090228969
License date	Dec 09, 2021
Licensed Content Publisher	John Wiley and Sons
Licensed Content Publication	Chemistry - A European Journal
Licensed Content Title	Crosslinker Copolymerization for Property Control in Inverse Vulcanization
Licensed Content Author	Tom Hasell, Justin M. Chalker, Helen Willcock, et al
Licensed Content Date	Jul 8, 2019
Licensed Content Volume	25
Licensed Content Issue	44
Licensed Content Pages	8
Type of use	Dissertation/Thesis
Requestor type	University/Academic

Format	Electronic
Portion	Figure/table
Number of figures/tables	2
Will you be translating?	No
Title	Sulfur copolymers for coatings, composites and mining applications
Institution name	Flinders University
Expected presentation date	Feb 2022
Portions	Figure 2 and 5
Requestor Location	Mr. Maximilian Mann Biological Science Road

Bedford Park, SA 5042 Australia Attn: Flinders University |
| Publisher Tax ID | EU826007151 |
| Total | 0.00 AUD |

Terms and Conditions

TERMS AND CONDITIONS

456

JOHN WILEY AND SONS LICENSE
TERMS AND CONDITIONS

Dec 09, 2021

This Agreement between Mr. Maximilian Mann ("You") and John Wiley and Sons ("John Wiley and Sons") consists of your license details and the terms and conditions provided by John Wiley and Sons and Copyright Clearance Center.

License Number	5205110160798
License date	Dec 09, 2021
Licensed Content Publisher	John Wiley and Sons
Licensed Content Publication	Chemistry – A European Journal
Licensed Content Title	Reactive Compression Molding Post-Inverse Vulcanization: A Method to Assemble, Recycle, and Repurpose Sulfur Polymers and Composites
Licensed Content Author	Justin M. Chalker, Louisa J. Esdaile, Luke C. Henderson, et al
Licensed Content Date	Jun 18, 2020
Licensed Content Volume	26
Licensed Content Issue	44

457

Licensed Content Pages	10
Type of use	Dissertation/Thesis
Requestor type	University/Academic
Format	Electronic
Portion	Figure/table
Number of figures/tables	1
Will you be translating?	No
Title	Sulfur copolymers for coatings, composites and mining applications
Institution name	Flinders University
Expected presentation date	Feb 2022
Portions	Figure 2A
Requestor Location	Mr. Maximilian Mann Biological Science Road Bedford Park, SA 5042 Australia Attn: Flinders University
Publisher Tax ID	EU826007151
Total	0.00 AUD

458

CCC Marketplace™

Order Confirmation

Thank you, your order has been placed. An email confirmation has been sent to you. Your order license details and printable licenses will be available within 24 hours. Please access Manage Account for final order details.

This is not an invoice. Please go to manage account to access your order history and invoices.

CUSTOMER INFORMATION

Payment by invoice: You can cancel your order until the invoice is generated by contacting customer service.

Billing Address

Mr. Maximilian Mann
Biological Science Road
Bedford Park, SA 5042
Australia

+61 (4)48106964
max.mann@flinders.edu.au

PO Number (optional)

N/A

Customer Location

Mr. Maximilian Mann
Biological Science Road
Bedford Park, SA 5042
Australia

Payment options

Invoice

PENDING ORDER CONFIRMATION

Confirmation Number: Pending

Order Date: 31-Dec-2021

---

1. Polymer chemistry

0.00 AUD

Article: Processes for coating surfaces with a copolymer made from sulfur and dicyclopentadiene

Order License ID	Pending	Publisher	Royal Society of Chemistry
ISSN	1759-9962		
Type of Use	Republish in a thesis/dissertation	Portion	Image/photo/illustration

LICENSED CONTENT

459

Publication Title	Polymer chemistry	**Country**	United Kingdom of Great Britain and Northern Ireland
Article Title	Processes for coating surfaces with a copolymer made from sulfur and dicyclopentadiene	**Rightsholder**	Royal Society of Chemistry
		Publication Type	e-Journal
Author/Editor	Royal Society of Chemistry (Great Britain)	**URL**	http://www.rsc.org/Publishing/Journals/PY/Index.asp
Date	01/01/2010		
Language	English		

REQUEST DETAILS

Portion Type	Image/photo/illustration	**Distribution**	Worldwide
Number of images / photos / illustrations	6	**Translation**	Original language of publication
Format (select all that apply)	Electronic	**Copies for the disabled?**	No
Who will republish the content?	Academic institution	**Minor editing privileges?**	Yes
		Incidental promotional use?	No
Duration of Use	Life of current edition		
Lifetime Unit Quantity	Up to 499	**Currency**	AUD
Rights Requested	Main product		

NEW WORK DETAILS

Title	Sulfur copolymers for coatings, composites, and mining applications	**Institution name**	Flinders University
		Expected presentation date	2022-02-04
Instructor name	Maximilian Mann		

ADDITIONAL DETAILS

Order reference number	N/A	**The requesting person / organization to appear on the license**	Maximilian Mann

REUSE CONTENT DETAILS

Title, description or numeric reference of the portion(s)	Figures 1-6	**Title of the article/chapter the portion is from**	Processes for coating surfaces with a copolymer made from sulfur and dicyclopentadiene
Editor of portion(s)	Mann, Maximilian; Zhang, Bowen; Tonkin, Samuel J.; Gibson, Christopher T; Jia, Zhongfan; Hasell, Tom; Chalker, Justin M	**Author of portion(s)**	Mann, Maximilian; Zhang, Bowen; Tonkin, Samuel J.; Gibson, Christopher T; Jia, Zhongfan; Hasell, Tom; Chalker, Justin M
Volume of serial or monograph	N/A		

460

| Page or page range of portion | 1-8 | Issue, if republishing an article from a serial | N/A |
| | | Publication date of portion | 2022-01-01 |

Total Items: 1 **Total Due: 0.00 AUD**

Accepted: All Publisher and CCC Terms and Conditions

461

SPRINGER NATURE LICENSE
TERMS AND CONDITIONS

Dec 09, 2021

This Agreement between Mr. Maximilian Mann ("You") and Springer Nature ("Springer Nature") consists of your license details and the terms and conditions provided by Springer Nature and Copyright Clearance Center.

License Number	5205101209363
License date	Dec 09, 2021
Licensed Content Publisher	Springer Nature
Licensed Content Publication	Nature Chemistry
Licensed Content Title	The use of elemental sulfur as an alternative feedstock for polymeric materials
Licensed Content Author	Woo Jin Chung et al
Licensed Content Date	Apr 14, 2013
Type of Use	Thesis/Dissertation
Requestor type	academic/university or research institute
Format	electronic
Portion	figures/tables/illustrations
Number of figures/tables/illustrations	1

462

High-res required	no
Will you be translating?	no
Circulation/distribution	1 - 29
Author of this Springer Nature content	no
Title	Sulfur copolymers for coatings, composites and mining applications
Institution name	Flinders University
Expected presentation date	Feb 2022
Portions	Figure 5a
Requestor Location	Mr. Maximilian Mann Biological Science Road Bedford Park, SA 5042 Australia Attn: Flinders University
Total	0.00 AUD

Terms and Conditions

Springer Nature Customer Service Centre GmbH
Terms and Conditions

This agreement sets out the terms and conditions of the licence (the **Licence**) between you and **Springer Nature Customer Service Centre GmbH** (the **Licensor**). By clicking 'accept' and completing the transaction for the material (**Licensed Material**), you also confirm your acceptance of these terms and conditions.

1. Grant of License

1. 1. The Licensor grants you a personal, non-exclusive, non-transferable, world-wide licence to reproduce the Licensed Material for the purpose specified in your order only. Licences are granted for the specific use requested in the order and for no other

463

Rights and Permissions Chapter 5

JOHN WILEY AND SONS LICENSE
TERMS AND CONDITIONS

Dec 09, 2021

This Agreement between Mr. Maximilian Mann ("You") and John Wiley and Sons ("John Wiley and Sons") consists of your license details and the terms and conditions provided by John Wiley and Sons and Copyright Clearance Center.

License Number	5204980088621
License date	Dec 09, 2021
Licensed Content Publisher	John Wiley and Sons
Licensed Content Publication	Macromolecular Chemistry and Physics
Licensed Content Title	Chemically Activated S S Metathesis for Adhesive-Free Bonding of Polysulfide Surfaces
Licensed Content Author	Maximilian Mann, Paris J. Pauling, Samuel J. Tonkin, et al
Licensed Content Date	Nov 23, 2021
Licensed Content Volume	0
Licensed Content Issue	0
Licensed Content Pages	7

464

Type of use	Dissertation/Thesis
Requestor type	Author of this Wiley article
Format	Electronic
Portion	Full article
Will you be translating?	No
Title	Sulfur copolymers for coatings, composites and mining applications
Institution name	Flinders University
Expected presentation date	Feb 2022
Requestor Location	Mr. Maximilian Mann Biological Science Road Bedford Park, SA 5042 Australia Attn: Flinders University
Publisher Tax ID	EU826007151
Total	0.00 USD

Terms and Conditions

TERMS AND CONDITIONS

465

JOHN WILEY AND SONS LICENSE
TERMS AND CONDITIONS

Dec 08, 2021

This Agreement between Mr. Maximilian Mann ("You") and John Wiley and Sons ("John Wiley and Sons") consists of your license details and the terms and conditions provided by John Wiley and Sons and Copyright Clearance Center.

License Number	5204480439511
License date	Dec 08, 2021
Licensed Content Publisher	John Wiley and Sons
Licensed Content Publication	Macromolecular Chemistry and Physics
Licensed Content Title	Chemically Activated S S Metathesis for Adhesive-Free Bonding of Polysulfide Surfaces
Licensed Content Author	Maximilian Mann, Paris J. Pauling, Samuel J. Tonkin, et al
Licensed Content Date	Nov 23, 2021
Licensed Content Volume	0
Licensed Content Issue	0
Licensed Content Pages	7

466

Type of use	Dissertation/Thesis
Requestor type	Author of this Wiley article
Format	Electronic
Portion	Figure/table
Number of figures/tables	1
Will you be translating?	No
Title	Sulfur copolymers for coatings, composites and mining applications
Institution name	Flinders University
Expected presentation date	Feb 2022
Portions	Abstract figure
Requestor Location	Mr. Maximilian Mann Biological Science Road Bedford Park, SA 5042 Australia Attn: Flinders University
Publisher Tax ID	EU826007151
Total	0.00 AUD

Terms and Conditions

TERMS AND CONDITIONS

467